

LEVEL II

0

AGARD-CP-283

AGARD-CP-283

AGARD

ADVISORY GROUP FOR AEROSPACE RESEARCH & DEVELOPMENT

7 RUE ANCELLE 92200 NEUILLY SUR SEINE FRANCE

AD A093658

AGARD CONFERENCE PROCEEDINGS No. 283

Electromagnetic Effects of (Carbon) Composite Materials upon Avionics Systems

DTIC
ELECTE
S JAN 14 1981 D
D

DDG FILE COPY

NORTH ATLANTIC TREATY ORGANIZATION



DISTRIBUTION AND AVAILABILITY
ON BACK COVER

DISTRIBUTION STATEMENT A

Approved for public release;
Distribution Unlimited

81 1 13 074

14

AGARD-CP-283

NORTH ATLANTIC TREATY ORGANIZATION
 ADVISORY GROUP FOR AEROSPACE RESEARCH AND DEVELOPMENT
 (ORGANISATION DU TRAITE DE L'ATLANTIQUE NORD)

AGARD Conference Proceedings No. 283

**ELECTROMAGNETIC EFFECTS OF (CARBON) COMPOSITE
 MATERIALS UPON AVIONICS SYSTEMS**

Edited by

F.S. Stringer
 ADXR/FS
 R.177 Bldg

Royal Aircraft Establishment
 Farnborough, Hants, GU14 6TD
 UK

11

12 372

Accession For	
NTIS GRA&I	<input checked="" type="checkbox"/>
DTIC TAB	<input type="checkbox"/>
Unannounced	<input type="checkbox"/>
Justification	
By	
Distribution/	
Availability Codes	
Dist	Avail and/or Special
A	

DTIC
 ELECTE
 JAN 14 1981
 S D D

Copies of papers and discussions presented at the 39th Technical Meeting, of the Avionics Panel of AGARD, held in Lisbon, Portugal on 16-19 June 1980.

DISTRIBUTION STATEMENT A
 Approved for public release

400 043

THE MISSION OF AGARD

The mission of AGARD is to bring together the leading personalities of the NATO nations in the fields of science and technology relating to aerospace for the following purposes:

- Exchanging of scientific and technical information;
- Continuously stimulating advances in the aerospace sciences relevant to strengthening the common defence posture;
- Improving the co-operation among member nations in aerospace research and development;
- Providing scientific and technical advice and assistance to the North Atlantic Military Committee in the field of aerospace research and development;
- Rendering scientific and technical assistance, as requested, to other NATO bodies and to member nations in connection with research and development problems in the aerospace field;
- Providing assistance to member nations for the purpose of increasing their scientific and technical potential;
- Recommending effective ways for the member nations to use their research and development capabilities for the common benefit of the NATO community.

The highest authority within AGARD is the National Delegates Board consisting of officially appointed senior representatives from each member nation. The mission of AGARD is carried out through the Panels which are composed of experts appointed by the National Delegates, the Consultant and Exchange Programme and the Aerospace Applications Studies Programme. The results of AGARD work are reported to the member nations and the NATO Authorities through the AGARD series of publications of which this is one.

Participation in AGARD activities is by invitation only and is normally limited to citizens of the NATO nations.

The content of this publication has been reproduced directly from material supplied by AGARD or the authors.

Published October 1980

Copyright © AGARD 1980
All Rights Reserved

ISBN 92-835-0277-9



*Printed by Technical Editing and Reproduction Ltd
Harford House, 7-9 Charlotte St, London, W1P 1HD*

THEME

In recent years composite materials have attracted aircraft designers for structural and aerodynamic reasons. These materials have promised lighter, cheaper and possibly stronger airframes and component parts with consequent aircraft performance improvement. Demonstrations have occurred on real aircraft, including combat aircraft wings and helicopter rotor blades.

Despite the physical potential of composites there is debate over their overall benefit technically and the implications of their use. There must be an assessment of the real cost of aircraft as a weapon system when avionics are fully installed. Relevant research is already being conducted in many areas but more work is required. Results of recent studies have not been widely disseminated. The objectives of this meeting were to appraise NATO Nations of the technical status of the problem, provide an opportunity for exchange of views on the Electromagnetic implications of composite materials to aircraft designers, scientists and engineers of various disciplines, and to give operational requirements staffs a more complete understanding of the overall effects of such materials on aircraft design.

PROGRAM AND MEETING OFFICIALS

CHAIRMAN: Mr F.S.Stringer
ADXR/FS
R.177 Bldg
Royal Aircraft Establishment
Farnborough, Hants, GU14 6TD
UK

MEMBERS

Dr J.Taillet
Directeur Scientifique de la
"Physique Générale"
ONERA
29 Avenue de la Division Leclerc
92320 Chatillon-sous-Bagneux
France

Mr M.G.Jube
Sous-Directeur à la Prospective
Aérospatiale
37 Bld de Montmorency
75016 Paris
France

Prof. Dr M.O.Kiciman
Civil Engineering Department
ODTU
Middle East Technical University
Ankara
Turkey

Dr Ing. M.Vogel
DFVLR e.v.
8031 Oberpfaffenhofen
Post Wessling/obb
Germany

Mr W.F.Ball
Avionics Division
Naval Weapons Center (Code 4041)
Dept. of the Navy
China Lake, CA 93555
USA

Mr R.Baggess
Wright Patterson Air Force Base
Dayton, Ohio, 45433
USA

AVIONICS PANEL

CHAIRMAN: Dr Ing. M.Vogel
DFVLR e.v.
8031 Oberpfaffenhofen
Post Wessling/obb
Germany

DEPUTY CHAIRMAN: Mr Y.Brault
Thomson CSF
Division Equipments
Avioniques et Spatiaux
178 Bld Gabriel Péri
92240 Maikoff
France

↓
CONTENTS :

	Page
THEME	iii
PROGRAM AND MEETING OFFICIALS	iv
CHAIRMAN'S REPORT	vii
	Reference
<u>SESSION I – MATERIALS AND APPLICATIONS</u>	
CURRENT AND PROJECTED USE OF CARBON COMPOSITES IN UNITED STATES AIRCRAFT by R.W.Leonard and D.R.Mulville	1
EFFET DE L'ENVIRONNEMENT EN SERVICE SUR LES MATERIAUX COMPOSITES par G.Jubé	2
APPLICATION OF CARBON FIBRE COMPOSITES TO MILITARY AIRCRAFT STRUCTURES by T.Sharples	3
<u>SESSION II – CHARACTERISTICS, MEASUREMENTS, MODELLING AND STANDARDS</u>	
ELECTROMAGNETIC SHIELDING CHARACTERISTICS OF ADVANCED COMPOSITES by D.F.Strawe	4
THEORETICAL CALCULATION OF RF PROPERTIES OF CARBON FIBRE LAMINATES by D.C.Brewster	5
RF RESISTIVITY AND SCREENING CHARACTERISTICS OF CFC MATERIALS by D.A.Bull, G.A.Jackson and B.W.Smithers	6
THE MEASUREMENTS OF ELECTRICAL CONDUCTIVITY IN CARBON/EPOXY COMPOSITE MATERIALS OVER THE FREQUENCY RANGE OF 75 MHz to 2.0 GHz by W.F.Walker	7
EMC, LIGHTNING AND NEMP-PROTECTION – NEW REQUIREMENTS FOR APPROVED SPECIFICATIONS WHEN USING CFRP by D.Jaeger and K.H.Rippl	8
THE ELECTRICAL EFFECTS OF JOINTS AND BONDS IN CARBON FIBRE COMPOSITES by J.Brettle, K.J.Lodge and R.Poole	9
<u>SESSION III – SPECIFIC TOPICS AND RESEARCH PROGRAMS</u>	
THE UK MINISTRY OF DEFENCE PROGRAMME ON THE ELECTROMAGNETIC PROPERTIES OF CARBON FIBRE COMPOSITES by J.M.Thomson and R.H.Evans	10
PROGRAMME FRANCAIS D'ESSAIS EN VOL SUR LES EFFETS ELECTROMAGNETIQUES DE LA Foudre par J.C.Alliot et D.Gall	11
AIRCRAFT MANUFACTURERS APPROACH TO THE E.M.C./AVIONICS PROBLEMS ASSOCIATED WITH THE USE OF COMPOSITE MATERIALS by G.Barton and I.P.MacDiarmid	12
CONDUCTIVITY MODIFICATION OF BORON FIBERS by R.Y.Kwor and C.A.Paz de Araujo	13

	Reference
TENSION INDUITE DANS LES CABLES A L'INTERIEUR DE STRUCTURES FERMEES METALLIQUES ET EN CARBONE EPOXY SOUMISES A UNE IMPULSION DE COURANT TYPE Foudre par D.Gall	14
ELECTROMAGNETIC INTEGRATION OF COMPOSITE STRUCTURE IN AIRCRAFT by G.L.Weinstock	15
<u>SESSION IV – ELECTROMAGNETIC EFFECTS UPON RADIATION PATTERNS, ELECTROSTATIC AND LIGHTNING PROBLEMS</u>	
ESSAIS EN VOL POUR L'ETUDE DES PERTURBATIONS RADIOELECTRIQUES D'ORIGINE ELECTROSTATIQUE par P.Laroche, R.Weber et D.Gall	16
THE BEHAVIOUR OF CFRP PANELS IN METAL AIRCRAFT DURING SIMULATED LIGHTNING STROKES by B.J.C.Burrows and A.W.Hanson	17
INFLUENCE ON ANTENNA GAIN AND POLARIZATION PURITY OF REFLECTORS MANUFACTURED FROM CARBON FIBRE COMPOSITE MATERIALS by L.Heichele	18
LIGHTNING THREAT DEFINITION FOR COMPOSITE AIRCRAFT by P.Geren	19
<u>SESSION V – PROTECTION AND TRADEOFF METHODS</u>	
ELECTRICAL/ELECTROMAGNETIC CONCERNS ASSOCIATED WITH ADVANCED COMPOSITE MATERIALS IN AEROSPACE SYSTEMS by C.L.Blake and J.C.Corbin, Jr	20
IN DEPTH STUDIES OF COMPOSITE AIRCRAFT ELECTROMAGNETIC PERFORMANCE by J.Birken	21
ELECTROMAGNETIC COUPLING TO ADVANCED COMPOSITE AIRCRAFT WITH APPLICATION TO TRADE-OFF AND SPECIFICATION DETERMINATION by R.Wallenberg, E.Burt and G.Dike	22
DISCUSSIONS, with Addendum by G.Davis and F.L.Vogel	D
LIST OF ATTENDEES	A

Electromagnetic Effects of (Carbon) Composite Materials
upon Avionics Systems

Chairman's Report

AGARD. Avionics Panel
39th Technical Specialists Meeting
Lisbon, Portugal.
June, 1980

1. GENERAL INFORMATION

The meeting was arranged between 16-19 June 1980. The first three days were devoted to the technical presentations and discussion, the fourth was reserved for a technical visit to the Civil Engineering Facility, Maritime Research Centre, Lisbon.

The total registered attendance was 93 and this number of delegates was mostly present right up to the closing ceremony. The number of papers presented was 22 with only two being offered as reserves for papers withdrawn late in the preparatory period; for national reasons.

Nearly all of the papers were invited, this proved successful since the material and the presentations were of a high standard and they fitted reasonably within the framework of the session titles.

Five sessions were arranged. Each author was allowed 30 minutes for presentation allowing 15 minutes for discussion time. This proved useful since slow speech was possible, to aid the interpreters, and themes could be developed adequately. The deliberate limit set on the number of papers presented was therefore beneficial.

An unprecedented number of questions and formal answers were offered. They have been recorded and edited for publication with the proceedings of the meeting.

2. SCOPE OF THE TECHNICAL COVERAGE

Despite the physical potential of composite materials for aircraft engineering, especially carbon fibre composites (CFC), there has been debate over their true benefit technically and the implications of their use. The promise of cheaper, lighter and possibly stronger airframes with consequent aircraft performance improvement has encouraged aircraft designers to include such structures as components in demonstrator aircraft and to plan for a wide application of CFC in future aircraft designs. The impact of electromagnetic effects generated by the introduction of composites has been the subject of research but no serious discussion had occurred prior to this specialist meeting on an international scale, so far as could be determined. Neither had there been a forum for an exchange of views and experience on this subject between the airframe designers and the avionics and electronic systems engineers. To establish this latter point, the meeting was arranged to follow closely in time the meeting of the Structures and Mechanics Panel of AGARD held in Greece in March 1980 when composite materials were discussed. The Avionics Panel Specialist Meeting in Lisbon was opened by the Panel Chairman, Dr Martin Vogl and the delegates were welcomed to Portugal by Captain Mascarenhas PAF on behalf of General Bourbonne. The first presentation was offered by Mr M.G. Jubé, Chairman of the STP; it included a summary of the proceedings and conclusions of the STP meeting which set the scene for the AVP discussions in Lisbon. The Lisbon programme was divided into five Sessions comprising:

- Session I Materials and Applications
- Session II Characteristics, Measurement, Modelling and Standards
- Session III Specific Topics and Research Programmes
- Session IV Electromagnetic Effects upon Radiation Patterns, Electrostatic and Lightning Problems
- Session V Protection and Trade-off Methods

3. SESSION I

The summary of the SMP meeting outlined several of the fabrication techniques employed and referred to many of the areas in aircraft construction which will employ composites in future. The paper by Messrs Leonard and Mulville gave a most valuable insight into the use of CFC in the USA. The paper by Mr T. Sharples describing the application to military aircraft structures summarised the advantages to the Structural engineer and he gave a very useful survey of the factors which reduce the effectiveness of CFC. An important statement covered the effects of moisture effects, variability in mechanical performance with lay-up arrangements and the resulting material strengths. It was encouraging to note that the airframe manufacturers were aware of electromagnetic effects such as EMC, screening, bonding and earth returns but there was a general air of surprise among delegates at the great extent to which CFC was to be employed in both fixed wing aircraft and helicopters of the future. Mr Leonard and Mr Sharples were questioned closely as can be noted from those questions and answers included in the proceedings.

4. SESSION II

Measurement of Electrical Characteristics

The presentations suggested that no generally accepted test methods exist. Thus it is very difficult to compare measurement data. However, the most important parameters were established as

resistivity/conductivity
anisotropy
inhomogeneity

Papers by Strawe/Geren (4), Smithers (6) and Walker (7) dealt with measuring methods and measurement data.

Existing Standards

The impact of electrical characteristics of CFC upon existing standards and specifications for test methods of avionic systems have not yet been taken into account. This is especially true of external EMC. Design guides for electronic equipment should include such parameters.

Theoretical Understanding

The theoretical understanding of CFC is not yet fully complete, especially non-linear effects.

Bonding

In view of power earth returns and lightning current-carrying capability, more research is needed upon bonding methods when using CFC. Such research will require close liaison between structural and avionics engineers to achieve the optimum benefits of CFC application.

5. SESSION III

Six papers were presented in this session which covered some specific topics relating to lightning effects and to the use of boron fibers.

The first paper was written by Mr R.H. Evans and Dr J.M. Thomson, both of the Royal Aircraft Establishment at Farnborough. Dr Thomson presented the paper. It described the CFC work in the UK dating back to 1970 and indicated its relationship as part of the far wider MOD(PE) programme on electromagnetic effects. Overall, the UK programme is aimed at ensuring that adequate information on CFC utilization is available for aircraft and flight weapon systems projects to allow quantitative clearance for service introduction. The paper gave a preliminary assessment of the electromagnetic impact of CFC as identified to date by the programme. Major problem areas identified were:

- a. HF penetration of the CFC aircraft skin, expected to be worse than with the already difficult aluminum skin.
- b. Bonding and jointing - the major problems lie not with CFC itself, but with the bonding and jointing of the material.

The paper concluded by indicating the future direction of the programme which was probably half-way through its life.

The second of this session dealt with a French Programme studying the electromagnetic effects of lightning. The paper was prepared by Mr J.C. Alliot of ONERA and Mr D. Gall of CEAT, and presented by Mr Alliot.

Directed by the French Aeronautical Technical Services, a flight test programme to evaluate the electromagnetic disturbances caused by lightning was defined which has been in hand since 1978. The aircraft utilized is a TRANSALL C-160 from the Air Force, which carries instrumentation to detect the phenomena associated with direct or proximity hits, lightning current (pulsed and direct), skin currents at different points of the structure, interior and exterior electromagnetic fields, and overloads upon a variety of equipment. Various recorders permit the characterization of the aircraft electrical status during lightning strikes.

The effects of electromagnetic radiation upon structural panels made of composite materials was of particular interest to define protection systems. After a number of modifications to the instrumentation employed during the 1978 tests, new experiments are planned for the summer 1980 with the following objectives:

- i Obtain qualitative information regarding the electromagnetic energy coupling modes caused by lightning.
- ii Understand the effects of a variety of structural panels made of composite materials when subjected to lightning.
- iii Evaluate the electric state of a vehicle when subjected to lightning.

- iv Characterize the electrical wavelengths on the aircraft structure under lightning conditions.

A paper by Mr Ian MacDiarmid, of British Aerospace, Warton, and Mr Glenn Barton of Westland Helicopters Limited, was delivered jointly. It first described lightning strike tests conducted on CFC panels for the Jaguar aircraft. The results indicated were that no significant change in the EMC clearance of the aircraft resulted from introduction of CFC panels. A second set of tests described were conducted on composite rotor blades for flight clearance. The rotor blades had a carbon trailing edge with a Glass Reinforced Plastic spar and titanium erosion shield. With this composite rotor, the concern was that of certifying a design which provided an adequate electrical path to conduct moderate severity lightning strikes. Test results showed no degradation in rotor structural strength. Further improvements are under way. Other work described on the paper outlined the investigation of longer term problems relating in general to CFC effects on avionic systems, including CFC fuselage investigations, conductivity measurements and an earth return study.

Paper four, by Mr R.Y. Kwor and Mr C.A. Paz de Araujo of the University of Notre Dame, described some research work being conducted on Boron Fibers. The paper was read by Dr J. Walker of the Rochester Institute of Technology and the characteristics and typical application methods of these fibers were reviewed. Boron fibres are noted for their low dc conductivity. The research was aimed at evaluating methods for increasing this conductivity so that its application might be practical. Tests were conducted on both carbon diffused boron and nickel-plated boron. The conclusion showed that carbon doping cannot be used because of limitations of mechanical properties. Nickel, on the other hand, proved to be very compatible with boron, yielding excellent improvements in conductivity. It appeared to take considerable effort to prepare the boron for test and the cost-effectiveness of using it as a substitute material would have to be evaluated.

A fifth paper described the voltage induced in wiring cables in the interior of closed metallic and carbon epoxy structures when subjected to a pulse of current as might be caused by lightning. It was written by Mr D. Gall and presented theoretical and experimental results on the mechanism of induced overvoltage on electric wiring located inside closed structures when subjected to lightning currents. The contribution of two parameters, diffusion of skin currents and the internal electromagnetic field, was discussed for two types of structures: aluminum alloy and carbon fibres. It was shown that the frequency spectrum of lightning at maximum power is at frequencies lower than 100 KCZ and that carbon fibres offer 3000 times less protection than aluminum alloy in both overvoltage and effects of electromagnetic conditions due to lightning.

The last paper of Session III was written and delivered by Mr G. Weinstock of McDonnell Aircraft. This paper revealed an extensive amount of effort in CFC applications by MCAIR for both the F-18 and AV-8B aircraft. The aircraft have extensive applications of graphite/epoxy composite material. The paper described and discussed these extensive studies and test programs at MCAIR backing the introduction of the G/E material to these aircraft. The work evaluated G/E shielding capability noting that the principal reason for shielding ineffectiveness was the reduction associated with discontinuities at seams and joints (agreeing with results of the MOD(PE) programme described in paper number one). It has been shown that improvements in G/E joints can be made and are effective. Other study results indicated that G/E ground planes for Antenna (UHF and L band) allow proper antenna functioning. Further, adequate lightning protection can be accomplished. Mr Weinstock stated that he had not yet found any electromagnetic G/E issue that could not be handled as part of a typical aircraft development program.

In summary, there was some agreement between several of the papers. The problems encountered to date seem to be responding with care and the application of good engineering practice.

6. SESSION IV

In particular this Session concentrated upon the electromagnetic effects upon radiation patterns, electrostatic and lightning problems. Four papers covered this field by authors from the US, France, Germany and the UK. An interesting topic for discussion was the effect of introducing metal skins by vacuum deposit or other means. Pilot protection was another topic which will need further research. A very important aspect raised in discussion but not in the presentations was the application of fibre optics to ensure adequate EMC.

7. SESSION V

Session V covered Protection and Trade-off Methods. Again the discussion highlighted a certain unease in the avionic fraternity that protective methods might not be sufficient. The possible need for harder avionic systems to meet the demands created by CFC applications indicated that the delegates were not entirely satisfied with the state of the art. It is likely that much more research will be needed on this topic.

8. In conclusion it was evident that future systems designers will require guidelines to meet the extra electronic demands generated by the application of CFC to aircraft structures. It is clear that the wide application of CFC may be commonplace in the not too distant future. The claim by some airframe manufacturers that there was no problem in meeting lightning EMC and electrostatic demands was evidently received with some scepticism by several delegates. It was stressed many times that from now on airframe and avionic systems designers must liaise closely as designs develop. The meeting revealed several new innovations, particularly new electrostatic dischargers and data upon CFC electromagnetic tests. It will be necessary to standardise dimensions in the analysis of data however to prevent prolonged argument over

the relevance of some research results. A means of ensuring this could be an early consideration of the topic by one of the NATO project committees.

The programmes presented are regarded by many research engineers as half complete. There was some encouragement from delegates that another review such as the Lisbon Specialists Meeting should be held as those programmes neared completion to assess the recommended solutions to problems which have arisen and will no doubt continue to arise.

F S STRINGER
Programme Chairman

CURRENT AND PROJECTED USE OF CARBON
COMPOSITES IN UNITED STATES AIRCRAFT

by

Robert W. Leonard
National Aeronautics and Space Administration
Langley Research Center
Hampton, VA, USA, 23665

and

Daniel R. Mulville
Department of the Navy
Naval Air Systems Command
Washington, D.C., USA, 20361

Abstract

Because of demonstrated weight savings and potential manufacturing cost savings, carbon composite materials are beginning to be used in commercial transports, general aviation aircraft, military fighter aircraft and helicopters. Current production applications of carbon composites range from the secondary structures of new commercial transports to wing primary structures of fighters, and current development efforts assure their future application to fuselages, and even whole airframes, for performance gains and fuel efficiency. Laminate construction characteristics, that may be relevant to avionics system design, vary widely.

INTRODUCTION

The term "composite structures," as now generally used and as specifically used in this paper, refers to structures comprised of filaments of one material--with relatively high strength or stiffness per unit mass--embedded in a homogeneous matrix of another, usually softer, material. While "fiberglass" composites, consisting of glass filaments in epoxy, have been extensively used for some time in aircraft secondary structures (1), a primary focus of current interest is composites composed of fine carbon filaments in epoxy (or another polymer) because of their combination of very high strength and stiffness with potentially low cost. Research on structures molded from carbon composite systems dates from the mid-1960's (2) and has been strongly supported by the United States Government through the Department of Defense, and the National Aeronautics and Space Administration. Included has been extensive research on electrical properties and the effects of lightning strikes on carbon composites (3,4).

While current applications in commercial transport aircraft are confined to secondary structure, carbon composites are already being applied, in military aircraft, to empennage and wing primary structure and limited use in fuselage structure has begun. Moreover, development efforts toward future extensive use of carbon composites in empennage, wing, and fuselage primary structures are underway or planned.

This paper briefly reviews the pertinent characteristics of carbon composite structures. It then outlines their current and projected use in commercial transports and other civil aircraft, in military fighter aircraft, and in helicopters. Typical examples are cited to display relevant details of composition and construction.

CHARACTERISTICS OF CARBON COMPOSITE STRUCTURES

The benefits of carbon fiber composite materials arise from their higher strength/density and stiffness/density ratios compared to available metal alloys and other composites. This is illustrated in figure 1, (5). As illustrated by the typical ranges of values in figure 1, the specific strength and stiffness of fiber composite materials vary, not only with the relative fractions of fiber and matrix, but also with the ply stacking sequence and the directional relationships of applied loads to the directions of fibers in the plies which make up a composite laminate. Because practical aircraft structures are subjected to a varied spectrum of flight and other loads leading to different multiaxial stress states at each point of the structure, full-time alignment of fibers with stress directions is not possible. Nor is such alignment generally desirable from the standpoint of acceptable defect and damage tolerance or acceptable durability since concentration of too much strain energy in today's somewhat brittle carbon fibers can lead to imperfection sensitivity and to violent failures. Added to this are low design-ultimate-strain limits (about 3000 $\mu\text{in/in}$ for commercial transport applications) which must be imposed on today's composite structures to assure acceptable long term performance of currently available epoxy matrix materials. Thus, practical aircraft applications of carbon fiber composites now and in the near future generally relate to the lower strength and stiffness values in figure 1. In spite of this, they offer component weight savings in the 20-30% range and, with further gains possible through production of tougher fiber and matrix materials, the future of carbon fiber composites in aircraft structures seems assured.

Property variations already exist of course among the fiber and matrix materials in use today. Table 1 summarizes some of the basic physical properties (6) of fiber materials that are produced in sufficient quantities for current applications. The conductivity of individual fibers varies somewhat as indicated by the relative electrical resistance values in Table 1 (7). These were measured by passing low levels of Direct Current through 1-cm-long fibers clamped between gold contacts. Substantially higher electrical resistance values for carbon fibers may be feasible, as indicated by the comparable results in Table 2 for three fibers that have not been developed to readiness for structural applications.

The conductivity of epoxies and other polymeric matrix materials is essentially zero so that cross-fiber conductivity of composite arrays depends on the degree of fiber-to-fiber contact and, thus, on fiber volume fraction. Inductive coupling between fibers is also a factor and the electrical conductivity of finished composite laminates is clearly a function of the fiber directional array and stacking sequence in the laminate. For example, measured directional conductivities of a spectrum of symmetric orthotropic laminates, composed of plies of unidirectional tapes, is given in Table 3 (8).

Not reflected in such results is the recent introduction of bidirectional carbon cloth (fig. 2), which is "pre-pregged" (impregnated with raw epoxy or other resin) after weaving, and thus may provide more nearly isotropic conductivity within a cloth layer. Cloth is often combined with tape in a laminate and is frequently used as the inner surface layer of skins and stiffener flanges to control fiber breakout in drilling of cured composites. Exterior surfaces, whether cloth or tape, will be painted in virtually all applications and use of aluminum mesh or flame sprayed metal coatings over critical areas for lightning protection is not uncommon. Metal fasteners, as well as these metal coatings, will always be electrically isolated from the graphite with a nonconductive sealant or layer to prevent galvanic corrosion of the metal surface at the interface.

CARBON COMPOSITE STRUCTURES IN CIVIL AIRCRAFT

Applications of carbon fiber composites to commercial transports and other civil aircraft have lagged behind applications to military aircraft because, in civil applications, composites must not only save substantial weight relative to competing metal designs, but must be cost competitive as well. For civil transports, additional constraints are the inherently great sensitivity of certifying authorities to the safety implications of new technology, the concern of users that unexpected problems may cause revenue losses from down time, and the necessary conservatism of manufacturers whose warranties include life guarantees. For these reasons, introduction of carbon composites into commercial transports can only occur gradually, beginning with "secondary structure," i.e., with components whose failure will not threaten the safety of the aircraft and which can be quickly replaced if failures occur within the aircraft lifetime.

Transport Secondary-Structure Applications

Current applications of carbon fiber composite structures in commercial transport aircraft are limited to flight service of prototype secondary structures. The most extensive such application to date is the flight of 27 Boeing 737 aircraft with up to four composite spoilers on each aircraft (fig. 3). The spoilers have covers of aluminum-core honeycomb construction with carbon epoxy skins consisting of 61% fibers in a [15/-45/90₂/45/-15] laminate formed with tape.* Three different carbon/epoxy systems employing both Union Carbide T-300 and Hercules AS (Courtaulds A) fibers have been used (9). Their development and flight service has been supported by the National Aeronautics and Space Administration (NASA) and Boeing has recently projected their commitment to production on 737 aircraft as early as 1980 (10,11).

A second current application, supported by NASA in the context of its Aircraft Energy Efficiency Program, is development and flight service of 20 composite upper-aft rudders for the Douglas DC-10 (fig. 4). This is a two-spar, multirib structure (fig. 5) with solid carbon/epoxy spars, ribs, and skins consisting of 70% Union Carbide T-300 fibers in tape arranged in [0/±45]_s** laminates. The aluminum alloy straps and a cable to the forward rudder hinge bracket provide a conductive path for lightning. The first rudders began flight service in 1977 and all have now been committed to flight.

*Fiber fractions designated in this paper will, in every case, refer to volume. The arrangement of tapes and bidirectional cloth plies to form a laminate will be designated by specifying fiber direction in degrees for each ply, or group of identically oriented plies (whose number is denoted by a subscript) progressing from the outer to inner surface for skins and spars. For bidirectional cloth, the direction of the "warp" fibers is indicated. The 0° direction (denoted by 0 without the degree symbol) will refer to the outboard spanwise direction for wing and empennage mounted structures and the forward direction for fuselage mounted structures.

**Where a subscript s follows the brackets, symmetry with respect to the centerline of the laminate thickness is indicated and the directional designations refer to only the plies in the outer half-thickness.

Current commercial flight applications of limited numbers of prototype secondary composite structures also include selected components developed in industry IRAD programs. For example, secondary components which have been committed to flight on the Douglas DC-9 and DC-10 aircraft, along with the DC-10 upper aft rudder, are also illustrated in figure 4. Included are engine cowls and examples of lightly loaded fuselage surface structure (landing gear door, tail cone) and internal floor structure as well as vertical tail trailing edge surface panels which close the gap between the control surfaces and the rear spars.

Further commercial transport applications of carbon composite control surface structure in the near future have been accelerated by development of two additional such composite structures in the NASA Aircraft Energy Efficiency Program. One is a composite inboard aileron for the Lockheed L-1011. This is a two-spar rib-stiffened structure where both covers are relatively thin sandwiches with syntactic/epoxy cores (epoxy, filled with hollow glass microspheres) and carbon/epoxy face sheets consisting of 61% Union Carbide T-300 fibers in 3 plies of tape. The layup for each cover is [45/0/135/syn]_s, where syn designates the syntactic/epoxy layer. The front spar is carbon/epoxy tape in the layup [45/0/135/0/90]. No lightning protection is prescribed. Ten shipsets of L-1011 carbon composite ailerons will be produced for flight service.

The third NASA-supported control-surface structures effort is development of composite elevators for the Boeing 727. Their construction (fig. 6) employs sandwich covers and a minimum number of spars and ribs with sandwich webs. The sandwich covers have nomex cores and carbon/epoxy face-sheets consisting of 64% carbon fibers in layups illustrated in figure 7. Lightning protection consists of a 0.51 mm (0.02 inch) thick, 5.1 cm (2 inch) wide aluminum alloy strap encircling the elevator surface over the outer 99 cm (39 inches) of length (fig. 8). Five shipsets, manufactured in the NASA program with Union Carbide T-300 fibers, have been committed to flight service with one of Boeing's customers for the new 767; nine more T-300 shipsets are being assembled with company funds for flight service.

The B-727 elevator development has led to Boeing commitment to production application of generically similar carbon composite sandwich construction in all the control surfaces (elevators, rudder, ailerons, and spoilers) of both the 767 and 757 aircraft for introduction into airline service in 1982 and 1983 respectively. As shown in figure 9 for the 767, carbon fiber use on these aircraft, in a hybrid composite with Kevlar fibers, extends also to the fixed trailing edge panels behind the wing and tail rear spars, the wing-body fairings, landing gear doors, engine cowls and wing leading edge access panels. The carbon fiber is again Union Carbide T-300 in a tape inner layer which, with an outer Kevlar cloth ply, makes up the face sheets of nomex-core honeycomb sandwich. Carbon fiber composites used in the 767 total some 1300 Kg (2900 lb). Note also, in figure 9, the extensive use of fiberglass and Kevlar composites.

While current plans for fuselage interior composite secondary structure on the Boeing 767 (fig. 9) cite fiberglass floor panels (fig. 10), the use of carbon fibers in such structure appears to be growing. For example, limited use of carbon composite floor panels is already occurring on a small number of the Boeing 747's and 747SP's produced and recent projections (10,11) indicate that by 1983, use of carbon composites, as a customer option, may be extended to greater floor panel areas, the overhead storage bins, and ceiling panels. In fact, carbon composite ceiling panels and storage bins (fig. 10) are also projected for the Boeing 707, 727, 737, 757, and 767 aircraft with some of these applications possibly occurring as early as 1981. And carbon composite floor beams and panels on half the Lockheed L-1011's produced, beginning in 1983, is also projected (10). The matrix materials in such applications will probably be phenolics, but electrical properties should be comparable to carbon/epoxy structures. Of course, in every case, this internal carbon composite structure is entirely surrounded by a metal fuselage shell.

Transport Primary-Structure Applications

Early production applications of carbon composites to commercial transport primary structure are unlikely, but such structure will reach the prototype flight service stage in 1981 in the context of NASA's Aircraft Energy Efficiency Program. Primary structures under development in this program include the Boeing 737 Horizontal Stabilizer box (fig. 3) which is a two-spar structure with eight ribs and I-stiffened skins consisting of 62% Union Carbide T-300 fibers. The skins have 5 to 15 plies of bidirectional cloth and 2 to 4 plies of tape with the outer surface layers tape oriented in the $\pm 45^\circ$ directions and the inner surface layer cloth. Skin stiffeners, spars, and ribs are also largely cloth construction with six or more layers. Lightning protection is provided by aluminum flame spray over the outer 48 cm of the stabilizer box plus metal tip, leading edge, and trailing edge structure (fig. 3).

A second carbon composite primary structure under development in the NASA program, is the vertical fin box of the Lockheed L-1011 (fig. 11). Its construction is illustrated by figure 12. The covers are hat stiffened skins with 10 to 40 plies of tape in the skins and 20 full-length plies of tape in the hat stiffeners. The outer and inner skin plies are oriented in the $\pm 45^\circ$ direction. The spars have 20 to 24 plies of tape in their webs and 10 to 12 plies in their caps. Most ribs have aluminum truss members for webs. The fiber is again Union Carbide T-300 and the fiber volume fraction is 62% to 68%. No external lightning protection for the fin covers is currently planned, although a special conductive joint is provided between the covers and metal leading and trailing edge structure.

The third commercial transport carbon composite primary structure, under current development in the NASA program is the Douglas DC-10 vertical stabilizer (fig. 4). This structure is an array of 4 spars and 13 ribs all of which have sine-wave webs consisting

of 2 to 5 layers of bidirectional cloth. Covers are sandwich, with 58-ply spar and rib caps built in and nomex honeycomb with 2 45° cloth plies in the outer face sheet and 1 45° ply for the inner face sheet. Laminates are 65% Union Carbide T-300 fibers. As shown in figure 13, the vertical stabilizer has two antennae near its upper end and lightning protection is provided by an aluminum flame spray coating over the whole surface (except the antennae) plus aluminum tip and leading edge structure, and conductive joints at the rudder hinges and skin panel edges.

Production applications of the carbon composite empennage primary structure being developed in the NASA ACEE Program are unlikely because economically the competitors are metal components well down the manufacturing cost curve. However, new designs of empennage, for aerodynamic or other reasons, could well be produced as early as the mid-1980's in generically-similar carbon composite forms.

The application of carbon composites to commercial transport wing primary structures was studied in the NASA ACEE Program (12,13,14) and electromagnetic effects was identified as a major technology issue. Wing primary structure will include many plies of carbon tape or cloth near the root, with thicknesses near the tip on the order of thicknesses of the above-cited empennage structures. While application of carbon composites to commercial transport wing and fuselage primary structures is certain if fuel costs continue to rise, such applications are unlikely to occur before 1990. Thus, for current and near-future applications of carbon composites to wing and fuselage primary structures, one must look to smaller aircraft for private or military use.

"General Aviation" Aircraft Applications

Application of carbon composites to secondary structures of general aviation aircraft has only just begun with the use of carbon/epoxy flaps and spoilers on the Cessna Citation III. In spite of this late start by the general aviation industry, one manufacturer (LearAvia Corporation) has already launched the development of the world's first "all-carbon-composite" production aircraft, the Lear Fan 2100.* This is a 10-place, twin-engine turboprop aircraft with a 12.2 meter (40 foot) wing span and a 12.2 meter (40 foot) fuselage length. Tooling preparation is underway and production of some structural parts for the first (prototype flight test) vehicle has begun.

As shown in the exploded view of the Lear Fan's air frame and propulsion elements in figure 14, the only elements with substantial metal content, besides the engines, drive train, transmission, and landing gear, are an aluminum nosewheel-well structure and the fuselage floor, which is paneled with an aluminum layer electrically connected to the wheel-well structure to form a conductive path front-to-back at the floor line. Avionics boxes are mounted on the nosewheel-well structure to provide a ground plane and electrical conductors are routed along the underside of the floor.

Exterior skin construction (fig. 14) consists of 4 or more plies of T-300 woven carbon/epoxy cloth (Fiberite "8-harness Satin") except for the tip of the forward fuselage cone which is a Kevlar/epoxy radome. The fuselage is reinforced with carbon/epoxy frames and stringers and pressure bulkheads are nomex-core honeycomb with woven cloth carbon/epoxy face sheets. The wings have three tip-to-tip channel-section spars and a number of ribs consisting of multiple layers of the woven carbon/epoxy cloth. Empennage construction is similar. There is some use of carbon/epoxy tape in the caps of the various stiffening elements. Design specifications call for maintaining slightly less than 60% fiber volume fraction throughout.

Lightning protection for the entire fuselage of the Lear Fan 2100 is intended since its full length is a direct strike zone. Aluminum strips are planned on the radome and an aluminumized fiberglass or aluminum flame spray layer will be applied over the rest of the fuselage surface. An alternate system under investigation involves aluminum wire interwoven with graphite fabric. Other areas requiring this protection are the wing roots, tips and trailing edges.

CARBON COMPOSITE STRUCTURES IN MILITARY AIRCRAFT

The United States' military services have led the way in both research and development toward carbon composite structures and in their production applications. Secondary structure, of course, came first. Carbon/epoxy underwing fairings on United States Air Force F-111's were introduced into service on production aircraft in 1971 and speed brakes on Air Force F15's were converted to carbon/epoxy, beginning in 1975. Production applications of carbon composites to empennage primary structure quickly followed, building on extensive earlier applications of boron composites. For example, the Air Force F-16, with a carbon/epoxy horizontal stabilizer and carbon/epoxy vertical stabilizer skins, first flew in 1976. Because a detailed review of these would add little to what has been said above, we will move on instead to examples which include the earliest applications of carbon composites to wing primary structure and illustrate the outlook for such applications to fuselage primary structure. We will also review the status of carbon composite applications to helicopters and the outlook for extensive helicopter applications.

*The authors are indebted to Mr. R. Tracey and colleagues of LearAvia Corporation, Reno, Nevada for the information on the Lear Fan 2100 which is presented in this paper.

Fighter Aircraft Primary-Structure Applications

Beginning in the latter half of the 1970's, two United States Navy aircraft emerged with extensive applications of carbon/epoxy composites in production structure (15). One of these is the F-18 (fig. 15) in which carbon composites comprise almost 10% of the structural weight and over 50% of the surface area. They are used in the wing skins and the horizontal and vertical tail primary load-carrying boxes, as well as in wing and tail control surfaces, the speed brake, leading edge extension, and miscellaneous doors.

The F-18 carbon composite wing skins are 70% Hercules AS (Courtaulds A) fibers in a solid quasi-isotropic laminate. Thickness varies from root to tip with the minimum thickness equivalent to 40 5-mil plies of tape in a layup consisting of 48% each 0° and ±45° plies and 4% 90° plies. Construction of the tail primary structure is comparable.

The most ambitious military use of composites to date is on the United States Navy's AV-8B (fig. 16) where 26% of the structural weight is carbon-epoxy structure. Carbon composite components, with 70% Hercules AS (Courtaulds A) fibers, include the wing load-carrying box and forward fuselage primary structure as well as the horizontal stabilizer, elevators, rudder, overwing fairing, ailerons, flaps and lift-augmentation devices. Construction of the AV-8B wing and associated secondary structure is illustrated in figure 17. The wing skins are one-piece tip-to-tip laminates with a minimum thickness equivalent to 20 5-mil plies of "unidirectional broadgoods" in a layup composed of 15% each 0° and 90° plies, 30% each ±22½° and ±45° plies, and 10% ±67½° plies. The skins are mechanically fastened to a multi-spar sub-structure with sine-wave webs where the material is bidirectional woven cloth. Aluminum leading edge and tip structures channel lightning currents around the carbon/epoxy fuel-carrying box.

As also seen in figure 17, skins of the wing trailing edge secondary structures are also unidirectional broadgoods and sub-structure is bidirectional cloth, except for the flap slot door which is full-depth-honeycomb construction. Construction of the horizontal stabilizer is similar to the wing, except for use of tape in the covers and flat, laminated webs in the spars.

The AV-8B carbon composite forward fuselage development was initiated some two years ago (16,17). This structure envelops the crew station and AV-8B equipment and systems; therefore, development testing has included assessment of electromagnetic effects. It is all carbon/epoxy, stiffened solid laminate with longerons, bulkheads, and frames (fig. 18). The sidewalls are co-cured with hat stiffeners; skins are bidirectional cloth construction with a minimum thickness of 5 plies in a [45/0/45/0/45] laminate. The floor, bulkheads, and frames are the same basic construction as the sidewalls with cloth webs and co-cured hat stiffeners.

Because substantial further weight reduction through advanced composites can only be achieved by fuselage applications and mission requirements establish a need for 12-15% further reduction in system structural weight of some aircraft types, a current major development thrust toward fuselage applications is underway (16). Two United States Navy programs are addressing carbon composite structures for the center and aft fuselage sections of V/STOL patrol aircraft, for example (18,19); one of these is an all carbon/epoxy stiffened-skin design while the other is a hybrid Kevlar/carbon/epoxy design. Relative to this thrust, questions of systems compatibility, including electromagnetic interference and electromagnetic pulse effects, are recognized as key technical issues (16).

It is apparent that carbon composite structural applications in fighter, and other military aircraft will continue to increase, and that carbon composite fuselage construction must be expected in future military aircraft. Whether fixed-wing military aircraft will approach "all-composite" construction still remains to be seen; but projections of 50% advanced composite structure by weight may be found (16).

Helicopter Applications**

The limited current use of carbon composites on production helicopters is typified by use of carbon fibers for rotorblade reinforcement. However, extensive use of fiberglass and Kevlar in fuselage secondary structure is already common and fuselage applications of carbon filaments can be expected soon. For example, figure 19 shows projected use of carbon on the Hughes Advanced Attack Helicopter (AAH) where development of the carbon composite tail boom and vertical stabilizer have already begun. Use of carbon fibers in the tail boom and fin of the Sikorsky UH-60 Blackhawk (also known as the Utility Tactical Transportation Aircraft System) is also projected, but in a hybrid combination with Kevlar. Various miscellaneous applications, to landing gear struts, rotor hubs, rotor gear boxes, etc., are also being explored.

*Though they have the width of bidirectional cloth, "unidirectional broadgoods" have the structural and electrical characteristics of tape in that they consist of about 95% parallel carbon filaments and about 5% interwoven transverse dacron filaments.

**The authors are indebted to J. Waller, T. Mazza and A. Gustafson of the Applied Technology Laboratories U.S. Army Research and Technology Laboratories, Fort Eustis, Virginia, for the information contained in this section and the associated figures.

Carbon fibers used in current helicopter structures applications are the same as those used in fixed-wing aircraft structures; most current applications involve Union Carbide T-300 fibers. The tail-boom configuration, however, lends itself to efficient fabrication by filament winding and this approach, with realistic limits on filament tension, leads to structures with fiber volume fractions as low as 50%. Thus, cross-fiber conductivities, and possibly laminate conductivities, may be relatively low in such applications.

Even more extensive applications of carbon composites in the more distant future are likely to follow from the U.S. Army's Advanced Composite Airframe Program (ACAP). As illustrated in figure 20, this program is exploring composites application to virtually every element of fuselage structure and both tail surfaces. Primary structure is carbon or carbon/Kevlar hybrid composite while secondary structure is fiberglass. Five contractors are completing preliminary designs of composite advanced versions of one of their existing aircraft; the program will continue with two contractors proceeding to detail design, ground test, fabrication by each of one advanced composite vehicle, and flight demonstration about 3 years hence. Lightning protection specifications are such as to generally require addition of some form of protective metal screen.

Such an extensive application of carbon composites to military helicopters will not likely occur for at least five years. However, competitive pressures may stimulate earlier introduction of some of the advanced components explored in the Advanced Composite Airframe Program, since three of the five preliminary designs are derivatives of commercial helicopters.

SUMMARY

Current carbon composite applications to commercial transports are limited to secondary (non-flight-critical) structures, but this use is already extensive on two new Boeing aircraft and will soon be widespread, involving fuselage as well as wing and tail secondary components. Carbon composite empennage primary structure for transports is also under development and production applications can be expected by the mid-1980's. Development of composite wing and fuselage structure for commercial transports is certain to follow as fuel costs rise.

"General aviation" aircraft applications of carbon composites have only just begun, but may soon lead the way with the first all-carbon composite aircraft structure, which is already under development for the 10-place Lear Fan 2100.

In the meantime, military aircraft production commitments of carbon composite structure have already progressed to empennage and wing primary structure and to part of a fuselage structure in two United States Navy fighter aircraft. Moreover, need for performance gains is forcing the rapid development of capability for further application of carbon composites to complete fuselages.

Helicopter production applications of carbon composites are also projected to soon include tail booms and other primary structure and the United States Army is vigorously exploring the potential of all-composite airframes, with use of carbon fibers in primary structure, for possible future applications.

In summary, carbon composite materials are already finding limited use in both civil and military aircraft structures to exploit their weight-saving potential for improved performance or fuel efficiency. Since these needs are growing, and a manufacturing-cost-savings potential is also recognized, wider use of composites in the near future may be expected. Carbon composites generally involve fiber volume fractions in excess of 60% in a variety of orthotropic sandwich or solid laminates. Bidirectional woven carbon cloth, common in recently designed structure, may provide higher, more uniform laminate conductivities than tape.

REFERENCES

1. Buffam, H. E. and Thompson, V. S. Transition from Glass to Graphite in Manufacture of Composite Aircraft Structure, NASA Conference Publication 2036, Part I, Proceedings of the CTOL Transport Technology-1978 conference held at Langley Research Center, Hampton, VA, USA, February 28-March 3, 1978, p. 331.
2. Advances in Structural Composites, Proceedings of Society of Aerospace Materials and Process Engineers 12th National Symposium and Exhibit, Anaheim, CA, October 10-12, 1967.
3. Force, R., Geren, P., Strawe, D. and Schmidt, A. Investigation of the Effects of Electromagnetic Energy on Advanced Composite Aircraft Structures and their Associated Avionic/Electrical Equipment-Phase II, Vol. 1, Final Report. Report D180-20186-4 for the Naval Air Systems Command by the Boeing Company, September 1977.
4. Fisher, F. A. and Plumer, J. A. Lightning Protection of Aircraft, NASA RP-1008, October 1977.

5. Vosteen, L. F. Advanced Composites for Aircraft. Presented at the ASCE Annual Convention, Pittsburgh, PA, April 25, 1978.
6. Advanced Composite Design Guide, Vol. IV (3rd Edition), Air Force Flight Dynamics Laboratory, Contract No. F33615-74-C-3075, January 1977.
7. Taback, I., Tanguy, J. S., Salmirs, S., Butterfield, A. J. and Bartron, T. R. Experimental and Analytical Studies for the Graphite Fiber Risk Assessment, NASA CR-159214, 1980.
8. Gajda, W. J. Measurement of the Electrical Properties of Composite Materials in the Frequency Range of DC to 30 MHz, AFSC RADC-TR-79-203, August 1979.
9. Stoocklin, R. L. Development, Manufacturing, and Test of Graphite-Epoxy Composite Spoilers for Flight Service on 737 Transport Aircraft, NASA CR-132682, October 1976.
10. Pocinki, L., Kaplan, L. and Cornell, L. Advanced Risk Assessment of the Effects of Graphite Fibers on Electronic and Electrical Equipment. Final Phase II Report. NASA CR-159210, 1980.
11. Clarke, R. B. Review of Accident and Incident Data and Development of Carbon Fiber Use Projection. Report on Task Assignment No. 1, Carbon/Graphite Fiber Risk Analysis and Assessment Study for the National Aeronautics and Space Administration, Contract No. NAS1-15510, December 1978.
12. Harvey, S. T. and Michaelson, G. L. Advanced Composites Wing Study Program, Vol. 1- Executive Summary, NASA CR-145382-1, Vol. 2-Final Report, NASA CR-145382-2, National Aeronautics and Space Administration, Contract No. NAS1-15003, August 1978.
13. Watts, D. J. A Study of the Utilization of Advanced Composites in Commercial Aircraft Wing Structure-Executive Summary, NASA CR-158902-1,-Final Report, NASA CR-158902-2, National Aeronautics and Space Administration, Contract No. NAS1-15004, July 1978.
14. Sakata, I. F. Ostrom, R. B. and Cardinale, S. V. Utilization of Advanced Composites in Commercial Aircraft Wing Structures-Executive Summary, NASA CR-145381-1,-Final Report, NASA CR-145381-2, National Aeronautics and Space Administration, Contract No. NAS1-15005, August 1978.
15. Weinberger, R. A., Somoroff, A. R. and Riley, B. L. U.S. Navy Certification of Composite Wings for the F-18 and Advanced Harrier Aircraft, AGARD Report No. 660 (Certification Procedures for Composite Structures) April 1977.
16. Minecci, J. J. and Hess, T. E. "Composite Fuselage Development for Naval Aircraft." Presented at the Society of Aerospace Materials and Process Engineers (SAMPE) meeting, San Diego, CA, May 6-8, 1980.
17. "YAV-8B Program Engineering Investigations of Composite Applications" U.S. Navy Contract No. N00019-76-C-0666, McDonnell Aircraft Company.
18. "Advanced Composite Center Fuselage Program" U.S. Navy Contract No. N62269-78-C-0017, Grumman Aerospace Corporation.
19. "Advanced Composite Aft Fuselage Program" U.S. Navy Contract No. N62269-78-C-0502, Vought Corporation.

TABLE 1. Physical Properties of Available Carbon Fibers

MANUFACTURERS AND FIBER DESIGNATIONS	MASS DENSITY GM/CM ³	ULTIMATE STRENGTH, 10 ⁹ N/M ²	YOUNGS MODULUS, 10 ⁹ N/M ²	ELECTRICAL RESISTANCE, K OHMS *		
				MAX.	MIN.	AVE.
UNION CARBIDE T-300	1.74	2.24	234	6.5	5.5	6.2
HERCULES (COURTAULDS)						
AS (A)	1.80	2.07	193	4.9	3.2	4.0
HTS	1.72	2.41	248	5.2	3.4	4.3
HMS	1.88	2.07	365	3.9	2.0	2.3
CELANESE						
GY-70	1.97	1.72	531	4.1	1.6	2.9
C-6000	1.76	2.76	234	8.4	4.3	6.4

* APPROXIMATE VALUES FOR COMPARISON PURPOSES, OBTAINED WITH 1 CM LENGTH SINGLE FIBERS CLAMPED BETWEEN GOLD CONTACTS (REF 7).

TABLE 2. Electrical Resistances of Early Experimental Fibers (Ref 7)

FIBER DESIGNATIONS	ELECTRICAL RESISTANCE, K OHMS *		
	MAX.	MIN.	AVE.
DE-110	320	160	200
DE-112	20	14	16
DE-114	89	75	80

* APPROXIMATE VALUES OBTAINED FOR COMPARISON WITH TABLE 1 VALUES BY THE SAME PROCEDURE.

TABLE 3. Measured Conductivities of Some Orthotropic Layups (Ref 8)

LAYUP*	MEASURED CONDUCTIVITY (mhos/m) for current in the:	
	0° DIRECTIONS	90° DIRECTIONS
[0 / 90] _s	7000	3000
[0 / 45 / 90] _s	5000	1700
[0 / ±45 / 90] _s	8000	2500
[0 / ±45 / 0 / 90] _s	5333	1540
[0 / ±45 / 0 / 90 / 90] _s	5000	2500
[0 / 90 / ±45 / ±45 / 90 / 0] _s	2500	5000

* s denotes a symmetrical layup; that is, one half the number of layers are specified from left to right as they exist from the outer surface to the center of the laminate.

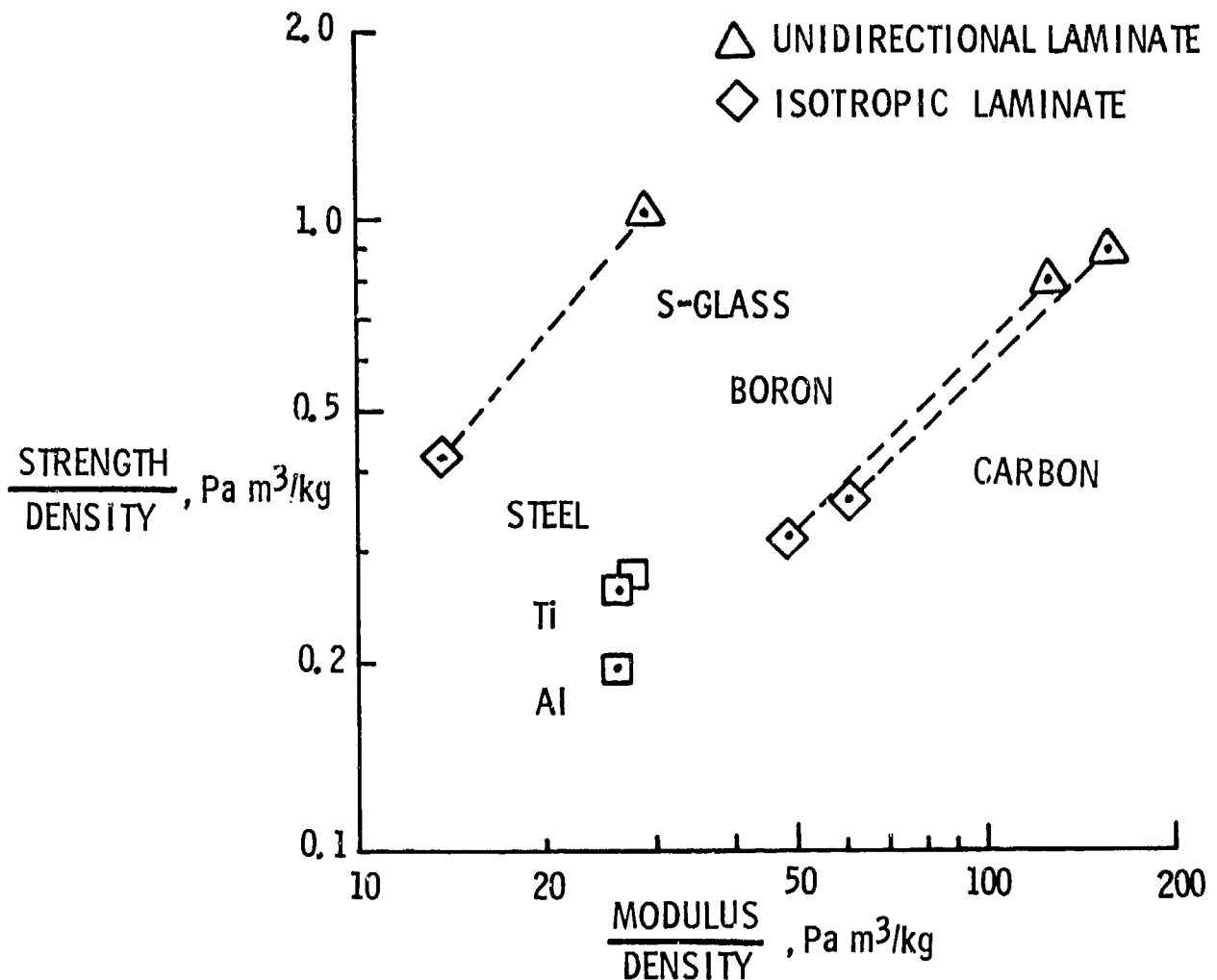


FIGURE 1. Specific Strength and Stiffness of Composites and Metals

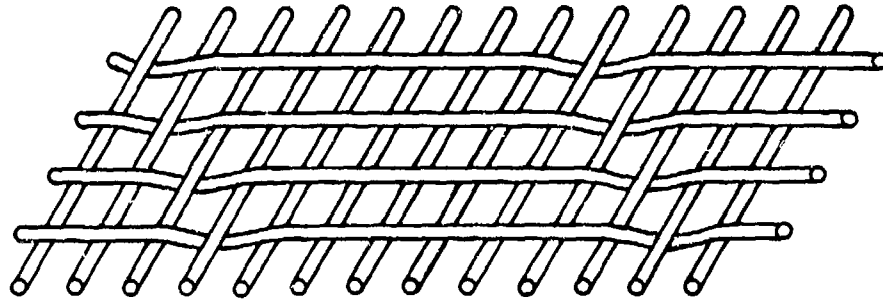


FIGURE 2. Typical Bidirectional Weave of Carbon Cloth

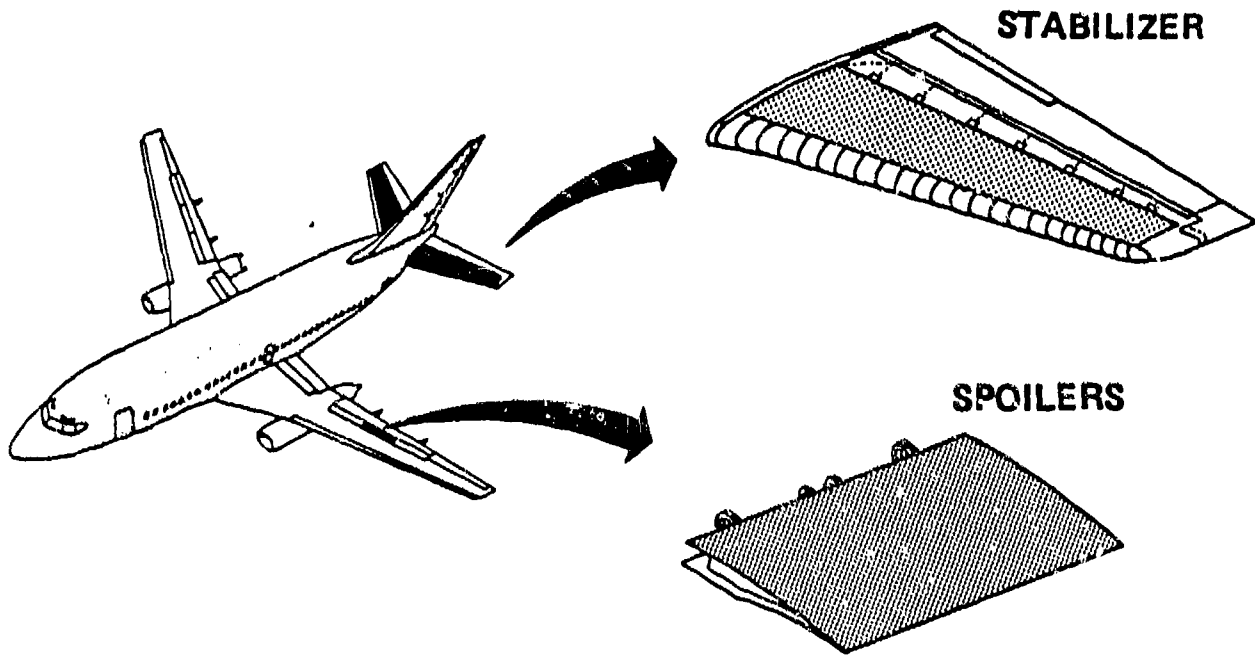


FIGURE 3. Carbon Composite Spoilers and Horizontal Stabilizer on the Boeing 737

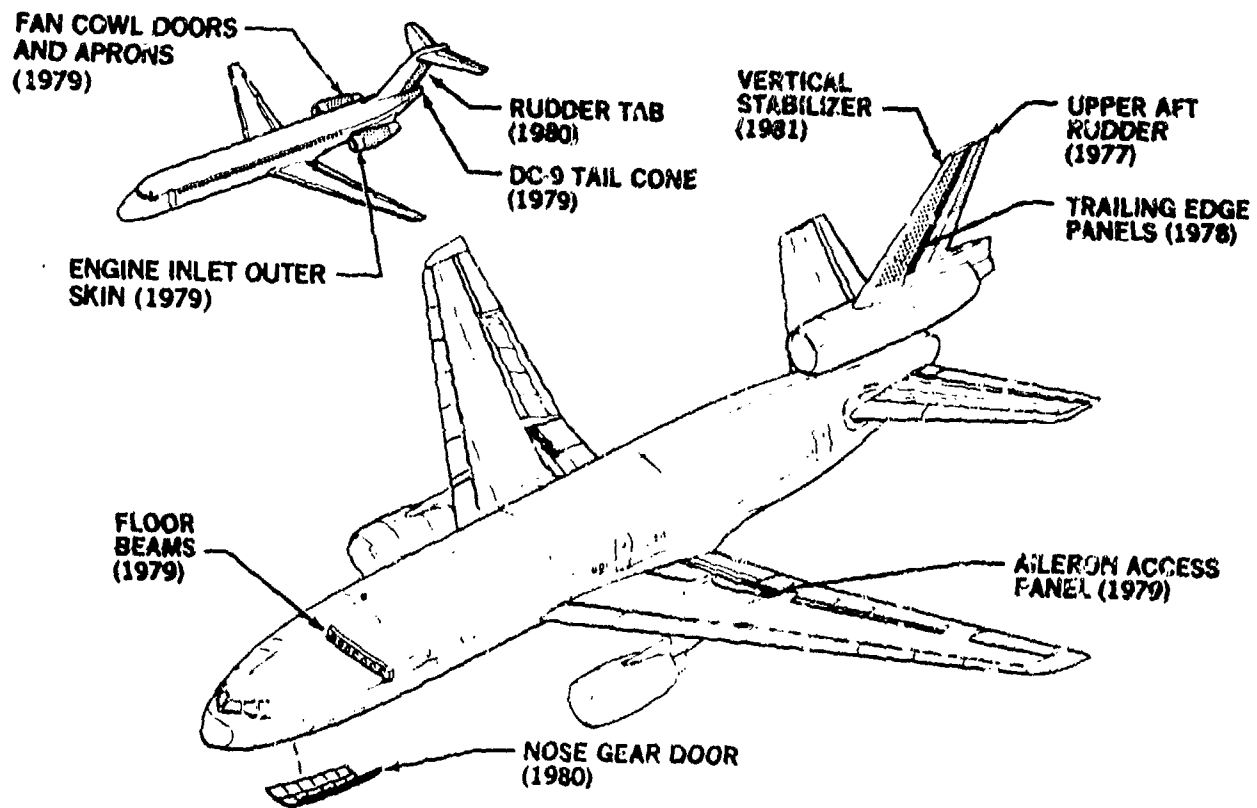


FIGURE 4. Douglas Carbon Composite Structure Applications

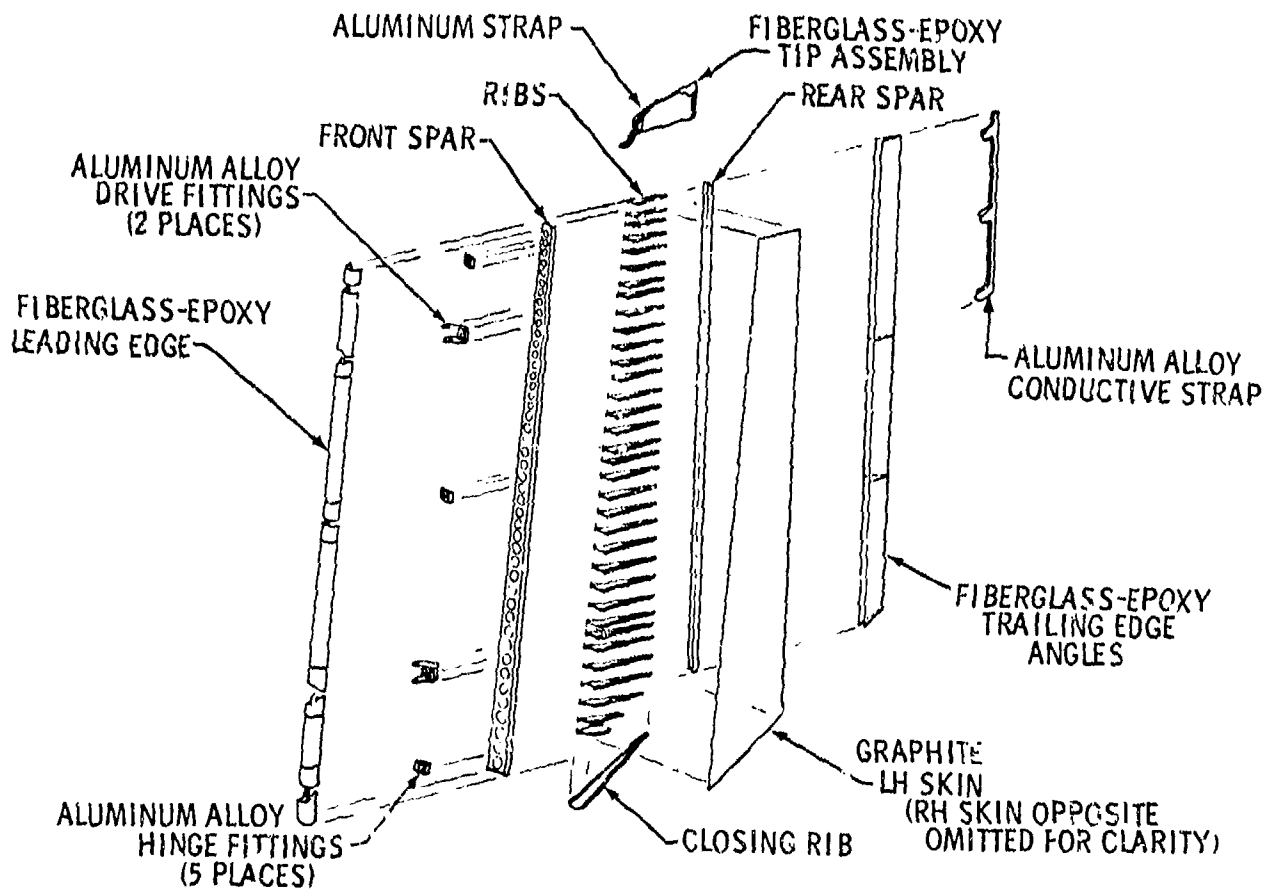


FIGURE 5. Construction of the DC-10 Composite Upper Aft Rudder

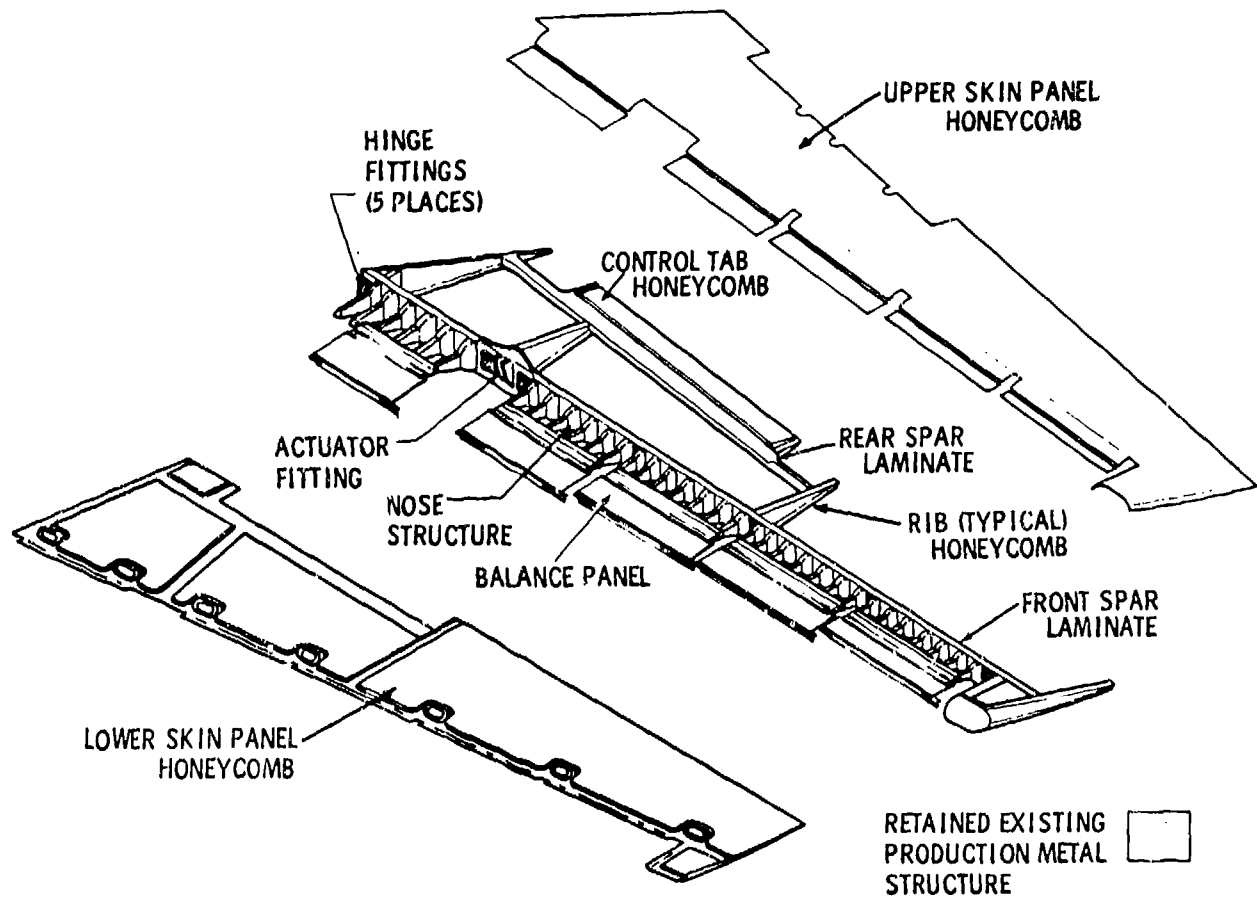


FIGURE 6. Construction of Composite B-727 Elevators

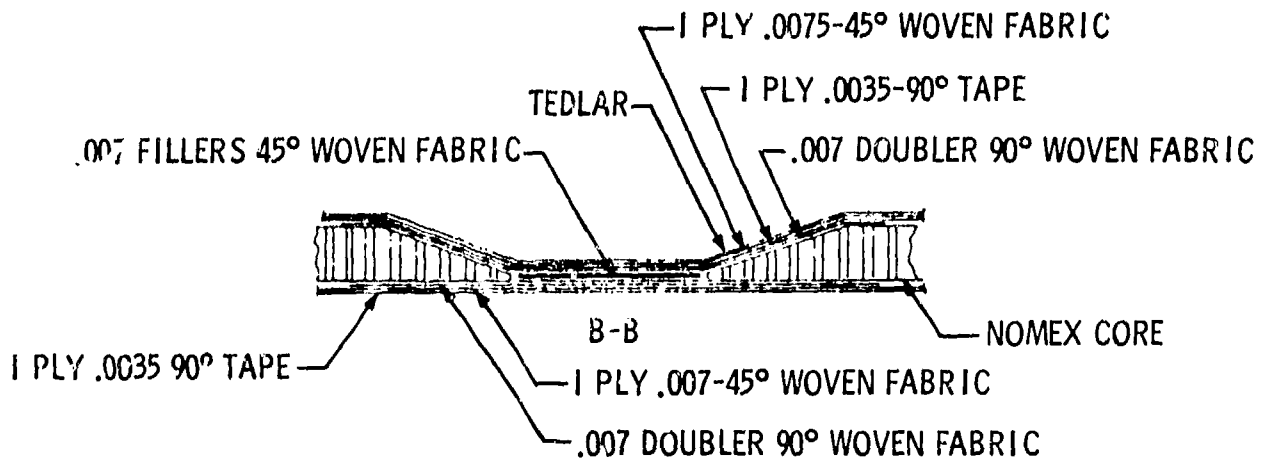


FIGURE 7. Layup of Composite B-727 Elevator Skins at Rib Location

STATIC DISCHARGE FITTINGS

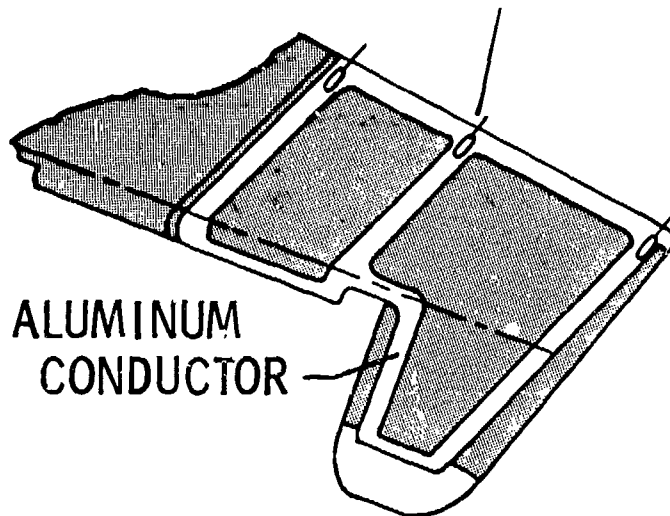


FIGURE 8. Composite B-727 Elevator Lightning Protection

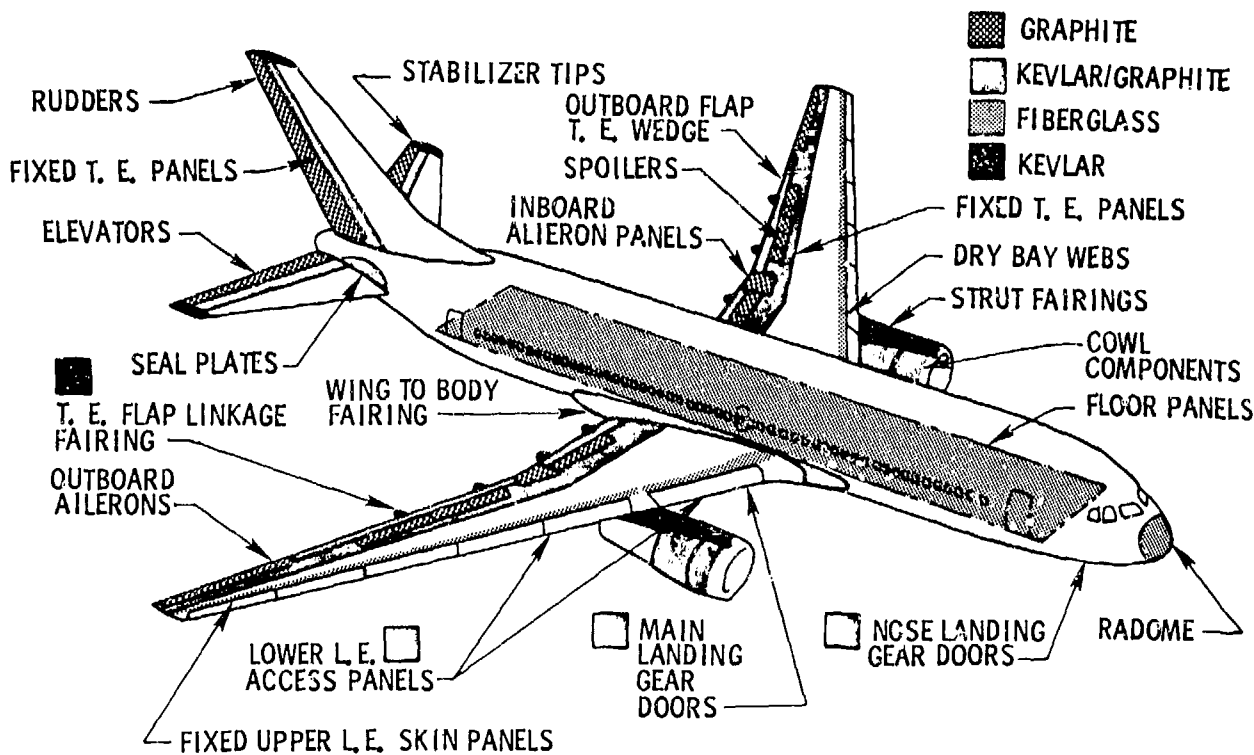


FIGURE 9. Composite Structure on the Boeing 767

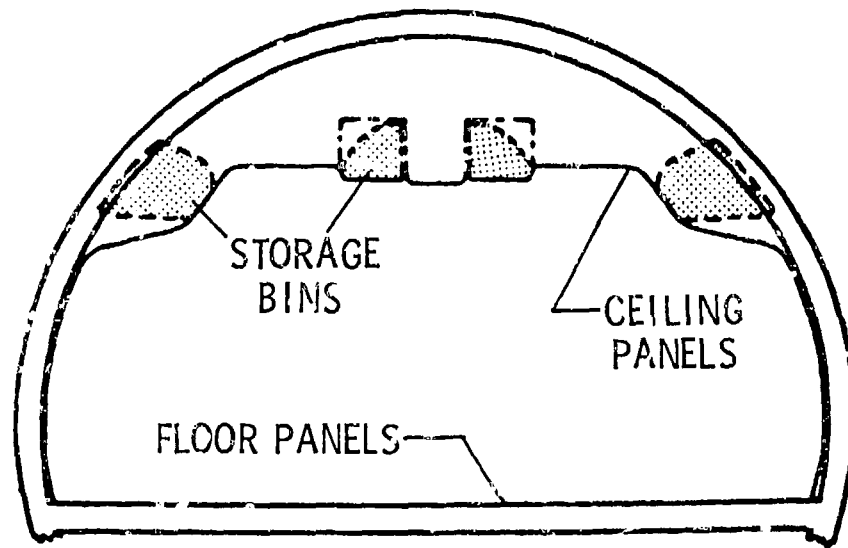


FIGURE 10. Ceiling Panels and Overhead Storage Bins

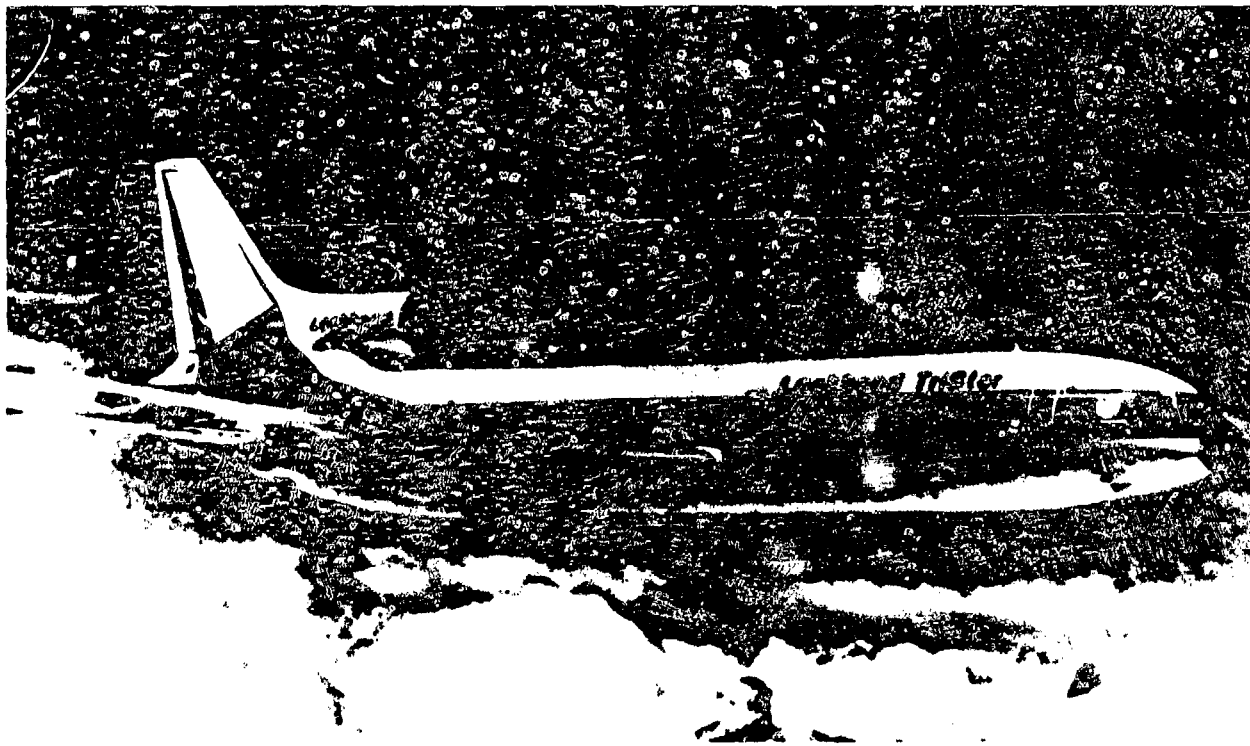


FIGURE 11. L-1011 Advanced Composite Vertical Fin (ACVF)

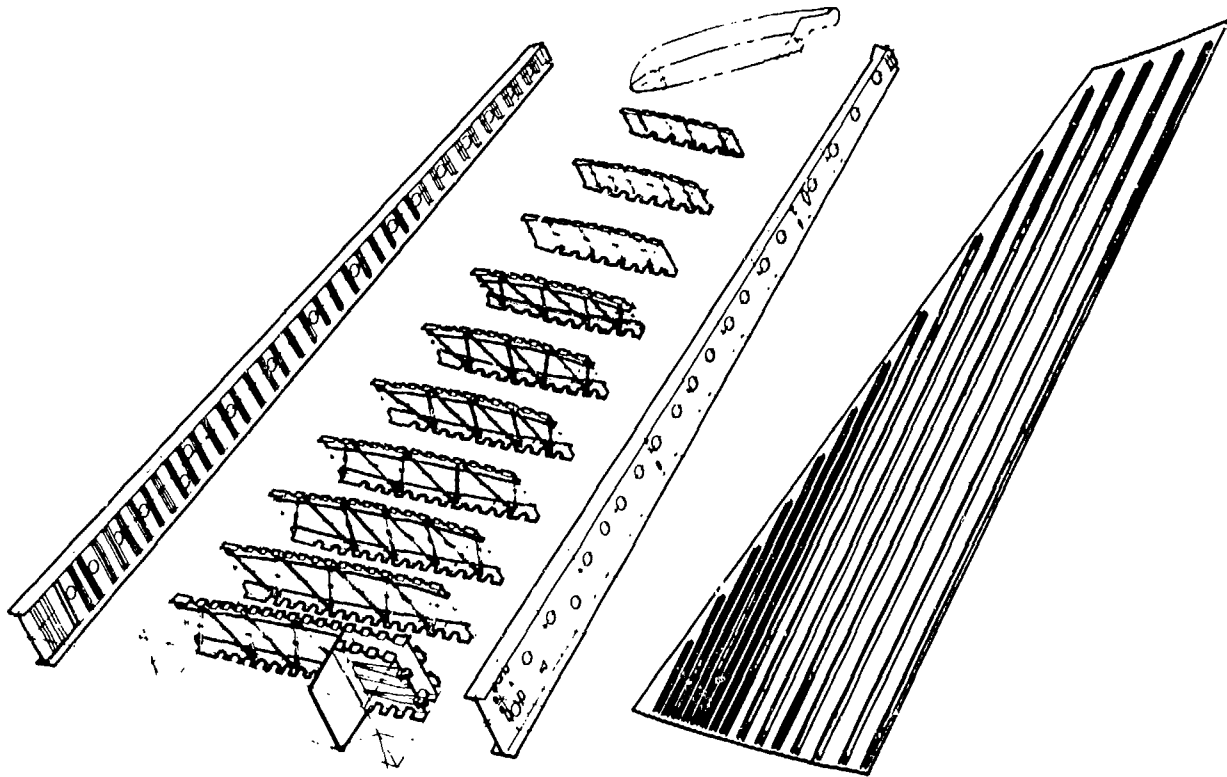


FIGURE 12. L-1011 ACVF Structural Configuration

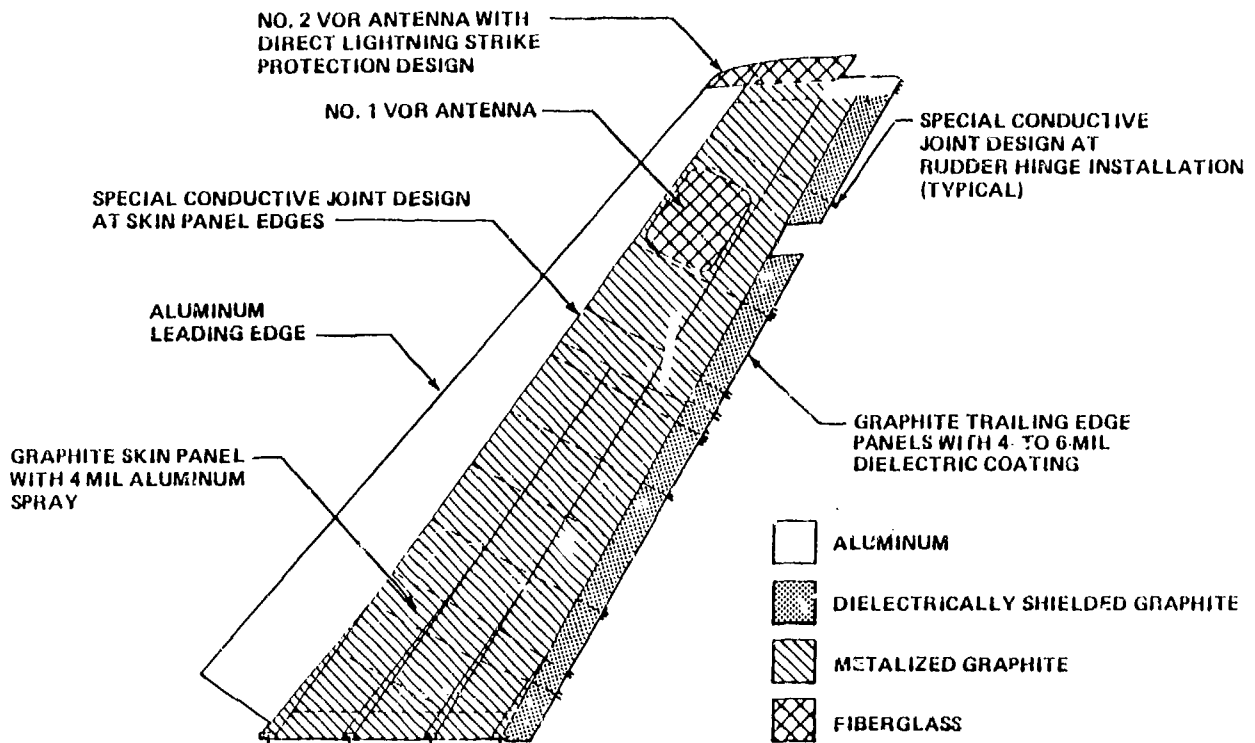


FIGURE 13. Lightning Protection System of DC-10 Composite Vertical Stabilizer

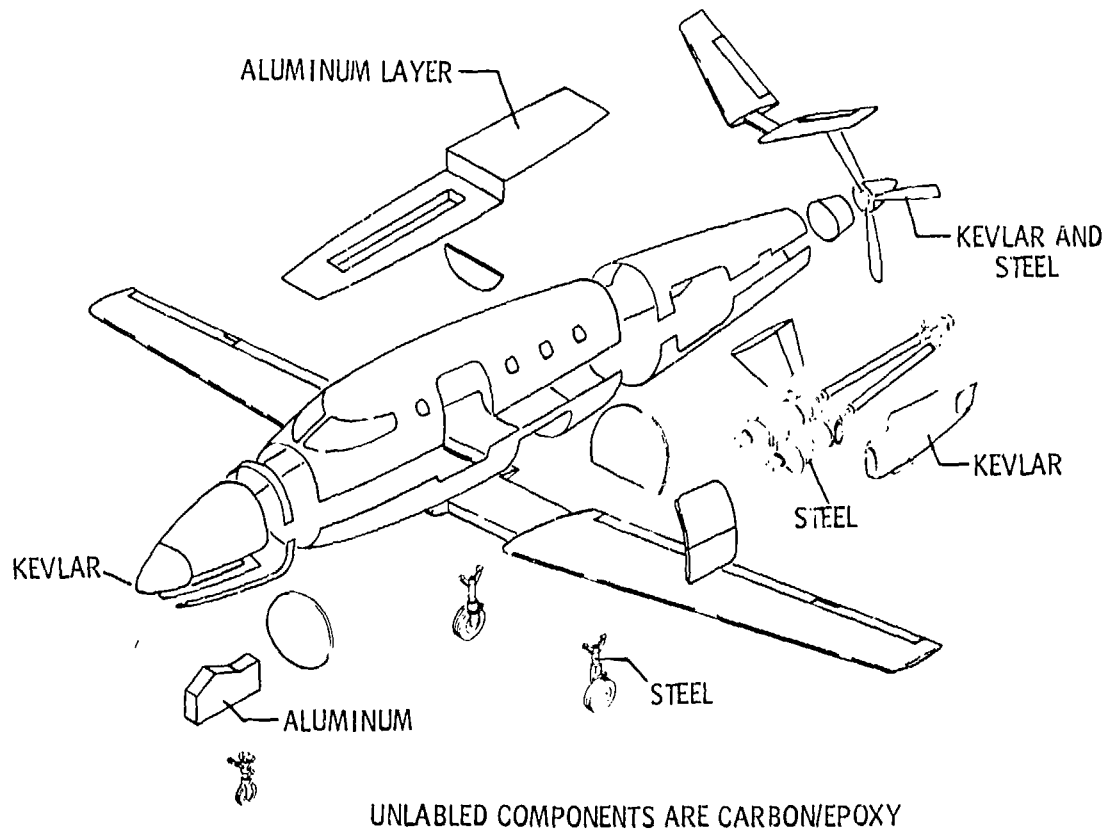


FIGURE 14. Airframe Elements of the All-Carbon-Composite Lear Fan 2100

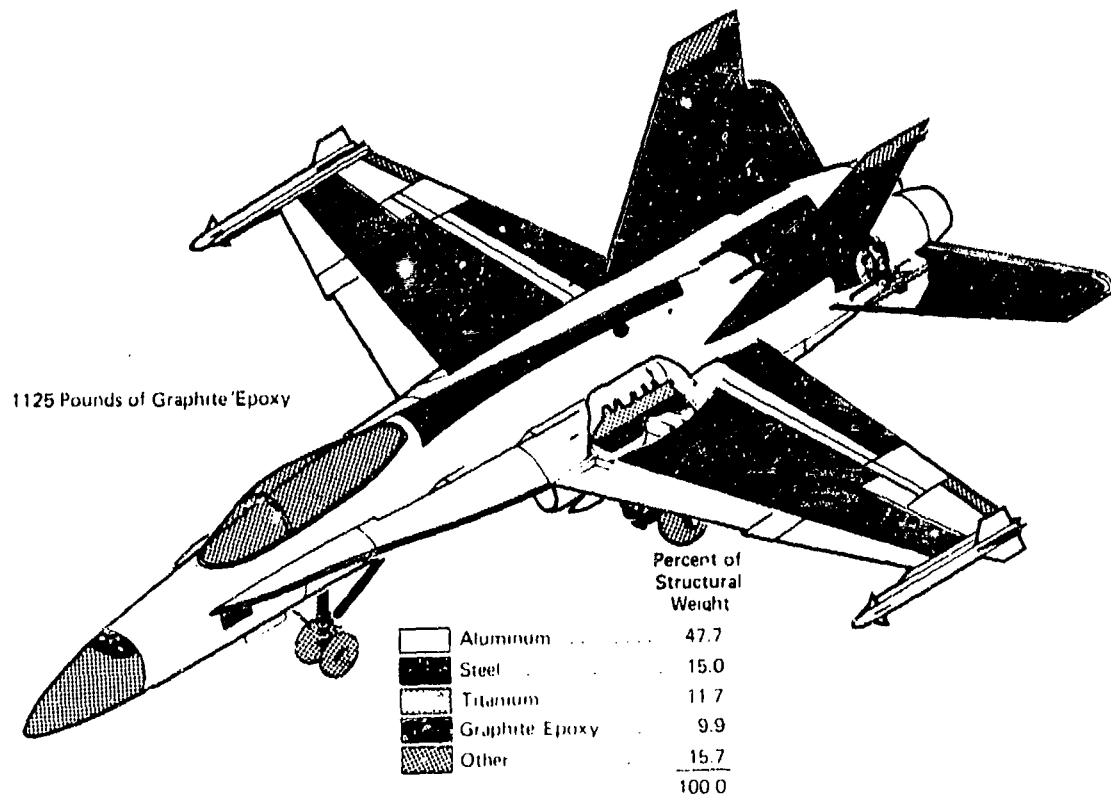


FIGURE 15. Carbon Composite Structures on the F-18

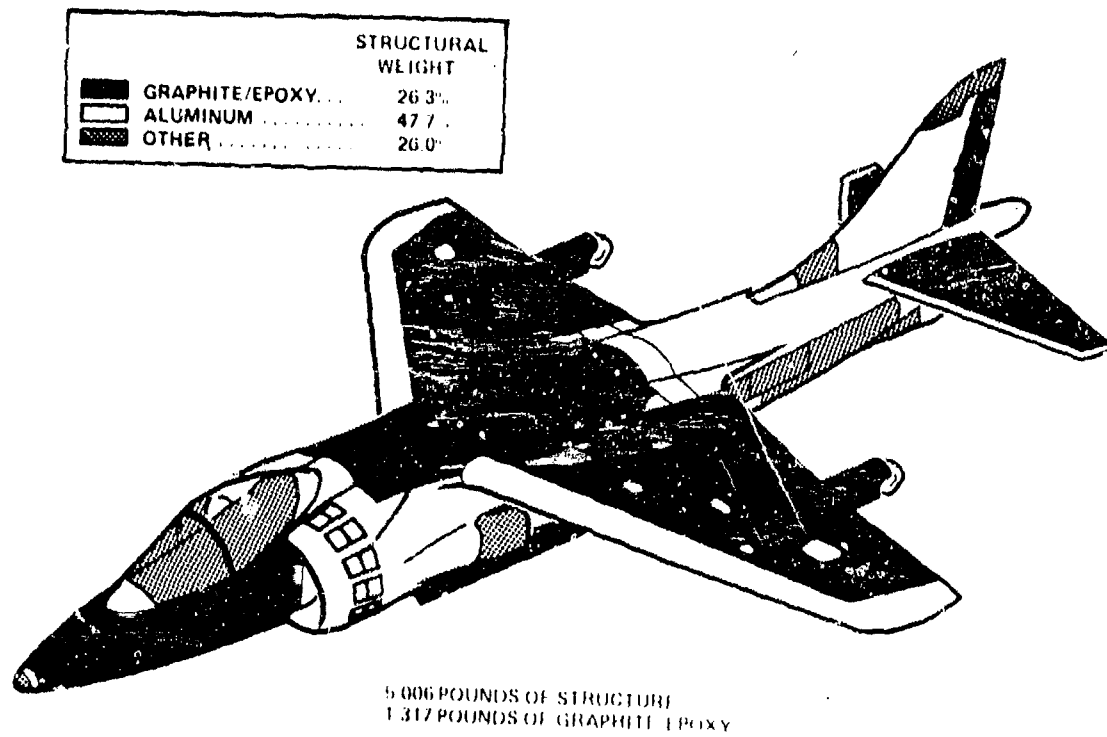


FIGURE 16. Carbon Composite Structures on the AV-8B

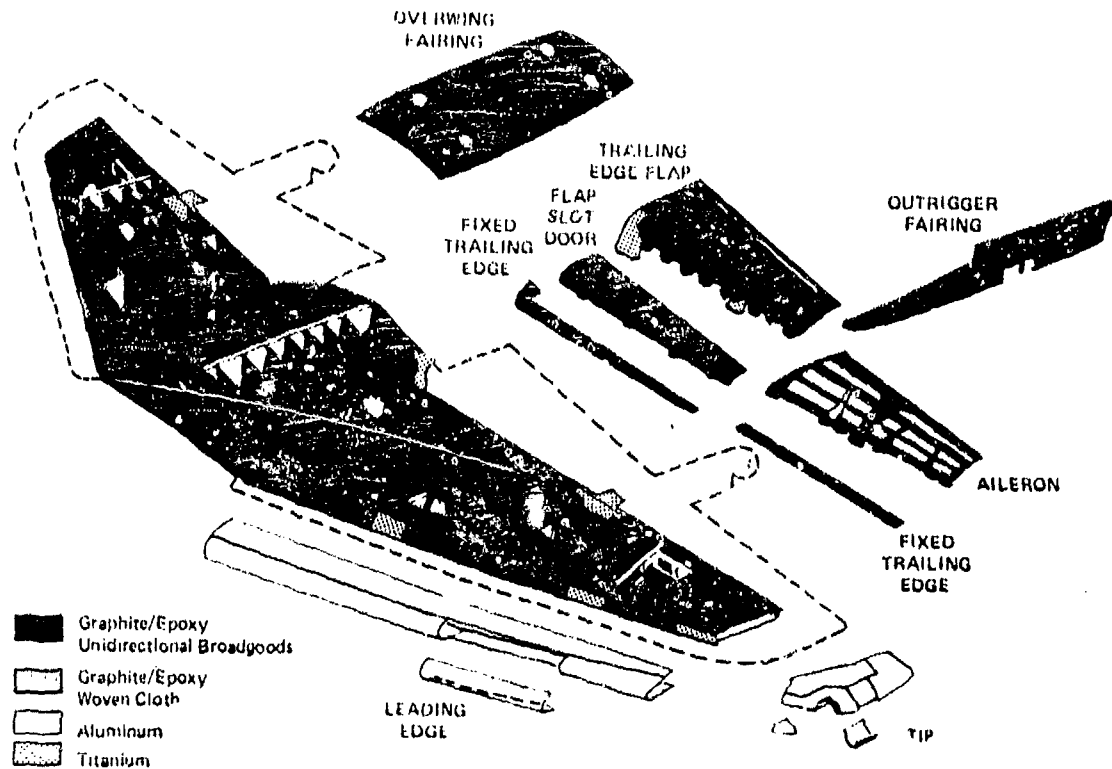


FIGURE 17. Construction of AV-8B Carbon Composite Wing

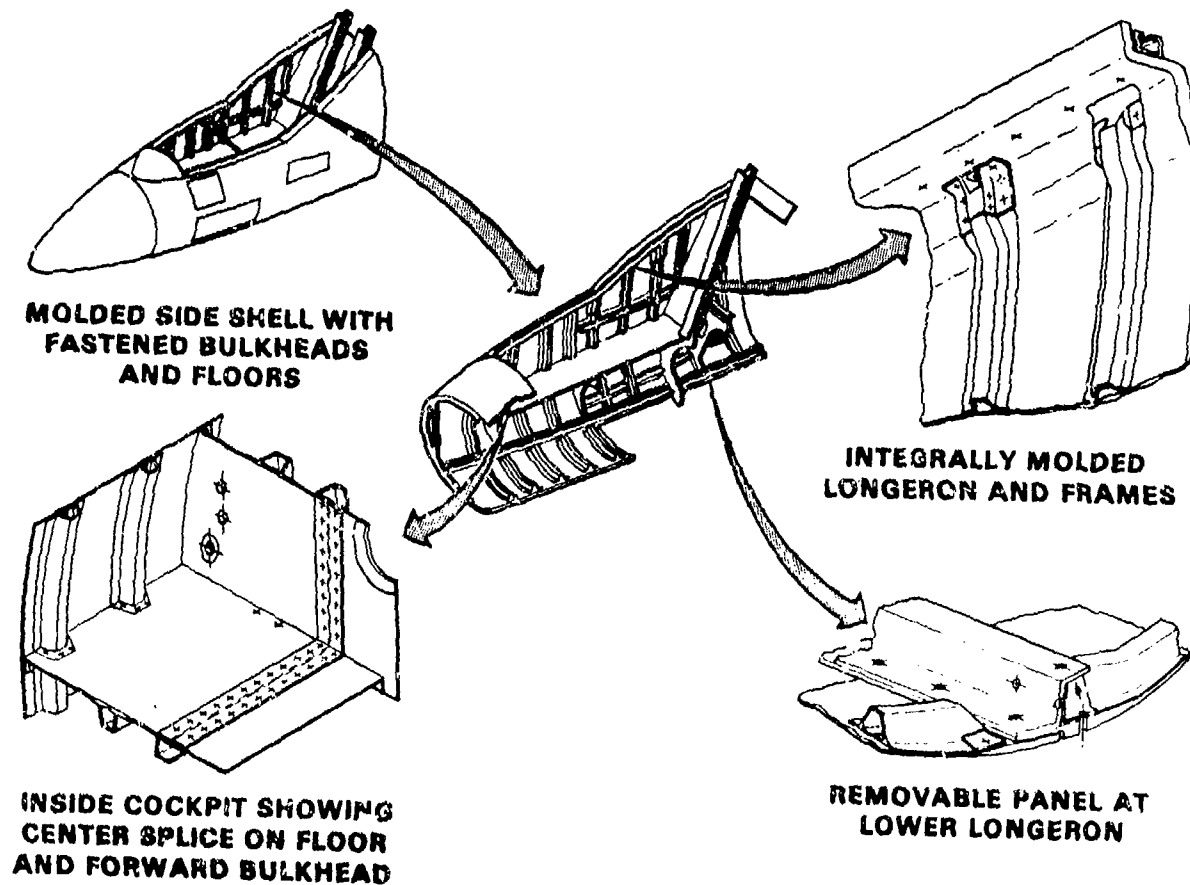


FIGURE 18. Construction of AV-8B Carbon Composite Forward Fuselage

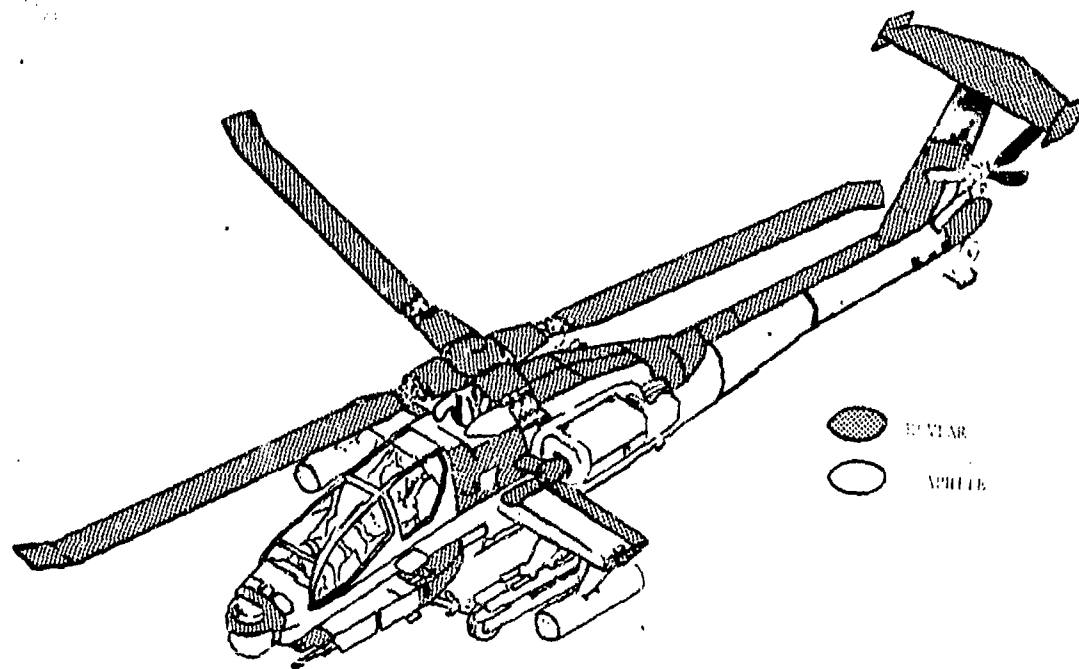


FIGURE 19. Potential Near-Term Composite Use on the Hughes AAH

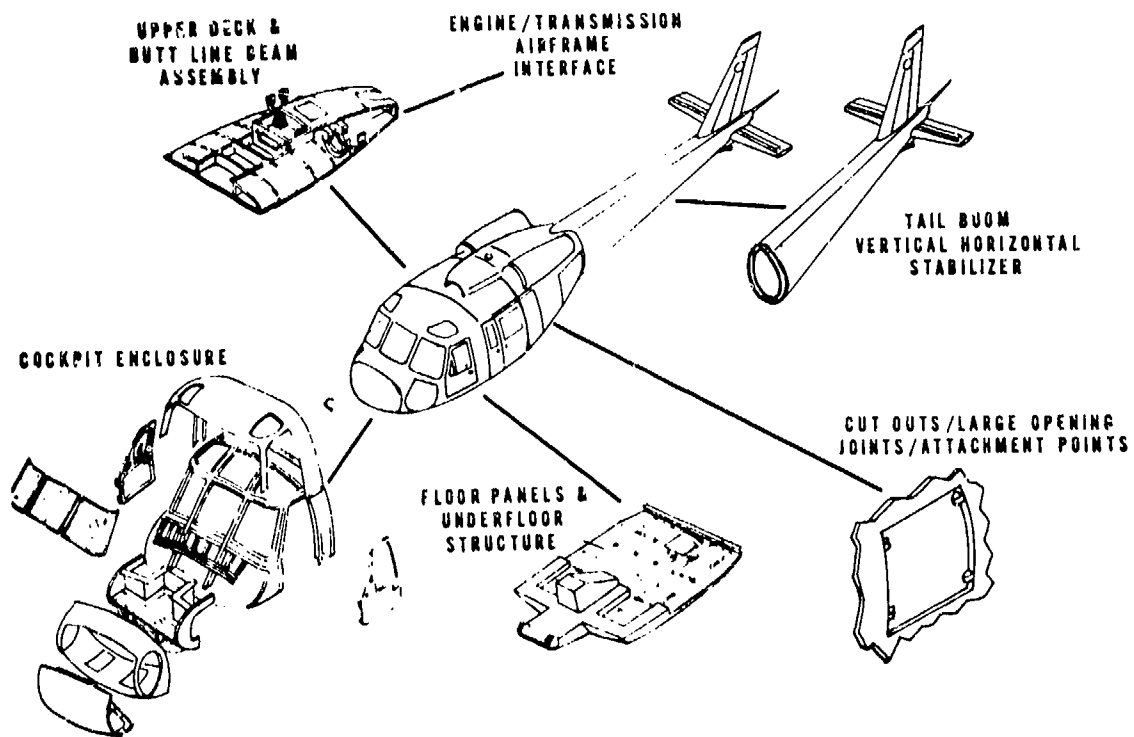


FIGURE 20. U.S. Army's Advanced Composite Airframe Program (ACAP)

**EFFET DE L'ENVIRONNEMENT EN SERVICE SUR LES MATERIAUX COMPOSITES
(RESUME DU CONGRES D'ATHENES - AVRIL 80)**

par

George Jubé
Aérospatiale
Paris, France

Les 21 communications qui constituaient ce congrès, réparties en 5 sessions ont, sinon apporté la réponse à toutes les préoccupations, au moins permis de faire le point des connaissances et de l'expérience actuelles sur le comportement des matériaux composites soumis à l'ensemble des agressions physiques et mécaniques que l'on a aujourd'hui l'habitude de regrouper sous le vocable d'"environnement".

Une chose est certaine: chacun des auteurs était dans sa spécialité, un spécialiste éminent, et souvent reconnue comme exprimant l'opinion la plus qualifiée, de telle sorte que l'ensemble des exposés constitue vraiment la documentation la plus récente et la plus pertinente sur les divers aspects de ce vaste sujet.

La première session était consacrée aux effets physico-chimiques de l'environnement. Elle comportait quatre exposés d'où deux problèmes étaient particulièrement pris en considération. Tout d'abord, la sensibilité du composite à l'humidité. Il s'agit d'une question importante qui a justifié, chez tous les constructeurs et les organismes de recherche, une immense somme de travail. La tenue à l'humidité est en effet la préoccupation majeure des utilisateurs de plastiques armés, la manifestation essentielle du vieillissement dont la crainte se substitue, dans l'usage des polymères, à celle de la corrosion des métaux.

Cette crainte se fonde sur un grand nombre d'essais de laboratoire où l'influence de l'humidité est d'autant plus mise en évidence qu'elle se trouve en combinaison avec un autre phénomène physique: chaleur, fatigue etc.

Pendant longtemps on s'est borné à constater le phénomène et à se contenter de mesurer la perte de résistance qui en résulte. Ceci a donné lieu à des méthodes expérimentales dites de "vieillissement accéléré" dans lesquelles on s'efforçait d'accentuer, en général par la chaleur, l'effet de l'ingestion d'eau sur la résistance et la cohérence de la structure. Ces méthodes, souvent extrêmement sévères, avaient plus ou moins la prétention de représenter un analogue, par concentration du temps, avec le phénomène d'exposition naturelle en service.

Cette analogie ne fut jamais parfaitement démontrée et les essais accélérés ont eu surtout le mérite de déterminer un classement dans la susceptibilité du matériau, le seuil admissible d'acceptation demeurant encore sujet de discussion.

Depuis quelques années, le phénomène de diffusion de l'humidité dans la matrice organique est accessible au calcul et des théories ont été établies qui permettent de prévoir, dans une ambiance donnée, la quantité d'eau absorbée au bout d'une certaine durée d'exposition. On peut alors, théoriquement du moins, relier cette notion à celle de l'évolution de la résistance, de la rigidité dans des conditions d'imprégnation identiques. Une certaine corrélation entre les calculs et les essais a pu être ainsi observée, en considérant toutefois que la détermination des coefficients de diffusion caractéristiques de chaque résine et destinés à être incorporés dans le calcul n'est encore accessible que par la voie expérimentale.

Les auteurs ont ainsi confirmé l'influence de l'humidité sur les composites, d'autant plus sensibles qu'il s'agit de parois minces. M. Bergman (RFA) a montré que l'absorption d'eau dans les revêtements peu épais de panneaux sandwichs pouvait provoquer des pertes de résistance allant jusqu'à 50%. L'eau introduite dans les cellules du nid d'abeilles peut même, en cas d'échauffement ultérieur, provoquer le décollement sous la pression de la vapeur.

Toutefois, comme le souligne M. Edge de la BAE, les essais de laboratoire conduisent généralement à accentuer le phénomène d'absorption bien au-delà des valeurs réellement observées en pratique. Elles tendent à atteindre la limite de saturation du matériau alors que les mesures effectuées sur les éléments en service montrent qu'il semble exister un seuil d'équilibre qui dépasse rarement un taux d'humidité de 1%, valeur pour laquelle les pertes de propriétés mécaniques sont minimales.

Les conclusions des divers auteurs n'en demeurent pas moins prudentes et comportent le souci d'une hypothèse conservatrice de forte absorptivité. Le cas d'un séjour prolongé en ambiance tropicale, par exemple, peut se rencontrer et déplacer défavorablement le seuil d'équilibre observé en régions tempérées.

L'autre problème, qui retient particulièrement l'attention des expérimentateurs est les comportements en ambiance spatiale, et notamment dans le vide.

L'utilisation des composites se développe sur les satellites et le risque d'altération par dégazage n'est plus aujourd'hui considéré comme très important. Les travaux rapportés par M. Tennyson (Canada) et M. Barboni (Italie) montrent que des propriétés importantes comme le coefficient de dilatation que l'on sait déterminer par le calcul, d'après l'orientation des couches, sont légèrement affectées dans le vide. Il en est de même, de façon toutefois non inquiétante, pour les propriétés mécaniques, encore que l'agent éliminé par le phénomène de dégazage soit généralement, et ici encore, l'humidité.

La seconde session, sur l'environnement superposé à la sollicitation mécanique, s'est attachée à établir les lois d'endommagement de la structure composite selon des spectres conventionnels, avec ou sans superposition de l'effet de l'humidité et de la chaleur. Cette combinaison s'est montrée, comme on pouvait s'y attendre, nettement plus défavorable au matériau que l'effet d'un facteur isolé.

Il n'a malheureusement pas été possible d'établir des règles pouvant permettre de prédire, la durée en fatigue et une poursuite de l'expérimentation, par exemple, sous des cycles simulant un nombre de vols, s'avère nécessaire.

L'ensemble des dégradations observées suggère néanmoins qu'avec les limites de sécurité actuellement appliquées dans les structures, la tenue à la fatigue n'est pas un problème inquiétant. On peut d'ailleurs ajouter qu'il s'agit même là d'un avantage très important du composite sur le métal.

La troisième session était consacrée aux sollicitations mécaniques aléatoires, et notamment à l'effet des impacts accidentels.

Un exposé de M. Torres (France) sur la remarquable résistance des pales d'hélicoptères en composite, illustré d'un film montrant le sectionnement de madriers de 20 cm de côté a vivement impressionné l'auditoire et contredit, dans ce cas particulier, la réputation peu flatteuse du composite à cet égard.

Le phénomène de l'impact sur les composites a été analysé par M. Dorey (Royaume Uni) qui a observé une bonne corrélation entre l'essai Charpy et la ténacité. L'impact provoque une réduction importante de la résistance qu'il est possible d'améliorer par des couches de tissus de Kevlar ou de verre disposées en surface.

M. Card (USA) a rapporté une série d'essais très significatifs sur l'impact de panneaux sous chargement en compression. Les essais ont montré l'existence d'un seuil où un impact de 15 joules provoque l'effondrement du panneau lorsque la déformation imposée est de 3%, valeur relativement modeste et fréquemment atteinte dans les dimensionnements actuels. L'essai est effectué avec une résine à faible allongement (1%) et il est considéré qu'une plasticité portée, par exemple à 4% améliorerait considérablement les résultats.

M. Aoki (RFA) indique, de son côté, que résistance à la fatigue est nettement moins affectée par le choc que la tenue statique. On retrouve ainsi un comportement caractéristique des composites et déjà observé dans les zones percées pour fixation.

En conclusion de cette session, on considère que le comportement aux impacts est encore insuffisamment analysé (celui de métaux ne l'est d'ailleurs pas, lui-même, de façon parfaite) et nécessite la poursuite des expériences. Ici encore, on s'interroge sur l'influence de l'humidité, encore rarement prise en compte dans les essais, ainsi que sur l'historique de la pièce avant l'impact et son état d'endommagement.

La session 4 traitait des phénomènes physiques atmosphériques, foudre, précipitations génératrices d'érosion etc.

MM. Rouchon et Gall (France) et Schneider (USA) ont montré que la réaction du composite à la foudre est très différente de celle des métaux mais que le dommage est moins alarmant qu'on avait pu le supposer à l'origine, la foudre n'ayant pas l'effet destructeur que l'on craignait.

Il faut cependant souligner l'importance du choix du nid d'abeilles et le problème posé par la continuité électrique au droit des joints. Il existe des revêtements de protection efficaces, dont on souligne que l'effet n'est pas proportionnel à l'épaisseur.

Une très grave préoccupation, qui a failli il y a 3 ans compromettre le développement des matériaux composites, est le risque de dispersion des particules de filaments dans l'atmosphère lors d'un accident suivi d'incendie. Il avait été avancé que ces particules pourraient, en se déposant sur les équipements électriques et électroniques provoquer des courts-circuits aux très graves conséquences.

M. Bell (USA) a montré avec quel sérieux et avec quels moyens considérables la NASA avait pris le problème.

L'analyse des causes, la production des fibres en dimension et en quantité, leur dispersion ont été décrites en détail ainsi que l'évaluation financière des dommages encourus.

La partie expérimentale a été également considérable, avec les essais en laboratoire sur équipements ménagers et industriels ainsi que de spectaculaires expériences en soufflerie et l'interception des panaches de fumée "grandeur nature" par d'immenses filets suspendus à des ballons.

La conclusion démontre la faiblesse du risque, mais la nécessité de développer des formes inoffensives du matériau: résines cokéfiabiles, revêtements enfermant la fibre dans une gaine non conductrice ainsi que l'intérêt des fibres non graphitiques.

En ce qui concerne l'érosion, M. Torres (France) a montré les résultats de protections diverses de bord d'attaque d'hélicoptères. M. Springer (USA) a développé un modèle mathématique simplifié qui relie le phénomène à la notion de fatigue. Il définit ainsi un période d'incubation, suivie de celle où l'enlèvement de matières commence à se manifester. Le modèle semble bien se vérifier par les essais, mais l'incubation est plus courte de plusieurs ordres de grandeurs qu'avec les métaux. Ceci confirme la nécessité de protéger le composite dans les zones soumises à l'érosion.

En conclusion de cette 4ème session, comme le remarque le rapporteur, M. Barboni (Italie) le phénomène atmosphérique qui comporte le risque le plus grave est aussi le plus simple: la pluie.

Enfin la cinquième session était consacrée à une revue générale du comportement en service, les orateurs représentant les constructeurs et utilisateurs étant choisis parmi ceux ayant accumulé l'expérience la plus significative.

Le sujet des pales d'hélicoptères a été traité par MM. Barnard (Westland, UK) et Brunsch (MPB-RIA) auxquels on doit ajouter M. Torres (SNIAS, France) dont l'exposé avait été prononcé en Session III. L'expérience extrêmement satisfaisante du composite dans cette application est aujourd'hui unanimement reconnue.

Deux problèmes demeurent toutefois incomplètement résolus:

- L'érosion en extrémité de pale pour laquelle la remise en état de la protection n'a pas encore atteint un stade de définition satisfaisant.
- Les difficultés de réparation par l'utilisateur (remarquons que la réparation sur le terrain des pales métalliques n'a jamais été conseillée).

L'expérience de la NASA, sur les structures d'avions de transport dont elle a suscité le développement et qu'elle surveille en service, met en évidence le très faible niveau de dégradation observé. Les durées d'exploitation dépassent aujourd'hui 5 années et l'accumulation des heures de vol atteint 2,5 millions réparties sur 200 éléments. On est frappé par le fait que la reprise d'humidité, crainte majeure, n'atteint pas 1% après s'être stabilisée dès les premiers mois. On constate également que des résines (ex: Narmco 5209) dont l'emploi a été entre-temps abandonné sur la foi des résultats défavorables de laboratoire à cet égard ne se comportent finalement pas plus mal que les autres en ambiance réelle.

L'US Air Force dont l'introduction d'éléments en vol remonte à 1969 a également accumulé une expérience considérable. L'utilisation des composites sur les ailes d'armes s'est progressivement développée, depuis les portes et les empennages, jusqu'aux caissons de voilure produits aujourd'hui, en attendant les fuselages.

L'expérience montre le comportement sans reproche des composites bore-epoxy, formule produite au début et, à peu près exclusivement jusqu'en 1972. Les assemblages par collage des éléments de reprise en titane, notamment, n'ont jamais donné lieu à préoccupation.

L'armature de filaments de carbone, introduite par la suite a présenté à l'usage quelques cas de délaminages locaux et de craquelures sur les bords des éléments. Les phénomènes d'importance et de gravité limitées n'ont d'ailleurs aucun caractère systématique et laissent penser qu'ils relèvent de cas d'espèce. Des procédures de réparation ont été mises au point.

D'une manière générale, les formations estiment que la maintenance des éléments en composite leur cause moins de travail que celle des éléments métalliques correspondants. La principale difficulté réside encore dans la procédure d'inspection par ultra-sons qui est souvent laborieuse et mal adaptée au dessin des pièces. Un système intégré (dénommé ISIS) fournissant une visualisation générale de la pièce sur écran vient d'être mis au point et doit être très prochainement expérimenté sur les Bases pour contrôle de routine.

L'expérience de l'US Navy, qui exploite ses appareils dans les conditions d'environnement particulièrement sévères, corrobore parfaitement celle de l'Air Force. Les inévitables endommagements sont à relier aux tribulations du service bien plus qu'aux phénomènes physiques de l'ambiance. Les procédures de réparation ont fait l'objet d'un développement particulièrement attentif et leur efficacité dans le rétablissement des propriétés initiales a été démontrée aussi bien par les essais au sol que par l'expérience en vol.

En résumé, l'expérience en vol qui est déjà considérable sur les éléments secondaires et qui aborde maintenant les structures principales, s'avère dans l'ensemble extrêmement favorable. Elle a converti au composite les utilisateurs dont l'attitude d'origine était, comme on le comprend, extrêmement réservée. Il semble bien que le développement remarquable de l'application aux pales d'hélicoptères doive se reproduire sur les structures d'avion, et les projets en cours,

qu'il s'agisse d'avions d'armes ou de transport, font au composite une place de plus en plus large. La limitation d'emploi devient aujourd'hui davantage de caractère technologique et industriel.

Le principal problème qui demeure est celui du contrôle de qualité.

Il s'agit d'une part des progrès nécessaires de l'appareillage et de la méthodologie notamment pour les examens en service sans démontage des éléments. Par ailleurs on manque encore de données sur le seuil d'admissibilité des défauts, sur la justification d'un rebut et les pratiques actuelles, extrêmement prudentes et conservatives font de sorte que le coût du contrôle lui-même et les conséquences de sa sévérité constituent un élément déterminant du prix de revient des structures en composite.

En conclusion, on constate que cet important congrès a mis successivement en évidence deux tendances que l'on pourrait à première vue qualifier d'opposées.

Les gens de la Recherche et de l'expérimentation en laboratoire ont décrit un ensemble de phénomènes qui indiquent clairement que l'usage des composites comporte un certain nombre de limitations. L'influence de l'humidité, des chocs, leur combinaison défavorable avec les autres facteurs de l'environnement, la sensibilité particulière de la sollicitation en compression, sont autant de sujets qui n'auraient pas manqué de freiner le développement des matériaux composites s'ils avaient été connus à ce point il y a une dizaine d'années.

Auprès de ces facteurs d'inquiétude, l'expérience en service se traduit d'une façon assez contradictoire par la satisfaction, l'optimisme, l'absence de difficultés majeures et en fin de compte une vigoureuse poussée en avant, dans laquelle les utilisateurs emboîtent le pas aux promoteurs.

Il est difficile de ne pas être tenté, dans ce dilemme, de rejeter les avertissements des scientifiques et de consacrer le triomphe de la pratique sur la speculation théorique.

La question n'est pas aussi simple, car les phénomènes mis en évidence en laboratoire sont indéniables. Il leur manque simplement les données statistiques qui permettraient de définir leur degré de probabilité. D'un autre côté, il est vraisemblable que les éléments mis en service avaient bénéficié d'une fabrication relativement bien surveillée, effectuée dans des ateliers travaillant dans des conditions de fabrication prototype. Qu'en sera-t-il lorsque le composite sera produit en série avec des défauts à la limite des conditions d'acceptation, lesquelles auront bien dû, entre temps, être quelque peu libéralisées?

La solution finale se trouve donc à la convergence des deux cheminements, lorsque les deux tendances se rejoindront et se compléteront dans une appréciation raisonnée du risque.

Un nouveau rendez-vous est déjà pris, entre-temps, tous les éléments sont réunis pour que le matériau composite poursuive, sous surveillance, sa croissance et son développement.

APPLICATION OF CARBON FIBRE COMPOSITES TO
MILITARY AIRCRAFT STRUCTURES

By

T. Sharples
British Aerospace: Aircraft Group
Warton Division
Warton Aerodrome
Preston PR4 1AX
Lancashire
England

SUMMARY

The main purpose of the paper is to give a detailed description of where Composites are most likely to be used in the structure of future Military Aircraft with an indication of the type of Composite material and the structural form. This is with the intention of setting the scene for the later sessions when the main theme of Electromagnetic effects upon Avionics Systems will be taken up.

The advantages of using CFC are identified together with the main factors which have to be considered in design; this is followed by a statement on the realistic potential in terms of mass savings followed by a short discussion on the possible economic benefits.

Before closing with a brief recognition of the more obvious EMC problem areas, the paper describes the most likely structural configuration for each major structural component, relying liberally on sketches.

1. INTRODUCTION

The main purpose of this paper is to give a fairly detailed description of where Carbon Fibre Composites (C.F.C.) are most likely to be used in the structures of future military aircraft together with an indication of the type of material and structural configuration. This is with the intention of setting the scene for the later sessions when the main theme of the meeting (electromagnetic effects of carbon composite materials upon Avionics Systems) will be taken up.

2. ADVANTAGES OF C.F.C. TO THE STRUCTURAL ENGINEER

2.1 Static Strengths

Carbon Fibre materials have lower mass densities and higher mechanical strengths than metallic materials currently used for aircraft structures, and therefore they are seen to offer significant advantages to the Structural Engineer.

Basic Uni-directional strengths of 2½ to 4 times those of conventional light-alloys coupled with 40% lower density are readily achievable and a strength comparison chart can be seen in Fig.1.

2.2 Fatigue Resistance

Tests have shown that the fatigue performance of C.F.C. notched specimens is such that the endurance limit is around 65% of the static ultimate. This applies for most structural layups under typical flight-by-flight fighter wing spectrum loading and it should be noted that, unlike metallic materials, the critical fatigue loading is in compression and not tension. This compares with an endurance of about 30% of ultimate for typical light-alloys if we consider damage tolerance requirements. As typical maximum working stresses are less than 60% of ultimate, it would appear that no special allowance is necessary in C.F.C. structures to achieve the required in-service fatigue lives.

Fig.2 shows a comparison of C.F.C. and light alloy fatigue performances.

3. FACTORS WHICH REDUCE THE EFFECTIVENESS OF C.F.C.

3.1 Effect of Layup

A longitudinal layup of C.F.C. has little or no resistance to loads applied perpendicular to the main fibre. The majority of structures have to cater for loads in all directions which means that there are very few structural applications for a purely 0° layup.

A typical layup can be taken as having 50% of 0° fibres with the remainder being a mixture of 90° and ± 45° to carry shears and lateral loads. This reduces the laminate strengths to about half of that of a fully 0° laminate since the 90° fibres have no strength along the 0° axis and the modulus of the ± 45° layup is only 20% of the 0°.

3.2 Notch Sensitivity

Stress concentrations have to be considered in the design of composites since they play an important part in determining the strength of a laminate. The material has little or no plastic zone, which in metals serves to nullify the effect of stress concentration, and therefore notch factors have to be taken into account in the static design.

Current manufacturing technology requires the use of bolts to attach the various components and a typical bolt hole in a laminate containing 0° fibres will approximately halve its strength.

Certain measures can be taken to reduce notch sensitivity, for example by incorporating low-modulus material in way of the bolt holes, or even to remove the need for bolting by developing all-bonded assemblies.

However, consideration of manufacturing defects and local in-service damage will almost certainly result in similar notch factors being applicable.

3.3 Environmental Degradation

Matrix-dependent properties of CFC structures (such as compression and shear) are sensitive to the uptake of moisture at temperature. This occurs because of the reduction in glass transition temperature (which effectively reduces the allowable working temperature of the material) and tests have shown that reductions in compression strengths of about 30%, under typical fighter aircraft environmental conditions, apply to the currently available materials.

It is widely believed that practicable protective measures can only delay the uptake of moisture and work continues in this field as well as towards developing improved resin systems.

3.4 Variability

It is necessary to make an allowance for statistical variability of material properties.

Variability can be expected to come from the basic material constituents, manufacture of the components and from construction of the structural components.

Analysis of tests to date have shown that typical mean test values should be reduced by about 20% to obtain minimum design allowables.

3.5 Resulting Material Strengths

After taking into account all the considerations mentioned above, structural laminate strengths for typical fighter aircraft environments can be calculated.

Figs 3 and 4 compare CFC design allowables for varying amounts of O^o with those for current light-alloy and titanium. These have been divided by the relevant densities to reflect weight benefits.

It can be seen that CFC tension properties show a distinct benefit compared with a much reduced advantage for compression, mainly because of environmental degradation.

4. REALISTIC POTENTIAL

Design studies have been carried out to apply C.F.C. in major structures and these applications have demonstrated that Composite Structures can be lighter than their metal counterparts. An indication of the conclusions drawn from the various structures is given below, together with the expected weight savings for each of the major structural components.

4.1 Summary of Experience

The effect of the use of Composites on the structural weight can vary depending on the structural complexity, load levels and complexity of geometric shape.

Lightly loaded structures, such as front fuselage which tend towards minimum thickness design in metal, show mass savings which approximate to that obtained by direct replacement of the metallic components by composites.

At the other extreme, a highly loaded structure with unavoidably complex ply layups, such as the root region of a strength design wing structure - especially if it contains a joint, would show negligible mass savings. Most structures lie in between these two extremes and the following table indicates a realistic potential for mass saving. Note that this is based mainly on strength design. It is possible that wings, fins and tailplanes will have a stiffness requirement and, if this dominates, this could lead to an even greater mass saving advantage by using CFC.

Component	Mass Saving on Compositised Structure	Composite Utilisation	Total Mass Saving
Wing	20%	70%	14%
Fin	45%	40%	18%
Tailplane (or Foreplane)	45%	40%	18%
Front Fuse	40%	40%	16%
Centre Fuse	17%	40%	7%
Rear Fuse	30%	50%	15%

Applying this to the structure of a typical military aircraft shows a structural mass saving of about 12% for a composite utilisation of 40%.

Note that this does not include resizing benefits (See para 4.2).

4.2 Aircraft Resizing

The mass saving described in the previous paragraph would, if applied to an all-metal concept, result in an improved aircraft performance in terms of flight envelope and range. If the mass savings were anticipated from the outset, it would then be possible to resize in order to get the same performance out of a smaller, lighter aircraft.

In order to obtain maximum advantage of resizing, it would be necessary to change the engines, scaling them down in accordance with the reduced mass. It is realised that this is not always possible so the following resizing advantages are presented against two options; one assuming no engine change and one assuming complete resizing including the engines.

It can be seen from Fig.5 that for a composite utilisation of 40% the resized aircraft would show structural mass savings of 17% (no engine change) and 21% (with resized engine).

5. ECONOMIC BENEFITS

Although most of the R & D studies to date have been towards establishing a design technology, it has been possible to perform economic assessments from a production viewpoint and the following points give some indication of the current thinking. In arriving at the following cost comparisons between metal and CFC, consideration has been given to factory overheads. This has revealed that a CFC manufacturing plant would show up favourably when compared to the conventional production one, mainly because of a reduction in the number of manufacturing processes, a considerable reduction in the types of material to be stocked and the use of less costly equipment.

5.1 Component Manufacture

a) Metal Components

Producing metal components depends upon the material to be used and the processing (that is whether made from sheet metal or machined from billet).

If it is assumed that the material is light-alloy and 30% is made from sheet metal with 70% machined from billets, then an average cost per kg of 39 units can be identified. Of this 9 units come from the cost of the basic material, including a utilisation factor of 0.7 average.

b) CFC Components

In considering the manufacture of CFC components, the following key operations have to be performed; comparative costs are given below.

<u>OPERATION</u>	<u>COST/kg (units)</u>
. Material	25.5
. Layup	44 hand layup 4 M/C layup
. Preparation for cure	12
. Curing	1
. Post Cure (trimming etc)	8

It can be seen that hand layup costs dominate and it follows that attempts should be towards automating layups, since appropriate studies have shown the cost-effectiveness of such methods.

It is considered that in a properly equipped CFC production facility with a properly planned throughput of CFC components which have been designed with automation in mind, only 30% will require hand layup. Hence the average cost for CFC components is 62 units/kg.

5.2 Component Assembly

a) Metal Components

The assembly costs will vary according to the component in question (depending upon such things as fuel sealing, assembly of thick members with little curvature, assembly of thin sheet components of complex shapes, numbers of components in an assembly etc). An average cost per kg of 61 units applies to the assembly of current military aircraft structures manufactured by conventional methods.

b) CFC Components

There do not appear to be any special assembly problems associated with CFC components.

What can be claimed however is a reduction in cost compared with metal equivalents arising from the reduction in numbers of parts which make up each assembly.

It has been shown that the constituent parts of an assembly, whether it be a fuselage, wing or tailplane, are reduced by at least 50% by designing in CFC, and also that assembly cost is proportional to

the numbers of parts in that assembly. If consideration is given to reducing bolted joints and attachments by using co-cured and bonded methods of fabrication, then further cost savings could be claimed but for the purpose of this report a man hour reduction of 40% will be assumed.

Hence cost of CFC Assembly is 32 units/kg.

5.3 Resulting Costs

Material	Manufacturing Costs (Units/kg)	Assembly Cost (Units/kg)	Total Cost (Units/kg)
Metal	39	61	100
CFC	62	32	94

It is clear from the above figures that it costs more to manufacture components in CFC than in metal even when allowance is made for the more efficient material utilisation. Automated layup techniques offer significant cost reductions but at best the cost of CFC manufacture will be about 50% greater than for the metal equivalents.

However, there are significant cost savings to be obtained in component assembly where the considerable reduction in parts count which has been demonstrated by designing in CFC leads to about a 50% reduction in assembly costs compared with metallic structures.

The indications are that structures containing CFC should cost less than the all metal equivalents, especially if maximum advantage is taken of the structural mass savings. However, this would mean designing to maximise automated manufacturing techniques and having the necessary production development.

Fig 6 shows the cost saving potential.

6. STRUCTURAL CONFIGURATION

Para 4 describes the likely composite utilisation in the various structural components and in this para the description is extended to include structural configurations. Fig 7 shows a hypothetical fighter aircraft configuration.

6.1 Wing (see Fig. 8)

The torsion box will be of multispar construction and designed to carry fuel. The configuration may well be for a through wing (in which case there would be a determined effort not to have a centre-line joint) or for a wing which joins on to the fuselage at the body side. Current technology would require the skins to be bolted to the substructure but all-bonded assemblies are being pursued.

Component	Description
Main skins	Balanced CFC laminate containing approx 50% of spanwise fibres, with the majority of the remainder at $\pm 45^\circ$. Local reinforcing will be necessary at load inputs such as for flaps and pylons.
Main spars	Channel section made from $\pm 45^\circ$ CFC.
Intermediate Spars	Sine-wave construction using $\pm 45^\circ$ CFC. The spar caps will be mainly 0° with some 90° material for the radial loads.
Ribs	Channel or 'I' section construction using $\pm 45^\circ$ CFC. Note that in some cases light-alloy may be preferred depending upon the complication.
Leading Edge	Either GRP or CFC skins with a full-depth honeycomb.
Flaps	Sandwich construction using honeycomb with CFC skins.

6.2 Taileron/foreplanes (See Fig. 9)

These components are fully moveable, independently activated control surfaces.

The most likely construction is full depth L.A. honeycomb supporting CFC skins containing approximately 50% of spanwise fibres with the remainder being mainly $\pm 45^\circ$; a small amount of 90° being included for stability.

Attachment to the fuselage will be through a metal spigot or actuator arm bolted to the skins; CFC beams will be used to distribute the local load inputs.

Leading edge will be GRP or CFC with a full depth honeycomb and this will be bolted to the main box.

Trailing edge will be a full depth sandwich using CFC skins.

6.3 Fins (See Fig 10)

These will be of similar construction to the tailerons.

6.4 Fuselage (See Figs 11 - 21)

The application of CFC to fuselage is strongly configuration dependent influenced by the intake and duct complexity, the position of the engines and the wing. However, the following is an indication of where CFC is likely to be used, assuming the engines to be in the rear fuselage and the wing to be attached to the fuselage side.

Component	Description
Bulkhead Frames	Made from CFC using equal amounts of 0° , 90° and $\pm 45^\circ$. Stiffened by either swages or co-cured hat sections. Skin flanges separately attached to simplify the tooling.
Intermediate frames/ stiffeners	Channel or 'I' sections. May be made from cloth depending on the curvature.
Longerons	Top hat or 'I' sections made from $\pm 45^\circ$ with 0° in the flanges or caps. Could be co-cured or laid up integral with the skins.
Skins	Will vary from $\pm 45^\circ$ with longerons or 0° , 90° and $\pm 45^\circ$ in equal proportions with stiffeners, depending upon the loading.
Doors and Panels	Sandwich construction using honeycomb with CFC skins.

7. POTENTIAL EMC PROBLEM AREAS

It is recognised that an aircraft which contains a large amount of CFC structure may have unacceptable reductions in its electromagnetic functions.

Three of the rather obvious important problem areas are discussed below in an attempt to indicate the designers' understanding.

7.1 Screening

The higher specific resistance of CFC (compared to metal) suggests that the effectiveness of the surface in providing a screened enclosure may result in equipment operation problems.

Tests have been carried out on experimental sections of front fuselage structures to compare the performance of a CFC structure with that of a metal one. These are reported to have shown little difference in the shielding and what difference there was could most likely be handled by judicious siting of cables.

One important question which is yet to be answered is with regard to the effectiveness of screening at panel and door joints where the requirement for quick release and easy access may be at variance with the requirement for efficient screening. More research is required here in order to establish design rules for the attachment of Avionics bay doors for example where it is unlikely that cables can be resited.

7.2 Structural Earth Return for Power Supplies

Measurements of resistance indicate that CFC may not be suitable for providing earth return paths for electrical systems. A better understanding of this has to be obtained by tests on large scale structures since the provision of an alternative earth path would add weight.

In order to assess the significance of the problem, design studies are in hand to investigate the use of concentrated structural booms of both CFC and metal which may provide a continuous electrical path in typical CFC fuselage structures.

7.3 Bonding

It is recognised that effective electrical bonding of CFC structures will rely upon the provision of low resistance joints within the structure.

The move towards greater structural and manufacturing efficiency by eliminating mechanical fasteners and using bonded joints is likely to increase the joint resistance since the adhesive prevents good contact between the carbon fibres.

It is necessary to perform tests on properly representative structures to determine whether the joints offering good structural efficiencies are acceptable and, if not, to investigate improvements such as using conductive epoxies or the use of discrete pins through the joint. See Fig 22 for typical joint details.

8. CONCLUSIONS

The high specific strength of CFC offers weight saving potential to the aircraft structural engineers.

Design and manufacturing studies have shown that this potential can be realised and that for a maximum utilisation, where 40% of the aircraft structure is made from CFC, mass savings of about 12% can be expected. These savings can be increased to as much as 20% if the aircraft is resized for constant performance.

Cost studies indicate that, if full advantage is taken of automated techniques and the weight reductions, structures containing CFC should cost less than for the metal equivalents.

Work is continuing to assess the EMC problems in order to ensure that full advantage can be taken of these potential weight and cost savings on future military aircraft.

9. ACKNOWLEDGEMENTS

The writer wishes to thank British Aerospace for permission to publish this paper. Also his colleagues, in particular Mr. A. N. Rhodes for his inspiration and Messrs. Haresceugh, Rogers and Law for information on which it is based. The writer also wishes to acknowledge the generous support of Her Majesty's Government who are funding the development programmes.

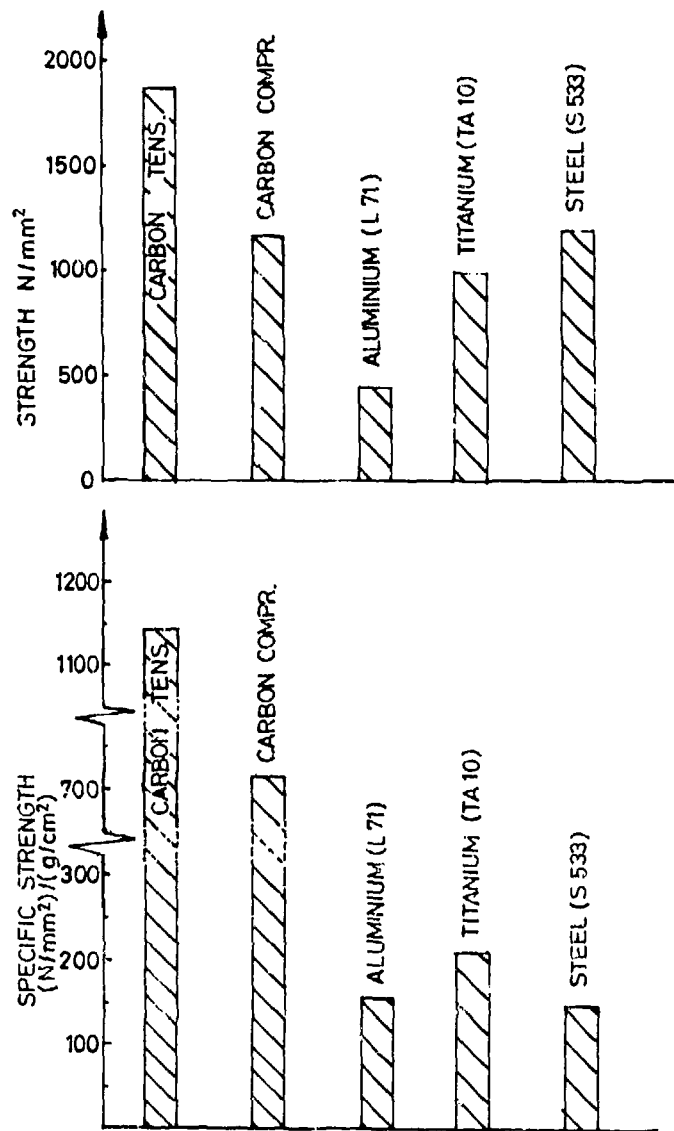


Fig. 1 Strength comparison with conventional aircraft materials

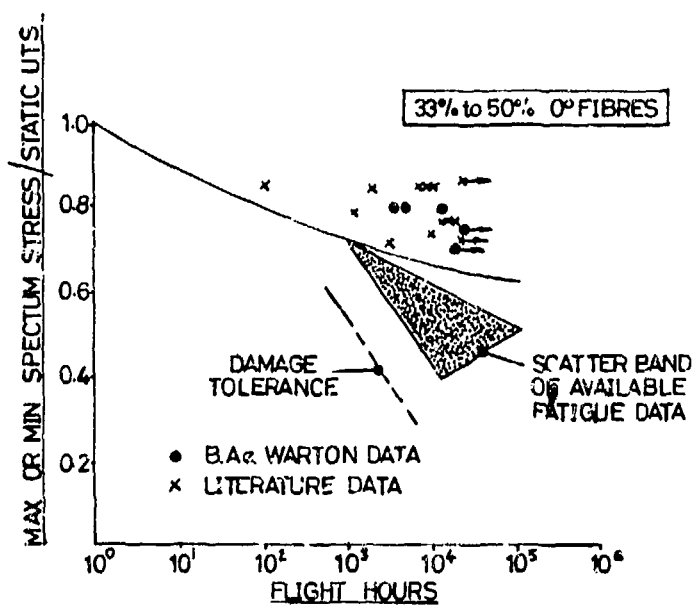


Fig. 2 Flight by flight fatigue behaviour of C.F.R.P.

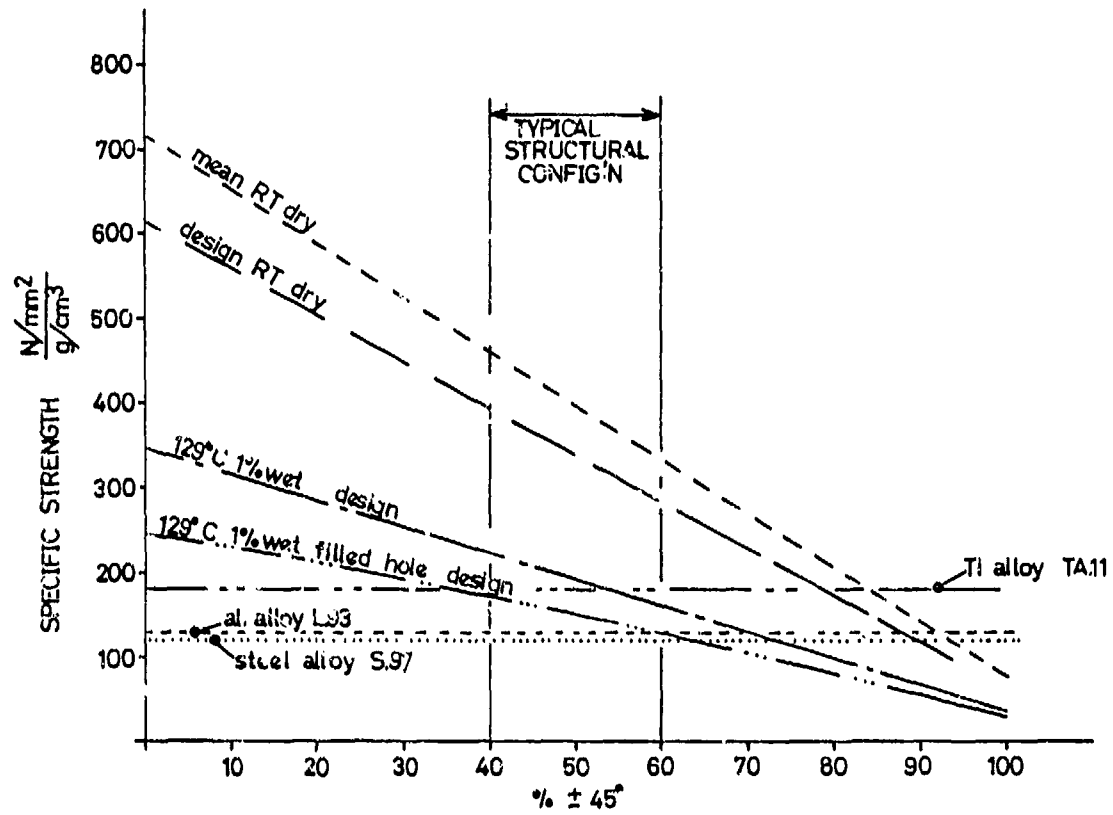


Fig.3 Specific compressive strengths of XAS/914 and common engineering materials

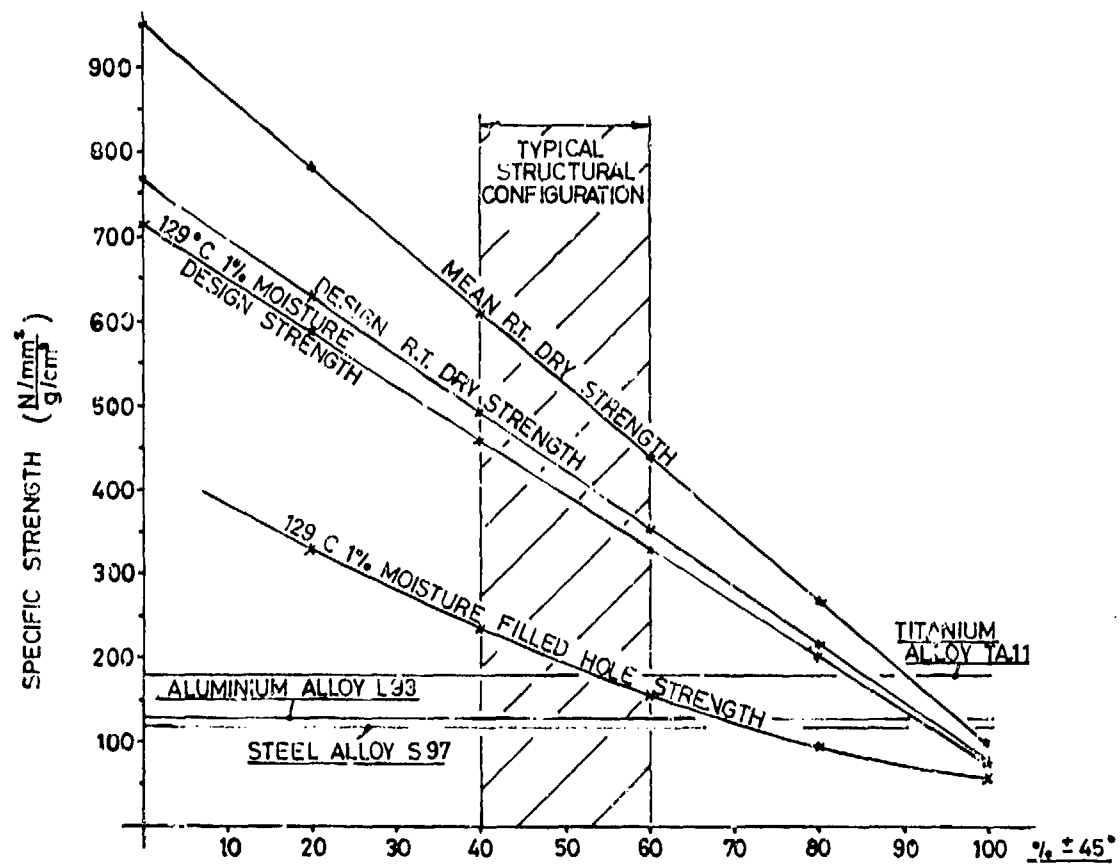


Fig. 4 Graph showing comparison of the specific tensile strength of XAS/914 with engineering materials

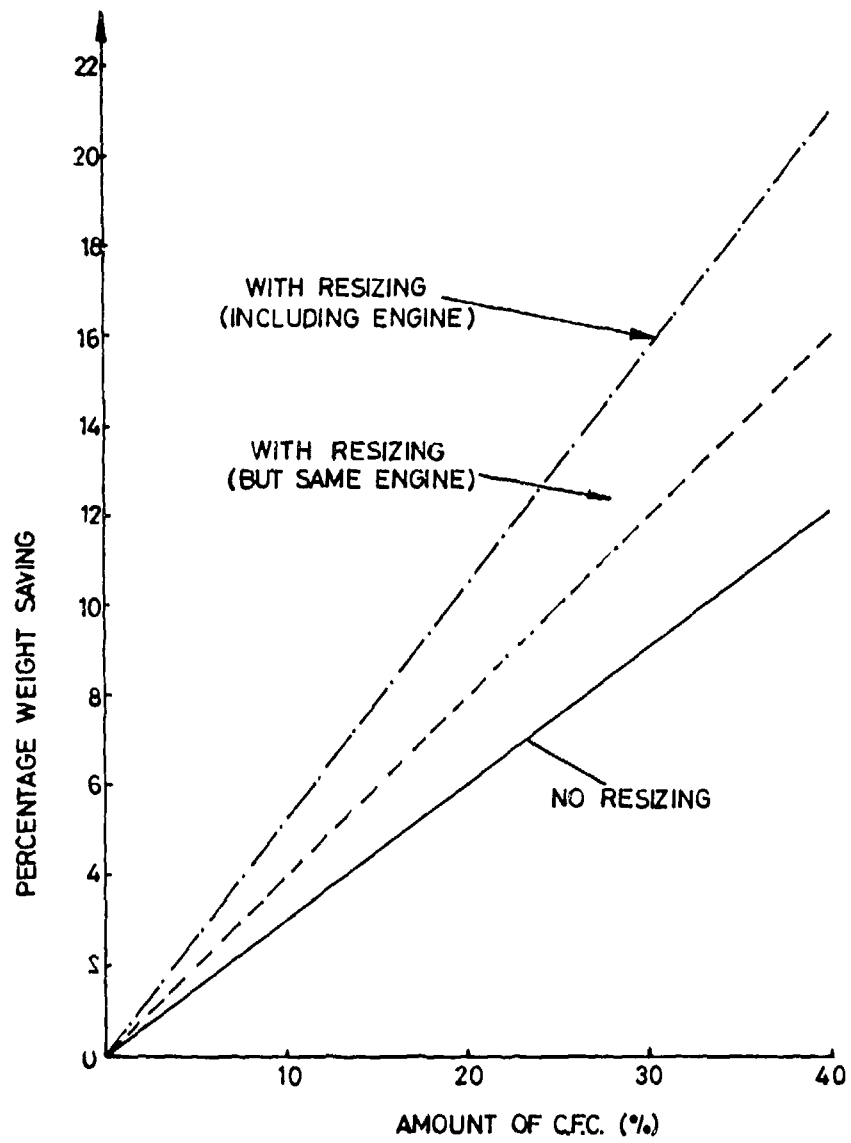


Fig.5 Potential structural mass saving (including the effect of aircraft resizing)

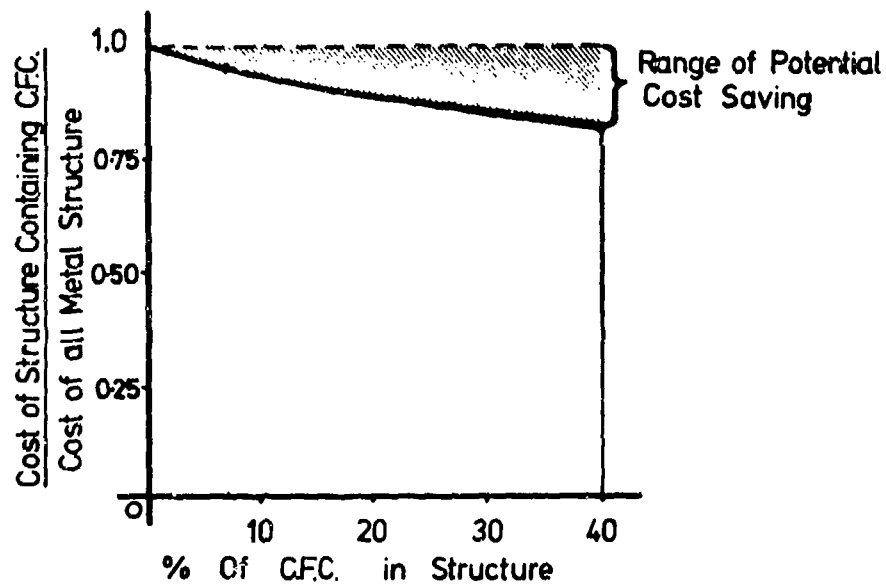


Fig.6 Cost saving potential of CFC structures

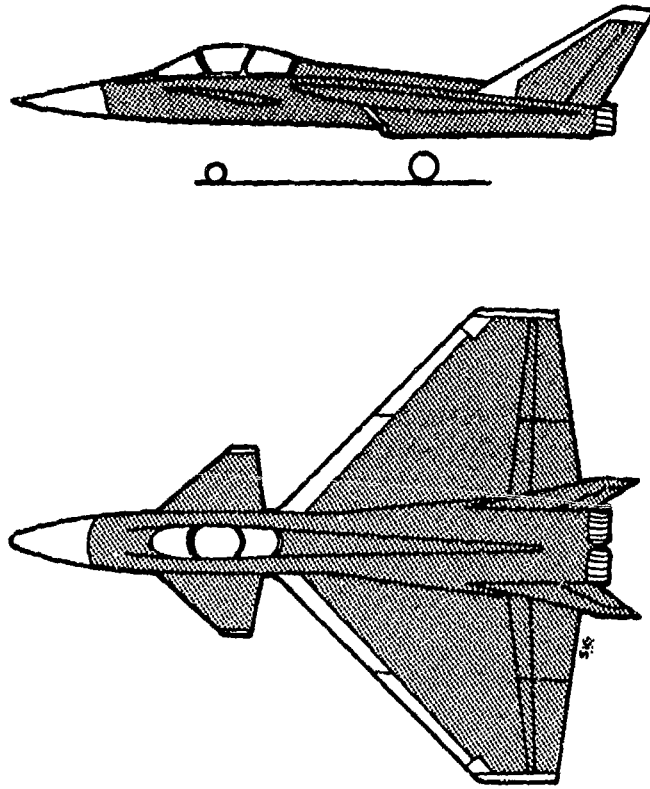


Fig.7 C.F.C. items for future concepts

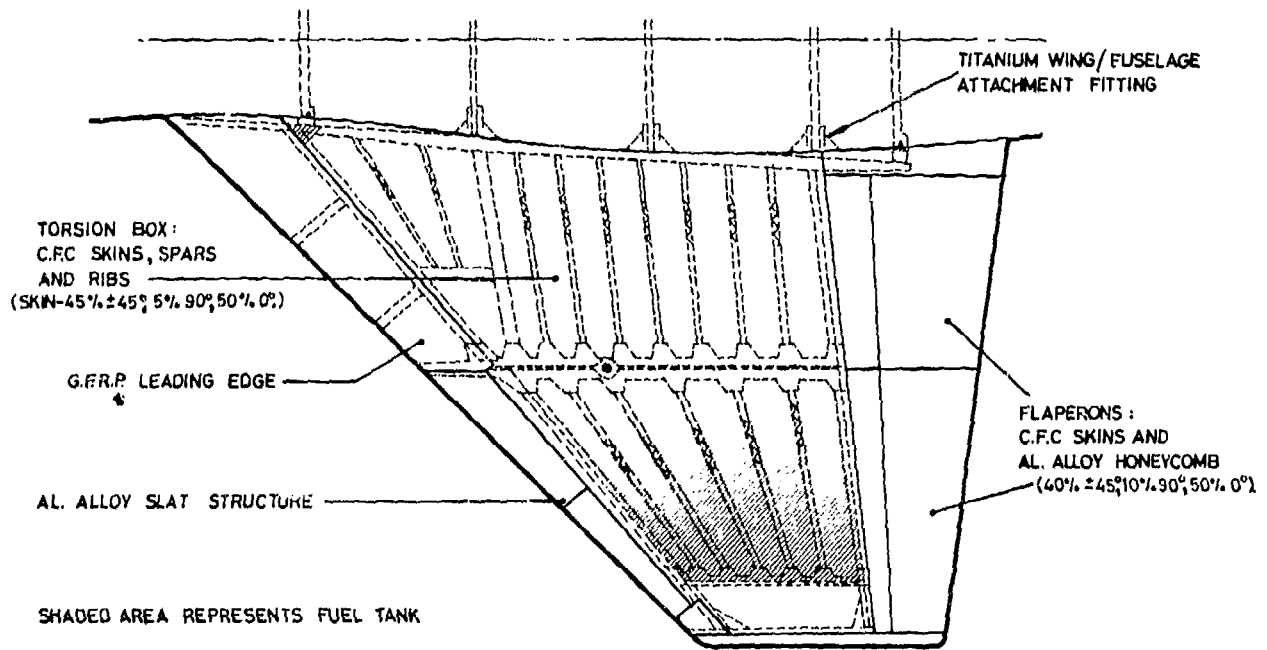


Fig.8 C.F.C. wing

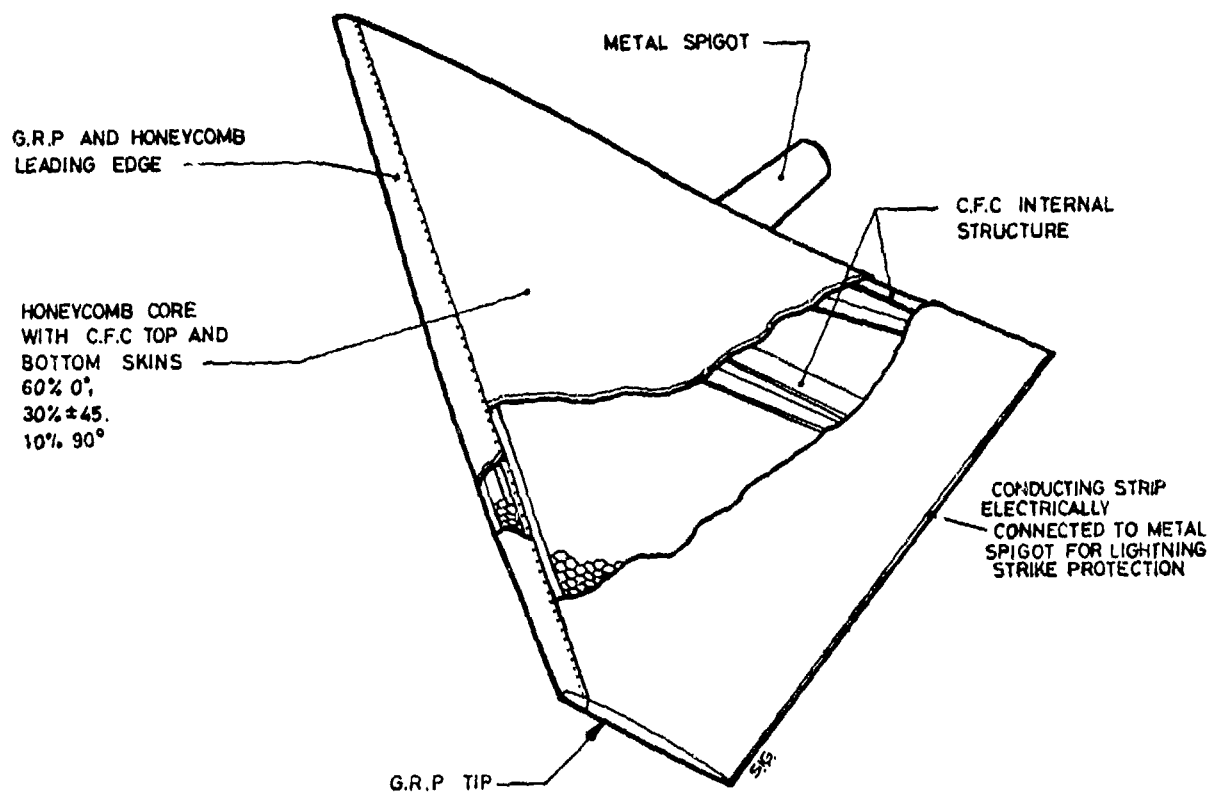


Fig.9 C.F.C. canard

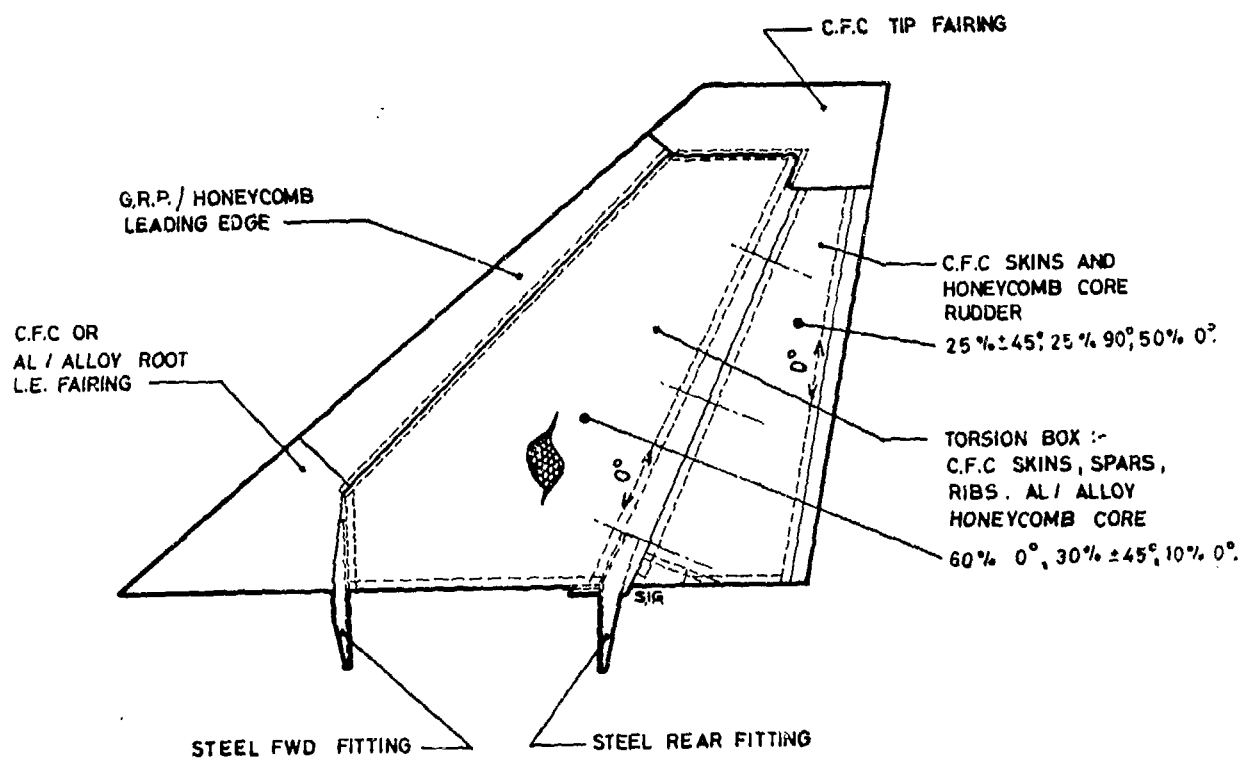


Fig.10 C.F.C. fin

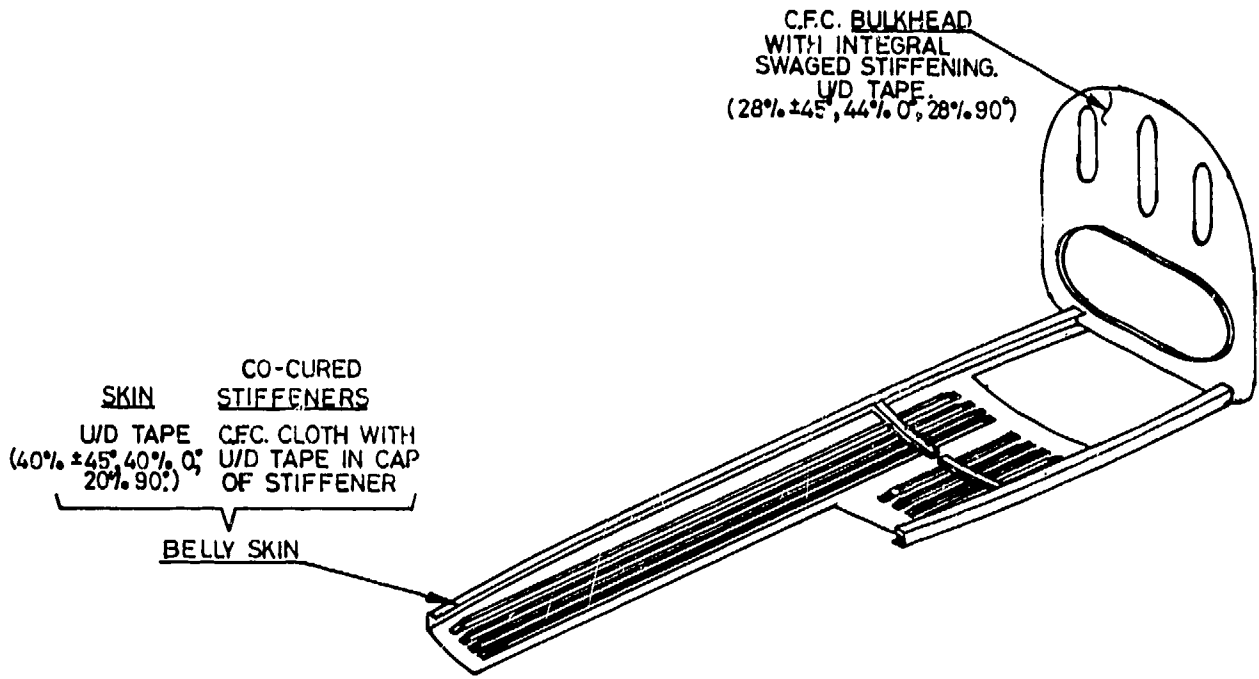


Fig.11 Front fuselage

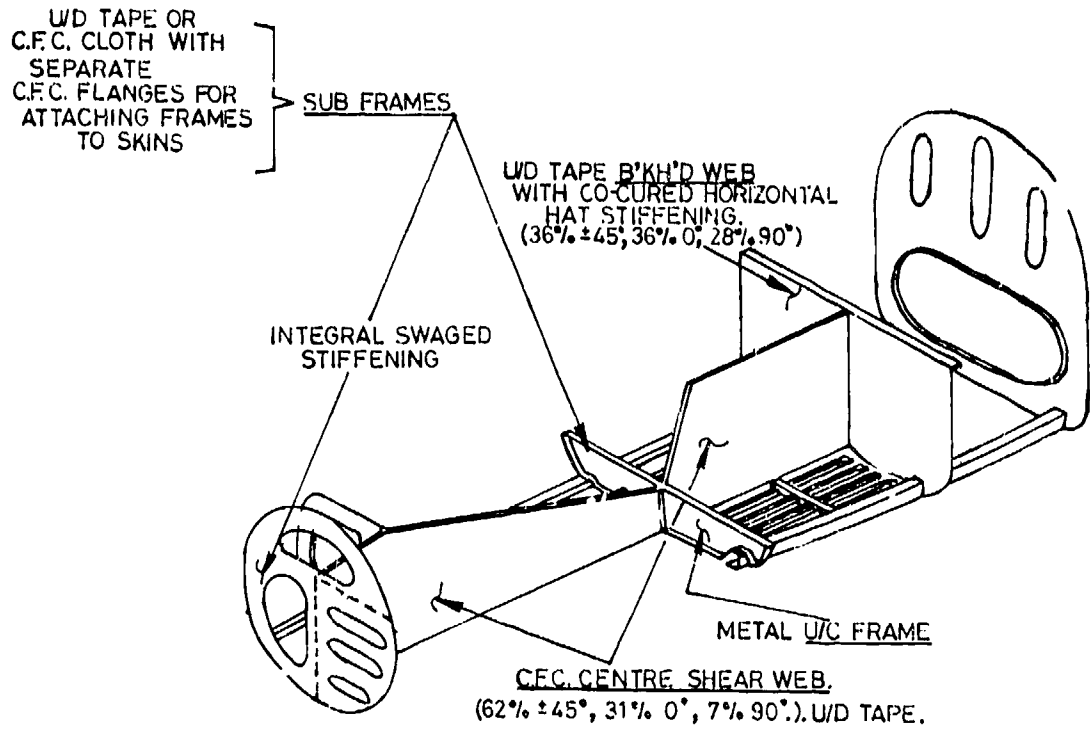


Fig.12 Front fuselage

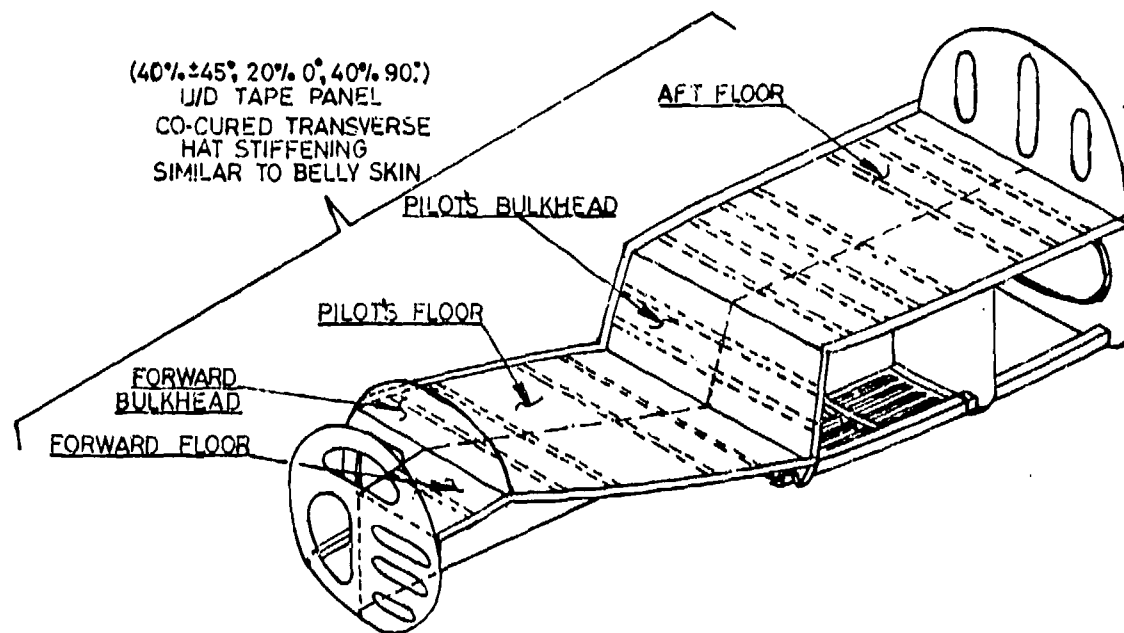


Fig.13 Front fuselage

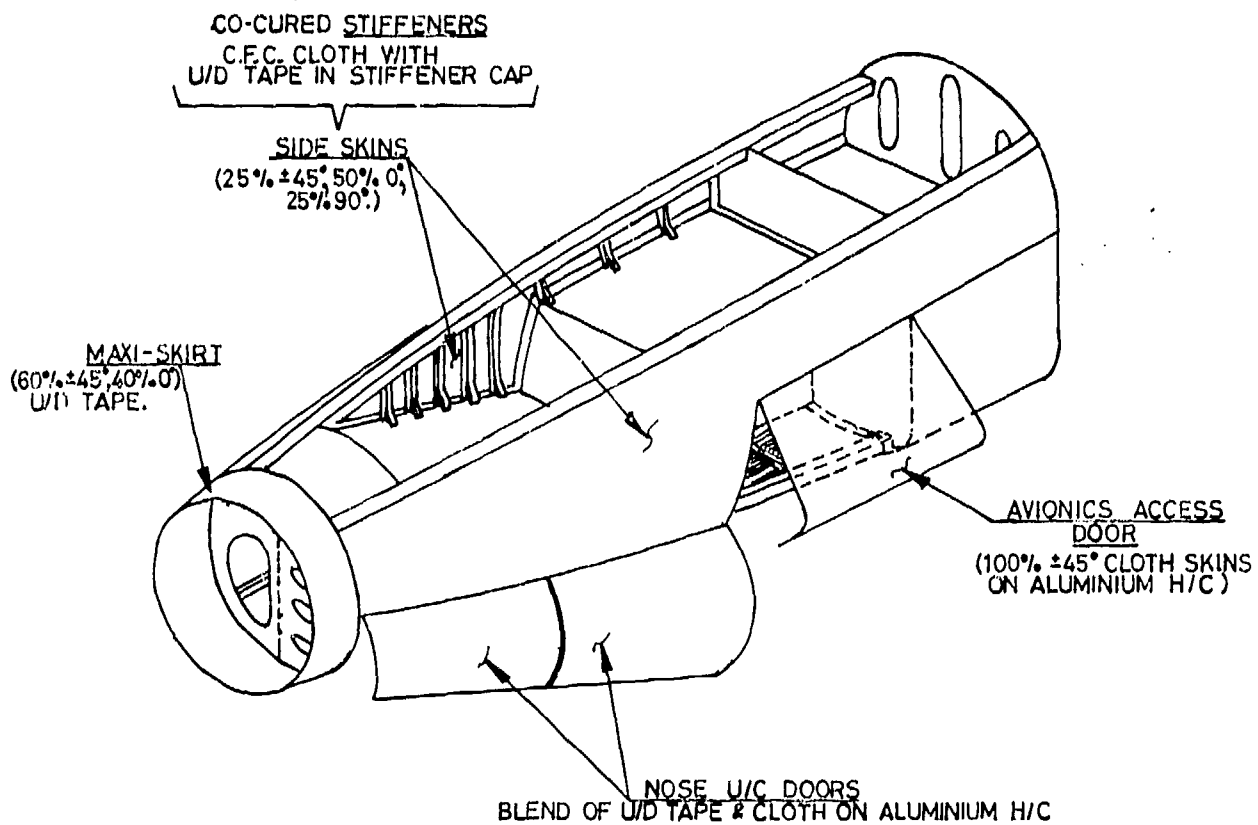


Fig.14 Front fuselage

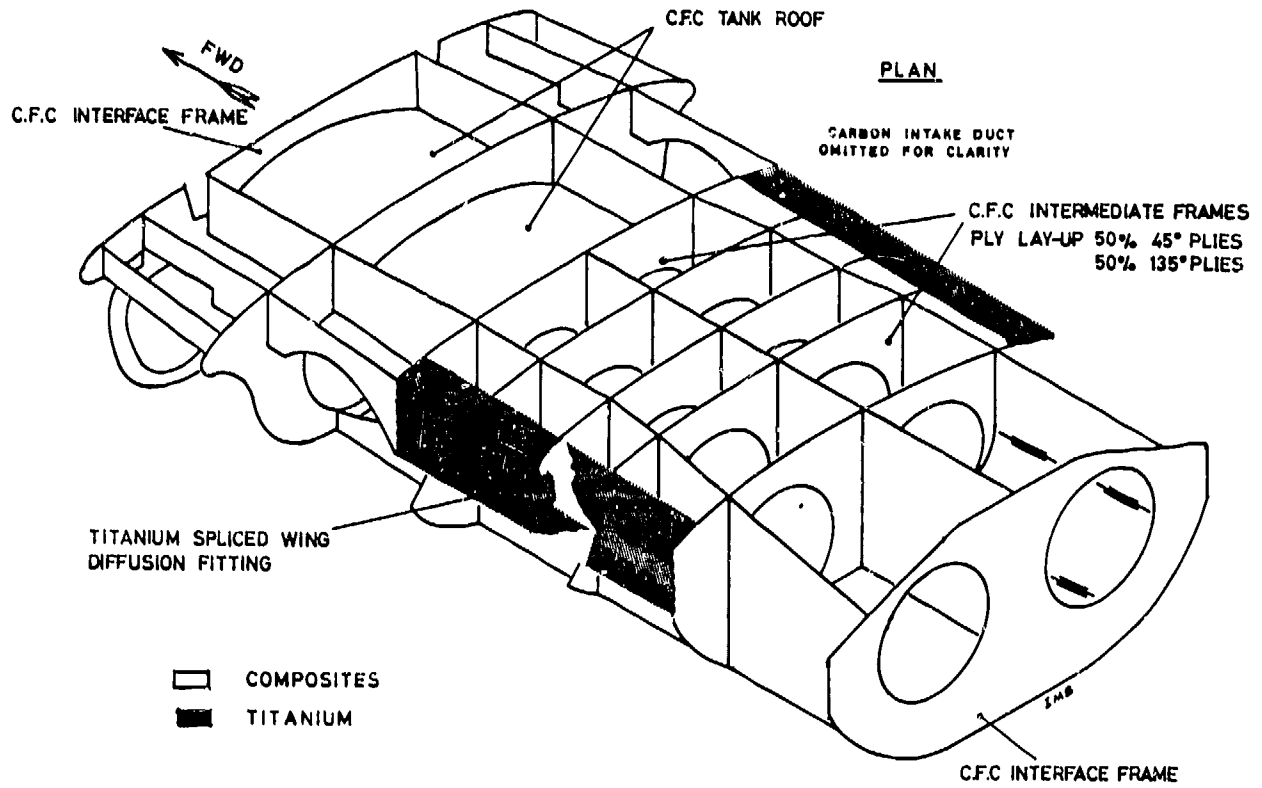


Fig. 15 Basic structure - centre fuselage

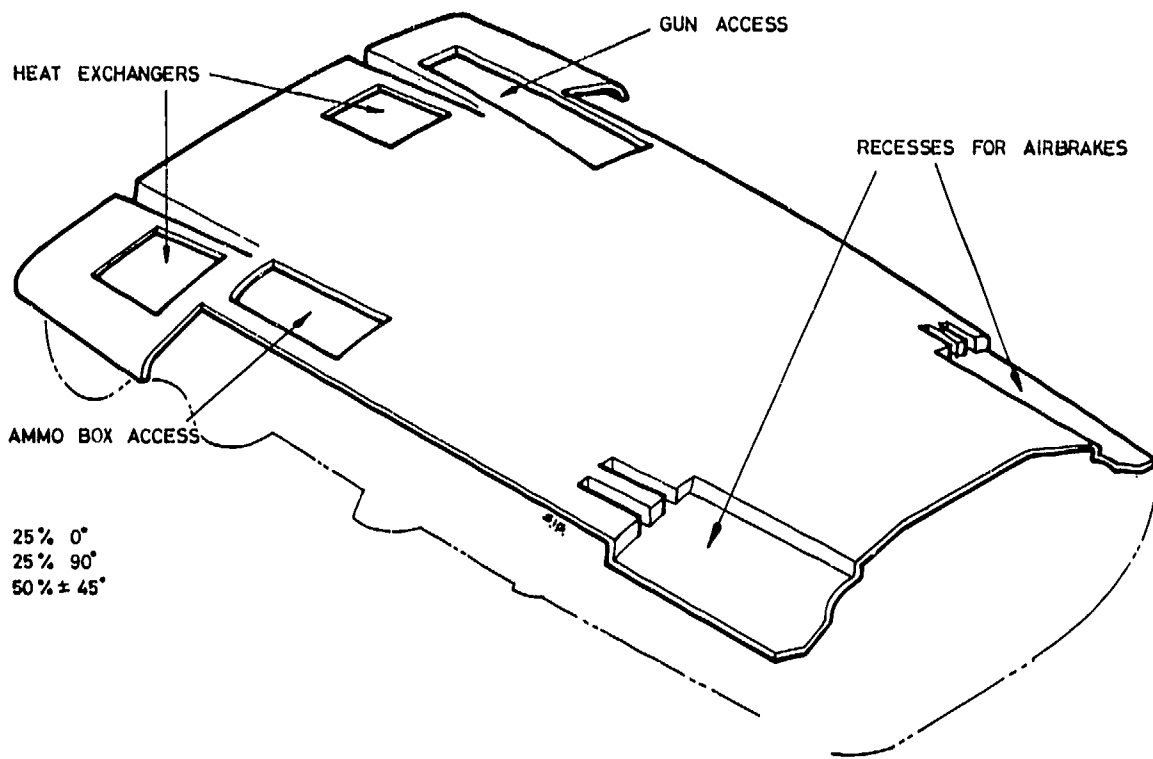


Fig. 16 C.F.C. centre fuselage top skin

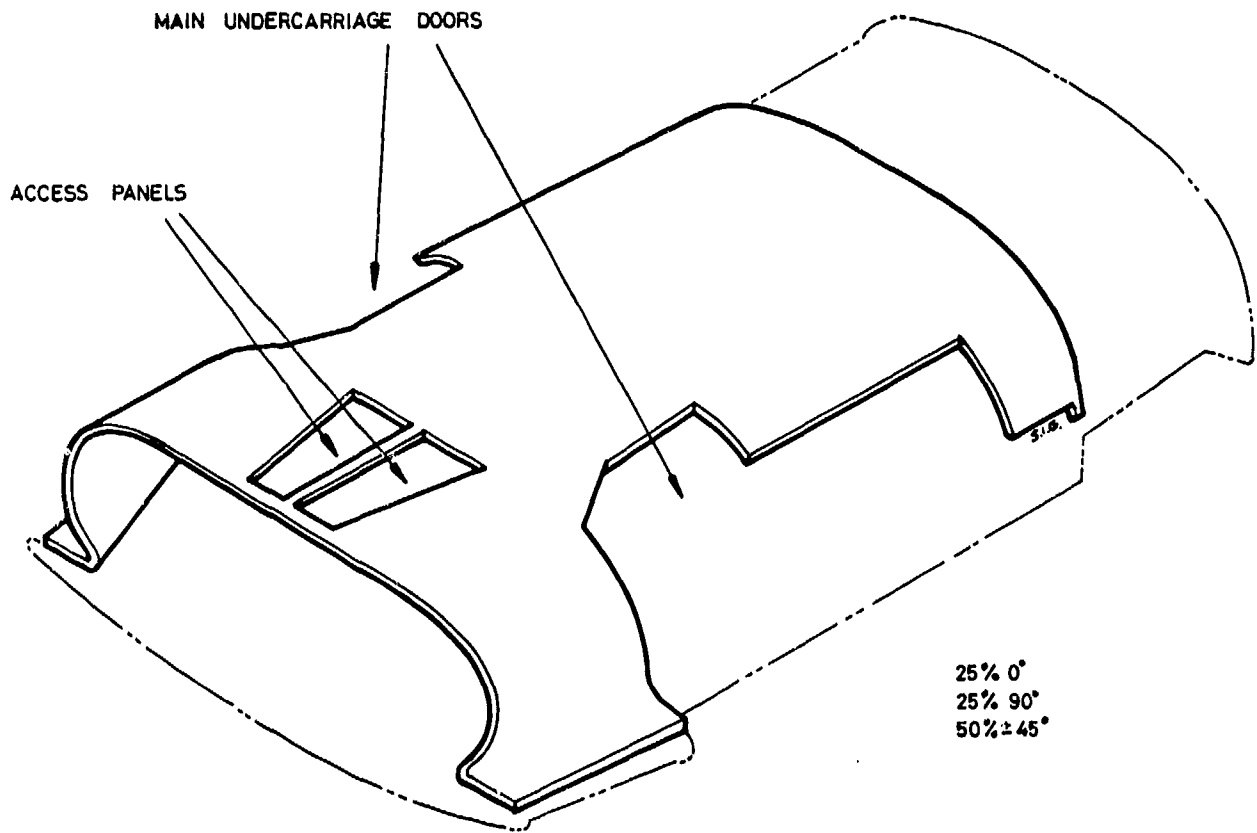


Fig.17 C.F.C. centre fuselage bottom skin

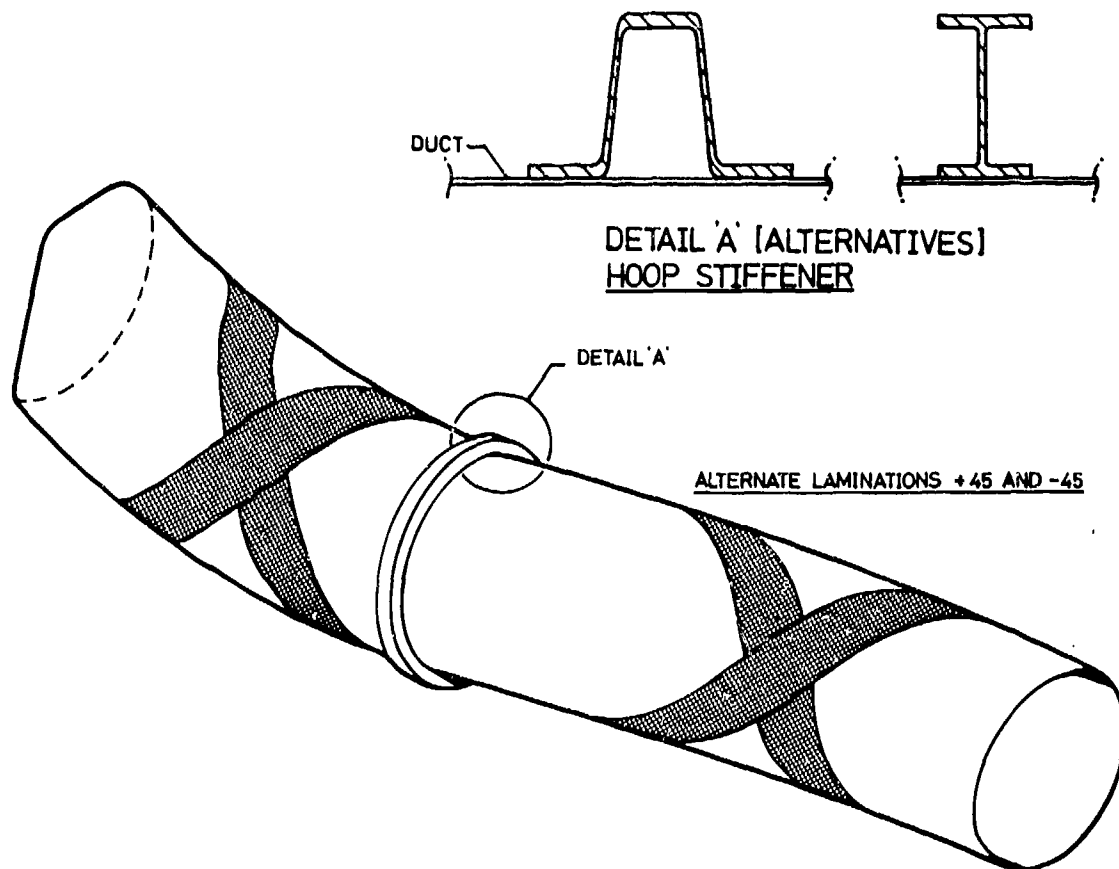


Fig.18 Carbon fibre duct (one piece) STN X5500 to X10200

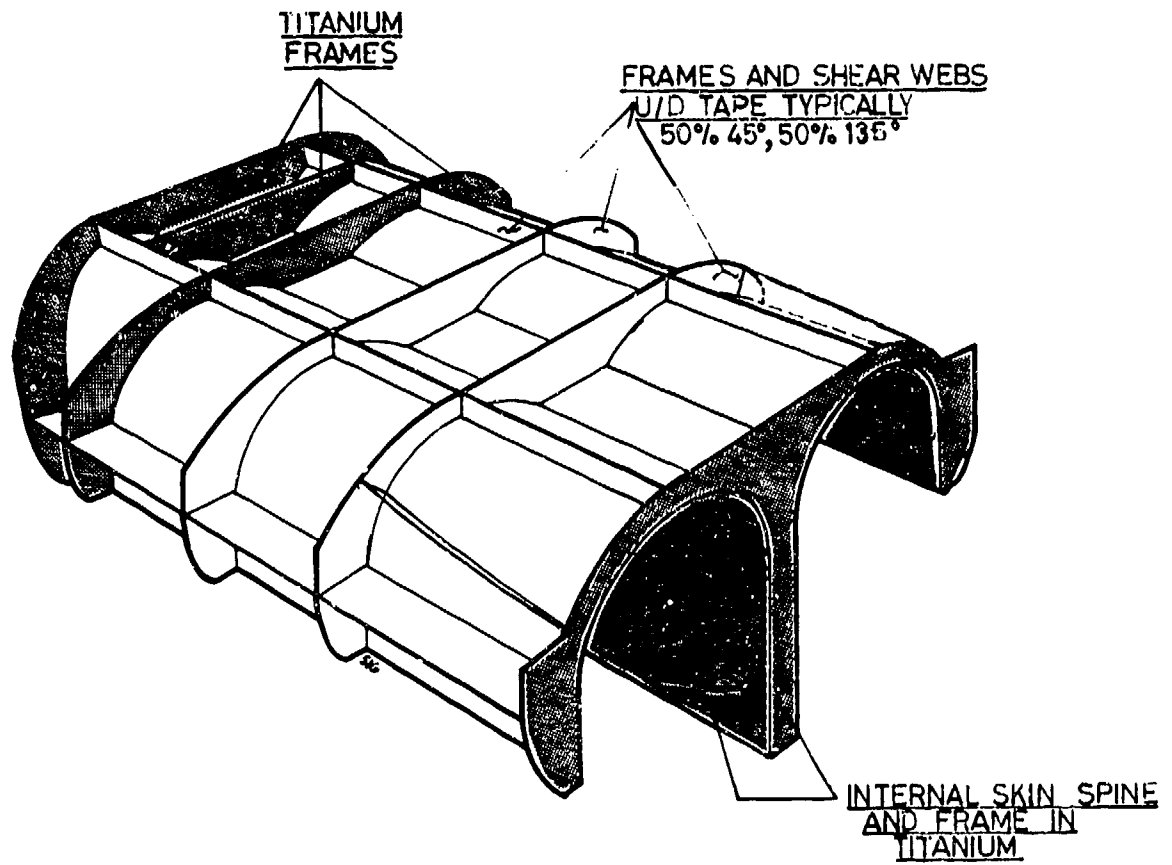


Fig.19 C.F.C. rear fuselage base structure

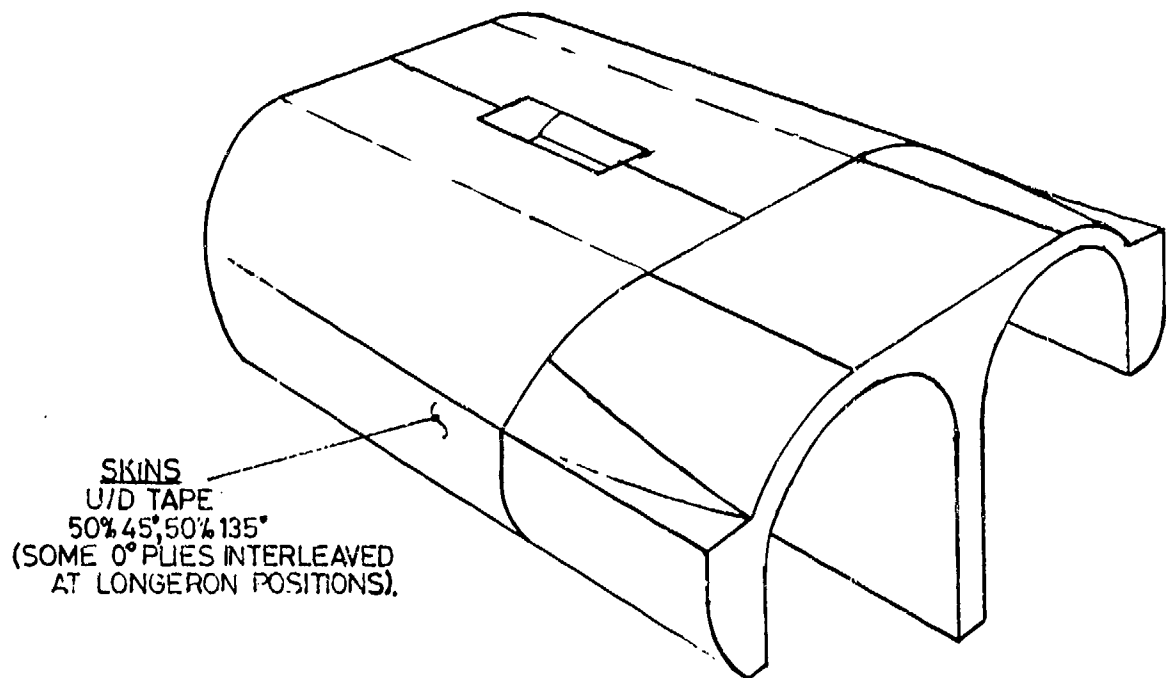


Fig.20 C.F.C. rear fuselage

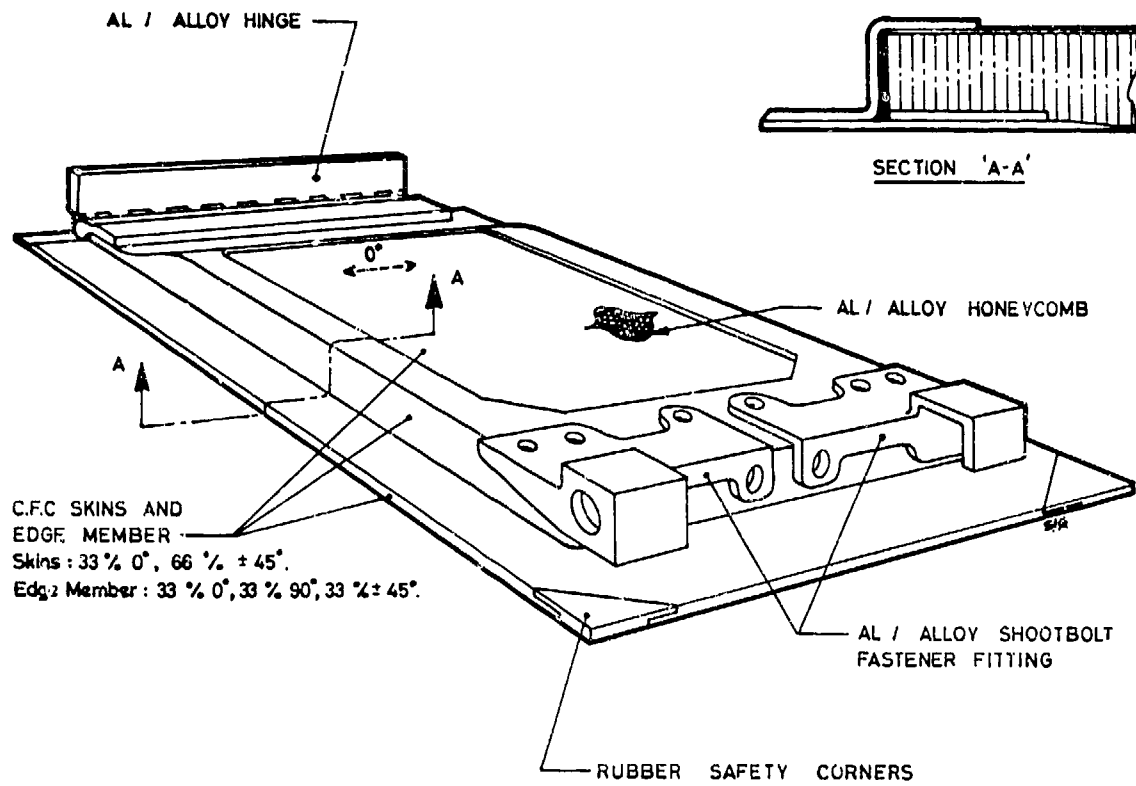


Fig.21 C.F.C. typical door

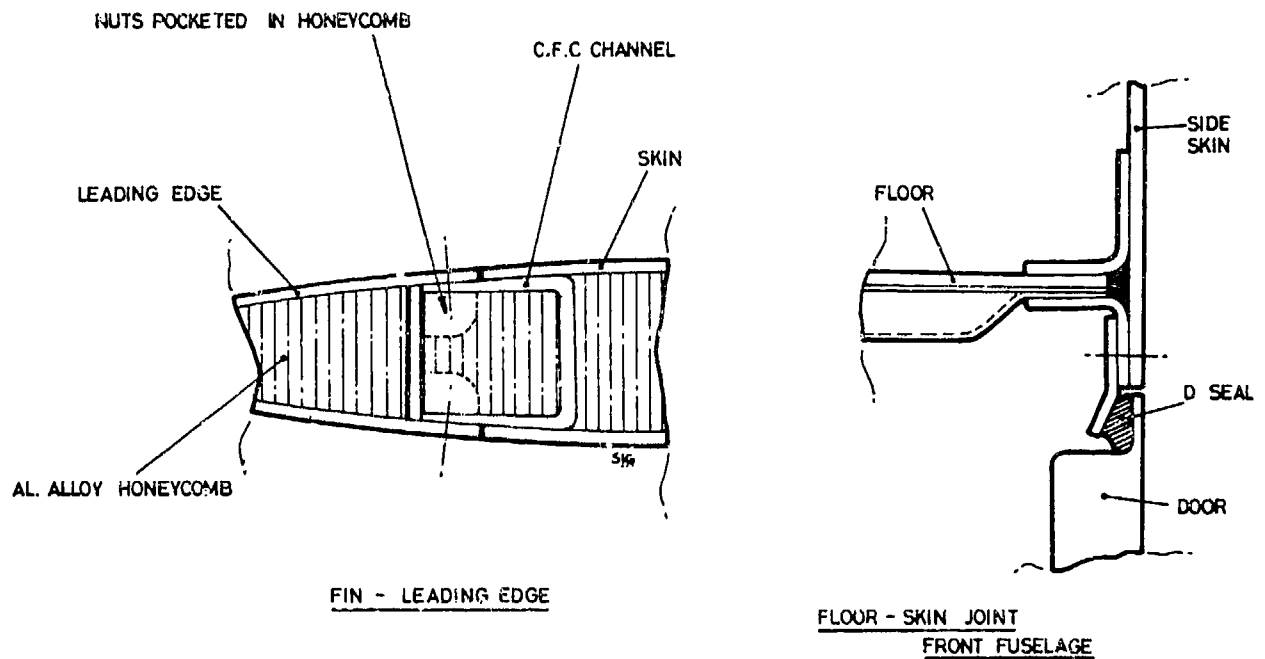


Fig.22 C.F.C. typical joints

ELECTROMAGNETIC SHIELDING CHARACTERISTICS
OF ADVANCED COMPOSITES

Dr. David F. Strawe

The Boeing Aerospace Company
Post Office Box 3999
Seattle, Washington 98124 U.S.A.

SUMMARY

A considerable body of data has been gathered on the basic electromagnetic (E.M.) properties of graphite advanced composite materials. This paper presents a sampling of that data relevant to the EM shielding applications. A basic set of shielding parameters is introduced which describes the intrinsic shielding characteristics of composite materials, enhanced conductivity coatings (metal foils, screens, flame spray, etc.), and electrical joints in those materials and coatings. Measurement concepts for these parameters are discussed which have been used over the frequency range 0 - 18 GHz.

Cross axis layups of graphite composites exhibit a uniform conductivity isotropic in the plane of the graphite filaments. This planar conductivity normally falls in the range of $1-2 \times 10^4$ mhos/meter. The third axis conductivity component, generally unimportant in shielding applications, is commonly an order of magnitude or more smaller. These composites can provide useful shielding from EM environments if they are electrically bonded in a continuous manner to the rest of the structure. Common mechanical joints between composite sections are highly resistive and unreliable electrical joints. Joining concepts which provide good electrical connections over wide frequency ranges have been developed and are described.

1.0 INTRODUCTION

Application of advanced composite materials to aircraft can provide significant weight reductions with consequent performance improvement over conventional metal designs. Boron filament, graphite-fiber, glass reinforced epoxy composites or hybrid combinations of these can be used to advantage. A major concern is the impact of composite materials application on the function of aircraft electrical and electronic components in the high EM fields due to lightning, nuclear EMP, radars, etc.

Unlike the metals they replace, materials such as boron, graphite, and S-glass permit the direct propagation or diffusion of exterior surface fields to the interior where they can produce voltages and currents at levels sufficient to upset or damage mission critical electronics. Even when diffusion is unimportant, joints in boron and graphite sections are likely to be poor electrically, allowing substantial field penetration.

Over the last decade a substantial body of data has been taken on electrical material and joint parameters in the 0-100 MHz frequency range. Graphite epoxy composites, metal foils and screens, flame spray coatings, and joints in these have been measured and reported extensively. Reliable means for measuring a wide range of parameter values have been developed, i.e., the "Quadrex" and "FPT" facilities. "Anechoic Chamber" measurements have provided some material and joint data in the microwave region.

In this paper the material parameters required for EM coupling analysis will be described along with measurement concepts. In addition, measured parameters for various composites and coatings are presented. Some conclusions regarding the shielding capability of advanced composites are listed.

2.0 FUNDAMENTAL CONCEPTS

2.1 Shielding Theory

The EM coupling problem can be solved with the following steps:

1. Calculate the induced exterior surface current and charge densities J_s and ρ_s .
2. Using J_s and ρ_s calculate interior "incident" fields in the absence of cabling whose response is ultimately to be calculated.
 - a. Use J_s and ρ_s to define interior shield surface sources.
 - b. Use these sources to calculate interior incident fields.
3. Using the fields of 2, calculate cable responses.

It is the specification of the interior shield surface sources (2a) with which we are most concerned here. In particular, it is the specification of shield material parameters which allow determination of these surface sources from the exterior responses J_s and ρ_s that we seek. A set of material shielding parameters will be introduced which will characterize any reasonably good nonmagnetic shielding material. The material may be a metal sheet, foil, or mesh; a composite laminate of good conductivity; or a composite coated with metal foil or mesh.

As a practical matter, only graphite among the composite laminates appears to offer good conductivity. Reliable, low-resistance composite joints have been obtained only in graphite laminates.

Material specifications are commonly given in terms of electric and magnetic shielding effectiveness (ESE and MSE, respectively). These are normally dB insertion loss field ratios for a particular shield geometry and incident field configurations of electrostatic, quasistatic magnetic, and plane wave form. The magnitudes of electric (magnetic) fields at a point inside the shield are related by these specifications to the external ambient. However, these are not true material descriptions since they depend upon shield configuration, shield dimensions, and field configuration, as well as the shield material itself. No convenient general method exists for determining shield interior fields from ESE and MSE taken in a special shield geometry and field configuration even when the shield is formed uniformly from one material type with perfect joints. A more general approach would require a specification for each material used to form the shield surface as well as the joints between material sections.

2.2 Mechanisms of Shield Penetration

Field penetration of shields takes place by coupling through apertures, by conduction on cables penetrating the shield, through imperfect electrical joints in shield materials, and by direct propagation (diffusion) through the shield material. If the shield material is mesh or screen (perhaps a coating on a poorly conducting composite laminate) coupling takes place through (ideally) a regular array of apertures in addition to diffusion through the mesh conductors. Both effects can be described by material parameters independent of screen size, shape, or shield geometry. In the following, only the material-related penetration mechanisms are considered, i.e., diffusion through conducting material, mesh aperture coupling, and imperfect material electrical joints.

Vance (Vance, E. F. - 1971) has shown that the effect of diffusion and magnetic aperture coupling can be lumped together into a transfer impedance in cable braid penetration analysis. This concept can be generalized (figure 1) to surface penetration. In this case the tangential electric field produced on the "back" side of a shield surface due to a surface current density J_s on the "front" side is given by

$$\bar{E}_t = z_s \bar{J}_s \quad (1)$$

The "back" side of the sheet is assumed to be terminated in a wave impedance much larger in magnitude than the surface impedance of the conducting surface. The above constitutes the defining equation for the "surface transfer impedance" z_s . In general, mesh asymmetries cause z_s to be a tensor quantity, but a scalar approximation is often sufficient.

The effect of electric aperture coupling is, following Vance (Vance, E. F. - 1971) and Kaden (Kaden, H. - 1952), considered to be due to an array of effective electric dipole moments on the back side of a mesh surface due to a normal electric field \bar{E}_n (with its associated penetration of mesh apertures) on the "front" side. The electric dipole moments per unit area, $\frac{d\bar{p}}{da}$, on the mesh surface, is normal to the surface as directed along \bar{E}_n .

$$\frac{d\bar{p}}{da} = P \bar{E}_n \quad (2)$$

This is the defining equation for the "surface electric polarizability" P .

Joints of reasonably low impedance can be conveniently described in terms of voltage V_j (open circuit) produced on the "back" side of a jointed surface section and the current density J_s on the "front" side which produces it.

$$V_j = \frac{1}{Y_j} J_s \quad (3)$$

This is the defining equation for the joint admittance per unit width Y_j of a joint (figure 1c). The reciprocal of Y_j is the transfer impedance of a unit width of a homogeneous joint and J_s is the current per unit width flowing across the joint.

2.3 Parameter Measurements

It is convenient to measure z_s , P , and Y_j in cylindrical samples of the shielding materials. Six-inch-diameter, 36-inch-long samples of jointed and unjointed materials were evaluated in a quadraxial test facility. A description of such a facility has been given by Knowles (Knowles, E. D. - 1969). Circumferential joints were formed in cylindrical samples and tested in a manner similar to connector joints (figure 2).

Reduction of parameter data from quadrax data is complicated at high frequencies by the sample electrical length. Straightforward transmission-line models for the quadrax can be used to reduce this parameter data. At low frequencies the reduction is purely geometrical; this is sketched here.

In figure 2 it can be seen that the quadrax response for a cylinder of length L and radius a is

$$V_L = \frac{I_{in}}{2} \frac{z_s L}{2\pi a} \quad (4)$$

The "voltage drop" across the cylinder transfer impedance $z_s L/2\pi a$ due to the exterior sample current I_{in} is $2V_L$. This drop splits equally between the inner line terminations $Z_1 = Z_0$. The surface transfer impedance z_s is calculated, using (4), from the quadrax transfer impedance V_L/I_{in} . Equation (4) gives the entire quadrax response when P and Y_j effects are negligible.

The joint admittance per unit joint width is determined from the sample joint transfer impedance, Z_j , where

$$Z_j = \frac{1}{Y_j 2\pi a} \quad (5)$$

When the joint is much "leakier" than the sample material the quadrax response is

$$V_L = I_{in} z_J/2 \quad (6)$$

When the unjointed portion of the sample contributes significant leakage this must be subtracted out using the z_s of the material and the unjointed length, L' , i.e.

$$V_L' = V_L - \frac{I_{in} z_s L'}{4\pi a} \quad (7)$$

Except for coarse meshes the contribution of P is usually negligible in the matched sample configuration of the quadrax. When its effect is small, it can be shown that the effect can be eliminated by merely averaging the inner line response voltages. To isolate P in this case the quadrax can be connected with an open-circuited drive line. The connection essentially eliminates the sample exterior current I_{in} and the z_s , Y_J contributions. P is determined from the transfer capacitance between outer and inner lines C_T . Vance (Vance, E. F. - 1971) and Kaden (Kaden, H. - 1959) have related the effective dipole moment of a small shield aperture to the transfer capacitance C_T it produces in a triaxial configuration. The dipole moments and transfer capacitances of the aperture array of a mesh can be collected and the relation between P and C_T written as

$$\frac{C_T}{L} = \frac{P C_{int} C_{ext}}{4\pi a \epsilon^2} \quad (8)$$

where ϵ is free space permittivity, and C_{int} and C_{ext} are the inner and outer line capacitance per unit length.

In general, the fields inside a shield constructed of jointed materials without apertures, except for those of mesh material, can be written as a linear combination of exterior J_s and ρ_s with parameters z_s , P , Y_J .

$$\begin{Bmatrix} E_{int} \\ H_{int} \end{Bmatrix} = \mathcal{H} \left[(z_s \bar{G}_{diffusion} + \frac{1}{Y_J} \bar{G}_{joint}) \cdot \bar{J}_s + P \bar{G}_p \cdot \bar{E}_n \right] ds \quad (9)$$

$$\text{where: } \bar{E}_n = \frac{\rho_s}{\epsilon_0} \hat{n}$$

2.4 Examples

Expressions for the electric and magnetic fields inside a small hollow mesh sphere can be adapted from standard sphere solutions (Kaden, H. - 1959). In a uniform field, E^{inc} and H^{inc} the fields at the sphere's center, can be shown to be given by

$$\begin{aligned} E &= E^{inc} \left(\frac{3P}{2\epsilon a} + \frac{j\omega\epsilon 4az_s}{3} \right) \\ H &= \frac{H^{inc}}{1 + \frac{j\omega\mu a}{3Z_s}} \end{aligned} \quad (10)$$

where a is the sphere radius. Comparison is shown in figure 3 between measured and calculated fields for a 30-inch-diameter sphere constructed of 18 mesh, 10-mil phosphor/bronze screen. Actually, the measured geometry was the equivalent hemisphere mounted on the floor of a plane wave simulator.

Similar expressions can be constructed for cylindrical shells. Fields have been predicted successfully in a number of cylindrical shells constructed of graphite laminates, metal foils and meshes, and graphites coated with foils and meshes.

Measured currents on axis parallel interior conductors also have been predicted with good accuracy using similar approaches and measured z_s and P data. Some examples are given in figure 4.

3.0 EMPIRICAL RESULTS

3.1 Test Specimens for HF Measurements

Tests were conducted on samples of (1) composite laminates, (2) metal foils, (3) metal screens, (4) aluminum flame spray, (5) aluminum honeycomb core, and (6) combinations of (2) through (5) with composite laminates. In most cases combinations were not bonded. An evaluation program showed that bonded and unbonded shielding materials have the same shielding effectiveness. Three principal reinforcing materials were evaluated: graphite, boron, and S-glass. The graphite fibers were T-300, HTS, and HMS, all impregnated with 5208 resin from Whittaker. The boron was Rigidite 5505 prepreg from AVCO and the S-glass was unidirectional Scotchply with a 1002 resin system from the 3M Corporation. These materials were selected because they have been extensively characterized mechanically and applied to structural components by industry.

Initial testing on a large number of the above materials was accomplished using flat-plate magnetic shielding effectiveness (MSE) techniques, i.e., measurement of the change in coupling between two closely spaced loops when a flat-plate sample of material is placed between the loops. This allowed the various materials to be ranked so only the most promising were used for detailed parameter measurements. For example, graphite composites (with or without metal coatings), in 0°/90° layups exhibited predictable shielding which was very significant for laminate thicknesses approaching those required for aircraft skin. Boron composites, on the other hand, were found to be difficult to join electrically and produced

unpredictable and mediocre shielding. S-glass composites provided no significant amount of shielding. All test specimens for the Quadrax tests were 6 inches in diameter and 36 inches long. The materials used were 24-ply T-300/5208 and 12-ply HTS/5208 for the composites, and a aluminum and copper foil and aluminum and phosphor/bronze screens for coating materials.

Joint configurations that were evaluated fell into three categories: (1) structural joints, (2) screen/graphite joints, and (3) coating joints appropriate in screen and foil overlays on composites. The desired joint parameter is the joint admittance, Y_j , and this was obtained from test data taken in the quadrax on 6-inch-diameter test specimens, usually about 3 inches long. The structural joints selected were typical of the joints in current use on composite structures, both composite-to-composite and composite-to-metal. The test specimens were all fabricated with $0^\circ/90^\circ$ construction (a double 90° at mid-plane). They were precompact and partially cured every 4 to 6 plies. Each nonmetallic cylinder end was provided with an electrical attachment to the quadrax test fixture by inserting a 2-inch-wide, 100-mesh PB screen one inch into each 90° center ply, and a single screen at the double 90° center plies.

The screen/graphite joint was developed to provide the electrical contact between the cylindrical graphite test specimens and the quadrax end-plates. It is fabricated by inserting screen between every other ply during layup.

Screen and foil coating materials, to be effective, must be joined electrically to coating materials on adjacent composite panels or to adjacent metal where composite attachments are made. The methods of joining that were tested are ultrasonic seam-weld, epoxied and cured at 90 psi, spot-weld, seam-weld, and spot-weld with doubler.

3.2 HF Test Results

Shielding material data, z_s and P , reduced from quadrax measurements are presented in figures 5 through 7. Figure 5 shows the results for the coating materials alone, i.e., aluminum and phosphor/bronze screens. The magnitude of z_s is shown as a function of frequency while P is independent of frequency for these samples and is only listed in the figures. Figure 6 shows results for the graphite laminates alone and figure 7 shows results for coated laminates. Examples of joint admittance data are shown in figure 8.

3.3 VHF and Microwave Measurements

Relatively little material and joint data has been taken above 100 MHz. Much of that is of questionable quality being apparently polluted by leakage around the sample. That involving small samples transverse to coaxial lines and waveguides are questionable due to unusual current distributions of abnormally thin anisotropic samples. Also, data involving closure of a box enclosure with a composite sample suffers from the current distribution problem and is therefore not extendable or usable in other applications of the same material since it cannot (or at least has not been) be reduced to basic material or joint data.

Microwave measurements of material and joint parameters are difficult owing to a shortage of wide-band receivers and power sources. Generally, measurements are made one octave at a time with different sources, amplifier, plug-ins, etc. for each band. There is a general sensitivity to local geometric detail because of the short wavelengths involved. Most of the credible data taken above 1 GHz has been obtained from transmission loss measurements in an anechoic chamber of some form (Force, R. D. - 1979) and (Strawe, D. F. - 1980). A schematic representation of this approach is shown in figure 9.

Figures 10 and 11 show a working anechoic chamber. This one consists of two open-ended, flanged, stainless steel boxes, two end plates, and a center plate which includes the sample holder. Two doors were built into one of the boxes to access the sample holder. The entire chamber was lined with a blanket type microwave absorber. Antennas are mounted on the end plates at opposite ends of the chamber. Two antennas are required to cover the 1 to 18 GHz frequency range. The two chamber compartments are separated by the center plate, which contains the material or jointed panel to be measured.

A simple butt type joint was fabricated in one 8-ply and one 16-ply panel. A sketch of a butt joint is shown in Figure 12. The joint consists of a slot or gap between two panels, a cap over the gap, and one row of fasteners on each side of the gap joining the three members together. This type of joint is found on the leading edge and wing skin of commercial aircraft.

Construction of sample joint 1 was accomplished by first cutting a 0.12 inch wide slot 14 inches long in a 16-ply panel, cutting a 3 inch wide by 15 inch long cap from another graphite epoxy panel (8-ply with 0° , 90° , 0° , 90° , etc. layup), machining two rows of holes in the cap and panel, then, fastening the cap to the panel. Each row of fasteners was 0.75 inches from the center of the slot in the panel. The fasteners were made of titanium coated with an aluminum epoxy paint which is electrically non-conductive. Each row contained 15 fasteners spaced one inch apart. The holes for the fasteners were a few thousandths of an inch larger in diameter than the shaft of the fastener. This is considered a non-interference fit. Countersinking of the holes was required to accommodate the head of the fasteners.

Sample joint 2 was constructed in an 8-ply panel in an identical manner as joint 1. However, before fastening the cap to the panel the mating surfaces of the panel and cap were lightly sanded to expose the graphite surface. In joint 1 the mating surfaces are epoxy, a non-conductive material. In addition the titanium fasteners used in joint 2 were uncoated and the holes were drilled slightly smaller than the shaft of the fasteners providing an interference fit. Thus, it was intended that joint 2 would be an improved version of joint 1 because of the electrical contact between fasteners and graphite fibers in the panel and cap, and between mating surfaces of the cap and panel.

After construction of the joint it was discovered that the coated fasteners in joint 1 made electrical contact with the graphite fibers in the panel. Examination of the fasteners showed that the coating had been removed or not applied properly around the head of the fastener. Every fastener in both jointed samples was found to be electrically connected to the graphite fibers. Thus the only major difference between joints 1 and 2 is the electrical contact in the mating surface area. Figure 13 contains

photographs of an unjointed graphite epoxy panel, and a complete joint. Figure 14 portrays the other side of the joint and the joint and cap prior to assembly.

The joint admittance of the test samples is deduced from their transmission data taken in the anechoic chamber. The transmission transfer function from input to output port is measured. It has the multiplier Y_J^{-1} so that Y_J can be determined by comparison of transmission data with that of a standard slotted panel. The joint admittance of a linear array of thin electrically short slots is easily calculated from standard formulas (Kaden, H. - 1959) and (Marcuvitz, N. - 1951). Since the test geometries and transmission factors are the same for unknown and standard slotted "joints" except for the joints and their Y_J 's, the ratio of transmission factors is the ratio of Y_J 's. Commonly, only the magnitude of Y_J is obtained because of difficulties in accurate phase measurements. If the transmission factors are defined as

$$T \equiv \frac{P_R \text{ (power received)}}{P_T \text{ (power transmitted)}} \sim |Y_J^{-2}| \quad (11)$$

Then

$$|Y_J| = |Y_J \text{ (std)}| \sqrt{\frac{T \text{ (std)}}{T}} \quad (12)$$

An array of thin electrically small rectangular slots layed out, as shown in Figure 15, with slot length W , width δ , center-center spacing S , and N parallel lines of slots has the joint admittance:

$$|Y_J| = \frac{24S}{N \omega \mu \pi W^3} \ln \frac{2W}{\delta} - 1 \quad (13)$$

As an example, slotted reference 2 consists of a single line ($N=1$) of rectangular slots with $S = 1"$, $\delta = .032"$, and $W = 0.2"$. The above formulation indicates that well below slot resonance at ≈ 25 GHz the Y_J is approximated by

$$Y_J = \frac{286}{f_{\text{GHz}}} \quad (14)$$

The joint admittance of the slotted reference 2 and that of joints 1 and 2 are shown in Figure 16. Note that below slot resonance, the reference slot array degrades monotonically with increasing frequency while joints 1 and 2 monotonically improve. The improved joint (2) is comparable to the slotted reference at S-Band but is 50 dB superior at Ku-Band. The surface sanding and interference fit of fasteners used in joint 2 lead to 10-30 dB improvement over its untreated baseline configuration joint 1. The accidental contact of the fasteners in joint 1 to the graphite fibers undoubtedly improves the joint over the more common isolated fastener used in practice.

4.0 CONCLUSIONS

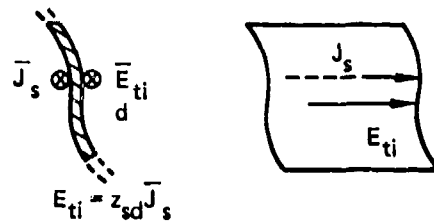
Much more data has been measured than could be presented in this paper. The conclusions that follow are based on a larger data base.

1. Single-component, multilayer, multidirectional composites composed of graphite tapes behave as 2 axis isotropic materials and can be described electrically by the surface transfer impedance z_s . Joints in these materials can be made with a very high admittance per unit width using screen inserts, so that the joints are effectively invisible electrically.
2. Graphite composites normally exhibit an in-plane isotropic conductivity of $1-2 \times 10^4$ Mho/meter for all frequencies up to 1 GHz (Strawe, D. F. - 1975; Force, R. D. - 1977). From 1-20 GHz there is evidence (Force, R. D. - 1977) to indicate a decline in σ by perhaps a factor of 2, although this may be a result of measurement error. Above 1 GHz graphite, in layups of 8 or more plies, is practically opaque, with dominate leakages coming from joints. For this case, the actual value of effective conductivity is unimportant. The material displacement current is always dominated by conduction current so that permittivity is also unimportant. Third axis (normal to sheet) conductivity is normally lower by over an order of magnitude.
3. Hybrid composites that isolate graphite plies with non-conducting plies (e.g., glass, Kevlar, etc.) will require that each graphite layer be continuous electrically at each joint to take advantage of the shielding afforded by each graphite ply. Such composites will, in general, not be describable by a z_s , P or Y_J material parameter as are the homogeneous materials where the conducting plies are in intimate contact. For many applications, hybrid composite shielding characteristics may be approximated using these parameters, but in others they will exhibit effects due to trapped inter-ply modules in the non-conducting material between the graphite plies. In these cases, flat-plate MSE will not have a uniqueness comparable to that of the simpler single-component graphite composites.
4. Boron composites at low and intermediate frequencies are anisotropic, poorly conducting materials for which no good joining technique could be found. This is in contrast to the graphite composites where an excellent electrical bond to the graphite fibers was achieved by inserting screen between alternate graphite plies. The shielding characteristics of boron composites cannot, therefore, be described by unique values for MSE, z_s or Y_J which are required for a general analysis.
5. Composites made of non-conducting materials such as S-glass and Kevlar cannot be described by the basic material parameters and have no significant shielding effect.

6. Uncoated graphite composites and composites coated with foil, screen, or flame spray must be electrically joined to neighboring structure, so as to form closed conducting shells, if they are to contribute optimally to the shielding of the interior. Ultrasonic seam welding of aluminum screen and foil coatings provides an optimum coating joint, once the appropriate welding schedule has been determined for the mesh size and alloy used.
7. The shielding characteristics of materials and joints with well defined z_s , P , and Y_j can be analyzed in a conventional manner, except that (a) large z_s may affect the exterior current response and will produce substantial interior responses due to direct penetration through the material, and (b) non-zero P will require a distributed electric aperture-coupling analysis in addition to the conventional diffusion-type analysis involving z_s .
8. Screens and foils can be incorporated within, or on the surface of, composites during fabrication without impacting the processing or curing schedule of the material. No incompatibilities in thermal expansion, voids, or delaminations have been detected. They are also not expected to compromise the structural properties.
9. Aluminum flame spray is an isotropic good conductor with conductivity 10 to 30 times below that of pure aluminum and a density 1/3 to 1/2 that of aluminum.
10. Standard butt joints with doubler and standard fasteners provide poor electrical joints in the 0-100 MHz range. They may be, because of the common use of corrosion protection coatings, a totally open circuit. This would seriously affect the penetration of attached lightning currents (and other HF region threats) into an aircraft interior. Although, required joint Y_j has not been established for aircraft skin applications. It appears that microwave leakage through joints will present a lesser problem than HF leakage.

REFERENCES

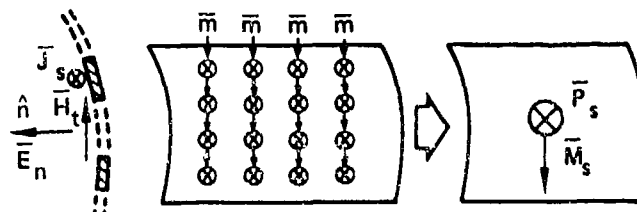
- Force, R. D. et al, Sept. 1977 "Investigation of Electromagnetic Energy Effects on Advanced Composite Structures and Their Associated Avionics/Electrical Equipment", Phase II, Vol. 1, Technical Report, D180-20186-4, Boeing Aerospace Company, Seattle, Washington.
- Kaden, H., 1959 "Wirbelstromer and Schirmung in der Nachrichtentechnik", Springer-Verlag, Berlin.
- Knowles, E. D. and Olsen, L. W., 1969, "Cable Shielding Effectiveness Testing", Boeing Aerospace Co., published by DNA as a Protection Engineering and Management Note, PEM-14.
- Marcuvitz, N., 1951, Waveguide Handbook, MIT Rad. Lab Series, Vol 10, McGraw-Hill Book Co., N.Y.
- Strawe, D. F. and Piszker, L. D., Sept. 1975 "Interaction of Advanced Composites with Electromagnetic Pulse (EMP) Environment", Boeing Aerospace Co., Document D180-19980-1, prepared for AFML/LC, Wright-Patterson AFB, Ohio 45439, Tech. Rep. AFML-TR-75-141.
- Strawe, D. F. and Piszker, L. D., Jan. 1980, "Investigation of Penetration of Electromagnetic Energy Through Joints in Advanced Composite Structures", Boeing Aerospace Co., D180-25240-2, prepared for Naval Air Systems Command, Arlington, VA.
- Vance, E. F. and Change, H., November 1971, "Shielding Effectiveness of Braided-Wire Shields", SRI Technical Memorandum 16.



$$E_{ti} = z_{sd} \bar{J}_s$$

$$z_{sd} = \frac{E_{ti} \text{ (INNER SURFACE TANGENTIAL ELECTRIC FIELD)}}{J_s \text{ (OUTER SURFACE SKIN CURRENT)}}$$

A. DIFFUSION



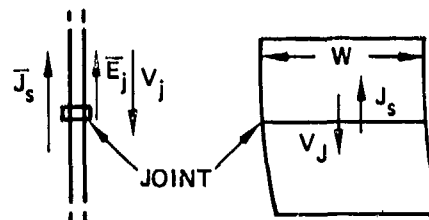
$$\bar{P}_s \text{ (ELECTRIC DIPOLE MOMENT/UNIT AREA)} = P \bar{E}_n$$

$$\bar{M}_s \text{ (MAGNETIC DIPOLE MOMENT/UNIT AREA)} = M \hat{n} \times \bar{J}_s$$

$$P \text{ (ELECTRIC SURFACE POLARIZABILITY)} = n a_E$$

$$M \text{ (MAGNETIC SURFACE POLARIZABILITY)} = n a_H$$

B. QUASISTATIC APERTURE COUPLING



$$V_j = \frac{I_{tot}}{Y_{tot}} = \frac{J_s W}{Y_j W} = \frac{J_s}{Y_j}$$

C. JOINT COUPLING

Fig.1 Surface coupling

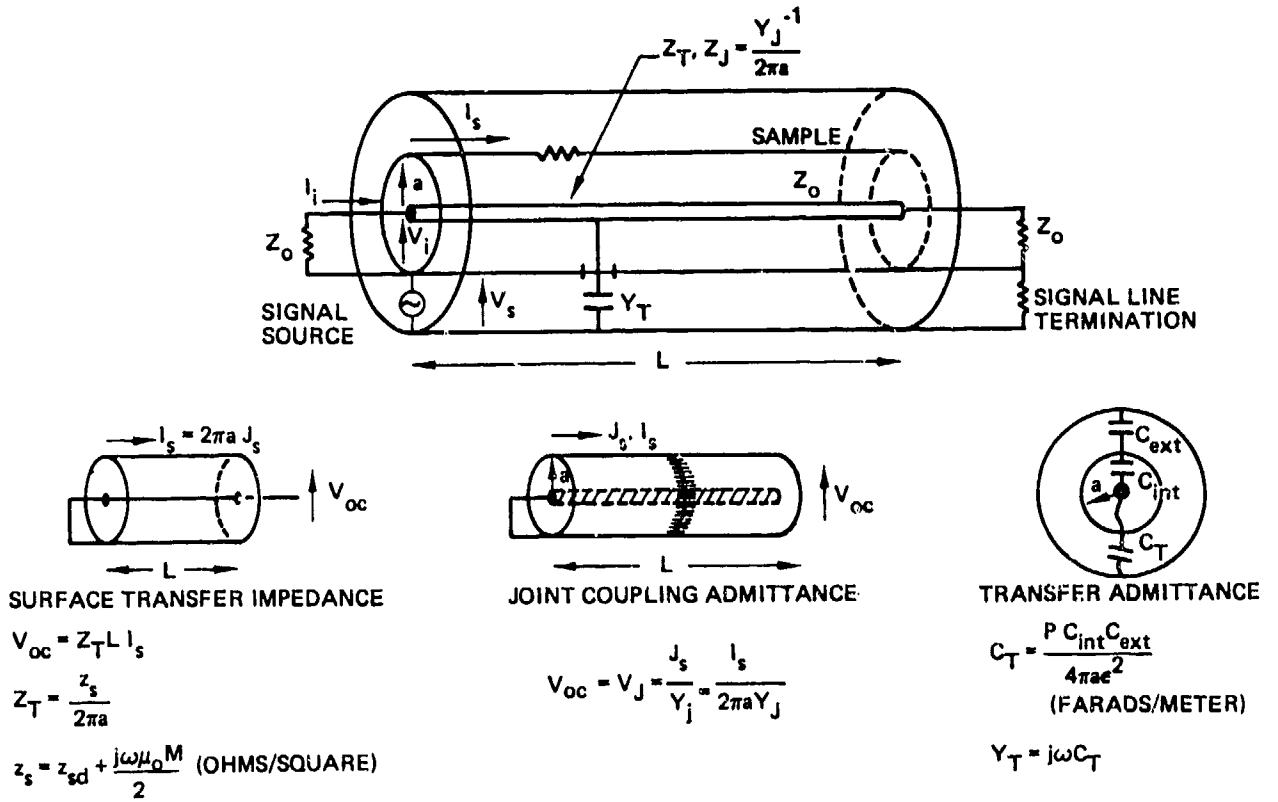


Fig.2 Quadaxial test concept for material parameter measurement

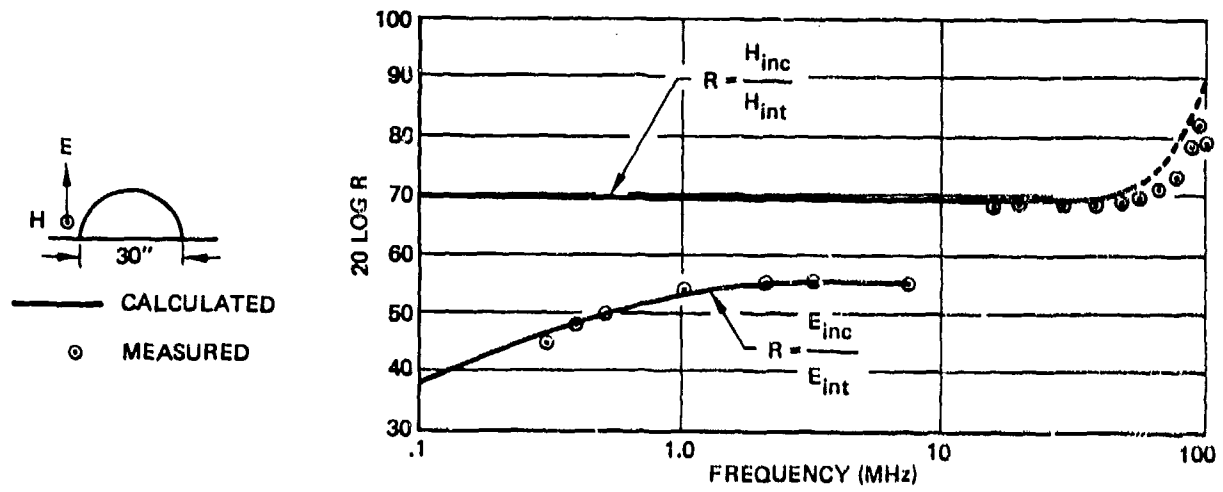


Fig.3 E and H field response at center of 18-mesh PBS hemisphere

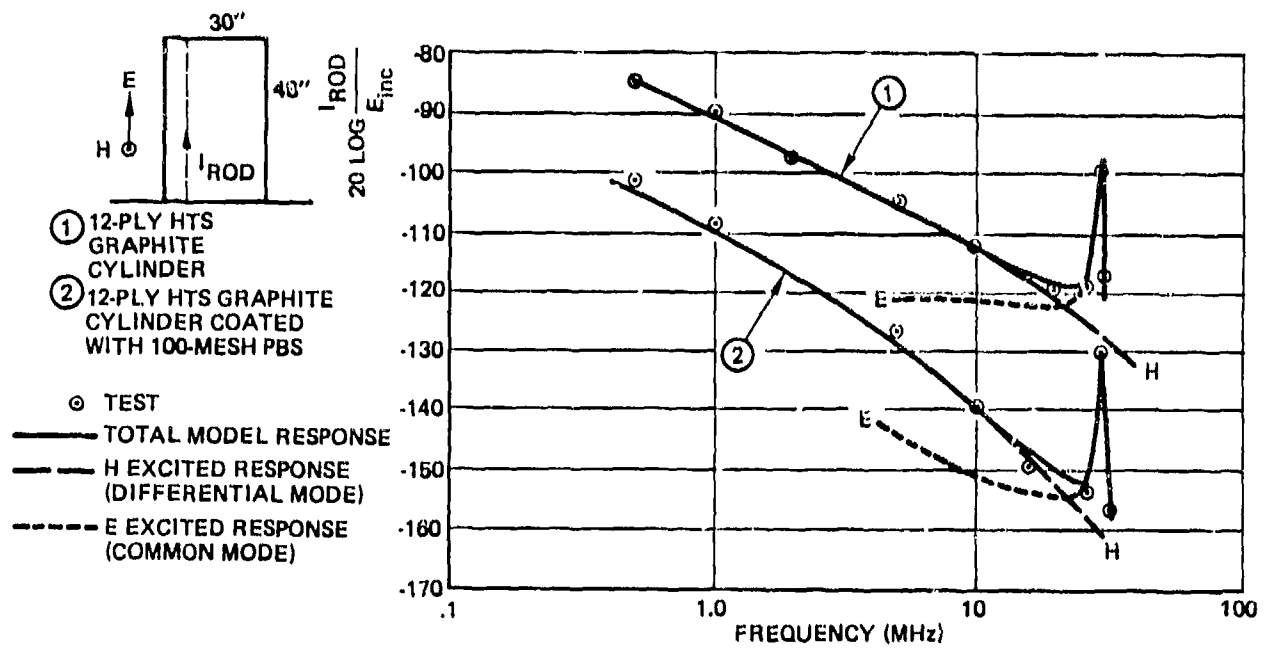


Fig.4 Validation interior current for a coated and uncoated graphite cylinder

- 1 — 40 MESH AL SCREEN
($P=1.05 \times 10^{-17}$ FARADS)
- 2 — 100 MESH AL SCREEN
- 3 — 120 MESH AL SCREEN (LOT A)
($P=1.26 \times 10^{-18}$ FARADS)
- 4 — 200 MESH AL SCREEN
($P=2.08 \times 10^{-18}$ FARADS)
- 1 18 MESH PB SCREEN
($P=7.10 \times 10^{-16}$ FARADS)
- 2 80 MESH PB SCREEN
($P=1.00 \times 10^{-16}$ FARADS)
- 3 120 MESH PB SCREEN
($P=7.56 \times 10^{-18}$ FARADS)
- 2 MIL AL ($P=0$)

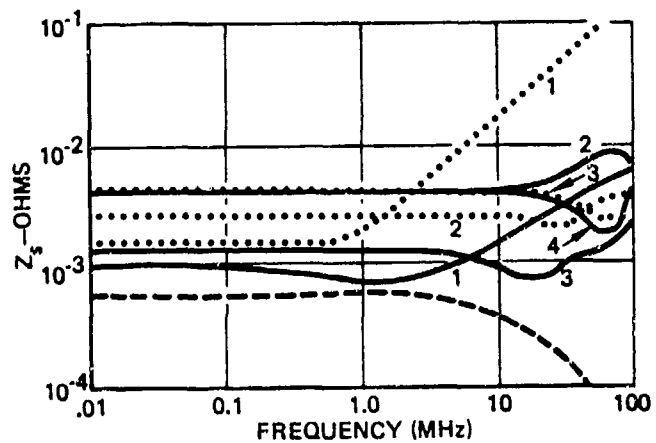


Fig.5 Measured surface transfer impedance for coating materials alone

- 1 - 8 PLY T300 ($P=0$)
- 2 - 12 PLY HTS ($P=0$)
- 3 - 24 PLY T300 ($P=0$)

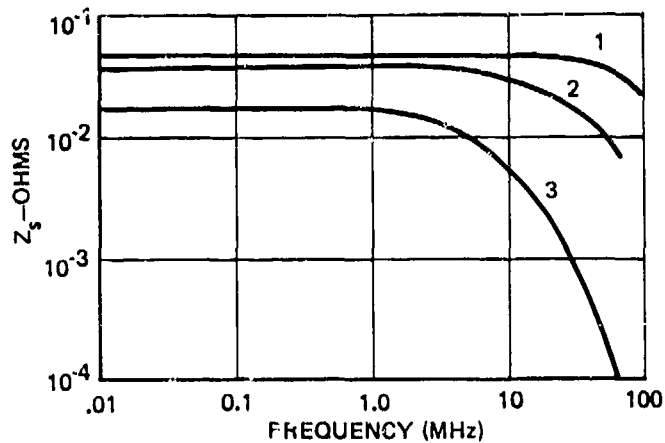


Fig.6 Measured surface transfer impedance for graphite laminates

- 1 - GRAPHITE + 120 MESH AL SCREEN (LOT A)
- 2 - GRAPHITE + 40 MESH AL SCREEN
- 3 - GRAPHITE + 2 MIL AL FOIL ($P=0$)

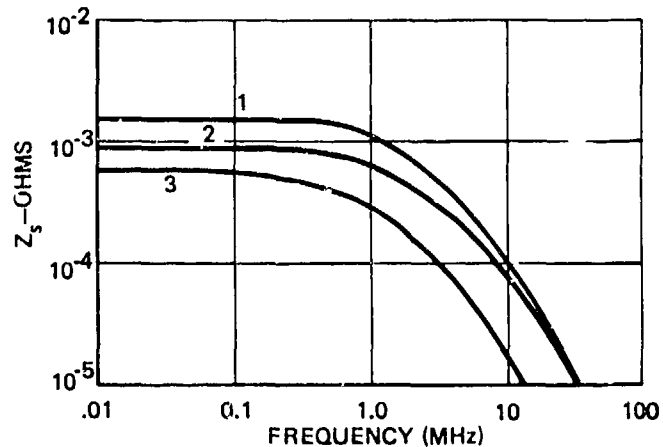


Fig.7 Measured surface transfer impedance for 24 ply T300 graphite with various coatings

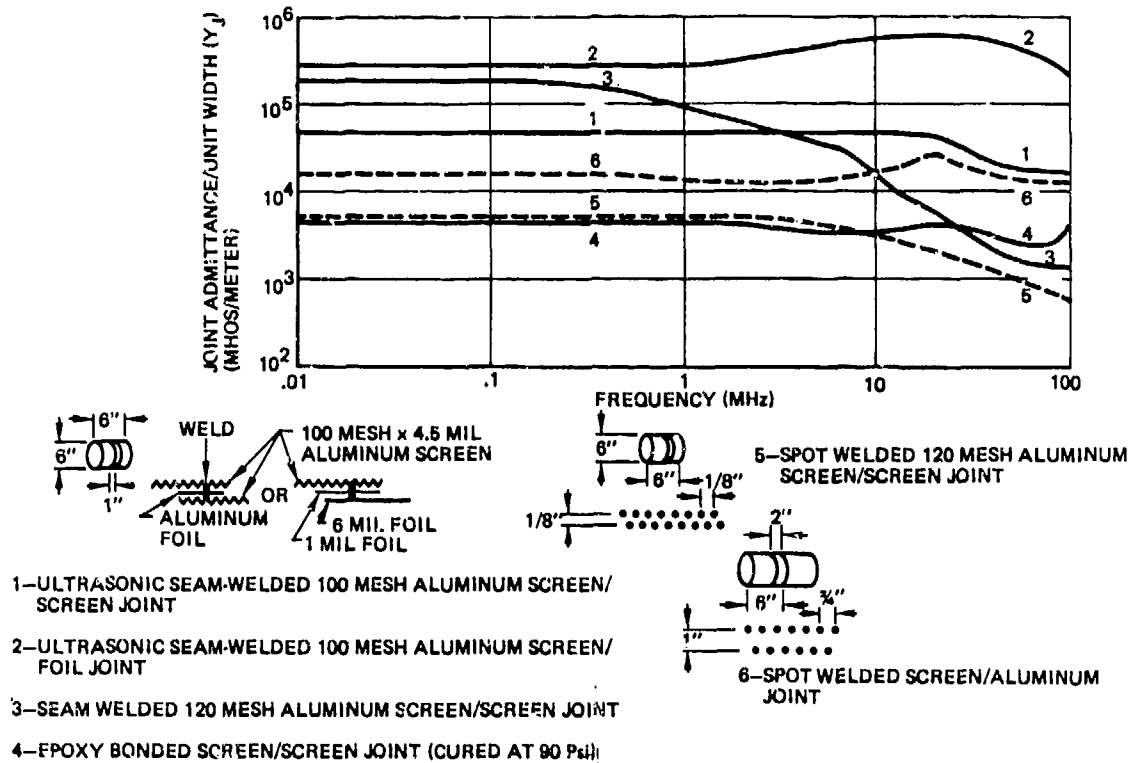


Fig.8 Measured joint admittances

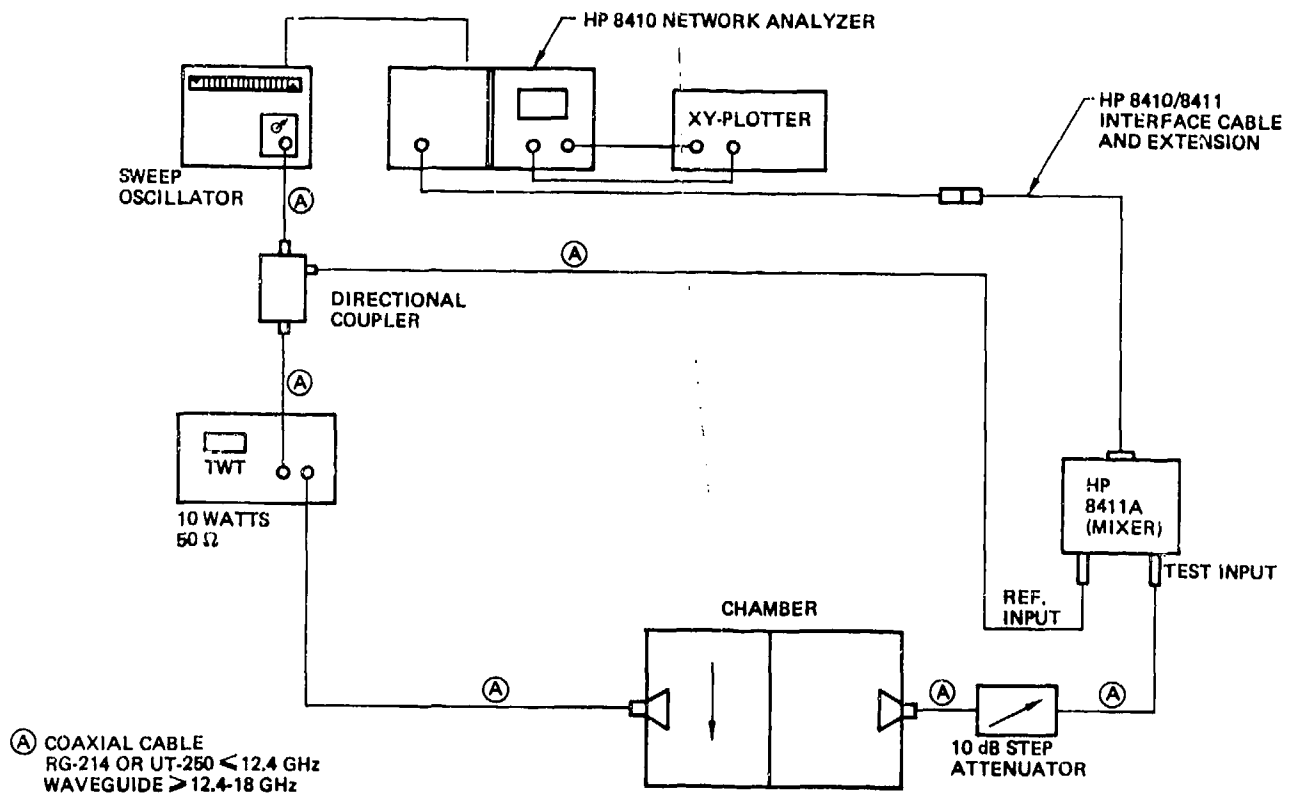


Fig.9 Instrumentation system block diagram

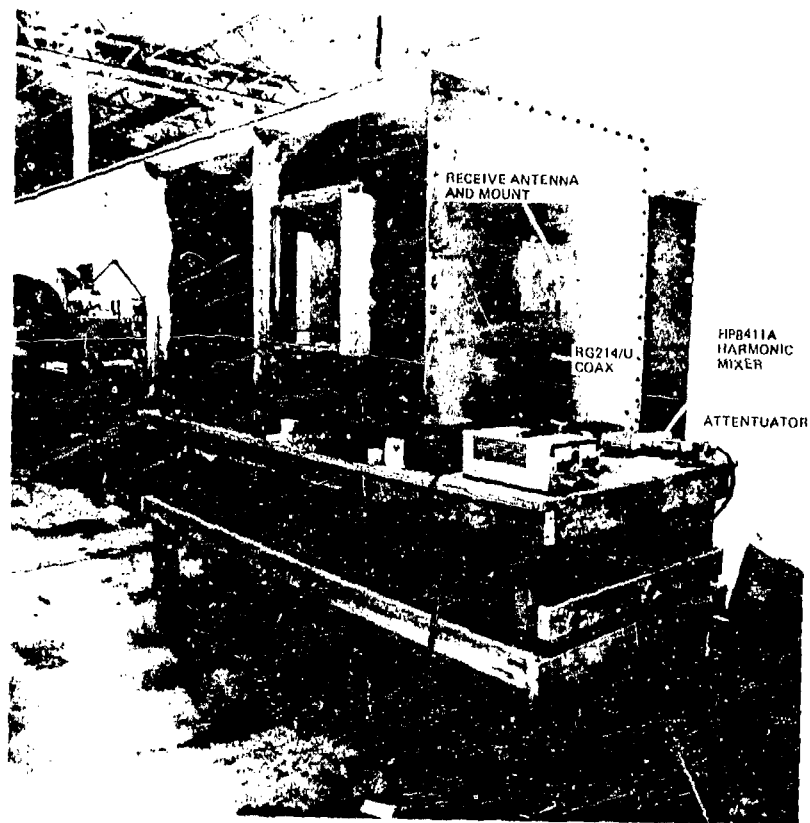


Fig.10 Peripheral test equipment receive side of chamber

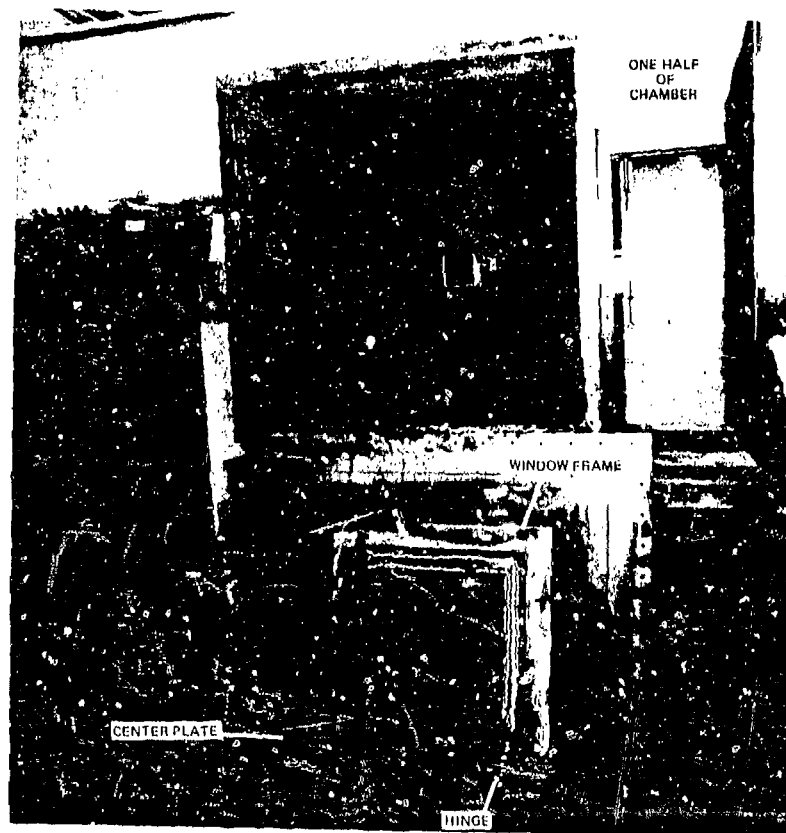


Fig.11 Center plate and sample holder

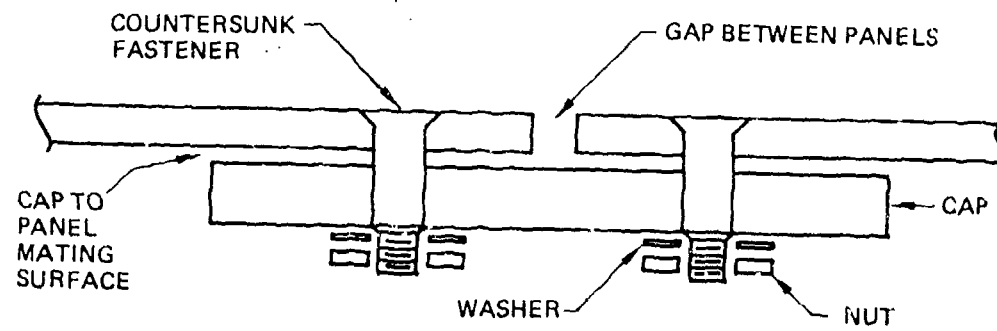


Fig.12 Cross-sectional view of a simple butt joint

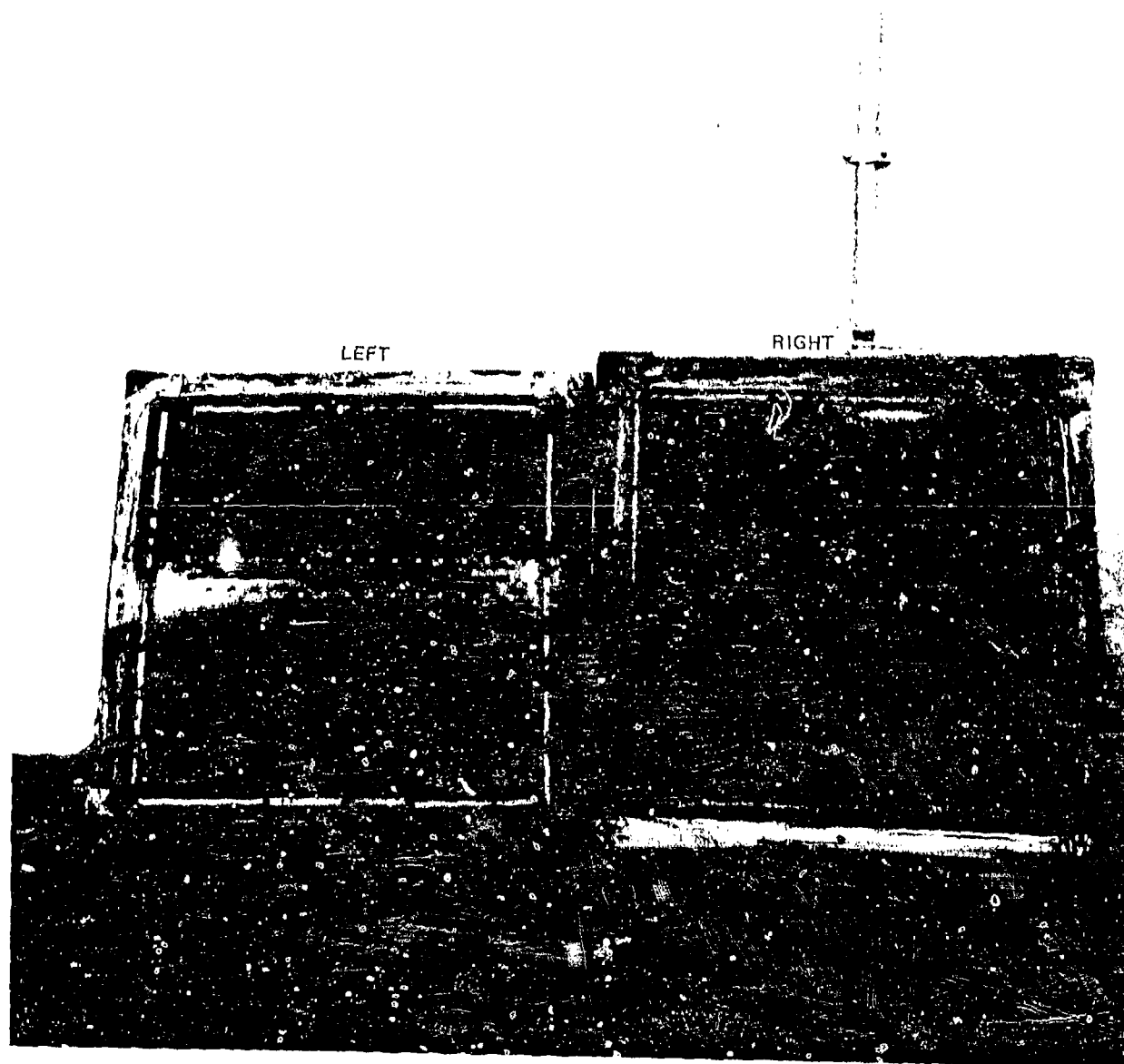


Fig.13 Left one side of a completed joint; right -- unjointed graphite-epoxy panel



Fig.14 Left - other side of jointed panel; right - joint before assembly

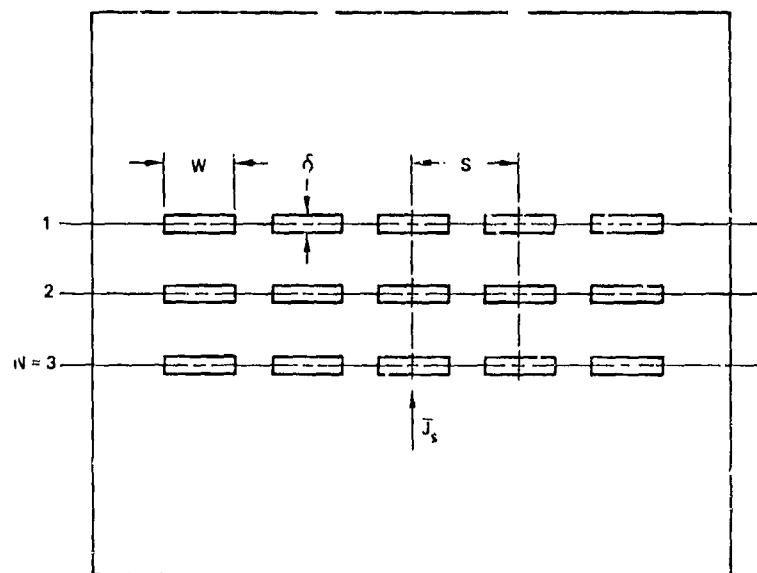


Fig.15 Reference slot array geometry

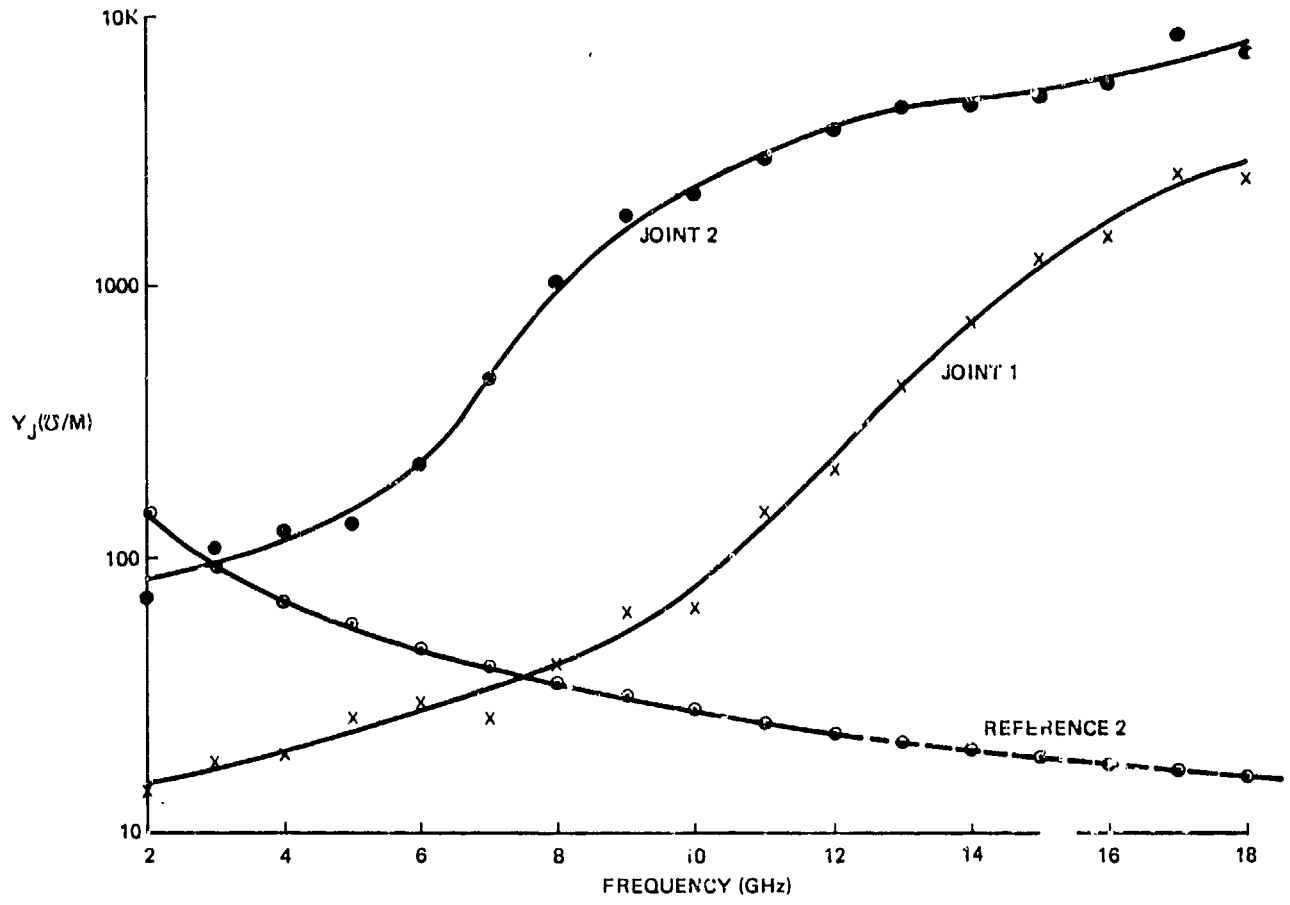


Fig.16 Joint admittance

THEORETICAL CALCULATION OF RF PROPERTIES
OF CARBON FIBRE LAMINATES.

D.C. Brewster

Marconi Research Laboratories,
GEC-Marconi Electronics,
Chelmsford, CM2 8HN,
U.K.

SUMMARY

The purpose of the work presented here was to find a mathematical theory to describe the electromagnetic behaviour of material consisting of a sequence of Carbon Fibre Composite laminae. The analysis applies to approximately-planar regions which are not near joints, bonds or other electrical discontinuities. The model adopted is an infinite sheet and each carbon fibre lamina is modelled as a homogeneous anisotropic conducting lamina. Some theoretical justification for this is given. An alternative theory based on replacing the entire sheet by a single homogeneous layer has also been considered and its range of validity investigated. The conductivities used were obtained experimentally from unidirectional samples by other researchers.

We calculate the shielding (0-1 GHz) of a plane wave normally incident on the infinite sheet and also the reflected field. We calculate the shielding improvement for a thin aluminium coating. We also investigate the variation of apparent resistivity with frequency.

We show that as regards shielding and reflection the infinite sheet can be characterized by surface and transfer impedances. These quantities can be used to calculate electromagnetic field shielding of finite objects. Some calculations (using the Fourier Transform) are given of shielding by a plane screen when illuminated by an Electromagnetic Pulse.

1.0 INTRODUCTION

In order to calculate certain electromagnetic properties of Carbon Fibre Composites, CFC, such as shielding, antenna behaviour, it is not immediately clear how to model the CFC. Each CFC lamina consists of a dielectric material within which the individual carbon fibres lie. It was decided to model a single lamina as a homogeneous conducting material which is anisotropic, i.e. has different conductivities in different directions. Some justification for this is presented later. The infinite carbon fibre sheet is now modelled as a sequence of laminae, each with the conductivity tensor orientated in a direction depending on the fibre direction. Using this model we have calculated the shielding (0-1GHz) of a plane wave normally incident on the infinite sheet. We have also calculated the shielding improvement if a thin aluminium coating is applied. We also estimate whether antenna performance is likely to be affected by the CFC. The variation of apparent resistivity with frequency is calculated and compared with experimental results obtained elsewhere.

We show that the infinite screen can be characterised by surface and transfer impedances. These quantities can be used to calculate electromagnetic field shielding of finite objects. The surface and transfer impedances are calculated by computer and no simple formula is available for them unless the frequency is low enough.

A much simpler model of a CFC sheet has also been considered. The entire sheet is replaced by a single homogeneous layer with a conductivity tensor that is obtained by an averaging process across all the individual laminae. Where possible the two theories have been compared.

2.0 DISCUSSION OF MAGNIFIED PHOTOGRAPHS OF CFRP LAMINATES

To obtain an adequate understanding of the electromagnetic behaviour of a CFRP panel it was felt necessary to obtain detailed knowledge of how the carbon fibres lie in a typical CFRP panel. This was done by photographing, under magnification, cross-sections cut through various CFRP lay-ups. Some of the photographs taken are given in diagram 1. In photograph A (magnification x 60) we can surmise the fibre directions from the appearance of the cross-section of an individual fibre. In lamina 1 the fibres are in the 0° direction. The angle here is measured between the fibre and the plane of the cut. The next lamina (lamina 2) is at 45° (approximately) since the fibre cross-sections are slightly elliptical. In lamina 3 the fibres are at 90° .

In photograph B (magnification x 600) the location of individual fibres is clearly discernible. The fibres have a diameter of the order of $8-10 \times 10^{-4}$ mm. In general the fibre locations are random in nature except that in some of the photographs, especially photograph C, there are regions where fibres are absent. These regions generally occur between laminae. This raises the problem of possible inter-lamina resistance. A discussion of this is given in Section 7.

3.0 MATHEMATICAL ANALYSIS OF A SINGLE LAMINA

We assume that the frequency is such that the diameter of each carbon fibre as well as the spacing between carbon fibres is small compared to the wavelength. This is clearly the case in the range 0-1GHz. Because of the complexity of the actual distribution of fibres within a lamina we aim to model a single lamina by a homogeneous material which is anisotropic i.e. has different conductivities in different directions. Such a material is called biaxial.

3.1 Conductivity Parallel to Fibres

We follow the theory presented in (Casey, K.F. 1976). We have studied this theory carefully to ascertain whether it is necessary to correct the familiar d.c. model of conductivity parallel to the fibres, when dealing with the a.c. case. The d.c. model asserts that σ_x , the conductivity parallel to the fibres, = $q\sigma_f$, where q is the volume fraction occupied by the fibres and σ_f is the conductivity of the carbon which the fibres consist of.

We make the following assumptions:-

- The distance between fibres is small compared to the wavelength.
- The fibre radius, b , say is small compared to the skin depth of the carbon which the fibres consist of.

In practice (b) is satisfied. The skin depth, δ_f , of the carbon is

$$\delta_f = \sqrt{\frac{2}{\omega \mu_0 \sigma_f}}$$

We estimate $\sigma_f = 7.7 \times 10^4$ mho/m. (This value is taken from (ERA, 1979) where they state that certain fibres have resistivity 1.3×10^{-5} Ω m.) At 1 GHz $\sigma_f \approx .057$ mm. Since b , is of the order of .01 mm condition (b) is satisfied.

The effect of (b) is that the component of electric field parallel to the fibre axis completely penetrates the fibre. We further assume that the current in a fibre is uniform across its cross-section. Choose coords. (x, y, z) such that x is in the fibre direction. z is perpendicular to the plane of the lamina. We model the lamina as a sequence of uniformly spaced fibres as shown in figure 2. The distance between the fibres in the y -direction is a and in the z direction is d .

Consider a plane CW-wave incident on the lamina. Assume that the x -variation of the field is e^{-jux} and y -variation e^{-jvy} . The range u, v is $-\infty$ to $+\infty$. The infinite range arises because the field generated by a localized source e.g. an antenna external to the lamina consists of such plane waves where u, v can vary from $-\infty$ to $+\infty$. The time variation is $e^{j\omega t}$.

We consider a particular row of fibres assumed to be in the plane $z=0$. Let the origin $(0,0,0)$ be on the axis of some fibre. We analyse the electrical properties of this row of fibres by considering the situation depicted in figure 3. It consists of the row of fibres embedded in the epoxy resin which extends indefinitely in all directions. This amounts to assuming that successive rows of fibres interact only via the plane wave reflected and transmitted by a row. This is justified in (Casey, K.F. 1976) who shows that the reactive field interaction between adjacent rows is negligible. The electric field incident on the row of fibres is

$$\underline{E}^{inc} = (E_x^{inc}, E_y^{inc}, E_z^{inc}) e^{-jux} e^{-jvy} e^{-jwz}$$

w is determined by $w = \sqrt{k_m^2 - u^2 - v^2}$.

$k_m^2 = \omega^2 \epsilon_m \mu_0$, where ϵ_m is the permittivity of the resin. The square root for w is chosen to represent a wave travelling in the $+z$ direction, i.e. if $u^2 + v^2 < k_m^2$ the w is real and positive; if $u^2 + v^2 > k_m^2$, w is negative pure imaginary.

Let $I_0 e^{-jux}$ be the bulk current flowing in the fibre whose axis passes through $(0,0,0)$. Then the current flowing in the fibre whose axis passes through $(0, na, 0)$ is $I_0 e^{-jux} e^{-jvna}$. Here $-\infty < n < \infty$. The bulk current is assumed uniformly distributed through the fibre: All field quantities calculated below are assumed calculated within the fibre passing through $(0,0,0)$. The x -component of the vector potential due to $I_0 e^{-jux}$ is

$$-\frac{\mu_0 j}{4} I_0 e^{-jux} H_0^{(2)}(\tilde{k}b), \text{ where } \tilde{k} = \sqrt{k_m^2 - u^2}$$

$H_0^{(2)}$ is the Hankel function of the second kind.

The x component of the vector potential due to the current in the n th fibre is

$$\begin{aligned} & -\frac{\mu_0 j}{4} I_0 e^{-jux} e^{-jvna} H_0^{(2)}(\tilde{k} \sqrt{z^2 + (y-na)^2}) \quad (n \neq 0) \\ & = -\frac{\mu_0 j}{4} I_0 e^{-jux} e^{-jvna} \sum_{m=-\infty}^{\infty} J_m(\tilde{k}x) H_m^{(2)}(\tilde{k}|n|a) e^{-im\phi} \end{aligned}$$

This formula is taken from (Abramowitz and Stegun, 1965) equation 9.1.75. The average of this value within the fibre is (approximately)

$$-\frac{\mu_0 j}{4} I_0 e^{-jux} e^{-jvna} H_0^{(2)}(\tilde{k}|n|a)$$

This requires the assumption that $|\tilde{k}b| \ll 1$.

The x-component of the vector potential due to all the fibre currents in the row is

$$A_x = -\frac{\mu_0 j}{4} I_0 e^{-jux} \left[H_0^{(2)}(\tilde{k}b) + \sum_{n \neq 0} e^{-jvna} H_0^{(2)}(\tilde{k}|n|a) \right].$$

The following expression can be derived (assuming $va \ll 1$),

$$\sum_{n \neq 0} e^{-jvna} H_0^{(2)}(\tilde{k}|n|a) = \frac{2}{av} + \frac{2j}{\pi} \log(\tilde{k}a/2\pi);$$

we derive

$$\begin{aligned} A_x &= -\frac{\mu_0 j}{4} I_0 e^{-jux} \left[\frac{-2j}{\pi} \log(\tilde{k}b) + \frac{2}{av} + \frac{2j}{\pi} \log(\tilde{k}a/2\pi) \right] \\ &= -\frac{\mu_0 j}{4} I_0 e^{-jux} \left[\frac{2}{av} + \frac{2j}{\pi} \log(a/2\pi b) \right]. \end{aligned}$$

The electric field E_x due to the fibre currents is

$$\begin{aligned} E_x &= -\frac{j\omega}{k_m^2} (k_m^2 - u^2) A_x \\ &= -\frac{\omega\mu_0}{2} I_0 \frac{\sqrt{2}}{k_m^2} \left[\frac{1}{av} + \frac{j}{\pi} \log(a/2\pi b) \right] \quad \dots 1 \end{aligned}$$

The total x-component of electric field is

$$E_x^{\text{tot}} = E_x^{\text{inc}} + E_x = I_0 / (\pi b^2 \sigma_f). \quad (\text{By definition of } \sigma_f)$$

$$\text{Thus } I_0 \left[\frac{1}{\pi b^2 \sigma_f} + \frac{\omega\mu_0}{2} \frac{\sqrt{2}}{k_m^2} \left[\frac{1}{av} + \frac{j}{\pi} \log(a/2\pi b) \right] \right] = E_x^{\text{inc}}$$

From (Casey K.F., 1976) we have that the electric field due to all the fibre currents, averaged along the y-axis is

$$E_x^{\text{av}} = \frac{\omega\mu_0}{2} \frac{\sqrt{2}}{k_m^2} \frac{1}{av} I_0 e^{-jux}$$

We now define the average conductivity σ_x for the region $|z| \leq d/2$ by

$$\frac{I_0}{ad\sigma_x} = E_x^{\text{av}} + E_x^{\text{inc}} \quad \dots 2$$

Then from 1 and 2

$$\begin{aligned} \sigma_x &= \frac{1}{ad} \left[\frac{1}{\pi b^2 \sigma_f} + \frac{\omega\mu_0}{2} \frac{\sqrt{2}}{k_m^2} \frac{j}{\pi} \log(a/2\pi b) \right]^{-1} \\ &= q\sigma_f \left[1 + \frac{\omega\mu_0}{2} b^2 \sigma_f \frac{\sqrt{2}}{k_m^2} j \cdot \log(a/2\pi b) \right]^{-1} \quad \dots 3 \end{aligned}$$

Thus if

$$\frac{\omega\mu_0}{2} b^2 \sigma_f \left| \frac{\sqrt{2}}{k_m^2} \log(a/2\pi b) \right| \ll 1 \quad \dots 4$$

we deduce $\sigma_x = q\sigma_f$

With $\sigma_f = 7.7 \times 10^4$, $b = 1 \times 10^{-5}$, $a = 2.3 \times 10^{-5}$, $\epsilon_m = 3.5 \epsilon_0$

condition 4 becomes

$$\left| 1 - \frac{u^2}{3.5k^2} \right| \ll \frac{4 \cdot 10^4}{F} \quad \dots 5$$

where F is the frequency in MHz. $k^2 = \omega^2 \epsilon_0 \mu_0$

The criterion 5 amounts to a restriction on the value of u . When considering surface currents on aircraft this means that they mustn't vary too rapidly compared with the wavelength. At 1GHz the condition 5 is roughly

$$|u/k| \ll 12.$$

This appears to be satisfied for most cases.

We deduce that the single row of fibres depicted in figure 3 behaves as a homogeneous layer of thickness d with conductivity $\sigma_x = q\sigma_f$ in the x-direction. Thus the sequence of rows of fibres in figure 2 behaves like a homogeneous lamina with x-conductivity $q\sigma_f$.

When we turn to the chaotic arrangement of fibres shown in photo B figure 1 it seems reasonable to deduce, in the light of the above analysis of a simplified model of a CFRP lamina (i.e. a regular array of fibres), that correction terms to the volume fraction theory for x-conductivity will be negligible in the frequency range of 0-1GHz.

The value of σ_x used in our subsequent analysis is obtained from experimental work (ERA, 1979) on uni-directional material. $\sigma_x = 4.76 \times 10^4$ mho/m.

3.2. Conductivity Perpendicular to the Fibres

We investigate the average conductivity of a simple lamina in the two directions y and z . z is perpendicular to the plane of the lamina, see figure 2.

A theory for the d.c. case can be based on some formulae given in (Bueche F., 1972).

The presence of conductivity in the y and z directions arises because of the formation of infinite chains of contact between fibres. Infinite chains of contact between fibres do not give rise to net conductivity in the y and z direction and so to estimate σ_y and σ_z it is necessary to know the proportion of fibres involved in infinite chains of contact. Formulae for this quantity are given in (Bueche F. 1972). We specialize these formulae to the 2-dimensional case where the "particles" are circular.

Let q be the volume fraction occupied by the fibres.

Let q_{max} be the maximum possible volume fraction occupied by the fibres.

q_{max} is determined by the densest possible packing of the fibres, and $= \pi/(2\sqrt{3})$

Put $\alpha = q/q_{max}$. If y is the smallest root of the equation:-

$$\alpha(1-\alpha)^4 = y(1-y)^4$$

then the fraction of fibres, w_f , involved in infinite chains of contact is given by

$$w_f = 1 - (1-\alpha)^2 y / (1-y)^2 \alpha.$$

q is typically .6 and we deduce

$$w_f = .9985$$

i.e. virtually 100% of fibres are involved in infinite chains of contact.

Infinite chains of contact between the fibres which are responsible for the conductivity in the z -direction involve the contact resistance R_z . R_z is defined as the resistance, for a unit length in the x -direction, between two fibres. We also define R_y , analogously, when dealing with infinite chains involved in the y -conductivity. R_y and R_z may be different because even though photograph B of diagram 1 appears to indicate little difference between y and z direction, the process of CFRP panel construction, involving pressure in the z -direction may produce $R_z < R_y$. An estimate of the resistivity in the y and z -directions is now possible, in terms of R_z and R_y .

$$\rho_z = \pi R_z / 4q \text{ and } \rho_y = \pi R_y / 4q.$$

This result is based on a simplified model shown in figure 4. The fibre diameter is $= 2b$. Then $q = \pi b^2 / 2a$.

From figure 4 we can deduce immediately that $\rho_z = R_z a / 2b$.

The epoxy matrix is assumed insulating.

Unfortunately the above theory really only provides a qualitative description of the nature of the y and z -conductivity. Estimation of R_y and R_z seems impossible. We must rely on measurements.

According to (Baskerville M.W., 1978)

$$\sigma_z (=1/\rho_z) = 40 \text{ mho/m}$$

$$\sigma_y (=1/\rho_y) = 100 \text{ mho/m}$$

These are based on measurements of a unidirectional sample. According to (ERA, 1979).

$$\sigma_y = 105.3 \text{ mho/m}$$

σ_z was not measured.

Because of the uncertainty of σ_z we have used both $\sigma_z = 40$ and 105.3. It turns out that for shielding calculations the precise value is not too important provided it is not too low. The value of σ_y used was 105.3 mho/m.

The above analysis is purely d.c. We have not attempted to construct an a.c. model. Except for purely unidirectional material, the conductivity σ_x (being considerably larger than σ_y and σ_z) dominates the shielding properties of a CFRP sheet. In view of this and the likely complexity of the problem, we have not felt it is worthwhile attempting a detailed a.c. analysis of y and z -conductivity. We have made the assumption that we can use σ_y and σ_z in our time harmonic analysis.

4.0 THEORETICAL ANALYSIS OF A SEQUENCE OF ANISOTROPIC CONDUCTING OR DIELECTRIC LAMINAE.

Figure 5 shows an infinite sheet consisting of a sequence of laminae. We suppose that the z axis is normal to the plane of the sheet, and we have chosen Cartesian coordinates (x', y', z) with origin on one of the faces as shown.

Assume an incoming plane wave $\underline{E}^{\text{inc}}, \underline{H}^{\text{inc}}$, with propagation vector $\underline{k}^{\text{inc}} = (u', v', w) = k(\sin\theta\cos\phi, \sin\theta\sin\phi, \cos\theta)$, is incident on the sheet. The time variation, suppressed, is $e^{j\omega t}$. Then

$$\underline{E}_{x'}^{\text{inc}} = E_x^0 e^{-j(u'x' + v'y' + wz)}$$

and similarly for the other components.

w is determined by

$$w = \sqrt{k^2 - u'^2 - v'^2}$$

$$k^2 = \omega^2 \epsilon_0 \mu_0, \omega \text{ is the angular frequency.}$$

The quantities u', v' are always real. w is real and positive if $u'^2 + v'^2 < k^2$ or negative pure imaginary if $u'^2 + v'^2 > k^2$.

Suppose the r^{th} lamina lies between $z = z_{r-1}$ and $z = z_r$. The r^{th} lamina of thickness d_r , has a combined conductivity and permittivity tensor (σ^r), which is diagonal with respect to a set of axes (x, y, z) which vary with each lamina. The angle between the axes (x, y, z) and the fixed axes (x', y', z) is θ_r .

$$\sigma^r = \begin{pmatrix} \sigma_x^r + j\omega\epsilon_x^r & 0 & 0 \\ 0 & \sigma_y^r + j\omega\epsilon_y^r & 0 \\ 0 & 0 & \sigma_z^r + j\omega\epsilon_z^r \end{pmatrix}$$

The equations obeyed by \underline{E} and \underline{H} in the r^{th} lamina are

$$\underline{\nabla} \times \underline{E} = -j\omega \underline{H}$$

and
$$\underline{\nabla} \times \underline{H} = j\omega \underline{D}$$

where
$$\underline{D} = \frac{1}{j\omega} \sigma^r \underline{E}$$

Now
$$\begin{pmatrix} x \\ y \end{pmatrix} = \begin{pmatrix} \cos \theta_r & \sin \theta_r \\ -\sin \theta_r & \cos \theta_r \end{pmatrix} \begin{pmatrix} x' \\ y' \end{pmatrix}$$

Define
$$\begin{pmatrix} u \\ v \end{pmatrix} = \begin{pmatrix} \cos \theta_r & \sin \theta_r \\ -\sin \theta_r & \cos \theta_r \end{pmatrix} \begin{pmatrix} u' \\ v' \end{pmatrix}$$

It can be verified that

$$ux + vy = u'x' + v'y'$$

In the r^{th} lamina we assume that the field variation is of the form $e^{-j(ux+vy+w_1z)}$. The variation $ux + vy$ arises because of the boundary condition that at each interface between laminae the tangential component of \underline{E} and \underline{H} is continuous. The boundary condition ensures that the variation in the plane of the lamina is the same as the incident field.

$$\text{Let } \beta^2 = u^2 + v^2 + w_1^2 \text{ and } n_x = u/\beta, n_y = v/\beta, n_z = w_1/\beta.$$

Define $k_x^2 = -j\omega\mu_0(\sigma_x^r + j\omega\epsilon_x^r)$, $k_y^2 = -j\omega\mu_0(\sigma_y^r + j\omega\epsilon_y^r)$ and $k_z^2 = -j\omega\mu_0(\sigma_z^r + j\omega\epsilon_z^r)$.

From the analysis given by (Collin 1960) on TEM waves in anisotropic dielectric media, p. 98 equation (106), we have

$$\frac{n_x^2 k_x^2}{\beta^2 - k_x^2} + \frac{n_y^2 k_y^2}{\beta^2 - k_y^2} + \frac{n_z^2 k_z^2}{\beta^2 - k_z^2} = 0$$

Now $n_z^2 = 1 - n_x^2 - n_y^2$ and so

$$\frac{u^2}{\beta^2} \cdot \frac{k_x^2}{\beta^2 - k_x^2} + \frac{v^2}{\beta^2} \cdot \frac{k_y^2}{\beta^2 - k_y^2} + \left(1 - \frac{u^2}{\beta^2} - \frac{v^2}{\beta^2}\right) \cdot \frac{k_z^2}{\beta^2 - k_z^2} = 0$$

$$\text{Thus } u^2 k_x^2 (\beta^2 - k_y^2) (\beta^2 - k_z^2) + v^2 k_y^2 (\beta^2 - k_x^2) (\beta^2 - k_z^2) \\ + (\beta^2 - u^2 - v^2) k_z^2 (\beta^2 - k_x^2) (\beta^2 - k_y^2) = 0$$

The constant term of this cubic in β^2 is zero, and so β^2 has two possible values which can be shown to be

$$\beta_1^2 = \frac{1}{2k_z^2} \left[-u^2(k_x^2 - k_z^2) - v^2(k_y^2 - k_z^2) + k_z^2(k_x^2 + k_y^2) - \sqrt{Q} \right] \quad \dots (1)$$

$$\beta_2^2 = \frac{1}{2k_z^2} \left[-u^2(k_x^2 - k_z^2) - v^2(k_y^2 - k_z^2) + k_z^2(k_x^2 + k_y^2) + \sqrt{Q} \right]$$

where $Q = (k_z^2(k_x^2 - k_y^2) - u^2(k_x^2 - k_z^2) - v^2(k_y^2 - k_z^2))^2 + 4k_z^2 v^2(k_y^2 - k_z^2)(k_x^2 - k_z^2)$.

$$\text{Define } w_1 = \sqrt{\beta_1^2 - u^2 - v^2} \quad \text{and} \quad w_2 = \sqrt{\beta_2^2 - u^2 - v^2}$$

Thus 4 waves are possible in the r^{th} lamina.

Wave 1 has field variation $e^{-j(ux+vy+w_1z)}$, Wave 2 has field variation $e^{-j(ux+vy+w_2z)}$

Wave 3 has field variation $e^{-j(ux+vy-w_1z)}$, Wave 4 has field variation $e^{-j(ux+vy-w_2z)}$

We now calculate \underline{E} and \underline{H} associated with the four waves.

$$\text{Wave 1. } E_x = E_x^1 e^{-j(ux+vy+w_1z)}, E_y = E_y^1 e^{-j(ux+vy+w_1z)}, H_x = H_x^1 e^{-j(ux+vy+w_1z)}, H_y = H_y^1 e^{-j(ux+vy+w_1z)}$$

From (Collin, 1960), p.99, equation (11), we have

$$D_x : D_y = \frac{n_x^2 k_x^2}{\beta^2 - k_x^2} : \frac{n_y^2 k_y^2}{\beta^2 - k_y^2}$$

$$\text{Now } D_x = \frac{1}{j\omega} (\sigma_x^r + j\omega\epsilon_x^r) E_x \quad \text{and} \quad D_y = \frac{1}{j\omega} (\sigma_y^r + j\omega\epsilon_y^r) E_y$$

$$\text{Thus } E_x^1 = \frac{u}{v} \frac{\beta_1^2 - k_y^2}{\beta_1^2 - k_x^2} \cdot E_y^1 = \alpha_1 E_y^1$$

From $\nabla \times \underline{E} = -j\omega\mu_0 \underline{H} = -j\beta \times \underline{E}$ where $\beta = (u, v, w_1)$ we deduce $\omega\mu_0 H_x^1 = vE_z^1 - w_1 E_y^1$.

$$\text{Thus } H_x^1 = n_1 E_y^1 \quad \text{where} \quad n_1 = w_1 \frac{(k_z^2 - k_y^2)}{\beta_1^2 - k_x^2} \cdot \frac{1}{\omega\mu_0}$$

$$\text{Similarly } H_y^1 = \gamma_1 E_x^1$$

$$\text{where } \gamma_1 = \frac{uw_1}{v} \cdot \frac{(\beta_1^2 - k_y^2)(k_x^2 - k_z^2)}{(\beta_1^2 - k_x^2)(\beta_1^2 - k_z^2)} \cdot \frac{1}{\omega\mu_0}$$

Wave 3.

We replace w_1 by $-w_1$.

$$E_x = E_x^3 e^{-j(ux+vy-w_1z)} \text{ etc.}$$

We can deduce

$$E_x^3 = \alpha_1 E_y^3 \quad H_x^3 = -\eta_1 E_y^3 \quad \text{and} \quad H_y^3 = -\gamma_1 E_y^3$$

The reason for expressing waves 1 and 3 in terms of E_y is that this field component is always non-zero if $\sigma_x \neq \sigma_y$. If $\sigma_x = \sigma_y$ then a rotation of the (x,y) axes is carried out which guarantees $E_y \neq 0$. The analysis for waves 2 and 4 is obtained by replacing β_1^2 by β_2^2 . All field quantities are expressed in terms of E_x . This quantity can always be arranged to be non-zero.

$$\begin{aligned} E_y^2 &= \alpha_2 E_x^2 & \alpha_2 &= \frac{v}{u} \frac{\beta_2^2 - k_x^2}{\beta_2^2 - k_y^2} \\ H_y^2 &= \eta_2 E_x^2 \\ H_x^2 &= \gamma_2 E_x^2 & \eta_2 &= \frac{2^{-k_y} w_2 (k_x^2 - k_z^2)}{\omega \mu_0 (\beta_2^2 - k_z^2)} \end{aligned}$$

and

$$\begin{aligned} E_y^4 &= \alpha_2 E_x^4 \\ H_y^4 &= -\eta_2 E_x^4 \\ H_x^4 &= -\gamma_2 E_x^4 \end{aligned} \quad \gamma_2 = \frac{1}{\omega \mu_0} \frac{v w_2 (\beta_2^2 - k_x^2) (k_z^2 - k_y^2)}{u (\beta_2^2 - k_y^2) (\beta_2^2 - k_z^2)}$$

The total field, $\underline{E} = (E_x, E_y, E_z)$ and $\underline{H} = (H_x, H_y, H_z)$ in the r^{th} lamina is the sum of the four waves above. We need only consider $x' = y' = 0$ since the variation $e^{-j(u'x' + v'y')}$ is common to all laminae.

Let D be the matrix

$$D = \begin{pmatrix} \alpha_1 & \alpha_1 & 1 & 1 \\ 1 & 1 & \alpha_2 & \alpha_2 \\ \eta_1 & -\eta_1 & \gamma_1 & -\gamma_2 \\ \gamma_1 & -\gamma_1 & \eta_2 & -\eta_2 \end{pmatrix}$$

Then

$$\begin{pmatrix} E_x \\ E_y \\ H_x \\ H_y \end{pmatrix} = D \begin{pmatrix} e^{-jw_1 z} & 0 & 0 & 0 \\ 0 & e^{jw_1 z} & 0 & 0 \\ 0 & 0 & e^{-jw_2 z} & 0 \\ 0 & 0 & 0 & e^{jw_2 z} \end{pmatrix} \begin{pmatrix} E_x^1 \\ E_y^3 \\ E_y^2 \\ E_x^4 \end{pmatrix}$$

Thus the field components at $(0, 0, z_r)$ are related to those at $(0, 0, z_{r-1})$ by

$$\begin{pmatrix} E_x(0,0,z_r) \\ E_y(0,0,z_r) \\ H_x(0,0,z_r) \\ H_y(0,0,z_r) \end{pmatrix} = D \begin{pmatrix} e^{-jw_1 d_r} & 0 & 0 & 0 \\ 0 & e^{jw_1 d_r} & 0 & 0 \\ 0 & 0 & e^{-jw_2 d_r} & 0 \\ 0 & 0 & 0 & e^{jw_2 d_r} \end{pmatrix} D^{-1} \begin{pmatrix} E_x(z_{r-1}) \\ E_y(z_{r-1}) \\ H_x(z_{r-1}) \\ H_y(z_{r-1}) \end{pmatrix} = U_r \begin{pmatrix} E_x(z_{r-1}) \\ E_y(z_{r-1}) \\ H_x(z_{r-1}) \\ H_y(z_{r-1}) \end{pmatrix}$$

Define $T_r = \begin{pmatrix} \cos \theta_r & \sin \theta_r & 0 & 0 \\ -\sin \theta_r & \cos \theta_r & 0 & 0 \\ 0 & 0 & \cos \theta_r & \sin \theta_r \\ 0 & 0 & -\sin \theta_r & \cos \theta_r \end{pmatrix}$

Then we can transform from the co-ords (x,y) to the fixed co-ords (x', y') . Using the fact that tangential components of \underline{E} and \underline{H} are continuous across the inter-lamina boundaries we deduce

$$\begin{pmatrix} E_x, (0,0,z_n) \\ E_y, (0,0,z_n) \\ H_x, (0,0,z_n) \\ H_y, (0,0,z_n) \end{pmatrix} = \prod_{r=1}^n (T_{n-r+1}^{-1} \cdot U_{n-r+r} \cdot T_{n-r+1}) \begin{pmatrix} E_x, (0,0,z_0) \\ E_y, (0,0,z_0) \\ H_x, (0,0,z_0) \\ H_y, (0,0,z_0) \end{pmatrix}$$

Inverting this we derive

$$\begin{pmatrix} E_x, (x',y',z_0) \\ E_y, (x',y',z_0) \\ H_x, (x',y',z_0) \\ H_y, (x',y',z_0) \end{pmatrix} = \Lambda \begin{pmatrix} E_x, (x',y',z_n) \\ E_y, (x',y',z_n) \\ H_x, (x',y',z_n) \\ H_y, (x',y',z_n) \end{pmatrix}$$

The matrix Λ is evaluated by computer and it connects the field components from the illuminated and shielded sides. Using Λ , reflected and transmitted fields can be calculated when the incident field is known.

5.0 PLANE WAVE SHIELDING RESULTS

Figure 6 gives plane screen shielding for a normally incident electric field. The dashed curves are obtained by replacing the entire sheet by a single homogeneous but anisotropic layer. The conductivities of the layer are obtained by averaging across the laminae. Table 4 gives the lay-ups.

Table 1. Plane Wave Shielding (dbs), $E^{inc} // x'$

Sample	Thickness (mm)	Frequency					
		D.C.	3MHz	10MHz	30MHz	100MHz	300MHz
THIN1	.5	67.0	67.0	67.0	67.1	68.1	72.5
THIN2	.5	70.5	70.5	70.5	70.6	71.2	73.0
RAE	1.75	77.9	78.1	79.3	85.1	101.3	131.5
BAE1	1.85	78.4	78.6	80.1	86.7	104.2	134.6
BAE2	1.98	82.5	83.0	86.1	93.3	104.9	127.9
BAE2A	1.98	82.5	82.8	85.4	94.1	106.0	119.7
BAE4	1.19	74.6	74.6	74.9	77.1	86.3	104.7
BAE6	2.11	85.5	86.6	92.4	100.0	136.8	190.2
BAEP5	5.26	87.5	93.9	109.0	136.7	189.9	253.2
SMM	7.92	85.0	92.5	108.8	139.5	205.5	316.9
SMMA	27.92	85.0	108.9	129.2	164.4	235.1	350.2
SMMB	207.92	85.0	128.0	148.6	184.0	254.6	367.7
TEST	3.00	81.1	81.7	84.4	90.3	104.4	130.4
BAE2AL	1.985	89.8	92.4	100.7	113.9	132.7	160.1

Table 2. Plane Wave Shielding (dbs), $E^{inc} \perp x'$

Sample	Thickness (mm)	D.C.	3MHz	10MHz	30MHz	100MHz	300MHz
THIN1	.5	67.0	67.0	67.0	67.1	68.1	72.5
THIN2	.5	61.1	61.1	61.1	61.0	61.8	61.3
RAE	1.75	77.9	78.1	79.3	85.1	101.3	131.5
BAE1	1.85	78.4	78.6	80.1	86.7	104.2	134.6
BAE2	1.98	73.0	73.0	73.7	77.2	89.2	111.9
BAE2A	1.98	73.0	73.2	74.5	79.8	90.7	108.1
BAE4	1.19	74.6	74.6	74.9	77.1	86.3	104.7
BAE6	2.11	32.6	32.6	32.6	32.6	32.6	33.7
BAEP5	5.26	87.5	93.9	109.2	138.4	198.7	269.4
SMM	7.92	94.5	114.7	132.7	159.5	221.9	332.7
SMMA	27.92	94.5	133.7	153.1	184.2	251.6	366.0
SMMB	20.92	94.5	153.0	172.5	203.8	271.1	383.4
TEST	3.0	81.1	80.5	74.9	68.4	66.4	65.4
BAE2AL	1.985	86.8	87.4	90.9	99.4	116.4	144.4

5.1. Samples with Isotropic Averaged Conductivity.

For certain lay-ups the averaged conductivity tensor has equal conductivity in all directions parallel to the plane of the sheet. It was found that the agreement between the averaged theory and the more exact lamina analysis is quite good. The shielding at d.c. varied from 67.04db for THIN1 to 87.49 db for BAE5. As the frequency increased the shielding initially remained constant until about 10MHz for the RAE sample, and until about 3MHz for BAEP5. For higher frequencies the shielding improved.

5.2. Samples with Anisotropic Averaged Conductivity.

The agreement between the averaged theory and the lamina analysis holds only for a certain frequency range e.g. 0-20 MHz for BAE2, 0-10 MHz for BAE2A, 0-3 MHz for 8MM. If we consider the case of the incident field parallel to the direction of the smallest component of the averaged conductivity tensor the averaged theory and lamina analysis are in rough agreement however up to about 300 MHz. For the incident E field parallel to the higher component of the averaged conductivity we see that the shielding does not increase with frequency as rapidly as is indicated by the averaged theory.

Above 300 MHz the shielding behaviour of THIN2, for $E^{inc} \perp x'$, remained at roughly 61 db (to within ± 2 db) up to at least 10 GHz. This is in contradiction to the average theory.

5.3. Samples with Air Gaps.

The effect of introducing air gaps in samples is to increase the shielding when the frequency is sufficiently high. There is no such effect at d.c. (The sample 8MMA is the same as 8MM except that a 2 cm air gap is introduced in the centre of the sheet. 8MMB is similar except that the gap is 20 cm). This phenomena is a well-known property of double shields, (Rizk F.A.M., 1977).

6.0 APPARENT RESISTIVITY

In figure 7 we show the apparent resistivity, $\rho_{x'}$ and $\rho_{y'}$, calculated from the Λ matrix. Also shown are some measured results based on samples 5 mm wide. The two sets of results generally agree to within a factor of 2.

Table 3. Averaged Resistivities $\rho_{x'}$ and $\rho_{y'}$ at DC.

Sample	$\rho_{x'}$ $10^{-4} \Omega m$	$\rho_{y'}$ $10^{-4} \Omega m$	$\rho_{x'}$ (ERA) $10^{-4} \Omega m$	$\rho_{y'}$ (ERA) $10^{-4} \Omega m$
THIN1	.419	.419		
THIN2	.280	.834		
RAE	.419	.410	.56	.59
BAE1	.419	.419	.59	.61
BAE2	.280	.834	.31	.52
BAE2A	.280	.834	.31	.52
BAE4	.419	.419	.52	.55
BAE6	.210	95.0	.210	95.0
BAEP5	.419	.419	.45	1.0
8MM	.280	.834		
BAE2AL	.121	.170		

7.0 TRANSVERSE CONDUCTIVITY

The value of transverse conductivity (i.e. σ_z) used in the calculations reported so far has been of no significance because for normal incidence the induced currents flow entirely in the plane of the sheet. It may be asked however whether σ_z plays a role in shielding for other than plane waves normally-incident. Three different values of σ_z were used, viz 1.0, 40.0, 105.3 mho/m. It was found that for plane wave shielding the precise value of σ_z is not important.

The lamina analysis assumes that the laminae touch along their surfaces. This amounts to assuming perfect electric contact. In practice there may be contact resistance between the laminae. In fact from some of the photographs, diagram 1, there may be regions at the interface where fibres are absent and the net result may be some form of contact resistance. To investigate whether these effects could affect the shielding characteristics of CFRP we considered the BAE2 lay-up but interposed at each interface between laminae a thin layer (.006 mm thick) of dielectric ($\epsilon = 3.5\epsilon_0$) was located. This has the effect of insulating the laminae from each other. However the alteration in shielding was generally small.

8. TRANSFER AND SURFACE IMPEDANCE

For samples without air gaps it was found possible to calculate the reflected and transmitted fields that arise for incident plane waves arriving at an arbitrary angle of incidence, by means of surface (Z_s) and transfer (Z_T) impedance tensors (i.e. 2×2 matrices). See figures 8, 9. The off-diagonal

elements of the transfer impedance are responsible for the difference between the averaged theory and lamina analysis seen in figure 6.

9.0 CFC GROUND PLANE

We consider an elementary electric dipole on a CFC ground plane. Even for an extreme example, viz. THIN2 (thickness .5 mm) at 1 GHz (maximum component of surface impedance tensor 1.6 ohms) and polar angle 89° , the far field reduction compared to a perfect ground plane was only 1.3 db. We conclude that as regards far fields for most applications the CFC can be assumed perfectly conducting.

10.0 PLANE SCREEN EMP SHIELDING

The peak value (1.0 v/m) of the chosen normally incident EMP ($\alpha = 6 \times 10^6$, $\beta = 8 \times 10^7$) occurs at 35 ns. It was found that the transmitted field had approximately the same polarization as the incident field.

Table 4. Peak Values of the Transmitted Electric Field.

Sample	$E^{inc} // x'$	$E^{inc} // x'$	$E^{inc} // y'$	$E^{inc} // y'$
	Peak Value V/m	Time of Peak (nanoseconds)	Peak Value (V/m)	Time of Peak (nanoseconds)
THIN2	2.97×10^{-4}	37	8.86×10^{-4}	36
BAE1	1.15×10^{-4}	58	1.15×10^{-4}	58
BAE2	6.79×10^{-5}	75	2.21×10^{-4}	47
BAE2AL	2.37×10^{-5}	120	4.08×10^{-5}	70
BMM	5.85×10^{-6}	436	3.16×10^{-5}	207

11.0 CONCLUSIONS

The mathematical theory presented above can be used to calculate the plane wave screening and surface and transfer impedances of CFC. Comparison has been made with a simpler theory whereby the entire CFC sheet is replaced by a homogeneous but anisotropic material. The simpler theory is valid below a certain frequency (approx. 30 MHz for 2 mm thick sample) but at higher frequencies does not always provide the correct polarization or magnitude.

12.0 ACKNOWLEDGEMENT

This work has been carried out under contract for the Procurement Executive, Ministry of Defence, U.K. The author also thanks the Technical Director, GEC-Marconi Electronics Limited for permission to publish.

REFERENCES

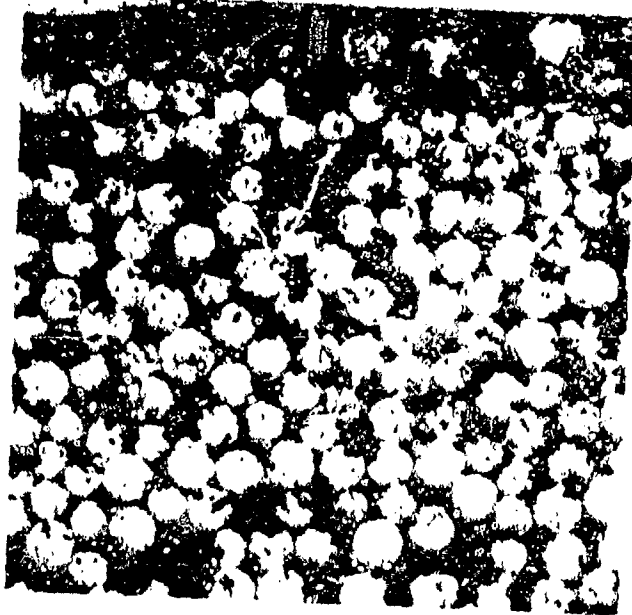
- Abramowitz M. and Stegun I.A., 1965, "Handbook of Mathematical Functions",
 Baskerville M.W., 1978, "A Short Study of the Anisotropic Resistance in Carbon Fibre Composites",
 Pleasey Research (Cassell).
 Bueche F., 1972, "Electrical Resistivity of Conducting Particles in an Insulating Matrix"
 J. Appl. Phys. Vol. 43, No. 11.
 Casey K.F., 1976 "EMP Penetration through Advanced Composite Skin Panels",
 AFWL Interaction Note 315.
 Collin R.E., 1960, "Field Theory of Guided Waves", McGraw-Hill Book Company.
 Electrical Research Association, 1979, "Measurements of R.F. Properties of Carbon Fibre
 Composite Materials (CFC), "No. 3320/R/2.
 Rizk F.A.M., "Low Frequency Shielding Effectiveness of a Double Cylinder Enclosure",
 IEEE, EMC-19, No. 1

Table 5. Lay up of examples considered

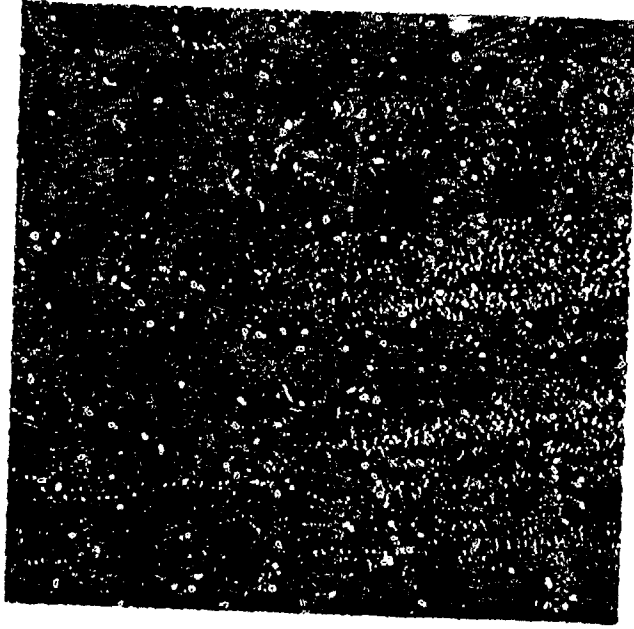
Name	Thickness (mm)	No. of laminae	Lay-up (w.r.t. to fixed axis x')
Thin1	.5	4	0 90 0 90
Thin2	.5	4	0 45 0 45
Rae	1.75	16	0 90 0 90 ...
Bae1	1.85	10	0 90 0 90 ...
Bae2	1.98	16	0 45 0 45 ...
Bae2a	1.98	16	45 45 45 45 0 0 0 0 0 0 0 0 -45 45 -45 45
Bae4	1.19	8	45 45 ...
Bae6	2.11	16	0 ...
Bae p5	5.26	40	90 45 0 45 45 0 45 90 ...
8MM	7.92	64	0 45 0 45 ...
8MMa	27.92	65	0 45 0 45 ... 0 32 laminae 2cm air gap ... 0 45 0 45
8MMb	20.792	65	0 45 0 45 ... 0 32 laminae 20cm air gap ... 0 45 0 45
Test	3.0	3	0 45 90
Bae2al	1.985	17	0 45 0 45 ... 0 16 laminae aluminium .005 mm



Lamina No 3 2 1
Photograph A (x60)



Photograph B (x600)



Photograph C (x60)

Diagram 1 Magnified photographs of sections through carbon fibre composite material

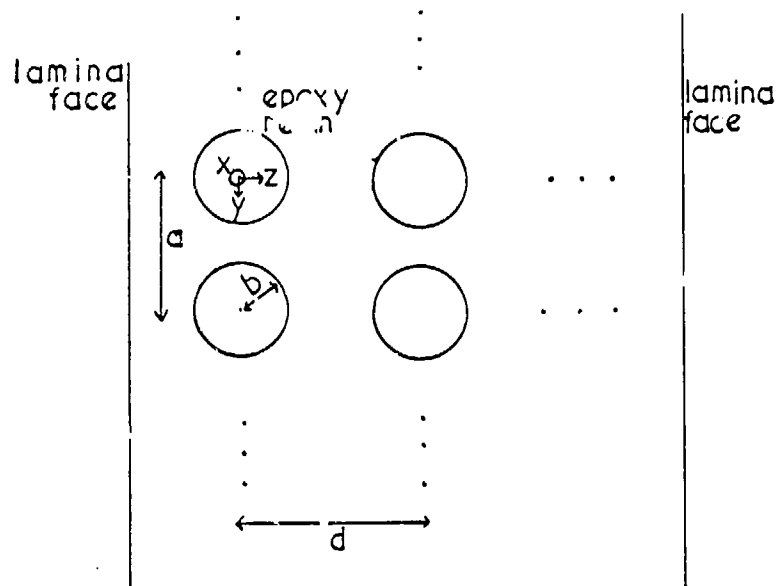


Fig.2 Simplified model of fibres in a lamina

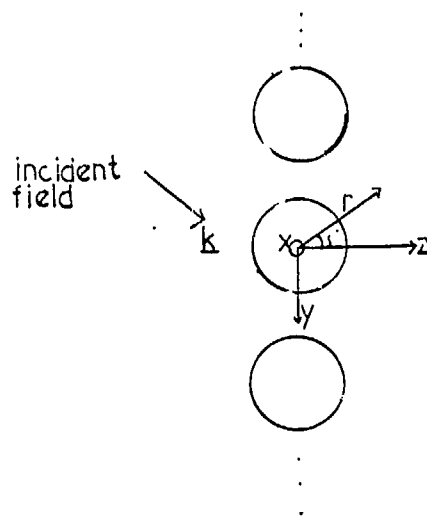


Fig.3 Single row of fibres in epoxy resin

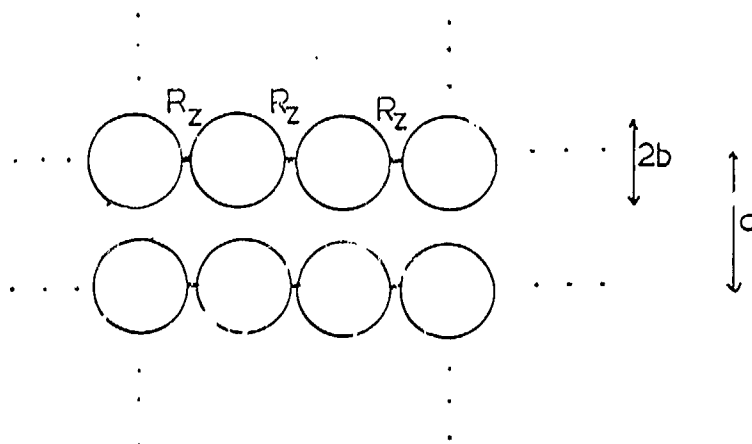


Fig 4 Model for transverse conductivity

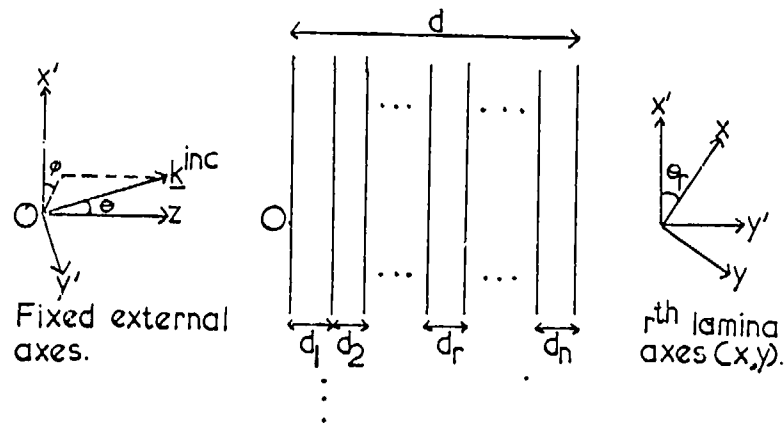


Fig.5 CFC sheet consisting of n laminae

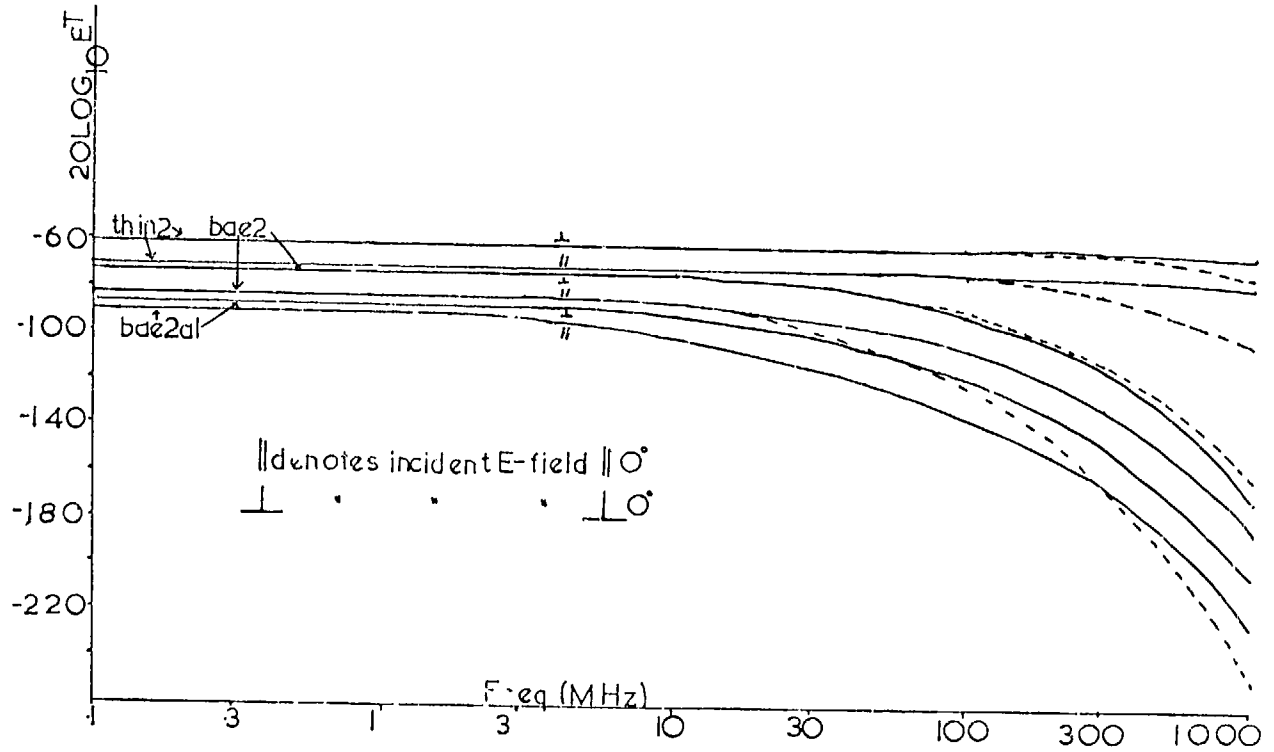


Fig.6 Plane screen shielding. Incident E-field IV/m, normally incident

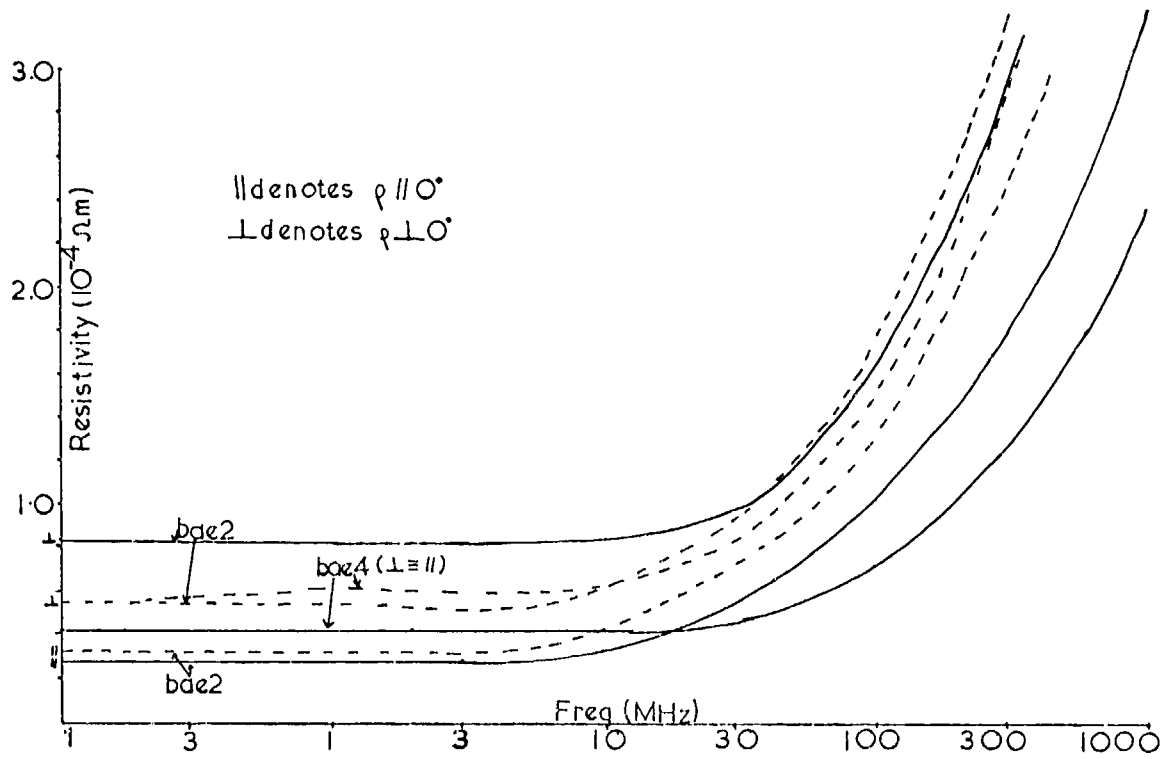


Fig.7 Variation of resistivity with frequency. Measured results, (ERA, 1979), shown as dashed curve

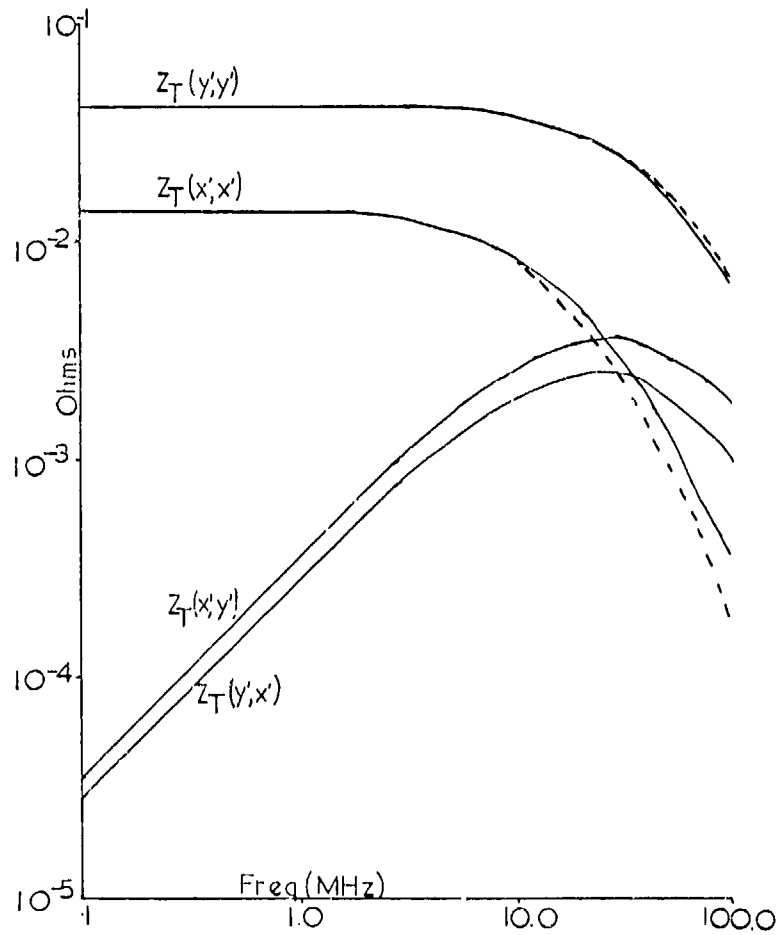


Fig.8 Magnitude of elements for Z_T matrix for BAE2 (----- Averaged Theory)

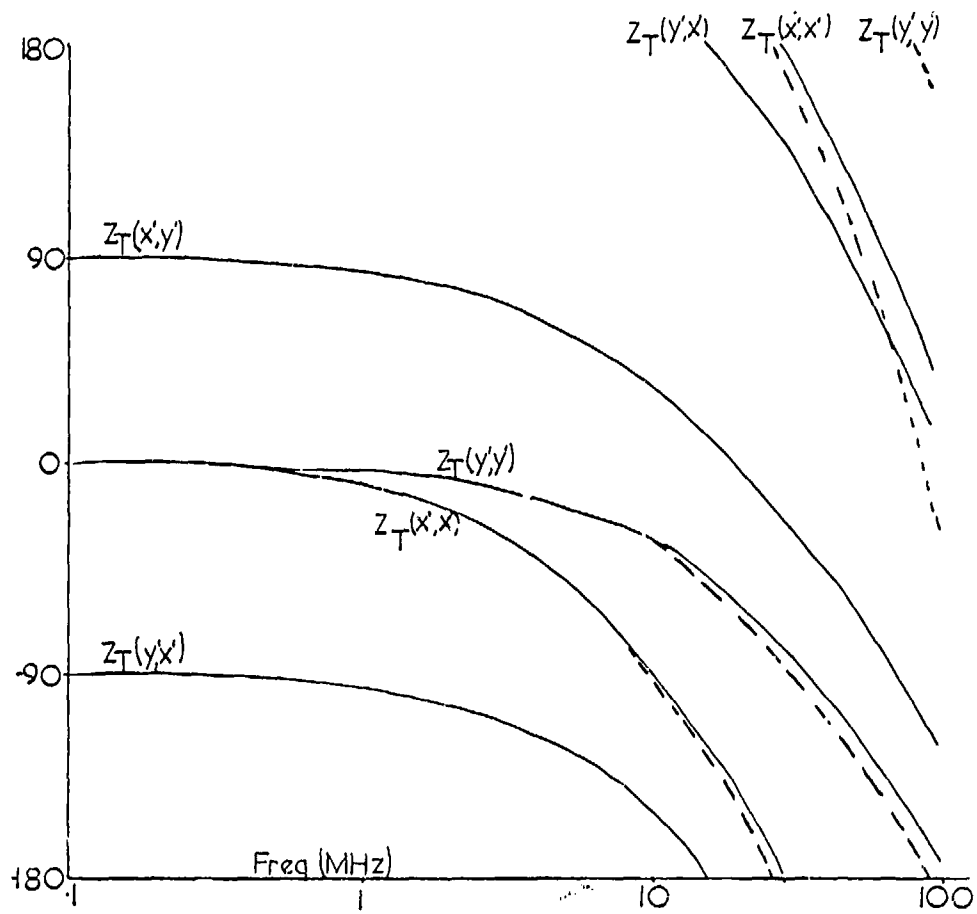


Fig.9 Phase of elements of matrix Z_T for BAE2 (----- Averaged Theory)

RF RESISTIVITY AND SCREENING CHARACTERISTICS
OF CFC MATERIALS

D.A. Bull, G.A. Jackson and B.W. Smithers

ERA Technology Ltd

Leatherhead

Surrey

U.K.

SUMMARY

A series of investigations have been made to determine both the electrical resistance characteristics of carbon fibre composite (CFC) samples and their screening properties.

Resistivity was examined from d.c. to 300 MHz and certain effects of environment were noted under d.c. test conditions.

The measurement of screening properties required much larger samples and test frequencies ranged from 150 kHz to 30 MHz for the magnetic mode and from 50 MHz to 1000 MHz for the electric mode.

This paper describes the methods and techniques employed with brief comments on some of the theoretical aspects of conduction and screening.

1. INTRODUCTION

Carbon fibre composite materials have been subjected to intensive examinations concerning their mechanical properties but their electrical properties, particularly at high frequencies, are much less well-known. The performance of CFC will be inferior to that of metal in respect of conductivity and screening and it is difficult to predict the performance of an aircraft containing substantial proportions of CFC material without a reasonable body of fundamental data.

ERA Technology was asked to examine a number of the basic properties of CFC materials including the present measurements of electrical resistance and screening. An interesting feature of the latter is the relationship between the results of attenuation assessment under both near and far field conditions.

2. CARBON FIBRE COMPOSITE MATERIALS

Although carbon fibres were produced commercially a century ago, the use of long fibres of controlled diameter embedded in a matrix to form a constructional material of great strength and lightness is a comparatively recent development. Progress has been such that these materials are now to be found in equipment for the leisure market, boat-building, automotive engineering as well as for our present concern, the aerospace industry. Carbon fibre composites have used, for example, in the AV8B wing, the HIMAT experimental model and in civil and military aeroplanes in the U.K.

Individual carbon fibres have a diameter of $7 - 8 \times 10^{-6}$ m and are grouped together in bundles of many thousands (often 10,000) to form a tow. Such tows are coated with resin and laid parallel and suitably spaced on a non-stick surface. A second sheet of non-stick paper or plastic film is placed on top of the tows, the latter having a circular cross-section at this stage. The tows are then rolled between the two sheets to flatten them so that filaments in adjacent tows meet, filling the gaps between them. A tow of circular cross-section may have a diameter of 2mm but after rolling, a spread up to 6mm or 12mm may occur (GILL, R.M., 1972). The accepted term for the composite at this stage is 'pre-preg' and can be stored in drums which if maintained at a suitably low temperature can have a satisfactory 'shelf-life'. The orientation of the tow is normally unidirectional and successive plies are laid as required to obtain the mechanical performance for particular applications.

A curing cycle at the necessary temperatures and applied pressure completes the production of a sheet or more complex shape as desired.

3. PREVIOUS WORK ON RESISTIVITY

Measurements of low-frequency conductivity (d.c. to 1 MHz) have been reported,

(SCRUGGS, L.A.; GAJDA, W.R., 1977). These measurements were made both for current flow parallel to and across the fibre direction in a unidirectional material. At the higher frequencies of this range, sample voltage was measured with an oscilloscope and current was derived from the voltage drop across a known resistor connected in series with the sample. Results gave a resistivity of the order $5 \times 10^{-4} \Omega\text{m}$ which was constant from d.c. to 1 MHz when current flow was parallel to fibre direction. The method is not suitable for use at frequencies very much higher than 1 MHz as the reactance of the sample soon becomes comparable with resistance.

Some more recent results (GAJDA, W.R., 1979) suggest d.c. resistivity (unidirectional CFC with current flow parallel to fibres) of $1.0 \times 10^{-5} \Omega\text{m}$. This value agrees more closely with those obtained at ERA than the earlier results of SCRUGGS and GAJDA.

Values of resistivity at 2 GHz similar to those at 1 MHz were found (WALKER, W.F. and HEINTZ, R.E., 1977), when using a CFC sample as a partition across a 50 ohm line. Using another method (strip line), however, these authors expressed doubts about the accuracy of results above 1 GHz. In the latter case the test sample was connected as a shunt path and treated as a lumped impedance. By introducing composite material (unidirectional) as part of the strip line WALKER and HEINTZ calculated resistivities of $1.2 \times 10^{-5} \Omega\text{m}$ at 1 GHz and $4.5 \times 10^{-5} \Omega\text{m}$ at 2 GHz.

Some more recent work (WALKER, W.F.; HEINTZ, R.E., 1979) extends these measurements down to 75 MHz by using long samples (6 feet). The authors suggest refinements for this technique but currently have no explanation for the manner in which conductivity decreases with frequency.

4. TEST METHODS FOR RESISTIVITY

The measurements of resistivity made at ERA and described below generally made use of a Q-meter (Marconi TF1245A). Small samples (25mm x 10mm and 25mm x 5mm) were used in the frequency range 1 MHz to 300 MHz. The Hewlett-Packard Vector Impedance Meter, Model 4815A, can measure complex impedance over the range 0.5 MHz to 108 MHz in a very convenient fashion, but is, unfortunately, limited in performance with small low resistance samples.

Where longer samples are available having a higher resistance the performance of the Vector Impedance Meter is somewhat improved, but the complexities of mounting each sample in a transmission line render the method less attractive (and less accurate) than the use of the Q-meter with small samples. Comparison measurements between Q-meter and Vector Impedance Meter methods are described below.

In the Q-meter method the measurement of R.F. resistance of samples is accomplished by including them in series connection in a resonant circuit as indicated in Figure 1. Figure 2(a) shows the test jig used at frequencies of 50 MHz and below. At frequencies above 50 MHz and up to 300 MHz shorter connections are required and Figure 2 (b) shows a 'standard' inductor, and inductor with test sample included. Figure 3 shows where electroless copper plating is used to enable soldered connections to be made to the samples.

In the jig of 2 (a), if :

Q_1 = Q value obtained with the test sample shorted

Q_2 = Q value obtained with the test sample in circuit and C_1 and C_2 are the corresponding indicated values of tuning capacitance for resonance then :

$$R_x = \frac{1}{\omega} \left[\frac{1}{C_2 Q_2} - \frac{1}{C_1 C_2} \right]$$

where R_x is the required value of the resistance of the sample.

All tests were conducted at room temperature and prevailing humidity conditions.

Additionally, resistance under direct current conditions was obtained by measuring the test sample voltage drop using a digital voltmeter, and comparing this with the voltage drop across a standard resistance connected in series with the sample.

A larger sample forming the inner conductor of a parallel-plate line, figure 4, was short-circuited at one end and the impedance at the open end was measured using a Hewlett-Packard 4815A Vector Impedance Meter at frequencies up to 100 MHz. When using the Impedance Meter with this sample (d.c. resistance 0.18 ohms) errors were minimised by obtaining probe readings at the '100Ω check' socket on the instrument, and with the probe tip shorted as well as with the sample connected.

5. ORIGIN AND STRUCTURE OF TEST SAMPLE MATERIALS

Ten types of material were available, all from U.K. sources. Details of structure and fibre and resin types are given in Table 1.

6. PREPARATION OF SAMPLES

Sheets of CFC material as supplied, were generally in rectangular form. Arbitrary orthogonal directions x and y were noted parallel to the sheet edges and samples were cut using a hacksaw and marked 'x' and 'y'. Additionally, samples were obtained by cutting at an angle of 45° to 'x' and 'y'. All edges were smoothed using a medium-fine grade of glass-paper and finished with fine grade carborundum paper. The 25mm x 10mm or 25mm x 5mm faces were not abraded as good adhesion and electrical contact were not required on these surfaces.

Samples were then wrapped in two layers of PVC adhesive tape of width 20mm so that a 2.5mm length at each end of the samples was exposed. The samples were then immersed in a sensitiser solution for 10 to 15 minutes, washed thoroughly and immersed in an electroless plating solution until an adequate deposit of copper was obtained. Details of this process were supplied by Plessey Research (Caswell) Limited and are to be found in the Appendix to this paper. The samples, Figure 3, were washed, dried and soft soldered into the jig of Figure 2(a), or the inductor end-pieces were soldered as required for tests at higher frequencies. Entry of current into the sample was largely at the 10mm x thickness or 5mm x thickness plated areas at the sample ends.

Direct electroplating using acidified copper sulphate solution and a suitable plating current resulted in a satisfactory mechanical bond, but d.c. tests revealed that the electrical bond was significantly inferior.

In connection with the short transmission line tests referred to in Section 4, a sample of unidirectional CFC material, H, 200mm x 12mm x 2.11mm was connected as shown in Figure 4. The sample was cut with fibres parallel to main current flow and electroless copper plated at each end, thus allowing it to be soft-soldered into the line.

7. RESULTS

7.1 Measurements On Small Samples Using Q-meter

Some examples of the results obtained are shown in Figures 5-6 and 5(a) - 6(a). Resistivities are generally lower for the narrower, 25mm x 5mm samples. This is consistent with the existence of a skin effect for current flow, since in the narrower sample the loss in effective cross-sectional area will be proportionately less than in wider samples as current retreats to surfaces and edges with rise in frequency.

This change in distribution of current over the cross-section, (skin effect), occurs because those parts of the cross-section which are circled by the largest number of magnetic flux lines have a greater inductance than other parts and hence a greater reactance. Those parts having the greatest reactance will carry the least current. With a flat strip, as used here, the current density is greatest at the edges, reduced at the flat surfaces and least in the centre. Hence, skin depth of current flow controls the resistance for alternating currents. From Maxwellian theory it can be shown (HUND, A., 1936) (WHINNERY, J.R., 1942) that current penetration depth is proportional to $f^{-1/2}$, and high frequency resistance is proportional to $f^{1/2}$ in a conductor of circular cross-section. Figures 5(a) - 6(a), where resistivity is plotted against $f^{1/2}$ show substantially linear relationships.

In the case of the unidirectional sample H(y), Figure 6, where the fibres are parallel to the direction of current flow, the d.c. resistivity is shown as 2.1 to $2.4 \times 10^{-5} \Omega$. These samples contain Super A fibres of d.c. resistivity about $1.3 \times 10^{-5} \Omega$. On this basis the fibre volume fraction is between 0.54 and 0.62. It has been indicated elsewhere (WHITNEY, J.M., 1978) that volume fractions vary from about 0.60 to 0.65.

TABLE 1
Test Material Data

Sample	Fibre	Resin	Number of plies and lay angles. (Detailed lay-up where known)
B	-	Phenolic	16 plies, 0° , 90°
C	SUPER A	Code 69	10 layers of cloth; 0° , 90°
D	SUPER A	BSL 914C	16 plies; 0°_8 , $\pm 45^{\circ}_8$
E	SUPER A	BSL 914C	16 plies; 0°_8 , $\pm 45^{\circ}_8$
F	SUPER A	BSL 914C	8 plies; $\pm 45^{\circ}$
G	SUPER A	BSL 914C	16 plies; 0°_8 , $\pm 45^{\circ}_8$
H	SUPER A	BSL 914C	Unidirectional; 0° , 16 plies
I	SUPER A	BSL 914C	40 plies; 0° , 90° , $\pm 45^{\circ}$ $0,0, + 45, -45, 0,0, 90,0,C, +45, -45, 0,0,0,0,0, +45-45,$ Centre $0,0,0,0,$ etc
L	SUPER A	BSL 914C	16 plies; 0°_8 , $\pm 45^{\circ}_8$
P5	HM (High Modulus)	Code 69	Quasi-Isotropic 90° , $+45^{\circ}$, 0° , -45° , -45° , 0° , 45° , 90° 8 layers repeated 5 times

Table 2 shows the range of resistivities obtained at a number of frequencies, and which are characteristic of samples or panels where good contact is maintained by copper plating at the current entry and exit surfaces. It may be expected that these resistivity results will be applicable to large panels with the same aspect ratios as the samples, e.g. 1.0m x 2.5m panel analogous to 10mm x 25mm samples and 0.5m x 2.5m panel to 5mm x 25mm samples.

TABLE 2
Ranges of Resistivities for CFC Materials

Frequency MHz	Ranges of resistivity-all samples except unidirectional $10^{-5} \Omega m$	Resistivity of unidirectional samples $10^{-5} \Omega m$	
		Parallel to lay	Perpendicular to lay
1	3 to 15	2	1100
10	5 to 15	6	1100
50	12 to 35	12	1300
100	17 to 60	16	*
300	32 to 150	30	*

* Measurement not possible.

The measurement technique was verified by measuring the resistance of a 22mm length of Eureka resistance wire of 0.13mm diameter from d.c. to 250 MHz and comparing these results with calculated values. Differences were negligible up to 50 MHz, but the measured value was 20% higher than calculated at 250 MHz. There is, however, a large transition in conductor dimensions where the thin wire joins the inductor strip used at 250 MHz and proximity effects may be significant at the higher frequencies. Q-meter accuracy is claimed as $\pm 5\%$ up to 10 MHz, rising to $\pm 12\%$ at 250 MHz and $\pm 20\%$ at 300 MHz. An assessment of overall accuracy in the determination of the resistivity of the CFC samples is difficult, but limits of $\pm 10\%$ up to 10 MHz, $\pm 20\%$ from 10 MHz to 50 MHz and $\pm 30\%$ from 50 MHz to 300 MHz are probably realistic. Repeatability of measurements has proved to be of a higher order, i.e. about $\pm 5\%$.

7.2 Measurements using Unidirectional Samples H(y) in a Transmission Line

As noted in Section 4 and shown in Figure 4 a sample of unidirectional CFC material H(y), was connected as part of a short-circuited transmission line. This sample was tested using the Hewlett-Packard Vector Impedance Meter Type 4815A, adopting the precautions noted in Section 4 above.

Figure 7 shows the results obtained and the resistance of the sample was found to increase markedly with frequency. The sample was then examined using the Q-meter and these results are also shown in Figure 7. A sample of this size is not well suited to the Q-meter technique, but the results obtained are comparable with those found using the Vector Impedance Meter. The resistivity values obtained by Q-meter at frequencies above 30 MHz are probably less accurate, as the jig method, Figure 2 (a), is inappropriate and an initial Q value, Q_0 , must be obtained by using a 'dummy' shorted transmission line in which a brass strip replaces the CFC sample.

Figure 8 shows the Vector Impedance Meter results again, but now these are compared with those found using the 25mm x 5mm sample of H(y) material, as previously shown in Figure 6. The length to width ratio for the transmission line sample is 16.7 compared with 5 for this Q-meter sample. Results differ by a maximum of 15% at frequencies up to 50 MHz. For such low resistance samples, (the 200mm strip has a d.c. resistance of 0.18 ohms), the accuracy of the Vector Impedance Meter is much reduced above about 50 MHz, and the use of the Q-meter (with smaller samples) is preferred.

In Figure 9 the resistivity of the transmission line sample as measured by the Vector Impedance Meter is plotted against a scale proportional to $f^{\frac{1}{2}}$. It will be seen that a linear relationship occurs suggesting the existence of a normal skin effect for current flow.

The measurements show that results obtained using a Q-meter are in good agreement with those made using the Vector Impedance Meter and both methods demonstrate the presence of skin effect.

8. THE CALCULATION OF R.F. RESISTANCE OF CFC SAMPLES

A method for the calculation of the resistance of samples over a range of frequencies would be of considerable value and the measurements made on the ten types of material listed in Table 1 could provide ample validation for such procedures.

Belevitch (BELEVITCH, V., 1971) has considered lateral skin effect in a fiat conductor of thickness t and width or lateral dimension w . His analytical treatment for conductors of elliptical cross-section is complete, but only partial solutions were obtainable, using numerical treatments, for conductors with sharp edges (e.g. rectangular cross-section).

In view of these limitations in the theoretical description of the high frequency behaviour of simple materials it appears that no rigorous treatment can be envisaged for the more complex case of CFC at the present time.

A simpler approach to this problem has been tried at ERA and the obvious sample for an initial consideration is H(y), the unidirectional material, with main current flow in the O° direction (i.e. in the direction of fibre-lay).

Haefner (HAEFNER, S.J., 1937) described a method based on experimental evidence, for calculating the alternating current resistance of conductors of rectangular cross-section - see also, Terman (TERMAN, F.E., 1943). Haefner's corroborative measurements were made at frequencies up to 8 kHz, but his examination of data from other sources suggested that good agreement between theory and measurement would be maintained at much higher frequencies. Figure 10 shows how the ratio R_{ac}/R_{dc} is related to a parameter p for various ratios of width to thickness of the cross-section of the sample.

Haefner's treatment has been applied to sample H(y), the unidirectional material, using the direct current resistivity as a basis for calculating resistivity at high frequencies. Measured and calculated values are shown in Figure C and the calculated values are seen to be about 20% lower than those measured at 100 MHz.

Considerable fibre to fibre contact occurs in CFC material of any construction and there is therefore, a strong tendency for skin effect to be developed as in a homogeneous material.

Proximity or coupling effects between bundles of fibres (tows) have been considered, and if existing, would modify the resistivity values calculated by Haefner's method and improve the agreement between measured and calculated results. Proximity effects are, however, insufficiently developed in a material having the resistivities of CFC materials to have an appreciable effect on the calculations.

A specimen of H(y) unidirectional material was cut 12mm wide and mounted and polished so that the circular fibre ends could be examined. Under microscopic observation the ply boundaries were clearly defined but no delineation of tow to tow boundaries within a ply were detectable. It is apparent that the measurements on samples H(y) of widths 5mm and 10mm were conducted on a material composed of parallel layers poorly insulated from one another. Measurements made perpendicular to the strips showed the resistivity to be about five times greater than that across the fibre direction. It has not been possible, so far, to make a theoretical prediction of the high frequency behaviour of such a composite material.

It is instructive, however, to consider the theoretical behaviour of an hypothetical CFC material of small dimensions, (1.57mm x 1.57mm cross-section and 10mm in length), where the tows (4 in number and 10^4 fibres per tow) can be regarded as discrete conductors when cross fibre resistivities are assumed to be as those found in samples of material type H.

Howe (HOWE, G.W.O., 1917) gives a method for calculating the ratio R_{ac}/R_{dc} for such a sample.

Table 3 shows the results obtained and these are compared with calculations using Haefner's method appropriate to a conductor of homogeneous cross-section.

The ratio R_{ac}/R_{dc} for the composite consisting of four discrete tows, shows that the grouping of thousands of fibres in a tow with fibre-to-fibre contact within each tow gives rise to a strong skin effect at frequencies above 10 MHz. At frequencies up to 100 MHz the ratio R_{ac}/R_{dc} is not very different from that found for a solid homogeneous cross-section.

TABLE 3

Comparison between discrete tow and homogeneous structures

Frequency (MHz)	R_{ac}/R_{dc} (Howe, 4 tows)	R_{ac}/R_{dc} (Haefner, homogeneous)
0.1	1.0	1.0
0.3	1.0	1.0
1	1.002	1.0
3	1.005	1.0
10	1.046	1.05
30	1.29	1.15
100	2.0	1.90
300	2.67	3.05
1000	4.06	5.44

9 THE EFFECT OF VARIOUS LIQUIDS ON THE DC RESISTANCE OF CFC SAMPLES

Environmental effects on CFC materials are of prime importance and work has been done concerned with the effects on direct current resistance for small samples immersed in a variety of liquids.

Water is an obvious candidate liquid and in order to reduce the time required to reach saturation, samples were immersed in boiling water for at least 72 hours, samples remaining immersed when not boiled. Total time of immersion was nearly 700 hours.

Samples were also boiled in a synthetic sea water solution for a least 72 hours and the total time of immersion exceeded 1000 hours. Sample construction is shown in Figure 11 with screws, nuts and washers for electrical connection. Although in the main test batch, such fittings were removed during boiling in sea-water, an additional sample was fitted with brass screws and boiled separately in sea water. Corrosion effects on these permanently fitted brass screws were found to be slight.

The increase in voltage drop for seven samples immersed in boiling water was about 30% for a 79 hour period of boiling. One other sample, composed of woven cloth, was unaffected by such treatment.

Samples immersed in boiling sea water fared less well, however, and some voltage drops increased by up to 100%. Some degree of variation may have been introduced by the repeated assembly and dismantling of the screw fittings during the boiling period. The sample boiled separately, only increased in voltage drop by 8% compared with a 40% increase for a sample of the same material boiled without fittings, although the effects of contamination by small amounts of copper and zinc cannot be discounted. Once again, a sample composed of woven cloth was virtually unaffected by boiling in sea water.

The immersion of samples at room temperature in WD40 protective fluid, hydraulic fluid and paraffin for periods ranging from 300 to 1400 hours had virtually no effect on voltage drop.

Some of the test samples boiled in water were re-measured for voltage drop after they had remained immersed at room temperature for a further 1400 hours after boiling ceased. They were then placed in a vacuum chamber at a pressure equivalent to an altitude of 21 km (about 35 torr) for a period of 16 hours. Voltage drops were measured after returning the sample to atmospheric pressure. No changes in voltage drop occurred as a result of this treatment.

10 SUMMARY OF RESULTS ON RF RESISTIVITY AND FLUID IMMERSION TESTS

Ten types of CFC material have been examined over the range d.c. to 300 MHz. In the case of unidirectional CFC the resistivity at d.c. and low frequencies and where main current flow is in the direction of the fibre lay is consistent with the expected fibre volume fraction of 0.60 to 0.65.

Skin effect develops in all samples in a manner similar to that for a homogeneous isotropic material when connections to the test samples are made in the manner described. The effect can be measured by Q-meter or Vector Impedance Meter techniques. The Q-meter is usable at frequencies up to 300 MHz whereas the Vector Impedance Meter is limited to 108 MHz, and is not well suited to the low resistance of CFC samples.

Water absorption to saturation has been found to increase the electrical resistance of samples 20% to 40% with the exception of a woven sample where no change in resistance occurred.

Immersion in boiling sea water increased the voltage drop of test samples by as much as 100% but the sample of woven cloth material was again unaffected by such treatment.

Immersion in protective fluid, hydraulic fluid or paraffin showed little effect on any sample.

No significant changes in voltage drop were produced after subjecting water saturated samples to an ambient air pressure equivalent to an altitude of 21 km for a period of 16 hours.

11 SCREENING

11.1 Previous work on screening

The literature concerned with screening by CFC is somewhat larger than that pertaining to resistivity and detailed comments cannot be made on it in a paper of this length. We would instance as examples papers such as those by (SKOUBY C.D., 1975), (STRAW, D; FISZKER, L., 1975) without intending the denigration of any other works published prior to or after these dates. The authors referred to above as well as others, described the use of a 'box' method for screening measurements and which is the method adopted at ERA for this purpose.

11.2 Definition

The purpose of screening is to provide some degree of isolation between a source of electromagnetic energy or transmitter and sensitive electronic equipment or receiver. The definition of screening ability is the ratio of the field strength in the unprotected free space situation to the corresponding value with the screen in place. The attenuation in the magnetic mode $A_H = H_1/H_2$ and in the electric mode $A_E = E_1/E_2$ where the subscripts refer to the field strength in 1 - free space and 2 - inside the enclosures. The definition relates to the tangential components of the field and makes no assumptions other than that adequate rejection of the component not being measured can be achieved by the measuring technique adopted. The important feature in the separation of the attenuation measurements into magnetic and electric mode values is the use of the appropriate receiving aerials.

11.3 Techniques of Assessment

The concept of the perfect enclosure may be introduced at this stage. This is not an

enclosure having infinite attenuation but one in which penetration is due to distributed transfer through the material of the screen only and not due to imperfections such as joints, seams, windows etc. In the absence of imperfections, the field within the enclosure is less affected by local distortion and the position of internal equipment for measurements is not so critical. However, ideal conditions such as these are rarely achievable in practice and the investigation on composite panels was no exception. The techniques which were employed involved the construction of a 1.0m³ copper box with one side replaced by the panel under test. The installation of the composite panel in the copper box inevitably results in departure from the concept of the perfect enclosure but the methods of assessment have been designed to ensure as far as possible that the attenuation of the complete structure is determined by distributed transfer through the composite panel. The incident electromagnetic field consists of separate but interrelated electric and magnetic components, complex in the near field but simple transverse E and H components in the far field. For any incident field the pattern of induced current flow in the screen is dependent on the particular component under consideration as shown in Figure 12. See also MIEDZINSKI, J., (1959). The composite panel was fitted to the copper enclosure and the transmitting aerial was orientated to ensure maximum flow of induced current in the panel.

The investigation was separated into magnetic and electric mode measurements, the former using loop aeriels and extending from 0.15 to 30 MHz while the latter used biconical aeriels and covered the range 50 - 1000 MHz. Separation into reflection and absorption losses has not been included in the investigation. However, several of the sample panels provided had a thickness of 2.0mm which is approximately equal to the penetration depth at frequencies around 2 MHz. Thus the attenuation at low radio frequencies is generally dominated by reflection loss while at higher frequencies the effect of absorption increases rapidly and becomes dominant in the v.h.f. band and above.

12. EXPERIMENTAL METHODS

Sample panels of either 1.0m² or 0.5m² were normally supplied with imperfect edges as a result of the curing procedure, and also had, by the nature of the curing, a resin-rich surface preventing good contact to the fibres. Before making any screening measurements, therefore, the rough edges were trimmed by file and abrasive paper.

Initial measurements of the screening performance of each sample were made, as described in sub-sections 12.1 and 12.2 before removal of the surface resin layer. Further measurements were required with as good a contact as could be obtained between the panels and test enclosure.

This was achieved by removing approximately 25mm of the top resin layer on all four sides of one surface of the sample and electroless copper plating the exposed carbon fibres of the surface together with the edges in the manner described in section 6. The general experimental arrangement is shown in Figure 13. The basis of all measurements was to set up transmitting and receiving aeriels at a fixed separation distance, generally one metre, and to obtain values of received field strength over the appropriate frequency range for a known transmitter output. The receiving system was then installed inside the copper box with the appropriate panel in place and the measurements were repeated.

Considerable care was taken to ensure that the physical conditions, separation distance etc., were maintained throughout the measurements.

12.1 Magnetic Mode

In the frequency range between 0.15 and 30 MHz the transmitter or power amplifier was used to energise loop aeriels having a diameter of 25 cms. Similar loops were used as receiving aeriels and formed part of the tuned input circuit in an amplifier which in turn was connected to an interference measuring receiver. The complete receiving installation was installed inside the copper enclosure and was battery powered. The loop aeriels were tuned to resonance at each test frequency in order to achieve maximum sensitivity and were also orientated for maximum reception of signal. In practically all tests the orientation was very close to the predicted position indicating that distributed transfer was the dominant mode of propagation through the screen. Tests were performed throughout the frequency range under the following conditions: 1. Free space, 2. CFC panel installed but with edges unplated, 3. Panel installed with edges plated, 4. Enclosure alone, open on one side.

12.2 Electric Mode

Measurements in the electric mode covered the frequency range from 50 to 1000 MHz. Considerable problems were encountered with attempts to employ rod or doublet aeriels particularly at lower frequencies, where lack of sensitivity determined the minimum frequency at which reasonable measurements could be made. Further investigations led to the development of scaled down biconical aeriels for transmission and reception which gave good coverage of the frequency range without the need for adjustment.

For reasons of operational convenience the transmitting biconical aerial was installed inside the enclosure under test and was fed through double screened coaxial cable from the power amplifier and signal generator. The latter were installed in a similar but separate screened enclosure to ensure that no parallel propagation paths existed. The receiving biconical aerial was installed at the appropriate distance outside the enclosure under test.

Coverage of such a wide frequency range inevitably meant that resonant effects were encountered, which tended to dominate the results. Cavity resonance in the test enclosure occurred at about 230 MHz but the effects were reduced to negligible proportions by the installation of resistive damping material around the internal walls.

13 RESULTS OF SCREENING MEASUREMENTS

The results that are included are representative of many others produced during the course of a very comprehensive investigation. The samples referred to in the paper employed XAS fibres and BSL 914C resin. In Figure 14 the attenuation in the magnetic mode is shown for frequencies between 0.15 and 30 MHz. The upper curve shows the attenuation for a sample with edges plated by the methods described and for which good all round contact was maintained with the metal box. The attenuation is not large rising directly with frequency as might be expected for a panel whose thickness, 2mm, was approximately equal to the penetration depth at about 2 MHz. The absorption loss is estimated to be less than 10dB at 1 MHz and probably no more than 40 dB at 30 MHz so that reflection loss largely determines the overall attenuation in the frequency range up to 30 MHz. However, the increasing attenuation at frequencies approaching 30 MHz indicates that the absorption loss is likely to become dominant in the v.h.f. band. It must be emphasised that the values of attenuation refer to the composite panel alone, allowance having been made for the contribution provided by the five sided enclosure. The reduction in attenuation due to poor joints is well shown by the lower curve which presents the results for the same panel before plating.

Figure 15 shows the measured values of attenuation in the electric mode over the frequency range from 50 to 1000 MHz, again for the same plated and unplated panel. The frequency range was restricted by the inefficiency of the small biconical aerials which were used. The fluctuations in the attenuation are due to imperfections in the measuring technique rather than to variations in the sample. In particular the effect of the open sided enclosure on the small high impedance biconical aerials is much greater than on the loop aerials used for measurement of magnetic attenuation. The values around 90 - 100 dB are comparable with the limit of measurement as it is extremely difficult to provide this degree of isolation between the transmitting and receiving systems, so that the inherent attenuation provided by the CFC panel is probably much greater than the values shown. The most significant factor is again the deterioration in attenuation when there is poor contact between the CFC panel and the metal enclosure. The reduction shown is about 40dB and is probably an underestimate.

Figure 16 shows the results of the measurements of attenuation in the magnetic mode for three different samples of composite panels. One panel was conventional 16 ply CFC whereas the other two consisted of two 4 ply sheets surrounding a honeycomb in-fill of aluminum and of Hexcel which is an insulating material. The mechanism of screening has not been investigated in detail but absorption loss is probably dominant at frequencies above 30 MHz while at lower frequencies attenuation is provided by multiple reflection in the complex panels. The overall result is a level of attenuation in the magnetic mode of comparable value with that provided by the 16 ply panel.

Figure 17 shows the attenuation in the magnetic mode for the same panel as used to obtain the results given in Figure 14 but obtained entirely under far field conditions. In the frequency range up to 1.5 MHz broadcast transmitters were used at distances of about 200 km and in the range 1.5 - 30 MHz a small local source was used at a distance of 200 metres which was at least one wavelength at the lowest test frequency. Comparison of the results in Figures 14 and 17 shows close agreement.

Calculation of attenuation based on resistivity may be performed using a number of procedures. These generally involve a calculation for a spherical shell of CFC material. If this is done, calculated values are up to about 10dB below measured values. Detailed investigations have not been made.

14 SUMMARY

This investigation, had, among its objectives the provision of information to fill a gap in current knowledge of the r.f. properties of composite materials. This paper has provided a description of the techniques of measurement of the screening attenuation for panels of CFC material. The good agreement achieved between attenuation measurements under near and far field conditions, although investigated at present only for the magnetic field, is nevertheless a good indication that consistent and repeatable results can be obtained by the techniques which have been devised.

It has been shown that CFC panels such as are presently being used in aircraft construction are inherently capable of providing high attenuation at frequencies in the v.h.f. band and above. In the h.f. band the attenuation of magnetic fields will fall approximately directly with reducing frequency and is unlikely to exceed 20dB at frequencies below 1 MHz. The importance of bonding the CFC panels to the main structure has been clearly shown and the method of electroless plating has been demonstrated as one possibility for achieving adequate bonding. Several aspects of the problem which still require detailed study are the attenuation in the electric mode at frequencies below 30 MHz, and the performance of bonded joints between CFC panels. Further corroboration is also needed of the agreement between near and far field measurements.

15 ACKNOWLEDGEMENTS

The work described in this paper was sponsored by the Procurement Executive, Ministry of Defence, and the authors wish to express their appreciation of the support in this investigation.

The authors also wish to thank the Directors of ERA Technology Ltd for their permission to publish this paper.

REFERENCES

- BELEVITCH, V., 1971. 'The lateral skin effect in a flat conductor'. Philips Tech. Rev., Vol 32. No 6/7/8. pp 221-231.
- GAJDA, W.R., 1979. 'Measurement of the electrical properties of composite materials in the frequency range of d.c. to 30 MHz'. Phase Report RADC-TR-79-203. Rome Air Development Center, New York 13441.
- GILL, R., 1972. 'Carbon fibres in composite materials'. Iliffe Books, London (Published for the Plastics Institute, London SW1).
- HAEFNER, S.J., 1937. 'Alternating current resistance of rectangular conductors'. Proc. IRE, Vol 25, pp 434-447.
- HOWE, G.W.O., 1917. 'The high frequency resistance of multiply-stranded insulated wire'. Proc. Roy. Soc. A, Vol. 93, pp 468-492.
- HUND, A., 1936. 'Phenomena in high frequency systems'. Mc Graw-Hill, p.333.
- MIEDZINSKI, J., 1959. 'Electromagnetic screening-theory and practice'. ERA Technical Report M/T 135.
- SCRUGGS, L.A. GADJA, W.R., 1977. 'Low frequency conductivity of unidirectional graphite/epoxy composite samples'. IEEE 19th EMC Symp. Record. pp. 396-402
- SKOUBY, C.D., 1975. 'Electromagnetic effects of advanced composites'. Final Report for Office of Naval Research, Dept. of the Navy (USA). NTIS Ref. AD O10882.
- STRAWE, D., PISZKER, L., 1975. 'Interaction of advanced composites with electromagnetic pulse environment. Technical Report AFML-TR-75-141.
- TERMAN, F.F., 1943 'Radio Engineers' Handbook'. McGraw-Hill, p.34
- WALKER, W.F., HEINTZ, R.E., 1977 'Conductivity measurements of graphite/epoxy composite laminates at UHF frequencies'. IEEE 19th EMC Symp. Record, August 1977, pp.410-413.
- WALKER, W.F., HEINTZ, R.E., 1979. 'Measurement of electrical conductivity in carbon/epoxy composite material over the frequency range 75 MHz to 2.0 GHz'. Syracuse University. Phase Report RADC-TD-79-255.
- WHINNERY, J.R., 1942. 'Skin effect formulas'. Electronics (USA), February, pp.44-48.
- WHITNEY, J.M., 1978. 'Moisture diffusion in fibre reinforced composites'. Technical Report AFML-TR-78-48.

APPENDIX

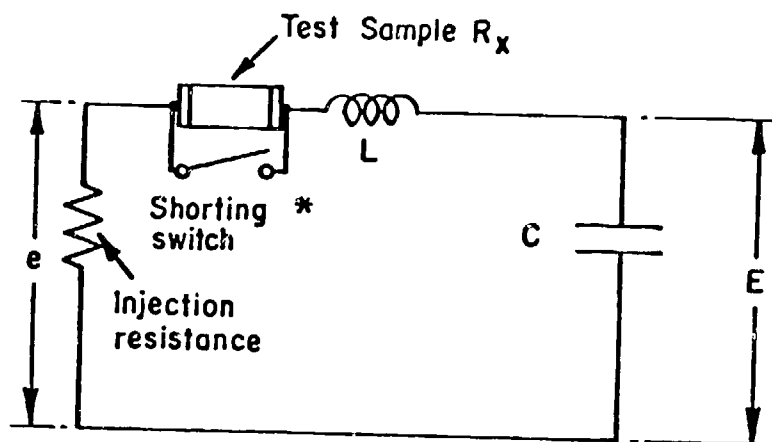
Electroless plating of CFC samples

Sensitizer (Note. This can be re-used)

Add 3.5g SnCl₂ to 20ml conc. HCl and add 5ml of 1% Pd Cl₂. Make up to 100ml with distilled water. Immerse the piece to be plated for about 5 minutes at room temperature and then rinse thoroughly (10 minutes).

Plating Solution

35g CuSO₄. 5H₂O; 170g sodium potassium tartrate; 50g NaOH. Make up to 1 litre with distilled water. Just prior to use, this solution, (or part of it), should have added to it formaldehyde solution in the ratio of 100mixture: 8 formaldehyde solution. The plated specimen should now be placed in this mixture, and left until plated. Plating occurs best on rough surfaces (it does not adhere well to the smooth outer layer of resin). The resulting copper layer is readily soldered but overheating is to be avoided.



$$Q = E/e$$

$$R_x = (1/\omega)(1/C_2 Q_2 - 1/C_1 Q_1)$$

$$C_x = \frac{C_1 C_2}{C_2 - C_1}$$

C_1, Q_1 , obtained with R_x shorted

C_2, Q_2 , obtained with R_x in circuit

Test samples are 25mm x 10mm (length x width)
and 25mm x 5mm.

* Jig with shorting switch
usable to 50 MHz, dual
inductor method used above
50 MHz. (See Fig. 2 (b))

Fig.1 Q-meter test circuit

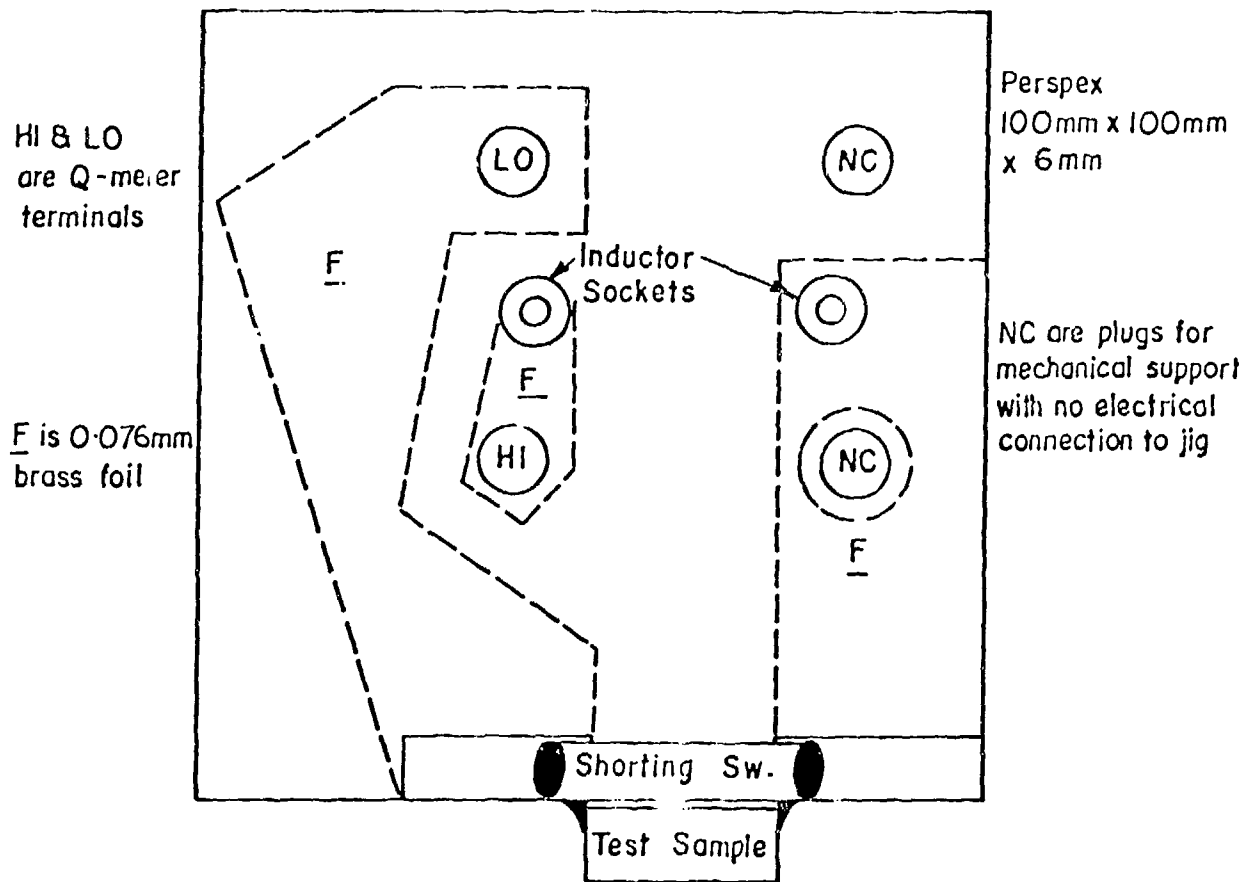
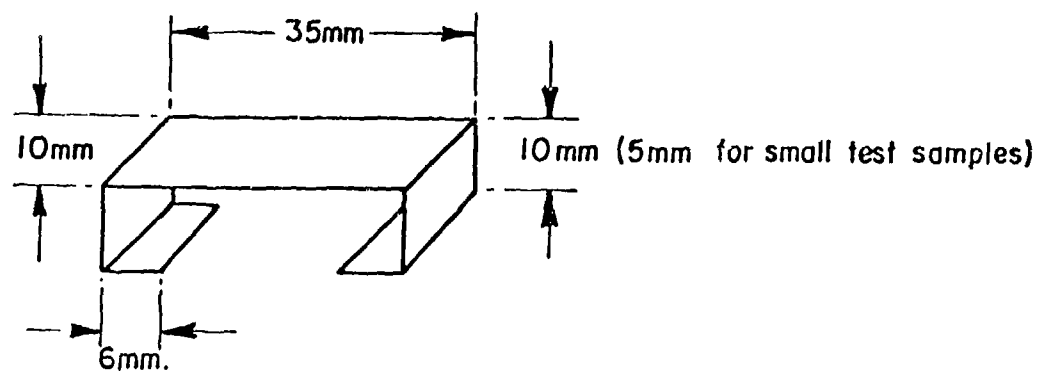


Fig.2(a) Test jig 1 to 50 MHz



Standard inductor for 100 to 300 MHz (0.076mm brass)

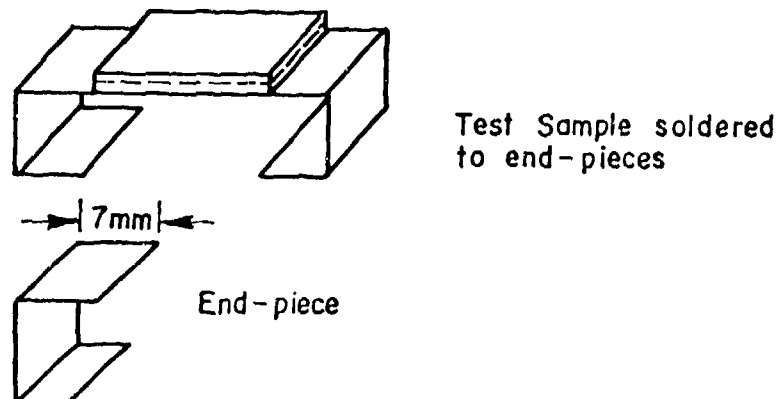


Fig.2(b) Testing samples at 100 to 300 MHz

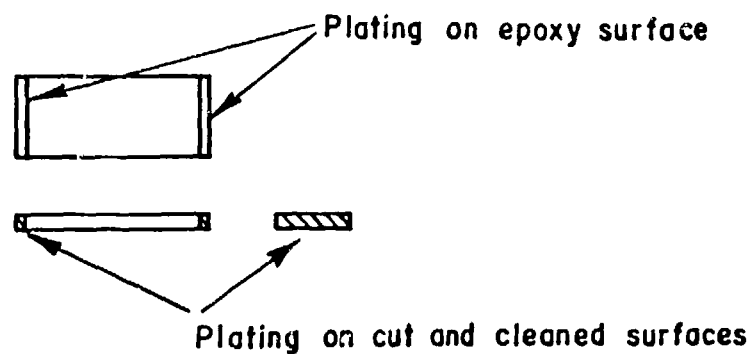


Fig.3 Plated sample

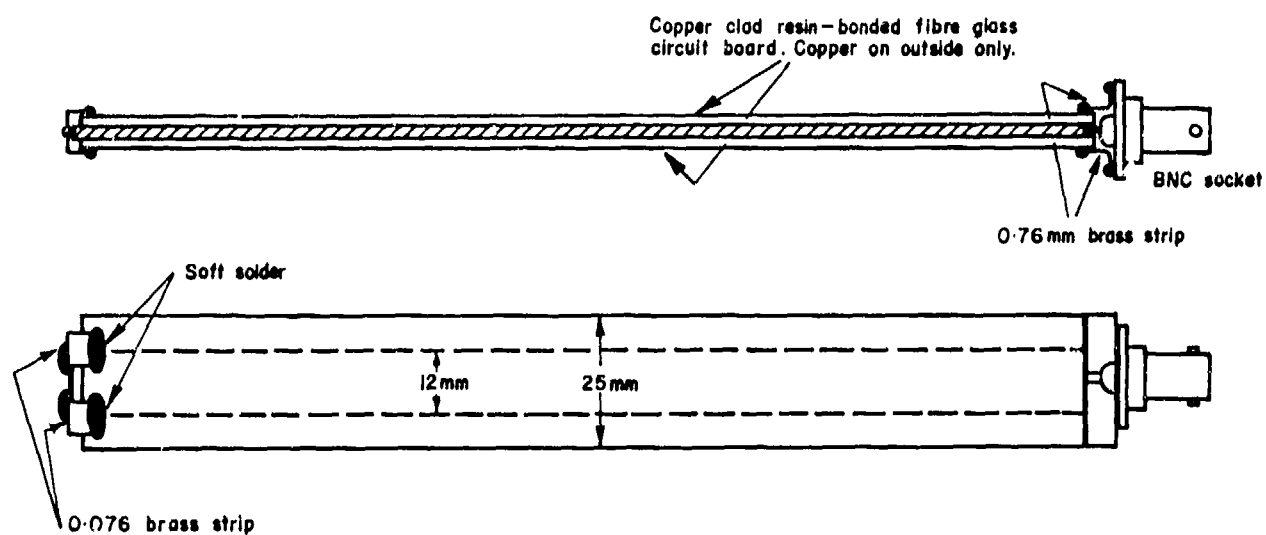


Fig.4 Transmission line sample of unidirectional material H(y), length 200mm, thickness 2.11mm

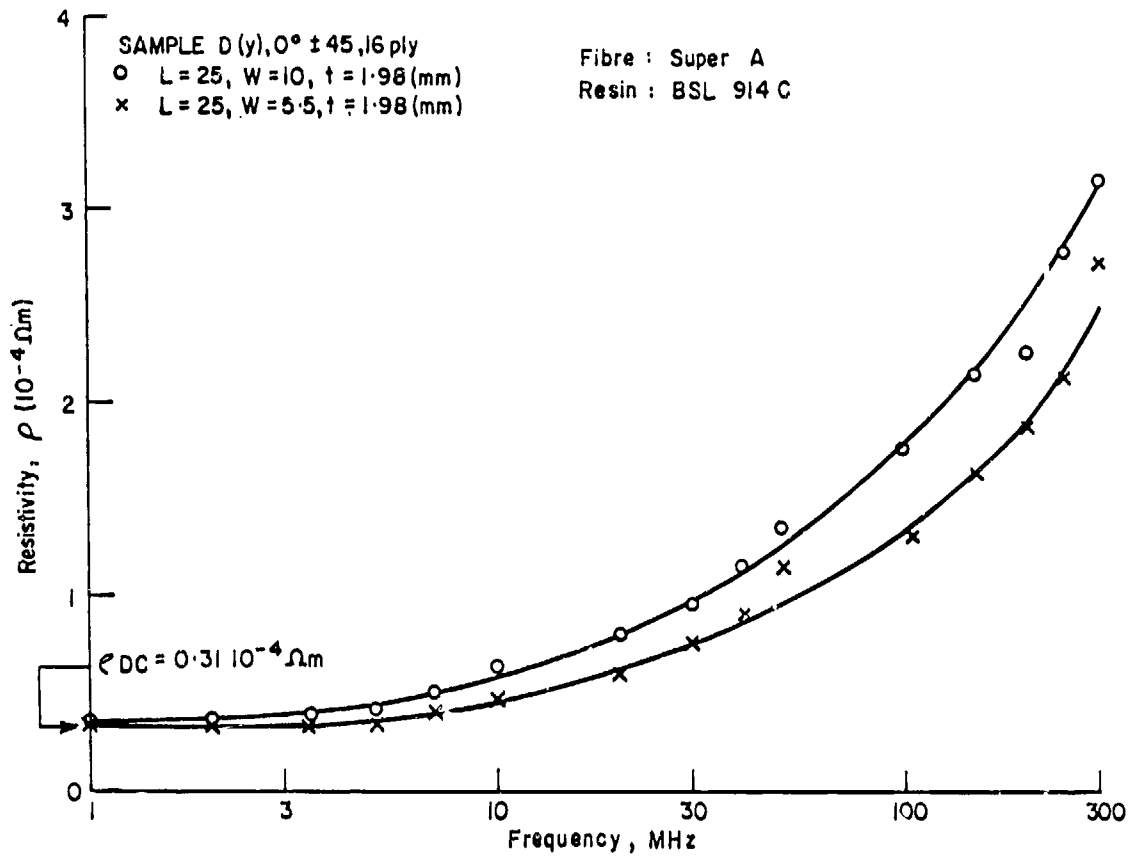


Fig.5 Typical resistivity-frequency characteristics

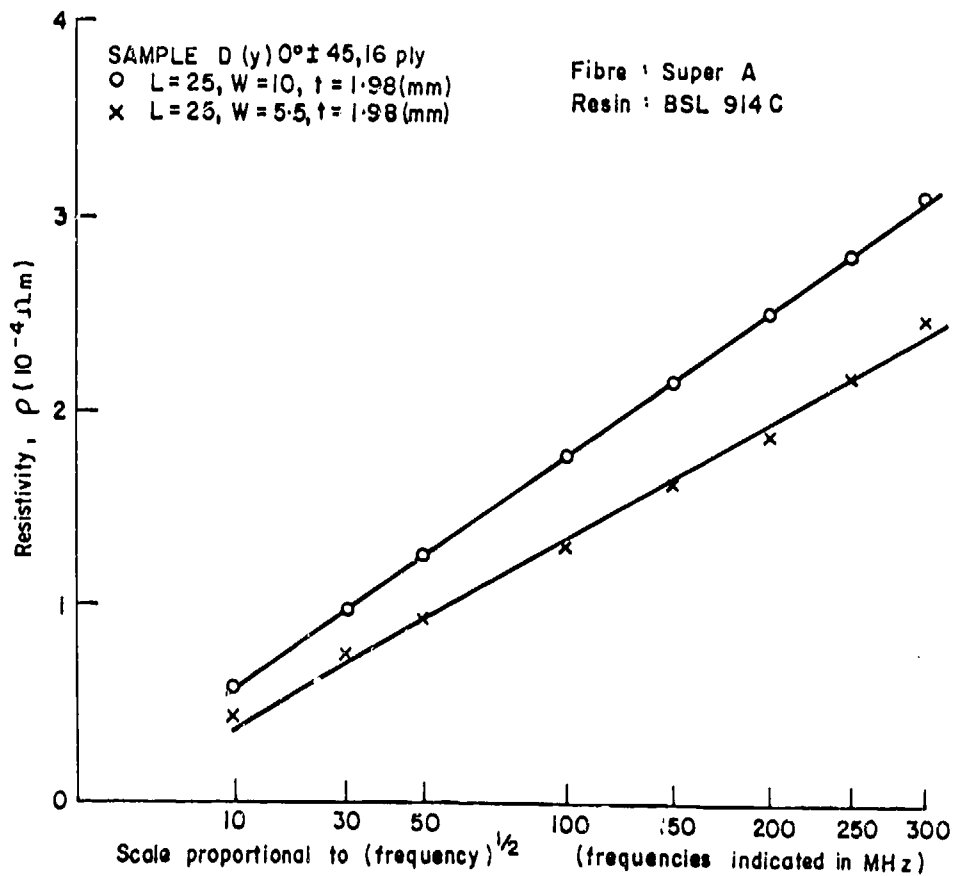


Fig.5(a) Typical resistivity-frequency characteristics

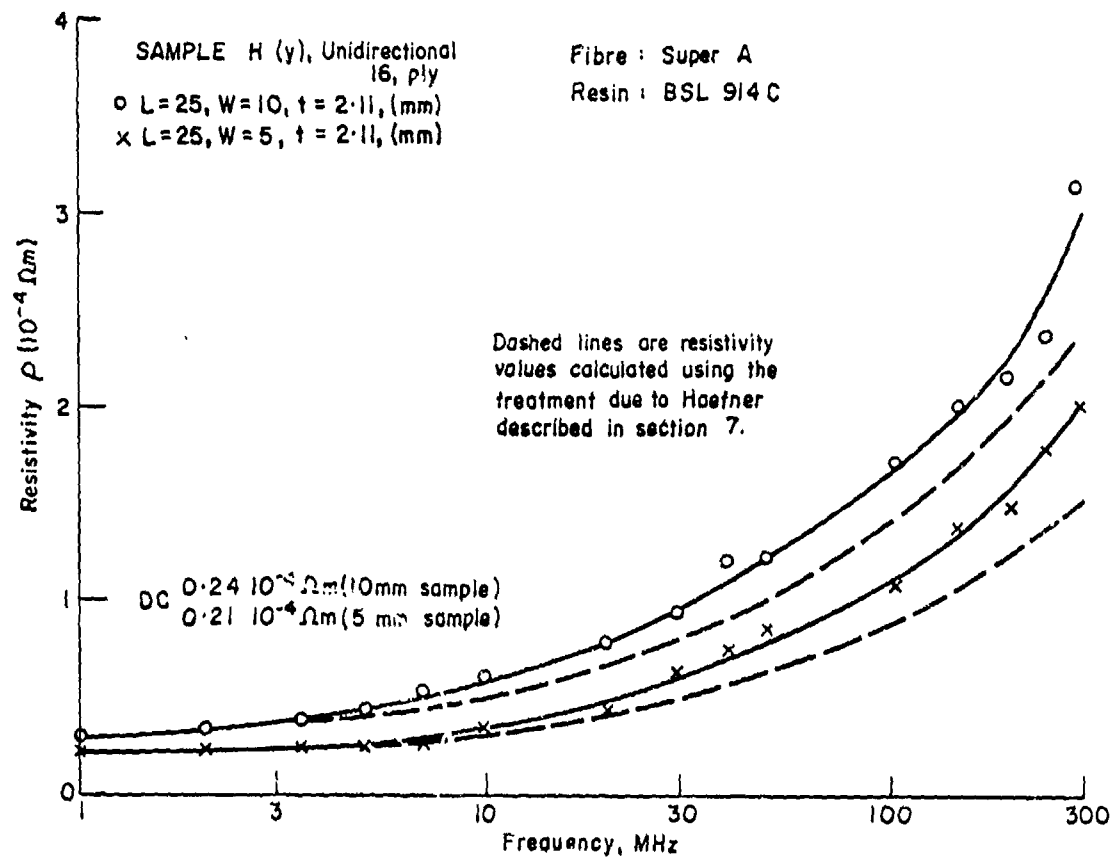


Fig.6 Typical resistivity-frequency characteristics

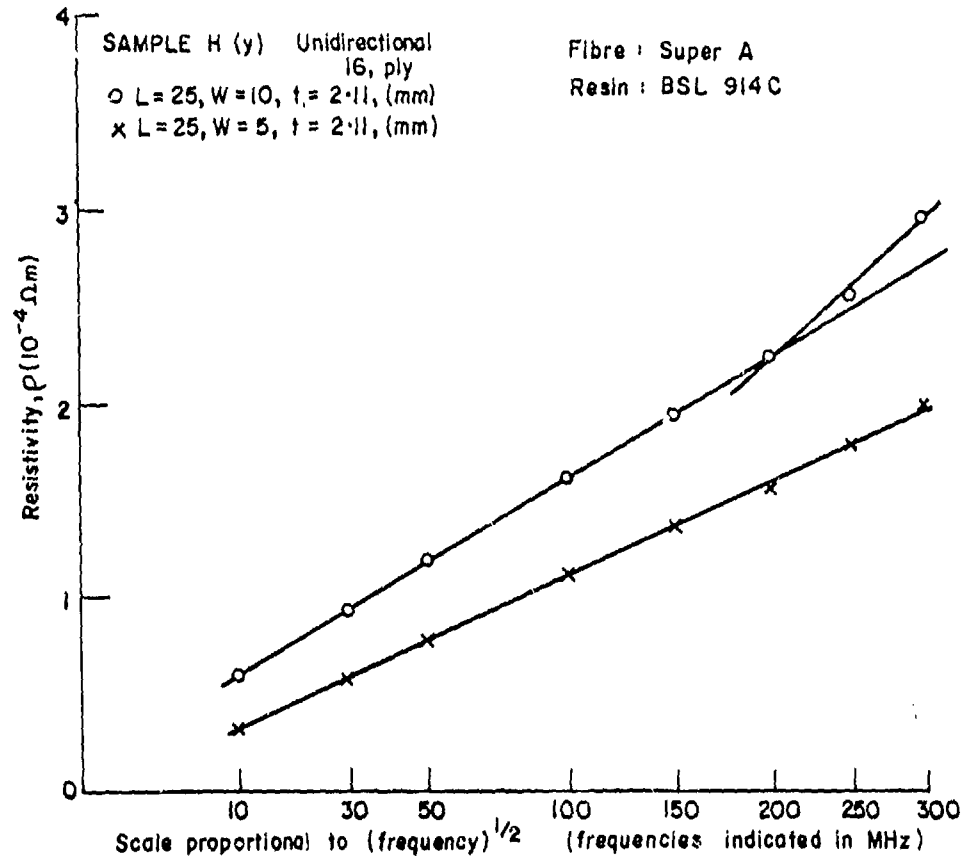


Fig.6(a) Typical resistivity-frequency characteristics

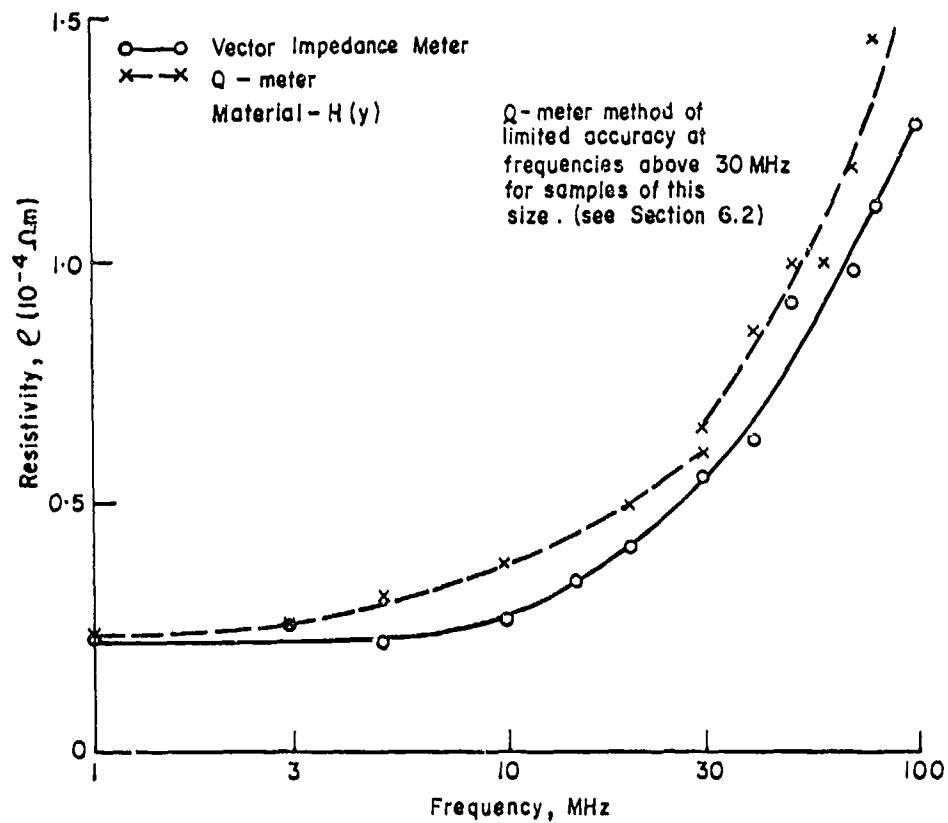


Fig.7 Transmission line sample 200mm x 12mm x 2.11mm (see figure 4) — resistivity measurements by vector impedance meter compared with those obtained using Q-meter

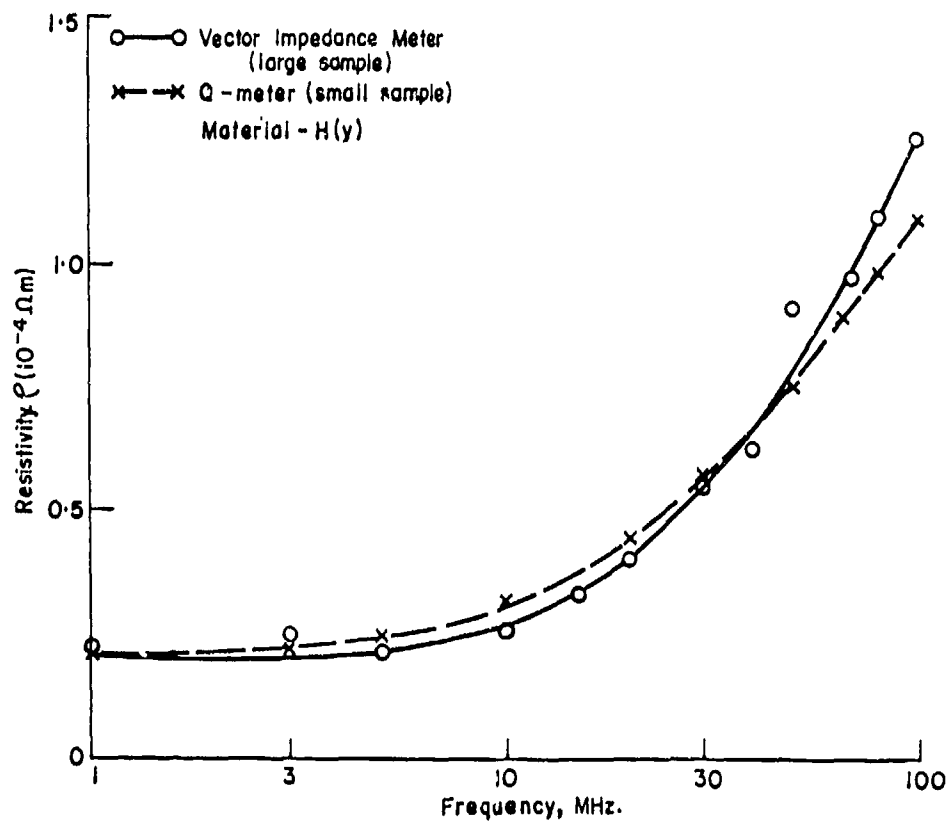


Fig.8 Transmission line sample 200mm x 12mm x 2.11mm (see figure 4) — resistivity by vector impedance meter, compared with measurements by Q-meter using 25mm x 5mm x 2.11mm samples of figure 6

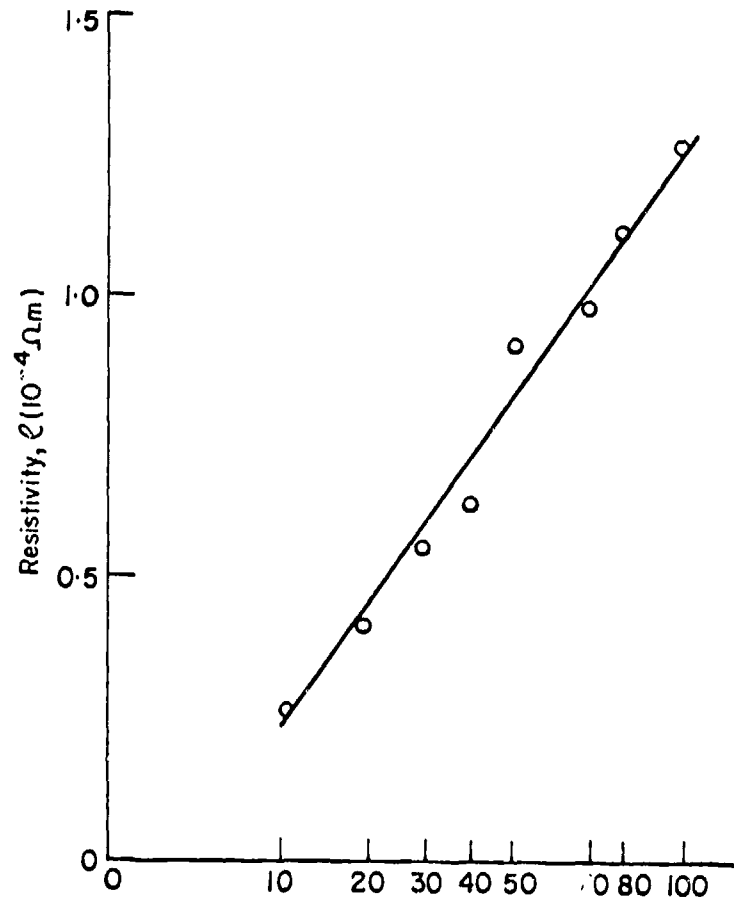
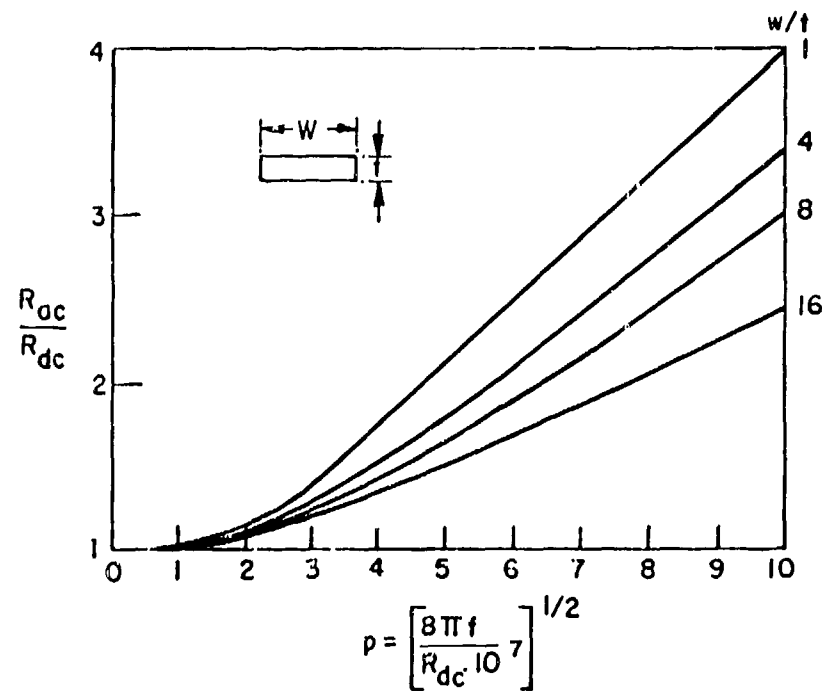


Fig.9 Transmission line sample 200mm x 12mm x 2.11mm. Resistivity measurements by vector impedance meter plotted against scale proportional to $(\text{frequency})^{1/2}$ (frequencies indicated in MHz)



f = frequency in Hz

R_{dc} = resistance of conductor in ohms per metre (direct current)

Fig.10 Resistance ratio for conductor of rectangular cross-section in terms of parameter p

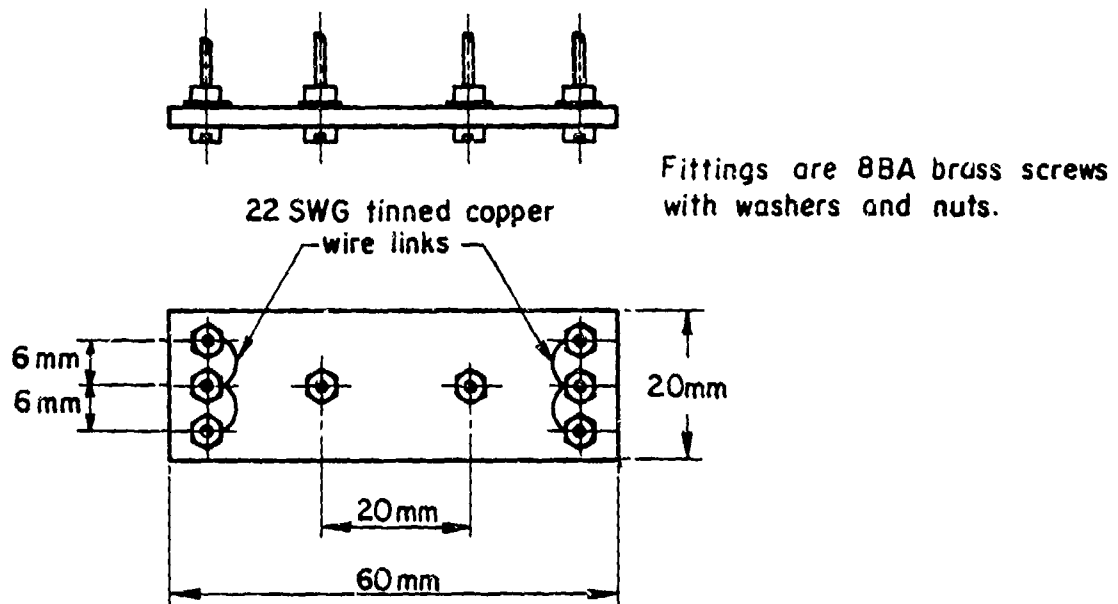


Fig.11 Samples for fluid immersion tests

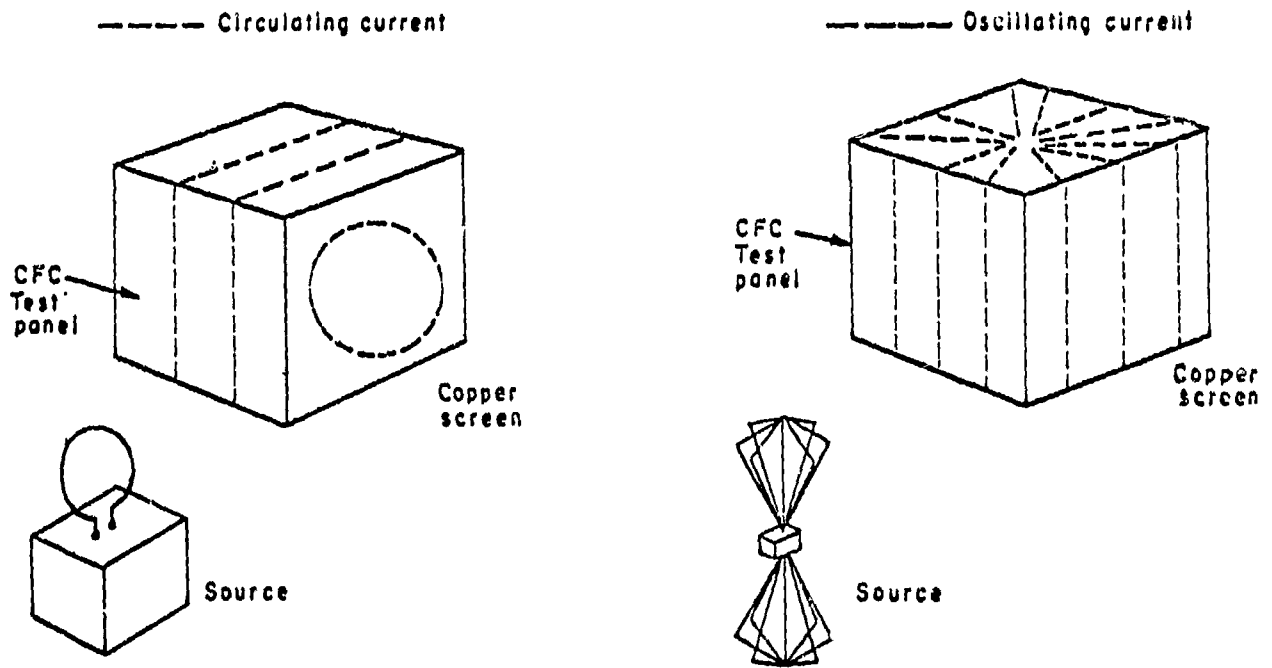


Fig.12 Patterns of current flow

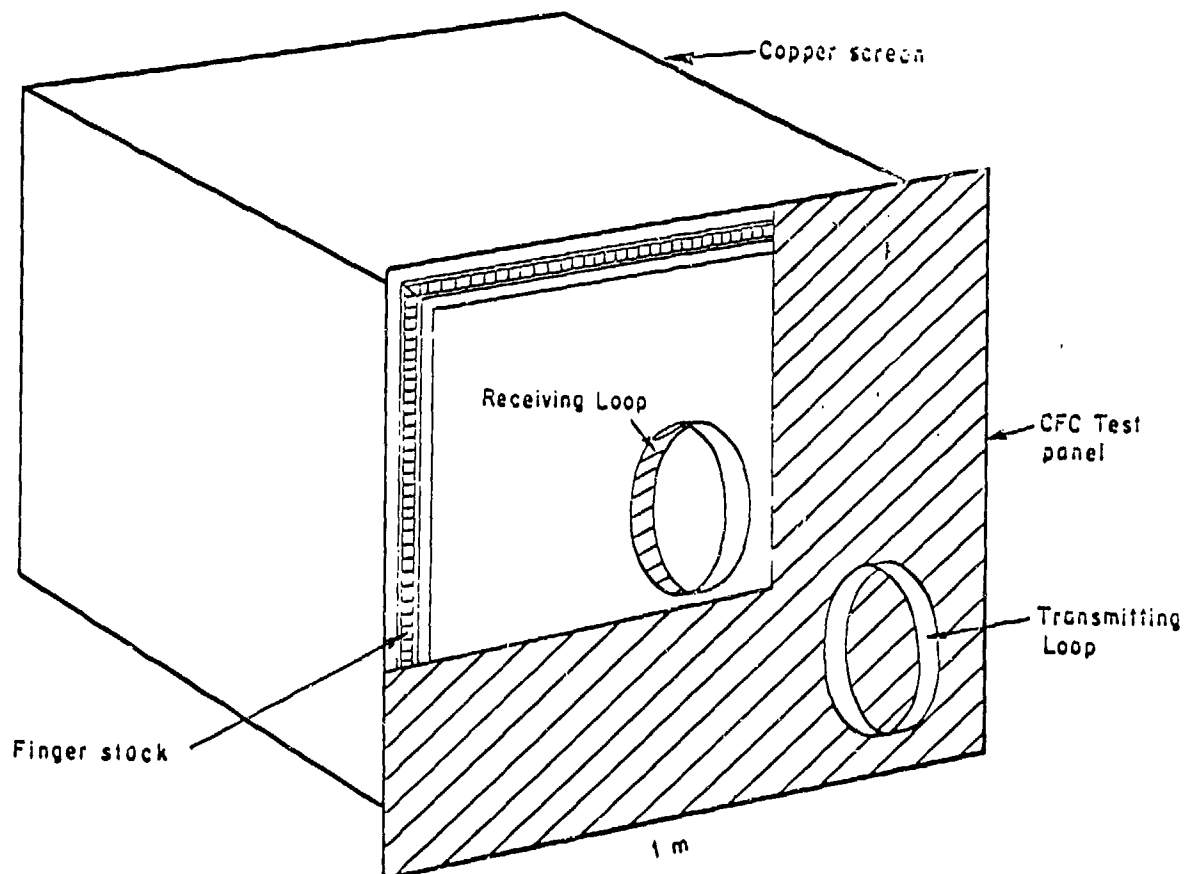


Fig.13 Experimental arrangement. (Loops coplanar)

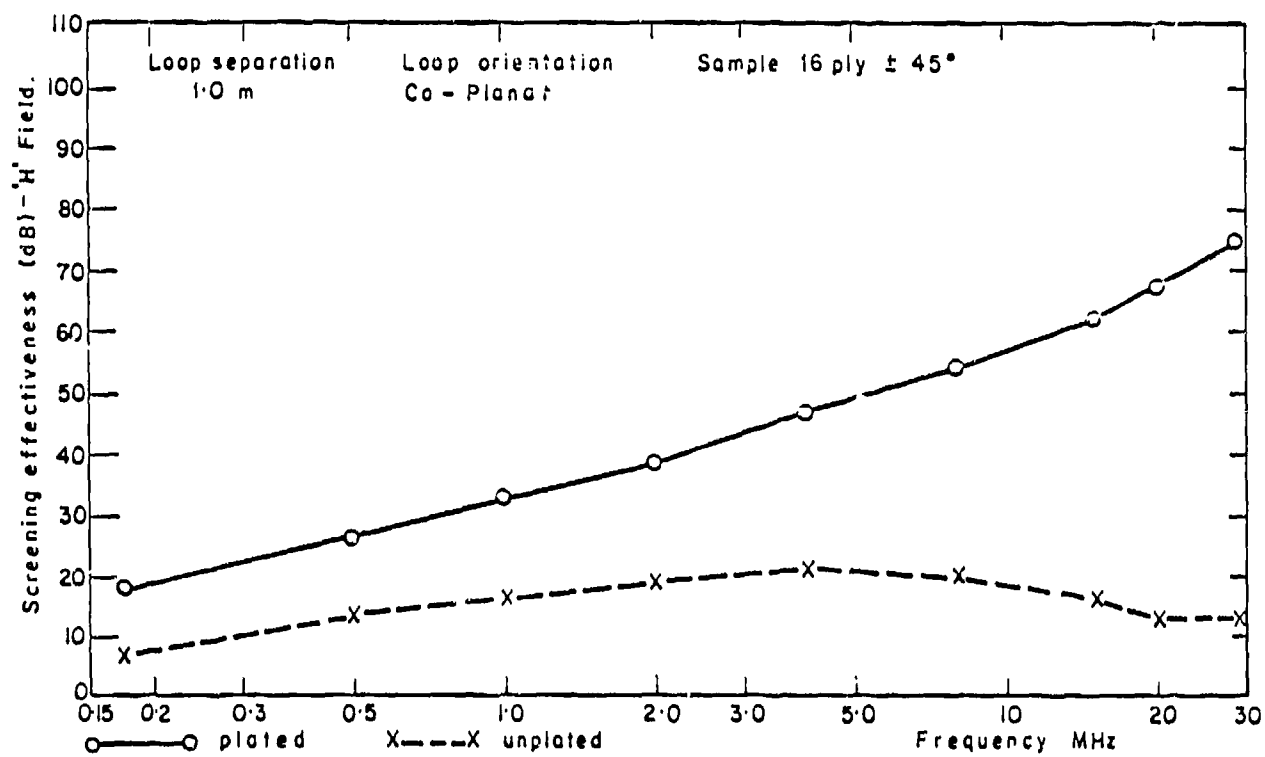


Fig.14 Magnetic attenuation

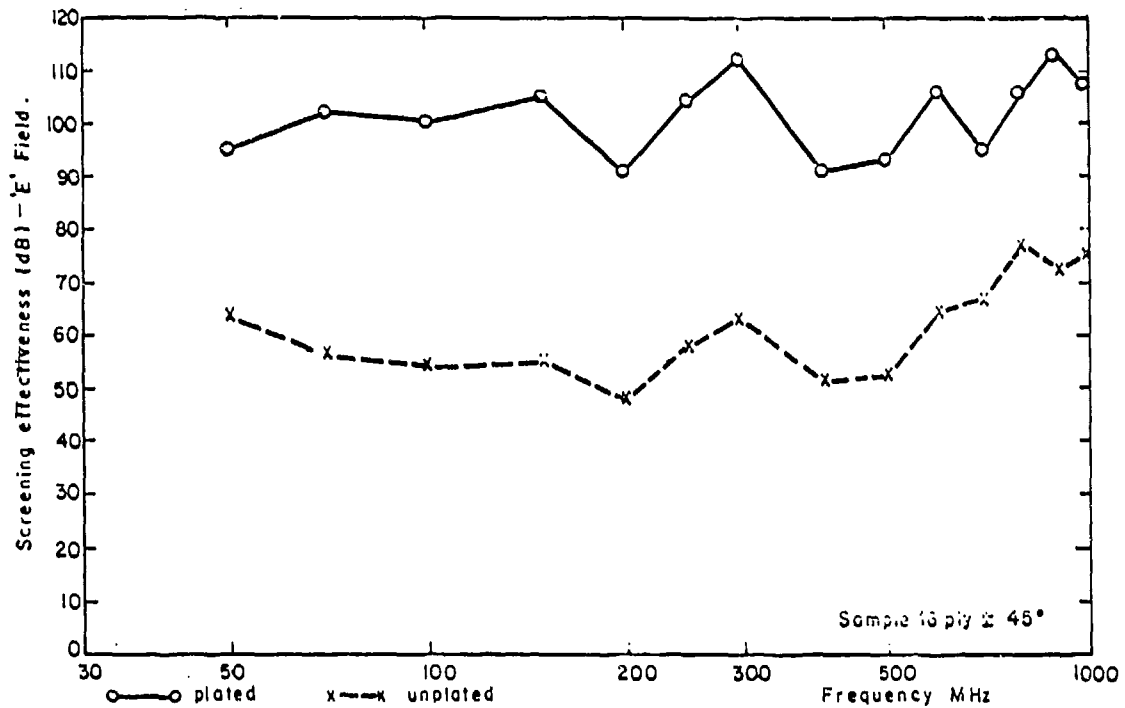


Fig. 15 Electric attenuation

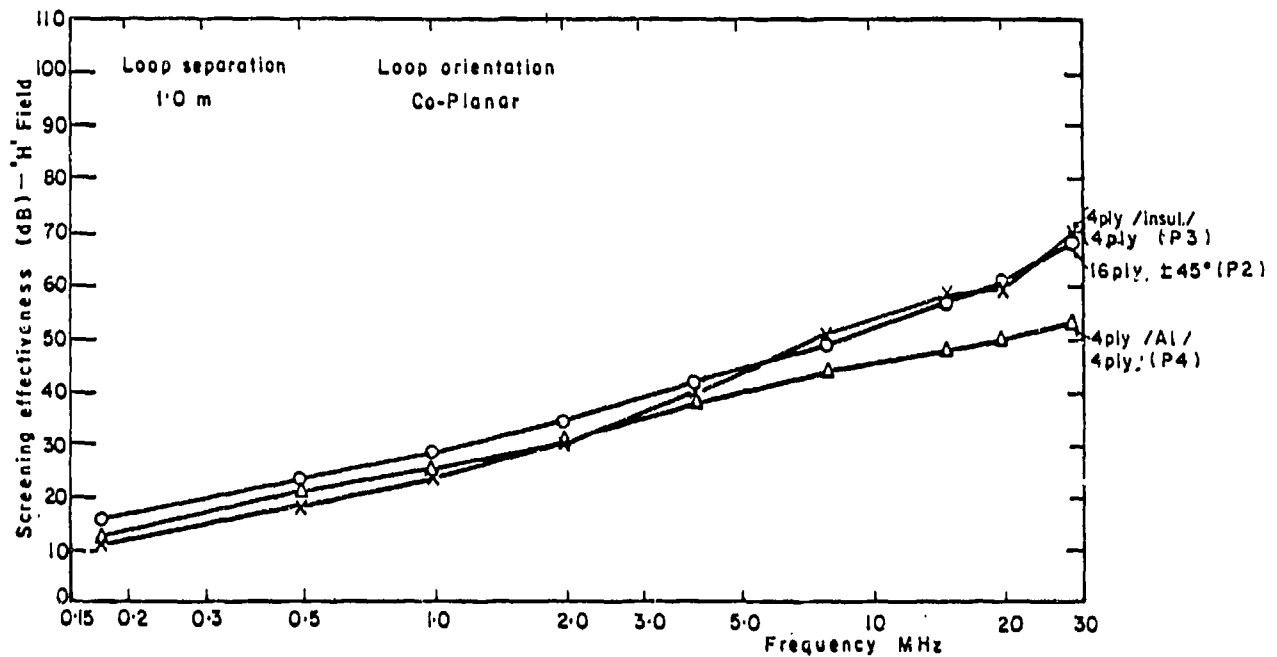


Fig. 16 Magnetic attenuation

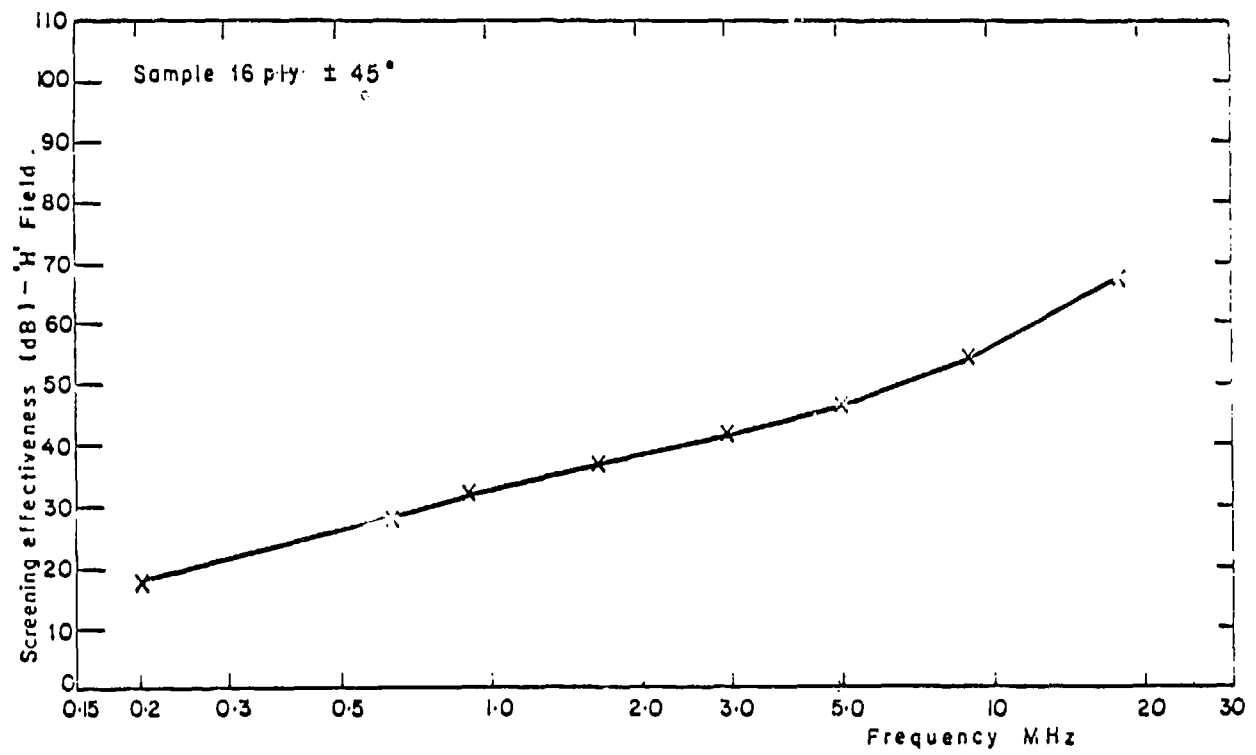


Fig.17 Magnetic attenuation - far field source

THE MEASUREMENT OF ELECTRICAL CONDUCTIVITY IN
CARBON/EPOXY COMPOSITE MATERIALS OVER THE
FREQUENCY RANGE OF 75 MHZ TO 2.0 GHZ

W. F. Walker
Electrical Engineering Department
Rochester Institute of Technology
Rochester, N.Y. 14623, U.S.A.

SUMMARY

A stripline technique for the measurement of longitudinal and transverse conductivity of graphite (carbon)/epoxy composite materials over the VHF/UHF (75 MHz to 2.0 GHz range) is described. The method is unusual in that it is essentially free of the uncertain effects of contact resistance between the sample and the measurement apparatus. The underlying theory of the method rests on the relationship between the conductivity of the sample and the lossy standing wave patterns established on the strip transmission line. The essentials of this theory are presented in the paper.

In addition to the presentation of the theory behind the method, the paper includes illustrations of experimental models of the test transmission line. Longitudinal and transverse conductivity measurements on graphite/epoxy are also presented as well as longitudinal measurements of boron/epoxy and aluminum in the 1.0 GHz to 2.0 GHz range.

1. INTRODUCTION

Any technique for the measurement of conductivity of carbon/epoxy composite materials over the 75 MHz to 2.0 GHz frequency range must contend with three major constraining conditions:

- a) Spurious contact resistance between the carbon/epoxy sample and the measurement apparatus must not interfere with the accuracy of measurement.
- b) The dimensions (in wavelengths) of the samples will be such that field and wave analysis methods will be required rather than "lumped circuit" analysis methods.
- c) Methods based on large-sheet, plane wave excitation at normal incidence will be impractical in all but the largest anechoic facilities.

The slotted strip-line method described here was devised with these conditions upper-most in mind.

2. THE SLOTTED STRIPLINE TEST APPARATUS

The basic geometry of the slotted stripline composite material tester is shown in Figure 2-1. The line is driven from a Radio Frequency (RF) generator at one end and left "open-circuited" at the other. The finite conductivity of the composite conductor produces dissipative voltage-standing-wave-patterns along the transmission line which are sensed by the probe. The E-Field squared-magnitude $|E^2|$ is then given by:

$$|E^2| = K[\cosh(2\alpha x + 2u) + \cos(2\beta x + 2\phi)] \quad (2-1)$$

where, K = a "gain constant" in (volts/meter)² depending upon source strength.

x = distance (meters) from the line end opposite the source.

α = real part (nepers/meter) of the propagation factor, γ .

β = imaginary part (radians/meter) of the propagation factor.

$\gamma = \alpha + j\beta$ = complex propagation factor along the line.

u = a "termination factor" (nepers) - equal to zero for a pure open-circuit termination.

ϕ = a "termination factor" (radians) equal to zero for a pure open-circuit termination.

A schematic representation of the test circuit and sketch of a typical lossy-line standing wave pattern are given in Figure 2-2. In the measurement of a sample, the squared-voltage-standing-wave-pattern is plotted and the parameters α , and β , are readily determined from this plotted data.

In samples of high conductivity along the axis of the slotted line (e.g. aluminum, carbon/epoxy and boron/epoxy with fibers parallel to the line axis) the skin depth is very small compared to the sample thickness. The admittivity $|\hat{Y}| = |\sigma_c + j\omega\epsilon_c|$ of these samples in the direction of propagation along the line is then given by:

$$|\hat{Y}| = |\sigma_c + j\omega\epsilon_c| = \frac{\omega\epsilon_d\beta_0^2}{\{[\alpha^2 - \beta^2 + \beta_0^2]^2 + 4\alpha^2\beta^2\}^{1/2}} \quad \text{mhos/meter} \quad (2-2)$$

where ω = operating radian frequency

ϵ_d = permittivity of the dielectric

$$\beta_o^2 = \omega^2 \mu_o \epsilon_d$$

μ_o = permeability of free space = $4\pi \times 10^{-7}$ $\frac{\text{henries}}{\text{meter}}$

a = thickness of the dielectric spacer in meters

In the frequency band reported here, the permittivity ϵ_c of the carbon/epoxy specimen is of the order of that of the epoxy alone with the result^c that $\sigma_c \gg \omega \epsilon_c$ and therefore $|\hat{\gamma}| \approx \sigma_c$.

3. OUTLINE OF THE UNDERLYING THEORY

3.1 Samples of High Conductivity

In the case of a unidirectional carbon fiber composite sample with fibers parallel to the slotted line axis, equation (2-2) has been used to relate sample admittance to the propagation parameters (α and β) on the line. In this case, the skin depth (depth of field penetration into the sample) is sufficiently small so that the line may be modelled as shown in Figure 3-1. The essential structure consists of a lossy (i.e. the composite) "half-space" facing a pure conducting "half-space" (aluminum) with a separating layer of dielectric (permittivity ϵ_d). The wave propagating along the line is then a "quasi TEM" sinusoidal wave propagating in the dielectric between the two half-spaces. This field geometry has been analyzed in the literature (Ramo, Whinnery, Van Duzer, 1967).

Ramo, Whinnery, and Van Duzer define three propagation constants, (γ , K_c and K_d) which characterize sinusoidal field behavior in "quasi-TEM" waves propagating^c between the two half-spaces of Figure 3-1.

$\gamma = \alpha + j\beta$ = complex propagation factor in the direction parallel to the plates

$K_c^2 = \gamma^2 + \omega^2 \mu_o \epsilon_c = (\text{propagation factor})^2$ in the lossy material in the direction normal to the plate surfaces

$K_d^2 = \gamma^2 + \omega^2 \mu_o \epsilon_d = (\text{propagation factor})^2$ in the dielectric between the plates in a direction normal to the plate surfaces.

The parameters ϵ_c , ϵ_d , μ_o and ω are:

ϵ_c = complex permittivity of the lossy material (F/m)

ϵ_d = permittivity of the dielectric (real) (F/m)

$\mu_o = 4\pi \times 10^{-7}$ henries/meter

ω = radian frequency of the propagation wave.

Equation (7), p. 381 of Ramo, Whinnery and Van Duzer relates these parameters to the geometry of Figure 3-1 (b) as

$$\tan(k_d a) = j \frac{k_c \epsilon_d}{k_d \epsilon_c} \quad (3-1)$$

This equation results from matching boundary conditions on the E and H fields at the interface between the lossy plates and the dielectric. "a" is equal to the spacing in Figure (3-1) (a) (and in the slotted line).

In the case of a lossy material such as the composites, the complex permittivity ϵ_c for the composite material can be expressed:

$$\epsilon_c = \epsilon_o k'_c + \frac{\sigma_c}{j\omega} \quad (3-2)$$

where, $\epsilon_o = 8.85 \times 10^{-12}$ farad/meter

k'_c = real part of the composite material dielectric constant (dimensionless)

σ_c = conductivity of the composite material in the direction of propagation (mhos/m)

For graphite/epoxy and boron/epoxy with fibers running in the direction of propagation, it may be anticipated that the losses will be relatively low in the stripline so that γ will be very nearly that for lossless boundaries. That is,

$$\gamma^2 \approx -\omega^2 \mu_o \epsilon_d \quad (3-3)$$

Then since,

$$K_d^2 = \gamma^2 + \omega^2 \mu_0 \epsilon_d \quad (3-4)$$

it will be true that,

$$|K_d^2| \ll \omega^2 \mu_0 \epsilon_d \quad (3-5)$$

With a small dielectric thickness "a", therefore, the term $(K_d a)$ will be much less than unity and the left hand side of equation (3-1) may be approximated by

$$\tan(K_d a) \approx K_d a \quad (3-6)$$

and there results,

$$K_d a \approx \frac{jK_c \epsilon_d}{K_d \epsilon_c} = \frac{-\omega \epsilon_d K_c}{j\omega \epsilon_c K_d} \quad (3-7)$$

or

$$K_d^2 a = \frac{\omega \epsilon_d K_c}{j\omega \epsilon_c} \quad (3-8)$$

Recalling that ϵ_c is complex, the term $(j\omega \epsilon_c)$ is the "admittivity" of the composite material and may be written

$$j\omega \epsilon_c = (\sigma_c + j\omega \epsilon_0 k'_c) \quad (3-9)$$

Equation (3-8) then becomes,

$$K_d^2 a = \frac{-\omega \epsilon_d K_c}{(\sigma_c + j\omega \epsilon_0 k'_c)} \quad (3-9)$$

Now, recall that $K_c^2 = \gamma^2 + \omega^2 \mu_0 \epsilon_c = \gamma^2 - j\omega \mu_0 (\sigma_c + j\omega \epsilon_0 k'_c)$, so that even for $\sigma_c \approx 1$ mho/meter, $K_c^2 \approx -j\omega \mu_0 (\sigma_c + j\omega \epsilon_0 k'_c)$ for frequencies up through 10^{11} Hz. Using this approximation and squaring equation (3-9) yields,

$$K_d^4 a^2 = \frac{(-j\omega \mu_0) \omega^2 \epsilon_d^2}{(\sigma_c + j\omega \epsilon_0 k'_c)^2} \quad (3-10)$$

The term K_d^4 may be expressed in terms of the real and imaginary parts of the propagation factor, γ , where $\gamma = \alpha + j\beta$. That is,

$$K_d^2 = \gamma^2 + \omega^2 \mu_0 \epsilon_d = (\alpha^2 + \omega^2 \mu_0 \epsilon_d - \beta^2) + j2\alpha\beta \quad (3-11)$$

Then the complex admittivity of the composite slab may be expressed as:

$$\hat{Y}_c = (\sigma_c + j\omega \epsilon_0 k'_c) = \frac{(-j\omega \epsilon_0) \omega^2 \epsilon_d^2}{K_d^4 a^2} \quad (3-12)$$

Equations (3-11) and (3-12) from the basis of the use of the slotted stripline for the measurement of composite material admittivity. By measuring the lossy standing wave pattern along the line, the real (α) and imaginary (β) parts of the propagation factor, γ , may be determined, and these, together with a knowledge of the dielectric material (ϵ_d), and "a", and the frequency, may be used in equations (3-11) and (3-12) to determine $(\sigma_c + j\omega \epsilon_0 k'_c)$.

In a practical example involving graphite/epoxy composites with unidirectional fibers running parallel to the direction of propagation, the following inequalities among α , β , and β_0 generally hold:

- β^2 is larger than β_0^2 but of the same order of magnitude
- $\beta_0^2 \gg \alpha^2$, where $\beta_0^2 = \omega^2 \mu_0 \epsilon_d$.

The result is that the angle of complex number K_d^4 in equation (3-12) is very sensitive to small percentage variations in the measurement of α or β . Correspondingly, the angle ascribed to $(\sigma_c + j\omega \epsilon_c)$ by the measurement process may be questionable. However, the magnitude of the admittivity of the sample $|\sigma_c + j\omega \epsilon_c|$ will be given to about the same accuracy as the measurement accuracy of α and β individually.

The procedure described above was used in all cases reported here except the case of a carbon/epoxy sample with unidirectional fibers transverse to the direction of propagation along the line. In this case the conductivity of the sample in the direction of line propagation (transverse to the fibers) is sufficiently low and the skin-depth sufficiently deep to permit the assumption of uniform current distribution over the cross-section of the sample. Under these circumstances the line can be modelled as a simple transmission line, as in Figure 3-2. For this model:

$$\begin{aligned} L &\approx \mu_0 \frac{a}{w} \\ C &\approx \epsilon_d \frac{w}{a} \\ R &\approx \frac{1}{\sigma w t} \end{aligned} \quad (3-13)$$

where a , t , and w are as indicated in Figure 3-2. μ_0 and ϵ_d are the permeability of free space and the permittivity of the dielectric spacer, respectively.

The line impedance z , and admittance y , per unit length are then,

$$\begin{aligned} z &= R + j\omega L \quad \text{ohms/meter} \\ y &= j\omega C \quad \text{mhos/meter} \end{aligned} \quad (3-14)$$

Accordingly, the propagation factor γ , will be:

$$\begin{aligned} \gamma &= \pm \sqrt{zy} = (R + j\omega L) (j\omega C) \\ &\approx \pm j\omega RC = \pm (1 + j) \frac{\omega RC}{2} \quad \text{for } R \gg \omega L \end{aligned} \quad (3-15)$$

and

$$\alpha \approx \frac{\omega RC}{2} \quad (3-16)$$

Equations (3-16) and (3-13) can then be used to relate the attenuation constant α to the sample conductivity σ , giving

$$\sigma \approx \frac{\omega \epsilon_d}{2\alpha^2 t a} \quad (3-17)$$

For this case, only the attenuation constant need be evaluated from the standing wave data.

4. DETAILS OF THE EXPERIMENTAL LINE

4.1 The "Six-Foot" Line

Two experimental lines were built and tested with carbon/epoxy, boron/epoxy, and aluminum test samples. One line (used at lower frequencies) was approximately 6 feet long and is shown (without the test sample in Figure 4-1). A cross-sectional view of the line with the test sample in place is shown in Figure 4-2. Excitation to the line is obtained by contact between the center conductor of a coaxial line with a beveled end of the test sample which has been covered with conducting paint (see Figure 4-3). Figures 4-4, 4-5, 4-6 show several "exposed" views of construction of the experimental six-foot line. Figure 4-7 shows the probe carriage, slab turner and detector assembly (essentially adapted from a General Radio 874-LSA coaxial line probe carriage).

4.2 The "10-Inch" Line

An earlier 10-inch line is shown in Figure 4-8 which used a slotted section of X-band (3cm.) wave guide as the outer conductor.

5. TYPICAL DATA AND CONDUCTIVITY RESULTS

Figure 5-1 shows a representative standing wave pattern (i.e., $|E^2|$ vs "x") obtained for a longitudinal, unidirectional carbon/epoxy sample measured at 300 MHz on the six-foot line. The lossy standing wave pattern is clearly evident. Wavelength, λ_g , on the line is readily measured (as indicated) from the cyclic nature of the pattern at the "open" end of the plot. The phase constant β_g is then calculated as:

$$\beta_g = \frac{2\pi}{\lambda_g} \quad (5-1)$$

The broken line on the plot represents the sketched estimate of the term, $K \cosh(2\alpha y)$, where "y" is the distance in meters toward the generator from the "open circuit" end of the line (157 centimeters on the distance scale). Two widely separated points on this broken line can be used to solve for the gain constant K and the attenuation constant α as follows (see Figure 5-1):

we have,

$$H_1 \approx K \cosh(2\alpha y_1) \quad (5-2)$$

$$H_2 \approx K \cosh(2\alpha y_2).$$

Then

$$\cosh(2\alpha y_2) = \left(\frac{H_1}{H_2}\right) \cosh(2\alpha y_1). \quad (5-3)$$

This last transcendental equation is then solved iteratively on a pocket calculator to yield α . The conductivity, σ , is then evaluated according to equation (2-2), given previously. In the case of Figure 5-1, the results were:

$$\begin{aligned} \beta_g &\approx 8.89 \text{ radians/meter} \\ \alpha &\approx .80 \text{ nepers/meter} \\ \sigma &\approx 5.03 \times 10^4 \text{ mhos/meter} \end{aligned} \quad (5-4)$$

Figures 5-2, 5-3, 5-4, 5-5 show representative standing wave data for unidirectional carbon/epoxy samples at frequencies of 150 MHz, 300 MHz, 600 MHz, and 2.0 GHz, respectively. The calculated conductivity values based on these measurements were:

Frequency	Conductivity (mhos/meter)
150 MHz	6.9×10^4
300 MHz	5.03×10^4
600 MHz	2.22×10^4
2.0 GHz	3.01×10^3

Figure 5-7 shows a standing wave pattern taken at 1.2 GHz on an aluminum sample. The constant "through" depths indicated a conductivity of the order of 10^7 mhos/meter.

Figure 5-8 shows a standing wave pattern for a unidirectional boron/epoxy sample @ 2.0 GHz. The calculated conductivity was 7×10^4 mhos/meter in the direction of the fibers.

6. SUMMARY

The work reported here is perhaps best viewed as a fairly thorough demonstration of the feasibility of the slotted stripline method over a broad range of frequencies and sample conductivities. In the process, the measured results gave a clear indication of the areas in which the method could be improved to the level where consistently accurate results could be obtained routinely.

6.1 Results on Experimental Lines

The 10-Inch Line

This line was effective above 1.0 GHz where at least one full cycle of standing wave pattern was attainable. Furthermore the mechanical precision of the line provided classic lossy-standing-wave patterns at frequencies between 1.0 and 2.0 GHz. The detector probe on this line was untuned, however, which resulted in considerable loss of sensitivity. This loss was not serious in the case of the highly conductive graphite/epoxy and boron/epoxy longitudinal samples, but prevented extended pattern measurement in the case of the highly lossy transverse graphite/epoxy measurement. Tuning the probe would have greatly increased the detector output and also suppressed harmonics (if present) in the signal generator which could greatly contaminate the standing wave pattern.

Due to the short circumferential distance around the sample strip within this line, it could be used readily up to about 5.0 GHz without danger of higher propagating modes.

The Six-Foot Line

The six-foot line was highly effective from 75 MHz to 2.0 GHz. Its lack of mechanical precision, principally with regard to uniformity of cross-section caused some noticeable perturbation of the standing-wave pattern along the line. Its "carcass", however, was simply a slotted length of stock aluminum channel extrusion. In a line with a more rigid structure, machined with a precision consistent with standard slotted line instruments, these perturbations would not occur.

There still remained some spurious radiation from the slot which interacted with the probe carriage on the six-foot line. It is felt that this interaction could be substantially reduced by a deeper slot into which the inner and outer (shield) conductors of the probe could extend.

6.2 Recommendations for Refinement of the Method

Basic Line Cross-Section

A Sketch of a proposed improved line cross-section is shown in Figure 6-1. In comparing this with the cross-section of the experimental line, a number of features are worth emphasizing:

- a) The entire structure is more rigid. This, coupled with machining of the sample bed and probe carriage track will provide the uniformity in cross-

section necessary for pure lossy-line standing-wave patterns.

- b) The circumferential distance around the sample strip is reduced allowing for operation at higher frequencies.
- c) The slot is considerably deeper to better contain the field and shield the probe.

Probe Design

Two improvements are suggested in connection with the probe and its carriage.

- a) Take advantage of the shielding features of a deeper slot by carrying both the inner and outer conductors of the probe deeper into the slot. Probe depth adjustment should be retained, however.
- b) In any given band of operation, the tuning circuit for the probe should have a single adjustable resonant peak. Since the system itself is capable of operation over a broad band, this precaution prevents inadvertent tuning to signal harmonics, as is possible with "stub-tuning."

7. ACKNOWLEDGEMENTS

The work reported here was supported by the U.S. Air Force Rome Air Development Center. The work benefited greatly from the support and guidance of Dr. Roy F. Stratton, the RADC Project Engineer. This paper has drawn almost entirely on U.S. Air Force Reports: TR-78-56 and TR-79-255, where the work is first reported.

References

- 1- RADC-TR-78-156, "Electromagnetic Properties and Effects of Advanced Composite Materials: Measurement and Modeling", J. L. Allen, et al., June 1978.
- 2- RADC-TR-79-255, "Measurement of Electrical Conductivity in Carbon/Epoxy Composite Material over the Frequency Range 75 MHz to 2.0 GHz", W. F. Walker and R. E. Heintz, October 1979.
- 3- Ramo, S; Whinnery, J.; Van Duzer, T., 1965, "Fields and Waves in Communications Electronics", John Wiley & Sons.

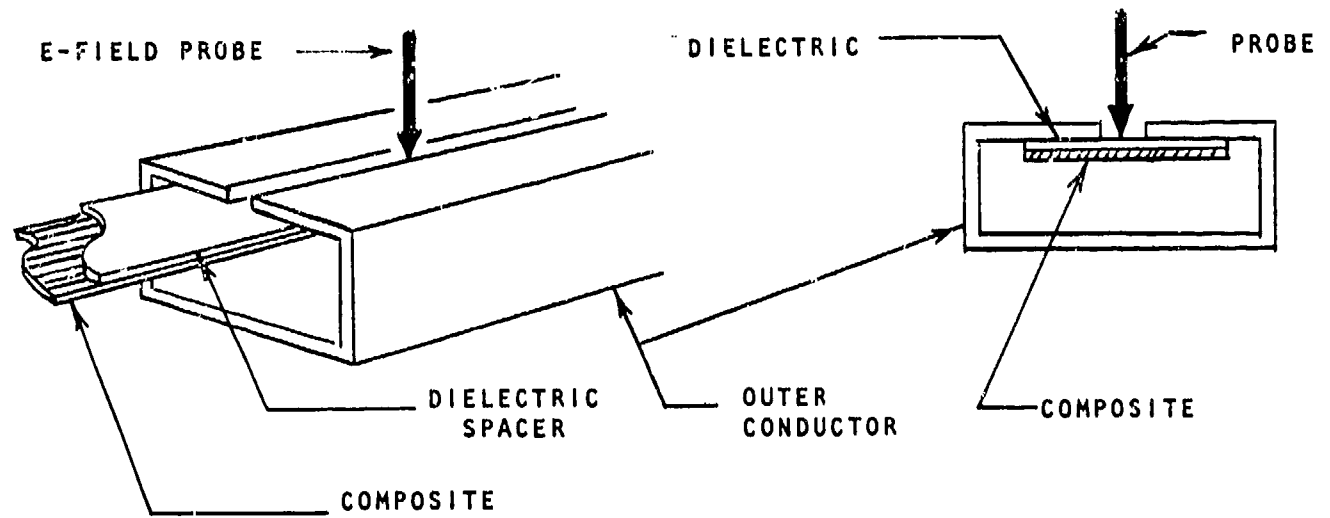
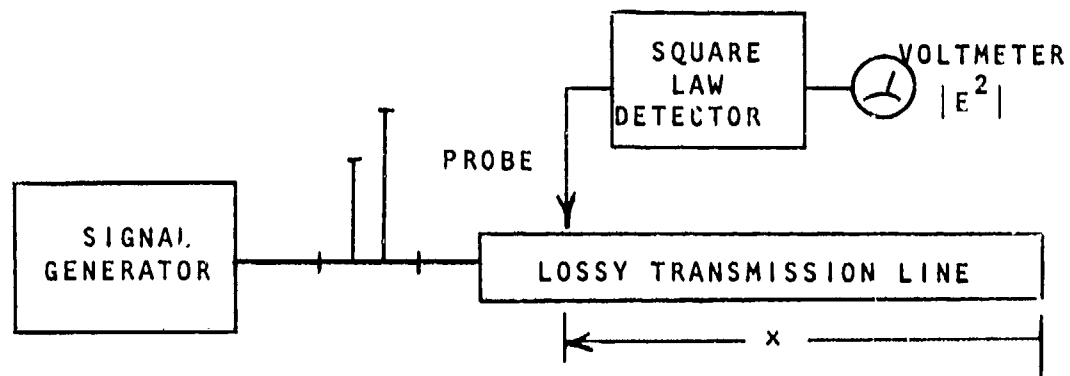
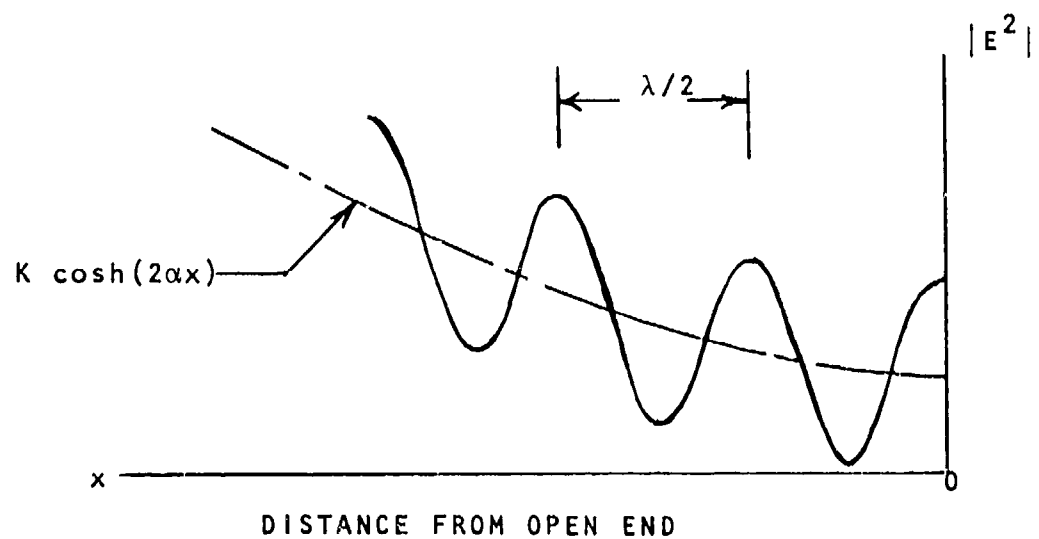


Fig.2-1 Slotted stripline geometry



a) EXPERIMENTAL BLOCK DIAGRAM



B) STANDING WAVE PATTERN

Fig.2-2 Measurement circuit and standing wave pattern

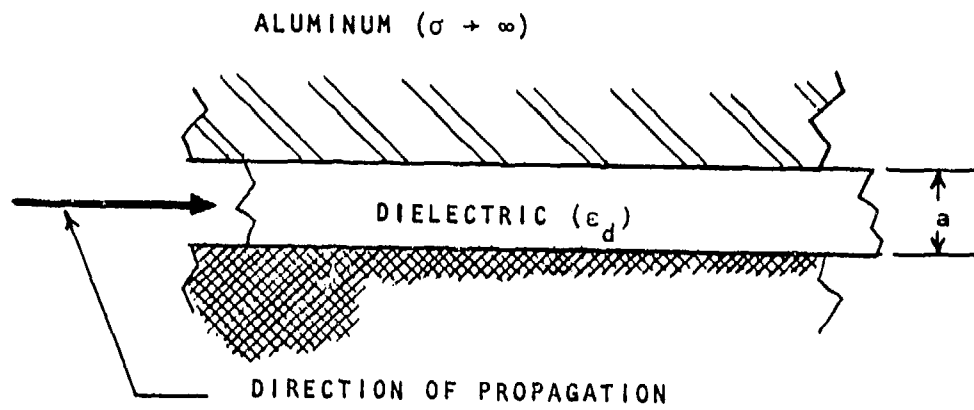
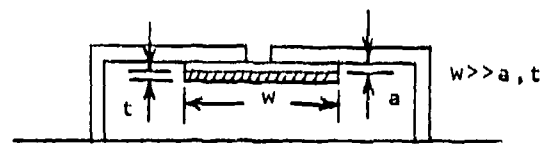
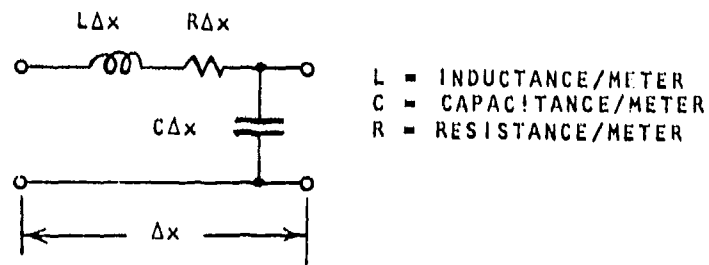


Fig. 3-1 Propagating field geometry



a) LINE CROSS-SECTION



b) DIFFERENTIAL LINE ELEMENT

Fig. 3-2 Low conductivity transmission line model

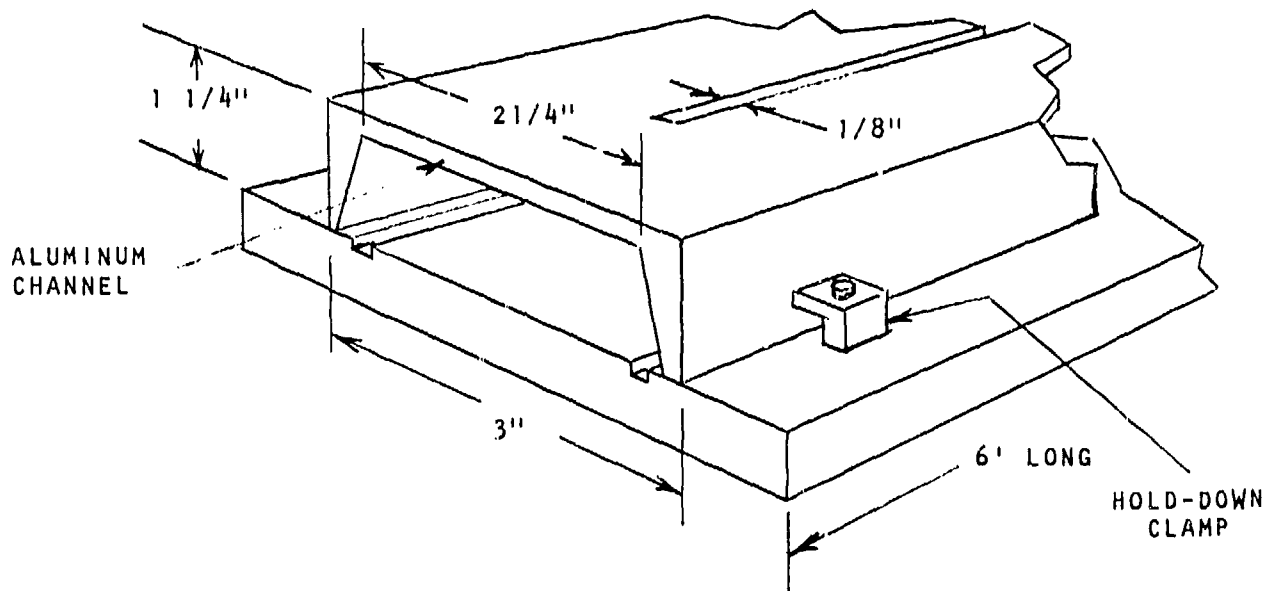


Fig. 4-1 Basic geometry of the six-foot line

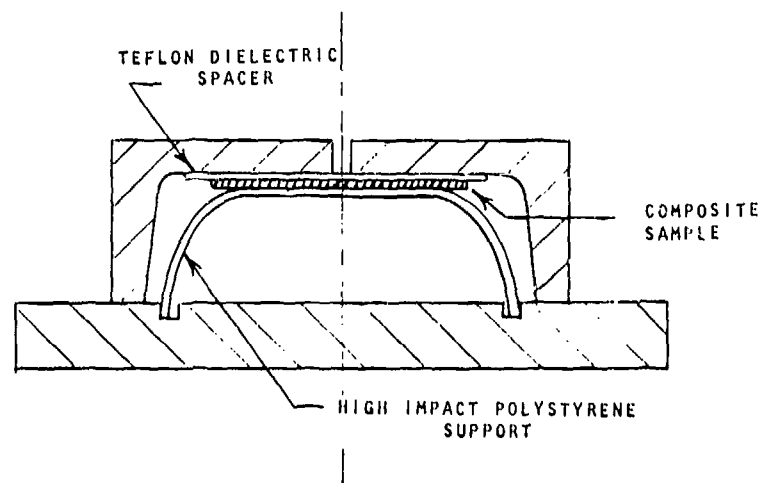


Fig.4-2 Cross-section of the six-foot line

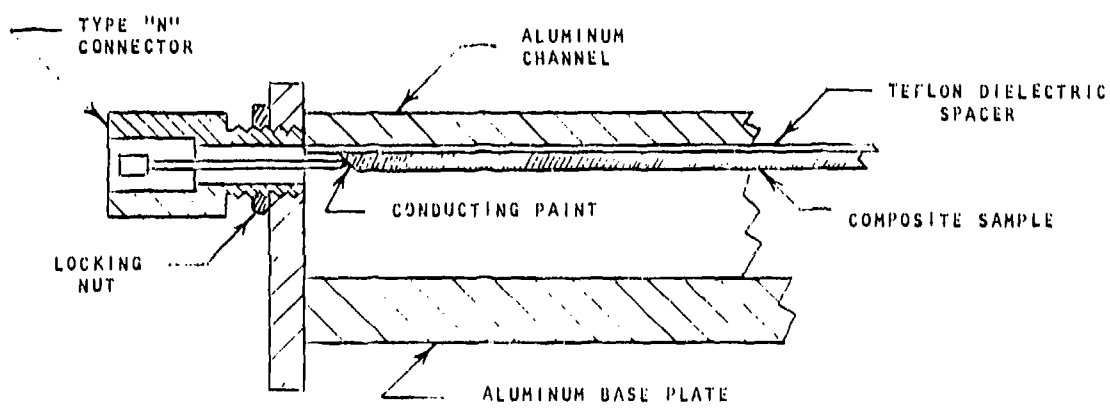


Fig.4-3 Excitation of the six-foot line

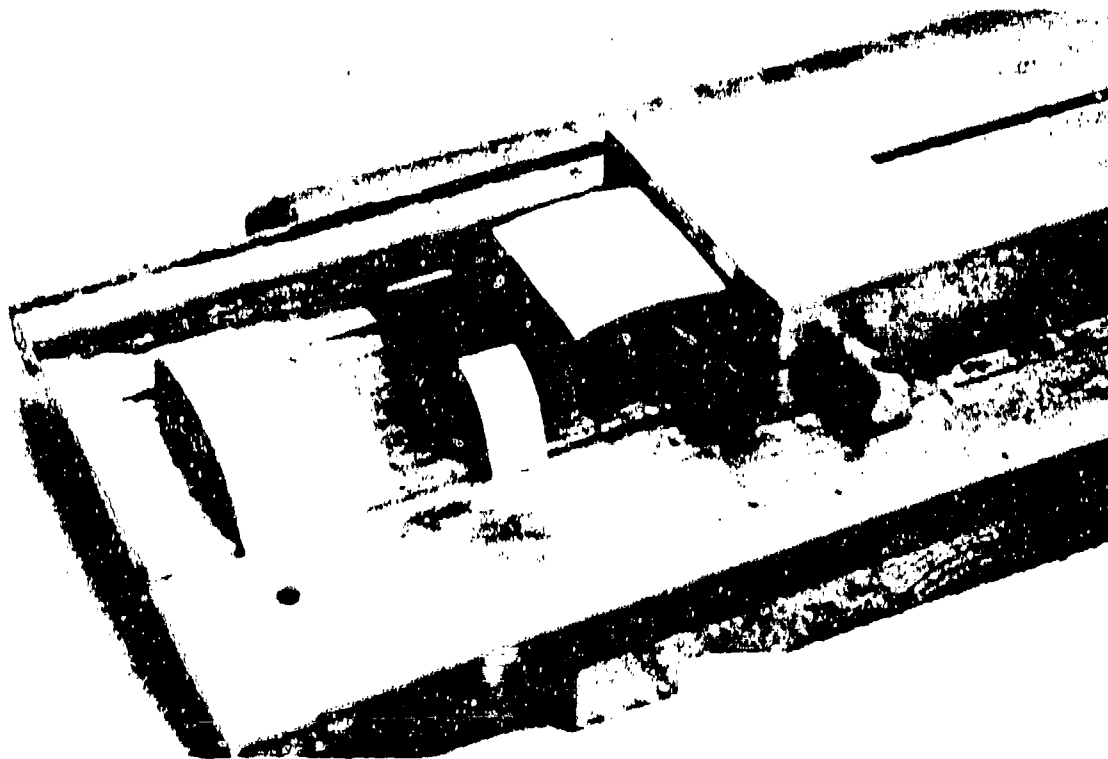


Fig.4-4 "Exposed" view of six-foot line with composite center conductor

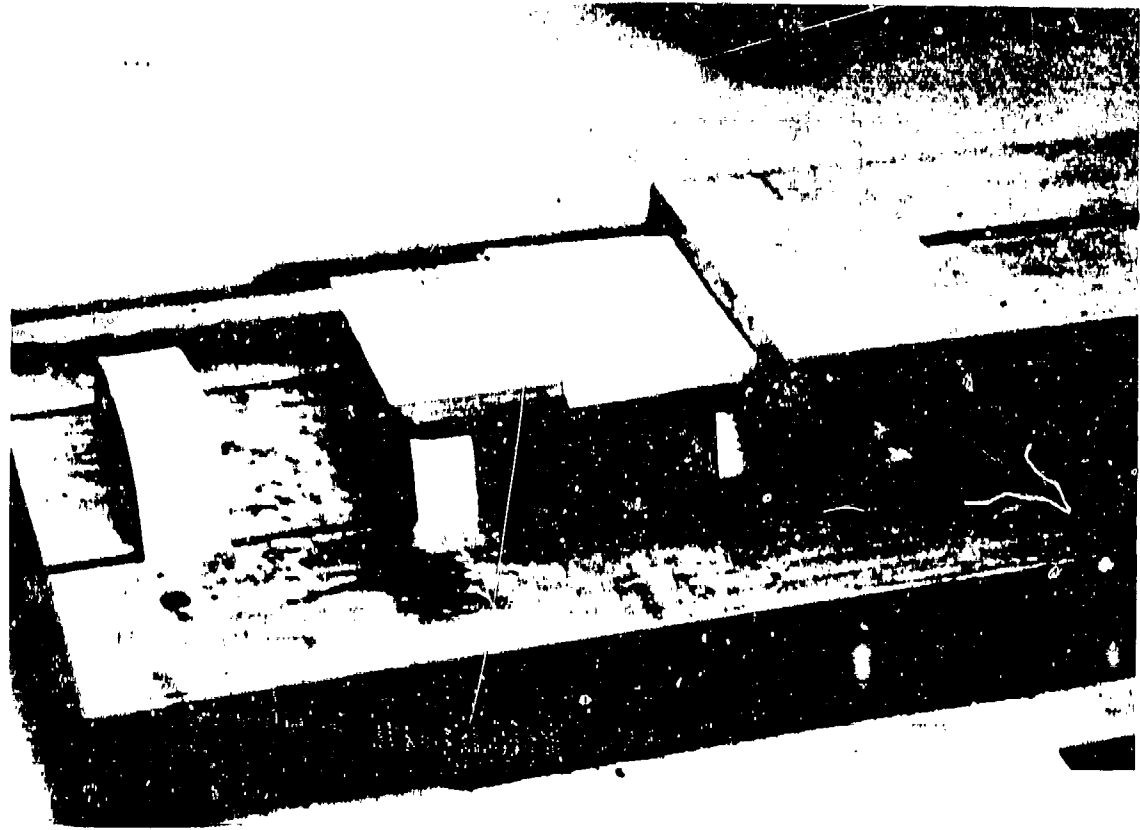


Fig.4-5 "Exposed" view of six-foot line with aluminum center conductor

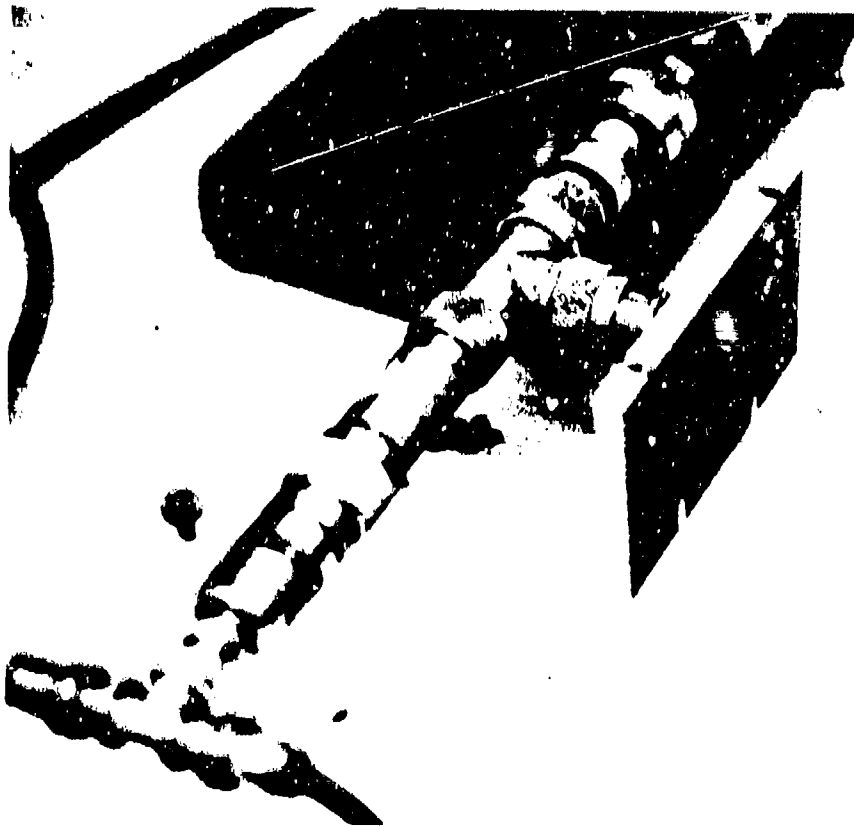


Fig.4-6 End plate and coaxial connector for the six-foot line

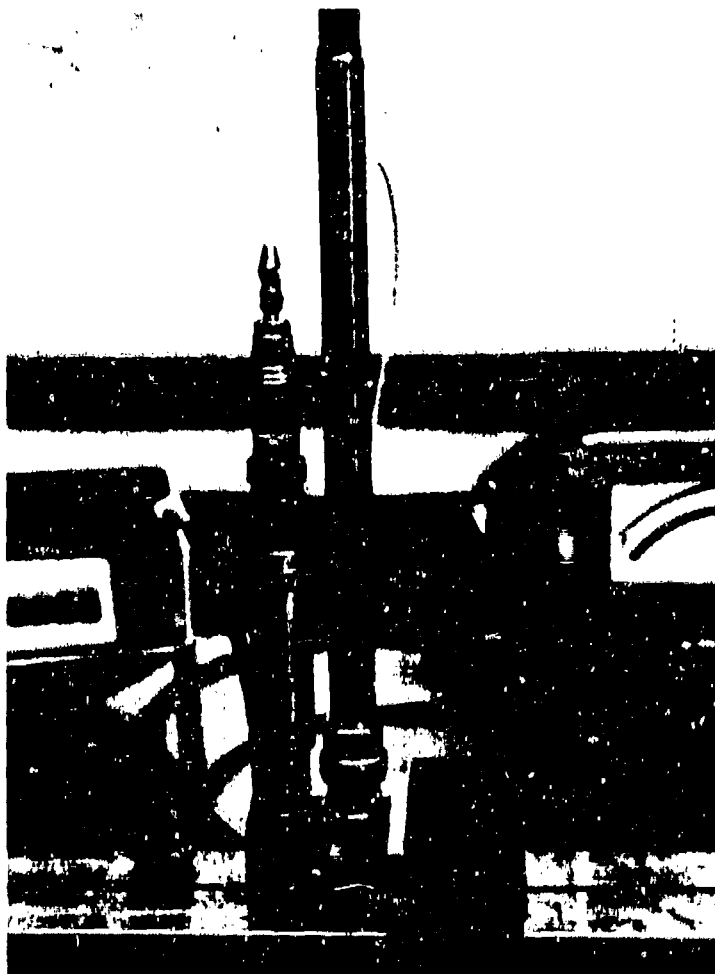


Fig.4-7 Probe carriage assembly for the six-foot line



Fig.4-8 "Exposed" view of the ten-inch slotted line
with composite sample

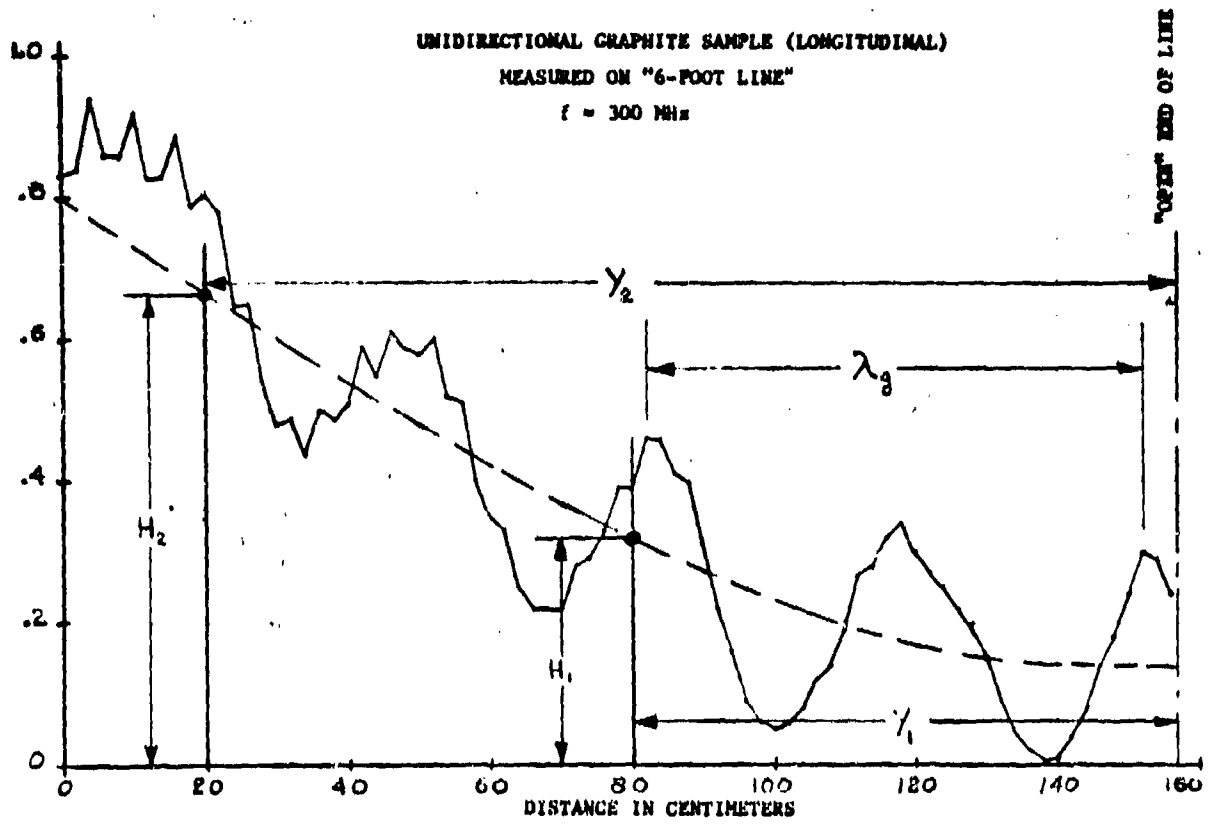


Fig.5-1 Standing wave pattern @ 300 MHz for longitudinal unidirectional graphite/epoxy sample

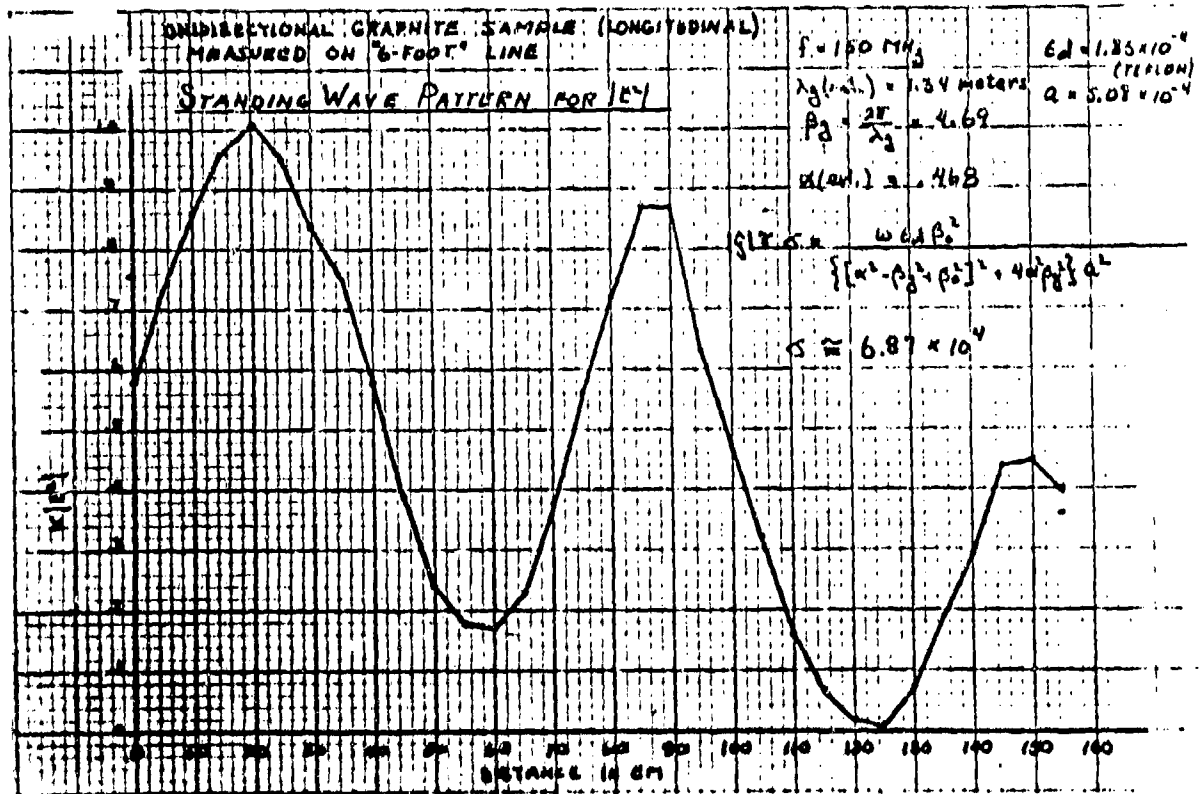


Fig.5-2 Standing wave pattern @ 150 MHz for longitudinal unidirectional graphite/epoxy sample

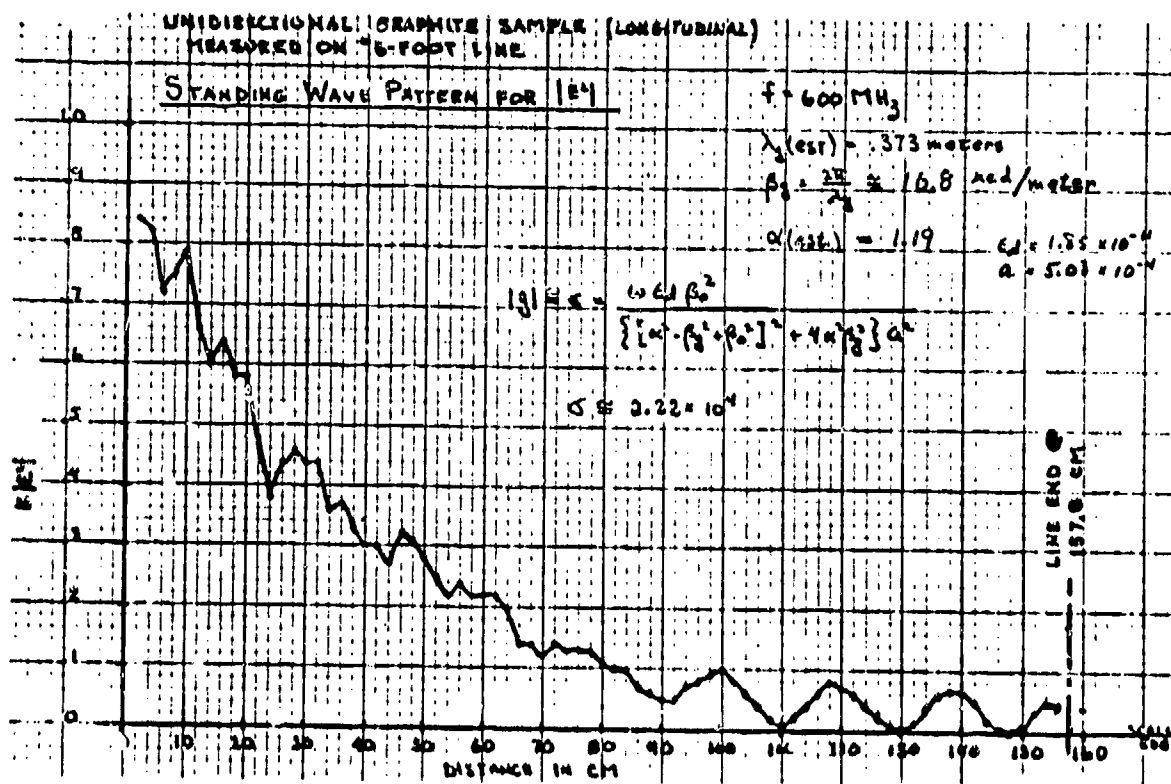


Fig.5-3 Standing wave pattern @ 300 MHz for longitudinal unidirectional graphite/epoxy sample

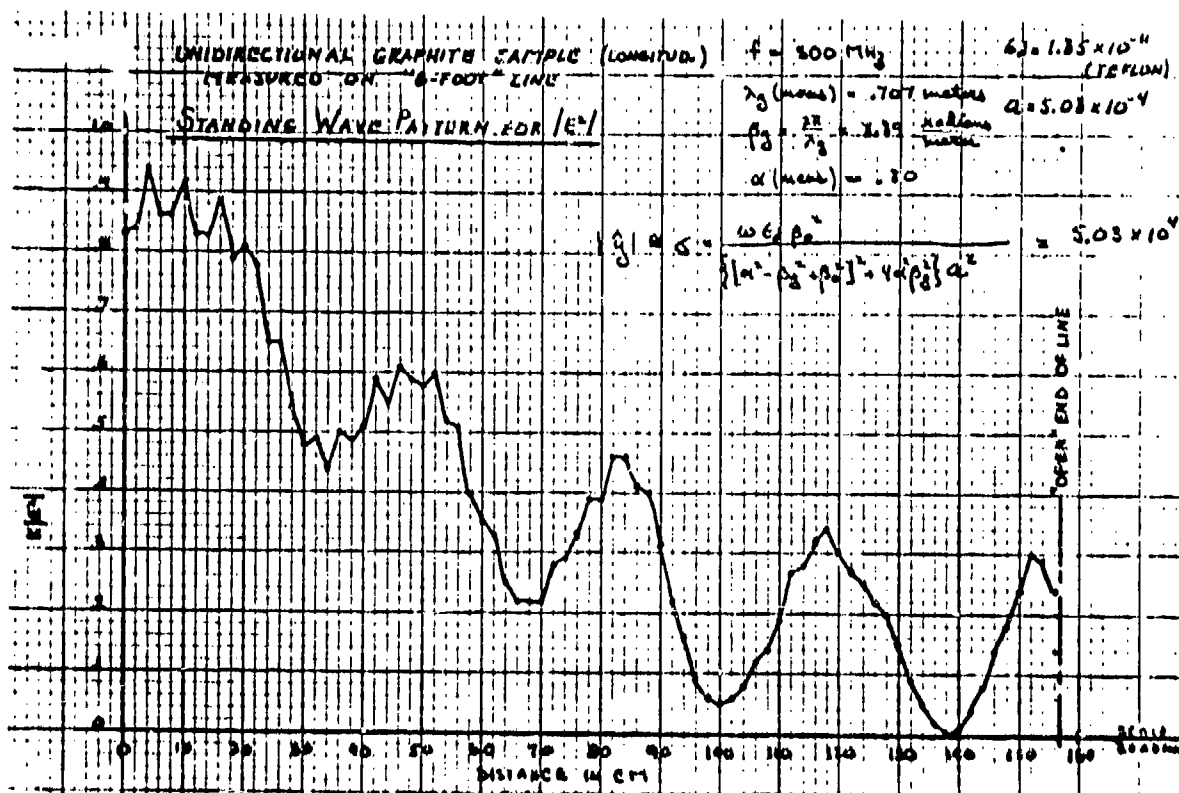


Fig.5-4 Standing wave pattern @ 600 MHz for longitudinal unidirectional graphite/epoxy sample

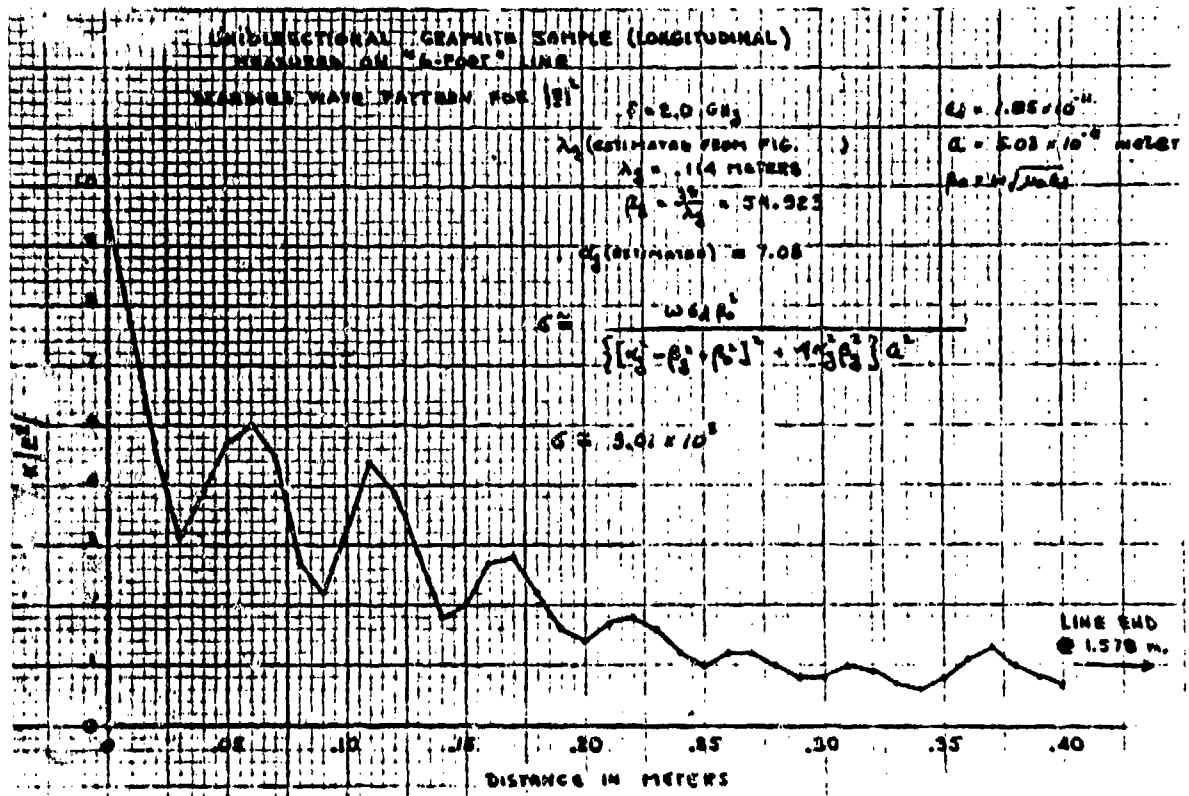


Fig.5-5 Standing wave pattern @ 2.0 GHz for longitudinal unidirectional graphite/epoxy sample

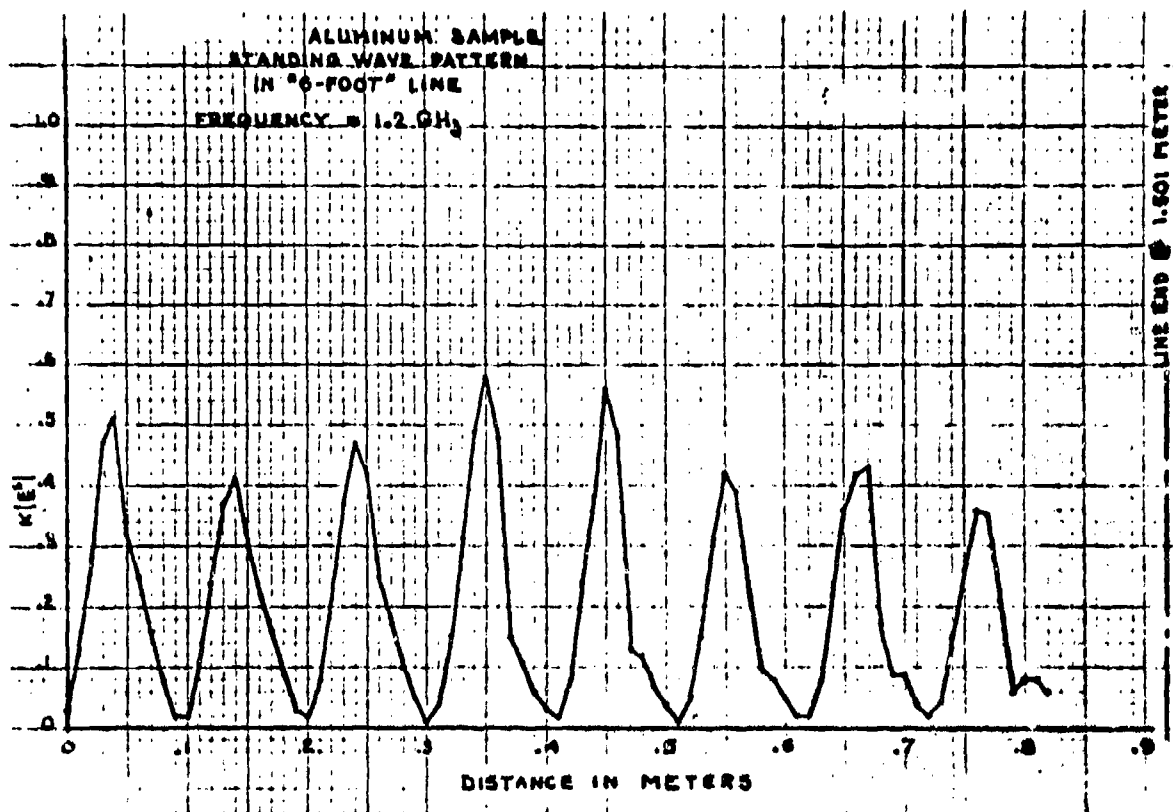


Fig.5-7 Standing wave pattern @ 1.2 GHz for an aluminum sample

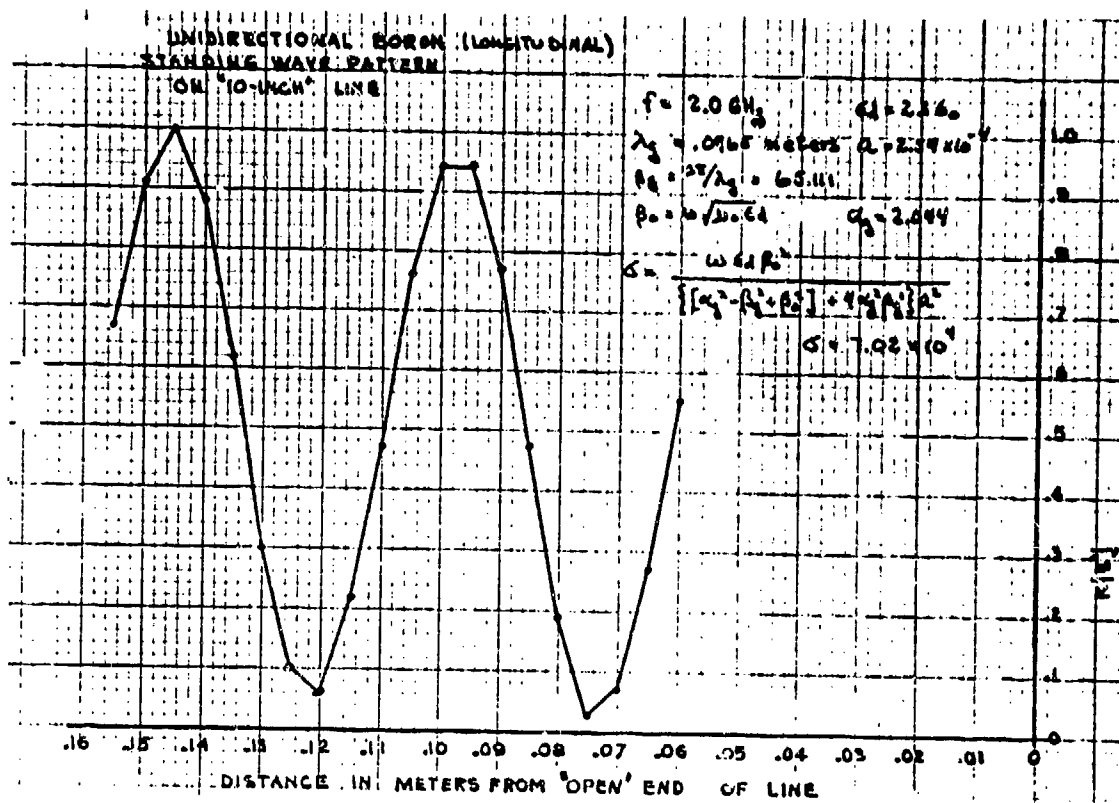


Fig.5-8 Standing wave pattern @ 2.0 GHz for a longitudinal unidirectional boron/epoxy sample

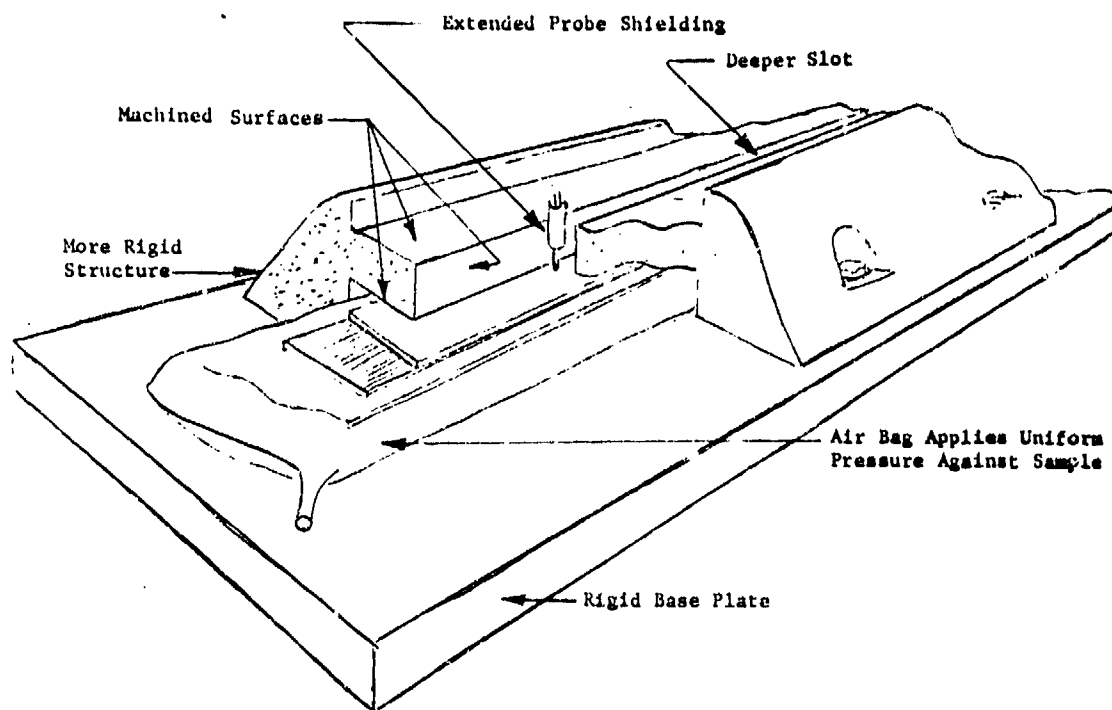


Fig.6-1 Sketch of improved line structure

EMC, LIGHTNING AND NEMP-PROTECTION-NEW REQUIREMENTS FOR

APPROVED SPECIFICATIONS WHEN USING CFRP

D. Jaeger / K.H. Rippl
Messerschmitt-Bölkow-Blohm
- Apparate -
D-8012 Ottobrunn - Germany

SUMMARY

The use of CFRP (Carbon Fibre Reinforced Plastics) in modern aircraft achieves good advantages for mechanical strength and is weightsaving, compared with aluminum structures (e. g. up to one ton weightsaving for fighter aircraft). This could be very important for flight performance and mission success. In spite of the advantages there are also some disadvantages in using CFRP materials. These are mainly unwanted electromagnetic effects on electronic equipment, caused by EMI (Electromagnetic Interference) lightning, electrostatic discharges, and NEMP (Nuclear Electro-Magnetic Pulse). The reason for these problems is lower shielding effectiveness of the aircraft structure compared to aluminum. Specifications used for aircraft today do not pay regard to the requirements of the new materials. For NEMP-protection there are no adequate specifications available in Western Europe. Proposals are made in this paper how the existing documents should be modified.

1. INTRODUCTION

To achieve proper performance of aircraft avionic systems, unwanted electromagnetic effects related to the fields of EMC (Electromagnetic Compatibility), lightning-, electrostatic- and NEMP-protection must be considered (Fig. 1). How important a good control of these effects is, can be seen from Fig. 2.

Absolutely necessary for the function of all electronic equipment integrated in the system is internal EMC. The necessity to manage the other problems like external EMC and lightning protection (and partly electrostatic effects), depends on the probability of an aircraft coming into a dangerous situation, in relation to the above problems. It is therefore a matter of safety requirements for the whole system if it has to operate without any fault or degradation under all possible circumstances. A good compromise between cost and probability of a hazard must be found. A special requirement is NEMP-protection. The electromagnetic effects resulting from the explosion of a nuclear bomb exhibit a serious threat to the electronic equipment of an aircraft. For all these problems several specifications and regulations are existing (Fig. 3). They may be used by the aircraft manufacturer as a basis for proper design and by the customer as a guideline for control. Most of these documents have been used successfully during many years and they are helpful today as well. But, as later discussed, some details do not pay regard to the new CFRP aircraft structures.

MIL-STDS 461A/462/463 are well-known standards for EMC on equipment and subsystem-level. Regulations for spikes and transients on power lines in aircraft are given in MIL-STD 704A. MIL-STD 1385 deals with EED's (Electro-Explosive-Devices) in an electromagnetic environment. It represents the only specification for the management of "external EMC"-problems. MIL-B-5087B contains some design principles for bonding and is in our case especially interesting for lightning protection and handling of electrostatic phenomena. MIL-E-6051D is the only existing system-specification for all electromagnetic problems discussed in this paper. As it is not only applied on aircraft but also on other weapon systems, it can only be a general guideline for the required "state of the art" in these fields. Detailed design criteria are shown in the "AFSC-Design Handbook" which has become a useful resource for proper management of "unwanted electromagnetic effects".

This summary contains only a selection of papers which are currently used in military aircraft avionics design. It should be mentioned that the so called "VG-Normen" are prepared in Germany at the present time and that they become effective as they are edited. They are intended to be more flexible and can therefore easier be adapted to the specific characteristics of new materials and techniques.

To get a better impression, how avionic systems in a modern CFRP-aircraft may be exposed to unwanted electromagnetic influence, a short overview shall be given on the related areas.

2. ELECTROMAGNETIC COMPATIBILITY

Fig. 4 is a "classical" EMC picture and shows how coupling of electrical signals occurs. The susceptible electronic equipment may be influenced by conductive coupling, if an unwanted current runs the same path as the wanted signal or if the interfering voltage is directly present at the equipment. Inductive and capacitive coupling is mainly present between cables and structure, while radiated coupling can happen between antennas and cabling and any other equipment, if high frequency signals are involved. These principles can be adopted for all kind of electromagnetic effects.

Internal EMC, for example, (Fig. 5) stands for unaffected, simultaneous operation of all electrical/electronic equipment in the aircraft. The interaction problem between non-antenna-equipment is mostly solved by the consequent observation of MIL-STDs 461/2 and MIL-E-6051D. More difficult to realize is the requirement that radiation from high-power transmitters should not have any influence on other equipment, as well as no electrical/electronic equipment should degrade the receiver performance. A major role in prevention of those hazards plays the shielding effectiveness of the aircraft structure, as demonstrated in Fig. 6. Fig 7 shows measurement results for the magnetic field shielding effectiveness of aluminium and CFRP material. For both materials, attenuation is increasing with frequency, while there is no attenuation measured for CFRP material below 100 kHz. But these theoretical relations cannot be fully transferred to an existing aircraft structure, because there are apertures and gaps in the airframe, which set a limitation for the shielding effectiveness, also depending on the frequency. If we assume some 40 dB as a natural limitation, a region can be seen in the diagram where the magnetic shielding effectiveness is fairly important for the different materials. This frequency range lies between 0 and approx. 10 MHz with the worst case around 100 kHz. It can easily be seen that this effect must have an influence on the requirements of the existing standards.

Regarding the internal EMC-problem again, the lack of shielding effectiveness in this certain frequency range could generate worse conditions in a CFRP aircraft for radiated emission and radiated susceptibility than in aluminium aircraft. According to MIL-STD 462, for example, all radiation tests for equipment must be performed with the test sample and its cabling on a metallic ground plane (Fig. 8), which represents the aircraft structure. The limits for electromagnetic fields, impinging on the susceptible equipment are related to this specific test set up. Fig. 9 shows the actual limits for "radiated susceptibility test RS03" according to MIL-STD 461 (3). The important frequency range is marked and some interesting transmitters are shown which could affect the electronic equipment of an aircraft. Besides broadcasting and navigational stations which possibly may produce an external EMC-problem under certain circumstances, the often used airborne HF-SSB transmitter becomes important for internal EMC. The consequence is, that the specified field strengths should be increased if a CFRP-structure is provided for the aircraft. The value depends on the design of the structure, but worst case requirements could be 20 - 30 dB higher than before.

Equivalent problems arise in connection with radiated emissions (Test RE 02). Fig. 10 shows the limit according to the same standard. In the critical frequency range there are some important navigational receivers installed in many aircraft, probably also short-wave receivers. In relation to CFRP-structures, a modification of these limits seems to be necessary. The range is shown in the diagram.

Another problem arises when the limits for "conducted susceptibility" are discussed (Fig. 11). Looking only upon the mechanism of conductive coupling, no provisions seem to be necessary by using new materials. But there is another, secondary effect which is the radiated coupling between antennas and electrical power leads. This could become important for internal EMC considerations (e. g. in connection with short-wave transmitters). The same requirements may be applied to the "radiated part" of conducted emissions originating from any involved electrical equipment. The limits according to MIL-STD 461A are shown in Fig. 12. How much the existing limits have to be altered, is not very easy to be calculated, because it depends on the design of cabling and cable shielding as well as on design of the whole system. Regarding "external EMC"-requirements, Fig. 13 shows the expected field strengths at the surface of an aircraft in relation to the distance from external transmitters.

There are no regulations existing concerning the external EMC-problem besides for EED's. By the use of CFRP materials for aircraft structures, this subject becomes more important especially in the lower frequency range. Regarding the attenuation curve of the different materials, provisions against this effect seem to be necessary. How stringent the applied test values should become, depends on the degree of safety which is required. In most cases 100 - 150 V/m are sufficient for any kind of air vehicle, including lightweight helicopters. To test the specified requirements, intensified tests on system level are necessary.

Fig. 14 shows a summary of new EMC requirements as a result of this chapter. Point 4 gives some advice how to manage the new situation. The use of twisted pairs, for example is not completely new, but now necessary for power leads as well. Some effort will also be necessary to introduce a good cable shield connection at both ends of the cable. The measures discussed above will have a widespread influence on other aircraft specifications.

3. STATIC ELECTRICITY

Electrostatic effects are threatening aircraft avionics if there is a charge accumulation on the surface or inside the aircraft or if a separation of charges by external fields or friction occurs (Fig. 15). The interference will happen if the charges are compensated again by a sudden or continuous (sparkling) current.

As seen from Fig. 16 the electromagnetic noise produced by these currents may reach the receiver input via antennas and thus reduces the operational performance of navigation and communication equipment. The frequency spectrum of "coronas" and "streamers" lies in the lower frequency region. Therefore ADF, Decca, OMEGA and probably short wave receivers will be affected. If we remember the attenuation curve of aluminium and CFRP material there could be an additional increase of noise at the antenna input by using composite

materials. The value depends widely on the system's design and the location of the antennas and the spark source. Discharges inside the aircraft can be another interference source. Short duration pulses are mainly dangerous for digital equipment. But in this case disadvantages by using composite materials seem to be not significant. The existing specification handling electrostatic effects is MIL-B-5087B and MIL-E-6051D. The design principles described herein should be observed for metallic aircraft as well as for aircraft with composite structures to prevent electromagnetic interference. In addition test procedures for system tests should be provided to test the system's performance under these conditions.

4. LIGHTNING

The lightning threat to aircraft depends on the probability of a stroke (Fig. 17) which is a function of flight level, geographical region of the operation, type of aircraft and other parameters. Experience shows that in average an aircraft is struck one or two times every 10 thousand hours of operation. How dangerous such a stroke is depends on its characteristics, like maximum current, rise time, charge, action integral and number of successive pulses. The mechanical destruction of lightning (Fig. 18) can be very dangerous for an aircraft. Nevertheless "indirect effects" of lightning may be dangerous as well if electronic equipment, which is critical for flight safety, is damaged or degraded.

Following the coupling mechanism as described before, lightning can generate high voltage and high currents in electronic circuits.

Fig. 19 shows the frequency distribution of a series of measured lightning spectra as a summary of several investigations. It is interesting to see that the maximum lies in a frequency range where CFRP structures have less shielding effectiveness than conventional metallic airframes. This means that magnetic fields from a direct stroke are invading without significant attenuation into the avionic compartment. Similar effects may result from near-by-strokes.

Fig. 20 shows the values of magnetic field strengths which are present near a lightning path in relation to the distance. They will be compared later-on with existing requirements.

Some important statements of MIL-B-5087B, which is the most representative specification for lightning protection today, are listed in Fig. 21. The table contains some "mechanical aspects" which mainly represent a guideline for aircraft construction. The document concludes that a maximum peak voltage on powerlines of about 500 V may be experienced (Calculated from the over all-resistance of the fuselage). The document defines also a very simple lightning stroke which is only adequate for metallic aircraft. Conductive composites are only mentioned as "problematic for bonding". But there are also some other documents available which are helpful for lightning protection as shown in Fig. 22.

MIL-E-6051D for example defines some general requirements for system tests. In addition, values for spikes on power lines are specified. But they are much too low for lightning purposes.

Spikes according to MIL-STD 461/2 are also too low in this context. MIL-STD 704 (also STANAG 3456) defined spikes for power lines which have higher peak voltage, but a recent revision cut down the requirements.

The only test for magnetic fields is described in MIL-STD-461/2. Fig. 23 shows the test set up for test RS02. The magnetic field strength produced in this test-set-up depends on the dimensions of the equipment under test.

Fig. 24 shows the relationship between dimensions and field strength.

If we remember the diagram of Fig. 20 it is easily to be seen that the applied field strengths are not enough for safety against lightning strokes.

Fig. 25 summarizes the existing lightning protection requirements. To solve special lightning problems, SAE-committee AE4-L published a paper called "Lightning Qualification Test Techniques for Aircraft and Hardware" which shall become a MIL-Standard and is proposed as STANAG 3659AE by the Military Agency of Standardization (Fig. 26).

In this document a new lightning stroke is specified for testing which pays regard to composite materials. The tests include also system tests on the electrical effects of lightning and electrostatics, but only for the complete vehicle. No limits are defined for electrical equipment. For these purposes additional test methods and limits are to be found.

5. NEMP

The last electromagnetic effect with which this paper intends to deal with is NEMP. As seen in Fig. 27 different characteristics for "exoatmospheric" and "endoatmospheric" NEMP must be assumed.

The threat to aircraft seems to be very similar to the electrical component of lightning. But the pulse duration and rise time is different.

Comparing the spectra of the exoatmospheric and the endoatmospheric explosions (Fig. 28/29), the endoatmospheric NEMP seems to be more dangerous for CFRP aircraft because of its low-frequency distribution. But considering that other effects of nuclear weapon are damaging an aircraft as well, a "balanced protection" regarding all these effects will be necessary.

This means that field strengths of some kV/m are sufficient for the endoatmospheric NEMP.

In Germany the NEMP requirements are fairly new. There are no specifications available besides the threat parameters. Only design guides could be recommended for NEMP-hardening (Engineering Design Handbooks AMCP 706-335 through 338, Design Engineer's Nuclear Effects Manual (DENEM), (SRD), DASA Handbooks 2114-1/2 and DASA TREE Handbook 1420). Design principles should base on their consequent observation. In USA some other classified regulations are in use, and NEMP-tests are performed on equipment and system level. In Germany "VG-Normen" will bring some better management of NEMP hardening problems. First drafts are expected at the end of 1980.

6. CONCLUSION

A summary of the present situation on applicable documents for the above mentioned electromagnetic effects on avionics in CFRP aircraft is given in Fig. 30. For EMC more stringent requirements are recommended. New test methods for system tests are necessary especially for external EMC considerations. For the electrostatic effects a consequent observation of the existing specifications seems to be adequate. For lightning protection the new SAE proposal could be helpful against mechanical destruction and partly against electromagnetic interference. But not all necessary aspects are handled. Therefore additional regulations should be worked out, even new test methods. For NEMP hardening no adequate specifications are available. New documents should pay regard to international experience.

As demonstrated above, a lot of paper-work has to be done in relation to CFRP materials in aircraft, before hardware considerations are possible. But a great deal of work for the different fields can be done together because problems are very similar (e. g. low frequency, spikes). Time and money can be saved if these activities are well coordinated.

REFERENCES

1. MIL-STD-461A (USAF) Electromagnetic Interference Characteristics; Requirements for Equipment (Notice 3) Feb. 1969
2. MIL-STD-462 (USAF) Electromagnetic Interference Characteristics; Measurement of (Notice 2) May 1970
3. MIL-STD-463A Definitions and System of Units, Electromagnetic Interference and Electromagnetic Compatibility Technology. June 1977
4. MIL-STD-704A Electric Power; Aircraft Characteristics and Utilisation of (Notice 3) USAF, Apr. 1973
5. MIL-STD-1385 Preclusion of Ordnance Hazards in Electromagnetic Fields; General Requirements for Apr. 1972
6. MIL-E-6051D Electromagnetic Compatibility Requirements System incl. Amendment 1 (USAF) July 1968
7. MIL-B-5087B (ASG) Bonding, Electrical, and Lightning Protection, for Aerospace Systems incl. Amendment 2, Aug. 1970
8. VG 95372 Elektromagnetische Verträglichkeit Übersicht (Beiblatt 1: Veröffentlichte Normen für EMV, VG 95370 - VG 95377) Bundesamt für Wehrtechnik und Beschaffung, Normenstelle Elektrotechnik, August 1979
9. AFSC Design Handbook Air Force Systems Command, Andrews AFB, Maryland
10. AMCP 706-235 Engineering Design Handbook Hardening Weapon Systems against RF Energy Army Material Command, Washington, D.C. Feb. 1972
11. N. Cianos, Oetzel, Pierce Structure of lightning noise, especially above HF. Lightning and Static electricity conference, Ohio, 1972
12. Lightning Qualification Test Techniques for Aircraft and Hardware SAE-AE4-L, proposal

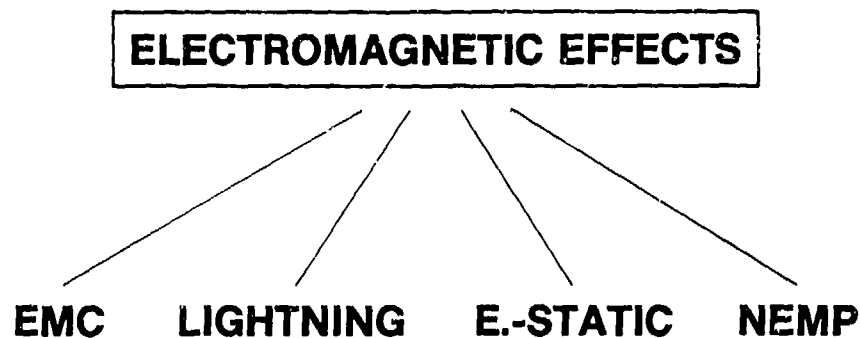


Fig.1 Survey of important electromagnetic problems

SUBJECT		SIGNIFICANCE
EMC	INT.	ABSOLUTELY NECESSARY FOR OPERATION
	EXT.	SAFETY PROBLEM
LIGHTNING		SAFETY PROBLEM
E-STATIC		MAINLY SAFETY PROBLEM
NEMP		SPECIAL REQUIREMENT FOR MISSION AND OPERATION

Fig.2 Significance of different electromagnetic fields

SPECIFICATION, DOCUMENT	APPLICATION
MIL-STD-461/ 462/463	EMC OF EQUIPMENT AND SUBSYSTEMS (ESPECIALLY INT. EMC)
MIL-STD-704	IMPORTANT FOR SPIKES AND TRANSIENTS ON POWER LINES
MIL-STD-1385	RF-ENVIRONMENT FOR SYSTEMS WITH ELECTRO-EXPLOSIVE-DEVICES (EXT. EMC RELATED TO SAFETY PROBLEMS)
MIL-B-5087B	BONDING AND LIGHTNING PROTECTION (GENERAL RULES FOR DESIGN AND CONSTRUCTION)
MIL-E-6051D	GENERAL REQUIREMENTS FOR THE DIFFERENT ELECTROMAGNETIC EFFECTS (DEFINITION OF SAFETY MARGINS, ETC.)
AFSC-DESIGN- HANDBOOK	DESIGN PRINCIPLES

Fig.3 Summary of mostly used documents

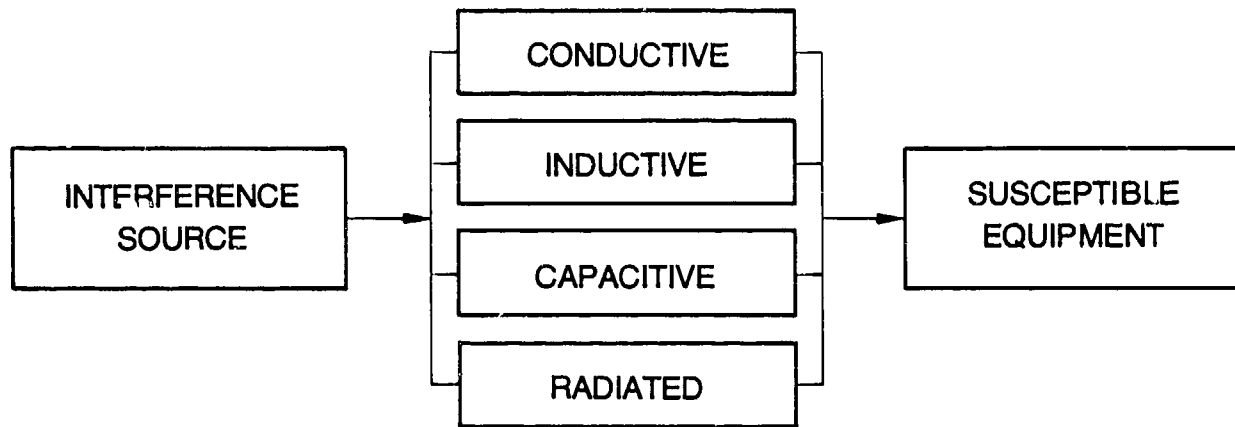


Fig.4 Coupling mechanism

EXTERNAL AND INTERNAL EMC-PROBLEMS

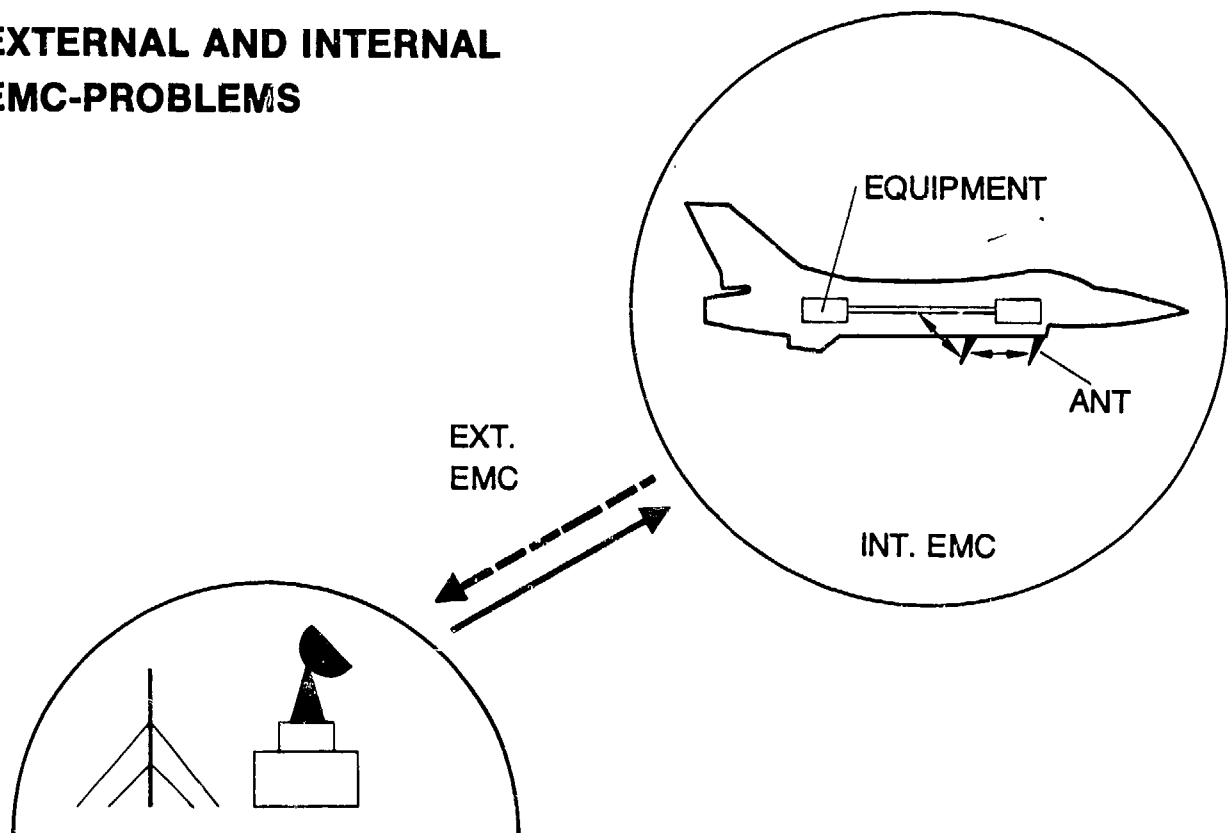


Fig.5 External and internal EMC-problems

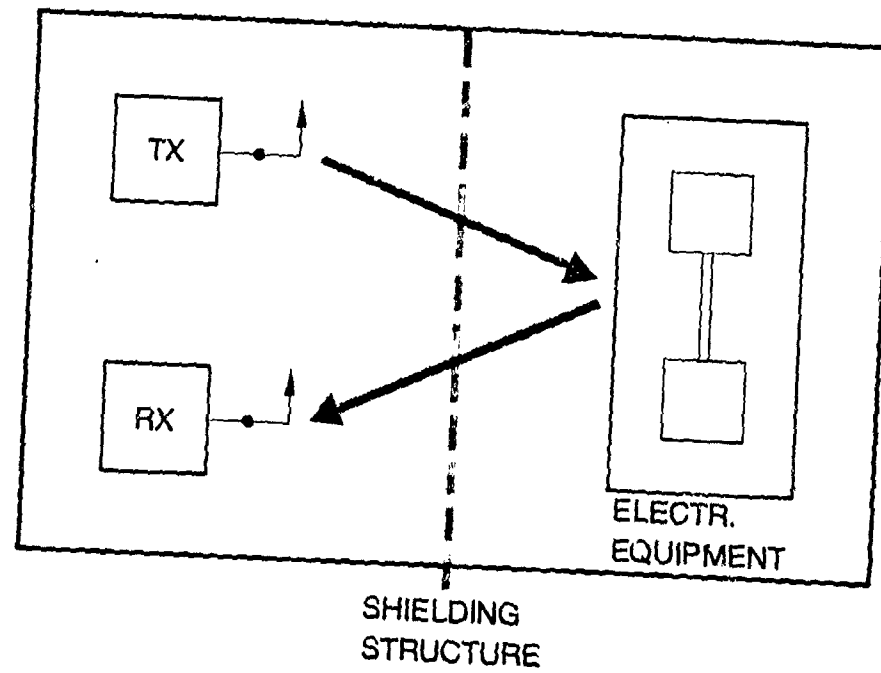


Fig.6 Example for internal compatibility problems

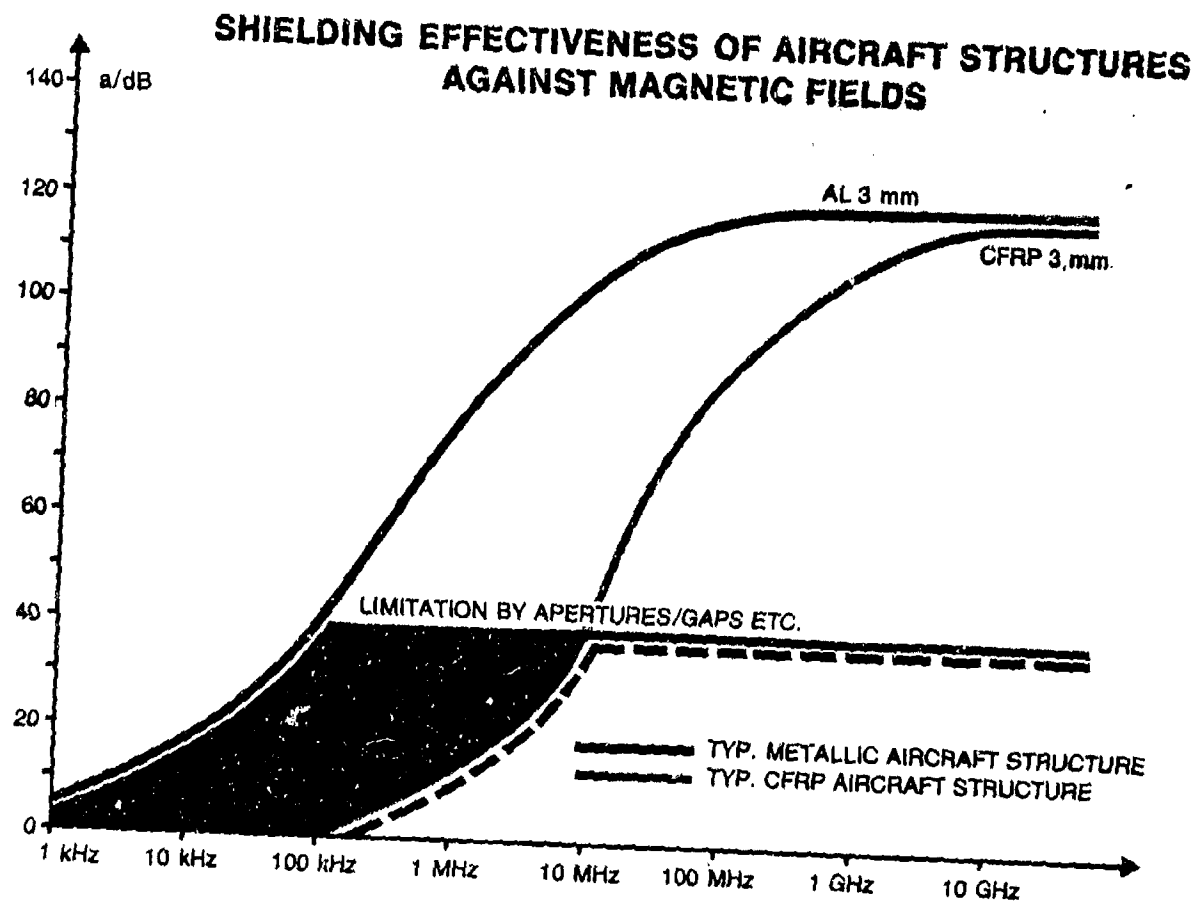


Fig.7 Shielding effectiveness of aircraft structures against magnetic fields

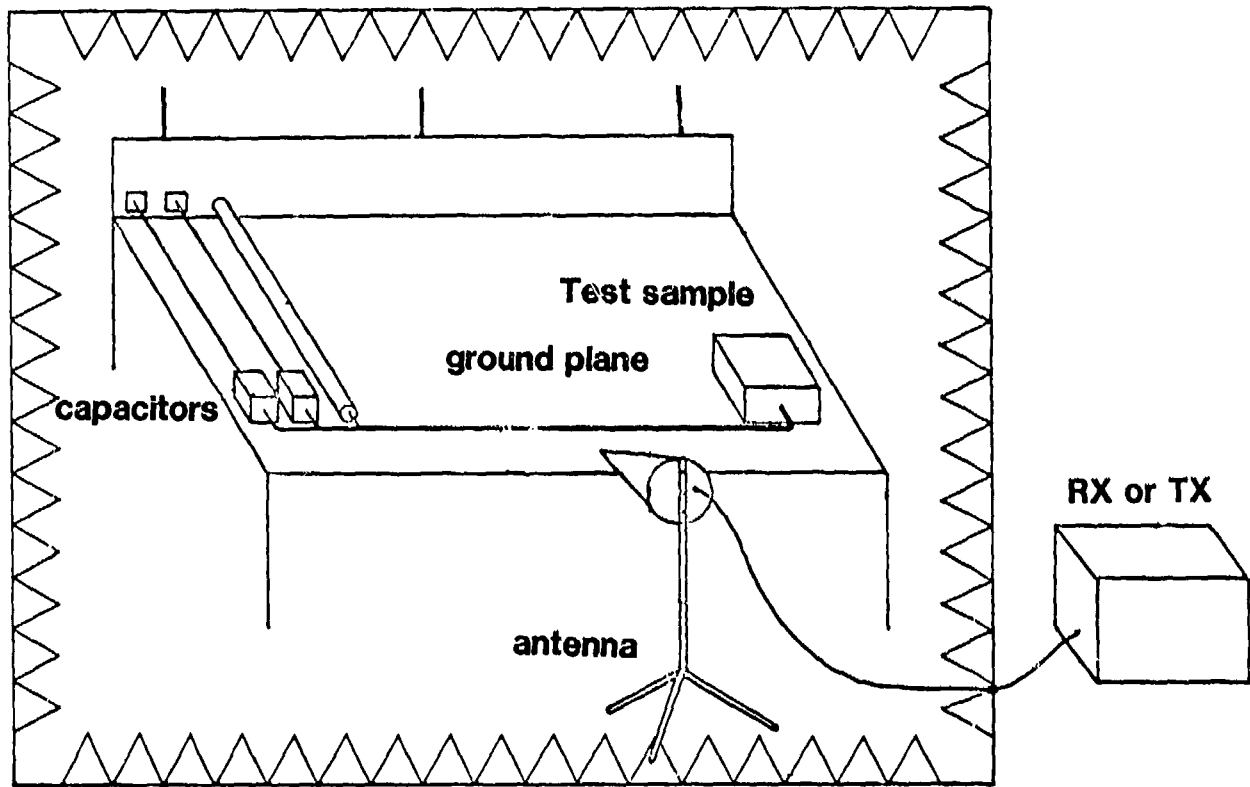


Fig.8 Typical test-set-up for 'radiated emission' and 'radiated susceptibility' tests

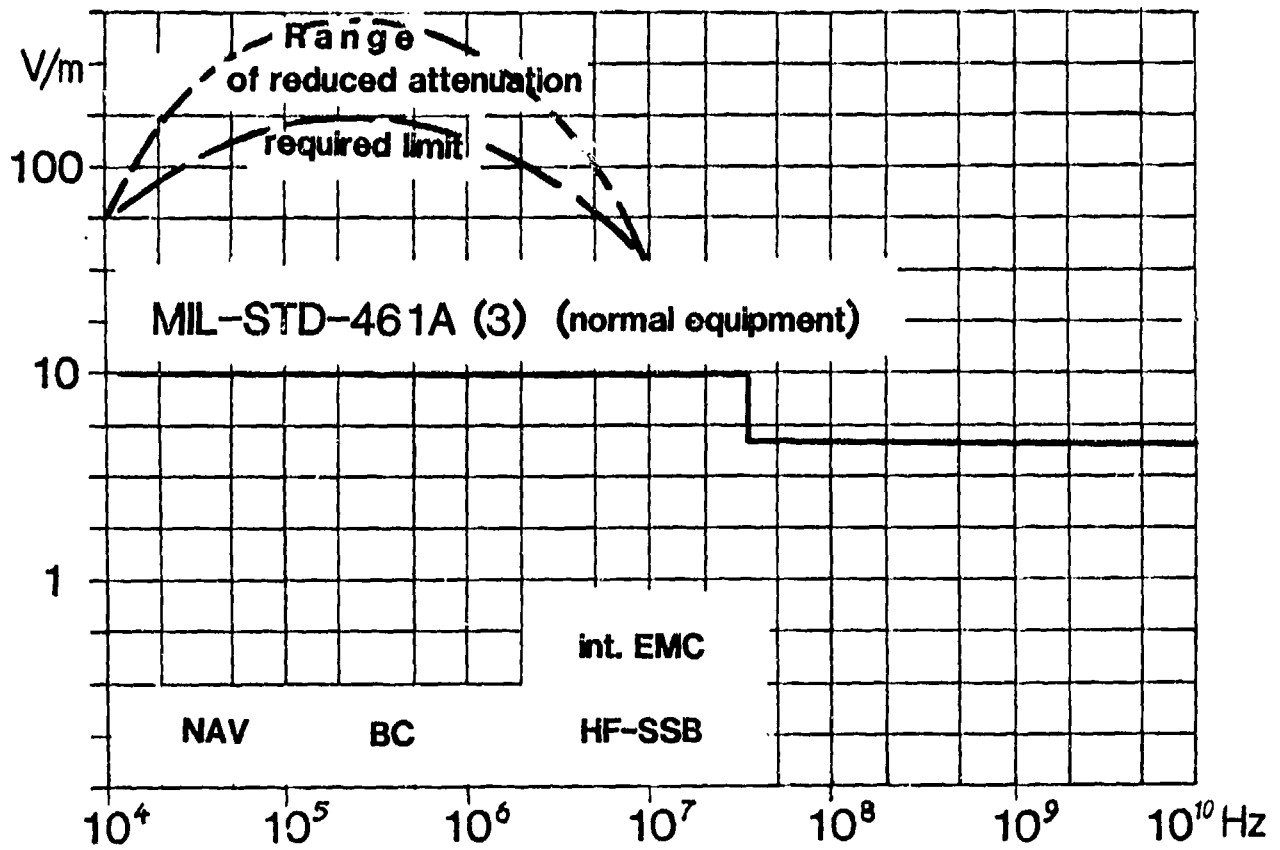


Fig.9 Limits for "radiated susceptibility"-test

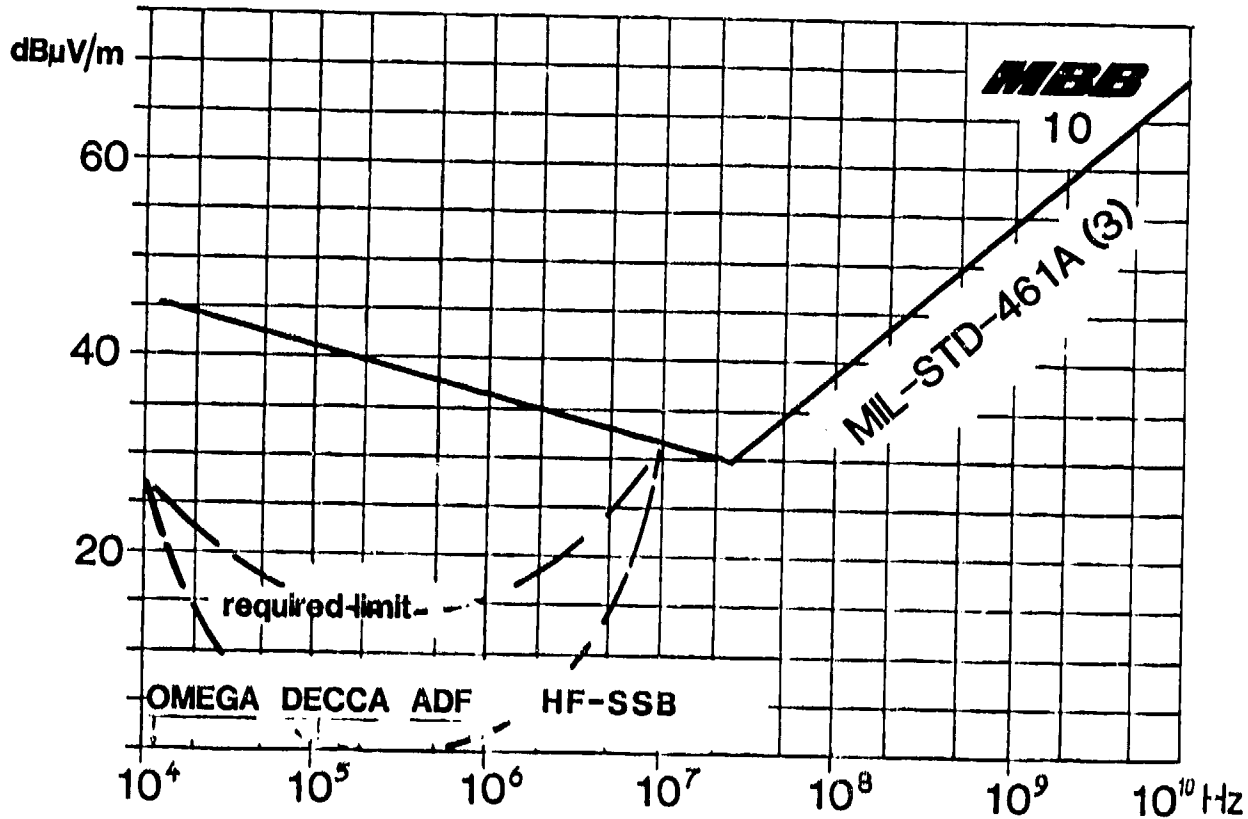


Fig.10 Limit for "radiated emission"-test

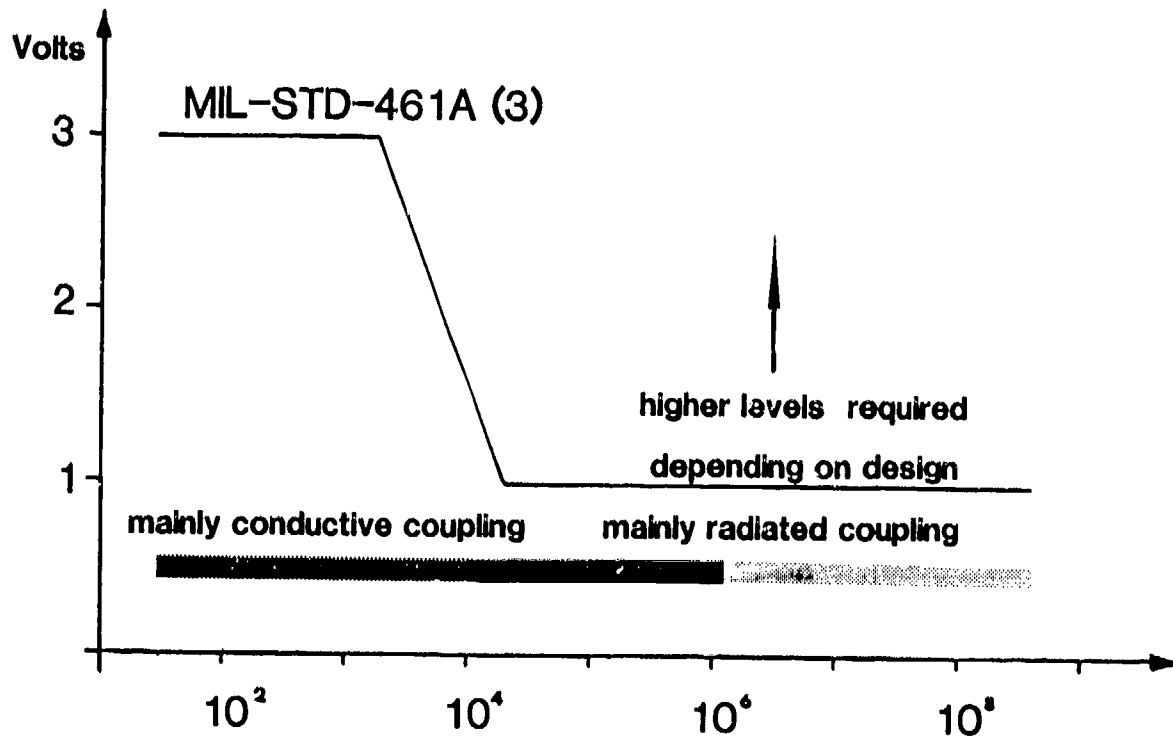


Fig.11 Limits for "conducted susceptibility" test

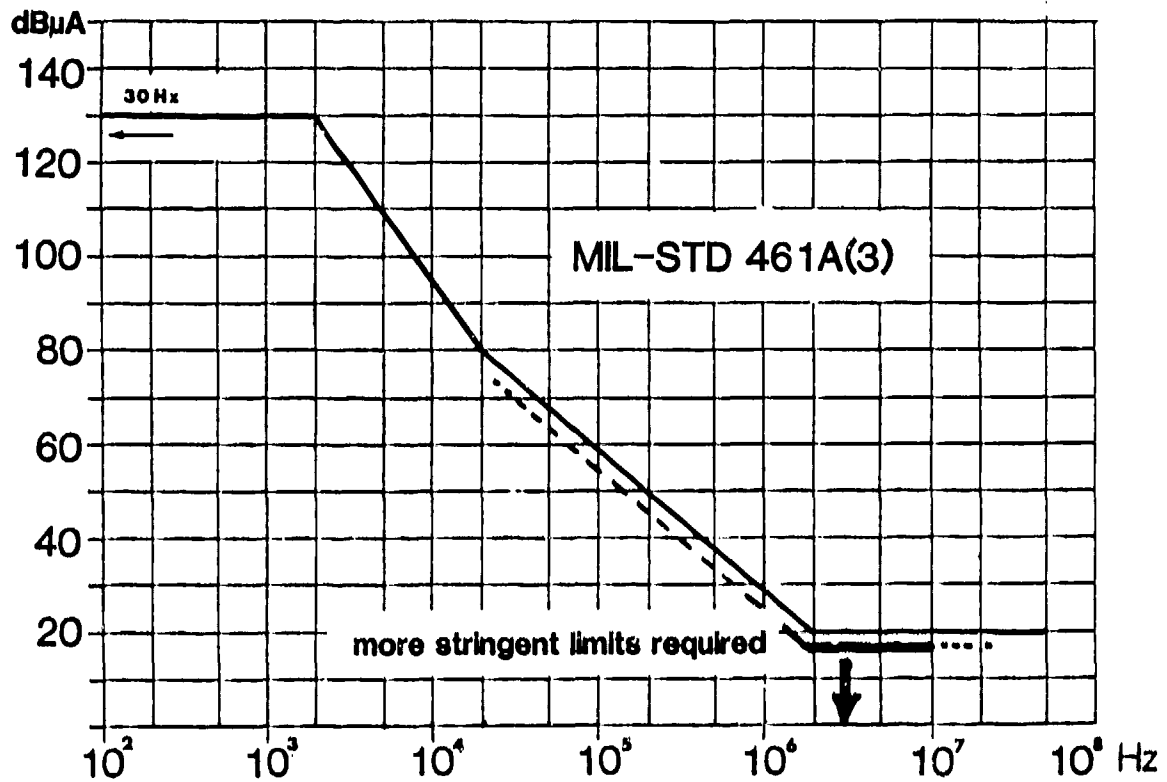


Fig.12 Limits for emitted interference on power lines

TRANSMITTER	DISTANCE				
	32 m	100 m	320 m	1 km	3,2 km
LF-, MF- BROADCASTING	153 $\frac{V}{m}$	51 $\frac{V}{m}$	17 $\frac{V}{m}$	5,6 $\frac{V}{m}$	1,9 $\frac{V}{m}$
SHORT WAVE RADIO	99 $\frac{V}{m}$	33 $\frac{V}{m}$	11 $\frac{V}{m}$	3,6 $\frac{V}{m}$	1,2 $\frac{V}{m}$
VHF BROADCASTING	99 $\frac{V}{m}$	33 $\frac{V}{m}$	11 $\frac{V}{m}$	3,6 $\frac{V}{m}$	1,2 $\frac{V}{m}$
TELEVISION	225 $\frac{V}{m}$	75 $\frac{V}{m}$	25 $\frac{V}{m}$	8,3 $\frac{V}{m}$	2,8 $\frac{V}{m}$
RADAR (PEAK)	1350 $\frac{V}{m}$	450 $\frac{V}{m}$	150 $\frac{V}{m}$	50 $\frac{V}{m}$	17 $\frac{V}{m}$

Fig.13 External EMC: Fieldstrengths of different RF-sources

1. MORE STRINGENT REQUIREMENTS FOR EQUIPMENT

- RADIATED SUSCEPTIBILITY
- RADIATED EMISSION
- CONDUCTED SUSCEPTIBILITY
- CONDUCTED EMISSION

2. INTENSIFIED EMC-TESTS ON SYSTEM-LEVEL

ESPECIALLY EXT. EMC.

EXTERNAL EMC-TESTS EXTENDED TO AVIONICS

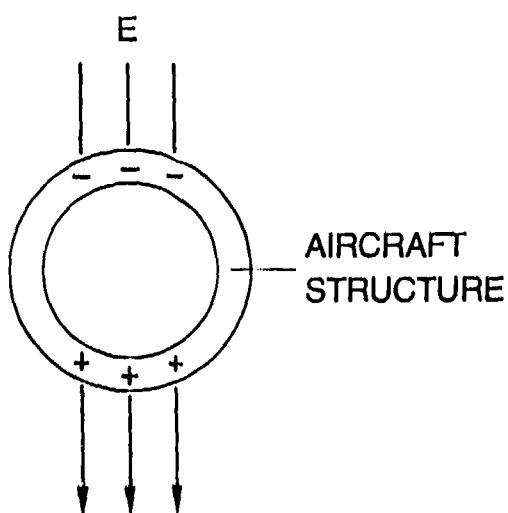
3. NEW TEST METHODS ARE NECESSARY

E.G. COUPLING BETWEEN CABLING AND ANTENNA SYSTEMS

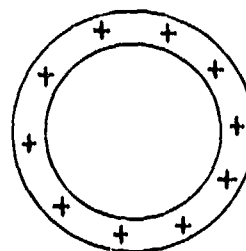
4. NEW PRINCIPLES FOR CABLING, SHIELDING AND GROUNDING MAY BE REQUIRED

- "TWISTED PAIRS"
- CAREFUL CABLE SHIELD CONNECTION AT BOTH ENDS

Fig.14 Summary of new EMC-requirements



SEPARATION OF CHARGE
BY EXTERNAL FIELDS
(E.G. IN THUNDERSTORMS)



CHARGE GENERATION BY
- SURFACE FRICTION
- EXHAUST OF ELECTRICALLY
CHARGED PARTICLES
- MOTION OF PLASTICS
ETC

Fig.15 Electrostatic phenomena

1. INTERFERENCE IN NAVIGATION- AND COMMUNICATION EQUIPMENT VIA ANTENNAS

- CORONA-EFFECT
 - SURFACE-STREAMERS
- IMPORTANT ESPECIALLY FOR LOW FREQUENCY SYSTEMS (ADF, DECCA ETC.)

2. INTERFERENCE CAUSED BY DISCHARGES INSIDE THE SYSTEM

SHORT DURATION PULSES OF HIGH AMPLITUDE AND SHORT RISE TIME.

EFFECTS ON

- ELECTRIC/ELECTRONIC (DIGITAL EQUIPMENT!!!)
- EED-CIRCUITS

Fig.16 Effects of E-static discharges

DEPENDS ON

- PROBABILITY OF STROKES
(FLIGHT LEVEL, TYPE OF AIRCRAFT, GEOGRAPHICAL REGION ETC.)
CA 1-2 TIMES PER 10000 HOURS OF OPERATION
- CHARACTERISTICS OF LIGHTNING STROKE
(MAXIMUM CURRENT, RISE TIME, CHARGE, ACTION-INTEGRAL, NUMBER OF PULSES)

Fig.17 Threat to aircraft caused by lightning strokes

1. "MECHANICAL" EFFECTS

(CAUSED BY THERMAL AND MAGNETIC FORCES)

- DAMAGE OF STRUCTURE
- DAMAGE OF EXTREMITIES LIKE RADOM, POSITION LIGHTS, ETC.
- MELTING OF TACKLE LINES
- ETC.

2. ELECTRICAL EFFECTS

- CONDUCTIVE COUPLING CAUSED BY CURRENTS ON THE STRUCTURE
- HIGH MAGNETIC FIELDS INSIDE THE AIRCRAFT
(CAUSED BY DIRECT AND NEAR-BY-STROKES)
- HIGH VOLTAGE SPIKES ON POWER- AND SIGNAL LINES

Fig.18 Effects of lightning

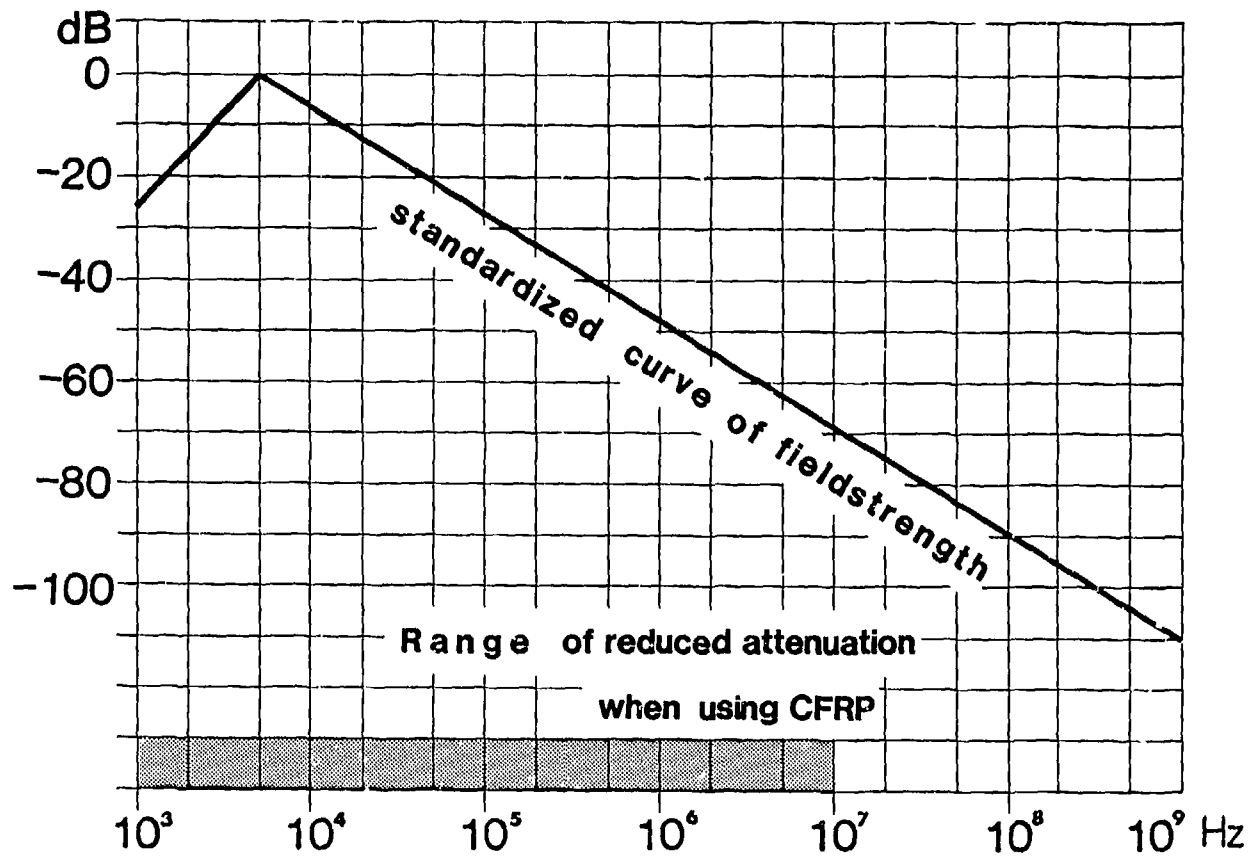


Fig.19 Typical spectrum of lightning strokes

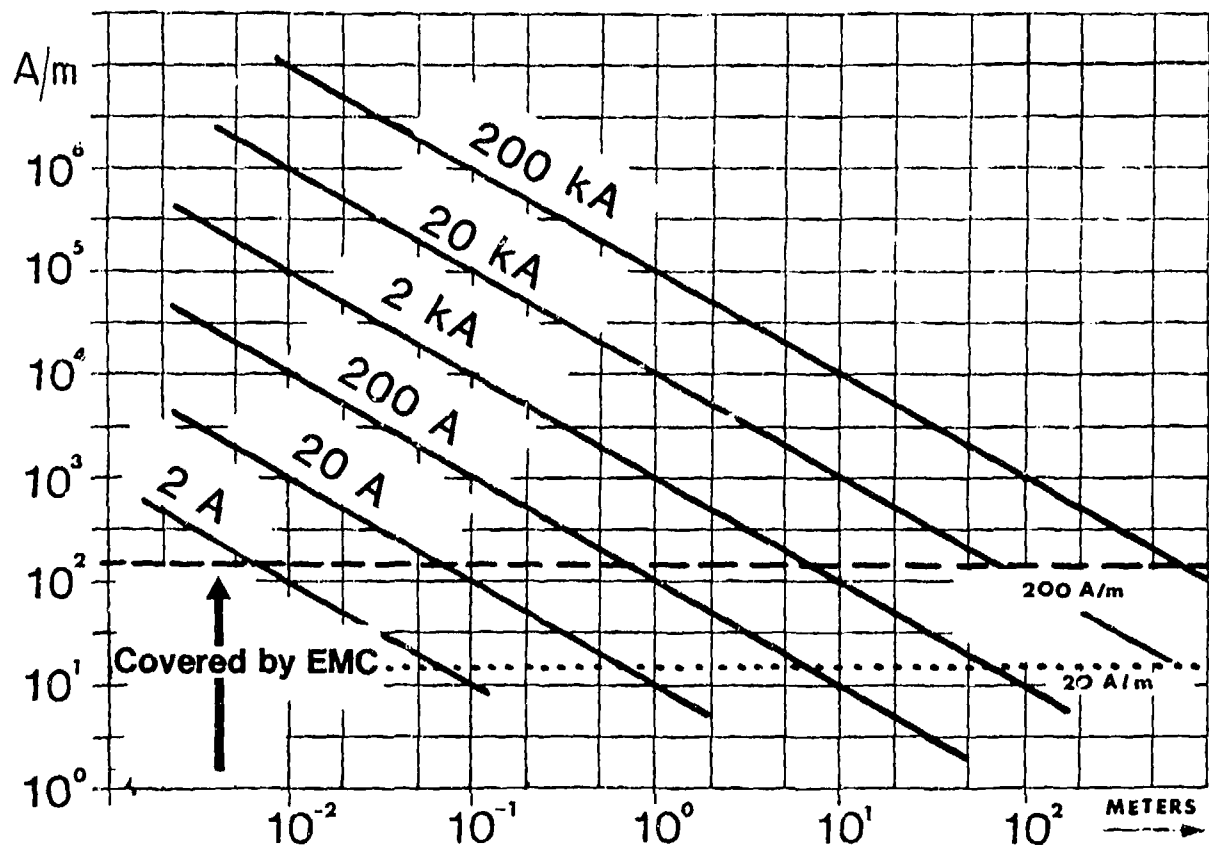


Fig.20 Magnetic fieldstrength near a lightning path

"MECHANICAL" ASPECTS	REQUIREMENTS FOR EXTERNAL PARTS OF THE AIRCRAFT – SELECTIONS OF MATERIAL – THICKNESS OF MATERIAL – RESISTANCE BETWEEN PARTS OF FUSELAGE
"ELECTRICAL" ASPECTS	REQUIREMENTS FOR "OVER-ALL-RESISTANCE" OF THE FUSELAGE – VOLTAGE DROP OF MAX. 500 V PERMISSIBLE – ± 500 V SPIKES ON POWER LINES
OTHER	VERY SIMPLE LIGHTNING PARAMETERS (200 KA; 20 μ S (50%); 100 kA/ μ S)

Fig.21 Important statements of MIL-B-5087B

DOCUMENT	CONTENT
MIL-E-6051D	– GENERAL REQUIREMENTS FOR SYSTEM TESTS – SPIKES + 50% AND – 150% OF LINE VOLTAGE (E.G. + 42 AND – 14 V FOR 28 V LINE) DURATION: < 50 μ S, OR SEE OTHER REQUIREMENTS APPLICABLE ONLY ON POWER LINES
MIL-STD 461/2/3	– SPIKES ACCORDING TEST CS06 (2 x LINE VOLTAGE) APPLICABLE ONLY ON POWER LINES – MAGNETIC FIELD ACCORDING TEST RS01 LIMITS TOO LOW FOR LIGHTNING
MIL-STD 704 (Stanag 3456)	– SPIKES ± 600 V ON POWER LINES, TRANSIENTS HAD BEEN COMPATIBLE WITH MIL-B5087B LATER: REQUIREMENTS OF MIL-E6051D IN FORCE

Fig.22 Comparison of other MIL-requirements

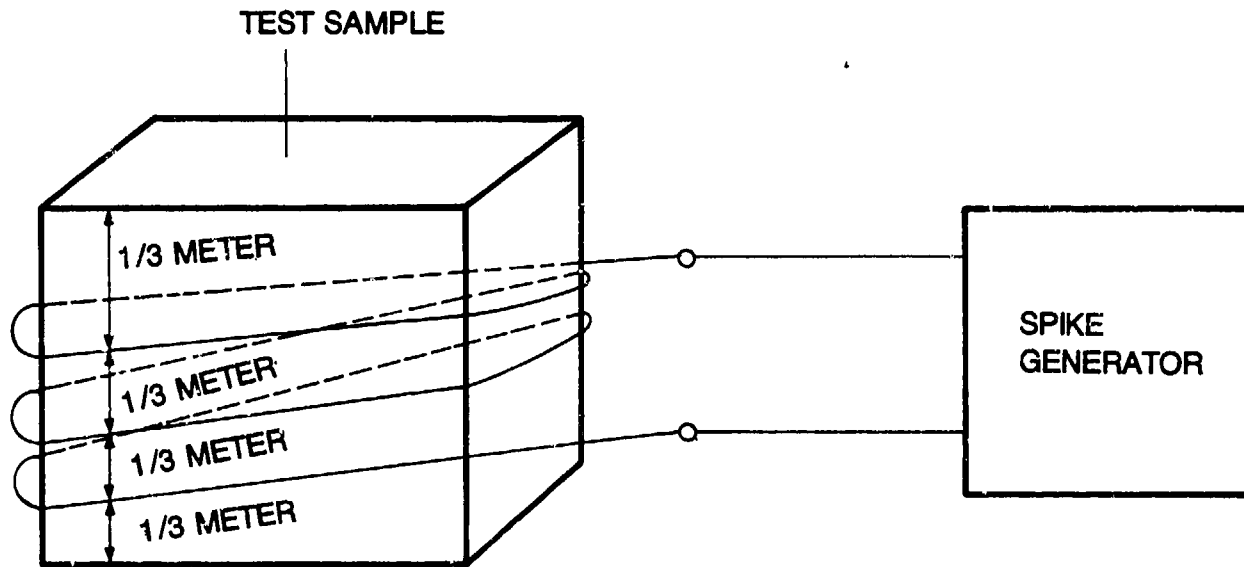


Fig.23 Test-set-up for magnetic-field-test

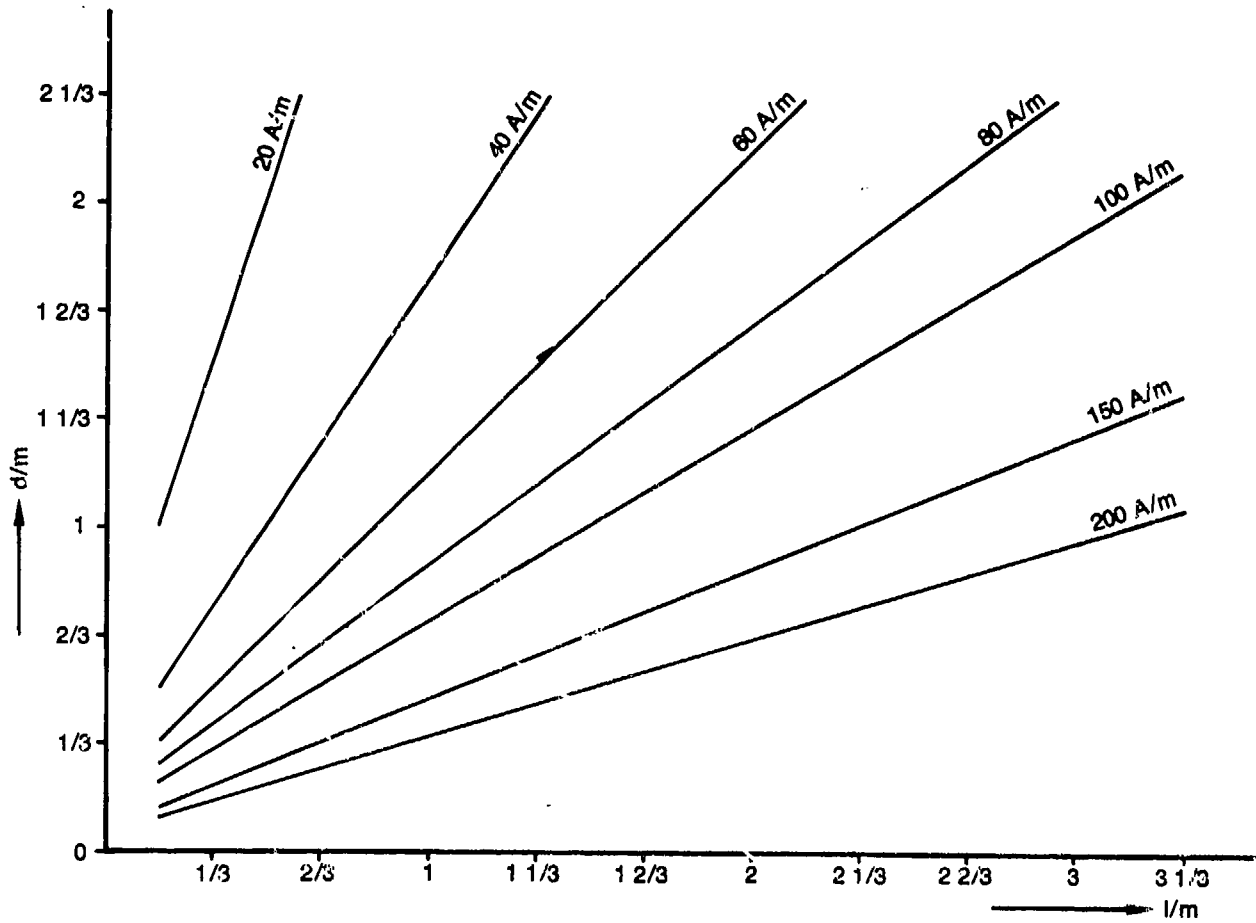


Fig.24 Limit for magnetic-field-test (RS02)

		EXISTING REQUIREMENTS	REMARKS
"MECHANICAL" ASPECTS		MIL-B-5087B	NOT ADEQUATE TO CFRP-AIRCRAFT; SAE PROPOSAL NOT IN FORCE
ELECTRICAL ASPECTS FOR EQUIPMENT	MAGNETIC FIELD	MIL-STD 461/2/3	NOT ADEQUATE
	SPIKES ON POWER LINES	MIL-STD 461/2/3 MIL-E-6051	NOT ADEQUATE
	SPIKES ON SIGNAL LINES	NO DOCUMENT	NO REQUIREMENTS
ELECTRICAL ASPECTS FOR SYSTEM		MIL-B-5087B ONLY SOME DESIGN GUIDELINES	NOT ADEQUATE

Fig.25 Summary of lightning protection requirements

"MECHANICAL EFFECTS"	<ul style="list-style-type: none"> - STRIKE AND RESTRIKE DEFINED (ADEQUATE LIGHTNING STROKE FOR CFRP STRUCTURES)
"ELECTRICAL EFFECTS"	<ul style="list-style-type: none"> - APPLICABLE ON EXTERNALLY MOUNTED HARDWARE - ONLY SYSTEM-TEST! - NOT APPLICABLE FOR AVIONIC EQUIPMENT TESTS

Fig.26 Important statements of SAE-AE4-proposal

A) EXOATMOSPHERIC PULSE

AMPLITUDE: CA. 50 KV/M
 RISE TIME: SOME NANOSEC
 P.-WIDTH: 0.5 MICROSEC
 PULSE IS PRESENT IN A WIDE-SPACED AREA;
 ALMOST NO OTHER WEAPON EFFECTS

B) ENDOATMOSPHERIC PULSE

AMPLITUDE: DEPENDS ON DISTANCE
 RISE TIME: SOME NANOSEC
 P.-WIDTH: SOME 100 MICROSEC
 ALL OTHER WEAPON EFFECTS ARE PRESENT DEPENDING
 ON DISTANCE IN DIFFERENT RATIOS.
 IF "BALANCED PROTECTION" FOR AIRCRAFT:
 NEMP SOME KV/M

Fig.27 NEMP-threat to aircraft

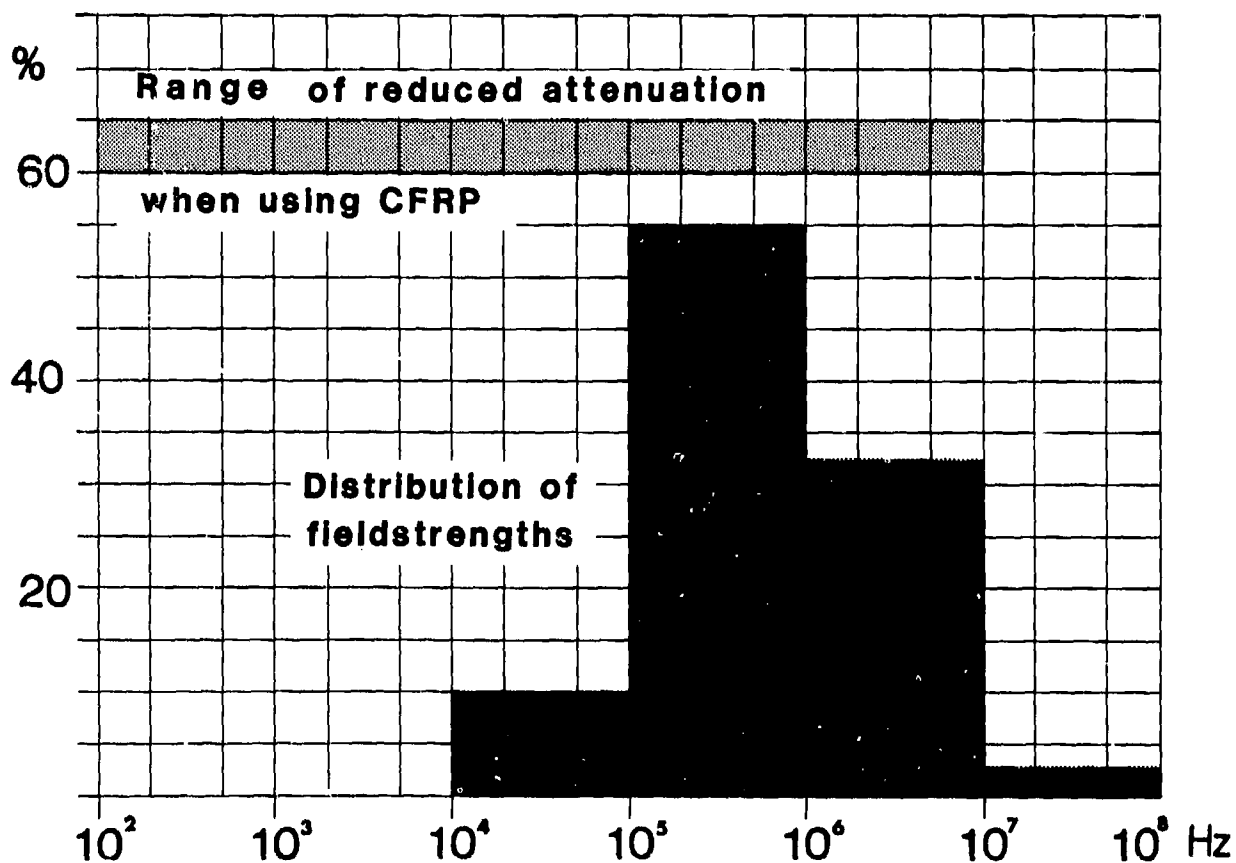


Fig.28 Typical spectrum of exoatm. NEMP

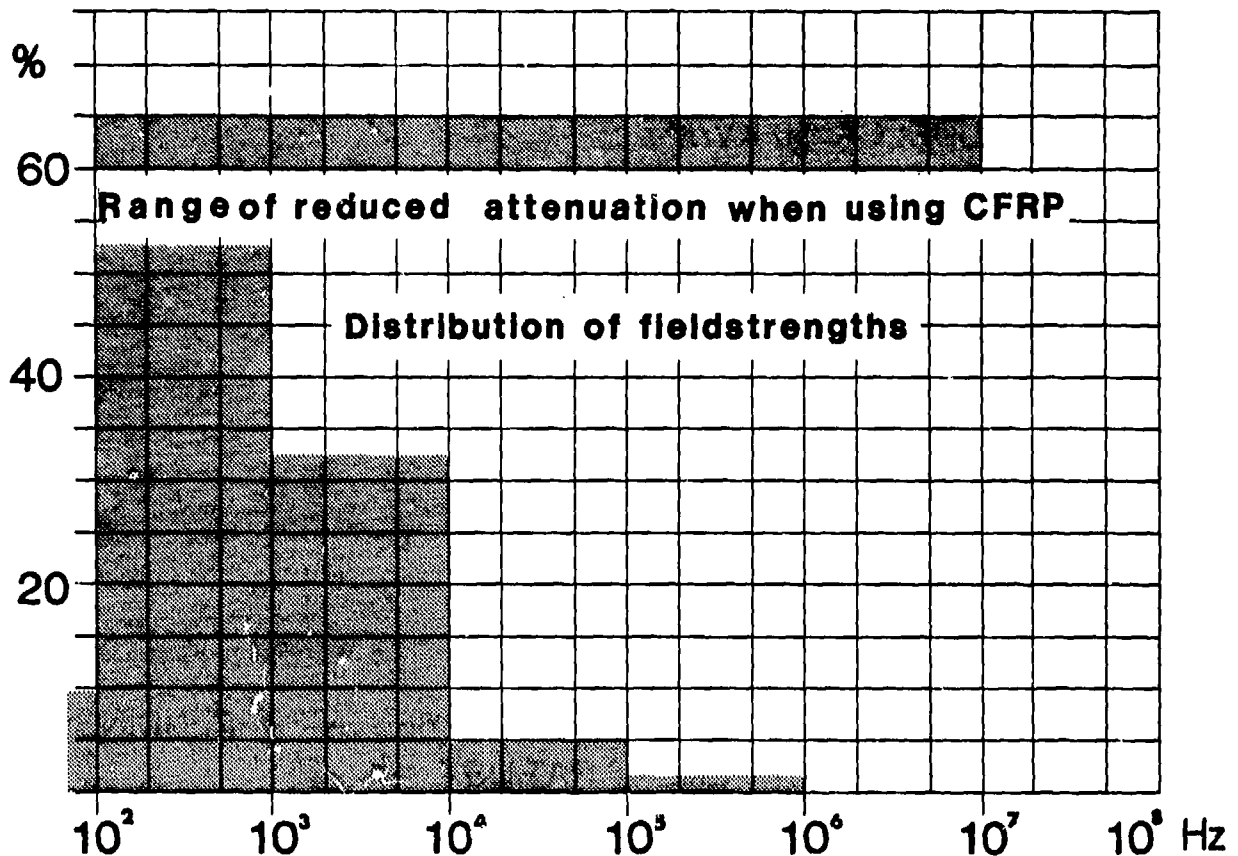


Fig.29 Typical spectrum of endoatm. NEMP

SUBJECT		PROBLEMS	CONCLUSIONS
EMC		<ul style="list-style-type: none"> - SUSCEPTIBILITY AGAINST RF-ENERGY - RADIATED EMISSIONS - CONDUCTED SUSCEPTIBILITY - CONDUCTED EMISSIONS - SYSTEM MEASUREMENT 	MODIFICATION OF LIMITS NEW TEST METHODS NECESSARY
E-STATIC		—	OBSERVATION OF ALL APPLICABLE PRINCIPLES
LIGHTNING	MECH.	SAE-DOC. NOT YET IN FORCE	SOLVED BY SAE-DOC.
	EL.	<ul style="list-style-type: none"> - SPIKES ON POWER LINES NOT ADEQUATE - NO MEASUREMENT OF SPIKES ON SIGNAL LINES - MAGNETIC FIELD TEST NOT ADEQUATE - NO SYSTEM TESTS SPECIFIED 	MODIFICATION OF LIMITS NEW TEST METHODS AND LIMITS NECESSARY FOR SIGNAL LINES AND MAGNETIC FIELD TESTS
NEMP		THREAT SIMILAR TO LIGHTNING NO ADEQUATE SPECIFICATIONS AVAILABLE	NEW TEST METHODS NECESSARY FOR EQUIPMENT AND SYSTEM TESTS

Fig.30 Present situation on applicable documents for CFRP-aircraft

THE ELECTRICAL EFFECTS OF JOINTS AND BONDS IN CARBON FIBRE COMPOSITES.

J. Brettle*, K.J. Lodge* and R. Poole†

* Plessey Research (Caswell) Limited
Allen Clark Research Centre
Caswell, Towcester, Northamptonshire.
U.K.

† Plessey Electronic Systems Research
South Leigh House,
Havant, Hants., U.K.

SUMMARY

The types of joint investigated in this work included dry compression joints, bolted joints and adhesively bonded structures. Their electrical properties were evaluated from dc up to 50 MHz, as well as certain specific higher frequencies. A variety of pretreatments and assembly methods were investigated. All the joints as initially produced to current aircraft practice had too high an impedance for the electrical requirements of an airframe. Various methods of reducing the joint impedance have been proposed and subjected to electrical and environmental tests. It is now possible to produce electrically 'invisible' bolted joints and adhesive joints with much improved conductivity. It has been found possible to permanently alter the joint impedance by the passage of a current through the joint. This effect has been investigated and a possible mechanism of this effect suggested.

The investigation of the possible production of radio frequency intermodulation products at joints have been carried out, but few intermodulation products have been found from any of the joints examined other than butt joints made with exposed carbon fibres in the joint.

1. INTRODUCTION

1.1. DC and Low frequencies

If carbon fibre composites (CFC) are to be used in aircraft then joints of some form will be inevitable, be they between CFC and CFC or CFC and metal. These joints represent discontinuities in the structure, and designers need to know the effect of these discontinuities on the overall material properties. Much work has been reported on the structural aspects of joints and bonds but to date only a limited amount of published information is available on the effects of joints and bonds on the electrical properties of the airframe. Ideally, we would prefer electrically invisible joints in a superconducting material at all frequencies from d.c. to many GHz.

At first glance, CFC is electrically not a very promising material, consisting of moderately conducting carbon fibres in an insulating matrix, usually epoxy resin. It might be assumed that such an arrangement would be highly anisotropic, with conduction only in the direction of the fibres, but much work, both practical and theoretical, has shown that provided that there is sufficient inter-layer current diffusion, multidirectional lay-ups above a few centimeters in size can be regarded as being effectively isotropic (1,2). These findings apply only to the bulk, as the conditions near the surface are somewhat different in that there is an epoxy rich layer of resin on the composite surface which has been squeezed out of the prepreg during curing.

1.2. Mechanism of RF Conduction in Carbon Fibre Composites

Most of the high-frequency currents flowing in a conductor do so at or near the surface. For this reason, the quality of electrical joints and bonds important to DC and power frequencies in an aircraft structure becomes of less concern as the frequency increases. In a carbon fibre structure, when the bulk conductivity may be of the order of 500 times worse than in aluminium, the skin depth of conductivity at 1MHz is of the order of 2mm. The capacitance between two overlapping or butting surfaces may be sufficient to ensure adequate RF conductivity even though the surfaces may be electrically insulated at DC.

1.3. Effects of Possible Conduction Non-Linearities

One postulated draw-back to the use of carbon-fibre in areas where RF conductivity was required was the possible non-linear effects of joints and bonds in the material, or indeed of non-linear effects in the material itself. Such non-linear effects become important in a compact structure such as an aeroplane, which carries a number of radio transmitters capable of simultaneous operation, whilst at the same time operating receiving equipment from adjacent aeriels. If there are any non-linear effects in the vicinity of the aerial system, it is possible that intermodulation products of the transmitted signals will combine to form unwanted signals at the receiver frequencies, thus greatly desensitizing the receiver. If there are two transmitters, of frequencies f_1 and f_2 , then in the presence of a non-linearity frequencies f_{1p} may be generated where

$$f_{1p} = mf_1 \pm nf_2$$

and m , n , are any integer, possibly large. The possibilities of interference occurring in such a non-linear structure should therefore be considered. If either f_1 or f_2 in the

example above is wideband modulated, then the possibilities for generation of unwanted frequencies are greatly increased.

2. EXPERIMENTAL DETAILS

2.1. Materials

The CFC used in this work was predominantly of two lay-ups both supplied by an aircraft manufacturer and made to their specifications. The prepreg used was Ciba-Geigy Fibredux 914C - XAS-5 and the lay-ups were a 16 ply, 0°_4 , $\pm 45^{\circ}_8$, 0°_4 , and a 40 ply quasi-isotropic (90° , $+45^{\circ}$, 0° , -45° , 0° , $+45^{\circ}$, 90°)₅ lay-ups. The d.c. resistivity of these and other CFCs used have been reported earlier (1).

The bolts used were 5mm diameter titanium alloy countersunk or hexagonal headed bolts typical of those used on current military aircraft although for comparison, aircraft quality steel or brass fasteners were used on some joints. For the adhesive joints, unless otherwise stated, Redux 319A film adhesive was used. This is a high temperature, aluminium filled, film adhesive with an incorporated nylon spacing scrim.

2.2. Experimental Work

For accurate electrical measurements of CFC or joint characterisation, it is essential that the contact between the CFC and the rest of the measuring circuit has as low a resistance as possible. Achieving this involves very careful cutting of the composite, to ensure that the epoxy resin is not smeared over the ends of the carbon fibres and that the damage to the fibres themselves is minimised. For a minimum contact resistance, electrical contact has to be made to as many of the exposed fibre ends as possible. In this work, this was achieved by electrolessly plating the ends of the composite with copper (3). This could be subsequently thickened up by soft soldering, or by electroplating. The leads from the measuring circuit could then be soldered directly onto the sample.

Direct electroplating onto the composite could also be used, but although this has sufficient adhesion, the electrical resistance was higher than the electrolessly plated samples. The resistance contribution from the electrolessly plated contacts was calculated from measurements of the resistance of different lengths of CFC and was found to be very much smaller than the material or joint resistances, having a contact resistance, unit area of less than $2 \times 10^{-8} \Omega m^2$ (inversely proportional to contact area) or expressed as a contact conductance per unit area, 5×10^7 mho/m².

2.3. Measurement Technique

All dc resistance and low frequency impedance measurements were made using a four contact technique to monitor the potential drop across the sample under test. Unless otherwise stated, the test current used was 10mA, 80Hz and was measured via the voltage across a standard non-inductive resistor. Contacts were normally soldered to the ends of the sample except in the case of potential mapping where sharp scalpel blades were pushed into the composite surface.

The effective series resistance (ESR) and other equivalent circuit values were determined using a Marconi Circuit Magnification Meter, type TF 1245A and associated oscillators up to frequencies of 50MHz. This was the 'Q meter' method which has been described elsewhere (4). At frequencies above 50MHz the samples become electrically 'too large' for realistic results to be obtained by this method.

2.4. Investigation of Non-Linearity in Carbon Fibre Material

For the reasons discussed in 1.3 it was required to establish to what extent, if at all, carbon fibre materials would contribute to the generation of intermodulation products (I.P.). For ease of experimental technique and interpretation, a harmonic generation method was used, illustrated in Figure 1. A high power signal generator, whose output is carefully filtered to remove all harmonics, drives an aerial to illuminate the sample under test. A second aerial, covering the second and third harmonics of the driving signal, picks up any harmonic signal on a synchronous receiver. Due to the sporadic nature of harmonic returns, a statistical analysis is performed on the sample, the results being displayed on an HP 3721A correlator. Typical results are shown in Figure 2.

The majority of measurements have been made with a transmitting frequency of 430 MHz. Some more limited results have been obtained at 220 MHz and 1200 MHz. Samples measured have included specimens of single sheets of material of various thicknesses, bonded assemblies, screened assemblies, assemblies bonded to metal, flame sprayed panels and various cut and damaged specimens. Measurements were taken in an anechoic chamber for the 430 MHz results and out of doors for the remaining frequencies. Second and third harmonics were examined in each case.

3. ELECTRICALLY ALTERED JOINT RESISTANCE

One of the most significant results found in this work was the fact that the initial resistance of an 'as made' joint was not stable, but could be altered by the passage of an electric current across it. The effect was roughly proportional to the size of the current so that after the resistance had been changed, a subsequent, larger current would alter the resistance again, whereas a subsequent, smaller one would not. The effect seems to be permanent and has been seen with current densities as low as $0.01A/m^2$. Both alternating

and direct currents produce this effect, but a.c. seems to be the more 'efficient'. In the majority of cases, the resistance of a joint has been lowered, but on two occasions the resistance of a joint increased due to the passage of current.

This effect has been seen on all types of joints examined in the work. It was found with dry joints, held together by external pressure, although not with joints whose mating surfaces had been abraded, despite joint temperatures in excess of 210°C. Bolted joints with abraded mating surfaces also did not show this effect, but although the effects were masked by the presence of the electrical short circuit provided by the bolts, it could still be found on the 'as received' joint. Adhesively bonded joints showed the largest effects, with both abraded and unabraded mating surfaces, in some cases showing a joint resistance change over four orders of magnitude.

Although potential mapping of the surface of the joint showed no variation, the effect seems to be very localized. Cutting a joint which had shown a large resistance drop into a number of thin slices gave smaller joints whose resistances varied by a ratio of 1:10⁹. It was impossible to distinguish any marks produced by the passage of small currents across the joint but the passage of large current densities (up to 300,000A/m²) produced burnt areas of free carbon fibres, devoid of epoxy resin (Figure 3).

It was to minimise the effect of this current induced resistance change that all work, except where stated to the contrary, was carried out at 10mA at 80Hz. In addition an electrical history of each joint was kept.

4. DRY JOINTS

An examination of the surface of CFC shows that the epoxy rich surface layer takes up the shape of either the bleed cloth or the smooth backing plate used in manufacture, (Figure 4) and in a plain lap joint, any electrical contact into the composite must be through this material. On the smooth, tool face side of the material there will be many points where the carbon fibres are exposed and contact can be made, but on the bleed cloth side, the situation will be different. Figure 5 shows decorated CFC surfaces, where using an electrochemical technique copper has been deposited only where the carbon breaks through the epoxy resin. As can easily be seen, the breakthrough points occur almost entirely at the bottom of the 'valley' caused by weave of the cloth. If two of these surfaces are brought together, as in a dry joint, then the carbon to carbon contact points are at best going to be separated by twice the "hill" to "valley" distance, giving a separation in this case of ~60µm. Provided no loose fibres cross this gap, then the voltage required to pass a current is very high. Assuming the potential required to discharge across dry air at atmospheric pressure to be around 3Kv/mm (5), this would require a potential of ~180V across 60µm assuming clean contacts. Experiments with dry joints held together under pressure have shown that for low clamping pressures, continuous conduction does not occur until voltages of around 200 volts and that with increasing pressure this voltage drops. When the pressure reaches ~20 x 10⁶ N/m², conduction can be obtained at applied potentials of less than one volt. Short, intermittent discharges occur before the onset of continuous conduction, presumably due to closer gaps between individual, misaligned fibres (Figure 6). As these contact and take the total current flow they presumably overheat and burn out.

5. BOLTED JOINTS

5.1. DC and Low Frequency Properties

The layout of the bolted joints used in this work is shown in Figure 7, the dimension of the joint being determined by the bolt separation and these followed normal aircraft practice. The bolt holes were drilled so as to minimise the damage to the side walls of the hole. This is very important as badly drilled holes can give rise to high and irregular joint resistance. Trace A in Figure 8 shows the joint resistance of a CFC/CFC joint in which the holes have been drilled too quickly, giving a high resistance compared to that of trace B, a correctly drilled joint.

Most of the joints used in this work were made with countersunk bolts as this was thought to give better electrical contact due to the increased CFC/metal interface area. However, measurements showed that a hexagonal headed bolt had a 64% lower resistance (at dc) than a countersunk one. This was thought to be due to the pilot of the countersinking bit damaging the surface of the lower bolt hole and increasing the bolt/CFC resistance. Despite this, this work continued to use this method of countersinking as it was felt to be more in line with aircraft practice than alternative methods.

It is also aircraft practice to 'wet' assemble joints using sealants and trace C in Figure 8 shows the effect of assembling a correctly drilled countersunk joint using a polysulphide type sealant. It can be seen that the use of sealant has only a limited effect above a moderately high bolt tightening torque.

The impedance values of these joints remain at their dc levels until frequencies of ~0.7MHz, above which they start to fall. (Figure 9). Also shown on this graph is the effective series resistance (ESR) of these joints derived from the 'Q meter' and these are also around the dc resistance values upto ~10MHz, above which they start to increase.

These values of joint resistance, even with the correct hole drilling, are too large for practical purposes and efforts have been spent on reducing the joint resistance. Potential mapping of the joints was carried out to try and locate the source of the resistance in

the joint. Figure 10 shows a cross section of a countersunk bolted joint with the potential differences between the points shown marked on. Where there are three values shown, they refer to the three bolts on the sample, the first value being the bolt furthest into the plane of the paper. Although a constant test current was used, because of the multiplicity of possible parallel paths it is not possible to convert these potential drops into resistance values, although the potential drops are a reasonable indication of the size and location of these resistances.

From these tests and from joints made with interleaved non conducting spacers, it is evident that the majority of the current crosses the joint via the bolts. In Figure 10, it is evident that most of the resistance is located in the bolt head/CFC countersink interface. Joints made with steel or brass bolts do not show the high resistance in this area and it was assumed that it was due to the titanium oxide film present on the bolt. Removing this film with a nitric acid/hydrofluoric acid etch significantly lowers the joint resistance as can be seen in Figure 11. Unfortunately, the removal of this anodised layer would not be permitted in aircraft practice, nor would the use of steel or brass bolts!

The nuts used to make most of these joints were hexagonal headed cadmium plated aircraft quality steel units. Conduction into the composite nearest to the nut must be either via the bolt shank or through the epoxy resin under the nut head, and a study of the potential differences in this region suggest that most of the conduction is via the nuts, Figure 12. This is despite the presence of the epoxy rich layer on the surface of the composite. Removing this layer and replacing the nut with countersunk steel nuts did not significantly lower the resistance in this area.

Other attempts to lower the joint resistance centred on the sides of the bolt holes. Coating the insides of the holes with a conductive coating should ensure that all the exposed carbon fibres are placed in contact with the bolt if the bolt makes contact with any one part of the hole. Several coating methods and metals have been examined and provided all have the same thickness and surface finish, all give essentially the same results. In all cases the joint resistance was very low, giving a practically invisible electrical joint (Figure 12). Any further improvements in the joint conductivity would make a negligible contribution to the overall conductivity which is dominated by the properties of the material.

An alternative approach to the reduction of joint resistance is the provision of another electrical path across the joint. The simplest way is to abrade the mating surfaces of the composite to give direct carbon to carbon contact. This considerably lowers the joint resistance which is not significantly increased by the use of sealant (Figure 4). However, as this method relies on individual carbon to carbon contact, the joint resistance is still too high. It can be reduced still further by coating the abraded surfaces with metal, which connects all the exposed fibres together. Coating the cut end also provides an alternative current path, obviating the need for the surfaces to be abraded (Figure 15).

5.2. The Impedance of Bolted Joints in the Range 0.1 - 50MHz

Two frequency dependent properties of these joints have been examined, their impedance and their effective series resistance (ESR). Although identical at low frequencies, these could show increasing divergence at higher frequencies.

The joint impedances tend to fall into three types (Figure 16). These are those impedances which tended to fall as the frequency rose. These included the untreated, standard joints and those made using sealants, Figure 9. The second type of joints are those whose impedance rose at the same rate as the ESR and these included abraded joints and those bolts who had the anodized coating removed. The final group were those whose impedance rose faster than the ESR and these included joints which had been metal coated. In all cases, the ESR was constant upto ~ 3 -5MHz, after which the value rose steadily.

6. ADHESIVELY BONDED JOINTS

6.1. DC and Low Frequency Properties

Due to the thick layers of adhesive which are present in bonded joints in addition to the epoxy resin on the CFC surface, they are extremely sensitive to the effects of current passage as discussed earlier. Consequently, reproducible results have been difficult to obtain. It would appear that for joints made to a similar design to Figure 4, an initial resistance (measured at 1mA DC) would be in the 1-2k Ω region. Abrading the joint surface prior to bonding lowers the resistance by about one half. The passage of currents from as low as 0.01A/m² will alter this value and resistances in the m Ω region have been obtained after passage of current densities of upto 700A/m². A change of this magnitude is, however, accompanied by considerable heating and a rather acrid smell!

Attempts to lower the joint resistance of the bonded joints have centred on reducing the adhesive resistance. Although the adhesive used (Redux 319A) is metal filled and has a lower volume resistivities than other adhesives, the use of a silver filled epoxy adhesive lowered the resistance of a joint to that comparable to a good bolted joint ($\sim 100\mu\Omega$) Redux 319A has a nylon scrim incorporated into the film for control of the glue line thickness. When this was replaced by metal gauzes of the same thickness the joint resistance was reduced to less than 1% of the joint as made with nylon scrim. There was no effect of the current dependent resistance in joints made with metal scrims. A variety of conducting scrims were used including stainless steel and carbon fibres.

Conducting overlays over the joint also reduced the joint resistance by providing alternative current paths avoiding the high resistance adhesive layer.

6.2. The Impedance of Bonded Joints in the Range 0.1 - 50MHz.

An impedance versus frequency plot is shown in Figure 17 and is typical of all the bonded joints not incorporating a metal filler or gauze. The impedance starts to fall above 0.5MHz and falls in a similar fashion to the ESR. The straight line drawn on Figure 17 shows the calculated impedance drop for a capacitor of the same size and spacing and a dielectric constant of 4.

7. INTERMODULATION PRODUCTS

In general, most measurements with single sheets of material, or with bonded assemblies, or assemblies bonded to metal, gave negative results. Exceptions were two experimental trim tabs, each containing a metal hinge and from experience it was considered that the hinge was the probable source of the harmonic radiation. When two cut edges were placed together loosely, however, a strong third harmonic signal was observed, accompanied by a weak second harmonic signal (see Figure 2). These signals are weaker than those typically received from a metallic assembly. Results from specimens that had been deliberately cracked also showed some small amount of third harmonic generation present.

8. ENVIRONMENTAL TESTING

For any of these improved joints to be of practical value, they must be able to withstand the wide variety of environmental conditions to which an aircraft is subjected, without any degradation of their properties. Therefore, a series of environmental tests have been proposed and the new jointing methods subjected to them.

The initial test has been exposure to accelerated corrosion conditions. There is no standard test for CFC and so the 1000 hour salt spray corrosion test has been used, as this would allow direct comparison with earlier work on metallic joints (1). Exposure of metal/CFC couples to this test showed that, with one exception, corrosion had started within 150 hours and got progressively worse during the duration of the test. The exception to this was the silver coated samples which showed no signs of corrosion at the end of the one thousand hours.

Several types of bolted and bonded joints were exposed to this test, and although all of the nuts showed evidence of corrosion, none of the electrical properties, either at dc or at higher frequencies were effected (Figure 19). The adhesively bonded samples however, although showing no visible signs of corrosion, had a dc resistance 15% higher than the uncorroded specimens, even though their high frequency properties remained the same.

The adhesion of the metal coating to the CFC was tested by measuring the shear strength of lap joints made with the coated samples. Satisfactory adhesion was obtained with electroplated samples, but the flame sprayed samples only gave reasonable adhesion when the surface was heavily shot blasted prior to coating (Figure 20). This resulted in a degree of surface roughness and damage to the carbon composite which is unacceptable to the aircraft industry.

These adhesion tests also showed that the use of metal gauzes in place of the nylon scrims did not lower the joint adhesion significantly, and that the passage of large current densities ($20\text{KA}/\text{m}^2$) across an adhesively bonded joint chars and burns the adhesive in the vicinity of the conduction point and may reduce the joint adhesion, Figure 21.

9. DISCUSSION

A major feature of this work is the effect of the passage of current on the resistance of the joint. This effect may have been seen before, an indium-CFC joint at Culham Lightning Studies Unit progressively lowered its resistance with increasing current passage, but the phenomenon was interpreted at the time as a result of the indium ageing (6). The effect may have serious consequences not only in the EMC field, but also on the structural integrity of the joint and its resistance to corrosion.

From the evidence of the types of joint where this effect is found and other work carried out at Caswell, it seems that the effect is associated with the epoxy rich surface layer and the heat generated by the passage of the current. The passage of electric current down an individual fibre into the composite matrix can be followed to the point where the heat generated by the current, and presumably the current itself, is diffused into the rest of the composite, by the softening of the epoxy resin next to the fibre and movement of the fibre itself. In the actual area of contact, where the fibre is carrying all the current, the heat was found to be sufficient to remove the epoxy resin completely, even if the sample had been coated with electrically conducting paint. Individual fibres could be made to glow incandescently for several seconds without burning out, by the passage of only small, milliamp size, currents. In the composite, the only method of dissipating this heat is conduction down the fibre or by evaporation of the epoxy resin in the immediate vicinity of the heat source. As a result of this, there will be an increased area of exposed carbon fibre, possibly with individual loose fibres, Figure 3. Subsequent testing will show a reduced resistance. In the few cases of increased resistance, it is possible that the 'twitching' of the conducting fibre breaks contact with the mating face, or that the local current is sufficiently high to burn out the conducting fibres.

Such a theory, whilst explaining why the effect is found only on samples which have not been

abraded (abraded adhesively bonded samples have simply replaced the epoxy rich layer with an adhesive layer), does not explain how the effect occurs at very low current densities. Because of the need to locate the area of conduction, all visual evidence for this effect has been from samples subjected to high current densities. Under these conditions high current, low voltage arcs can occur (5), but it is not clear what happens at the very low current region which has insufficient energy for sparking. Initial contact may be due to local high potential gradients caused by close proximity of loose fibre ends, or by direct contact, but more work is needed in this area.

Whatever the cause of this effect, it has serious consequences in other areas. The removal of the plastic matrix from the fibres will lower their ability to transmit stresses within the matrix and may cause localized failure. There is some evidence (Figure 21) that the passage of the current will destroy an area of adhesive in a bonded joint. Although the strength drop seen in this work was severe, it is thought that due to the small size of the sample that it was not a representative result, as the size of the burnt out area of adhesive would tend to remain the same, irrespective of the size of the joint.

There has been a tendency to assume that bonded aluminium/CFC joints would be safe from galvanic corrosion due to the insulating effect of the resin and the adhesive. If however, passage of a current through the joint results in a permanent low resistance path through the adhesive, then very rapid galvanic corrosion can occur. This is potentially the more serious problem as one way to prevent this effect occurring is to provide an electrically conducting path across the joint. This would prevent the structural damage, but would accelerate the corrosion of any incompatible metals present.

An improved electrical connection will be needed even for bolted joints as the resistance of a joint assembled without any special pretreatment is still too high to be satisfactory. A bolted joint should have a fairly low resistance as it is provided with a solid metal shorting path across the interface. However, due to structural constraints as to the strength, weight and corrosion resistance of the joint, the shorting path is usually made from titanium or its alloys. The oxide film present on the titanium causes a high joint resistance and removal of this oxide (Figure 9), or replacement of the titanium with some metal with a less resistant oxide would considerably lower the joint resistance, but is not practical due to the above mentioned constraints.

The actual path taken by the current through a bolted joint is by no means clear. It might be thought that all the current would cross the joint line by means of the bolt, but the existence of a current modified resistance effect in bolted joints shows that there is still sufficient "driving force" to create new current paths independent of the bolts. The constriction seems to be the interface between the carbon fibre composite and the metal, be it of the shank or the head. The effect of oversized bolt holes (Figure 8) would suggest the main conduction path was via the bolt shaft, but the attempt to bypass this interface by providing countersunk nuts and bolt heads with increased CFC/metal interface area, gave improvements of only limited value (Figure 10). This would seem to imply that conduction also occurs via the underside of the hexagonal headed bolt and that this conduction is almost as good as that obtained by the countersunk bolt against the exposed carbon fibre of the countersink. The reason for this may be that the pressure generated under the nut and bolt head is high enough to damage the epoxy layer sufficiently to obtain a low resistance path through it. In the case of dry, compression joints the load necessary to obtain this condition was $\approx 20 \times 10^6 \text{ N/m}^2$. Due to the uncertainties of the friction, and the presence of relative motion and other factors, it was not possible to calculate the exact pressure beneath the nut and bolt head of samples used in this work. However, from published information (7) and rough calculations it appears that it is entirely feasible that the stress of $20 \times 10^6 \text{ N/m}^2$ may be reached by a bolt tightening torque of 2Nm, thus allowing a relatively low resistance path from the nut or bolt head into the composite. This low resistance path formed at $\approx 2 \text{ Nm}$ would then explain the shape of the torque/resistance curves seen with bolted joints (Figure 8).

It seems likely that both the CFC/metal conduction paths are operating at the same time, but the exact balance of the current routes will depend on a number of factors, such as surface preparation, the state of the oxide layer etc.. Slight variations in these factors could alter the balance and significantly alter the overall joint resistance.

Attempts to improve the conduction of a bolted joints have used two approaches. One, to increase the numbers of contacts available and two, to improve the contact between the two sides of the joint or between the composite and the bolt. The first has been achieved by either abrading the surface so as to expose many carbon fibres, or to plate the carbon fibre surface so as to connect together all the exposed fibres. Thus contact to one is equivalent to contacting all the fibres and the current is therefore more readily, quickly and uniformly conducted into the body of the composite. Some methods such as coating the insides of bolt holes, use both approaches as the plating contacts all the exposed fibres in the hole and at the same time constricts the hole, making more intimate contact with the bolt. Using these approaches, it has been possible, depending on the method and materials used, to produce ideal, electrically 'invisible' bolted joints.

Their electrical properties at higher frequencies depend on the pretreatment the joints have received. The bolted joints which had no pretreatment, and those which were wet assembled had impedances which fell below the E.S.R.. In all these cases, there was a layer of epoxy or polysulphide type sealant between the two faces of the joint and it seems likely that despite the presence of an electrical short via the bolts, the sample is reacting as a capacitor with a low parallel resistance path. Samples which had been abraded and had no sealant between their faces had many direct carbon to carbon contacts and so any capacitance

the joint may have had was masked by the resistance of these contacts. The impedance of these joints was the same as the ESR. The third type, which comprised of the samples with metal coated bolt holes rose faster than the ESR. This may have been due to a resonance effect caused by the inductance of the metal 'tubes' or it may simply be due to the inductance of the system being detected at the much lower resistance levels found in these joints.

Because of the thick layer of resin and adhesive between the faces of an adhesive bond it is especially sensitive to the current dependent resistance effect, and it is difficult to determine what the normal conductive state of this joint would be. As the main adhesive used for this work is a high temperature adhesive and is loaded with aluminium powder, the normal conduction may be by a percolation effect. The passage of current must modify this, possibly by carbonization of the resin between the aluminium particles. There is certainly evidence of intense localized heating following the passage of a large current through these joints and it could be assumed that the same effect occurs, on a smaller scale, with lower current densities.

To obtain electrically conducting adhesive bonds, a conducting path through the adhesive must be made. Loading the adhesive with silver greatly improved the conduction, but only when the epoxy rich surface layer was removed. This was true of all the adhesive bonds, as it appears that the number of contacts through the surface layer of epoxy is a limiting factor in improving the joint conduction, and for an 'improved' joint the surface layer must be removed. This is not such a serious problem as might be thought as adhesive bonds tend to be made with abraded CFC surfaces. The use of silver loaded adhesive is a problem however, and not only from cost and weight aspects, as the amount of metal which needs to be added to the adhesive to ensure conductivity is such as to seriously reduce the strength of the adhesive. The provision of metallic conducting paths via the use of metal gauzes does not reduce the bond strength, but does not produce as low a bond resistance as the silver loaded adhesive. However, further work with different materials, size and weave may improve this.

The behaviour at high frequencies of the bonds made with metal gauzes and the abraded and silver filled adhesive was similar to those of bolted joints, and would suggest the presence of many, essentially resistive, parallel paths across the joint. The behaviour of the other bonded joints however is not so easily explained, as what appears to be a capacitive drop occurs at an order of magnitude too low a frequency. This may be a size effect, or some change in the electrical properties of the adhesive. One interesting fact which may or may not be significant is that the upturn in the ESR above 30MHz (Figure 17) occurs at the point at which the curve would have intersected the ESR curve for a bolted joint if they were plotted together. This may be a coincidence or may possibly be a consequence of the size of the samples. When all the ESR's of the joints made to this size of sample are plotted on the same graph (Figure 22), their values of 40-50MHz tend to lie in the region 0.5-1.5 Ω , irrespective of their initial values which ranged from 25m Ω to 50 Ω . This may be due to the measurement system used but later results in this work show that the construction of the joint tends to become electrically unimportant at RF frequencies and this may be the first indication of that.

Whilst it may not be too important how a joint is made at high frequencies, it is still necessary to improve the 'as made' joint conduction at dc and lower frequencies. It is possible to construct electrically perfect joints, but these are not galvanically compatible, nor are they easy to make on a production basis. Improved jointing methods which are both compatible with carbon fibre composite and capable of being used on a real engineering basis have been produced. These are electrically considerably better than the untreated joints but go only partway to perfection. More work is needed to combine the desirable properties of both methods of fastening.

It should be noted that the type of joints examined here represent the simplest types of joint and composite and in practice the joints will be much more complex. The composites could be combined with non-conducting composites such as glass or Kevlar, either as inter-layers or as surface faces. The composite could incorporate honeycombs, or be foam or metal filled and the jointing method may be used in combination with other fastening methods. In such cases the electrical aspects of each material and joint will have to be considered individually until a sufficient body of information is built up to enable design rules to be established.

10. CONCLUSIONS

- 1) As initially made, joints in carbon fibre composites are not good electrically at dc and low frequencies.
- 2) Bolted joints can be made electrically transparent with suitable pretreatment, but such pretreatments are not environmentally stable, giving rise to galvanic couples with the carbon. It may be possible to use some of these jointing methods if a suitable form of protection can be found, possibly the use of sealants.
- 3) Adhesive joints can also be improved electrically, but not to the same extent as bolted joints.
- 4) The resistance of joints which contain a layer of epoxy resin or adhesive between the mating surfaces can be altered by the passage of an electric current through the joint. This effect has repercussions in the corrosion resistance and structural integrity of the joint.

- 5) The method used to construct the joint tends to be of less significance at higher frequencies.
- 6) It appears from the limited results available that carbon fibre materials, in bulk, or rigidly bonded or screwed assemblies, show no detectable harmonic generation, and hence no I.P. generation. They may well be better than aluminium in this respect. However, bare cut edges, if touching, may set up considerable third harmonic radiation. This could occur, for example, if a hatch cover vibrated against its mounting. It would appear desirable, therefore, that cut edges be suitably treated.

11. ACKNOWLEDGEMENTS

The authors would like to acknowledge the financial support and the provision of samples for this work from the Ministry of Defence (Procurement Executive) and British Aerospace, Warton Division.

12. REFERENCES

- 1) J. Brettle, M.W. Baskerville, 'Electrical Bonding in Aircraft'. Proc. Int. IEEE Symposium on EMC, Oct. 9-11, 1979, San Diego, Cal., U.S.A. pp. 124-130.
- 2) D.C. Brewster, "Theoretical calculation of rf properties of carbon fibre laminates" AGARD Avionics Panel Specialists' Meeting on the electromagnetic effects of (carbon) composite materials upon avionic systems. Lisbon Portugal, June 15-19, 1980.
- 3) Provisional U.K. Patent Application No. 79/04102. The Plessey Co. Ltd., 1979. See also Appendix of ref. (4).
- 4) "Measurements of rf properties of carbon fibre composite material (CFC)" ERA report No. 3320/R/2 Sept. 1979.
- 5) G.A. Farrall "Arcing phenomena at electrical contacts" Electrical Contacts 1969 pp. 119-144.
- 6) Private communication, CLSU .
- 7) Design News May 22nd 1972 27, 10, pp.68.

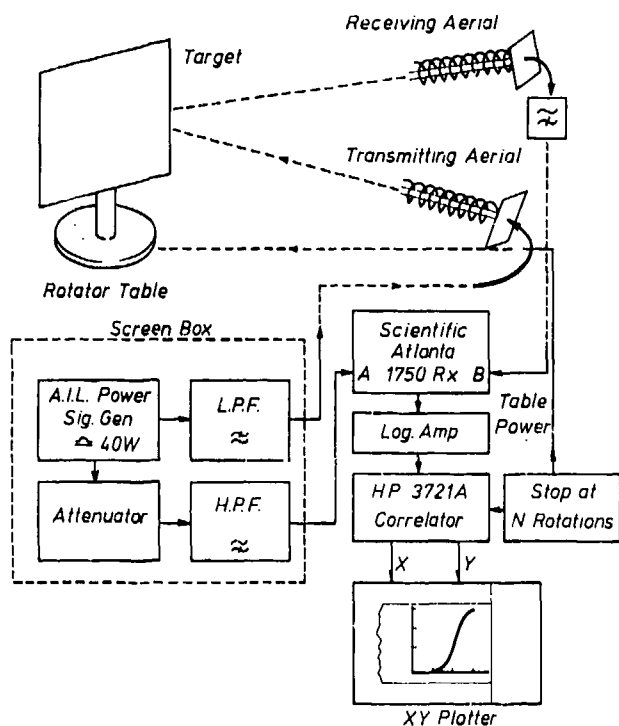
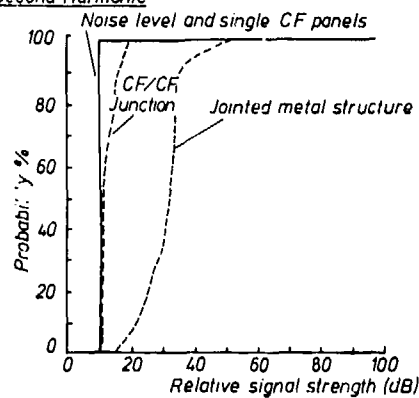


Figure 1 Test Equipment to Measure Harmonic Cross Sections

(a) Second Harmonic



(b) Third Harmonic

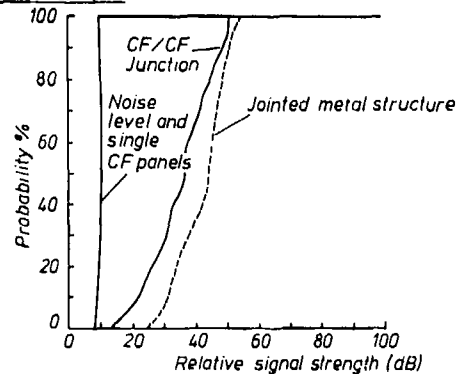


Figure 2 Second and Third Harmonic Probability Integral Plots for 430MHz

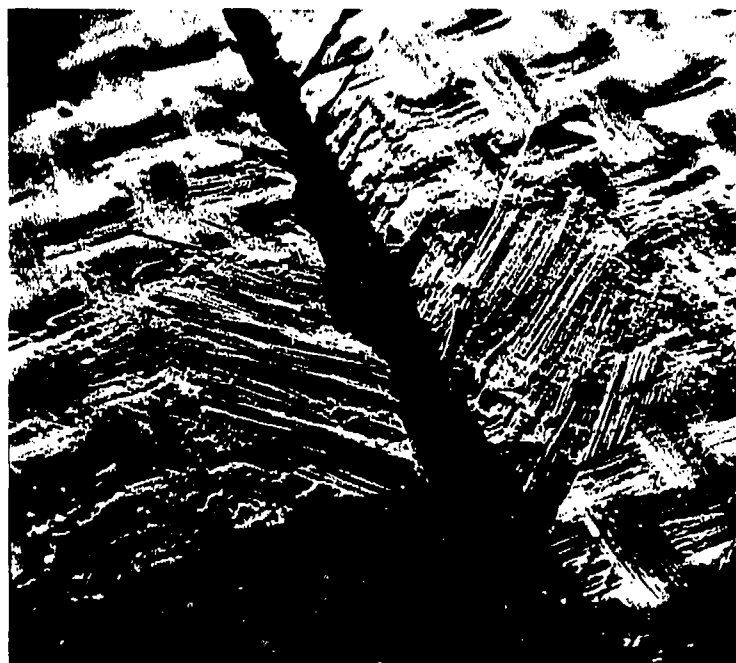


Figure 3 Scanning electron micrograph of carbon fibre composite showing site of the passage 8A current (x23)

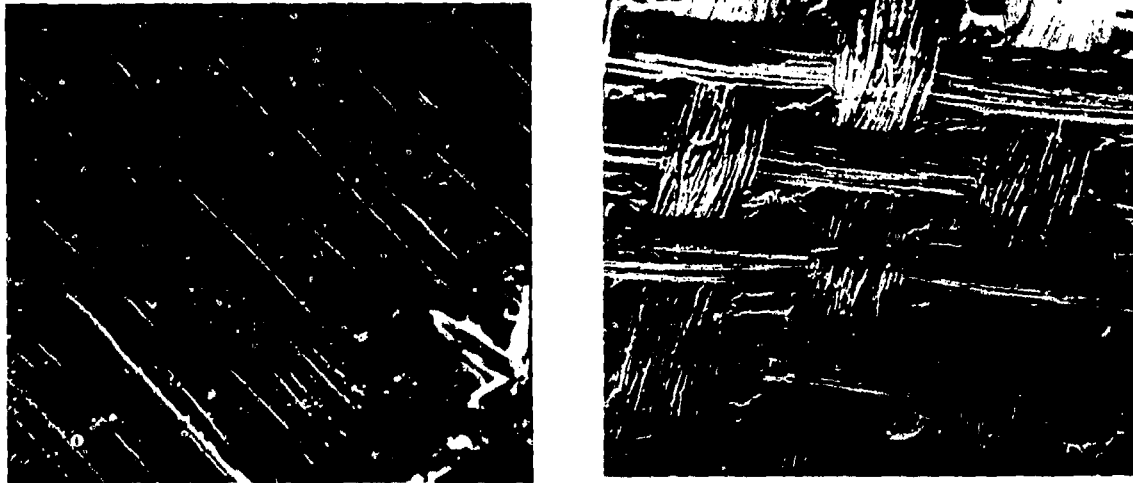


Figure 4 Scanning electron micrograph of carbon fibre composite showing (a) impression of tool face (x100)
(b) impression of bleed cloth (x48)

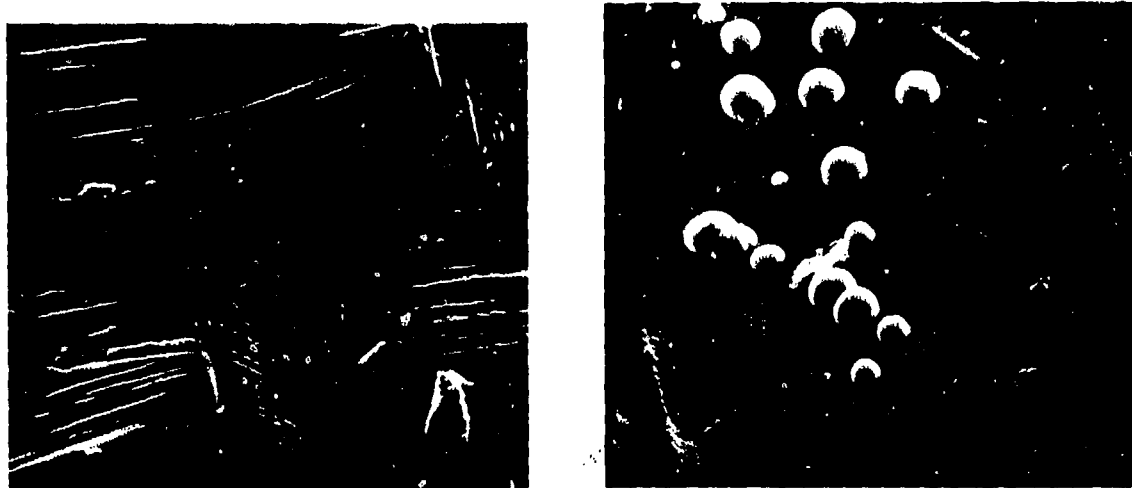


Figure 5 Scanning electron micrograph of carbon fibre composite showing impression of the bleed cloth. Where the carbon fibres break through the surface they have been decorated with copper nodules (a) x 100 (b) x 1,100

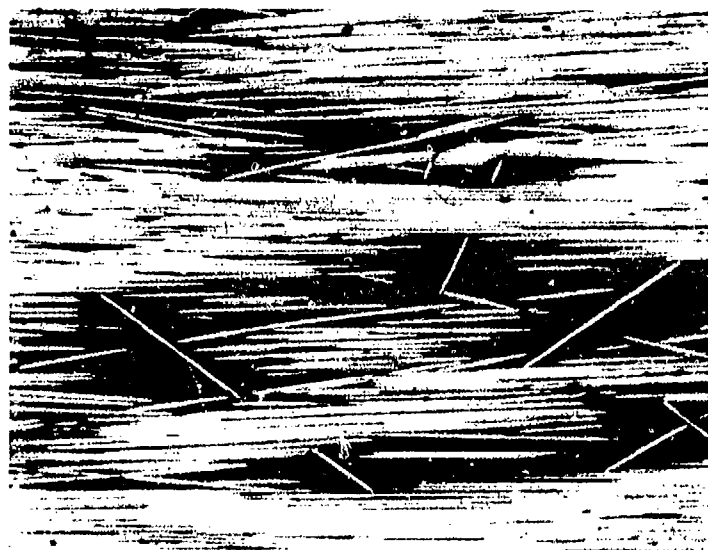


Figure 6 *Optical micrograph showing non-aligned fibres between ply surfaces x60*

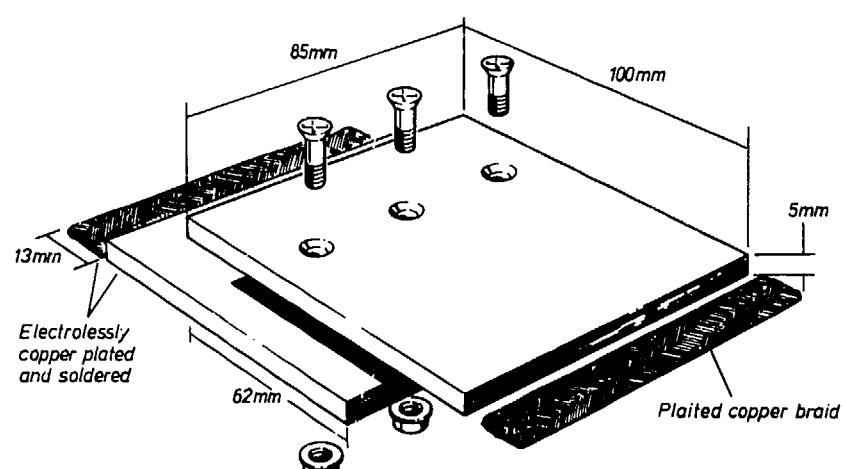


Figure 7 Layout of Bolted Joint in CFC

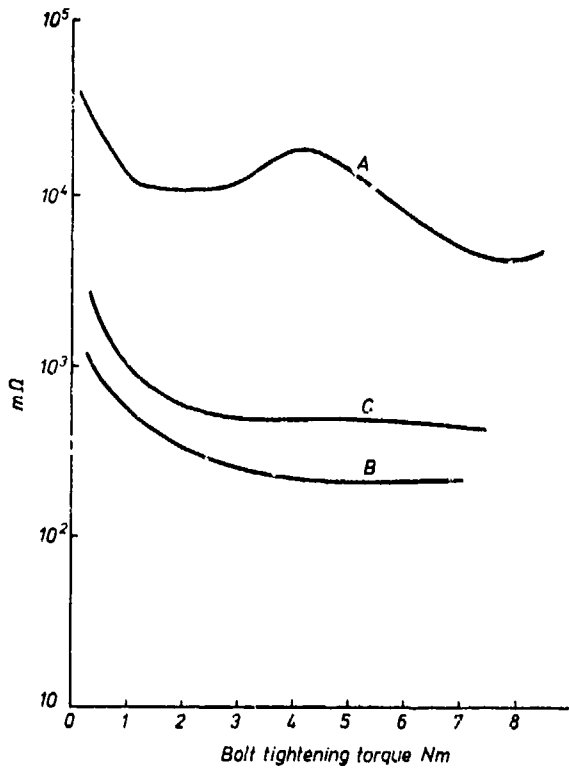


Figure 8 The effect of bolt tightening torque on the joint resistance

- A. Oversized holes
- B. Correctly drilled holes
- C. AsB, wet assembled with poly-sulphide type sealant

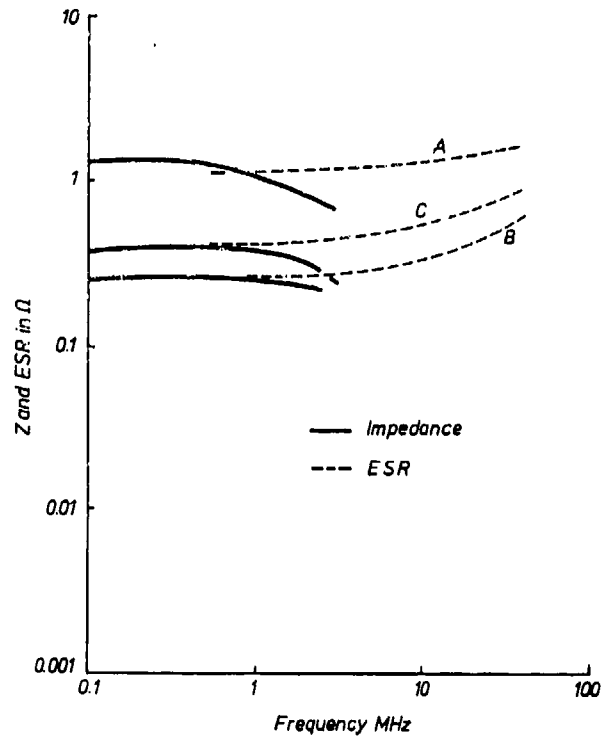


Figure 9 The effect of frequency on the impedance and ESR of the joints referred to in Fig 8

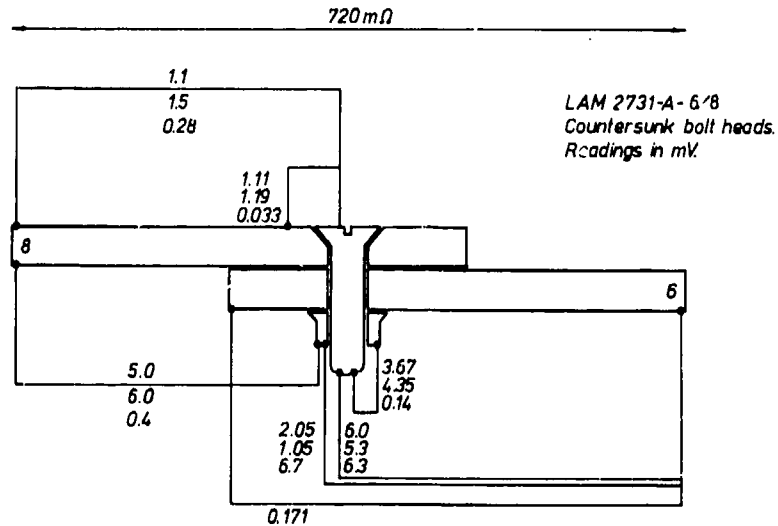


Figure 10 Potential drop across joint made with titanium alloy counter sunk bolts and cadmium plated steel nuts 10mA 80Hz test current.

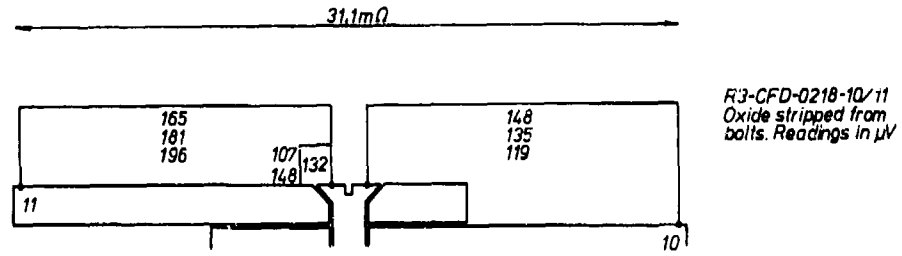


Figure 11 As Fig 10 but with oxide removed from the titanium alloy bolts

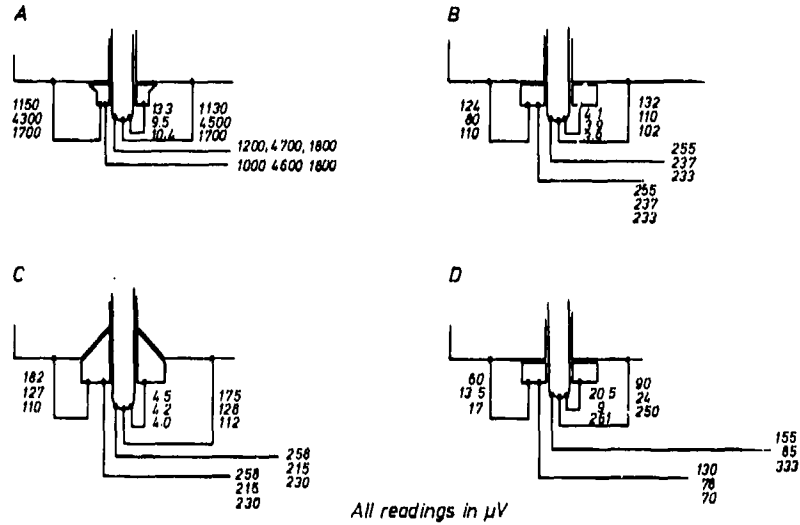


Figure 12 Potential drop across nut/CFC interface

- a. cadmium plated hexagonal steel nuts
- b. steel hexagonal nuts
- c. steel countersunk nuts
- d. brass hexagonal nuts

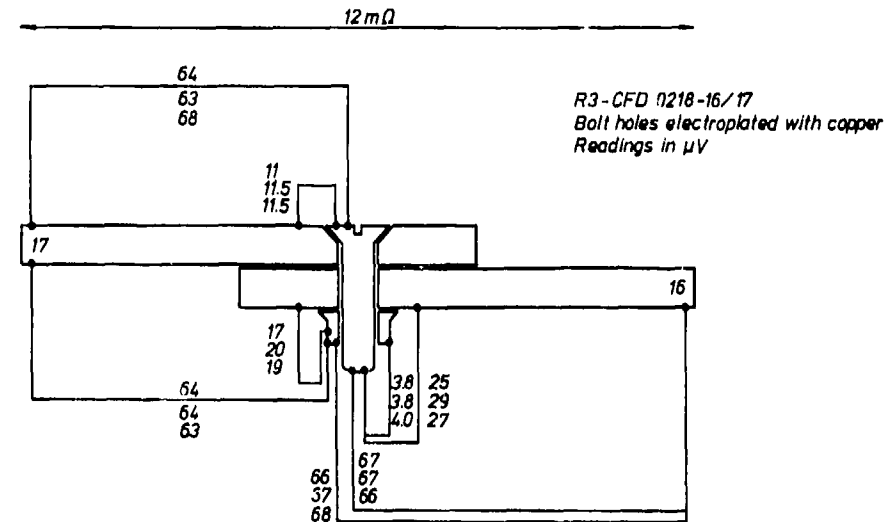


Figure 13 As Fig 10 but with the inside of the bolt holes electroplated with copper

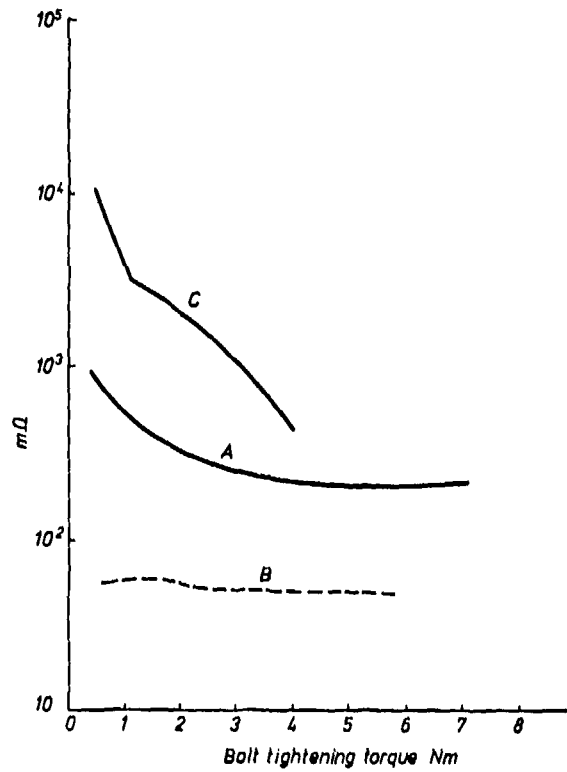


Figure 14 The effect of bolt tightening torque on the joint resistance
 A Correctly drilled holes
 B As A, but with mating surfaces abraded
 C As B, but wet assembled with poly-sulphide type sealant

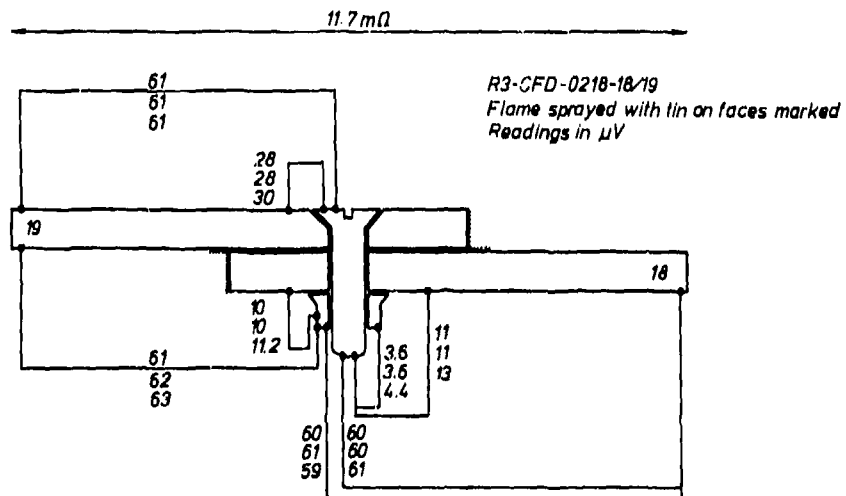


Figure 15 As Fig 10 but with ends and mating surfaces flame sprayed with tin

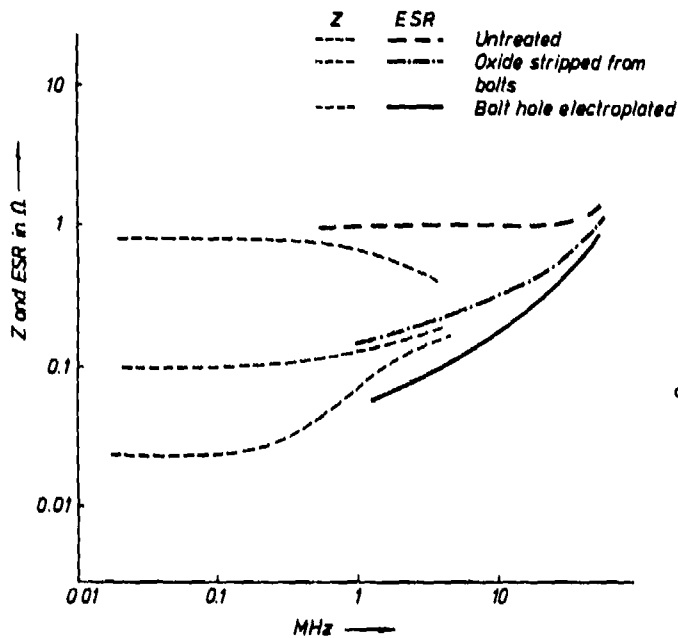


Figure 16 High frequency properties of CFC bolted joints with various pretreatments

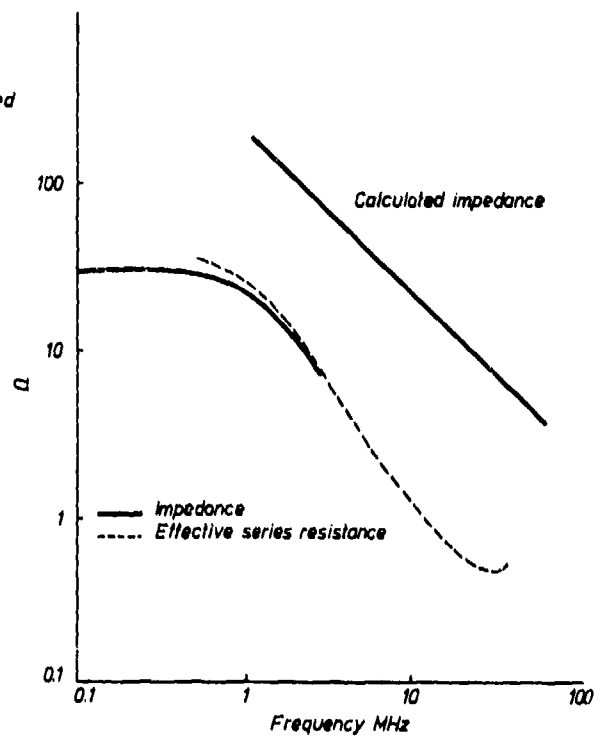


Figure 17 High frequency properties of bonded joints

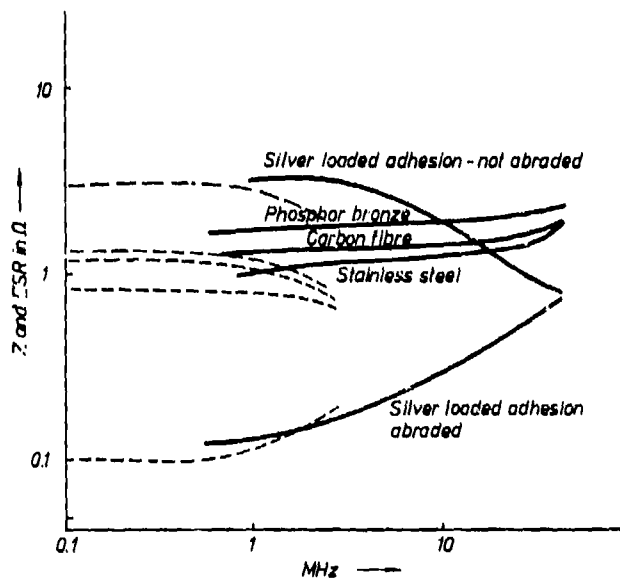


Figure 18 High frequency properties of modified CFC bonded joints

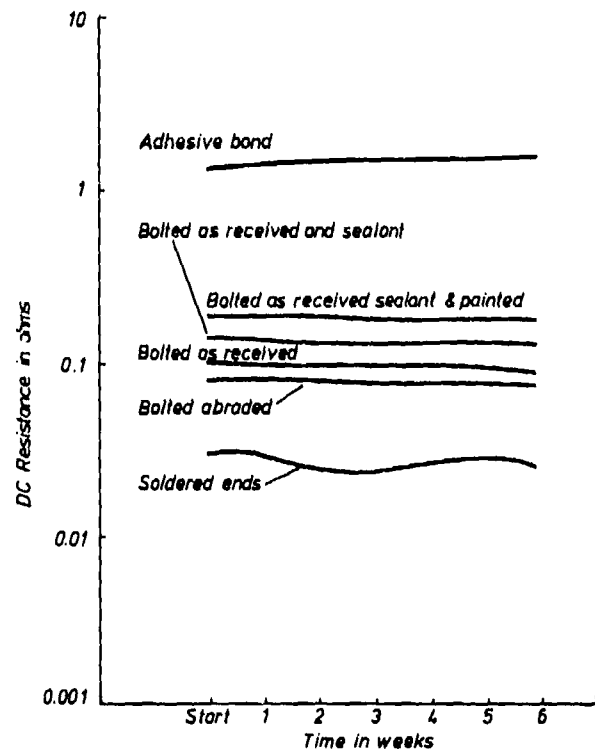


Figure 19 DC joint resistance of samples during corrosion test

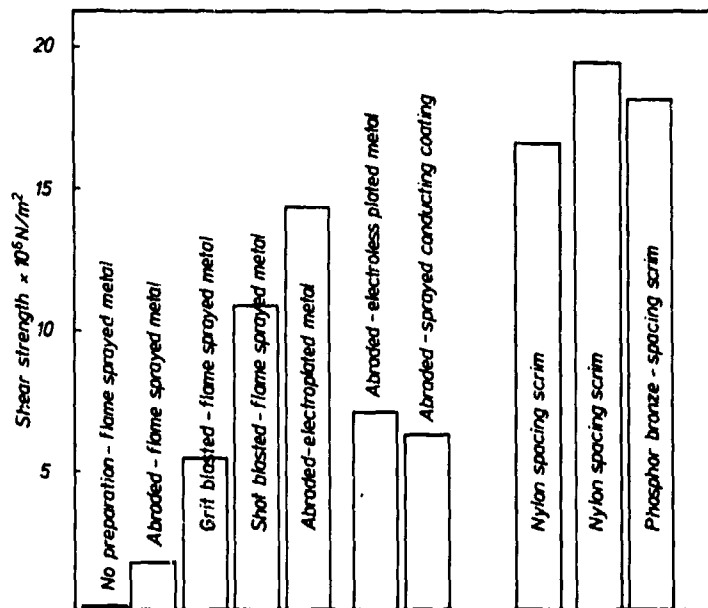


Figure 20 Shear strength of CFC lap joints made with various coatings and pre-treatments

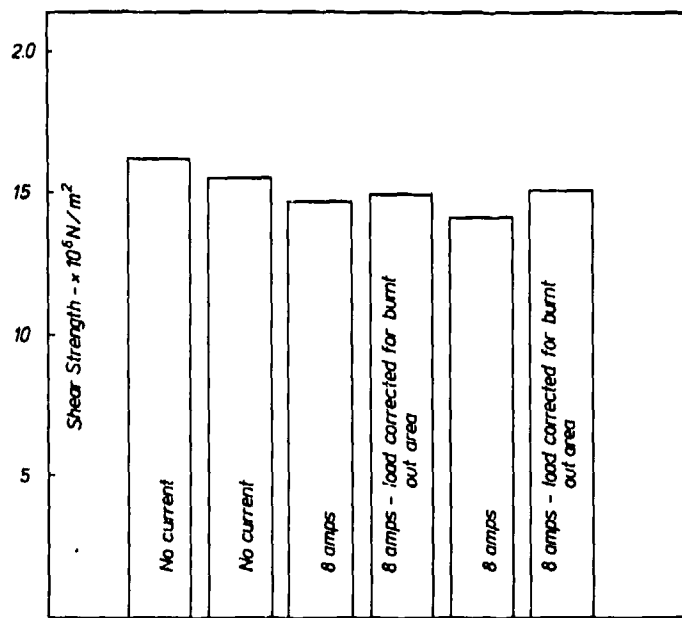


Figure 21 The effect of the passage of electric current through a CFC lap joint on its adhesive strength

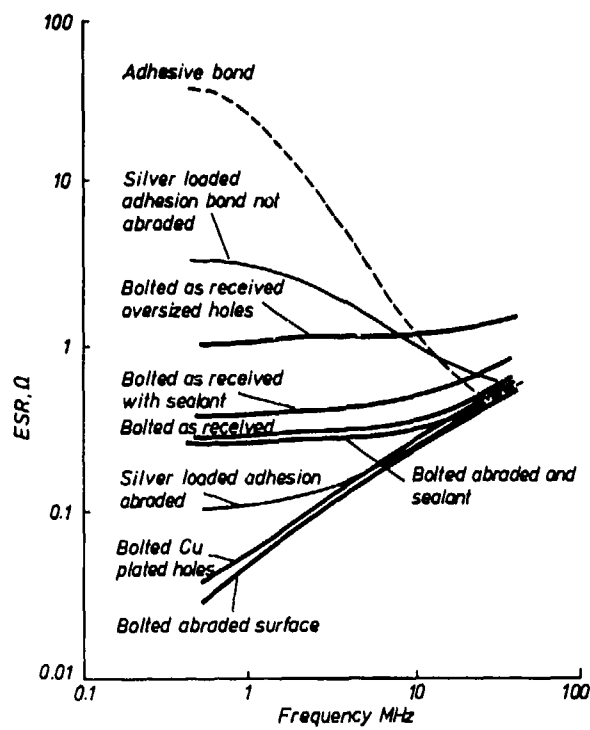


Figure 22 The ESR of some of the CFC joints made during this work

THE UK MINISTRY OF DEFENCE PROGRAMME ON THE ELECTROMAGNETIC PROPERTIES
OF CARBON FIBRE COMPOSITES

by

J.M. Thomson and R.H. Evans
Ministry of Defence (Procurement Executive)
Royal Aircraft Establishment
Farnborough, Hants, UK

SUMMARY

With some exceptions, UK work on the electrical properties of carbon fibre composites is regarded as part of an overall programme on electromagnetic effects (EMC, EMP, lightning, etc). The relationship of the CFC work to the remainder of the programme is discussed, and the principal investigations outlined and reviewed. One particular package - shielding measurements at RAE on a cockpit section manufactured by British Aerospace, Warton - is described in detail; for information on the remainder of the programme references are made to AGARD and other papers. It is shown that the major areas of concern are the bonding and jointing of the material and its characteristics at HF and below. This latter topic has an impact on shielding (including EMP and lightning sources) and aerial installation. Finally, the use which will be made of the information from these programmes is discussed.

1 INTRODUCTION

UK work on the electromagnetic properties of carbon fibre composites is generally regarded as part of an overall programme on electromagnetic effects (EMC, EMP, lightning, etc). The principal exceptions are where the work is concerned with the performance of CFC as an aerial counterpoise and the question of whether a CFC structure can be used as a power earth return. Nonetheless, these aspects are usually considered along with the purely EMC topics and much of the work that is done is directly applicable to them.

The UK electromagnetic effects programme is described elsewhere (Thomson, J.M., 1979). It is loosely split into packages investigating the sources of electromagnetic interference, its propagation through the fuselage, and its coupling into the wiring of susceptible systems; further packages cover research into equipment and aircraft specifications, and 'design for compatibility'. Overall, the purpose of the programme is to ensure that adequate information is available for aircraft and flight weapons systems projects to allow a quantitative clearance for introduction to service to be formulated, particularly where flight safety or mission success critical systems are concerned.

The MOD(PE)* programme on the electromagnetic properties of CFC is therefore not an end in itself but part of a wider electromagnetic effects programme. In particular, CFC has an impact in two of the packages:

- (i) how electromagnetic energy propagates through the fuselage;
- (ii) how airframe design is affected in the quest for compatibility.

The work on aerial installation and power system returns is closely allied to these two topics. The UK programme as a whole is outlined in section 2.

From an electrical point of view composites for use in aircraft are basically of two types. Those that are electrically non-conducting, such as glass fibre reinforced plastic, behave essentially as 'open windows' (except that they can accumulate electrostatic charge) and may be treated accordingly. Moreover, only a small proportion of the total surface is likely to be constructed from such materials, although the special case of helicopters needs to be borne in mind. On the other hand, carbon fibre composites are electrical conductors, although poor ones compared to metal, and the trend is towards constructing quite a high proportion of the structure, particularly the surface, from such material. This paper deals entirely with the properties of CFC, but it should not be overlooked that there are hybrid composites under development, containing both carbon and glass fibres for example, and these will have even lower electrical conductivity.

The principal characteristics likely to make CFC different from aluminium alloy are:

- (i) it has high resistivity (about 25-150 $\mu\Omega\text{m}$ compared with 0.052 $\mu\Omega\text{m}$ for aluminium alloy);
- (ii) it has high surface resistivity, making it difficult to achieve good electrical contact at joints;
- (iii) it is not homogeneous, consisting of fibres embedded in plastic and not necessarily in continuous contact along their length;

* MOD(PE): Ministry of Defence (Procurement Executive).

Table 1

THE UK MOD PROGRAMME ON THE ELECTROMAGNETIC PROPERTIES OF COMPOSITES

Date started	Performing organisation	Work item	Comments
1970	RAE Materials Dept	Resistivity measurements.	Part of Materials R & D programme
1970	ERA	Direct damage lightning effects using high voltage facility.	Work completed
1973	Salford University	Resistivity measurements.	Part of Materials R & D programme
1977	CLSU	Lightning effects, direct and indirect (including resistivity and shielding measurements).	Work completed. PV work also undertaken
1977	RAE Radio and Navigation Dept	Resistivity measurements, dc - 900 MHz; ground plane efficiency measurements at UHF.	Work completed
1977	ERA	Basic properties (resistivity, etc) at dc and rf; shielding effectiveness; aerial performance; environmental effects (water, salt water, fuels, etc); work on large structure.	Work continuing
1978	Plessey Caswell	Electrical impedance of CFC and CFC/metal joints at dc and rf; methods of improving joints; some environmental effects.	Work continuing. PV work also undertaken
1978	RAE (in collaboration with BAe Warton and MRL)	Work on CFC cockpit section, including: (i) Engineering Physics Dept - shielding effectiveness (ii) Radio and Navigation Dept - aerial performance	Work completed
1978	MRL	Mathematical model of multi-layer CFC to predict rf impedance and shielding effectiveness.	Work continuing
1978	Plessey South Leigh	Non-linear effects (harmonic generation and intermodulation products).	Work continuing

NB: The UK aerospace industry has also undertaken or sponsored work, particularly at BAe Warton (resistivity measurements, system studies, electrostatic charging, lightning effects) and WHL Yeovil (shielding effectiveness).

Legend:

BAe	British Aerospace
CLSU	UKAEA Culham Laboratory Lightning Studies Unit
ERA	ERA Technology Ltd (formerly Electrical Research Association)
MRL	Marconi Research Laboratory, Great Baddow
Plessey Caswell	Plessey Research (Caswell) Ltd, Allen Clark Research Centre
Plessey South Leigh	Plessey Electronic Systems Research Ltd, South Leigh
PV	Private venture
RAE	Royal Aircraft Establishment
WHL	Westland Helicopters Ltd

- (iv) it is not isotropic; that is, if a sheet is made with all fibres aligned essentially parallel then the effective resistivity perpendicular to the fibre direction is much greater (about 500 times) than that along the fibres.

2 DEVELOPMENT AND SUMMARY OF RESEARCH AND MEASUREMENT PROGRAMMES

Table 1 lists the principal past and current MOD(PE) programmes on the electromagnetic properties of composite materials. As noted at the foot of the Table some of the MOD(PE) contractors have also undertaken private venture work for outside agencies, and some of the UK aircraft firms have also undertaken or sponsored R & D work in this area.

The work has been sponsored by both the electrical and the materials/structures branches of MOD(PE). In the earlier days when RAE Materials Department were pioneering the development of CFC its electrical properties were among the factors that allowed an insight into the characteristics and performance of the material. This was the basic reason for the work at RAE in 1970 and Salford University in 1973. Similarly, the vulnerability of the material to lightning strike needed to be assessed, so simulated lightning tests on various composite panels were made at ERA in 1970-1974 to assess superficial damage, loss of strength, and the effectiveness of possible protective coatings (Phillips, L.N., and White, E.L., 1975). Further work to investigate damage mechanisms in more detail and to include indirect effects (induced voltages in electrical systems) was initiated at CLSU in 1977 (Little, P.F., 1980).

On the other hand, the electrical branches of MOD(PE) have only begun to sponsor work on composites in the last few years. Apart from the work at CLSU, in which there has always been a strong interest, the two main planks of the programme have been the work at ERA, starting in 1977, and at Plessey Caswell, starting in 1978.

The ERA package includes work on the basic electrical properties of the material, its shielding effectiveness, its performance as an aerial counterpoise, and its performance when incorporated in a large structure (Bull, D.A., Jackson, G.A., and Smithers, B.W., 1980; Bull, D.A., and Jackson, G.A., 1980; Smithers, B.W., 1980). The Plessey Caswell package includes work on the electrical aspects of the bonding and jointing of CFC, both to CFC and to metal (Brettle, J., and Baskerville, M.W., 1979; Brettle, J., Lodge, K.J., and Watson, A.W.D., 1980). Also in this period resistivity measurements were made on CFC samples, and its performance as an aerial counterpoise at UHF was assessed (Bagley, G., 1977).

Simultaneously with the developing MOD(PE) interest the electrical design and development teams in the UK aircraft industry also became concerned about the possible impact of the use of CFC in future aircraft projects. Following informal discussions the aircraft industry and MOD(PE) met in August 1977 and agreed that research into the subject be encouraged. This reinforced the case for work already being undertaken, or being considered, at RAE, CLSU, ERA and Plessey Caswell, and also showed the need for further studies in areas not covered by the main programmes. Accordingly, MRL were asked to develop a mathematical model of CFC to predict its rf impedance and shielding effectiveness (Brewster, D.C., 1980), and Plessey South Leigh were asked to investigate whether non-linear effects would occur either in the material itself or in joints (Brettle, J., Lodge, K.J., and Watson, A.W.D., 1980). In addition BAe Warton made available a CFC cockpit section for electrical work; after some discussion, it was agreed that it would be most useful to carry out some experiments on it in a joint MOD(PE)/aircraft industry/avionics industry programme, to allow all parties to acquire some knowledge of the performance of the material. This work was done at RAE and is reported in section 3.

In addition to the MOD(PE) programme, the UK aircraft industry has also undertaken or sponsored work on the subject (Smith, K., and Barton, G., 1980). However, close liaison has been maintained between all parties throughout the programme and collaboration has generally been extremely good; this is facilitated by an advisory group which meets twice-yearly.

Thus in 1980, a co-ordinated UK programme has been in existence for more than 2 years, results are beginning to appear, their implications assessed, and future developments planned. These aspects are covered in sections 4 and 5.

3 JOINT MOD(PE)/AIRCRAFT INDUSTRY/AVIONICS INDUSTRY WORK ON AN EXPERIMENTAL COCKPIT SECTION

One interesting example of collaboration was the RAE/BAe Warton/MRL exercise on a closed compartment forming part of a CFC cockpit section. This had been built as a structural demonstrator and was made available by BAe Warton. Measurements were made of its shielding effectiveness and its performance as an aerial ground plane; the former are reported here.

The cockpit section is shown in Figure 1; its dimensions are approximately 2.25 m x 1 m x 1 m. Also shown is a replica in 20 gauge aluminium. This was built because it was recognised at the outset that results from the CFC section in isolation would not have much meaning and that most value would come from results comparing the performances of CFC and conventional construction. The aluminium replica was built in RAE, with the bonding being in accordance with current practices at BAe Warton.

It was also acknowledged that the shape of the specimen could reduce the absolute, if not the relative, value of the results: without nose, rear fuselage and wings, the cockpit section alone would not exhibit the resonance characteristics of a typical aircraft structure when illuminated by an external field. It also became apparent, from experience at other sites, that perhaps the more major differences arise not when complete substitution of CFC for metal is made but when sections of a metal fuselage are replaced by CFC: this is because the skin current distribution is substantially altered with a metal/CFC mixture.

Despite these limitations the work still had the valuable objective of obtaining a first-hand general idea of the performance of the material in a complete structure; it led to the development of the instrumentation necessary for such measurements, and to the transfer of RAE experience and expertise to the firms involved.

The measurements were made in the RAE shielded room facilities; it had been hoped to make open site measurements but low measuring sensitivity coupled with restrictions on the amount of power allowed to be broadcast prevented this. Certain instrumentation had to be developed for the work: this included small electric and magnetic field probes, a preamplifier for the small HF signals that were being measured inside the structures, and a fibre-optic link to connect the probes and the measuring set. Examples of the field probes are shown in Figure 2: from left to right are a three-axis electric field probe (about 100 or 200 MHz to 1 GHz depending on signal strength), a three-axis magnetic field probe (1-150 MHz), and a three-axis electric field probe (1-100 MHz). The fibre-optic link was developed for use with the 100MHz to 1GHz electric field probe to make the signals measured in this range immune to pick-up: at the transmit end the rf is converted to dc which controls the frequency of an audio oscillator; an audio signal is then transmitted down the fibre-optic link and at the receive end a frequency counter displays a reading proportional to the original field strength.

The work as a whole, including instrumentation, is being reported (Carter, N.J., and Hobbs, R.A., 1980). Figures 3 and 4 show typical results: Figure 3 is the magnetic field attenuation over the range 1-160 MHz with the incident propagation vector perpendicular to the fuselage axis, and Figure 4 is the electric field attenuation over the range 1.5 MHz to 12 GHz with propagation directed along the fuselage axis. In both cases comparison with the aluminium replica is shown. In general the results, subject to the provisos mentioned earlier, do not differ much from those of other UK workers, in that significant differences between aluminium and CFC occur only in the HF band, for magnetic field shielding. It is also interesting to note that a reasonably close scrutiny of the results shows tentatively that the frequencies of some of the resonances can be linked to the structure's dimensions - those at 33.25, 66.5 and 133 MHz in Figure 3 corresponding to a length of 2.25 m.

Table 2

PRELIMINARY ASSESSMENT OF THE ELECTROMAGNETIC IMPACT OF CARBON FIBRE COMPOSITES

Minor problem areas	Major problem areas
1 Direct damage lightning effects 2 Non-linear effects in airframes (harmonic and intermodulation product generation) 3 Aerial installation at VHF and above 4 Power supply earth returns 5 Shielding at VHF and above	1 CFC properties at HF and below lead to penetration through the material of energy from on-board and external sources, EMP and lightning; they also cause difficulty in HF aerial installation. 2 Bonding and jointing: without adequate electrical design there can be penetration of energy through joints and difficulties with HF installations.

4 PROVISIONAL CONCLUSIONS FROM THE PROGRAMME

The essential electrical difference between CFC and conventional metals used in airframes is its resistivity and rf impedance. At dc the resistivity of a wide range of CFC samples ranges from 25-150 $\mu\Omega\text{m}$ compared to 0.052 $\mu\Omega\text{m}$ for a typical aluminium alloy used in aircraft construction, a ratio of about 1000. In addition the resistance/frequency characteristic is of the same general form as that for homogeneous material, in that it appears to exhibit a skin effect, although there are some variations which have yet to be explained. The influence of these factors on the specification, design, construction and operation of aircraft (or weapons) with CFC in their structures has not yet been examined in detail.

Table 2 is a preliminary assessment of the electromagnetic impact of carbon fibre composites. The essential message from this Table is that the major problem areas will arise because of the characteristics of the material at HF and below; above this frequency range there is little difference in the electromagnetic effects of CFC and aluminium. These findings are true for more or less all the lay-ups examined.

It appears that direct damage lightning effects are not serious, though attention should be paid to structures containing a metal honeycomb and to adhesive joints. Electrical non-linearities have not been found in the material itself, but further work is in hand to investigate the behaviour of joints; in any event the effects of the generation of harmonics or intermodulation products at such a source would be restricted to the possible degradation of radio receiver performance. Aerial installation at VHF and above is not seen as a problem: work at RAE has demonstrated that the performance of the material as a ground plane at these frequencies is virtually indistinguishable from aluminium alloy. Although it will not be possible to use CFC for a power earth return, with careful design even with extensive use of composites the associated weight penalty may only be a few tens of kilograms, particularly if certain longitudinal structural members are retained in aluminium alloy. The shielding properties of the material itself may be *different* at VHF and above - not necessarily *worse* - but this will be due to the factor mentioned in section 3, that the pattern of surface current distribution, and hence penetration, is changed. Some limited work on aircraft incorporating composite panels tends to confirm this opinion. In any case, even in metal aircraft it is not wise to place reliance on the shielding afforded by the fuselage for the protection of sensitive electrical and electronic systems.

The characteristics of the material, and its differences from aluminium alloys, at HF and below are that its impedance is much higher and that it offers much less shielding to magnetic fields. These differences are important for several reasons. Firstly, in the EMC of aircraft systems, on-board HF installations cause considerable problems in conventional metal aircraft, so it is likely that there will be even more penetration of HF energy through CFC skins. This also applies when the aircraft is exposed to an external transmitter. Similarly, induced voltage lightning effects are likely to be more severe for the same reasons, as the typical lightning current has significant content at these frequencies. The frequency spectrum of EMP includes these frequencies, though it also extends higher into the VHF and UHF regions. Accordingly, it is possible that electromagnetic interference susceptibility specifications for electrical and electronic systems will need to be made more severe in the HF band. Furthermore, when an aircraft HF transmitter system uses a notch aerial, the whole structure acts as a radiating element. Whether a CFC or CFC/metal aircraft will be adequately efficient for this task is still being investigated. In total, the deficiencies of the material in the HF band may be serious enough to affect the requirements and specification (airframe and equipment) of the aircraft as a complete weapon system. As a palliative, until the advent of the 'all-composite' aircraft, the rf interference problem may be reduced by the judicious siting of cables to take maximum advantage of the shielding offered by the metal part of the airframe, but in addition it may be necessary to metallise the structure in particularly critical areas. This remedy could also be required for lightning protection.

The second major problem area uncovered by the research programme is that of bonding and jointing. Time and again the report has been that the limiting factor in the electrical performance is not the material itself but the joint. This obviously applies to use of the airframe to carry current from power (dc and rf) and lightning sources, to its use as an aerial ground plane, particularly at HF, and to the limitation of non-linear effects. More insidiously, an imperfect joint allows electromagnetic energy to penetrate the airframe and hence increase the likelihood of EMI susceptibility problems. However, the indications, particularly from the ERA and Plessey Caswell work, are that with careful attention to design and fabrication these difficulties can be overcome, and the impedance of the joint can be made comparable to or less than that of the material. Nevertheless, this is a highly important area where the materials and structures engineers must be made aware of the design measures necessary to meet this objective. It seems possible that in a year or so realistic and proven designs meeting electrical requirements can be recommended.

These two problem areas - properties at HF, and bonding and jointing - obviously come together on many occasions, and indicate where the major effects on the EMC of the complete aircraft weapons system will lie, and where the most attention is required.

5 THE FUTURE DEVELOPMENT OF THE PROGRAMME

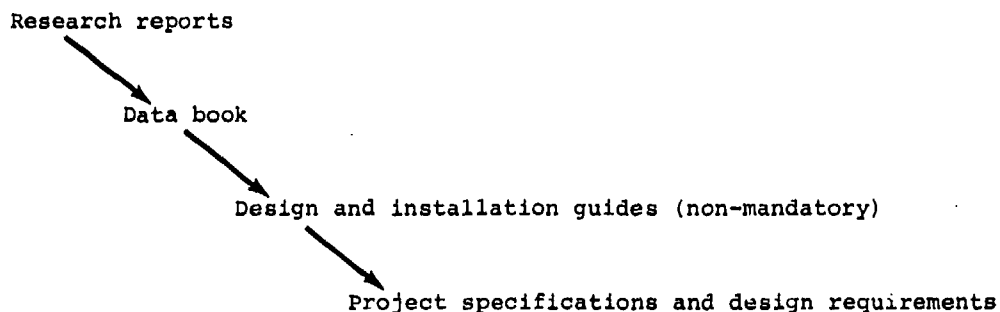
The UK programme as presently constituted comprises a certain amount of work at MOD(PE) research establishments and in the aircraft industry together with extramural research contracts with several firms. Thus, although it was launched in a co-ordinated manner and with consideration of overall requirements, and whilst it has been discussed regularly at an informal joint MOD(PE)/Industry advisory group, nonetheless the principal outputs so far are limited to research reports from the individual laboratories. These by themselves usually contain material that is not always directly applicable by the ultimate customers.

In addition we are now at a breakpoint in time where, having identified the main problem areas and initiated work to investigate them further, we must ensure that the results are in a form which provides maximum benefit to MOD(PE) and Industry. To evaluate the future direction of the programme it is useful to consider the customers and to identify their particular needs. In addition to MOD these include other government departments, organisations such as the Civil Aviation Authority, and the airframe, weapons and avionics industries. With this in mind it is possible to construct a table of organisations and their expectations from the general EMC programme and the particular topic of the electrical properties of composites:

Organisation	Requirement
Ministry of Defence and other government departments	Basic scientific knowledge
Airframe/weapons industries	How to specify aircraft/weapons/avionics
Avionics industry	How to clear aircraft/weapons to service
	How to build aircraft/weapons
	How to install avionics
	How to design avionics

Although this is a simple model, it is nonetheless useful. It shows, for example, that if the problem is to be explored fully there should be private venture investment from industry and indicates where this funding should be applied; most importantly, it identifies in which areas the principal outputs of the MOD(PE) programme should lie, and consequently assists in determining its aims and objectives.

It is evident that there are many different expectations from the research programme, and that the research reports at present being produced are unlikely to be sufficient to satisfy them all. In particular, it is evident that design information and guidance is a major requirement, and that the programme should be structured to provide this. A method of doing this, which is currently being debated within the UK, is to channel the results from the research programme into a hierarchy of outputs:



The first outputs are the research reports presently produced. The second output will be a data book, which will be a first attempt at distilling the results of the individual programmes (eg data on resistivity, bond impedance, non-linear effects, lightning effects, aerial performance) into one useful volume. The third output is the preparation of non-mandatory design and installation guides; probably a number will be required dealing, for example, with airframe design, avionics installation, aerial installation, etc. The fourth output will be the influence of composite structures in mandatory Project EMC and other specifications and design requirements.

Having this logical sequence of outputs means that the individual research contractors can see that their work is not merely an end in itself, but that it contributes to a greater whole; furthermore, it enables them to centre their efforts in areas which are ultimately going to be of most benefit to all of the potential customers for their work.

6 CONCLUDING REMARKS

The UK MOD(PE) research programme on the electromagnetic properties of carbon fibre composites is, perhaps, half-way through its life. Some preliminary observations on its results can be made, and useful information is starting to be fed into development programmes. Although two major problem areas and some minor ones have been identified these are not likely to be such as to inhibit the use of composites provided that there is close liaison between materials, structures and electrical specialists to ensure optimum overall design, particularly as regards bonds and joints. Other features which must be kept to the forefront are the increased weight of wiring, and cable screening, the likelihood of more severe EMC susceptibility requirements in the HF band, and the possibility of metallising in critical areas.

The UK programme has focussed initially on composites intended for aircraft structures; work may also be undertaken on composites for weapons structures, where these are different. Additionally, any development of hybrids such as carbon/glass composites must also include the evaluation of electrical properties, which may well be worse than those of carbon fibre composites.

Finally, some of the outputs of the UK programme, particularly in the jointing area, have already been accepted by the mechanical design offices of the aircraft industry and

influenced their activities. Such liaison must continue if the potential advantages of composites are to be realised in practice.

REFERENCES

- BAGLEY, G., 1977, "Notes on rf Properties of Carbon Fibre Reinforced Plastics", Unpublished MOD(PE) material
- BRETTE, J., and BASKERVILLE, M.W., 1979, "Electrical Bonding in Aircraft", IEEE EMC Symposium, San Diego, California, USA
- BRETTE, J., LODGE, K.J., and WATSON, A.W.D., 1980, "The Electrical Effects of Joints and Bonds in Carbon Fibre Composites", AGARD Avionics Panel Specialists' Meeting on Electromagnetic Effects of (Carbon) Composite Materials upon Avionics Systems, Lisbon, Portugal
- BREWSTER, D.C., 1980, "Theoretical Calculation of rf Properties of Carbon Fibre Laminates", AGARD Avionics Panel Specialists' Meeting on Electromagnetic Effects of (Carbon) Composite Materials upon Avionics Systems, Lisbon, Portugal
- BULL, D.A., JACKSON, G.A., and SMITHERS, B.W., 1980, "RF Resistivity and Screening Characteristics of Carbon Fibre Composite Materials", AGARD Avionics Panel Specialists' Meeting on Electromagnetic Effects of (Carbon) Composite Materials upon Avionics Systems, Lisbon, Portugal
- BULL, D.A., and JACKSON, G.A., 1980, "Assessment of Electromagnetic Screening Characteristics of Carbon Fibre Composite Material", IERE EMC Conference, Southampton University, UK
- CARTER, N.J., and HOBBS, R.A., 1980, "Some Radio Frequency Shielding Measurements on a Carbon Fibre Composite Front Fuselage Section", RAE Technical Memorandum (to be published)
- LITTLE, P.F., 1980, "Behaviour of CFRP Panels in Metal Aircraft during Simulated Lightning Strokes", AGARD Avionics Panel Specialists' Meeting on Electromagnetic Effects of (Carbon) Composite Materials upon Avionics Systems, Lisbon, Portugal
- PHILLIPS, L.N., and WHITE, E.L., 1975, "Effect of Simulated Lightning Strikes on Mechanical Strength of CFRP Laminates and Sandwich Panels", IEE/RAeS Lightning and Static Electricity Conference, UKAEA Culham Laboratory, UK
- SMITH, K., and BARTON, G., 1980, "Aircraft Manufacturers Approach to the EMC/Avionics Problems Associated with the Use of Composite Materials", AGARD Avionics Panel Specialists' Meeting on Electromagnetic Effects of (Carbon) Composite Materials upon Avionics Systems, Lisbon, Portugal
- SMITHERS, B.W., 1980, "RF Resistivity of Carbon Fibre Composite Materials", IERE EMC Conference, Southampton University, UK
- THOMSON, J.M., 1979, "The RAE Research and Development Programme on EMC for Aircraft and Flight Weapons Systems", IEEE EMC Symposium, San Diego, California, USA

Copyright

Controller HMSO London
1980

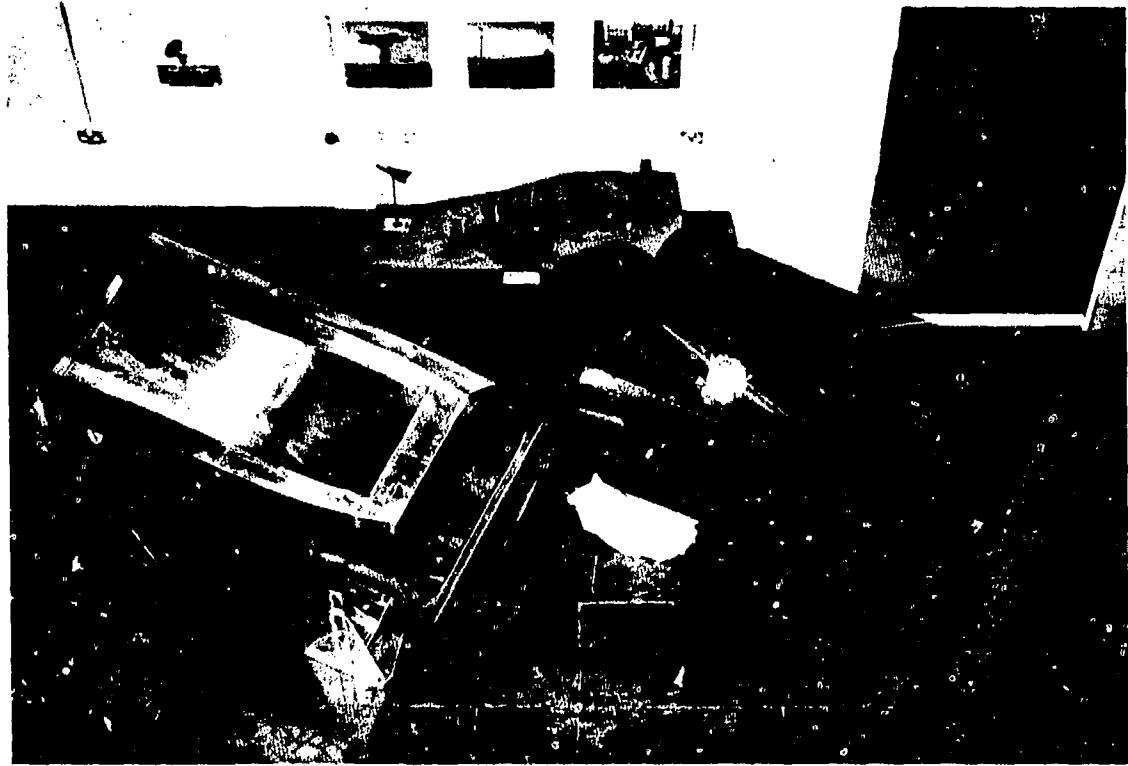


Fig 1 Aluminium and carbon fibre composite fuselage sections used for shielding measurements at RAE

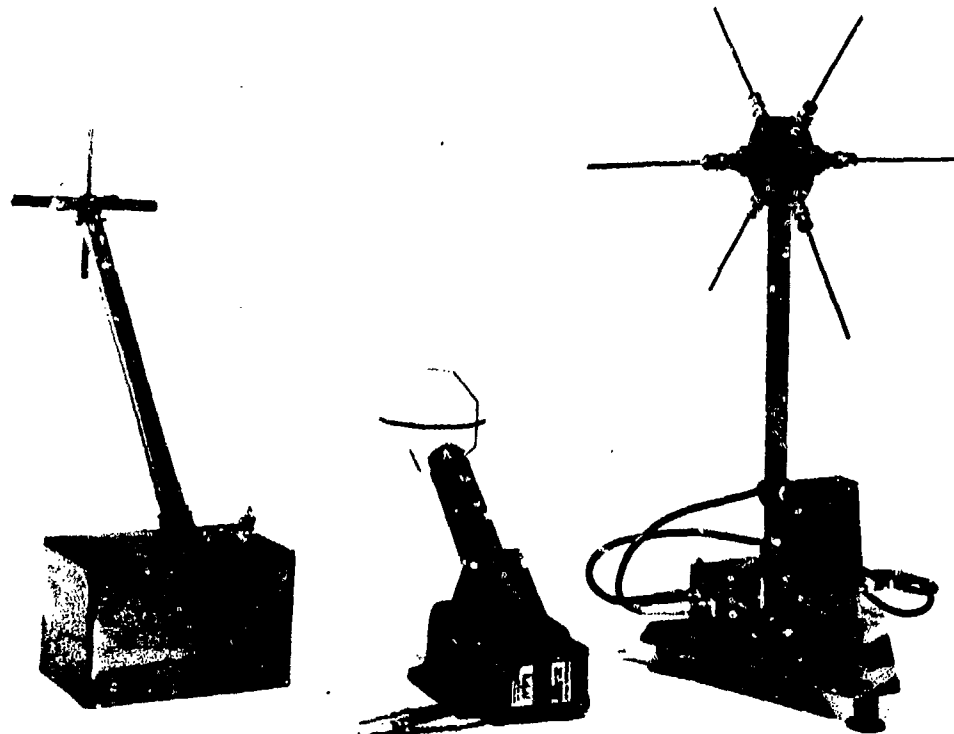


Fig 2 Field probes used for shielding measurements - (l to r)
E-field (100 MHz to 1 GHz), H-field (1-150 MHz),
E-field (1-100 MHz)

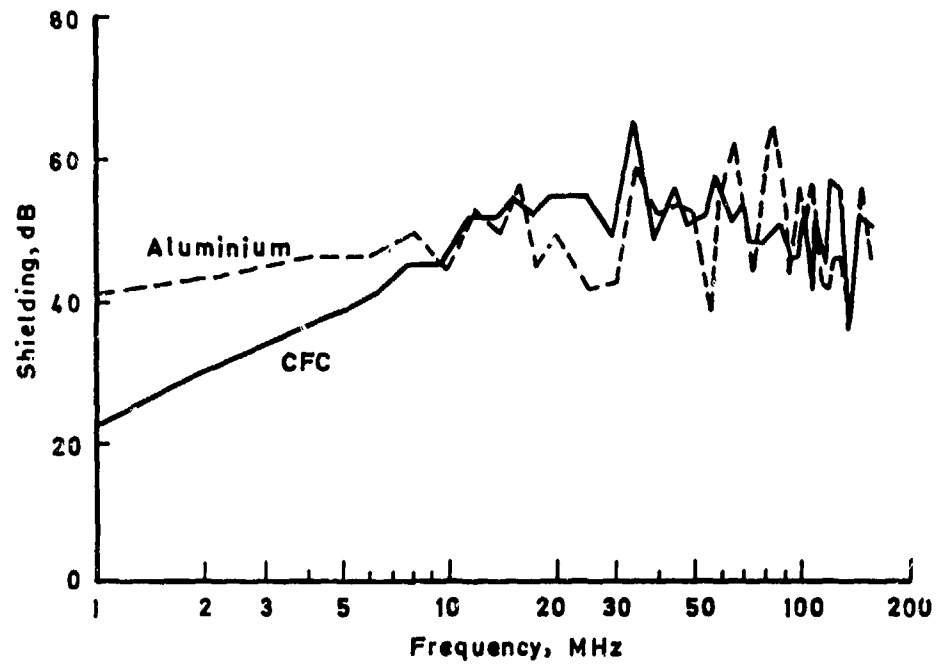


Fig 3 Magnetic field attenuation; propagation perpendicular to fuselage axis

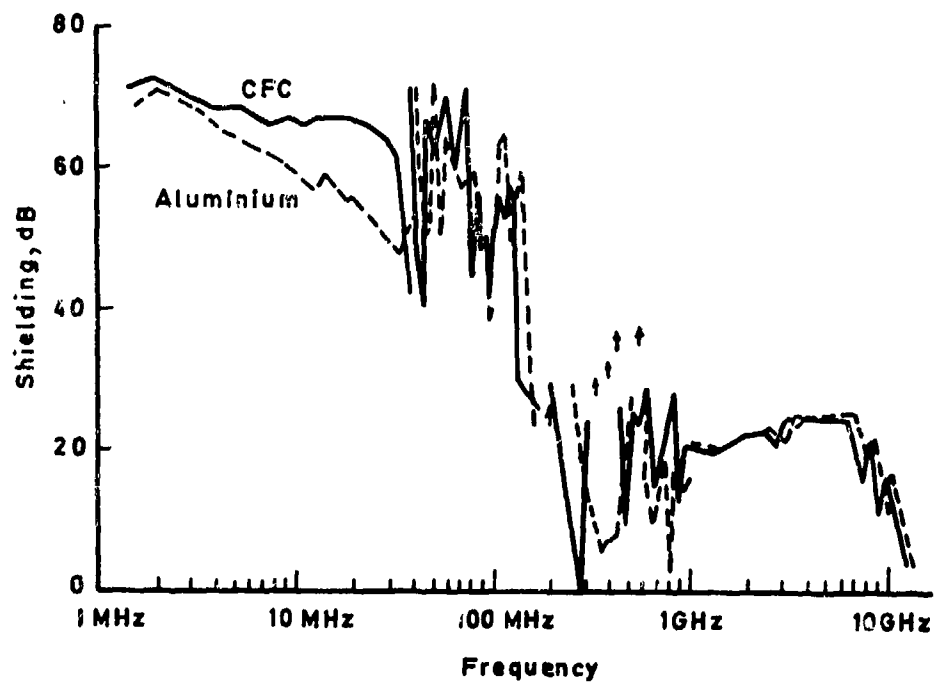


Fig 4 Electric field attenuation; propagation along fuselage axis

PROGRAMME FRANCAIS D'ESSAIS EN VOL
SUR LES EFFETS ELECTROMAGNETIQUES DE LA Foudre

J.C. Alliot
Office National d'Etudes et de Recherches Aérospatiales
92320 Châtillon - FRANCE

D. Gall
Centre d'Essais Aéronautiques de Toulouse
31056 Toulouse Cedex - FRANCE

RESUME

Sous l'égide des Services Techniques Français de l'Aéronautique, un programme d'essais en vol, destiné à évaluer les perturbations électromagnétiques de la foudre, a été défini et mis en oeuvre dès 1978.

Ce programme d'essais est réalisé par le CEAT, le CEV et l'ONERA ; l'avion utilisé est un TRANSALL C160 de l'Armée de l'Air, comportant une instrumentation appropriée à la détection des phénomènes associés aux foudroiements directs ou de proximité : le courant de foudre (composantes impulsionnelles et continues), les courants de peau en différents points de la structure, les champs électromagnétiques externes et internes, les surtensions sur divers équipements et circuits de bord ; différents capteurs permettent de caractériser l'état électrique de l'avion lors du foudroiement (potentiel d'équilibre, courant de charge d'origine triboélectrique, champ électrique atmosphérique extérieur).

Le comportement des panneaux de structure en matériau composite vis à vis du rayonnement électromagnétique est particulièrement étudié afin d'en définir les systèmes de protection. Après diverses modifications et adjonctions apportées à l'instrumentation utilisée lors des essais de 1978, une nouvelle campagne expérimentale se déroulera en 1980.

1 - INTRODUCTION

L'étude générale des foudroiements d'un aéronef en vol met en évidence deux types de problèmes (J. Plumer, B. Burrows, D. Clifford, 1978) :

- le premier est lié aux effets mécaniques de l'impact de la décharge sur la structure du véhicule (fusion, déformation, explosion, ...) ;
- le second, aux perturbations concernant les équipements électroniques embarqués, dues au rayonnement électromagnétique engendré par les décharges.

Dans l'état actuel des connaissances, on estime que les problèmes liés aux effets mécaniques de l'impact sont bien cernés et que des protections efficaces seront utilisées, de façon systématique, à court terme. Les actions mécaniques des décharges sur une structure sont, en effet, provoquées par des mécanismes dont les caractéristiques sont connues et peuvent être reproduites en laboratoire, en vraie grandeur. A l'inverse, les problèmes posés par les perturbations électromagnétiques sur les équipements électroniques embarqués sont beaucoup moins bien connus et font l'objet de nombreuses études.

A cela, plusieurs raisons peuvent être données :

- les caractéristiques du rayonnement électromagnétique engendré par les divers mécanismes d'une décharge atmosphérique (en particulier les décharges inter et intra nuages) sont encore mal connues et ne peuvent donc pas être simulées en laboratoire de façon satisfaisante ;
- les matériaux composites sont de plus en plus utilisés dans la construction aéronautique pour réaliser des parties de structure ; celles-ci constituent des passages privilégiés de l'énergie électromagnétique si des précautions particulières ne sont pas prises ;
- l'utilisation croissante des circuits intégrés digitaux, fonctionnant à bas niveau et présentant des impédances d'entrée et des bandes passantes élevées, pour réaliser les équipements avioniques (instrumentation d'aide à la navigation et de radio-communication, commandes électriques, calculateurs de bord, ...), se traduit par une plus grande susceptibilité des appareils aux rayonnements parasites.

L'analyse des résultats statistiques publiés sur les foudroiements directs des aéronefs en vol montre que la probabilité d'impact ne cesse d'augmenter au cours des années en raison de l'accroissement du trafic aérien qui impose, du moins pour les véhicules commerciaux, des plans de vol très stricts ; cette augmentation se traduit, sur certaines

lignes européennes, par un taux de foudroiement pouvant atteindre un événement pour moins de 1000 heures de vol. Les foudroiements les plus dangereux se produisent à basse altitude, au moment des phases d'ascension et de descente des véhicules ; ces foudroiements, en effet, se déclenchent entre un nuage et le sol, et s'accompagnent d'une onde de courant de forte amplitude, à variation très rapide, qui parcourt la structure et provoque la pénétration d'une énergie électromagnétique vers l'intérieur du véhicule.

Les Services Officiels Français de l'Aéronautique et les constructeurs ont, depuis une dizaine d'années, définis plusieurs programmes d'études expérimentales en laboratoire, visant à la protection des aéronefs contre la foudre. Ces études, basées sur la simulation des caractéristiques des décharges atmosphériques déterminées à partir de mesures effectuées au sol, ont conduit à la création d'un certain nombre de laboratoires d'essais spécialisés notamment celui du CEAT (Centre d'Essais Aéronautique de Toulouse) qui dispose de moyens de simulation à haute énergie pour étudier le comportement des structures. Pour les raisons évoquées précédemment, l'étude des mécanismes de couplage de l'énergie électromagnétique avec les équipements avioniques a conduit la Direction Technique des Constructions Aéronautiques à définir un programme d'essais en vol dont les objectifs à court terme sont les suivants.

- la définition et la mise au point de moyens de mesures, en vol, des paramètres électriques et électromagnétiques associés aux décharges atmosphériques ;
- l'étude des conditions d'initiation ou d'interception des foudroiements en vol (champ électrique inducteur, charge propre de l'avion, ...) ;
- la caractérisation des ondes de courant parcourant la structure du véhicule lors d'un foudroiement direct ainsi que la détermination de la répartition de ces courants sur la peau de l'avion ;
- la caractérisation des rayonnements électromagnétiques, engendrés par les foudroiements directs et de proximité, dans une gamme de fréquences s'étendant jusqu'à 200 MHz ;
- l'étude du "durcissement" des équipements avioniques.

L'objectif à plus long terme est l'établissement de recommandations et de normes pour protéger les équipements contre les foudroiements.

L'avion retenu pour ces expérimentations est le C160 "TRANSALL" A04 de l'Armée de l'Air, qui a été muni de deux perches métalliques de 4 mètres de long, situées à l'avant et à l'arrière du fuselage, pour localiser le point d'impact et caractériser l'onde de courant parcourant la structure lors d'un foudroiement direct. Plusieurs essais préliminaires de foudroiements en vol ont été réalisés en 1978 (D. Gall, 1979) avec la collaboration de l'AIA (Ateliers des Industries Aéronautiques), du CEV (Centre d'Essais en Vol), du CEAT, de la SEPTIM (Société d'Etude et de Fabrication des Techniques Industrielles Modernes) et du CESTA (Centre d'Etude Scientifique et Technique d'Acquitaine).

Deux programmes d'essais en vol similaires sont actuellement menés aux Etats-Unis par l'"Air Force Flight Dynamics Laboratory" sur un avion C130 (K.J. Maxwell, 1979) et par le "NASA Langley Research Center" sur un avion F106 (F.L. Pitts, 1979). D'autres programmes, visant plus particulièrement l'étude du comportement d'un type particulier d'avion (Boeing 747) au foudroiement direct, sont en cours de préparation (G.J. VonBokern, 1978).

2 - CAMPAGNE DE FOUROIEMENTS EN VOL EFFECTUEE EN 1978

2.1 - Choix de l'avion

Compte-tenu du caractère très particulier de ces essais, l'avion "TRANSALL C160-A04" (figure 1) fut choisi pour les principales raisons suivantes :

- a) disponibilité de l'appareil,
- b) sécurité de l'appareil : les comptes rendus consécutifs aux foudroiements des "TRANSALL" montrent leur faible sensibilité à la foudre,
- c) avion lent : 170 noeuds en conditions turbulentes (la basse vitesse permet de minimiser les effets de balayage de la foudre),
- d) avion équipé d'un radar météorologique,
- e) avion cargo pouvant emporter un cadre (cage de Faraday) de grandes dimensions (2 m x 3,50 m x 2 m).

Afin d'assurer une sécurité maximale pendant les essais, des précautions particulières ont été prises :

- métallisation de toute la structure de l'aéronef,
- protection spéciale au niveau des bouchons de réservoir de carburant,
- vérification de la tenue mécanique de tous les équipements mis en oeuvre et, en particulier, des perches.

2.2 - Description de l'instrumentation de mesure

Au cours de cette campagne d'essais, l'instrumentation comportait (figure 2) :

- une première mesure du courant de foudre sur la perche avant et une seconde sur la perche arrière ;
- une mesure du champ magnétique en quatre points situés à l'intérieur de la structure de l'avion ;
- une mesure des courants de peau à l'intérieur et à l'extérieur de la structure ;
- une mesure des surtensions développées sur une ligne test située à l'intérieur du fuselage, ainsi que des mesures de surtensions sur le réseau de génération électrique et sur certains équipements de bord.

L'ensemble des moyens d'enregistrement était regroupé à l'intérieur du cadre blindé qui assurait une atténuation au champ électromagnétique parasite supérieure à 50 dB jusqu'à une fréquence de 100 MHz.

2.2.1 - Mesure du courant foudre

Les courants de foudre, impactant la perche avant et sortant par la perche arrière, étaient mesurés à l'aide de deux "shunts" coaxiaux d'impédance $1 \text{ m}\Omega$, ayant un temps de réponse de 80 ns. Chaque "shunt" était placé à l'intérieur des perches de quatre mètres de long (figures 1 et 3). Des atténuateurs insérés dans les lignes de transmission, permettaient la mesure de courants jusqu'à 160 kA. La transmission des informations était réalisée par câble triaxial ; leur acquisition était effectuée au moyen d'un magnétoscope SONY type AV3670 CE de 2 MHz de bande passante.

2.2.2 - Mesure du champ magnétique

Le champ magnétique était mesuré en quatre points à l'intérieur de l'avion : deux capteurs étaient placés dans le bord d'attaque de chaque aile ; deux autres sur le fuselage, à l'intérieur de la soute, légèrement en avant du plan des hélices et à 45° de part et d'autre de l'axe de symétrie de l'avion. Les capteurs utilisés, du type triaxiaux, avaient une constante de temps $\tau = 1 \text{ }\mu\text{s}$. Les informations étaient transmises par câble bifilaire torsadé blindé et l'acquisition était effectuée, en mode F.M., à l'aide d'un enregistreur magnétique Schlumberger ME 4050 de 400 kHz de bande passante.

2.2.3 - Mesure des courants de peau

Les courants de peau étaient mesurés à l'aide de boucles de "MOEBIUS". Quatre boucles étaient montées par paires, l'une à l'extérieur, l'autre à l'intérieur du fuselage, légèrement en avant du plan des hélices. Les modes de transmission et d'acquisition de ces informations étaient identiques à ceux des mesures précédentes.

2.2.4 - Mesure des surtensions sur la ligne test

La ligne test était constituée d'un fil de cinq mètres de long, placé à 0,22 m de la paroi intérieure du fuselage.

L'une des extrémités du câble était reliée à la masse de l'avion et la surtension était mesurée aux bornes d'une impédance insérée entre l'autre extrémité du câble et la masse de l'avion. Le signal de surtension était acheminé par un câble coaxial vers un magnétoscope SONY type AV 3670 CE de 2 MHz de bande passante, modifié en conséquence pour ce mode d'acquisition de données.

2.2.5 - Mesures des surtensions sur certains équipements de bord

Outre les mesures de surtensions sur le réseau de génération électrique de l'avion, divers équipements de bord avaient été instrumentés tels que : le dégivrage d'une glace copilote, le réchauffage de l'antenne anémométrique, l'indicateur de débit carburant, un feu de position, le radar météorologique, un récepteur VHF et un récepteur VOR. Des chaînes de transmission par fibre optique assuraient la transmission des signaux vers un enregistreur magnétique.

2.2.6 - Base de temps

Une base de temps était distribuée sur tous les enregistreurs magnétiques et permettait d'obtenir une précision de l'ordre de la seconde.

2.3 - Principaux résultats obtenus en 1978

Durant la campagne d'essais qui s'est déroulée, au dessus du territoire français entre mai et juillet 1978, sept vols correspondant à 17 heures de recherches de conditions orageuses ont permis d'intercepter 19 foudroiements dont 14 ont été enregistrés. Les principales conditions, relevées au moment des foudroiements, étaient les suivantes :

- altitude en vol : $10\ 000 < Z < 15\ 000$ pieds;
- vitesse de pénétration dans les nuages : 170 noeuds;
- température : $-5^\circ\text{C} < \theta < 0^\circ\text{C}$;
- type de nuages : cumulo-nimbus isolés ou en formation;
- précipitations : en général, grêle;
- turbulence : en général, moyenne;
- localisation du foudroiement : à la périphérie ou à l'intérieur (1 à 2 nautiques) du nuage.

Ces essais ont permis :

- de vérifier la bonne tenue mécanique de l'ensemble de l'appareillage en présence de forts courants (160 kA), ainsi que l'efficacité des perches utilisées pour localiser l'impact et visualiser l'effet balayant de la foudre ;
- de mettre en évidence, d'une part la nécessité de généraliser l'utilisation des fibres optiques pour transmettre les signaux de mesure et, d'autre part, la nécessité d'améliorer la fiabilité du matériel d'enregistrement magnétique ;
- de déterminer l'ordre de grandeur des principales caractéristiques des courants parcourant la structure de l'avion lors d'un impact sur la perche avant.

La figure 4 montre, à titre d'exemple, une forme d'onde de courant enregistrée sur la perche avant, d'amplitude voisine de 50 kA et correspondant vraisemblablement, d'après les observations de l'équipage, à un foudroiement direct de l'avion entre nuage et sol. L'analyse qualitative des foudroiements, observés en vol, met en évidence l'existence de deux types de décharges : celles constituées d'une succession d'impulsions brèves, de faible amplitude et d'une durée totale d'environ 10 millisecondes, et celles ne comportant qu'un nombre limité d'impulsions, de forte amplitude et beaucoup plus espacées dans le temps.

3 - PERSPECTIVES DE LA CAMPAGNE D'ESSAIS 1980

Une nouvelle campagne d'essais, tirant partie des enseignements de la première, se déroulera, au cours de l'été 1980, avec la participation de l'ONERA (Office National d'Etudes et de Recherches Aérospatiales). Les objectifs supplémentaires concernent notamment :

- la caractérisation de l'état électrique du véhicule,
- l'étude de la fonction de transfert, du point de vue électromagnétique, de divers types de panneaux réalisés en matériaux composites,
- la visualisation et l'enregistrement cinématographique de l'environnement nuageux (face à l'avion), de la perche avant et de l'écran du radar météorologique, ceci afin de corrélérer les foudroiements avec la situation météorologique locale.

L'ensemble de l'instrumentation décrite aux paragraphes 2.2.1 à 2.2.6 sera maintenue.

3.1 - Caractérisation de l'état électrique de l'avion

Deux phénomènes principaux peuvent contribuer à l'apparition de champs électrostatiques sur la structure d'un avion en vol : l'action du champ électrique atmosphérique ambiant et la présence d'une charge électrique propre sur la structure. L'acquisition de cette charge propre peut être due à trois processus d'électrisation (J.L. Boulay, 1979) :

- la triboélectricité (impacts de particules chargées ou non),
- les charges électriques évacuées par les propulseurs,
- les décharges partielles de type "couronne", provoquées par un champ inducteur intense d'origine atmosphérique.

En fonction des configurations de vol, l'un ou l'autre de ces phénomènes peut être prépondérant mais dans le cas général, l'état électrique du véhicule résulte de la superposition des deux états précédents.

On peut montrer (P. Laroche, 1980) que l'implantation de capteurs en quatre points de mesure, judicieusement choisis sur la structure, permet de déterminer la charge propre acquise par l'avion (ou son potentiel) ainsi que les trois composantes du champ inducteur ambiant.

3.1.1 - Mesure du potentiel électrique de l'avion

La mesure des composantes du champ électrique atmosphérique inducteur et du potentiel de l'avion est effectuée à l'aide de quatre capteurs, du type moulins à champ, développés par l'ONERA (P.Laroche, 1980).

Ces capteurs sont disposés dans des zones non soumises au courant d'origine triboélectrique et sont répartis sur la structure de façon à ce que chacun des capteurs soit découplé au mieux par rapport à deux composantes du champ extérieur. Les points d'implantation retenus sur l'avion "TRANSALL" sont indiqués sur la figure 5. L'obtention de la valeur du potentiel et de celles des trois composantes du champ extérieur nécessite la connaissance de coefficients de forme dont la valeur dépend de la géométrie du véhicule et des points d'implantation des capteurs. Ces coefficients sont déterminés, en laboratoire, grâce à une maquette conductrice, à échelle réduite, de l'avion (P.Laroche, 1980).

Le signal de mesure, issu de chaque capteur de champ, est enregistré en mode F.M. sur un enregistreur magnétique (figure 6).

3.1.2 - Mesure du courant d'impact

Le courant d'origine triboélectrique est détecté par une sonde d'impact, constituée par une métallisation de la glace frontale centrale du poste de pilotage. Le courant collecté circule à travers une impédance de charge réunie à la structure de l'avion ; la tension détectée aux bornes de cette impédance est amplifiée et acheminée vers un enregis-

treur magnétique (figure 6).

3.2 - Mesures électromagnétiques à large bande

3.2.1 - Généralités

Le but de ces mesures est la détermination simultanée des champs électromagnétiques à l'extérieur et à l'intérieur du fuselage de l'avion, au voisinage d'une ouverture, ainsi que l'analyse des signaux parasites engendrés sur une ligne test située à bord. Les résultats attendus doivent permettre de déterminer :

- l'importance relative des mécanismes de couplage de l'énergie électromagnétique avec un circuit électrique embarqué lorsque l'avion est soumis à un foudroiement direct ou de proximité
- la fonction de transfert, du point de vue électromagnétique, d'une ouverture radiotransparente de dimensions géométriques données ;
- la fonction de transfert de cette ouverture lorsqu'elle est recouverte d'un panneau réalisé en matériau composite ;
- les conditions d'initiation ou d'interception d'un foudroiement, en liaison avec les mesures des paramètres électriques de l'aéronef décrits au § 3.1.

Les champs électromagnétiques sont mesurés à l'aide des capteurs à large bande passante ; les signaux sont transmis au moyen de chaînes optoélectroniques et leur acquisition est effectuée simultanément par des magnétoscopes vidéo et par des digitaliseurs rapides. Ces derniers sont gérés, de façon automatique, par un ordinateur qui assure également le stockage des données.

Le premier mode d'acquisition, opérant de manière continue doit permettre de reconstituer l'historique complet de la décharge atmosphérique avec une bande passante de 10 MHz et le second doit permettre d'analyser des phénomènes, pendant une durée limitée mais avec une bande passante de 200 MHz.

L'ensemble de l'instrumentation d'acquisition des signaux est disposé à l'intérieur de la cage de Faraday qui utilise un réseau d'alimentation électrique autonome, découplé du réseau de l'avion.

3.2.2 - Capteurs de champ électromagnétique

a) A l'extérieur du fuselage

L'implantation des capteurs de champ électrique et de champ magnétique a été choisie de façon à pouvoir estimer les champs, au niveau de l'ouverture étudiée, avec une précision suffisante dans la gamme de fréquence envisagée. De plus, cet emplacement doit être situé dans une zone à faible probabilité d'impact de la foudre. La figure 7 indique l'implantation retenue, les deux capteurs sont placés sur le côté extérieur droit et centrés sur une génératrice du fuselage passant par le centre du hublot ; ces capteurs sont protégés par un carénage en fibre de verre traité anti-statique. L'orientation des capteurs est choisie de façon à permettre la mesure du champ électrique normal à la paroi et la mesure du champ magnétique tangent à la circonférence du fuselage.

Les capteurs utilisés sont des détecteurs actifs, du type asymétrique, commercialisés par la société Thomson-CSF (Département applications spéciales de l'instrumentation). Ces dispositifs délivrent un signal de sortie proportionnel à la grandeur physique à mesurer (module du champ électrique E ou du champ magnétique H) et comportent huit gammes de mesures programmables. Leur forme géométrique particulière permet d'effectuer des mesures de champ très intenses (± 316 kV/m ou ± 839 A/m) dans une gamme de fréquences comprise entre 100 Hz et 150 MHz pour le capteur E et entre 6 kHz et 150 MHz pour le capteur H (figure 8).

b) A l'intérieur du fuselage

La détermination des champs électromagnétiques à l'intérieur du fuselage, sur l'axe du hublot (figure 7), est réalisée par des capteurs développés par la même société, permettant d'effectuer des mesures en champ libre dans une gamme de fréquences comprise entre 1 kHz et 130 MHz pour le capteur E et entre 30 kHz et 130 MHz pour le capteur H . Le premier comporte cinq gammes de mesure, réparties entre 1 kV/m et 100 kV/m et le second en comporte trois, comprises entre 26,5 A/m et 265 A/m (figure 9).

Les signaux parasites induits sur la ligne test sont détectés, soit aux bornes d'une impédance de charge, soit à l'aide d'une sonde de courant radiofréquence.

3.2.3 - Chaînes de transmission optoélectroniques

Les signaux entre les capteurs de champ et les systèmes d'acquisition sont transmis par voies optoélectroniques (figure 10). Les chaînes utilisées permettent d'effectuer une transmission analogique des signaux, dans une gamme de fréquence comprise entre 500 Hz et 200 MHz, avec une dynamique supérieure à 40 dB.

Ce matériel, commercialisé par Electro-Optic Developments, a été modifié et adapté aux conditions du vol.

3.2.4 - Systèmes d'acquisition et de traitement des signaux

L'acquisition des signaux est réalisée simultanément (figure 10) :

- par enregistrement continu, en fonction du temps, sur un magnétoscope Grundig BK411 de

de 10 MHz de bande passante et de 40 dB de rapport signal sur bruit, modifié en vue de cette application particulière ;

- par mémorisation sur des enregistreurs de transitoires de 200 MHz de bande passante. Ce mode d'acquisition permet d'appréhender et d'analyser des signaux rapides dans une fenêtre de temps limitée et utilise des digitaliseurs 7912 AD Tektronix de 10 K mots de capacité mémoire. La gestion de ces digitaliseurs et le transfert des données vers une mémoire de masse, constituée par une bande magnétique digitale, sont obtenus de façon automatique par l'intermédiaire d'un ordinateur 4052 Tektronix suivant le synoptique représenté sur la figure 11.

Deux circuits "Trigger" et "Synchronisation" permettent respectivement, de commander une acquisition des digitaliseurs quelle que soit la polarité du signal analysé et de repérer sur l'enregistrement vidéo des magnétoscopes BK 411, l'instant de l'acquisition effectuée par les enregistreurs 7912 AD.

3.2.5 - Nature des panneaux étudiés

Les hublots expérimentés ont un diamètre de 380 mm et seront recouverts successivement de panneaux en :

- verre,
- verre traité (procédé SEFTIM),
- fibre de carbone,
- fibre de carbone avec grillage cuivre intégré,
- fibre de verre avec grillage cuivre,
- métal.

Les panneaux en fibres de carbone et de verre ont une épaisseur de 2 mm et le grillage en cuivre utilisé a une maille de 1,5 mm, un diamètre de fil de 90 µm et une densité de 68 g/m²

4 - CONCLUSION

Une première campagne d'essais de foudroiement en vol sur un avion "TRANSALL" (1978) a permis de montrer la faisabilité d'une telle expérimentation et de mieux définir les chaînes de mesure à mettre en oeuvre. Tenant compte de ces enseignements, de nouveaux essais sont prévus au cours de l'été 1980 avec pour objectifs :

- d'obtenir des informations quantitatives sur les modes de couplage de l'énergie électromagnétique, engendrée par un foudroiement direct ou de proximité, avec les équipements de bord ;
- de connaître l'affaiblissement introduit par divers types de panneaux réalisés en matériaux composites ;
- d'évaluer l'état électrique d'un véhicule au moment du foudroiement ;
- de caractériser les ondes de courant parcourant la structure.

REFERENCES

- Boulay J.L. "Elimination des perturbations radioélectriques d'origine électrostatique sur avions". La Recherche Aérospatiale n° 1979-2, pp. 101-120 (1979), TP ONERA N°1979-53.
- Gall D. "Mesures des caractéristiques de la foudre en altitude". Essai n° 76/65 0000 P4 et final. Centre d'Essais Aéronautiques de Toulouse (1979).
- Laroche P., Weber R., Gall R. "Essais en vol pour la réduction des perturbations radio-électriques d'origine électrostatique. Meeting AGARD/AVP "Electromagnetic Effects of (carbon) composite materials upon avionics systems, Lisbonne (Portugal), 16-20 juin 1980.
- Maxwell, K.J., Walko, L.C., Mangold, V.L. "Inflight Measurements of Lightning Characteristics". Workshop on Grounding and Lightning Technology, Report FAA-RD-79-6, 6-8 May 1979, Melbourne (Florida).
- Pitts, F.L., Thomas, M.E., Campbell, R.E., Thomas, R.M., Zaepfel, K.P. "Inflight Lightning Characteristics Measurement System". Workshop on Grounding and Lightning Technology, Report FAA-RD-79-6, 6-8 May, 1979, Melbourne (Florida).
- Plumer J., Burrows, B., Clifford, D. Conference on Aircraft for Lightning and Atmospheric Electricity Hazards. ONERA Châtillon (France), 14-21 septembre 1978.
- Von Bokern G.J., Piszker, L.D., Brick, R.O. "In-flight Lightning Data Measurement System for fleet Application", The Boeing Company Seattle Washington, Report FAA-RD-78-83, Final Report (1978).

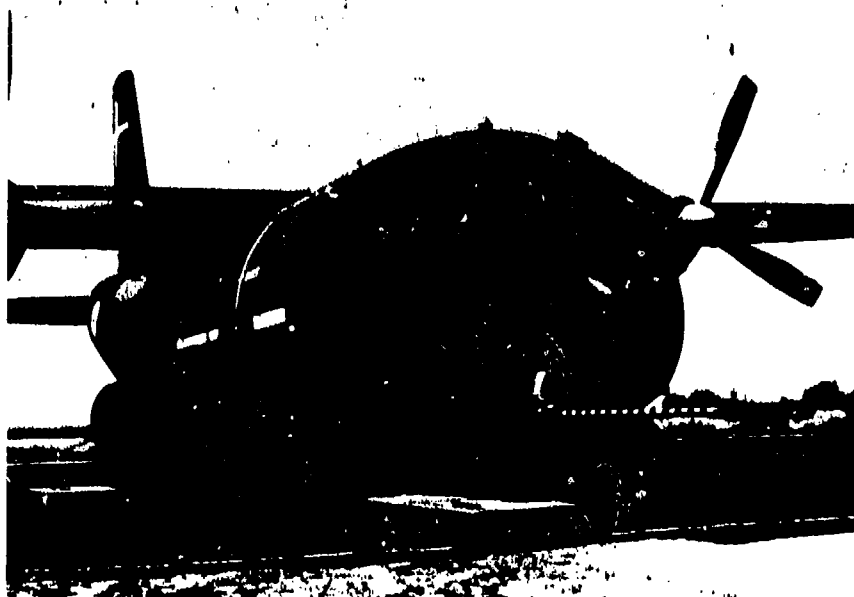


Fig. 1 - Photographie de l'avion "TRANSALL" C160-A04.

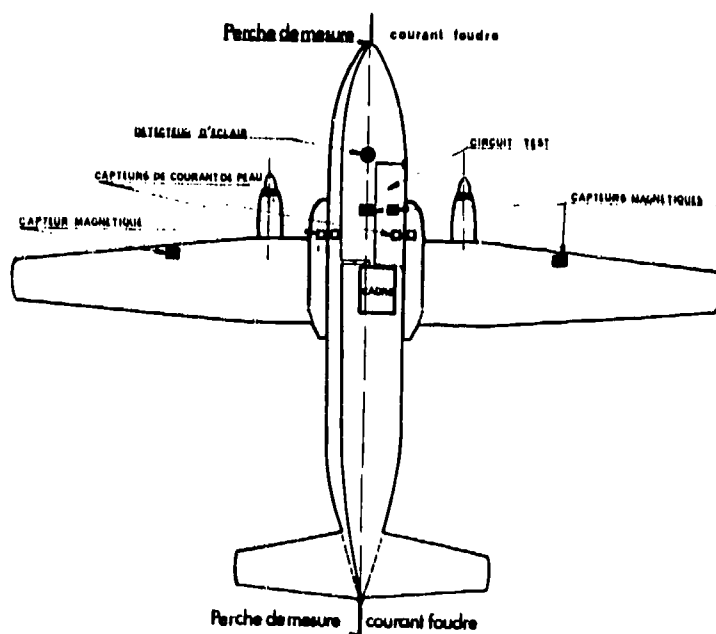


Fig. 2 - Représentation schématique de l'instrumentation utilisée au cours des essais en vol effectués en 1978.

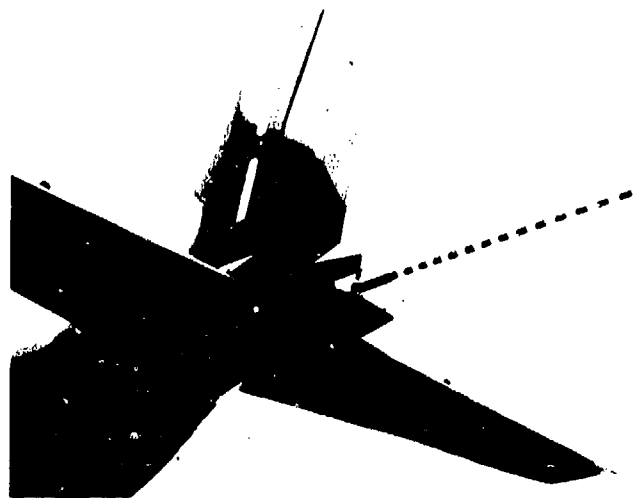


Fig. 3 - Photographie de la perche arrière.

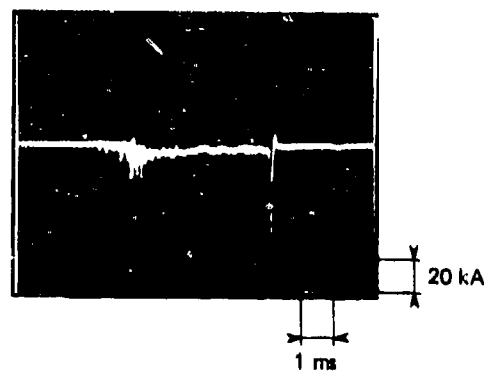


Fig. 4 - Forme d'onde du courant mesuré sur la perche avant du "TRANSALL" C160-A04.

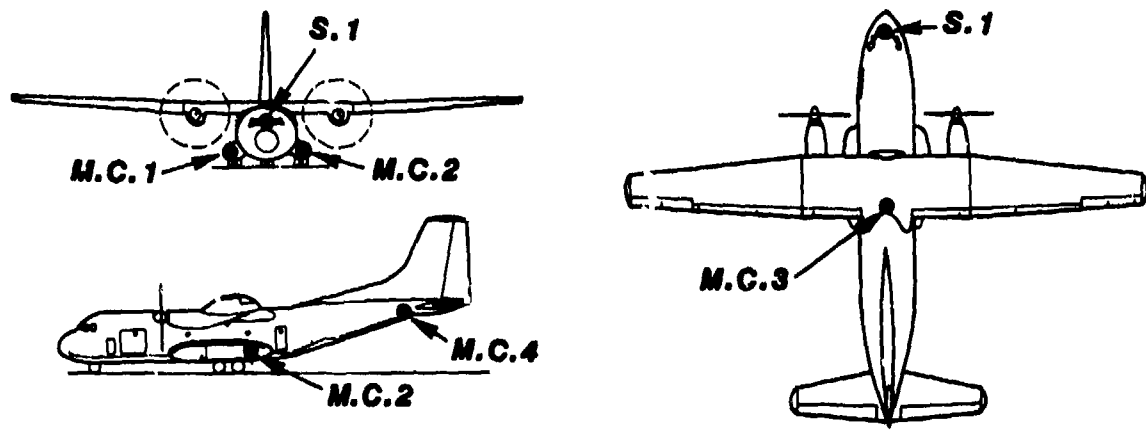


Fig. 5 - Implantation des quatre moulins à champ (M.C.) et de la sonde d'impact (S.I.) sur l'avion "TRANSALL" C160-A04.

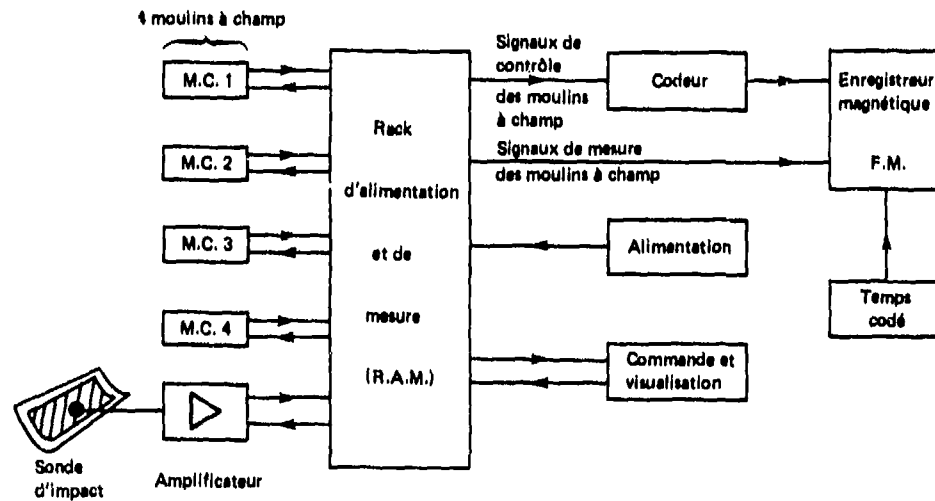


Fig. 6 - Représentation synoptique des chaînes de mesure du potentiel électrostatique de l'avion et du courant d'impact.

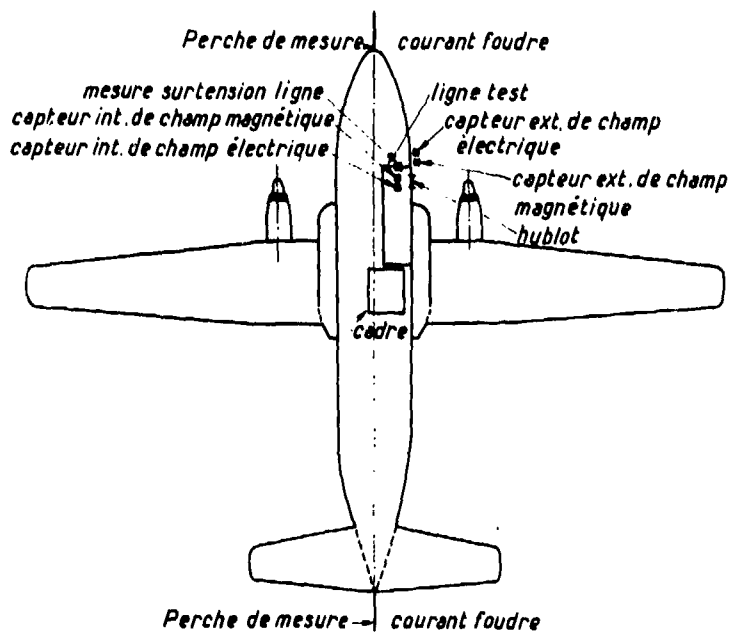
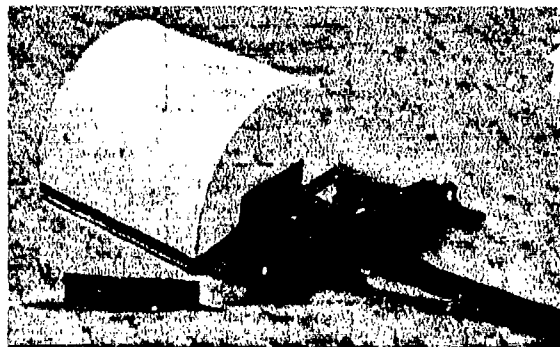


Fig. 7 - Implantation des capteurs de champs électromagnétiques sur l'avion "TRANSALL" C160-A04.

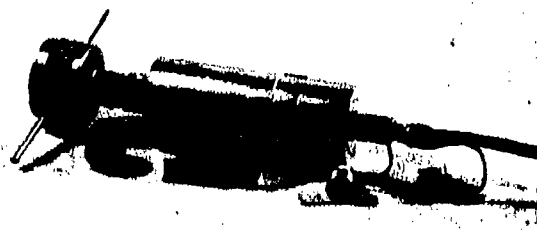


a) capteur E



b) capteur H

Fig. 8 - Capteurs de champs électromagnétiques du type asymétrique



a) capteur E



b) capteur H

Fig. 9 - Capteurs de champ électromagnétique du type symétrique.

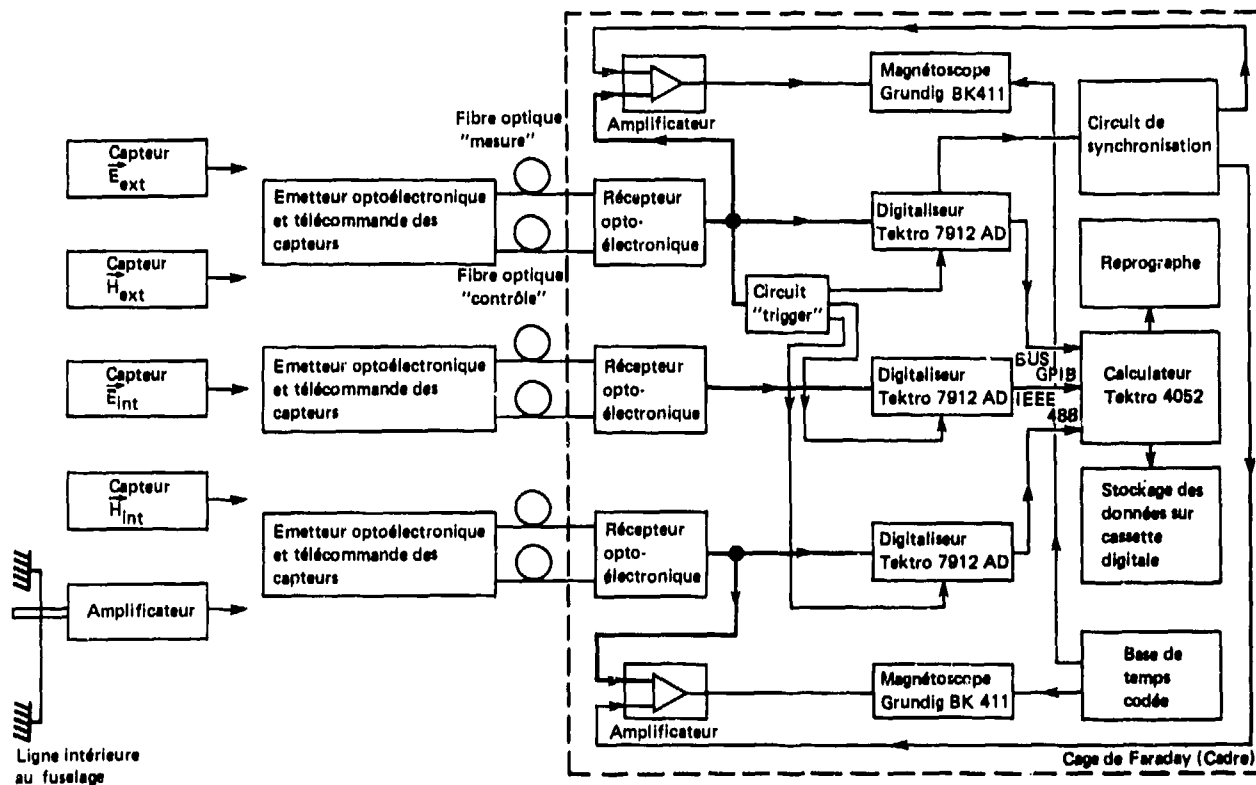


Fig. 10 - Schéma synoptique représentant les chaînes de mesure des champs électromagnétiques à large bande.

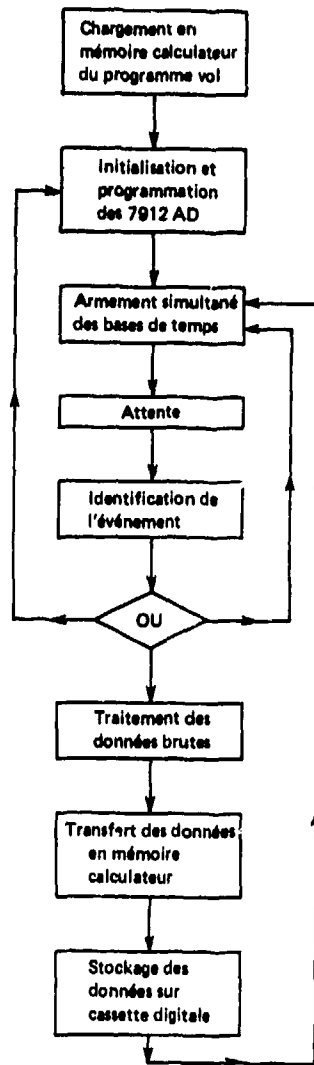


Fig. 11 - Déroulement du programme de gestion des 7912 AD et de stockage des données traitées à partir du calculateur 4052.

AIRCRAFT MANUFACTURERS APPROACH TO THE E.M.C./AVIONICS
PROBLEMS ASSOCIATED WITH THE USE OF COMPOSITE MATERIALS

by

G. Barton
Westland Helicopters Ltd.
Yeovil U.K.

I. P. MacDiarmid
British Aerospace, Warton U.K.

SUMMARY

The paper outlines, by giving detailed examples, the U.K. aircraft manufacturers approach to the E.M.C./Avionic problems associated with the use of Carbon Fibre Composites (C.F.C.).

The first two sections deal with examples of structures that required flight clearance within relatively short timescales, these are; the fitting of C.F.C. panels to Jaguar and Lightning Strike investigations on composite demonstrator rotor blades.

The remaining sections (3 to 5) outline work undertaken to address the long term problems of composite aircraft and their effects on avionic systems. This includes C.F.C. fuselage investigations, conductivity measurements and an earth return study.

1. JAGUAR CFC PANELS

The structural trend when introducing composites on aircraft has been to replace selected existing metallic panels with carbon fibre composite (CFC) panels. To assess the possible effects on avionic systems and the overall Electromagnetic Compatibility (EMC) of the aircraft each composite panel requires to be addressed considering such areas as material/lay-up and, position on aircraft, lightning strike effects, antenna performance, RF effects on systems/cables running beneath; etc. with the final objective to provide recommendations and supporting evidence for flight approval.

The introduction of CFC panels on the Jaguar aircraft is one such instance, and the following outlines the investigations undertaken and the subsequent programme of work.

The proposed CFC panels to be fitted on the Jaguar Aircraft are as listed below:-

Underwing Panel	EM4 18 0001
Rear Fuselage Spine Panel	EM4 28 0001
Rear Fuselage Tank Access Panels	CF18.010.001
	CF18.016.001

An initial investigation was undertaken considering the location of the panels which are shown in Fig.1.1 and the various systems/cables running beneath. It was concluded that only two areas of possible problems need to be considered further:-

1. Lightning Strike Effects
2. RF Effects (Possible deterioration in EM shielding properties)

1.1 Lightning Strike Effects

When it was initially proposed to use carbon fibre/aluminium honeycomb/carbon fibre sandwich panels on the aircraft a great deal of concern was expressed. This was because previous work on this type of sandwich panel indicated a possible hazard due to lightning currents flowing in the aluminium honeycomb. The damage noted arises mainly from current being forced to cross the dielectric glue line between aluminium ribbons. The subsequent instantaneous deposition of energy gives rise to three stages of failure depending upon the magnitude of the current densities. They are:

- 1) Blistering and arcing within the glue layer giving progressive failure of the bond up to complete separation of the ribbons. This occurs at very low current density.
- 2) Failure of the interface bond between the Carbon fibre and the aluminium honeycomb up to complete delamination of the Carbon fibre skin.
- 3) As current densities and action integral increase these two failure mechanisms can escalate into an explosive delamination of the carbon fibre skins.

When assessing the possible hazards due to lightning strike each panel was considered in turn and a great deal of attention given to the possible delamination problem. It was concluded that the rear fuselage tank access panels are the only panels with possible significant flight safety implications for the following reasons:

1. Delamination of this panel could cause a serious flight safety hazard.
2. These panels are in a high current density area and long before failure of these panels, sparking could occur at the metal to CFC interface resulting in ignition of fuel.

A programme of work was therefore undertaken to investigate the effects of lightning on the fuel tank access panels. In addition to performing a series of tests to determine the performance of the present design, various lightning strike protection finishes were also assessed during this programme of work, in case this proved necessary.

1.1.2 Simulated Lightning Strike Tests on the CFC Fuel Tank Access Panel

The work reported below was undertaken by UKAEA, Culham Laboratory, Abingdon, Oxfordshire and acknowledgement is given for the extracts used here from their report on this work.

The test conditions and levels subjected on the panels were derived from the Culham Laboratory Report "Recommended Practice for lightning Simulation and Testing Techniques for Aircraft". No CLM-R-163 dated May, 1977.

1.1.3 Test Specimens

A total of six specimens were supplied. They were:

- M.F.1. Standard Aluminium Panel of present production.
- J.F.2 Standard CFP/Aluminium honeycomb/CFP panel of the proposed demonstrator type.
- J.F.3 As J.F.2 with a 200 mesh stainless steel wire surface protection.
- J.F.4 As J.F.2 with Aluminium foil surface protection.
- J.F.5 As J.F.2 with flame sprayed Aluminium protection.
- J.F.6 Aluminium/Aluminium honeycomb/Aluminium sandwich panel.

In addition a mock up of that part of the fuel tank forming the immediate surroundings of the access panel was also supplied. In this mock up the method of fixing the panel to the tank was faithfully reproduced.

In addition to tests on the six panels mentioned above tests were also conducted on panels made at Culham. These were

- (1) A plain Carbon Fibre Epoxy Resin panel EPLA 4617 MPD having 8 laminates each 0.005 thick with the fibre lays at $0^{\circ}, 90^{\circ}, 90^{\circ}, 0^{\circ}, 0^{\circ}, 90^{\circ}, 90^{\circ}, 0^{\circ}$. to the direction of the current flow.
- (2) A SRBP panel.
- (3) A plain 2 mm thick Aluminium Sheet panel.

1.1.4 Test Techniques

Zone 3 Tests

The test panel was mounted in the simulated surround and this formed part of a parallel transmission line. The return conductor forming the other half of the system was placed opposite the outside of the panel. See fig.1.2.

This effectively simulated the natural lightning current distribution under zone 3 conditions in the panel and its immediate surround. The light tight box permitted photographic observation of possible sparking at the various current joints during the test pulse.

Zone 2a Tests

The simulated surround structure was reduced in size by removing some of the outer metal panel, and placed in the standard Culham large concentric feed arc test rig. This is designed to reduce the effect of the return conductor magnetic fields upon the arc movement, and thus more closely resembles the conditions of a natural lightning strike environment. The arc was struck between a jet diverting electrode and the test piece. This electrode diverts the electrode jet, which is not representative of a natural lightning strike, away from the test piece, and thus prevents unrepresentative damage from occurring.

1.1.5 Diagnostics

Zone 3

The total test current was measured by using a calibrated magnetic probe and a Rogowski coil. In addition two flat single turn coils were placed close to the surface of the access panels on both inner and outer sides. These coils covered half the effective width of the panel and were arranged to detect linkages with that component of the flux normal to the surface of the panel. This indicates the level of flux penetration of the panel. Reference levels were set by conducting tests with an aluminium panel and an insulating panel. Small holes were drilled into the CF/honeycomb/CF sandwich panel, into which probes were inserted to measure the honeycomb resistance.

The possible presence of sparking at the panel/surround interface was detected photographically.

Zone 2a

No special diagnostics other than normal current and voltage measurements were made for Zone 2a Tests.

1.1.6 Test Waveforms Used

Zone 3 Tests

The width of the simulated immediate surrounds of the panel is estimated as being one sixth of the total peripheral distance around the fuselage at the fuel tank position. At this point of the fuselage Zone 3 currents will be distributed fairly uniformly around the fuselage during natural strike conditions. The required test current parameters can be reduced therefore, by an appropriate amount from those recommended in the Culham Laboratory Report "Recommended Practice for Lightning Simulation and Testing Techniques for Aircraft" No. CLM-R-163 May, 1977. Thus the peak current can be reduced to one sixth i.e. from 200 kA peak to 33 kA peak, and the action integral can be reduced by a factor of 36 from $2 \times 10^6 \text{ A}^2\text{s}$ to $5.6 \times 10^4 \text{ A}^2\text{s}$. The actual waveform however is important in this case. The rise of the high current component must be short enough to ensure effective initial inductive sharing of the current between the aluminium surround and the CFRP Panel, but long compared to the redistribution time of current within the thickness of the panel, whilst the total pulse length must be long compared with the redistribution time of current between the carbon fibre sandwich panel, and the surrounding aluminium.

It will be noted from the table of results, that in all cases the action integral was lower than the $5.6 \times 10^4 \text{ A}^2\text{s}$ stated above, but that the peak current of 33 kA was achieved. The voltages measured in the flux loops however indicated that the high resistance of the CFRP panels played a significant part in the current distribution between the panel and the surround after the initial rise time, and that current had virtually ceased to flow in the carbon fibre before the end of the pulse. Clearly the action integral for a given peak current can only be increased by extending the duration of the pulse, and there was little point in extending the pulse beyond the time when no further current flowed in the carbon fibre. In addition such an extension of time can only be achieved by also lengthening the rise time thereby decreasing the di/dt , and the initial current sharing. A larger duration pulse therefore would have been a less severe test because of the slower rise time and in spite of the higher action integral. This is a very important point in establishing the complete validity of the tests.

Zone 2a Tests

The fuel tank access panel is in a region where a swept stroke reattachment could take place. There is not a high probability of such a reattachment, nevertheless in the event the panel could experience a restrike current plus some part of an intermediate or continuing current, in the form of an open arc on the panel. The likely damage mechanism therefore is the mechanical forces and current sharing between the CFC and the aluminium honeycomb during the restrike period, and the high charge transfer of the intermediate and continuing current phase. It is the latter which generates much of the arc root energy due to the tendency for the arc root to develop a near constant voltage.

The characteristics of the Zone 2a current waveforms therefore were a 100 kA short duration (oscillatory) pulse followed by triangular pulse having $\approx 2.7 \text{ kA}$ peak and a charge transfer of $\approx 40 \text{ coulombs}$.

1.1.7 Test Results

Zone 3 Tests

Zone 3 tests were conducted on a total of 5 panels. They were:

- (1) A present production aluminium panel and
- (2) A SRBP panel

(The results from these were used as reference levels representing a completely conductive, and a completely non-conductive panel, particularly with reference to the flux loops diagnostic). These were followed by:

- (3) A sandwich panel having aluminium honeycomb between aluminium sheets.
- (4) The Culham made CFRP panel.
- (5) The proposed sandwich panel having aluminium honeycomb between CFRP skins.

The Test levels used in these tests are given in table No. 1. There was predictably no response from the flux loop coils when an aluminium panel was tested. (Items 1 and 3 above). This confirms that the current density in the aluminium panels was the same as that in the surrounding aluminium section. With the XRB panel strong signals having similar characteristics were detected in both upper and lower flux loop coils confirming that no current flowed in the SRBP panel. In the case of CFRP panels (ITEMS 4 and 5) both with and without aluminium honeycombs, examination of the flux loop output curves again showed very similar characteristics between upper and lower coils with only very small differences in the curve profile during the very early phase of the pulse i.e. during the first 0.2 μsecs .

This indicates that appreciable current flowed in the CFRP panels during the initial rise time only, and for the greater part of the pulse little or no current flowed in the carbon fibre panel. No externally detectable damage was observed in the CFRP panels or in the honeycomb, and the resistance measurements conducted on the honeycomb did not indicate any significant latent damage to the honeycomb.

No sparking was detected inside the tight proof box.

Zone 2a Tests

The test wave-forms used on the various samples are given in table 2 together with an indication of the damage sustained. Photographs of the panels after testing are given in Figs.1.3 to 1.6. No damage was observed between the counter sunk screws and the CFRP. This is a very satisfactory result as the presence of the gasket forced all the current to flow through the screw/CFRP interface, and the absence of damage indicates a good current carrying interface.

In all cases where some form of surface protection was applied adequate protection was afforded to the Carbon Fibre. The protecting surface however was itself damaged and repairs would be necessary in practice. In the case of the foil and the flame sprayed aluminium repairs could be reasonably effected but the SS mesh protection may prove more difficult. In all cases it may be cheaper and quicker to replace the whole panel. Both the unprotected CFRP and the aluminium skin having a honeycomb centre were punctured on the outer skin, but otherwise both were intact. The results demonstrated that the damage sustained would not hazard the aircraft in flight nor would the damage be unacceptably extended by the aerodynamic forces on it during the remainder of the flight.

Conclusions

The Zone 3 tests indicate that the current sharing characteristics of this particular assembly gives very good protection to the CFRP and the aluminium honeycomb. The panel should therefore safely survive the zone 3 effects of a very severe strike to the aircraft. It must be stressed however that this conclusion refers solely to this particular panel in this particular position. Variations in the dimensions of the panel, its position on the aircraft, or other changes in the nature of the immediate surroundings (particularly changes in the conductivity of material surrounding the panel) could adversely affect its lightning performance.

The Zone 2a tests indicate that complete protection against arc root damage is possible. However there is very low probability of an arc root attachment to this panel, and in addition the damage likely to occur in such a rare event is extremely unlikely to hazard the aircraft in any way. The worst situation therefore is unlikely to cause more problems than the need to replace the panel after the strike, a requirement that might be necessary even if protection is applied. In view of this it was recommended that no surface protection was required on these particular panels.

1.2 R.F. Effects

The introduction of composites on aircraft raised the question of the possible reduction in the Electromagnetic Shielding properties of a composite airframe compared with the conventional aluminium structure. This therefore raised the problem of EMC of the Jaguar aircraft with CFC panels fitted. It was considered not necessary in this instance and indeed timescales did not allow, without good evidence to the contrary, to carry out absolute measurements of the shielding properties of the CFC panels and therefore a comparison type test was undertaken.

1.2.1 Test Philosophy

The size of CFC panels, where they are installed, the position of cables beneath, and their relation to other cable runs not passing beneath these panels influence the philosophy of testing and the results significantly.

When the problem of testing the 4 CFC panels was first approached the aircraft and drawings were examined to ascertain which systems were enclosed by the panels. It was found that one enclosed fuel, one enclosed a fuel contents sensor and fuel, and the other two covered wiring associated with the Autostabiliser and some other general wiring.

Since the Autostabiliser system has been subjected to a great deal of EMC testing both for onboard radio equipment transmissions and for RF environments it was felt that checking for degradation of the Autostabiliser system in the presence of onboard RF transmissions would be an indication of any reduction in screening due to changing the metal panels to CFC ones. It was not the intention to carry out absolute measurements of screening efficiency and field strength levels.

Consideration was given to the armament installation but as no armament cables run beneath any of these panels it was not considered necessary to test this system. Cross coupling 'down the line' between cables was considered. However, we investigated the installation and considered that there was adequate shielding between the cables beneath these panels and armament cables where they ran together in other parts of the aircraft. Had there been a significant deterioration in the shielding of the CFC panels, thereby permitting increased pick-up on the cables beneath the panels consideration would have been given to checking the armament system wiring to ensure cross-coupling between wiring does not affect the armament system. This proved to be unnecessary.

1.2.2 Results

The tests were carried out on a production Jaguar aircraft (S162) with the four CFC panels fitted as described earlier. The checks were in accordance with standard on-aircraft EMC clearance tests ensuring that specified power outputs were achieved.

1.2.2.1 Emissive Equipment Checks

Tailplane and rudder and all cockpit instruments were monitored for any deviations whilst the autostabiliser system was engaged and the following emissive equipments were activated over their operating frequency range.

TACAN

IFF

ILS

V/UHF

STBY UHF

RAD ALT

No interference was detected during these checks.

1.2.2.2 H.F. Transmission Checks

The results recorded for the CFC panels were taken during engine runs as our experience suggests that this is the worst case. (Because airframe vibration acts as a PFCU valve dither signal to increase system sensitivity to demodulated signals). The tests were carried out in a similar manner to that as in previous autostabiliser tests are compared to these earlier results as shown in Fig.1.7

The results show:-

- . That checks with CFC panels are similar to those obtained with metal panels.
- . The interference with CFC panels occurs within the same frequency range as that with standard metal panels.

The measurements did not suggest that CFC panels introduced a significant degradation.

1.3 Conclusions

From the results of these checks, using emissive equipment and HF transmissions, no significant degradation was observed from the fitting of CFC panels. No significant change in the EMC clearance of the aircraft therefore results from the introduction of these panels.

The results from the autostabiliser provide a useful comparison as th's system is known to respond to any excessive field. Only the HF transmissions resulted in noticeable interference and this was within the levels expected.

2. COMPOSITE ROTOR BLADES

Traditionally, helicopter rotor blades have been manufactured, with a light alloy spar trailing edge skins and tip fittings which presented a good fibre backed should a blade alloy spar trailing edge skins and titanium erosion shield necessitates the development of environmental protective systems.

W.H.L. have been developing demonstrator composite tail rotor blades, constructed as shown in figure 2.1 and lightning strike protection schemes have been considered during this demonstrator programme. The main objectives of this work are:-

1. Provide an adequate electrical path to conduct a strike of moderate severity
2. Ease of manufacture with a minimum of operations.

The initial phase of the work was to ascertain the suitability of the proposed connections between the erosion strip and the rotor boss to withstand the current of a simulated lightning stroke as defined in Culham Report CLM-R-163 "Recommended Practice for Lightning Simulation and Testing of Techniques for Aircraft".

2.1 Description of Test Pieces

(a) Straight connection (see Fig. 2.2)

This was a 9" length of the proposed erosion strip which was connected by two rivets to a 9" length of 3/8" copper braid and attached to a glass fibre backing strip. The other end was hard soldered to a brass connector which was bolted to a 3" x 2" x 1/4" block of aluminium at 90° to the line of the erosion strip representing the rotor boss connection.

(b) Angled connection (see Fig. 2.3)

This was similar to the "straight connection" except that at the boss end the aluminium block was in line with the erosion strip so that the braid turned through 90° bolting to the aluminium block.

(c) Titanium connection strip

This was a strip of titanium 2.5" x 0.8" x .020" cut from a small piece of the erosion strip. Suitable connectors were made so that test pieces and titanium strip could be mounted in the "quasi-concentric" rig in a vertical position. The rig was connected to both the 20 kV and 100 kV banks which could be used separately or in a combined waveform mode.

2.2 Test Current Waveforms

The tests were designed to check the specimen's ability to meet the requirements of component A of the lightning test waveforms (200 kA peak current and action integral = $2 \times 10^6 \text{ A}^2\text{sec}$).

Two possible failure mechanisms could result from Component A viz; failure due to the mechanical forces arising from the 200 kA peak current, and failure due to ohmic heating arising from the action integral of $2 \times 10^6 \text{ A}^2\text{sec}$. In order to separate these two effects, two separate tests waveforms were used. Firstly the mechanical failure mode was tested using a damped oscillatory pulse having a peak current of 200 kA and a rise of $\approx 6 \mu\text{s}$ and a total duration of $\approx 100 \mu\text{s}$. Following this, it was intended to assess the possible failure due to ohmic heating by using a unidirectional pulse having a total action integral of $2 \times 10^6 \text{ A}^2\text{sec}$. The samples a) and b) however failed on the high test current by mechanical forces in some areas and Ohmic heating in other regions although the action integral was well below the required $2 \times 10^6 \text{ A}^2\text{sec}$ during the high current pulse.

Similar wave-forms as above were used on the titanium connection strip, but the intensity level was reduced.

2.3 Test Procedure and Results

The "straight connector" was mounted in the standard Culham concentric test rig so that the erosion strip and the copper braid connection were in the zero magnetic field area.

A pulse having a peak current of 280-kA and an action integral of $.81 \times 10^6 \text{ A}^2\text{sec}$ was passed.

This produced considerable damage to the test piece. The copper braid was torn from the glass fibre backing and also showed signs of pinching but this was largely inhibited by the epoxy resin which had impregnated the braid. The hard-soldered connection between boss and braid had parted and the connector itself was bent at a right angle. The titanium had melted for about a $\frac{1}{4}$ " at the point where it connected to the copper braid (the cross section of the titanium was reduced at this point).

As no further tests were possible using the "straight connection" and the magnetic forces on the braid on the "angled connector" would be greater, it was decided to reduce the current level to the component D level to assess the ability of the test pieces to withstand a restrike. The "angled connection" was mounted in the same way as the "straight connection" and a pulse passed through it having a peak current of 102 kA and an action integral of $.11 \times 10^6 \text{ A}^2\text{sec}$. (note: Component D has $\hat{I} = 100 \text{ kA} \pm 10\%$ and an action integral of $0.25 \times 10^6 \text{ A}^2\text{s} \pm 10\%$).

This pulse did not part the braid from the glass fibre backing but at the boss end only a few strands of braid remained attached to the connector. At the riveted end where the titanium narrowed it had melted but not lost any metal, the metal having cooled in position.

Five tests were conducted passing the current through a 2" length of titanium .020" thick and 0.8" wide. The severity levels of the tests and a summary of the results is given in table 3 below. The results after scaling showed that the erosion strip which was $2 \frac{3}{16}$ " wide reach a temperature of about 600°C when subject to a component A pulse.

TABLE 3

SHOT	TEST PIECE	I kA	$I^2 t$ $\text{A}^2\text{sec} \cdot 10^6$	RESULT
1	.8" x 2" x .020" TITANIUM STRIP	123	.22	No change or damage, some heating
2	"	150	.22	Metal turned blue, slightly buckled.
3	"	165	.286	Metal red hot, increase in buckling.
4	"	182	.36	Metal red hot, further distortion.
5	"	8.0	.74	Test piece completely melted and blown from the test rig (after $\approx 60 \text{ ms}$).

The results indicated that neither the braid connections nor the reduced section of the titanium strip at the riveted connection were capable of withstanding the heating effect or magnetic forces of a Component A waveform. The titanium erosion strip whilst not itself being damaged would become too hot for the epoxy resin bonding to the rotor blade.

2.4 Further Work

Following these results in addition to improving the braid bonding, it was considered desirable to provide a display of visual evidence of being struck by lightning without causing structural damage to the blade. The split tag method was devised, the theory being the inner and outermost parts of the tag are large enough to carry a maximum strike (200 kA) so that the gap between, bridged only by the titanium tang would act as a fuse and show discolouration with only a small charge. A large one would blow this fuse and should the end of the shield turn up it would be flexible enough to distort without damaging the main area of the shield.

Initial work on the braid showed that a tubular tinned copper braid 4mm inside diameter 3.5 sq.mm cross sectional area will carry a peak current of 200 kA. However during tests the braid shrank in section and length causing the break in the braid. It was therefore decided to compress the length of the braid (bunching) to give a greater degree of flexibility to absorb this shrinkage. The brass cuff tag and the annealed copper spade tag at the shield end are silver soldered with Easy-Flow No.2 and both tags slotting inside of the braid, as shown in Fig.2.4

To obtain airworthiness approval for a limited number of flying hours for the composite rotor blade the split tag-method shown above was employed in a complete blade and tests undertaken to assess the integrity of the tip plate, carbon skins, erosion shield and braid assembly. It was planned to start testing with a low severity strike and work up to a severe level in increments, but only two strikes were performed as detailed:-

	1st Strike	2nd Strike
Peak Current	36 kA	116 kA
Action Integral	$0.09 \times 10^{-6} \text{A}^2 \text{secs}$	$0.77 \times 10^{-6} \text{A}^2 \text{secs}$
Rise Time	24 ms	27 ms
Total Duration	200 ms	300 ms

Following the first strike, slight delamination had taken place at the erosion shield, and the copper braid had deformed. On the application of the second strike considerable damage occurred which gave rise to the decision to strip the blade before proceeding further.

The erosion shield was carefully prised from the blade and the tip cap was unbolted and removed followed by an investigation of the full extent of the damage.

Debonding of the erosion shield had occurred, caused by ionization and subsequent explosion of the air gaps between adjacent balance weights situated between the erosion shield and the composite moulding. Carbon deposits, the debris from these explosions, are evident in these areas. Only a very small area (c. 10%) of the original shield blade bond remained intact after the second blast.

Vaporization of the free earthing braid between its tag and the braid surface had taken place (Figs 2.5 and 2.8). Severe damage to the rivets holding the braid to the erosion shield through the copper fusible link had also occurred together with some vaporization of the erosion shield at its extremity (Fig 2.11). Eventually, small holes had been blown in the erosion shield at the locations where it had debonded from the blade after the first blast. Thus these holes were considered a cumulative effect (see Fig. 2.11).

The rivets attaching the tip cap insert to the blade were slightly damaged (Figs. 2.7 and 2.11) and there was evidence of the burning of the P.R. 1221 sealant at the tip cap/insert interface.

No massive structural damage had been incurred by the composite section of the blade as the majority of the current had been carried by the more conductive erosion shield. The only damage present the small cracks in the carbon skin around the rivets, which attached the tip cap insert to the blade, and the localised scorching of the glass composite directly beneath the positions where arc-ing between the lead balance weights had taken place.

It was concluded that the structural strength of the blade had not been affected to any significant extent but the erosion shield would not stay attached to the blade under flight conditions following a severe lightning strike.

Further improvements to the lightning strike protection schemes for the composite blades are being investigated in particular the use of a 'one piece lead', leading edge balance weight which is cast integral with a one piece copper tag, giving an area of contact of $\frac{1}{2}$ " span. The remainder of the $2\frac{1}{2}$ " long tag is riveted to the erosion shield which has a tang reduced in length from the original. The protruding section of tag has a 6mm braid (C.S.A. 4.5mm²) held to it by a crimp connector. This braid will be bunched along its 9" span and held to the inner cuff eye tag by another crimp. The braid is restrained along its span with adhesive to the blade. It is expected by these changes to present 3 paths for the strike - shield, lead and the carbon Trailing Edge skins so reducing the amount of current in each component and the one piece lead should assist in reducing damage to the erosion shield as internal arcing will be minimised.

Tooling for casting this lead is being produced and a test blade allocated. It is programmed to undergo full threat lightning strike tests in the near future.

3. DISCUSSION OF THE IMPLICATIONS OF THE RESULTS OF SHIELDING MEASUREMENTS ON A C.F.C. FUSELAGE SECTION

In addition to measurements of the resistance of carbon fibre samples in the laboratory, shielding measurements have been carried out (1) on a mock-up front fuselage section constructed entirely of C.F.C. The results were compared with identical measurements carried out on a similar structure made from aluminium. In order to comment on the implications on the Aerospace industry of these results a brief summary of the results is given.

3.1 A Summary of the Shielding Results

Measurements of magnetic field shielding over the frequency range 1-150 MHz revealed that the C.F.C. fuselage exhibited lower shielding in comparison with the aluminium fuselage below 10 MHz. The largest

difference occurred at the lowest frequency (1 MHz) showing the C.F.C. fuselage to have 20dB less shielding effectiveness than the aluminium fuselage.

Comparison of electric field shielding for the two fuselages indicates very little difference in performance across the band 1 MHz to 10GHz.

These results, although useful as a first indication of any severe differences in performance between aluminium and C.F.C., should be viewed with caution. Shielding Effectiveness can only be quoted quantitatively in absolute terms with reference to an infinite sheet, or more practically, as a finite sheet forming part of the wall of a totally enclosed volume.

Although the C.F.C. structure was essentially totally enclosed and therefore topologically, behaving as an infinite sheet, the fuselage was constructed as a carbon fibre aircraft would be at the present time. There was therefore many slots and holes in the structure. These became resonant apertures at U.H.F. and microwave frequencies and the characteristics of these become the dominant influence on the results at these frequencies. Differences in performance between the aluminium and C.F.C. fuselage in the U.H.F. band and above could be attributed to differences in the apertures between one fuselage and another. Although a great effort was made to ensure the fuselages were identical it is unreasonable to expect no geometrical differences.

Although the fuselages were representative in shape, of a typical aircraft design they did not include any typical bay doors or hatches. It is these which provide the limitation to shielding effectiveness of a complete aircraft. The shielding results obtained therefore are somewhat higher than can be expected in practice.

3.2 The Implications of the Results

Because of the limitations of the measurements as outlined above, the results fall between two ideals. At one extreme, the results are not quantitative, absolute measures of shielding effectiveness, at the other, the fuselage has a better performance than could be expected from a final airframe design.

The results however are useful in confirming (or otherwise!) some initial misgivings about the E.M.C. implications of using a high percentage of C.F.C. in a future aircraft. These can be summarised as follows.

The shielding afforded by a C.F.C. fuselage at V.H.F. and above can be expected to be very similar to that obtained in a metal airframe providing care is taken over the design and bonding of bay doors and removable panels. As an extension to this and reinforced by the results of some antenna measurements carried out at R.A.E., Farnborough (2). The installation and satisfactory operation on a C.F.C. fuselage of antennas at V.H.F. and above is not anticipated to be a serious problem, providing, a careful bonding procedure is followed.

The area for most concern, highlighted by the shielding measurements is the poor shielding effectiveness of C.F.C. at frequencies in the H.F. band and below. Modern strike aircraft with a low altitude capability are required not only to operate, without interference problems, in the near-field of H.F. antenna but also to communicate effectively with a distant ground station. This requirement must be fulfilled by an on-board H.F. transceiver. The installation of such a system on-board a C.F.C. aircraft would create enormous problems with interference with flight safety critical avionics and it is questionable whether an efficient antenna system could be built into such an aircraft. Present systems (i.e. the H.F. notch) rely heavily on excitation of the whole airframe in order to launch an electromagnetic wave. The poor conductivity of C.F.C. would make this approach impossible.

4. D.C. CONDUCTIVITY OF CARBON FIBRE, COMPOSITE SAMPLES

It was decided that the E.M.C. laboratory at British Aerospace, Warton should carry out an investigation into the conductivity of various Carbon Fibre Composite (C.F.C.) samples prepared by the C.F.C. manufacturing facility at BAe, Preston.

The aim of the investigation was to establish the effect on conductivity of the number and orientation of the carbon fibre layers within the samples. This section of the paper describes those measurements and the theory developed which gives good agreement between theoretical and practical results.

4.1 Conduction of Direct Current Through C.F.C.

The form of carbon fibre composite material is such that the conductivity of a given sample is not homogeneous. In the case of a metal sample the conductivity is essentially the same for any direction of current flow through the sample. If conductivity measurements are made on a square sheet of C.F.C. of 'n' layers orientated such that all the fibres are parallel then two different conductivities would be obtained depending on the direction of current flow relative to the direction of the fibres. The situation is summarised in Fig. 4.1.

In this discussion, the analysis will concentrate on the conduction of current in the plane of the fibres although at certain points of the analysis the possibility of current conduction perpendicular to this plane is used.

4.2 Conduction of Current Along the Carbon Fibres

Simply, the 'n' layer sample can be represented by 'n' parallel resistors of equal value, as shown in Fig. 4.2. Although conduction between layers can take place (see later) the potential between layers at adjacent points in this case is negligible therefore, for this mode of conduction current flow between layers can be ignored.

The resistance R_T measured along the fibres of an 'n' layer sample is given by:-

$$R_T = \frac{R_1}{n} \quad (4.2.1)$$

where R_1 is the resistance along the fibres of each layer.

The conductivity is given by:-

$$\sigma = \frac{l}{R_1 A} = \frac{nl}{R_1 A} \quad (4.2.2)$$

where 'l' is the conduction path length and A is the conduction cross-section.

4.3 Conduction of Current Across the Carbon Fibres

This case can be treated in exactly the same way as conduction of current along the fibres, however, for conduction in a direction perpendicular to the fibres, the resistance of each layer R_1' is much greater than the resistance R_1 along the fibres.

$$\therefore \sigma = \frac{nl}{R_1' A} \quad (4.3.1)$$

where $R_1' \gg R_1$

4.4 Conduction of Current at 45° to the Direction of the Carbon Fibres.

For most practical applications in the aerospace industry, sheets of C.F.C. will consist of a number of layers of various orientations. If attention is restricted to combinations of 0° , 90° and $\pm 45^\circ$ orientations this covers the majority of the likely lay-up combinations to be used in the near future. The 0° and 90° orientations can be treated as described in the previous two sections. The $\pm 45^\circ$ orientation requires a more complex treatment.

Consider the case of no fibres connecting directly between sides AB and A'B' as shown in Fig. 4.3. If AB is at potential V_1 and A'B' is at zero potential, the variation of voltage is assumed to be exponential in the plane parallel to the y-axis. The potential variation along a line parallel to the y-axis is as shown in Fig. 4.4. The analysis is fairly lengthy and is described in detail in an internal BAE report (ADN 9006/3). For completeness it will be outlined below.

Using equations for potential gradient across the diagonal a relationship can be formed between current density near the centre of the panel and the potential across the panel.

By integrating the current density along the diagonal, the total current flow through the panel due to the voltage V_1 can be found, hence an expression for the resistance of a single layer of $\pm 45^\circ$ orientated CFC is given by:-

$$R_{45} = K^2 R_1 \quad \text{where; } R_1 = \frac{\rho t}{a} \quad \text{and } K = \frac{\rho t}{a}$$

4.5. Conduction in $\pm 45^\circ$ Orientated Layers

In the manufacture of composite materials, 45° layers are found in $\pm 45^\circ$ pairs. Consequently consider a $\pm 45^\circ$ panel as shown in Fig. 4.5.

The majority of fibres in layer '1', zone A_1 will be at or near potential V_1 . The majority of fibres in layer $i+1$ in zones A_2 and B_2 will be at or near zero potential. The two layers are connected with transverse resistivity ρ over an area $a^2/4$ and mean path length 't'. The resistance of this interlayer connection acts in series with the resistance along the fibres. The conduction path is shown in Fig. 4.6. The resistance of this path acts in parallel with the intrinsic layer resistance R_{45} . The equivalent circuit is shown in Fig. 4.7, analysis of this circuit leads to the following expression for the resistance of a $\pm 45^\circ$ orientated layer pair:-

$$\frac{R_1}{R_T} = 2 \left[\frac{1}{K^2 t} + \frac{1}{2 + \frac{4Kt}{a}} \right]$$

Using values from Table 4 it can be stated that:-

$$R_T = 0.96 R_1$$

In other words the resistance of a square $\pm 45^\circ$ layer pair is similar to the resistance of a single layer of the same dimension.

4.6 Measurement Technique

Square samples, 50 x 50 mm were prepared in four thicknesses of 4, 12, 16 and 24 layers. The lay-up orientations produced for each sample thickness are summarised in Table 4. These orientations were chosen as typical material to be used in a future airframe.

The square samples were prepared as shown in Fig. 4.8. Connection to the sample was made via a "wrap-around" layer of flame-sprayed copper as shown.

The resistance between the prepared ends was measured using a Sullivan Milliohmeter (Type 6666) which uses the four-point measurement technique. The basic principle of the method is to pass current through the sample from one contact to the other whilst measuring the voltage developed across the sample between two contacts coincident with the current source contacts. The system is shown in Fig. 4.9.

Ten samples of each thickness lay-up combination were measured (i.e. 120 separate measurements). The resistance values for the same type of sample were averaged to give average resistance values for each thickness/lay-up combination.

4.7 Treatment of Results

As stated in Sections 4.2 and 4.3, because of the nature of C.F.C. material, conduction through it can be treated as conduction through 'n' parallel resistors where 'n' is the number of layers of carbon fibre.

Ideally the 'n' resistors would all have equal value in a situation where contact to the C.F.C. was made exactly at the end. In practice this was not the case. The end contacts for the C.F.C. samples were as shown in Fig. 4.8.

It can be seen that effectively the resistance of the top and bottom layer is reduced by the flame-sprayed copper strip.

In practice, the total resistance R_T of a sample of 'n' layers all orientated in the same direction is given by

$$\frac{1}{R_T} = \frac{(n-2)}{R_1} + \frac{2}{R_i} \quad (4.7.1)$$

where R_i is the resistance of the top and bottom layer and is related to R_1 by

$$R_i = \frac{4R_1}{5} \quad (\text{from Fig. 4.9}) \quad (4.7.2)$$

This assumes that copper is a short circuit by comparison with C.F.C.

From equation (4.7.1)

$$R_1 = (n + 0.5) R'_T \quad (4.7.3)$$

Therefore the actual conductivity of the square sample becomes

$$\sigma_o = \frac{n}{(n + 0.5)R'_T t} \quad (4.7.4)$$

where 't' is the thickness as shown in Fig. 4.8. and R'_T is the actual resistance measured.

Equation (4.7.4) applies to all square samples in which the layers are all orientated in the same direction (i.e. 'a' type samples as in Table 4).

For samples consisting of n_1 layers whose fibres are orthogonal to the other n_2 layers a different correction factor must be derived.

A sample of the 'b' type (Table 4) with flame sprayed contacts can be represented by

$$\frac{1}{R_T} = \frac{(n_1 - 1)}{R_1} + \frac{5}{4R_1} + \frac{(n_2 - 1)}{R_1} + \frac{5}{4R_1} \quad (4.7.5)$$

where n_1 is the number of layers parallel to current flow.

and n_2 is the number of layers orthogonal to current flow.

From the results it is clear that $R'_1 \gg R_1$

$$\therefore \text{For } n_1 = n_2 \quad \frac{1}{R_T} = \frac{(n_1 + 0.25)}{R_1}$$

$$\text{i.e. } \sigma_{0,90} = \frac{n_1}{(n_1 + 0.25)} \frac{1}{R_T t} \quad (4.7.6)$$

The final type of sample investigated was of the form $0^\circ n_1, 90^\circ n_2, \pm 45^\circ p$, where 'p' was the number of $\pm 45^\circ$ layer pairs.

From Section 4.7 it is clear that a sample of this form can be treated as a parallel combination of n_1 layers conducting along the fibres and 'p' layer pairs conducting as described in Section (4.5).

That is the measured resistance of the sample is given by

$$\frac{1}{R_T} = \frac{3.84n_1 + 4p + 0.96}{3.84R_1} \quad (4.7.7)$$

The theoretical resistance of the sample is given by

$$\frac{1}{R'_T} = \frac{(n_1 + 1.042p)}{R_1}$$

The conductivity of this type of sample can therefore be calculated from the measured value of resistance R_T .

$$\sigma = \frac{3.84 (n_1 + 1.042p)}{(3.84n_1 + 4p + 0.96) R_T t} \quad (4.7.8)$$

4.8 Results and Conclusions

The results of the measurements are given in Table 4. It can be seen that the conductivity for all corresponding sample types is fairly consistent, with maximum scatter (approximately 17%) across the four thicknesses occurring in the unidirectional samples. Poor consistency is displayed by the conductivity results of unidirectional samples in which current is flowing across the fibres. This is thought to be due to variations in the effectiveness of the contact made by the flame-spray in these cases. However enough evidence is given to show that σ_{0}/σ_{90} is at least 1000. This verifies the initial theoretical assumption that for a sample containing $0^\circ, \pm 45^\circ$ and 90° orientated fibres, current conduction through the 90° fibres can be ignored.

The results also verify the theoretical treatment of $\pm 45^\circ$ layer pairs. Consider the 'b' and 'c' resistance measurement (ignoring the correction factor) for each thickness, it can be seen that the pairs of values are very similar. From this observation it can be concluded that a $\pm 45^\circ$ layer pair has a resistance of similar value to a single layer, carrying current along the fibres.

If the results are used to compare the resistance of a sheet of aluminium with a sheet of C.F.C. of N, 0° layers, N, 90° layers and 2N, 45° layers it is found that the C.F.C. has resistance of the order of 1000 times that of an aluminium sample of the same dimensions.

4.9 Earthing in Carbon Fibre Composite Airframes

As a result of the work on D.C. conductivity carried out at BAe, Warton and the conclusions obtained as quoted above in Section 4.8 it was decided that a theoretical study (3) should be carried out to estimate the weight penalty incurred due to extra wiring involved for providing an earth return in a C.F.C. airframe.

It is obvious from the results and conclusions of Section 4.8 that an airframe built exclusively from C.F.C. could not be used as an earth return. If a modern strike aircraft with a multi-role capability is taken as the example on which to base the study it can be shown (1) that the total earth and power cabling in such an aircraft has a weight of approximately 93 Kg. Assuming the maximum power and earth return voltage drop to be tolerated is 2.0V, D.C. and 4.0V, A.C. The increase in the weight of extra cabling for earthing in an airframe constructed from C.F.C. would be of the order of 216Kg. This figure represents an increase in total cable weight of 68%.

If earth return currents were accommodated in aluminium bars running the length of the fuselage, solely for this purpose, the weight increase could be reduced to 25Kg assuming the cross-section of the bars was optimised along the length, for minimum weight.

The weight penalty could be reduced still further if a number of longitudinal structural members of the aircraft were retained in aluminium alloy. These could then be used as the earth returns for the majority of equipment. Their total cross-section would need to be greater than 150 mm^2 in order to carry power earth return currents. Care would have to be taken to minimise earth loops caused by earthing via a small number of discrete paths.

5. CONCLUSIONS

The paper outlines the approach, of two British aircraft manufacturers, to obtaining more knowledge of C.F.C. as a material which may be useful in the manufacture of aircraft in the future.

One approach is to follow a demonstrator programme as highlighted in Sections 1, 2 and 3. This method of acquiring knowledge of C.F.C. is based on using the material in a practical application and learning by experience. Because we are still in the "early days" of learning about C.F.C. it is impossible to use it in a situation which involves flight safety. This limits the demonstrator programme to "mock-ups" placed in laboratory simulated situations or actual aircraft trials which do not degrade the flight safety in the event of failure.

The other approach to acquiring greater knowledge of the basic properties and disadvantages of C.F.C. is by small scale experiments on C.F.C. samples in the laboratory as outlined in Section 4. This approach will eventually yield an in-depth, fundamental understanding of the electrical properties of C.F.C. With this depth of understanding it would be possible to develop theories applicable to practical cases.

Experimental work with small laboratory samples, simplifies the testing of a large number of different lay-ups, surface preparations, bonding techniques etc. however the time taken to obtain results which can be of use in practical cases is significantly longer than timescales allow.

The demonstrator programme gives direct results, however trials of a number of different techniques is expensive and inconvenient.

The approach followed by British Aerospace and Westland Helicopters is a reasonable compromise whereby the results of small scale laboratory experiments have been used where possible in the design of demonstrator items.

From the work described in this paper it can be seen that the major problem still in need of a satisfactory solution, is one of bonding. Once this problem has been solved improvements in H.F. shielding effectiveness would depend solely on the conductivity of the materials included in the lay-up of the C.F.C. i.e. wire meshes or aluminium honeycombs. Satisfactory bonding techniques would also increase the feasibility of the installation of on-board H.F. antennas.

Another problem which has yet to be addressed is that of access panel, edge bonding. As mentioned in paragraph 3.1 a major cause of fuselage shielding degradation is the slots and gaps occurring around the edges of access panels. This problem exists on aluminium alloy aircraft, it is very likely to be significantly worse on a C.F.C. fuselage.

These two problems will be investigated via a combination of laboratory experiments and demonstrator programmes with continued close liaison between the laboratory based research workers and the structural engineers.

REFERENCES

- (1) Carter N. J. and Hobbs R. A., "Some Radio Frequency Shielding Measurements on a Carbon Fibre Composite Front Fuselage Section", Tech Memo, R.A.E. Farnborough August, 1979.
- (2) Baguley G; "The Effects of a C.F.C. Ground Plane on V.H.F. and U.H.F. antennas"; Tech Memo, R.A.E Farnborough, Unpublished at the time of writing.
- (3) Baker R. W.; "Earthing in Carbon Fibre Composite Airframes - Part I"; Report No. MQ 1889, B.Ae Warton, January, 1979.

ACKNOWLEDGEMENTS

The authors wish to thank British Aerospace, Warton and Westland Helicopters, Yeovil for permission and support to publish this paper. In particular the authors are extremely grateful to Mr. I. C. Taig for permission to use the theory he developed as described in paragraph 4.4. & 4.5.

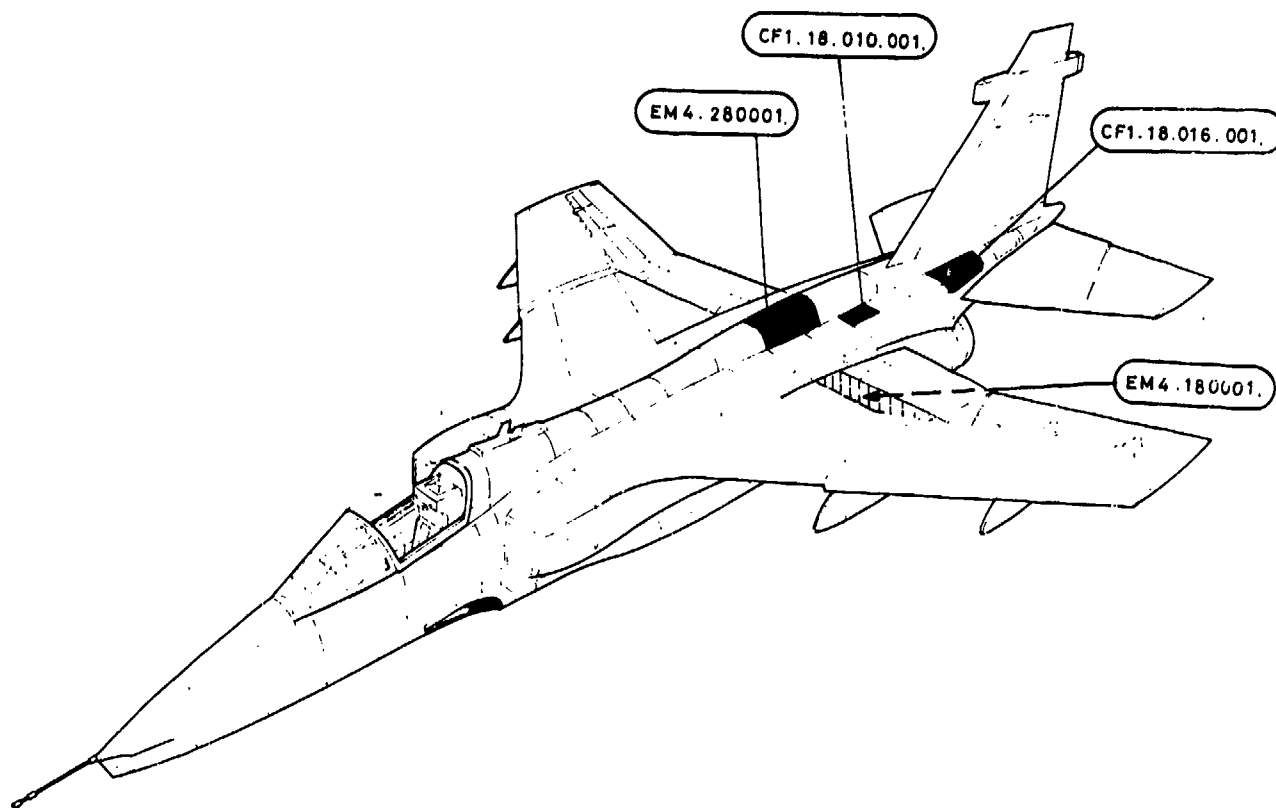


Fig. 1.1 CFC panel arrangement

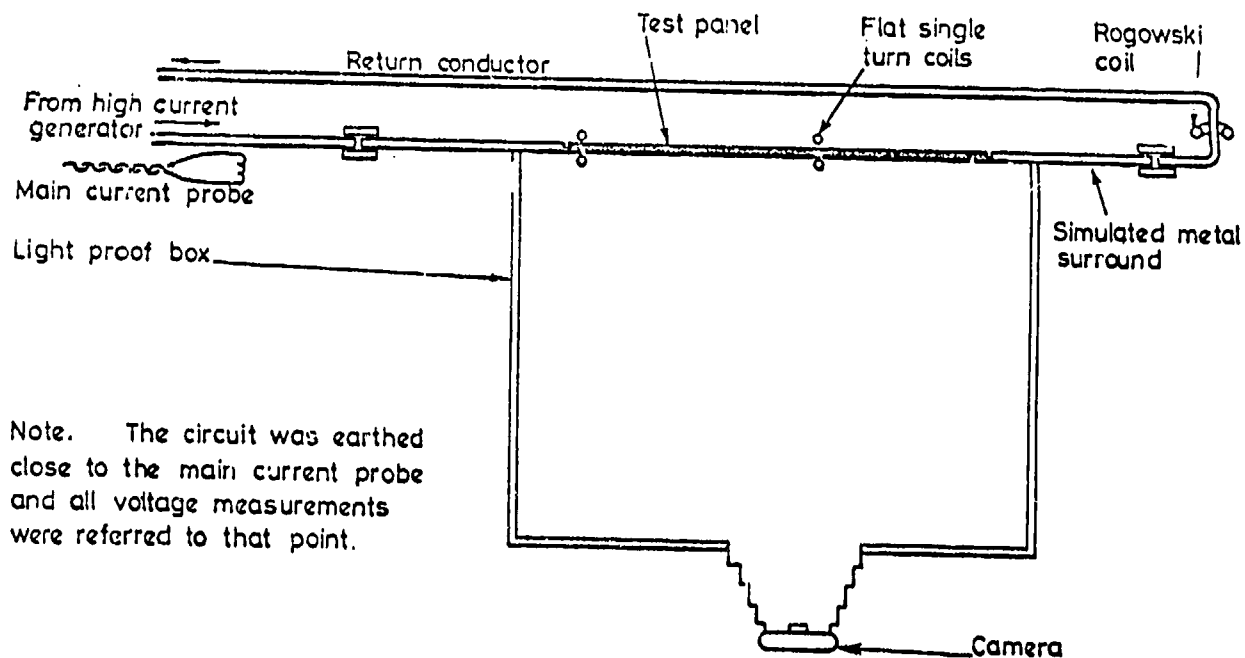


Fig. 1.2 Circuit arrangement for zone 3 tests

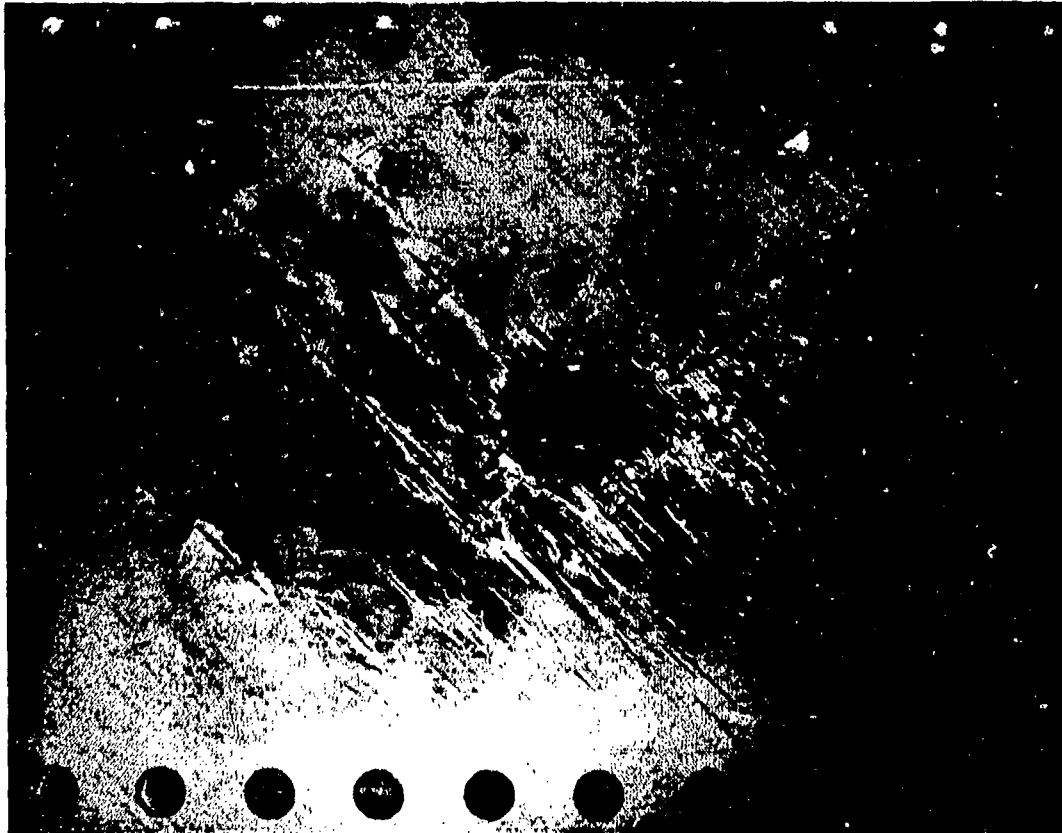


Fig.1.3 Damage to standard CFC panel from zone 2a tests

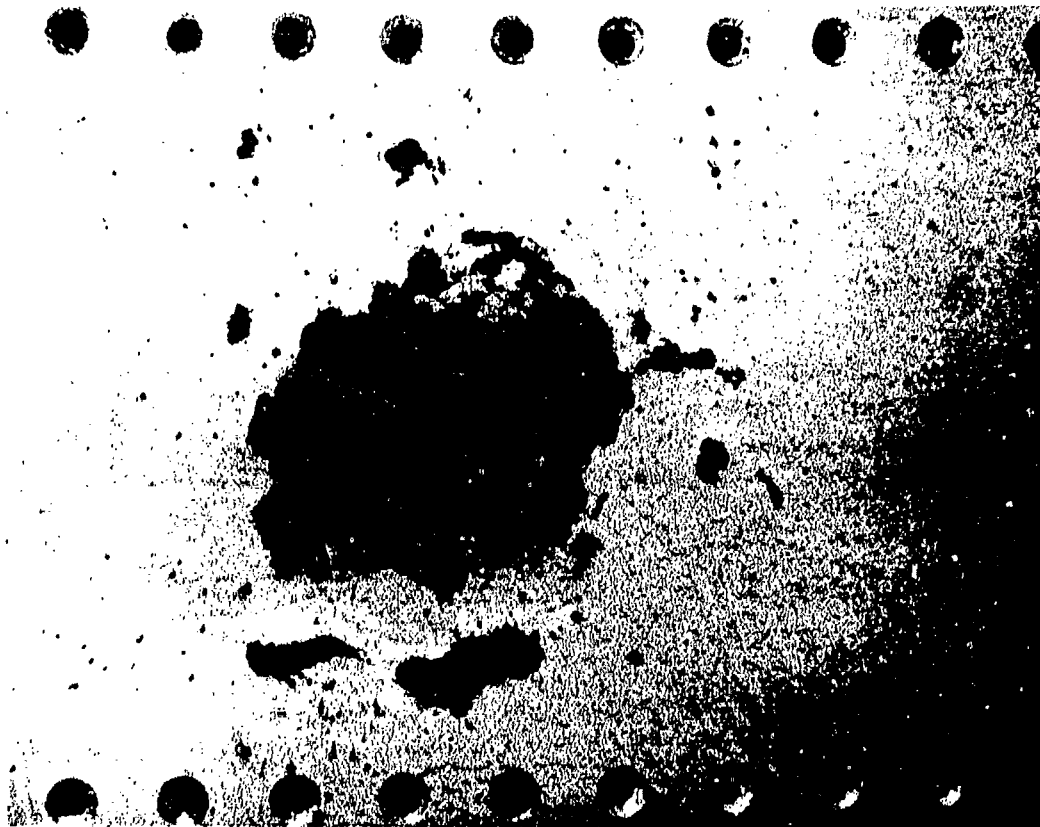


Fig.1.4 Damage to panel with flame-sprayed aluminium protection from zone 2a tests



Fig.1.5 Damage to panel with aluminium foil protection from zone 2a tests



Fig.1.6 Damage to panel with stainless steel mesh protection from zone 2a tests

TABLE I

Severity Levels of Zone 3 Tests

Panel	Peak current kA	Action integral A^2s	Honeycomb Resistance	
			Before	After
Aluminium skins with Aluminium Honeycomb	33	0.74×10^4	-	-
	33	0.74×10^4	-	-
	37	0.96×10^4	-	-
Standard Aluminium production panel	33	0.74×10^4	-	-
	34	0.92×10^4	-	-
	34	0.92×10^4	-	-
Standard proposed CF panel	14	0.15×10^4	1.25	0.63
	11	0.08×10^4	0.63	0.69
	18	0.28×10^4	0.69	0.65
	31	No Record	0.65	0.65
	41	1.71×10^4	0.65	0.59
Culham CFRP	22	-	-	-
	35	1.2×10^4	-	-
	35	1.0×10^4	-	-
	36	1.1×10^4	-	-
	33	0.8×10^4	-	-
	33	0.4×10^4	-	-
Insulating Panel SRBP	22	-	-	-

Note. There was very little change in the honeycomb resistance after the initial discharge. In previous work this pattern has been observed where very small currents have flowed in the honeycomb. Examination by sectioning and/or mechanical testing of samples showing this type of resistance change has always revealed minor change only to the honeycomb nodes, the level of which has always been too low to afford performance, or be detectable by non-destructive testings.

TABLE 2

Table of Zone 2a Test Current Parameters and
Damage Sustained

Panel	Component D		Component B		Damage
	Peak current kA	Action Integral A^2s	Peak current kA	Coulombs C	
Standard Proposed CFRP	100	1×10^5	2.7	40	15 mm diameter hole in top skin. Erosion of a few honeycomb cells. Small number of broken fibres over 120 mm diameter area. No damage to back skin.
CFRP with flame sprayed Aluminium	100	1.2×10^5	2.8	39	Erosion of aluminium over 100 mm diameter area. Slight scorching of top skin. No other observed damage.
CFRP with Alu- minium foil.	100	1.1×10^5	2.7	40	Erosion of aluminium foil over 40 mm diameter area. Damage to foil where it formed overlap joints. Slight scorching of CF skin. No other damage.
CFRP with Stainless steel mesh	100	1.1×10^5	2.7	34	Patches of eroded mesh, largest 30 mm diameter. Minor damage to CFRP in one area. No damage to back of panel.
Aluminium with Honey- comb.	110	1.3×10^5	2.7	39	Puncture of top skin in two places (2 mm diameter holes). tracks over surface.

X - RESULTS TAKEN FROM PREVIOUS EMC CHECKS
O - CARBON FIBRE PANEL CHECKS ON AIRCRAFT

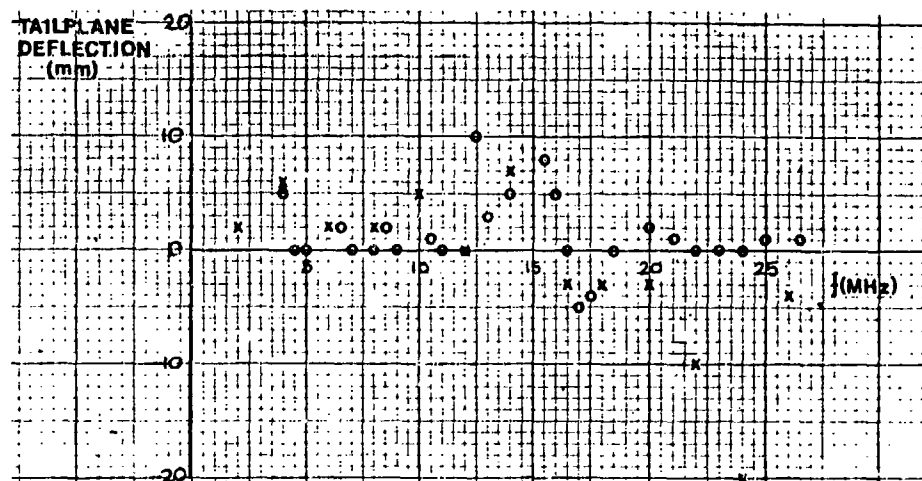


Fig. 1.7 Comparison of test results

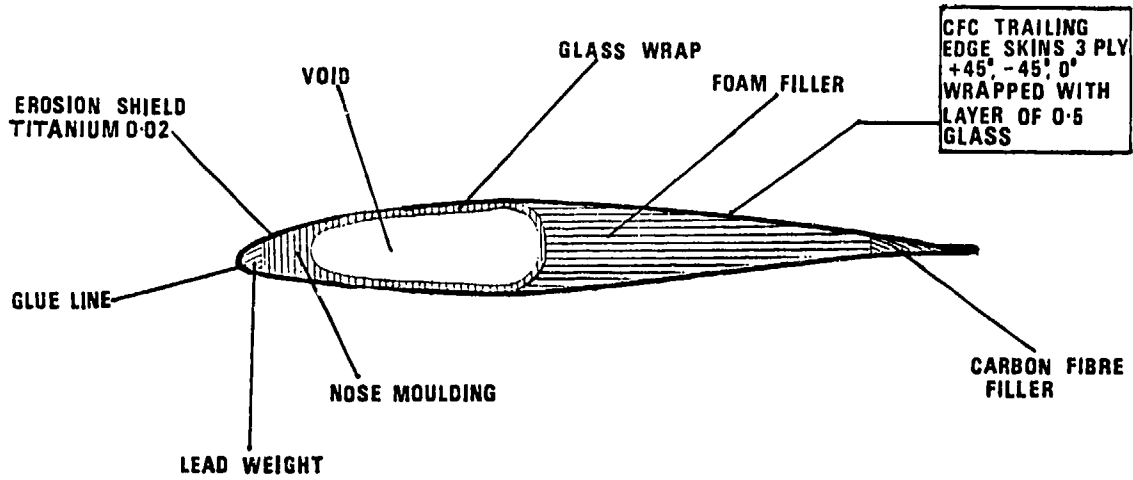


Fig.2.1 Composite tail rotor blade

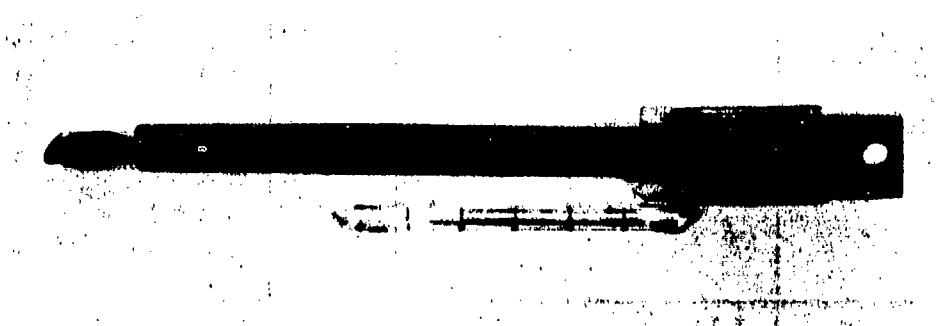


Fig.2.2 Connection between erosion strip and rotor boss – straight connection



Fig.2.3 Connection between erosion strip and rotor boss – angled connection

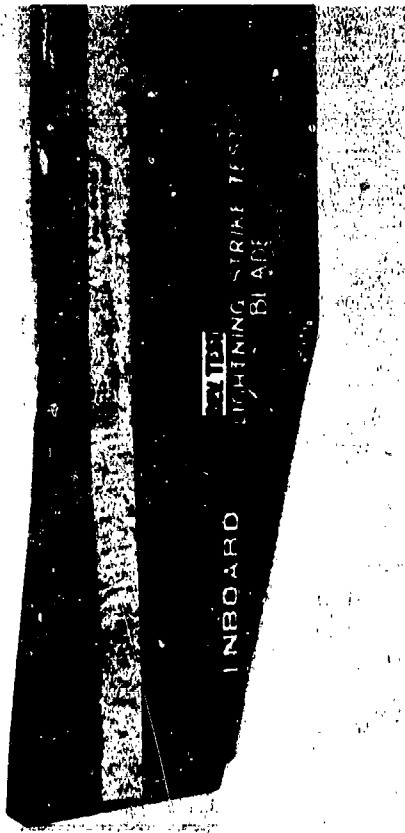


Fig.2.5 Inboard root-end

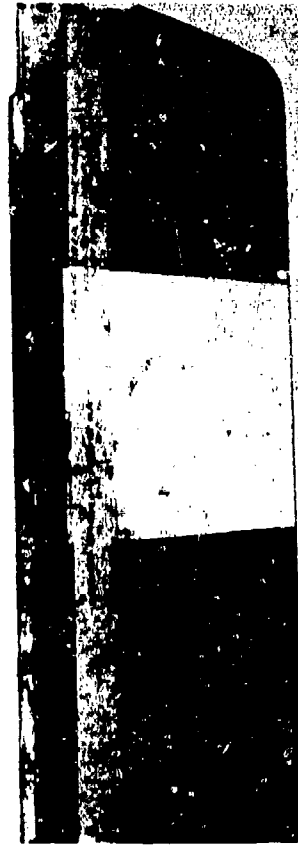


Fig.2.7 Inboard tip-end

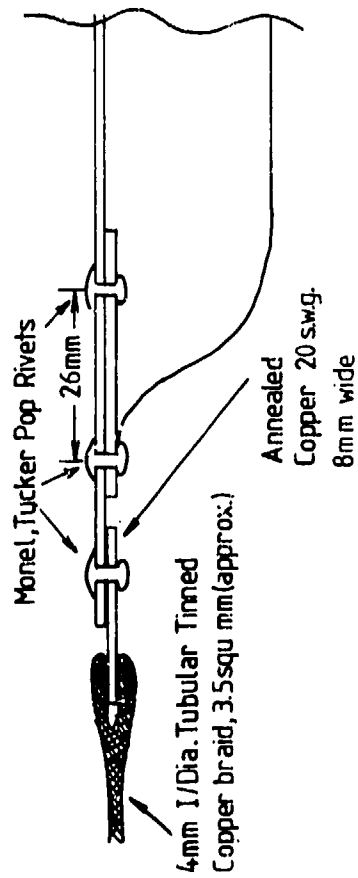


Fig.2.4 Section through leading edge showing proposed connection



Fig.2.6 Inboard centre



Fig.2.9 Outboard centre



Fig.2.11 Root-end of the erosion shield

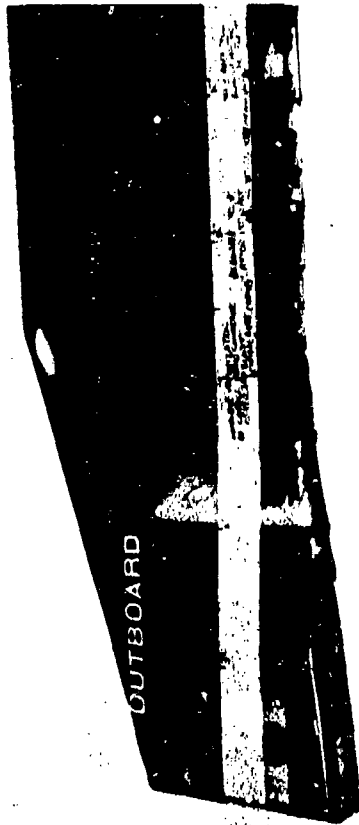


Fig.2.8 Outboard root-end



Fig.2.10 Outboard tip-end

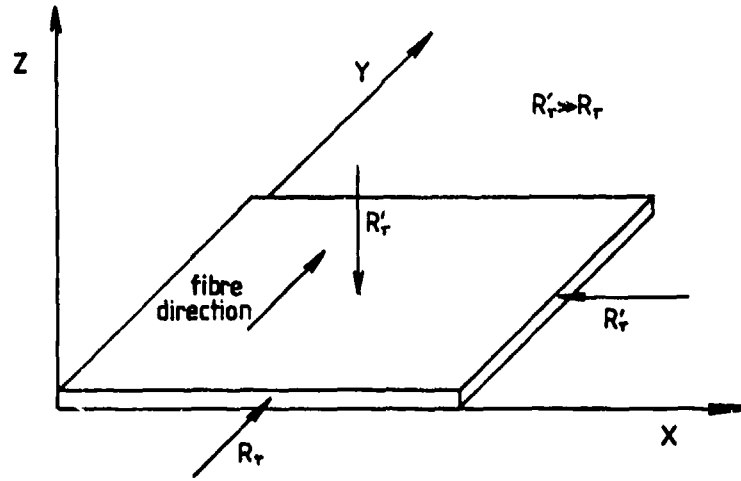


Fig.4.1 Non-homogeneous conductivity

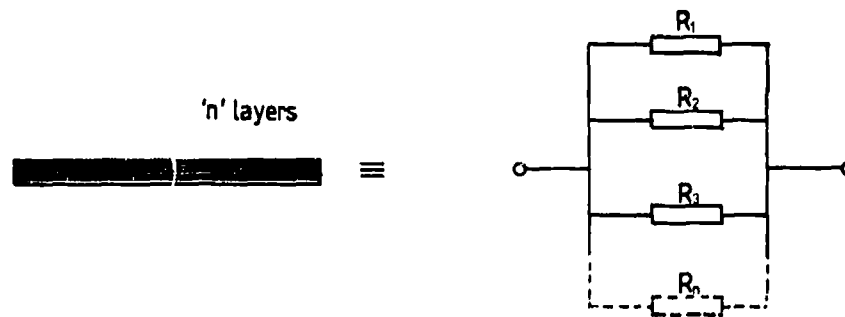


Fig.4.2 Equivalent circuit of a CFC sample

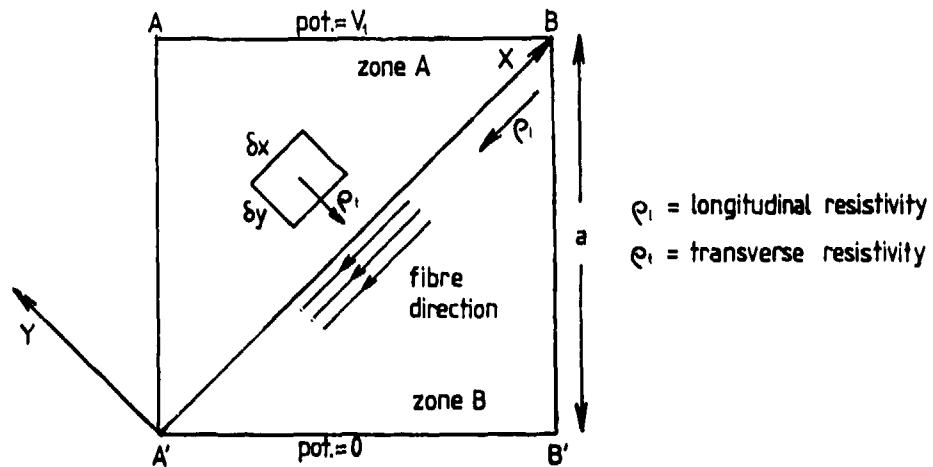


Fig.4.3 A 45° square sample of thickness 't'

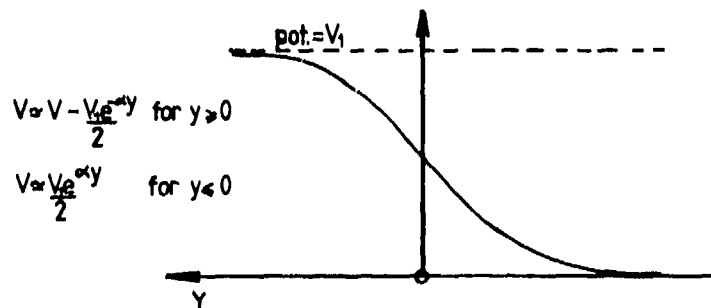


Fig.4.4 Potential gradient from A to B'

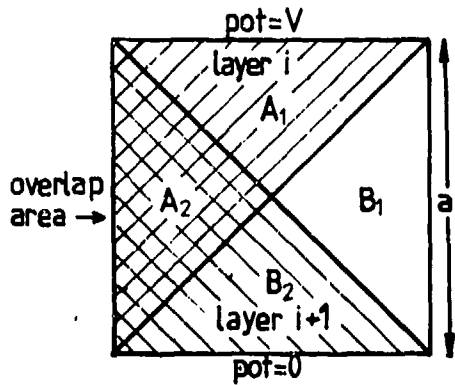


Figure 4.5

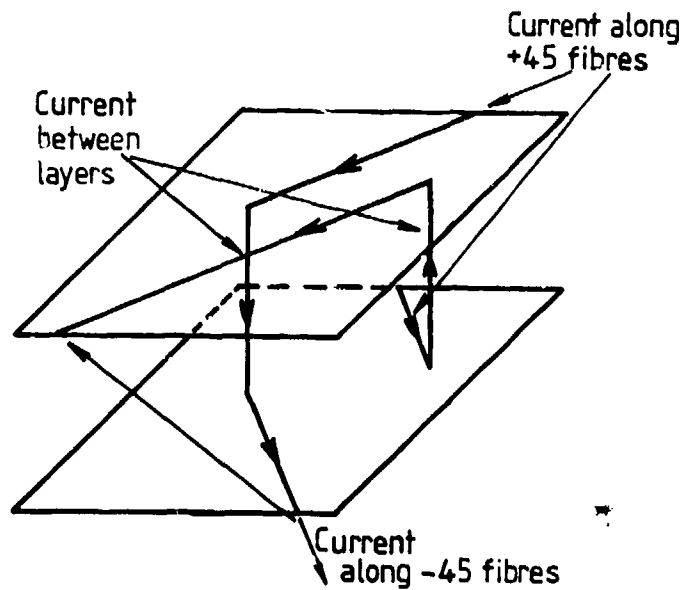


Fig.4.6 Current conduction between $\pm 45^\circ$ layer pairs

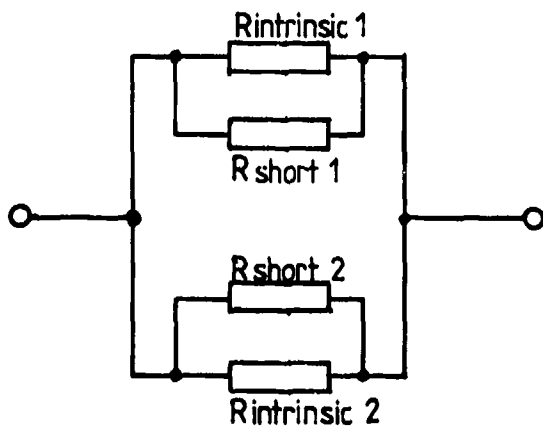


Fig.4.8 A typical test sample

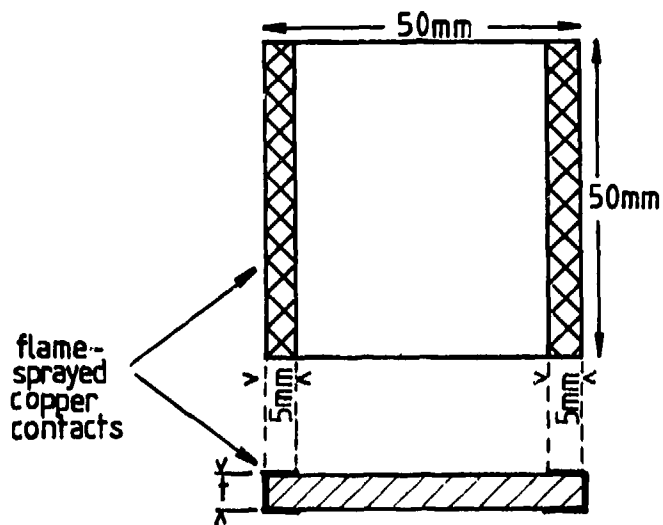


Fig.4.7 Equivalent circuit of a $\pm 45^\circ$ layer pair

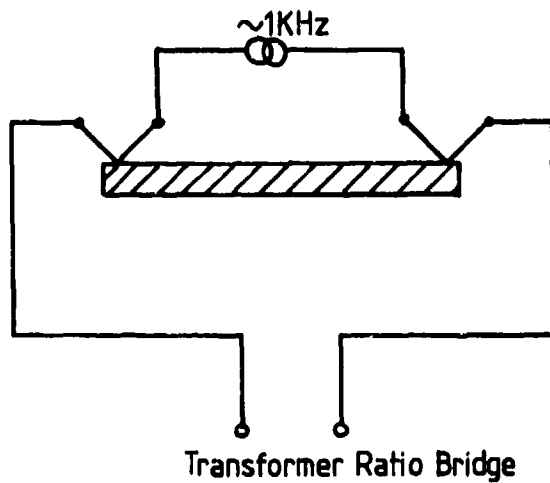


Fig.4.9 Resistance measurement technique

CONDUCTIVITY MODIFICATION OF BORON FIBERS

Richard Y. Kwor and Carlos Alberto Paz de Araujo
Department of Electrical Engineering, University of Notre Dame
Notre Dame, IN 46556

SUMMARY

Boron fibers have high specific strength and specific modulus, and are widely used in advanced composite materials. Its weakness lies in the low d.c. conductivity. Two possible ways of increasing the fiber conductivity to alleviate electromagnetic effects are investigated. The first is the doping of boron fiber using high temperature carbon diffusion. It is found that if the temperature is kept low enough not to deteriorate the mechanical properties of the fiber ($< 850^{\circ}\text{C}$) then there is no conductivity enhancement even after 24 hours of heat treatment. The second method is to electro-plate the boron fibers with Ni. Plated near room temperature, the Ni forms a thin sheath around the boron fiber which retains its superior mechanical properties. The electrical property of the plated fiber is characterized and the effect of high temperature (up to 1100°C) on the Ni-B system is investigated using a scanning electron microscope.

1. INTRODUCTION

Boron fibers have been widely used in Advanced Composite Materials (ACM). These materials consist of oriented layers of fibers embedded in an epoxy matrix. Because of the high tensile strength and high Young's modulus of boron fibers, boron-ACMs have begun to be used as structural and surface components of modern aircraft. The density of boron fibers further enhances its attractiveness for aerospace applications. A measure of the true potential of a material for aerospace applications comes from the values of its specific strength and its specific modulus (the strength and modulus divided by the density). The mechanical properties of boron fibers are unexcelled in the combination of the two quantities described above. Compared with graphite, another common fiber used in composite materials, boron does not have the potential hazardous environmental problem caused by flying fiber fragments.

Boron has a very small d.c. conductivity at room temperature. Immediate questions arise concerning the shielding effectiveness against electromagnetic interference and electromagnetic pulse effects. Further, because of its low conductivity, boron composites cannot withstand a lightning strike without damage. A solution to the problem of lightning susceptibility and shielding is necessary if the composite material is to achieve its full potential in aerospace applications.

Boron is a classical semiconductor and doping techniques could be used to enhance its conductivity. Carbon is a known dopant which when in relatively large quantity can significantly increase the conductivity of boron. This paper describes the attempt to dope boron fiber with carbon at temperatures up to 900°C . Problems associated with the process and the reason for its failure will be assessed.

The second approach of increasing the conductivity of the composite material is to cover the fiber with a conductive coating. Among several candidate metals, nickel (Ni) is the most attractive. It forms a strong bond with the boron fiber and makes an excellent electrical contact. If the Ni coating is thin, there will be no mass density increase problem. Furthermore, Ni is ferromagnetic. Its high permeability can improve the shielding effectiveness of the composite material. The Ni coating technique using electroplating and the conductivity measurement of the Ni-clad boron fibers will be presented here, along with a study of the temperature effect on the Ni-B system.

All the boron fiber specimens employed for this work were supplied by AVCO Systems Division with a nominal diameter of 8 mil ($203\mu\text{m}$). These fibers were chemically vapor deposited by hydrogen reduction of boron trichloride on a resistively heated tungsten wire substrate of approximately $20\mu\text{m}$ in diameter. We hereby refer to these fibers as B-W fibers.

2. EXPERIMENTS ON CARBON DIFFUSION IN BORON FIBERS

2.1 General Background

Early alloying experiments showed that carbon dissolves rapidly in molten boron. (HAGENLOCHER, A., 1959, 1960) With 3% of carbon, the conductivity of boron increases by two orders of magnitude at room temperature. In other investigations, appreciable carbon diffusion into boron at 2035°C (still below the melting point of boron) was observed. (GEIST, D., 1965) Carbon diffusion at a much lower temperature range has also been reported. (STERN, D. R. and LYND, L., 1958) In experiments of hydrogen reduction of BCl_3 on heated graphite fibers, the surface temperature of the fiber was only in the range of 1030°C - 1125°C , yet the carbon concentration in the deposited boron reached as high as 4%. These results were encouraging for the prospect of doping boron fiber with carbon to increase its conductivity. However, due to the special properties of the B-W fiber, experiments of carbon diffusion in the boron fibers must be limited within the temperature range where the mechanical properties of the fiber are not degraded by heat treatment. Such a degradation for B-W fibers is well known and reported by several

researchers. (GILLESPIE, J. S., 1966; WAWNER, F. E., 1967; THORNTON, H. R., 1968) The B-W fibers have an "amorphous" or glassy structure described in several literatures (LAUBENGAYER, A. W. et al, 1943; TALLEY, C. P. et al, 1960; GILLESPIE, J. S., 1966; WAWNER, F. E., 1967; LINDQUIST, P. F. et al 1968). It was suggested that the fiber structure is not genuinely amorphous. Instead, it is a structure composed of microcrystals (20Å - 30Å) distributed throughout the microcrystalline matrix. The identifications of these microcrystals vary. Both α - and β - rhombohedral modifications of boron have been suggested. (HOARD, J. L. and HUGHES, R. E., 1967; OTTE, H. M. and LIPSITT, H. A., 1975) Submicron-size inclusions of well-crystallized α - and β - rhombohedral boron, distributed throughout the microcrystalline matrix, indicate the tendency of the boron to establish greater long-range order. Because of this unique structure of the fiber, some transformation takes place at elevated temperatures. The critical temperature for the transformation lies somewhere between 600°C and 980°C, depending on the ambient atmosphere and the surface condition of the fiber. And the nature and rate of transformation depend on the ambient, heat treatment duration, temperature and surface condition of the fiber. The surface of the B-W fiber transforms to the macrocrystalline structures at or above the critical temperature, thus weakening its mechanical properties. At or above 1300°C the transformation is predominantly β - rhombohedral. (DICARLO, J. A., 1975) The surface crystals formed between the critical degradation temperature and 1300°C has not been completely identified.

Fiber degradation was observed in our diffusion experiments. The critical temperature was near 900°C at pressures slightly below 10^{-5} torr. The SEM micrograph (Fig. 1a) shows the macrocrystalline structure on the degraded boron fibers. The picture of an untreated fiber is shown in Fig. 1b for comparison. A series of experiments were done to investigate possible carbon diffusion below the fiber degradation temperature. They will be described in detail in Section 2.3.

2.2 Method of Conductivity Measurement

Various contacting methods have been used in the electrical measurement of boron: platinum contacts, (DIETZ, W. and HERRMANN, H., 1965) fused platinum, (GREINER, E. W. and GUTOWSKI, J. A., 1957) tungsten tip, (SHAW, W. C. et al, 1957) fused silver, (NEFT, W. and SEILER, K., 1965) and alloyed gold (GEIST, D., 1965). In our experiments, a simple and reliable way was used--electroplated Ni. Electroplated nickel adheres strongly to the surface of the boron fiber and provides an excellent ohmic contact to the fiber. Besides being simple and easy, the process makes it possible to control the geometry of the contact area. This is important in the calculation of the fiber conductivity. The plating technique and bath composition will be described briefly in a later section of this paper. Detail information on the plating can be found in the reference. (ARAUJO, C., 1979) To find the conductivity of the fiber sample, Ni sheath of 1 cm length was plated on both ends of the fiber. The tungsten core of the fiber is much more conductive than the boron. In order to relate the measured conductance to the conductivity of boron the core was isolated from the nickel plating by covering the fiber tips with Apiezon-W wax, as shown in Fig. 2a. As described elsewhere (GAJDA, W., KWOR, R., and ARAUJO, C., 1979) the conductivity of boron is given by:

$$\sigma = \left(\frac{I}{V}\right) \left[\frac{\ln(R/a)}{\pi L}\right]$$

where V is the applied voltage, I is the measured current, L is the length of the sheath, R is the radius of the fiber and a is the radius of the tungsten core. (Fig. 2) The conductivity of sample fibers were found before and after diffusion experiment to see if there was any improvement.

2.3 Experiments

The sample fibers in our experiments were purchased from AVCO Corp. and the fiber diameter is 8 mils (203 μ m). All the sample fibers were cut into a length of 7 cm which we found to be a convenient length to work with. A critical factor for repeatable reliable measurements of conductivity, especially in the electroplating technique, is a clean boron surface. The sample fibers were first subjected to a routine organic solvent cleaning cycle in an ultrasonic cleaner: Trichloroethylene, acetone, methanol and de-ionized (DI) water. They were then dipped in hot concentrated sulfuric acid for 5 min. (90° - 100°C). This hot surfuric bath removes surface oxides and contaminations (ELLIS, R., 1960). After a thorough rinse in DI water, these fibers were then blown dry with pure nitrogen. Several control fibers were then plated with Ni and their conductances were measured. The remaining fibers were divided into three groups. The fibers in Group I were covered with a suspension of pure powdered graphite in DI water and those from Group II were coated with PELCO's #1603-15 colloidal graphite (aqueous base) solution, Group III were just of plain clean fibers. After those coated fibers had been dried under an infrared heat source, they were loaded individually into the quartz tube in a furnace. The tube was then evacuated to 10^{-5} torr prior to heat treatment. Temperatures ranging from 800°C to 1000°C were used. Three heating periods were chosen: 6 hours, 12 hours and 24 hours. The residual carbon on the heat treated samples was subsequently cleaned in an ultrasonic bath and the fibers were Ni-plated for conductivity measurement.

2.4 Discussion of Results

All the 1000°C treated fibers and some of the 950°C treated ones showed severe surface degradation. These fibers became very fragile and difficult to handle. Little

degradation was found on samples heat treated at 900°C. However, there was no clear indication of any increase in conductivity for graphite coated samples from both Group I or Group II. Measured resistances for these fibers varied from 1000 Ω to 2000 Ω , compared with the 800 Ω for the Group III Control samples. (The maximum variation of the resistance for the control samples was less than 8%.) The data did not show any consistent difference between the first two groups. We believe that carbon diffusion in boron fibers was not appreciable at this temperature range. We arrived at this conclusion partly because of the results from our experiments, partly because of the lack of other research results contradictory to ours. In comparison, Hagenlocker's and Geist's experiments were done at a much higher temperature and the high carbon diffusion rate can easily be explained. On the other hand, the carbon movement into boron in Stern and Lynds' experiment might not be due to simple diffusion since chemical reactions were involved. (However, the results did suggest a possibility of improving the conductivity of the boron fiber by modifying the chemical vapor deposition growth process for the fiber.) Our experiments showed that at temperature range below the critical degradation point, whatever amount of carbon which has diffused into the boron fiber does not enhance its conductivity. We do not see the solid state diffusion of carbon as a practical means to improve the conductivity of boron fibers.

3. CONDUCTIVITY ENHANCEMENT OF BORON FIBERS USING NI PLATING TECHNIQUE

3.1 Ni-B System

It is possible to increase the conductance of the boron fiber by electroplating them with a thin coat of some metal. There are many metals commonly used for contacts, but most of them, including Cu, In, Pb and Sn do not alloy or form compounds with B easily. Several of them do not even wet the boron surface. (HANSEN, P. M., 1958; ELLIOT, R. P., 1965; and SHUNK, F. A., 1969) Noble metals such as Ag, Au and Pt make good contacts when fused to boron (NEFT, W., 1965; GEIST, D., 1965; GREINER, E. W., 1957) but they are too expensive for fiber applications. Nickel, on the other hand, is one of few metals which alloy and form compounds easily with boron. There are five known B-Ni compounds: B_2Ni , BNi , B_3Ni_4 , BNi_2 and BNi_3 , (MOFFATT, W. G., 1977) and among all the binary systems of B, the B-Ni system has one of the lowest eutectic points (900°C, about 81 atom % of Ni). Meanwhile, as already mentioned before, it is quite easy to introduce Ni onto boron fibers using electroplating technique. The process is simple, economical and reliable. The Ni electroplating techniques are well developed. The aspects of research immediately related to the fiber applications are then two-fold: to investigate the property of Ni contact on boron fiber and to find the temperature effect on the Ni-B system. The latter is necessary because of the lack of information available in the temperature range below the critical degradation temperature of the boron fiber.

3.2 The Ni Plating Experiments

The plating solution used in the experiments was a modified Watts Bath. The main constituents of a basic Watts Bath are nickel chloride, nickel sulfate and boric acid. (METAL FINISHING, 1979) Some additional reagents were added for optimal result. Detail description of the bath and its preparation technique can be found in the reference. (ARAUJO, C., 1979) Temperature, agitation, PH level, anti-pitting reagents and anode-cathode current density were carefully controlled. By setting the bath temperature at 60°C + 2°C, the PH at 4.5 and plating current density at 500A/M² at the cathode (fiber), best results were obtained. As briefly mentioned in Section 2.3, the surface of the fiber must be free from contamination. Boron oxide on the surface causes uneven plating, therefore, must be removed with hot concentrated H₂SO₄ prior to plating. Due to the high resistivity of the boron fiber, the section of the boron fiber being plated had to be limited to 5 cm or shorter for uniform plating. For the Ni-B contact characterization, 1 cm. of Ni sheath ($\sqrt{12}$ μ m thick) was plated on each end of the boron fiber (with the end covered with Apiezon-W wax to isolate the tungsten core). The resistance measurements showed that the plated Ni provided excellent ohmic contacts to the fiber. There were no non-linear effects sometimes found in other metal contacts. The resistance of the 7 cm boron fiber with 1 cm. of plated-Ni as contact at each end is found to be 800 Ω (+8% variation for different samples). When the entire length of the fiber is coated with 4 μ m thick of Ni (W core not contacted), these fibers exhibit a resistance of 4 Ω .

3.3 Temperature Effects on Ni-covered Boron Fiber

Heat treatment produces various changes on boron fibers. In order to eliminate the effect of oxidation, the experiment was done in vacuum (approx. 10⁻⁵ torr). The Ni-covered samples were heated in an evacuated quartz tube to various temperatures ranging from 550°C to 1100°C for 6 hours. Figure 3 shows the furnace and the vacuum system.

The heat treated samples were analyzed using a scanning electron microscope. In addition, the resistances of these fibers were measured and compared.

3.4 Experimental Results

3.4.a Heat Treatment at 558°C

Fibers exposed to temperatures in this range show no apparent change of surface characteristics. The "corn cob" or nodular aspect of the surface is clearly visible in Fig. 4. There is some evidence of nickel sheath "peeling" away from the fiber at some

locations. This is believed to be due to the difference in the coefficients of thermal expansion of Ni and B. Underneath the Ni film, some B movement into Ni is seen. The interaction of Ni and B at this temperature produces compounds at the interface. The contact resistance was found to have increased. (Please refer to Table 1, the Summary of Electrical Measurement Data.)

3.4.b Heat Treatment at 678°C

Fig. 5 shows four identifiable regions on the heat-treated Ni-clad boron fiber. In Region A the Ni sheath has moved away from the fiber as a result of the difference in thermal expansion. There is no Ni-B interaction and the Ni sheath appears to retain the original qualities of the plated Ni -- smooth and without crystallites. Region C is where the Ni and B have been in direct contact, some nickel borides form and crystals are seen throughout the entire thickness of the Ni sheath. Under higher magnification, these crystals are clearly visible (Fig. 6). Region B is the boundary between A and C. Here the nickel-rich crystals have a different form as those in Region C (Fig. 7 and 8). Region D (Fig. 9) reveals the interface region between Ni and B, similar to that shown in Fig. 4. Significant increase in the conductances of these fibers occurs. The measured average value of conductance is 2.1×10^{-3} mho, an increase of 40% over the conductance of untreated fibers.

3.4.c Heat Treatment at 738°C

In this experiment, thinner Ni sheath ($\sim 6 \mu\text{m}$) was plated. Fig. 10 shows that whenever in contact with B, this thin sheath is completely converted to nickel-boron compounds. There is a mass transfer of B which has been in contact with the Ni. Nodules are still evident where the Ni sheath has been peeled off early before any reaction can occur. These Ni-B compounds have increased the fiber conductance significantly. (Table 1)

3.4.d Heat Treatment at 804°C

We now return to the thicker nickel sheath ($\sim 12 \mu\text{m}$ for 6 min. plating). The higher temperature brings about more expansion of Ni relative to B, and thus the dramatic result shown in Fig. 11. Fig. 12 shows a higher magnification of Region B of Fig. 11. Large crystallites are visible along with some unreacted Ni sheath. The average conductance of these samples is 3.88×10^{-3} mhos.

3.4.e Heat Treatment at 914°C

At temperatures above 900°C, surface crystal formation of the boron fiber becomes evident. The deterioration of the mechanical properties of the fiber is immediate. The samples become brittle and easily shattered (Fig. 13 and 14). The nickel sheath, on the other hand, has turned into nickel borides as shown in Fig. 15.

3.4.f Heat Treatment at 1011°C and 1112°C

At 1011°C, large crystals appear throughout the boron fiber and on the Ni sheath. Severe differential mass transfer of B underneath the Ni sheath is evident in Fig. 16. The same picture also shows an interesting result: there is no crystal seen in the cross sections broken after the heat treatment. On the other hand, Fig. 17 shows an end of a fiber treated at 1112°C. There are many crystals formed on the cross section exposed during heat treatment. This clearly indicates that the boron fiber transformation from "amorphous" to crystalline states is a surface phenomenon. In this temperature range, the surface degradation is very severe and cracks sometimes develop in the Ni sheath (Fig. 18 and 19). Because of the fragility of these samples, electrical conductivity data are not available.

4. CONCLUSION

It has been shown in this work that the simple and obvious doping technique using carbon diffusion cannot be used to increase the conductivity of B-W fibers. The main limitation is the deterioration of mechanical properties due to the surface degradation of the fibers. At 10^{-5} torr, this degradation temperature was shown to be near 900°C. No appreciable carbon diffusion occurs at this temperature after 24 hours of heat treatment. Since it is known that carbon diffusion occurs near 1100°C in the hydrogen reduction of BCl_3 on graphite fibers (STERN, D. R. and LYND, L., 1958), two approaches can be made in the future research of fiber conductivity modification using carbon. The first is to use inert gas atmosphere instead of vacuum for the ambient of heated fibers. It was reported (DICARLO, J. A., 1976 and GILLESPIE, J. S., 1966) that Ar environment offered a desired result of no surface crystal formation up to 1100°C (one hour treatment). It is worthwhile to perform some experiment to see if conductivity enhancement can be obtained at 1100°C in inert gas environment such as Ar, He, N_2 or even H_2 . The second approach is more basic in nature. In the early investigation of pure boron crystal growth, carbon was found to be one of the common impurities. The chief source of contamination had been the gas reagents such as BCl_3 and BBr_3 . If the introduction of carbon into B fiber is the main purpose, then it is conceivable that some carbon impurity can be deliberately added into the source gas and in the subsequent fiber growth the carbon can be incorporated into the boron fiber in a controlled manner. Research in this direction should be

very fruitful.

The study of Ni-clad boron fibers revealed that Ni makes excellent contact with boron. Nickel borides with higher conductivity than pure boron begin to form between 500°C and 600°C. The Ni-plated B-W fiber is seen to have high conductivity. With approximately 4 μm thick of Ni, the conductance of 7 cm. length of the 8 mil fiber increases by a factor of 200. While this increase is largely due to the Ni sheath itself rather than the boron fiber, it can be argued that since the plated Ni forms a strong bond to the fiber, it can be considered as a part of the fiber. Because the plating technique is a simple addition to the existing fiber manufacturing process, this method may prove to be very attractive. The fiber leaving the growth furnace can be fed via an In-Ga eutectic or a mercury contact into a plating bath near-by. The plating is done as the fiber is continuously moving through the solution. Such a system should be quite cost effective and easy to operate. The Ni-clad boron fiber can be a worthy alternative candidate for advanced composite materials.

ACKNOWLEDGEMENTS

This work has been supported by the Air Force Office for Scientific Research (AFOSR). The authors would like to express their sincere gratitude. Thanks are also due to W. J. Gajda, Jr. for his fruitful and enlightening discussions.

REFERENCES

- ARAUJO, C., 1979, Master Thesis, University of Notre Dame, Notre Dame, IN.
- BEHRENDT, D. R., 1976, "Longitudinal Residual Stresses In Boron Fibers", presented at the Symposium on Composite Materials Testing and Design--Fourth Conference, Valley Forge, PA.
- DICARLO, J. A., 1975, "Anelastic Deformation of Boron Fibers", presented at American Physical Society Meeting, Denver, CO.
- DICARLO, J. A., 1977, "Techniques for Increasing Boron Fiber Fracture Strain", presented at the 106th Annual Meeting of the American Institute of Mining, Metallurgical and Petroleum Engineers, Atlanta, GA.
- DICARLO, J. A., 1978, "Mechanical and Physical Properties of Modern Boron Fibers", presented at the Second International Conference on Composite Materials, Toronto, Canada.
- DIETZ, W. and HERRMAN, H., "Conductivity, Hall Effect, Optical Absorption, and Band Gap of Very Pure Boron", in Gaule, G. K. (ed.): Boron Volume 2, Preparation Properties and Applications, Plenum Press, pp. 107-118.
- ELLIOTT, R. P., 1965, "Constitution of Binary Alloys, First Supplement", McGraw-Hill Book Company, New York, NY.
- ELLIS, R., 1960, "Some Etching Studies on Boron", in Kohn, J. A., Nye, W. F. and Gaule, G. K. (eds): Boron-Synthesis, Structure and Properties, Plenum Press, pp. 135-139.
- GAJDA, W. J., JR., KWOR, R., and ARAUJO, C., 1979, "Low Frequency Electrical Conductivity of Boron Fibers", submitted to J. Appl. Phys.
- GEIST, D., 1965, "Electron Paramagnetic Resonance, Electrical Conductivity and Impurity Diffusion in Doped Boron", in Gaule, G. K. (ed.): Boron Volume 2, Preparation, Properties and Applications, Plenum Press, pp. 203-214.
- GILLESPIE, J. S., JR., 1966, "Crystallization of Massive Amorphous Boron", J. Am. Chem. Soc. Vol. 88, pp. 2423-2425.
- GREINER, E. S. and GUTOWSKI, J. A., 1957, "Electrical Resistivity of Boron", J. Appl. Phys. 28, pp. 1364-1365.
- HAGENLOCHER, A., 1958, "Halbleitereigenschaften von Bor", doctoral dissertation, Technische Hochschule, Stuttgart.
- HAGENLOCHER, A., 1960, "Semiconductor Properties of Boron", in Kohn, J. A., Nye, W. F. and Gaule, G. K. (eds): Boron-Synthesis, Structures, and Properties, Plenum Press, pp. 128-134.
- HANSEN, M., 1958, "Constitution of Binary Alloys", McGraw-Hill Book Company, New York, NY.
- HOARD, J. L. and NEWKIRK, A. E., 1960, "An Analysis of Polymorphism in Boron Based upon X-ray Diffraction Results", J. Am. Chem. Soc., Vol. 82, pp. 70-76.
- HOARD, J. L. and HUGHES, R. E., 1967, "Elemental Boron and Compounds of High Boron Content: Structure, Properties and Polymorphism", in the Chemistry of Boron and its Compounds, Muettterties, E. L. (ed.), John-Wiley and Sons, New York.
- LAUBENGAYER, A. W., HURD, I. T., NEWKIRK, A. E., and HOARD, J. L., 1943, "Boron I. Preparation and Properties of Pure Crystalline Boron", J. Am. Chem. Soc. Vol. 65, pp. 1924-1931.

LINDQUIST, P. F., HAMMOND, M. S. and BRAGG, R. H., 1968, "Crystal Structure of Vapor-Deposited Boron Filaments", J. Appl. Phys. 39, pp. 5152-5162.

Metal Finishing, 1979, Metals and Plastics Publications, Inc., Hackensack, NJ.

MOFFATT, W. G., 1977, "Binary Phase Diagrams Handbook", General Electric Company, Schenectady, NY.

NEFT, W., and SEILER, K., 1965, "Semiconductor Properties of Boron", in Gaule, G. K. (ed.): Boron Volume 2. Preparation, Properties, and Applications, Plenum Press, pp. 143-167.

OTTE, H. M. and LIPSITT, H. A., 1966, "On the Interpretation of Electron Diffraction Patterns from 'Amorphous' Boron", Phys. Stat. Sol., Vol. 13, pp. 439-448.

OTTE, H. M. LIPSITT, H. A., LINDQUIST, P. F., HAMMOND, M. L., BRAGG, R. H., 1967, "Further Comments on the Paper "On the Interpretation of Electron Diffraction Patterns from 'Amorphous' Boron"", Phys. Stat. Sol., Vol. 19, K99.

SHUNK, F. A., 1969, "Constitution of Binary Alloys, Second Supplement", McGraw-Hill Book Company, New York, NY.

SMITH, R. J., 1976, "Changes in Boron Fiber Strength Due to Surface Removal by Chemical Etching", NASA Technical Report TN D-8219.

STERN, D. R. and LYND, L., 1958, "High-Purity Crystalline Boron", J. Electrochem. Soc. 105, 676.

TALLEY, C. P., LINE, L. E., JR. and OVERMAN, Q. D., JR., 1960, "Preparation and Properties of Massive Amorphous Elemental Boron", in Kohn, J. A., Nye, W. F. and Gaule, G. K. (eds.): Boron-Synthesis, Structure and Properties, Plenum Press, pp. 94-104.

THORNTON, H. R., 1968, "Fabrication of Metal Matrix Composite Materials:", J. Comp. Materials, Vol. 2, pp. 32-42.

WAWNER, F. E., JR., 1967, "Boron Filaments:", in Broutman and Krock (eds.): Modern Composite Materials, Addison-Wesley, pp. 244-269.

Table 1. Conductances of Heat-treated Boron Fibers. (with Ni sheath at each end.)

Temperature (°C)	time of heat treatment(hrs)	G(mhos)
as grown	--	1.25×10^{-3}
558°	6	6.896×10^{-4}
678°	6	2.100×10^{-3}
738°(*)	6	5.88×10^{-3}
804°	6	3.508×10^{-3}
914°	6	6.536×10^{-3}

(*) Different thickness of nickel was plated (6µm). All other samples have a thickness of 12µm.

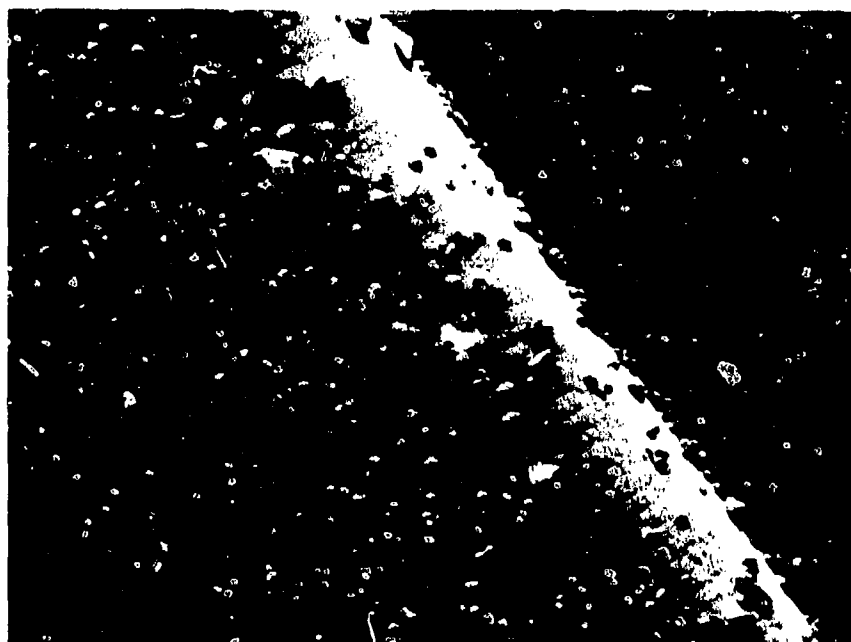


Fig. 1(a) Macrocrystalline structure of degraded fiber after 6 hours of 900°C treatment. (200X, 3° angle)

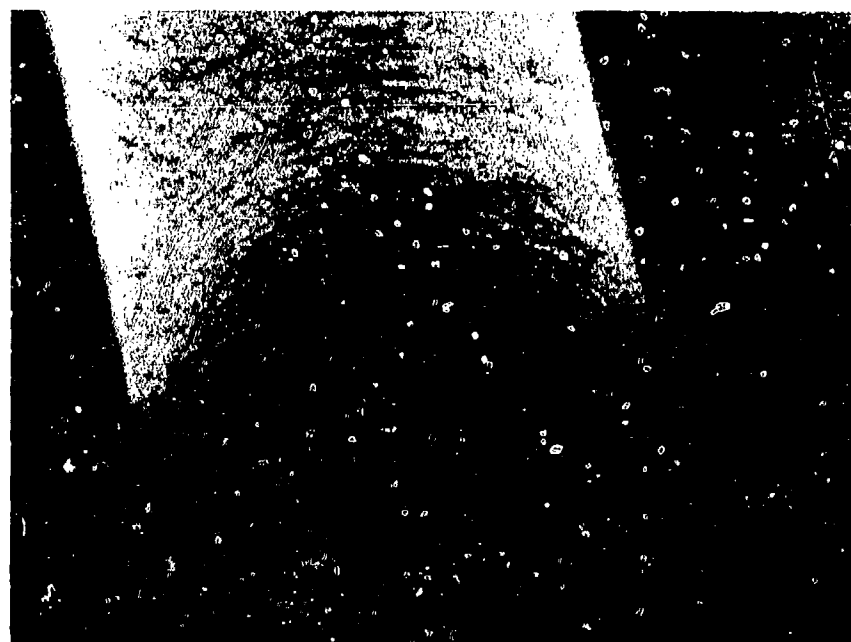


Fig. 1(b) Untreated "as grown" fiber. (200X)

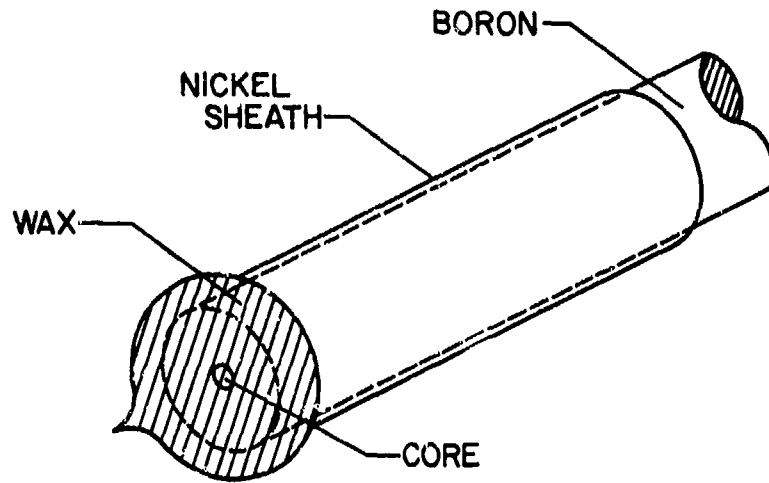


Fig. 2(a) Isolation of the Tungsten-boride Core.

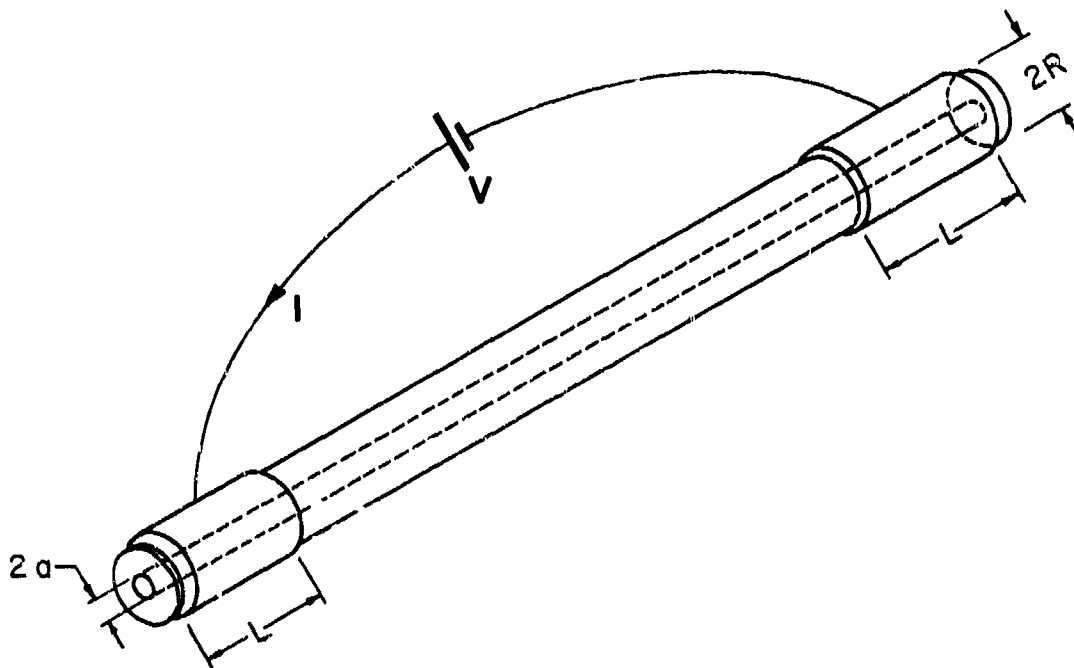


Fig. 2(b) Geometry of Contacts.

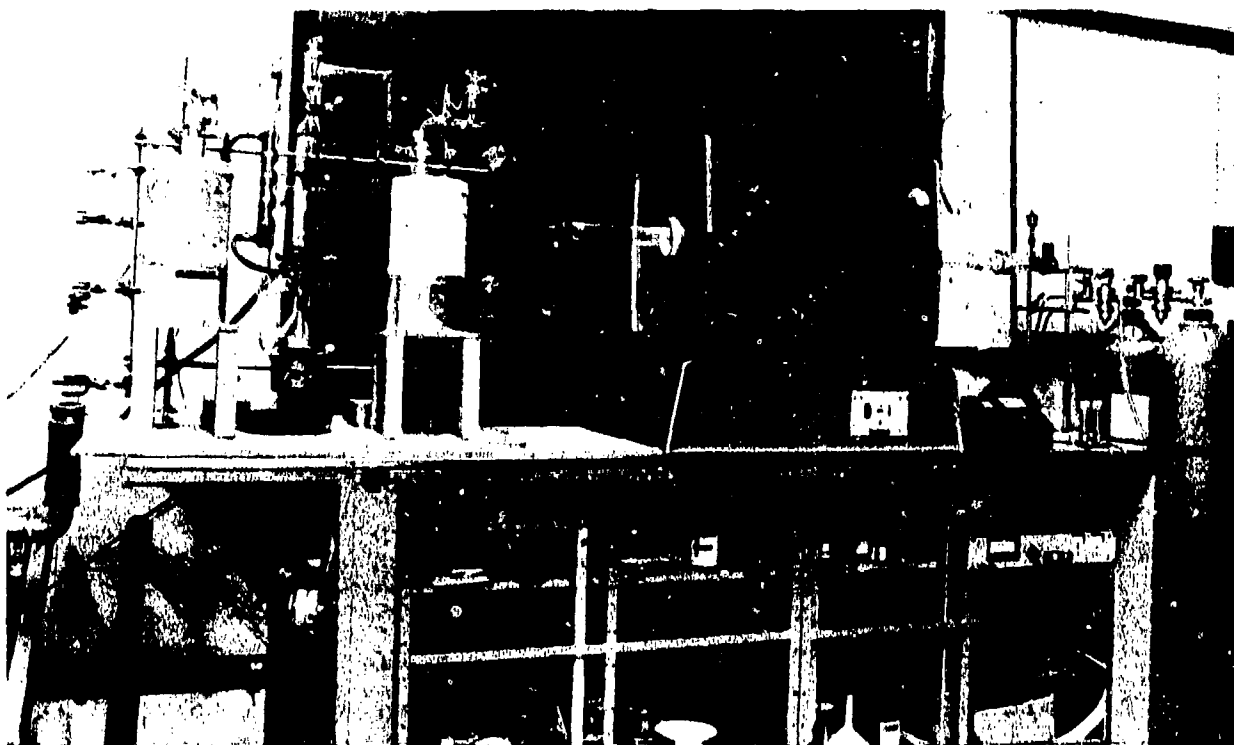


Fig. 3 The furnace and Vacuum System for Fiber Diffusion.



Fig. 4 Section of Ni-Clad boron fiber heated at 558°C for 6 hours. (500X, 57° angle)

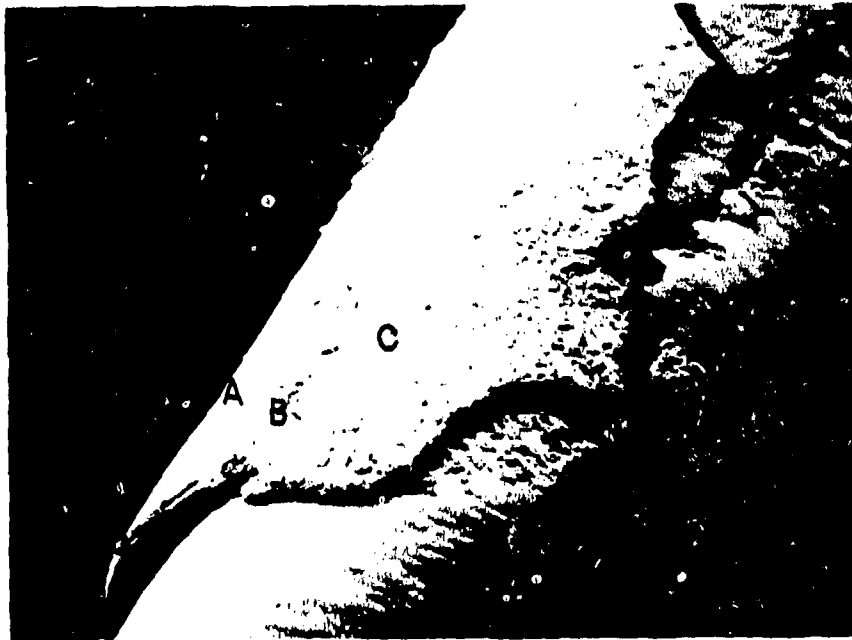


Fig. 5 Section of Ni-clad boron fiber heated to 678°C for 6 hours. Region A shows the Ni sheath retaining its surface characteristics. Region C shows places where the nickel is in contact with the fiber. Region B is the boundary of A and C. Region D shows the interface between Ni and B. (200X, 65° angle)

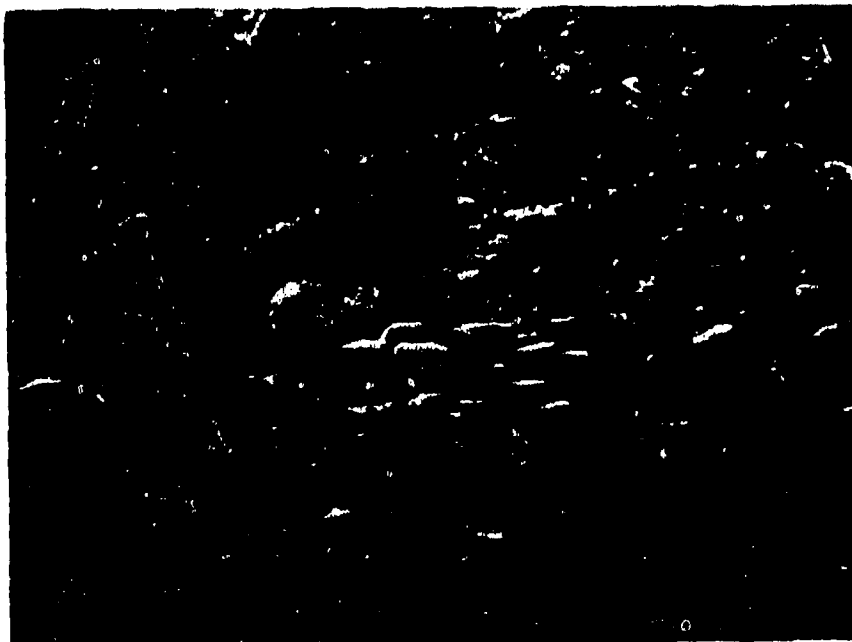


Fig. 6 Region C of Fig. 5 showing crystallites of nickel-boron compounds. (2000X, 65° angle)

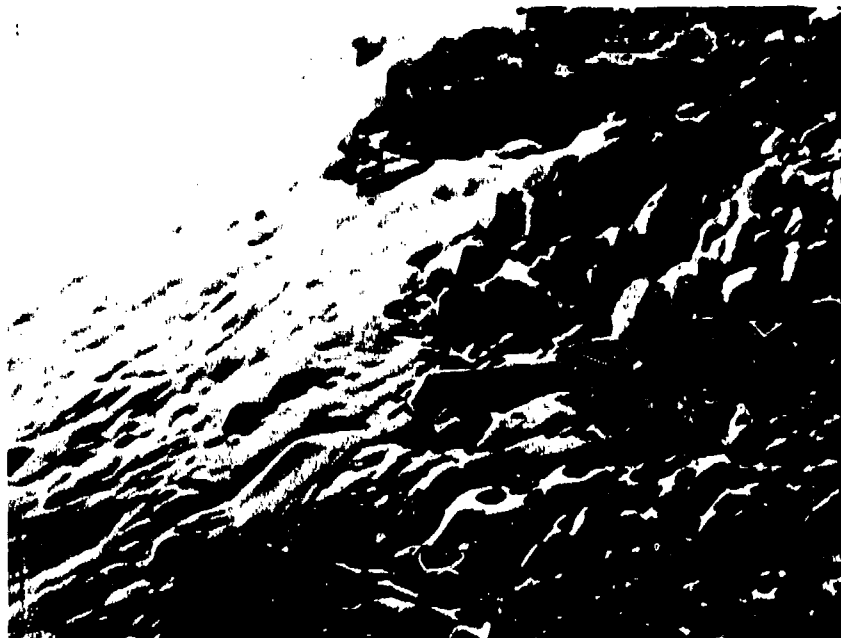


Fig. 7 Region B of Fig. 5 showing large nickel rich nickel-boride crystals. (2000X, 65° angle)



Fig. 8 Same crystals shown in Fig. 7 at higher magnification. (5000X, 65° angle)

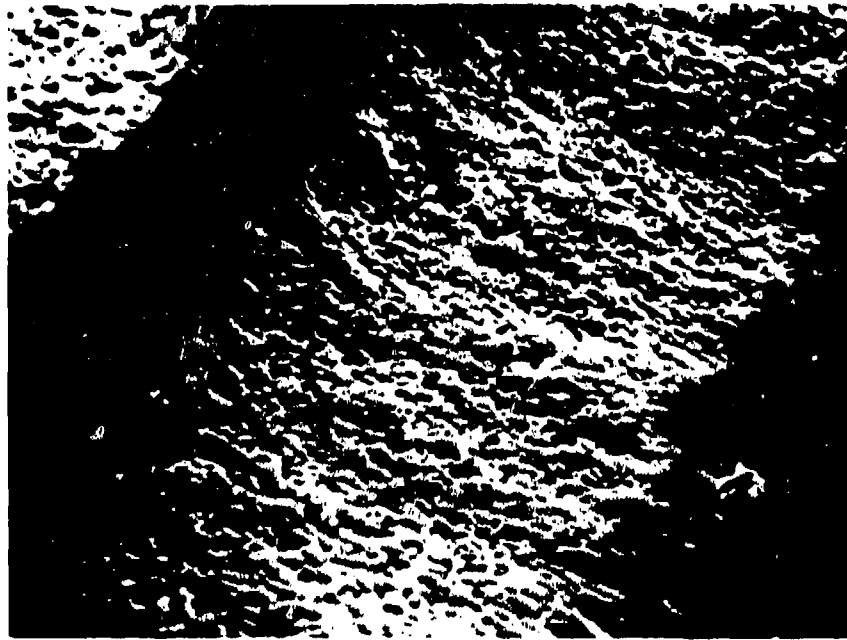


Fig. 9 Region D of Fig. 5 at 2000X, 65° angle.

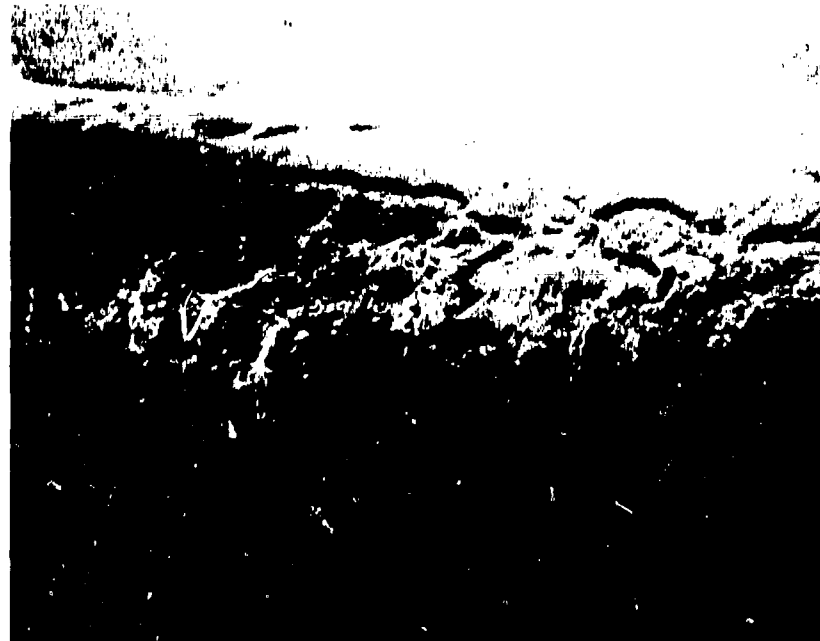


Fig. 10 Ni-clad fiber heated to 738°C, showing complete conversion of the thin (6 micron) nickel sheath. (200X, 68° angle)



Fig. 11 Ni-clad boron fiber heated to 804°C. (100X, 11° angle)

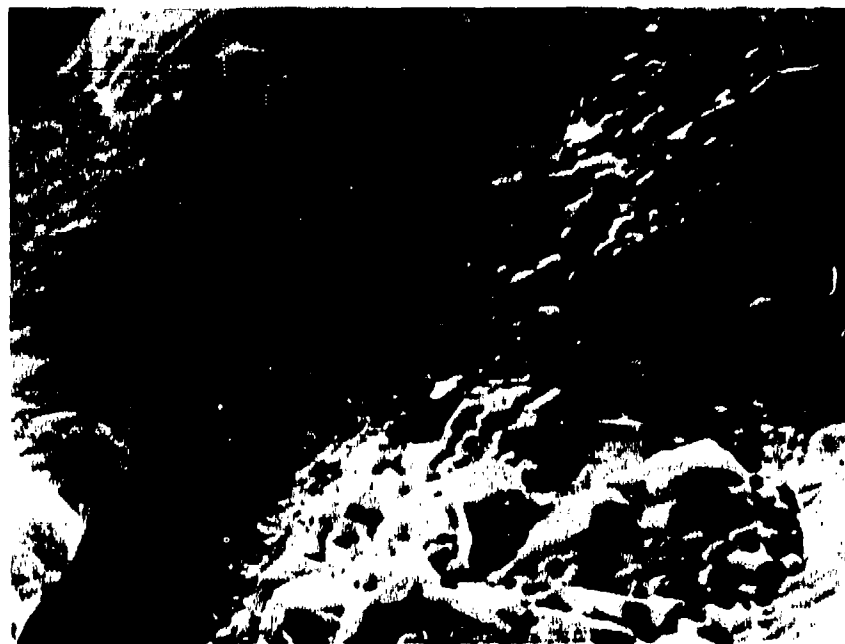


Fig. 12 Higher magnification of Region B of Fig. 11. (1000X, 11° angle)

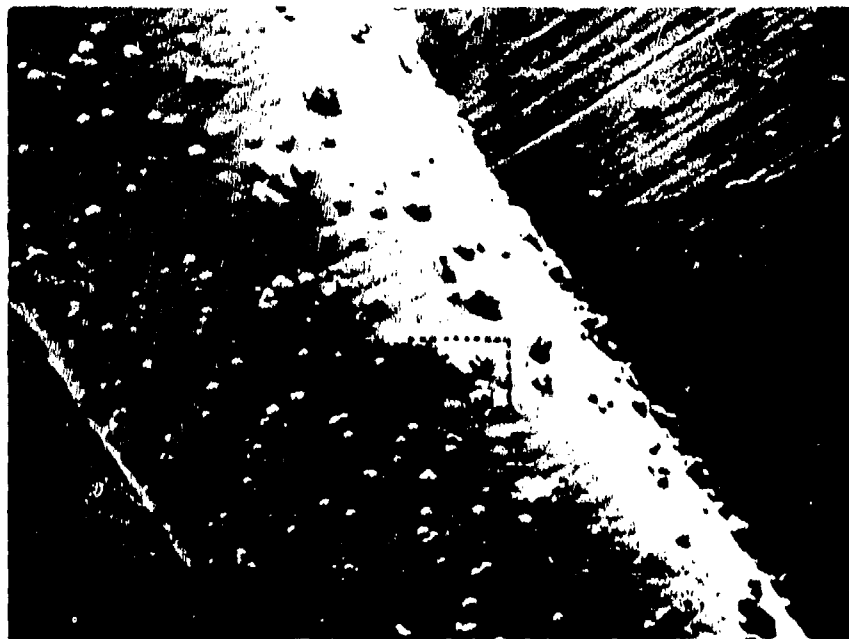


Fig. 13 At 900°C, some crystallites appear on the surface of the boron fiber. (200X, 3° angle)

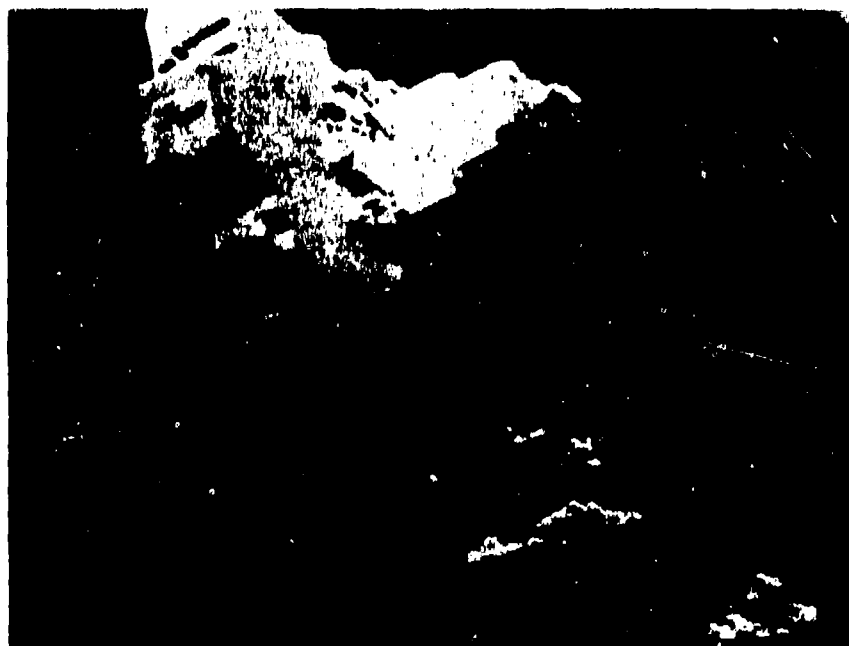


Fig. 14 Region A of Fig. 13 at 2000X, 3° angle.



Fig. 15 Ni sheath heated to 914°C. (2000X, 67° angle)

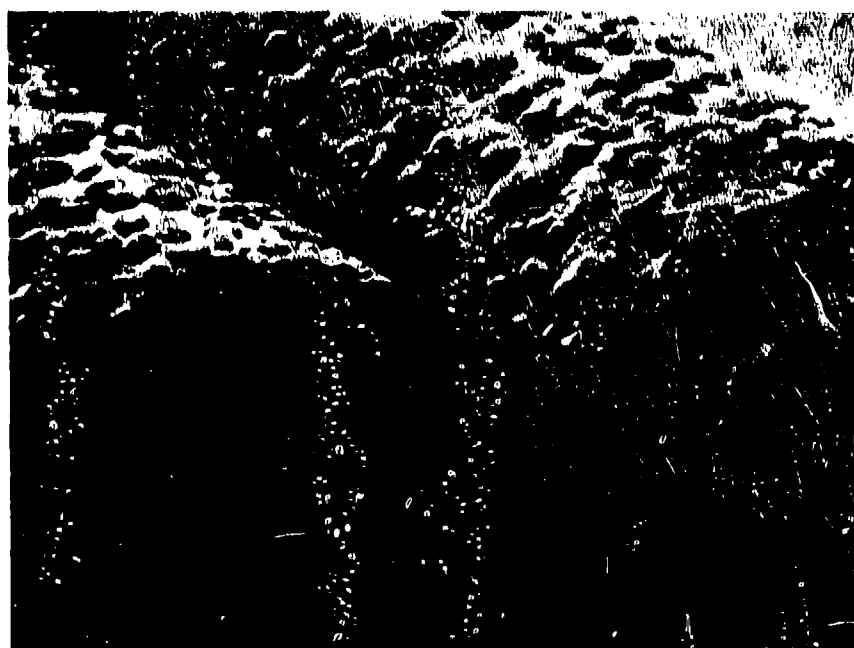


Fig. 16 Sections of Ni-clad boron fiber broken after having been heat treated at 1011°C. (200X)



Fig. 17 Boron recrystallization on the cross-section heated to 1112°C.
(200X, 75° angle)

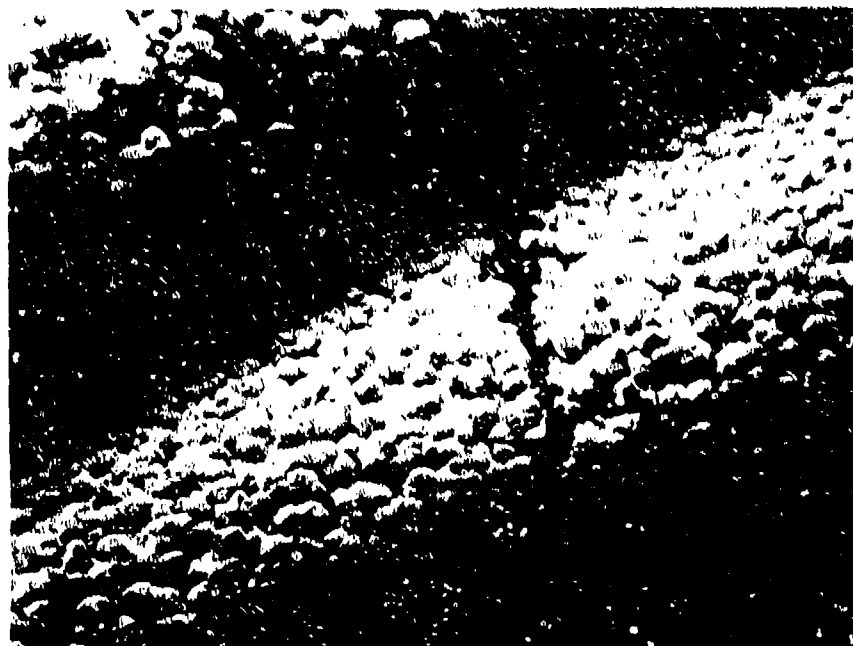


Fig. 18 Cracks in the nickel-boron sheath heated 1112°C. (200X, 41° angle)



Fig. 19 Higher magnification of Fig. 18 along the crack. (2000X, 41° angle)

TENSION INDUITE DANS LES CABLES A L'INTERIEUR
DE STRUCTURES FERMEES METALLIQUES ET EN CARBONE
EPOXY SOUMISES A UNE IMPULSION DE COURANT TYPE Foudre

par
Denis GALL
CENTRE D'ESSAIS AERONAUTIQUE DE TOULOUSE
23, avenue Henri Guillaumet
31 056 - TOULOUSE CEDEX
France

RESUME

Ce document présente les résultats d'études théoriques et expérimentales sur le mécanisme d'induction des surtensions dans les câbles électriques situés à l'intérieur de structures fermées, lorsque celles-ci sont parcourues par une impulsion de courant type foudre. La contribution des deux paramètres, diffusion du courant de peau et champ magnétique interne, est mise en évidence et comparée pour deux types de structure : alliage d'aluminium et fibre de carbone.

1 - INTRODUCTION

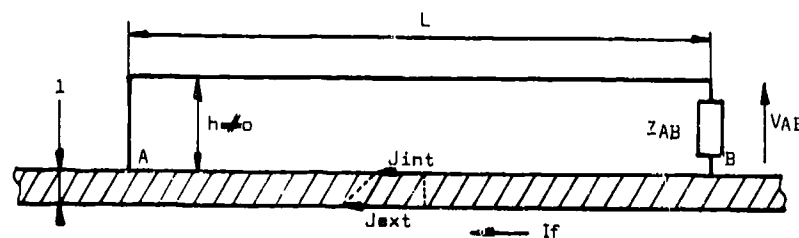
Lorsqu'un avion est foudroyé en vol, l'impulsion de courant électrique qui le parcourt circule généralement par son revêtement extérieur. Ce revêtement, constitué, jusqu'à ces dernières années d'alliages légers, bons conducteurs électriques, assure, outre, les fonctions aérodynamique et mécanique, la référence électrique de l'aéronef. On comprend dès lors, que le passage d'une impulsion de courant dans la structure est susceptible de perturber ou de modifier le fonctionnement des équipements électriques et électroniques de bord, l'importance et la forme de ces transitoires dépendant étroitement des caractéristiques électriques de la peau structurale.

L'étude présentée dans le document aborde, après un rappel sur les phénomènes de tension induite dans les câblages électriques, les problèmes nouveaux introduits par l'utilisation des fibres de carbone; ces problèmes sont mis en évidence en comparant les résultats obtenus sur une structure en alliage léger de 2 mm d'épaisseur et une structure en fibre de carbone de même épaisseur.

2 - TENSION INDUITE DANS LES CABLAGES ELECTRIQUES

2.1 - Circuit de simulation

Pour aborder ce problème, considérons la figure 1 qui représente une simulation simplifiée d'un circuit électrique de bord.



- Fig. 1 -

La peau de l'aéronef constituée d'un matériau de perméabilité magnétique μ et de conductivité électrique σ , d'une épaisseur l est parcourue par une impulsion de courant type foudre :

$$I_f = I \left(e^{-\frac{t}{T_D}} - e^{-\frac{t}{T_E}} \right)$$

Le câblage électrique est constitué d'un fil relié à la structure au point A (côté alimentation non représentée), cheminant à une hauteur h de la peau et alimentant un équipement d'impédance Z_{AB} . Ce circuit est situé à l'intérieur d'une structure entièrement fermée, c'est-à-dire ne comportant pas de fenêtres électromagnétiques.

2.2 - Tension induite

La surtension V_{AB} qui apparaît aux bornes de l'équipement, lorsque la structure est parcourue par l'impulsion de courant I_f est due à deux effets :

- un effet " résistif " de la structure
- un effet d'induction électromagnétique dans la boucle constituée par le câble et la structure

3 - EFFET " RESISTIF ", INFLUENCE DE L'EFFET DE PEAU

A l'intérieur d'un matériau conducteur, de conductivité donnée σ , en régime permanent de fréquence f , la densité de courant diminue en fonction de la distance de pénétration. On appelle épaisseur de peau d la profondeur à laquelle le champ $E = J/\sigma$ est une fraction $\frac{1}{e}$ de la valeur qu'il a dans le conducteur près de la surface.

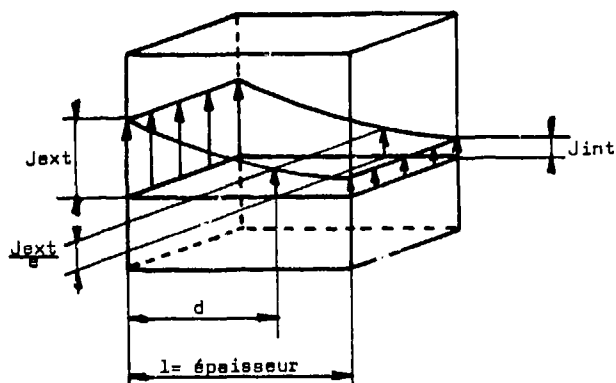


Fig. 2

$$d = \frac{1}{\sqrt{\mu f \pi \sigma}}$$

μ : perméabilité magnétique du matériau

σ : conductivité du matériau

L'analyse de la réponse indicielle de la peau permet de définir une constante de temps de pénétration T_p représentative du phénomène de diffusion.

$$T_p = \frac{\mu l^2}{\pi^2 \rho} \quad \rho \text{ résistivité}$$

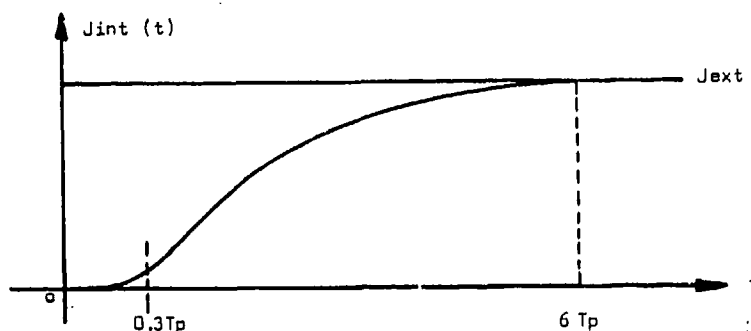


Fig. 3

L'application d'une densité de courant J_{ext} au temps $t = 0$ sur la paroi externe d'un conducteur conduit à l'apparition retardée $\tau = 0,3 T_p$ d'une densité de courant J_{int} sur la face interne, dont la valeur atteint lentement celle correspondant à un courant continu vers $t \sim 6 T_p$.

Or dans une configuration de câblage avion conventionnel (fig. 1), la peau servant de référence de masse électrique pour les équipements, le passage d'une impulsion de courant dans la peau est donc susceptible de générer une différence de potentiel entre les 2 points de référence.

$$V_{AB} = R_{dc} \times I \times f(T_p, I(t), t)$$

$$\text{avec } f(T_p, I(t), t) \in (0,1)$$

R_{dc} : résistance de la structure entre A et B mesurée en courant continu.

$$\text{si } l \gg d \text{ on a } f(T_p, I(t), t) \rightarrow 0$$

$$\text{si } l \ll d \text{ on a } f(T_p, I(t), t) \rightarrow 1$$

V_{AB} max est borné supérieurement par la loi d'ohm classique

$$V_{AB} \text{ max} = R_{dc} \times I$$

$$\text{avec } R_{dc} = \rho \frac{L}{S}$$

si ρ est faible R_{dc} est faible, T_p est grand et $f(T_p, I(t), t) \rightarrow 0$ car $l \gg d$.

3.1 - Application à des structures en alliage léger

Des essais ont été effectués sur une structure (fig. 4) en AU4G de 2 mm d'épaisseur ayant pour caractéristiques :

$$\rho = 3.10^{-8} \Omega \cdot m$$

$$T_p = 15 \mu s$$

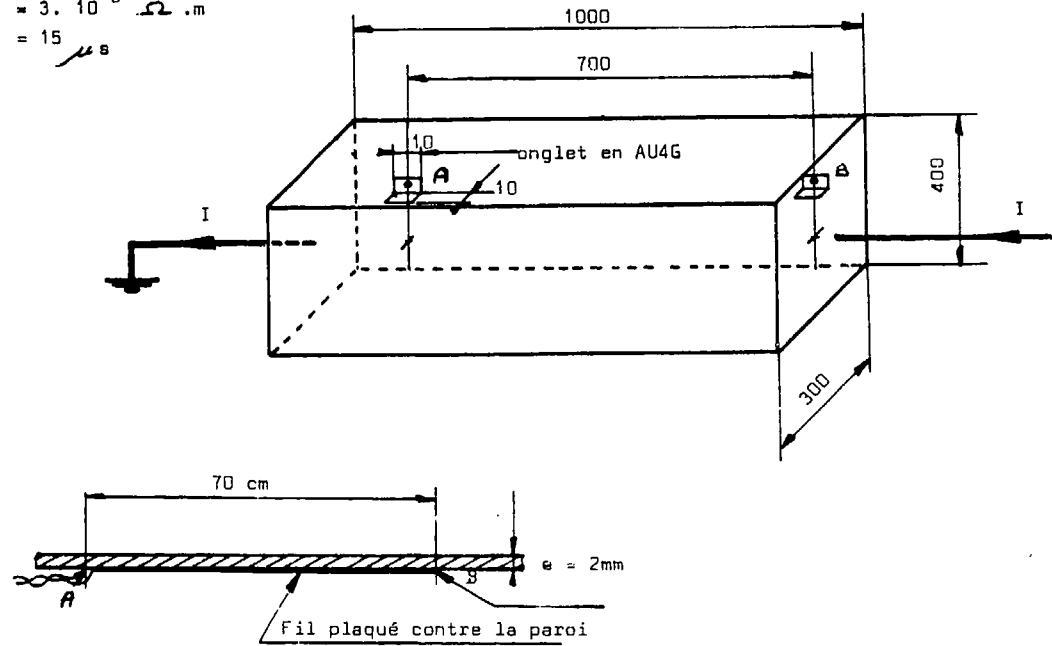
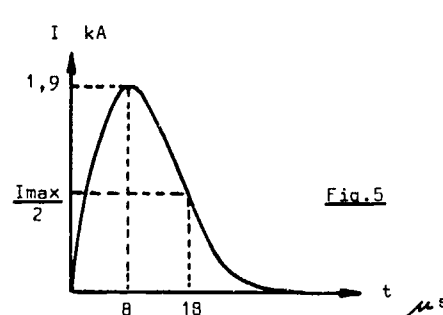


Fig. 4

Afin d'éviter toute influence de l'effet inductif, le fil de mesure a été plaqué contre la paroi de l'éprouvette.

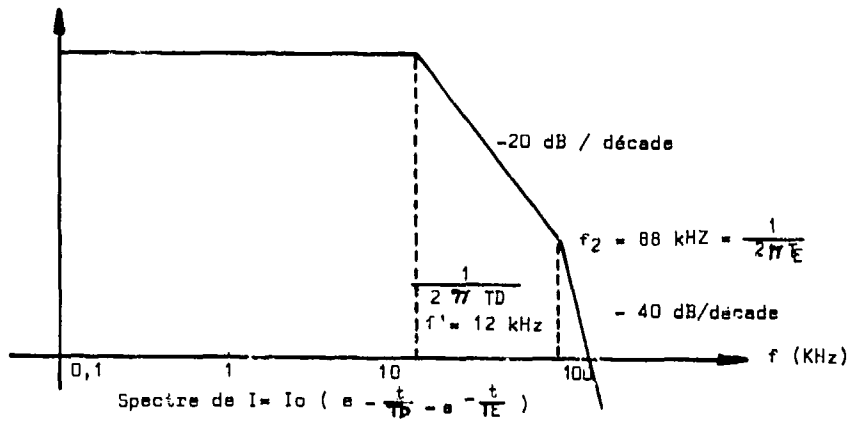
L'impulsion de courant utilisée est représentée figure 5.



$$I_f = I \left(e^{-\frac{t}{T_D}} - e^{-\frac{t}{T_E}} \right)$$

$$T_D = 1,3 \cdot 10^{-5} \text{ s}$$

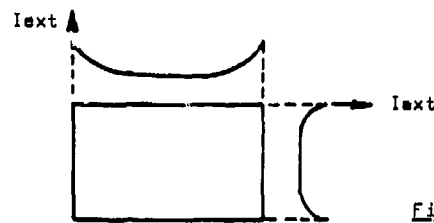
$$T_E = 1,8 \cdot 10^{-6} \text{ s}$$



Le spectre en fréquence de cette impulsion est représenté fig. 6

Fig. 6

Pour cette forme d'onde, et dans les conditions d'essai, en admettant une répartition uniforme de densité de courant externe, la valeur théorique donne $V_{int} = 8,5 \text{ mV}$, ($f(T_p, I(t), t) = 0,56$), la valeur mesurée a été de $V_{int} = 7 \text{ mV}$. La différence s'explique par les effets de bord qui introduisent une répartition non uniforme de courant (fig. 7).



En tenant compte de ces effets de bord l'écart est ramené à une valeur de l'ordre de 0,5 mV

Fig. 7

Si on extrapole ces résultats à $I = 100 \text{ kA}$, pour la forme d'onde de courant utilisée, on obtient une surtension par m de structure $V_{int} = 0,53 \text{ V/m}$. Il faut noter que la loi d'ohm classique s'applique à toutes les composantes spectrales du courant dont l'épaisseur de peau correspondante $d = \frac{1}{\sqrt{\mu f \pi \sigma}}$ est supérieure à l'épaisseur mécanique de la structure.

Dans le cas de l'AU4G de 2 mm d'épaisseur

$$f_c \leq \frac{c}{\pi l^2 \mu} \quad \text{donne } f_c \leq 2,4 \text{ kHz,}$$

on obtient donc le diagramme suivant fig. 7 bis.

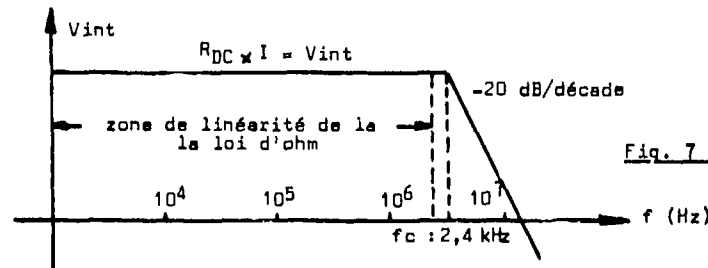
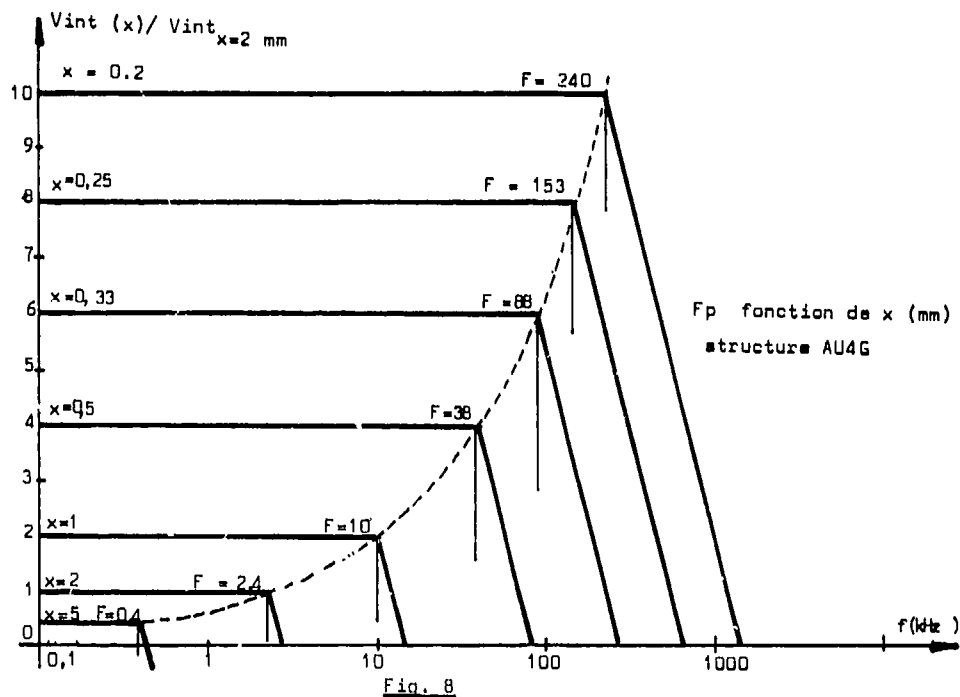


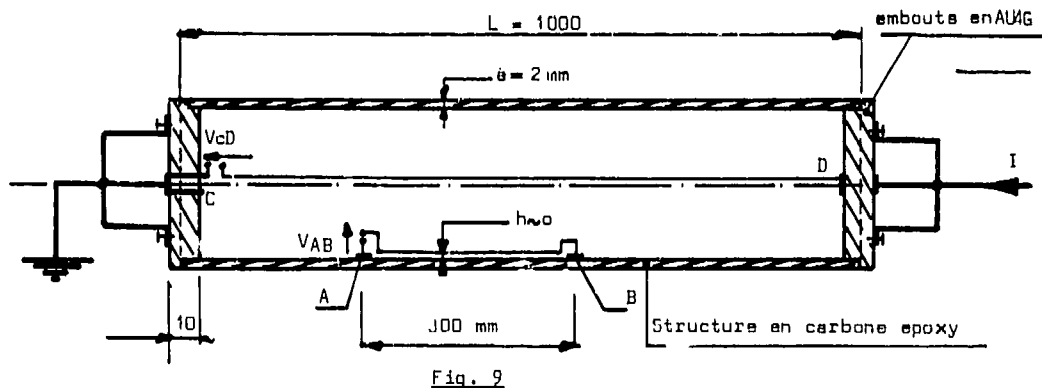
Fig. 7 bis

La figure 8 montre les courbes de réponses d'alliage léger de différentes épaisseurs.



3.2 - Application à des structures en fibre de carbone

Les essais ont été effectués sur le cylindre représenté figure 9.



Cette structure est constituée d'un cylindre en fibre de carbone de 2 mm d'épaisseur tissée par des plis à 90°, fermé à ses 2 extrémités par des embouts massifs en AU4G emmanchés à force à l'intérieur du cylindre.

Le courant I est injecté grâce à 4 reprises symétriques fixées sur chaque embout.

La résistance de ce cylindre vaut $92 \text{ m}\Omega$ soit $\rho = 11,6 \cdot 10^{-5} \Omega \cdot \text{m}$.

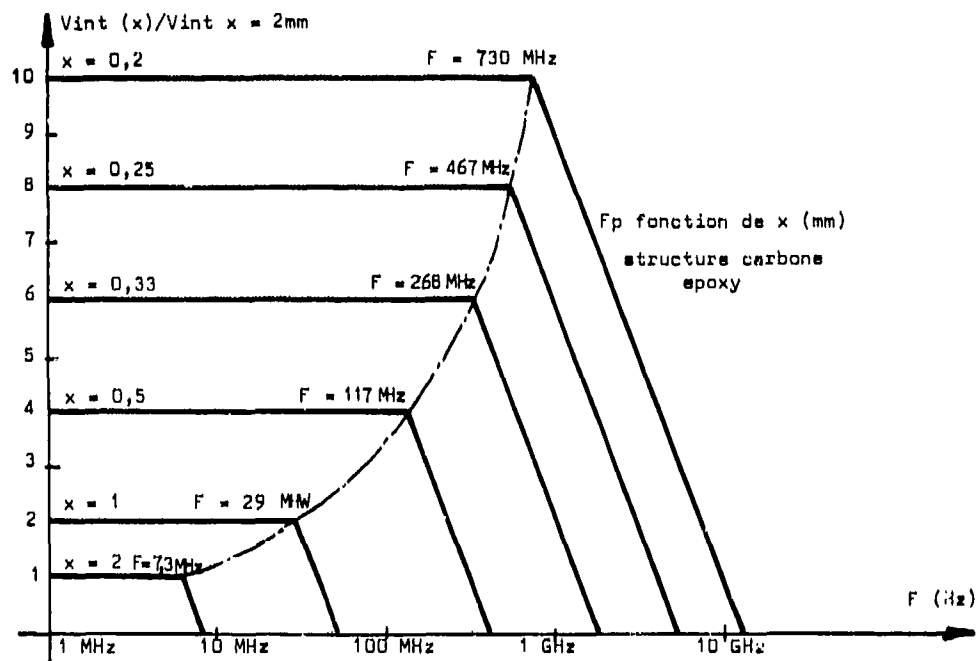
La constante de temps de pénétration est : $T_p = 4,4 \cdot 10^{-9} \text{ s} = 4,4 \text{ ns}$.

La fréquence f_c pour laquelle l'épaisseur de peau $d = \frac{1}{\sqrt{\pi f \mu \sigma}}$ est égale à l'épaisseur physique du matériau l est donnée par : $f_c = \frac{1}{\pi l^2 \mu \sigma} = 7,3 \text{ MHz}$.

L'application linéaire de la loi d'ohm reste donc valable sur le peroi interne de la structure de 2mm d'épaisseur pour les fréquences inférieures ou égales à 7,3 MHz.

Les essais ont été réalisés en injectant des impulsions de courant oscillantes amorties dont la pseudo fréquence max atteint une centaine de kHz. La relation $V_{ext} = V_{int}$ a été confirmée par les mesures. La vérification expérimentale à des fréquences supérieures à 7,3 MHz n'a pu être réalisée avec les installations utilisées.

La figure 10 montre les courbes de réponse de structures en fibres de carbone de différentes épaisseurs.



3.3 - Comparaison de l'effet de peau sur des structures en alliage léger et en fibre de carbone

Les résultats précédents montrent que la pénétration d'une impulsion de courant à l'intérieur de la peau d'un aéronef est directement liée aux caractéristiques du matériau et en particulier à sa résistivité ρ et par voie de conséquence à la constante de temps de pénétration $T_p = \frac{\mu l^2}{\pi^2 \rho}$.

Le diagramme figure 11 montre l'accroissement de l'aire d'application de la loi d'ohm, qui dans le cas d'une structure donnée varie dans le rapport des résistivités des matériaux. Dans le cas particulier des fibres de carbone, et de l'alliage léger, ce rapport est d'environ 3000.

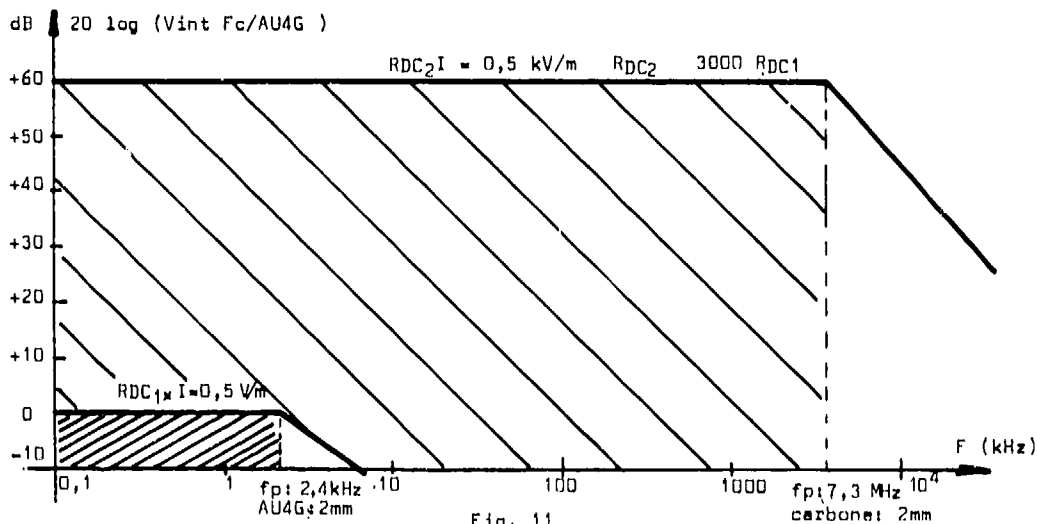


Fig. 11

4 - EFFET INDUCTIF DU AU CHAMP MAGNETIQUE INTERNE

Nous venons de voir la part que représente la composante " résistive " dûe à une des conséquences l'effet de peau dans la surtension qui apparaît aux bornes d'une impédance Z reliée à la masse. Nous allons maintenant évaluer la composante de la surtension due à l'induction électromagnétique $V = - \frac{d\Phi}{dt}$ à travers la surface que représente le câblage situé à une distance h au-dessus de la structure (fig. 1).

L'induction électromagnétique B_{int} est essentiellement créée par les filaments de courant qui circulent sur la face interne de la structure. Ce résultat fondamental a pour implication directe le fait que le champ magnétique interne apparaît retardé par rapport au courant qui l'a engendré. Son effet dans la génération de la tension induite est donc atténué, le $\frac{dB}{dt}$ étant le résultat du phénomène de diffusion à travers la peau.

4.1 - Champ électromagnétique à l'intérieur d'une structure en alliage léger AU4G de 2mm d'épaisseur

Le caisson qui a servi aux essais est le même que celui qui a été utilisé pour l'étude de l'effet résistif (fig. 4).

Le champ électromagnétique interne H_{int} est un champ dont l'évolution temporelle est en phase avec la densité de courant j_{int} et proportionnel à celle-ci. Ce phénomène est parfaitement mis en évidence sur les photos figures 12, 13, 14 qui représentent successivement :

- le courant total traversant la structure
- le champ magnétique relevé caisson ouvert c'est-à-dire obtenu par couplage direct : le champ électromagnétique est en phase avec le courant
- le champ magnétique relevé caisson fermé : le maximum du champ magnétique présente un retard de 68 μ s sur le courant injecté.



figure 12

Courant $I(t)$

$x = 20 \mu$ s/div
 $y = 0,18$ kA/div
 $t_{max} = 52 \mu$ s
 $I_{max} = 1,2$ kA

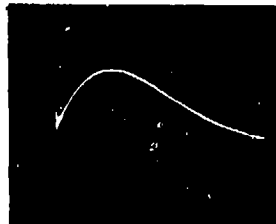


figure 13

Champ magnétique $H(t)$

caisson ouvert
 $x = 20 \mu$ s/div
 $y = 20$ mV/div
 $V_{max} = 52 \mu$ s
 $H_{max} = 67$ A/m

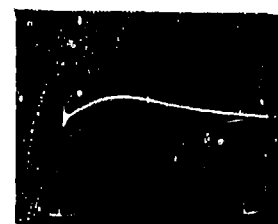


figure 14

Champ magnétique

caisson fermé
 $x = 50 \mu$ s/div
 $y = 10$ mV/div
 $V_{max} = 120 \mu$ s
 $H_{max} = 14$ A/m

Des mesures effectuées en injectant une impulsion de courant oscillante amortie ont permis de vérifier que l'atténuation apportée par la structure en alliage léger, de 2mm d'épaisseur (le niveau 0 db a été pris pour la pseudo période $T_0 = 450 \mu s$) suit parfaitement la courbe théorique - figure 15.

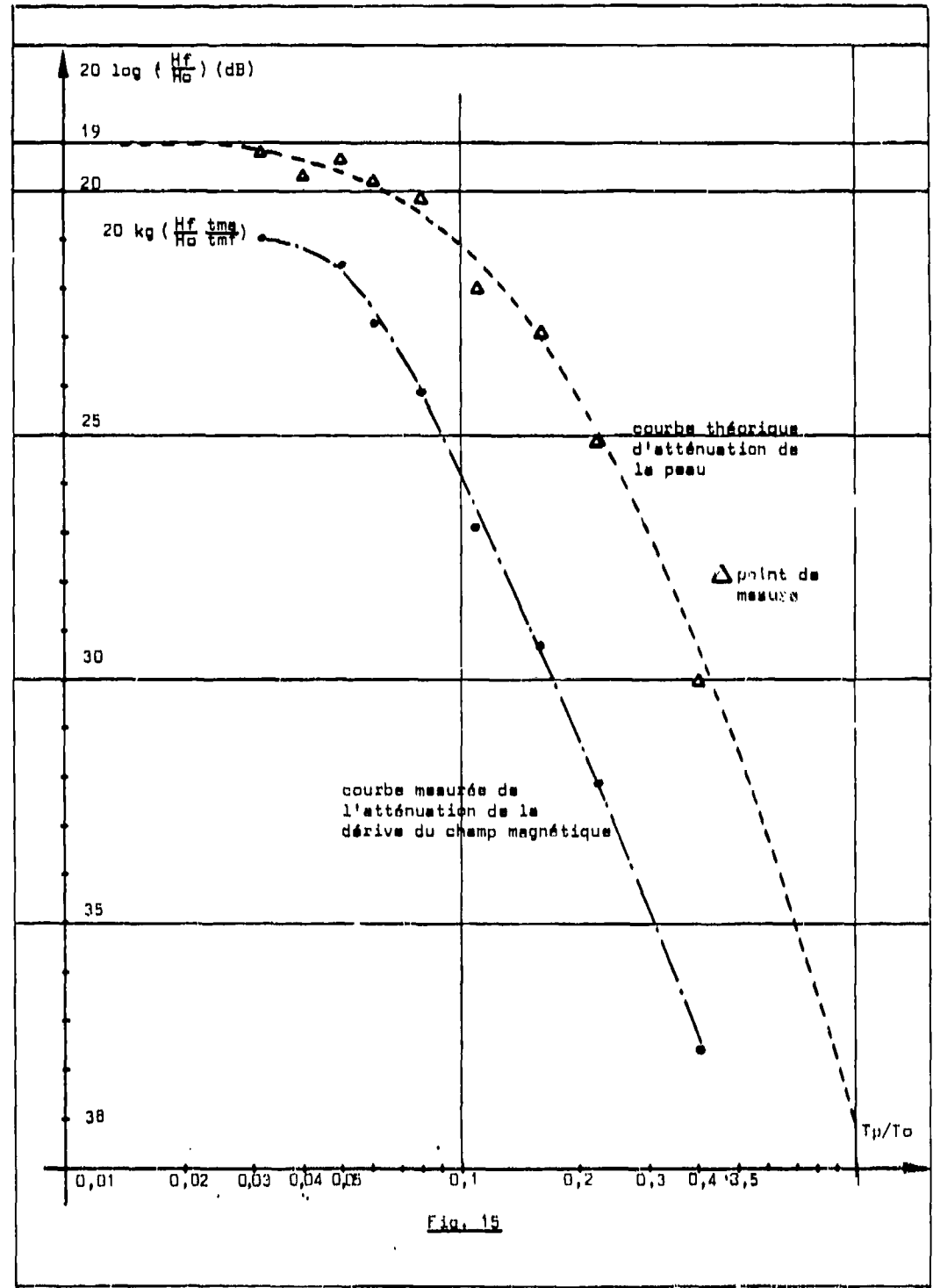


Fig. 15

Ce résultat confirme l'hypothèse selon laquelle le champ magnétique interne dans une structure fermée est essentiellement créé par le courant circulant sur le paroi interne de la structure.

4.2 - Champ électromagnétique à l'intérieur d'une structure en fibre de carbone de 2mm d'épaisseur

Des essais partiels ont été effectués sur le cylindre mis en oeuvre pour les études sur l'effet de peau.

Les installations utilisées n'ont permis que la génération d'impulsion de courant :

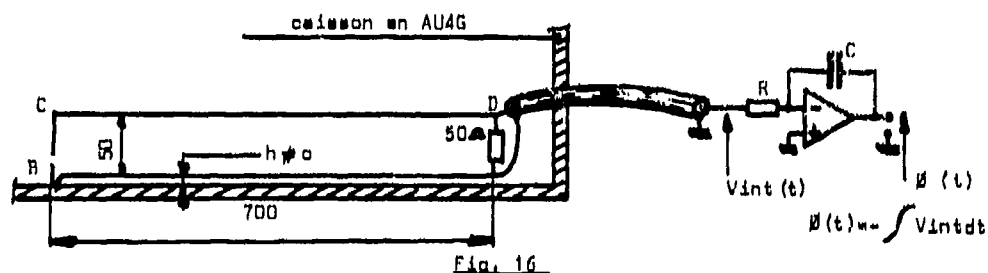
$$I(t) = I_0 \left(e^{-\frac{t}{T_D}} - e^{-\frac{t}{T_E}} \right) \text{ avec}$$

$$T_E = 1,8 \mu s \quad T_D = 11,8 \mu s$$

c'est-à-dire des impulsions dont le spectre de fréquence ne comportait pas de fréquences suffisamment élevées pour vérifier les calculs théoriques. Ces essais confirment cependant que les moyennes fréquences ne sont pas atténuées.

4.3 - Tension induite due au champ électromagnétique interne

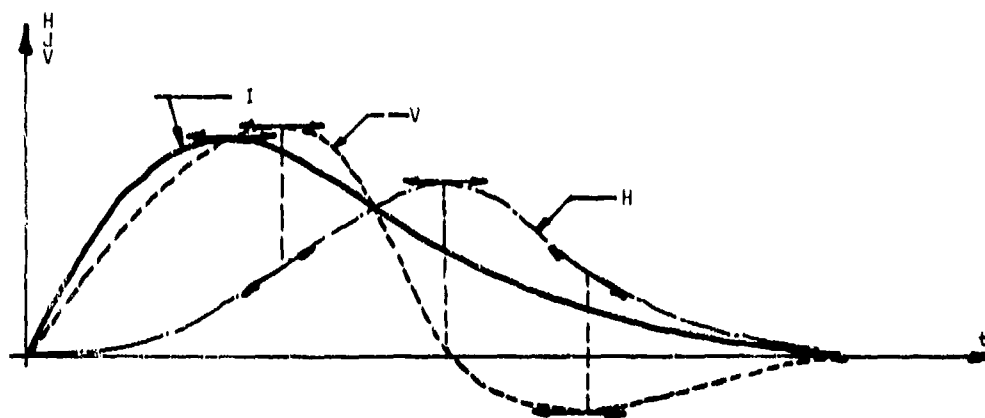
La tension induite due au champ électromagnétique interne a été mise en évidence en utilisant le montage représenté figure 16 dans le cas de structure en AU4G.



Les enregistrements effectués ont permis de vérifier que la tension induite due au champ électromagnétique interne vérifie bien la loi de LENTZ :

$$v = - \frac{d\phi}{dt} = - k \frac{dH}{dt}$$

Deux formes d'ondes de tension induite v peuvent donc apparaître aux bornes d'un circuit constitué d'une boucle avec 1 point unique à la masse.



- tension induite lorsque le champ magnétique interne est retardé (cas de l'AU4G)(Fig.17)

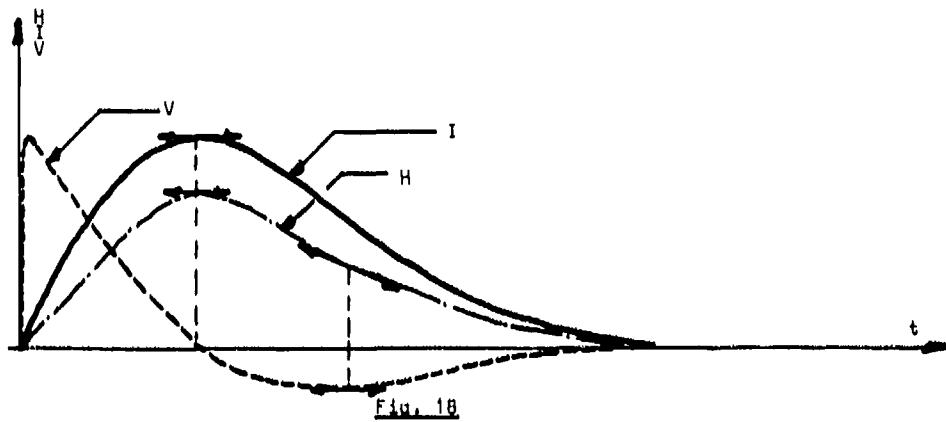


Fig. 18

- tension induite lorsque le champ magnétique interne est en phase avec le courant figure 18 (cas fibre de carbone) soumise à une impulsion de courant foudre.

4.4 - Comparaison des surtensions induites par le champ électromagnétique à l'intérieur de structures alliage léger et fibre de carbone

Les diagrammes suivants montrent le niveau des surtensions induites pour le champ électromagnétique d'une impulsion de courant de durée variable, à l'intérieur de structures fermées en ALU4 et fibre de carbone pour une boucle identique.

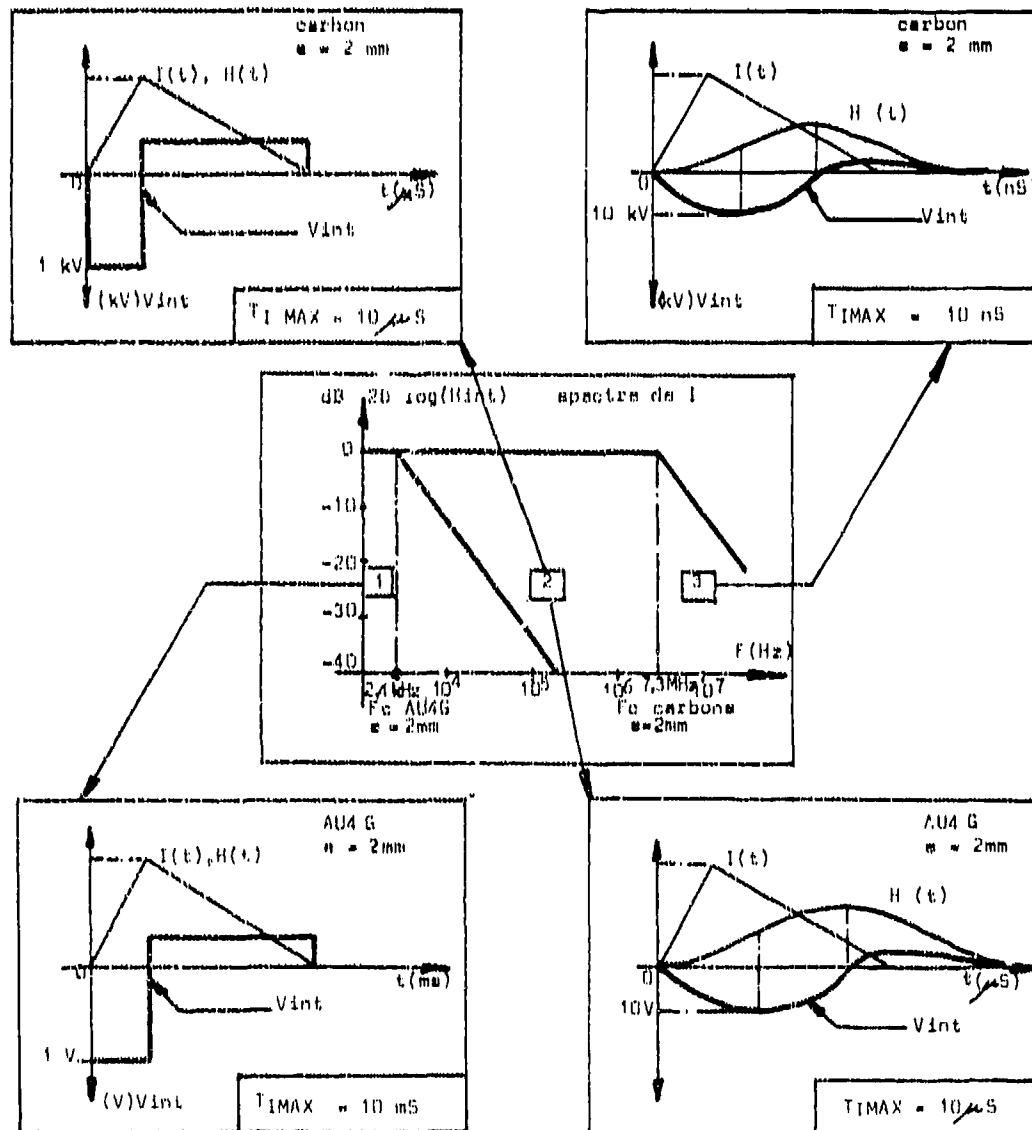


Fig. 19

5 - CONCLUSION

Le tableau suivant résume les observations dans le cas de structures en AU4G et fibre de carbone de 2mm d'épaisseur.

	Résistivité	Constante de temps de pénétration	Fréquence de coupure	Atténuation de $\frac{dH}{dt}$ à $f=100$ kHz	$U=RI$ pour $I=100$ kA continu	$U = \frac{dB}{dt}$ pour $l=1m$, $d=5cm$, $f=100$ kHz
AU4G	$3,4 \cdot 10^{-8}$	$15 \mu s$	2,4 kHz	- 60 dB	0,5 V	0,5 V
Carbone Epoxy	$1,2 \cdot 10^{-4}$	4,4 ns	7,3 MHz	0 dB	1,5 kV	0,5 kV
AU4G Carbone Epoxy	3000	~ 3000	~ 3000	60 dB	70 dB	60 dB

Il montre, compte tenu du spectre en fréquence de la foudre où le maximum d'énergie est situé à des fréquences inférieures à 100 kHz, que la fibre de carbone offre une immunité environ 3000 fois inférieure à celle d'un alliage léger, aussi bien en " chute de tension " qu'en transparence au champ électromagnétique.

ELECTROMAGNETIC INTEGRATION OF COMPOSITE STRUCTURE IN AIRCRAFT

G. L. Weinstock
McDonnell Aircraft Company
St. Louis, MO 63166
U.S.A.

Present U.S. Navy and Marine Corps aircraft being designed and produced by the McDonnell Aircraft Company, a Division of McDonnell Douglas Corporation, have significant portions of the skin and substructure fabricated from graphite/epoxy composite material. The F-18 Hornet has approximately 50% of its surface area composite and the AV-8B V/STOL utilizes composite material for its wing, tail and forward fuselage. Extensive analysis and testing has been performed during the last seven years to define those parameters necessary for successful electromagnetic integration of graphite/epoxy composite into these aircraft. Descriptions of the tests, analyses, and design processes including procedures, methods, results and design improvements are presented in this paper. The specific investigations addressed are: (a) basic material properties; (b) inherent electromagnetic shielding; (c) intermodulation effects; (d) effects on antennas; (e) panel shielding; (f) joint effects and improvements; (g) joint impedance; (h) access door design and improvements; (i) bonding; (j) large fuselage section shielding; and (k) complete wing shielding. The above tests and supporting analyses were performed on different types of composite construction, thickness, and size and were usually related to comparable aluminum articles. Some of the variations assessed and described in the paper are aluminum honeycomb, syntactic core and monolithic materials, combinations of lap and shear joints and selected metallic coatings.

Production designs developed for cost and weight effective incorporation of shielding and bonding improvement are noted in the text.

Introduction

McDonnell Aircraft Company (MCAIR), a Division of McDonnell Douglas Corporation, is producing aircraft for the U.S. Navy and Marine Corps that utilize significant amounts of graphite/epoxy (G/E) composite structure. Approximately 50% of the surface area of the F-18 Hornet is G/E, as is the wing, tail and forward fuselage of the AV-8B V/STOL aircraft. The growing use of G/E on military aircraft has raised questions regarding possible adverse electromagnetic effects. However, MCAIR has successfully been able to integrate G/E structure electromagnetically with high performance avionics subsystems.

The integration effort can be divided into three steps. The first step is to determine what external electromagnetic (EM) fields an aircraft may experience. Second, a practical susceptibility threshold is postulated. This susceptibility threshold includes all standard electromagnetic interference (EMI) suppression measures, such as: line filtering, wire shielding, bundle shielding, usage of balanced signal circuits and MIL-STD-461 compliance. The remaining differences between the external EM field level and the internal avionics EMI susceptibility threshold, must be supplied by airframe shielding. This is generally 15 to 30 dB.

The third step is to assess the actual aircraft structure and where required make the necessary design improvements.

Various analysis and test programs have been conducted to support MCAIR's program. They include the following topics as discussed in this paper:

- o Inherent Shielding
- o Panel Shielding
- o Joint Leakage
- o Joint Impedance
- o Fuselage Shielding
- o Syntactic Core Fuselage Shielding
- o Static Wing Shielding
- o Antenna Performance
- o Intermodulation Effects
- o Lightning Effects

Inherent Shielding

Investigations were initially performed to determine the inherent shielding properties of G/E. Washer specimens were cut from 1, 2, 4 and 8 ply G/E panels. These were tested in the coaxial line fixture shown in Figure 1.

The coaxial fixture was fabricated from aluminum and was actually an enlarged coaxial line with air dielectric. It had two identical sections, connected together with the test specimen between them (Figure 1). To determine the shielding of the specimens, a CW signal was inserted into one end of the fixture and the received signal was measured at the other end. This determined the inherent shielding level of the G/E specimens to a plane wave field.

The inherent shielding curve which was derived (Figure 2) provides only the upper limit of the shielding that can be obtained from G/E since it does not account for joint leakage. However, it is of major significance because it shows that its inherent shielding is far in excess of that required for the skins of military aircraft. Thus, successful aircraft can be designed using G/E fuselage and wings with no metal coating if joint and seam leakage is controlled.

These tests also showed that the shielding is predominantly by reflection rather than absorption, since the thickness of the panel (after accounting for polarization) had little effect.

Panel Shielding

Other tests were performed to determine panel shielding of G/E using a cubical copper box approximately 25 cm per side as shown in Figure 3. A parallel plate line was used as the plane wave source for frequencies below 70 MHz. For frequencies above 70 MHz, testing was performed in an anechoic chamber or outside on an antenna range, where the far field of an antenna was used as the plane wave source.

In these tests square panels were mounted on the open face of the fixture. The panel and fixture were then illuminated by a plane wave that was linearly polarized. The shielding was then computed by using the "panel on" and the "panel off" field strength readings taken via a rod antenna inside the box.

These tests were conducted for G/E panels of various thicknesses (1 ply, 2 ply, 4 ply, and 8 ply) and construction types (monolithic, honeycomb and syntactic core). Different types of panel attachment were also evaluated. These were: (1) contact mounting, where the panels were held tightly against the box, (2) conductive mounting, where the fibers of the G/E were conductively connected to the box by a conductive epoxy, (3) fastener mounted panels, where fasteners were used to connect the panels to the box, (4) capacitively mounted panels, where a conductive foil was wrapped around the panels and the flange on the box, and (5) panels with beryllium copper finger stock of various sizes mounted around the panel, both with and without a conductive foil. Typical results of these tests are shown in Figures 4, 5, and 6.

Panel/Joint RF Leakage Comparison Tests

The panel/joint tests were used to evaluate the RF leakage characteristics of various joint manufacturing techniques. The test articles consisted of thirteen panels of various configurations as shown in Table 1. Nine panels had joints and four solid panels were used for baselines. The jointed panels were constructed with various environmental seals, and some included other EMI protection devices.

Figure 7 illustrates the set-up for the joint leakage tests. The panels were mounted over the open end of a five-sided copper box and bolted to the flange surrounding its open end. Measurements were made by locating a signal source antenna inside the copper box and probing along the outer surface with a receiver probe.

Table 2 presents the performance of each panel. The leakage data was analyzed and the panels were assessed with respect to performance in preventing leakage. This was done for both E and H field leakage. Those joints that appear to perform best at preventing EM leakage were assigned a figure of merit of 100, and the other panels assigned numbers of lesser values.

The important conclusions to be drawn are:

- (1) Tin plating can provide appreciable improvement in the protection against electromagnetic field leakage through G/E single lap shear joints. The addition of finger stock does not provide a significant amount of protection above that which is obtained with the use of tin plating alone. Possible gains can be realized if the surface layer of epoxy is removed prior to plating the material with tin. This would provide better electrical contact with the current carrying fibers, and a better contact for the finger stock.
- (2) Finger stock appears to be most effective when bonding is desired between a metallic panel and a G/E panel. In this case both the electric field and the magnetic field leakage is lower. The magnetic field leakage is controlled more by the presence of tin plating on the G/E panel than with finger stock alone.
- (3) Tin plating of non-jointed G/E panel increases shielding effectiveness for both electric and magnetic fields.

Panel Joint Impedance Tests

The electrical bonding achieved with various methods of joint fabrication was also tested. DC resistance and RF impedances were measured across the joints to obtain the information relating to electrical current continuity.

Table 3 lists the panels that were used in the impedance tests. As stated above, the joints were single lap shear and double lap shear joints. Non-jointed panels were used for baselines.

Each test panel was injected with a current, by means of copper gloves electrically bonded to the panels on both sides of the joints. Seven measurement points were probed at discrete distances between the two copper contacting gloves. These points are indicated by the letters in Figure 8. The voltage drop at each point was recorded. Measurements were made from 14 KHz to 500 KHz.

Upon comparing the voltage drops at the joints of the various panels, it is evident that the effects of the impedances can be diminished by improvements added at the interface. The voltage drops across the "good" joints do not differ appreciably from that which is seen across any other two points on the panels.

Table 4 lists the results of these tests, comparing the various joints tested to the apparent impedance of the material from which they have been fabricated. The higher ratio of joint impedance to bulk material impedance indicates the degradation of current continuity by the joint. The addition of tin spray at the joint interface improves this ratio, in the frequency range tested, to a ratio of about one. That is, the joint is about as good as the bulk material, and its impedance is decreased. Therefore, the same procedures utilized to protect against EMI can also improve joint continuity for the currents on G/E structures.

Fuselage Shielding

Tests were conducted to determine the voltages induced in typical avionics wire bundles enclosed within G/E structures when irradiated by an external EM field and to provide comparison with metallic structure.

Two test boxes were fabricated, one of aluminum and one of G/E simulating the forward fuselage avionics bay. Figure 9 shows one test box in its location on the AV-8B aircraft and as it was constructed for these tests. The two boxes contained identical wire bundles and load terminations, routed along identical paths. The boxes contained doors, seams and joints to simulate the different types of apertures through which EM fields can penetrate an aircraft's skin. They were tested over a frequency range from 14 KHz to 18 GHz. Voltages induced on the cables were measured across the loads.

As shown in Figure 10 there were two cable bundles running along the length of the boxes. Each path was designed to parallel regions of possible electromagnetic leakage from the exterior regions of the boxes. The cables were intentionally routed close to joints and door seams to maximize induced voltage pickup. Within each cable was a single wire and twisted pair to be tested. These are typical wires used for data and control information transmission between equipment subsystems.

The low frequency (14 KHz to 100 MHz) portion of the test was performed outdoors at a site isolated from local EM interference. The high frequency (200 MHz to 18 GHz) portion was done in the MCAIR anechoic chamber.

Various test configurations were used, including combinations of open and closed side door panels, cable load terminations, and side orientations. Measurements were made at both the loaded and non-loaded ends of cables.

Results typical of the different test configurations (104 in all) are shown in Figure 11. The results show that in actual structures the leakage effects of joints for both aluminum and G/E are the dominant factor in shielding effectiveness and thus depending upon the actual aircraft there may be little difference between G/E and aluminum.

Syntactic Core Fuselage Tests

The effect of using syntactic core (micro-ballons) between thin layers of G/E was investigated. Two large samples representative of an aircraft fuselage with a removable door were fabricated, one of aluminum and one of G/E with syntactic core. Typical aircraft wiring was located inside each sample. The samples were then irradiated and the induced voltages on wires recorded.

The test set up and results are shown in Figure 12. The results show little difference between the G/E syntactic core sample and the aluminum sample.

Static Wing Shielding Tests

Tests were made on the shielding effectiveness of a representative G/E wing. The test article was the right side of a full size YAV-8B wing assembly with an EMI-tight termination box at the wing tip. Both the skin and substructure of the wing were fabricated from G/E. The leading edge was metal. The purpose of the tests was to compare the induced voltage in wire located under the metal wing leading edge with the induced voltage on the wires located under the G/E torque box section of the wing.

Wire cables were installed as shown in Figure 13. E and H field probes developed at the Navy Postgraduate School, were also installed in the torque box as shown. Each wire bundle consisted of one single wire, one twisted wire pair, one twisted shielded pair (TSP), one coaxial cable, and an additional TSP loop, which acted as a digital data link from the instrumentation box, along the wing to its tip and back.

The EMI measurements were made for incident RF fields from 14 kHz to 18 GHz, divided into a "low frequency" region (14 kHz to 100 MHz) and a "high frequency" region (200 MHz to 18 GHz). The high frequency measurements were made in the MCAIR anechoic chamber, as shown in Figure 14, and the low frequency tests were performed in an outdoor open area on the MCAIR complex, as shown in Figure 15.

The test setup generally consisted of an antenna positioned one meter away from the upper surface of the right wing.

The test results were similar to those previously shown and little difference was seen between the induced voltage on wires located under the G/E and metal.

Antenna Performance Tests

Pattern, gain and VSWR tests were conducted, to investigate antenna performance effects. Various test configurations were used to determine the effects in terms of the type of composite, the ground plane configuration, and the type of antenna mount. Metallic ground planes were used for reference tests.

In one test series G/E ground plane test specimens were used to conduct gain, pattern, and VSWR tests at 400 MHz, 1 GHz, and 10 GHz. Similar tests were made using metal ground planes for reference. UHF and TACAN blade antennas were used at 400 MHz and 1 GHz, respectively, while a radar beacon stub antenna was used at 10 GHz.

The tests for gain and pattern were run by using the test specimen as a ground plane for a receiving antenna, with the antenna and ground plane mounted on a rotator inside the anechoic chamber. The VSWR tests were performed by using the test specimen as a ground plane for a transmitting antenna.

Comparison of antenna patterns for all of the various ground plane specimens and all types of mounting shows only small pattern and gain changes, regardless of the ground plane or base mounting. Thus, composites form effective ground planes and metal is not needed. VSWR tests show that the slight changes in gain between various configurations is attributable to slight changes in input impedance.

INTERMODULATION EFFECTS

Concern has been expressed regarding intermodulation effects produced by the graphite fibers used in the composite matrix. However, this phenomenon is found only where a small number of fibers are involved and may be attributed to the "point contact" effect, where the tip of the graphite fiber forms a nonlinear junction with another material. No intermodulation effects have been found in the bulk material. In fact, MCAIR tests have shown that, within the limits of measurement, no harmonics are generated by passing high levels of current through the various types of G/E joints or bulk composite material used in airframe construction.

LIGHTNING

Structural Damage - Extensive testing has been performed to define current transfer capability of G/E. It has been demonstrated that G/E airframe structures have sufficient current carrying capability to withstand the high level lightning threat without damage, except in the immediate vicinity of the strike attach point. All damage can be eliminated by applying thin metallic coatings.

Lightning Induced Current/Voltages

The threat posed by induced coupling from nearby lightning is similar for G/E composite vehicles and metal. The primary reasons are:

- o For nearby lightning, the amplitude of the induced transient may produce upset but is not high enough to cause burnout, provided proper EMC measures have been taken to minimize the coupling in the low frequency regime where the composite airframe provides a poor shield. At these low frequencies, avionics equipment is relatively immune to interference. In the mid-to-high frequency region, the coupling occurs primarily through the aircraft apertures (i.e., radome, canopy, seams, cracks, etc.) and therefore is approximately equal to the coupling into a metal aircraft.
- o In cases where lightning-generated upset does occur, it does not present a problem for analog systems because the upset is in milliseconds and the linear constraints of the aircraft response are much longer. Digital systems upset can also be restricted to milliseconds or less provided the system is designed to reject the induced transients as "bad data" (by means of parity checks, redundant data, etc.) so that the "state" of the digital system is not permanently altered.

Lightning Attachment

Tests and aircraft strike histories clearly show that, for metal aircraft, lightning zones can be defined by attach point tests on a metallized scale model (except for non-conducting components-radomes, canopy, etc.). This method should also be valid for a vehicle utilizing composite parts if the composite conductivity is good enough to allow

the required current flow during the early strike phases. If the charge transfer and streamering which occur prior to the actual strike, are not inhibited, the zones for a partially composite vehicle can be determined from tests on a metal model.

While the conductivity of G/E ($\sigma_g \sim 10^4$ mho/m) is much less than metal ($\sigma_m \sim 10^7$ mho/m), it is much greater than that of a dielectric ($\sigma_d \sim 10^{-15}$ mho/m). Thus, G/E should behave more like a metal than a dielectric.

Tests were performed to determine conclusively if any significant differences exist between the attach point characteristics of metal and G/E composite.

To accomplish this, similar sized G/E and aluminum panels were fabricated. The panels were grounded and a high voltage probe was positioned 72 inches above and equidistant from the upper corner of each panel as shown in Figure 16. Using this arrangement, the attachment behavior of G/E and aluminum samples was directly compared. At each probe position, several arc attachments were initiated to determine the "preferred" attachment locations. For most tests both panels were grounded, but the horizontal test was repeated with the G/E panel ungrounded. The relative arc capture areas of each panel are summarized in Figure 16.

To investigate the arc attachment effects of metal beneath the G/E, a thin monolithic panel and the honeycomb panel were each tested with a sharp ground probe centered two inches below them. The tests showed the ground probe had no discernable influence upon arc attachment.

The results of all tests conducted during this effort show no measurable difference in attach point behavior between metal and G/E structure.

Conclusion

We at MCAIR have been addressing the electromagnetic effects of composites since 1971 and have been heavily involved in G/E electromagnetic integration into aircraft since 1974. The following summarizes our findings:

- o G/E has a significant amount of the inherent shielding capability.
- o The principal reason for shielding effectiveness reduction in G/E structures is discontinuities at seams and joints.
- o Our tests show little difference in shielding between G/E and aluminum structures because of joint effects.
- o Designs to improve G/E joint effects can be effective.
- o Antennas for UHF and L band systems function properly when using G/E ground planes.
- o Lightning protection designs are available if complete damage protection is required.

G/E aircraft structure can be designed to provide adequate electromagnetic shielding for avionics and electrical subsystems. To date, we have not found any electromagnetic G/E issue that cannot be handled as part of a typical aircraft development program.

TABLE 1
EMI LEAKAGE TEST PANEL LIST

<u>CONFIGURATION IDENT.</u>	<u>CONFIGURATION</u>	<u>JOINT</u>	<u>JOINT SEAL CONFIGURATION</u>
A	G/E Tape Mat'l	None	None
B	G/E Cloth	None	None
C	Aluminum	None	None
D	G/E (Tin Plated)	None	None
G	G/E-Aluminum	Single Lap Shear	Form-In-Place (FIP) Seal
H	G/E-Aluminum	Single Lap Shear	Tin Plated-FIP Seal
J	G/E-Aluminum	Single Lap Shear	FIP Seal
K	G/E-Aluminum	Single Lap Shear	FIP Seal-Finger Stock
L	G/E-G/E	Single Lap Shear	Tin Plated
M	G/E-G/E	Double Lap Shear	Fay Seal
N	Aluminum-Aluminum	Double Lap Shear	Fay Seal
P	G/E-Aluminum	Single Lap Shear	FIP Seal-Finger Stock
R	G/E-G/E	Single Lap	Tin Plated-FIP Seal-Finger Stock

TABLE 2
EMI TEST PANEL DATA
Relative Performance of Panels with Seams

Test	Panel Description	Seam Preparation (5)	Relative Performance ⁽¹⁾	
			E(2)	H(3)
N	Aluminum-Aluminum	None Double Lap Shear (DLS)	100	97
L	Graphite/Epoxy Cloth - Graphite/Epoxy Cloth	Tin Plated, Sealed	84	84
P	Aluminum - Graphite/Epoxy Cloth	Bonding Strip, Sealed	69	79
R	Graphite/Epoxy Cloth - Graphite/Epoxy Cloth	Tin Plated, Bonding Strip Sealed	64	78
G	Aluminum - Graphite/Epoxy Cloth	Sealed	58	99
H	Aluminum - Graphite/Epoxy Cloth	Tin Plated, Sealed	49	96
M	Graphite/Epoxy Cloth - Graphite/Epoxy Cloth	None (DLS)	50	4
K	Graphite/Epoxy Cloth - Graphite/Epoxy Cloth	Bonding Strip, Sealed	37	55
J	Graphite/Epoxy Cloth - Graphite/Epoxy Cloth	Sealed	10	68
C	Aluminum ⁽⁴⁾		99	99
D	Tin Plated, Graphite/Epoxy Cloth ⁽⁴⁾		95	89
A	Graphite/Epoxy Tape ⁽⁴⁾		80	71
B	Graphite/Epoxy Cloth ⁽⁴⁾		70	79

NOTES:

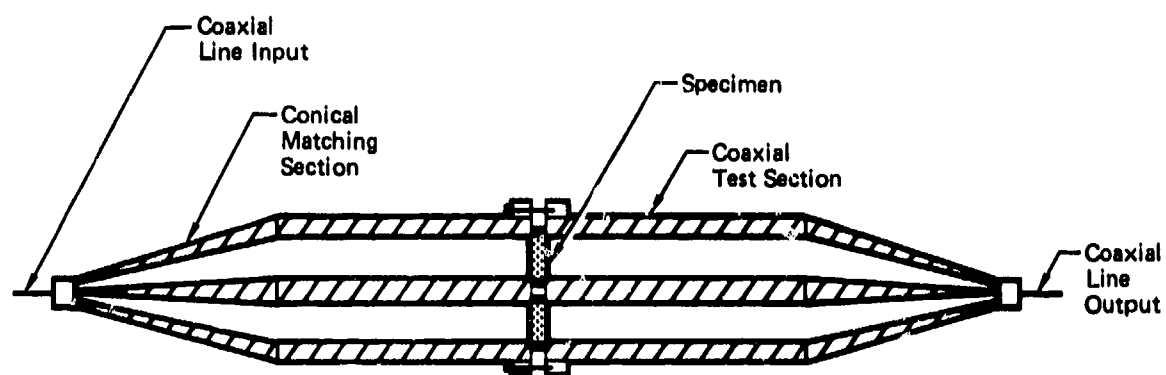
1. All panels show relationship to best panel whose value is 100
2. E (electric field)
3. H (magnetic field)
4. One piece panels (no seams)
5. Single lap shear (SLS) unless otherwise indicated

TABLE 3
JOINT IMPEDANCE TEST PANEL LIST

<u>CONFIGURATION IDENT.</u>	<u>CONFIGURATION</u>	<u>JOINT</u>	<u>JOINT SEAL CONFIGURATION</u>
B	G/E	None	None
C	Aluminum	None	None
G	G/E-Aluminum	Single Lap Shear	2-Ply Cured Fiberglass
H	G/E-Aluminum	Single Lap Shear	Tin Plate & Form-In Place Seal
J	G/E-Aluminum	Single Lap Shear	Form-In-Place Seal
M	G/E-G/E	Double Lap Shear	Fay Seal
P	Aluminum-G/E	Single Lap Shear	Fip Seal-Finger Stock
R	G/E-G/E	Single Lap Shear	Tin Plate-Fip Seal-Finger Stock

TABLE 4
RATIO OF IMPEDANCES

PANEL	TYPE	D.C. RESISTANCE (OHMS)	Ratio of Joint-Impedance to Bulk Material			
			14 KHz	42 KHz	112 KHz	500 KHz
J	All G/E SLS	0.03	7.0	10.4	5.9	1.8
M	G/E DLS	0.41	42.5	42.5	42.5	30.0
G	G/E-Alum SLS	0.013	2.3	2.4	2.1	2.8
H	G/E-Alum SLS	0.01	1.0	1.0	1.0	1.0
P	G/E-Alum SLS	0.013	1.0	1.0	1.0	1.0
R	G/E SLS	0.012	1.0	1.0	1.0	1.0
B	G/E Cloth	0.03	1.0	1.0	1.0	1.0
C	Aluminum	0.0	1.0	1.0	1.0	1.0



Washer Specimen Mounting Detail

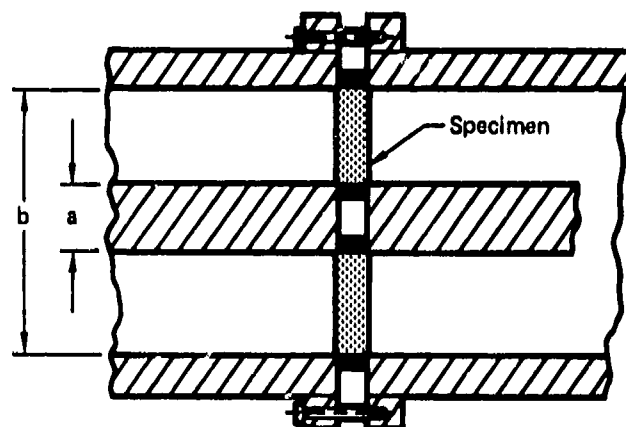


FIGURE 1 - COAXIAL FIXTURE

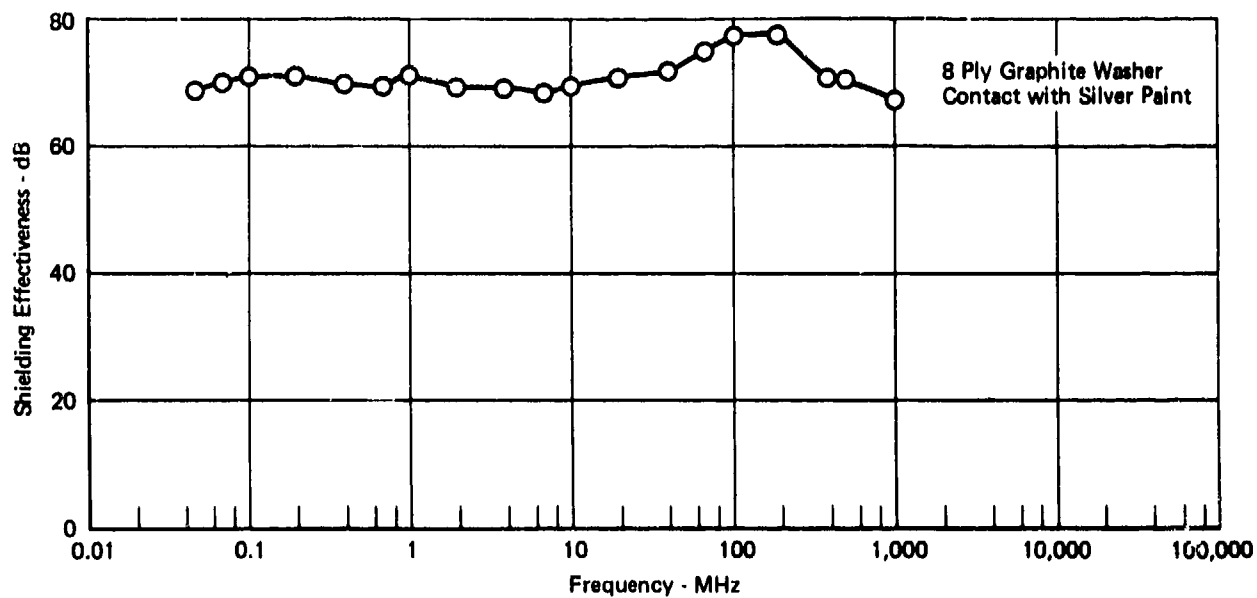


FIGURE 2 - PLANE WAVE SHIELDING MEASURED WITH COAXIAL LINE

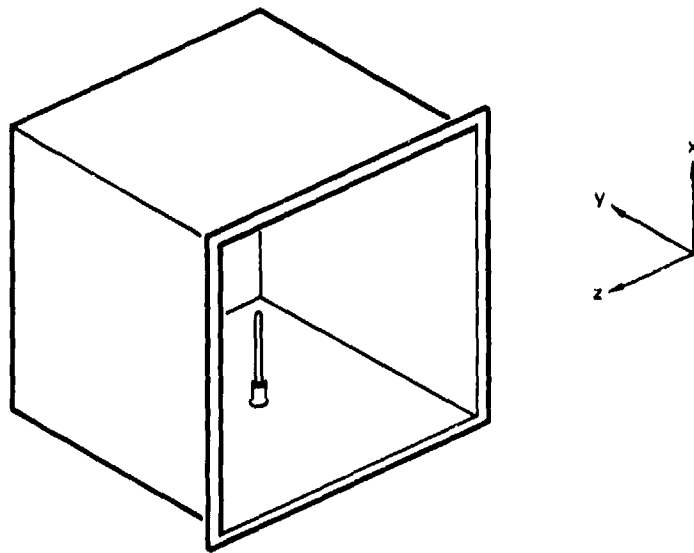


FIGURE 3 - CUBICAL BOX FIXTURE

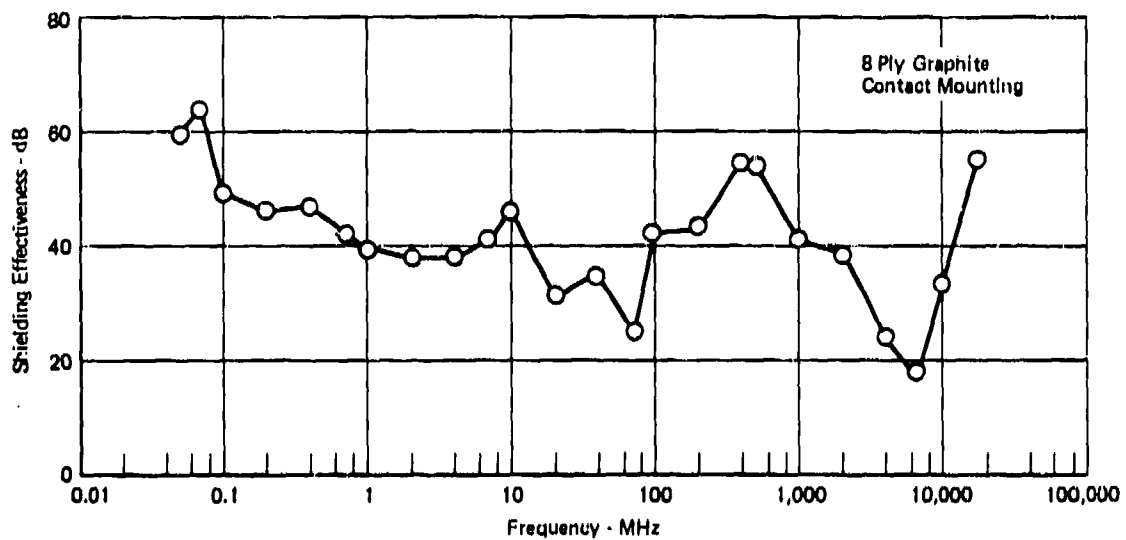


FIGURE 4 - ELECTRIC FIELD SHIELDING FOR GRAPHITE PANELS ON BOX

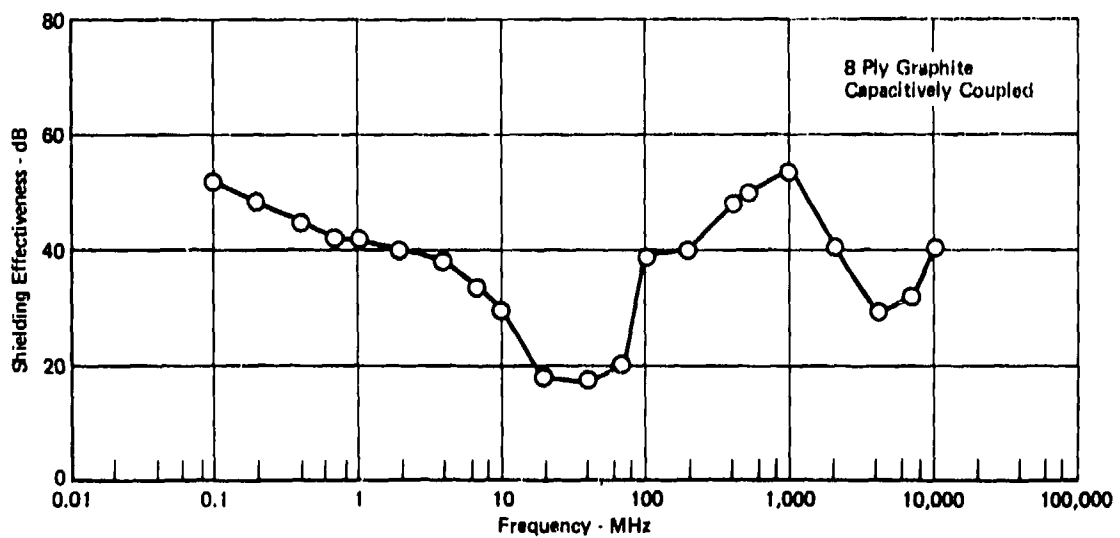


FIGURE 5 - ELECTRIC FIELD SHIELDING FOR GRAPHITE PANELS ON BOX (CAPACITIVELY COUPLED)

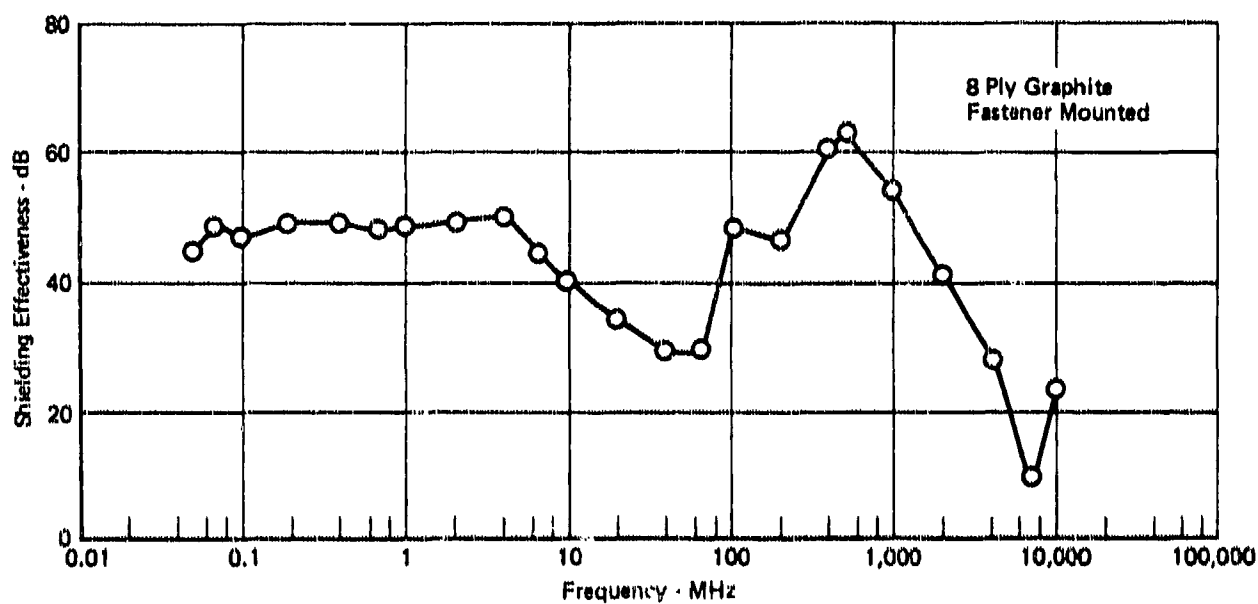


FIGURE 6 - ELECTRIC FIELD SHIELDING FOR GRAPHITE PANELS ON BOX (FASTENER MOUNTED)

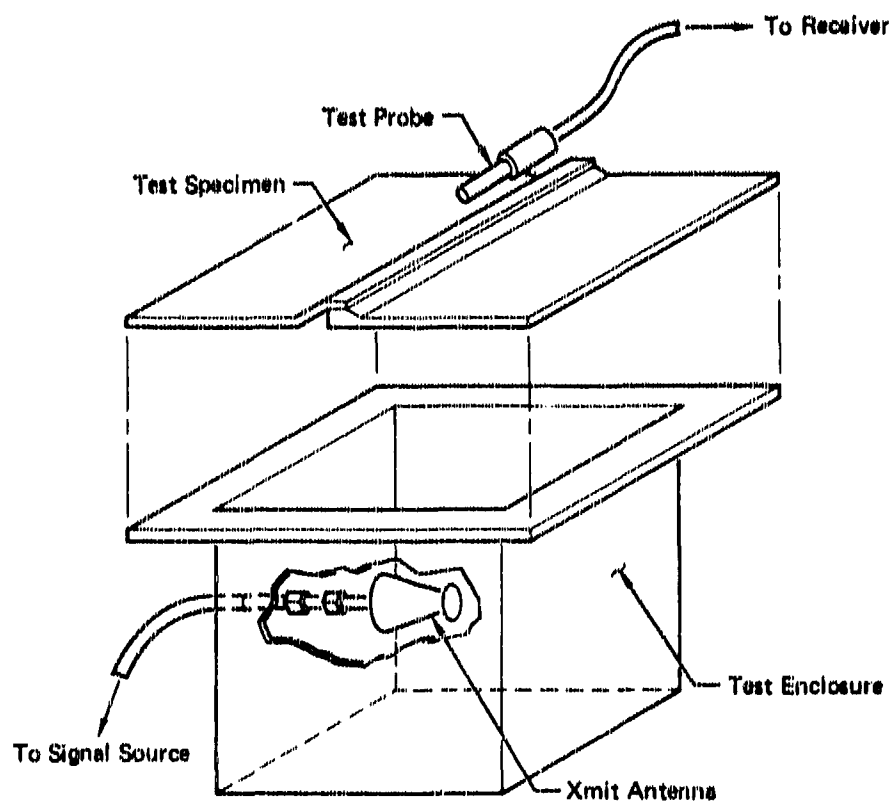


FIGURE 7 - TYPICAL TEST CONFIGURATIONS

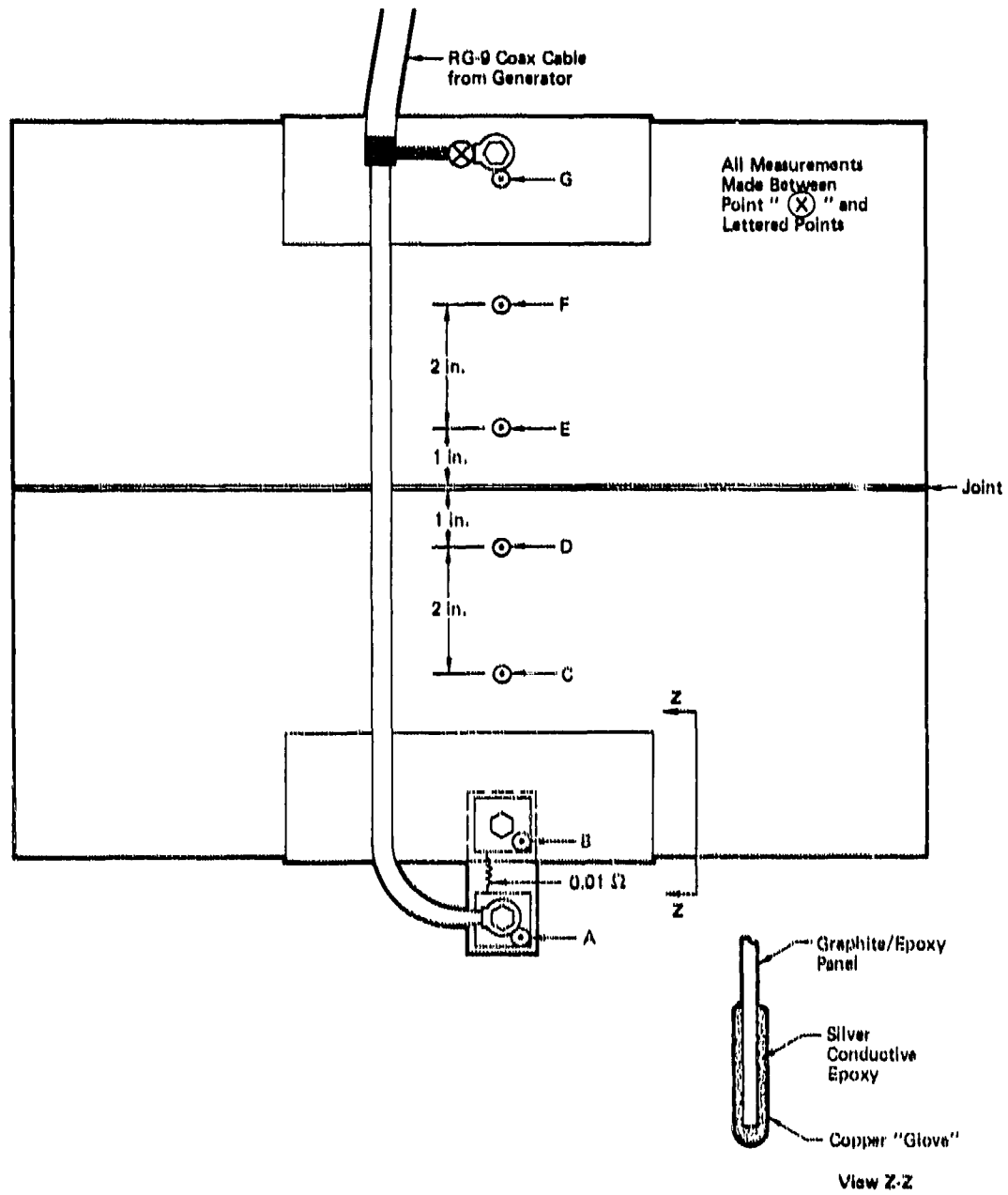


FIGURE 8 - CIRCUIT AND PROBE ATTACHMENT POINTS

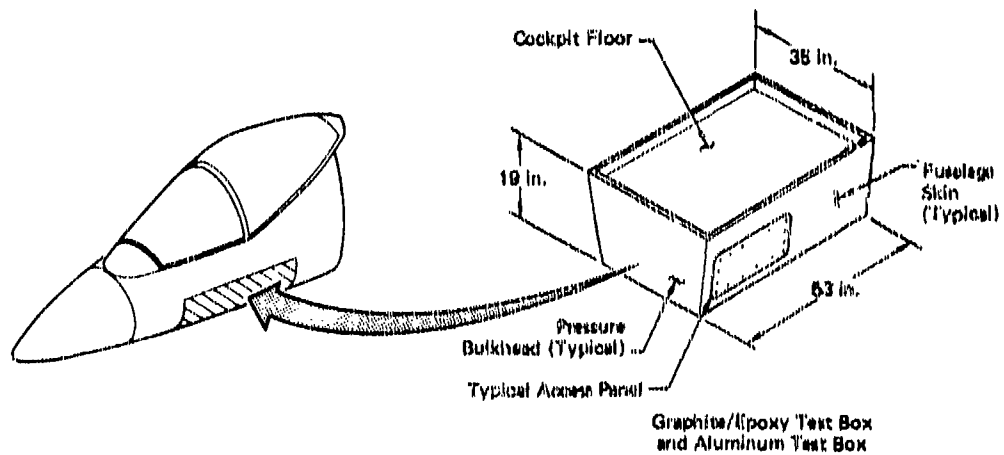


FIGURE 9 - FORWARD FUSELAGE EMI TEST ARTICLE

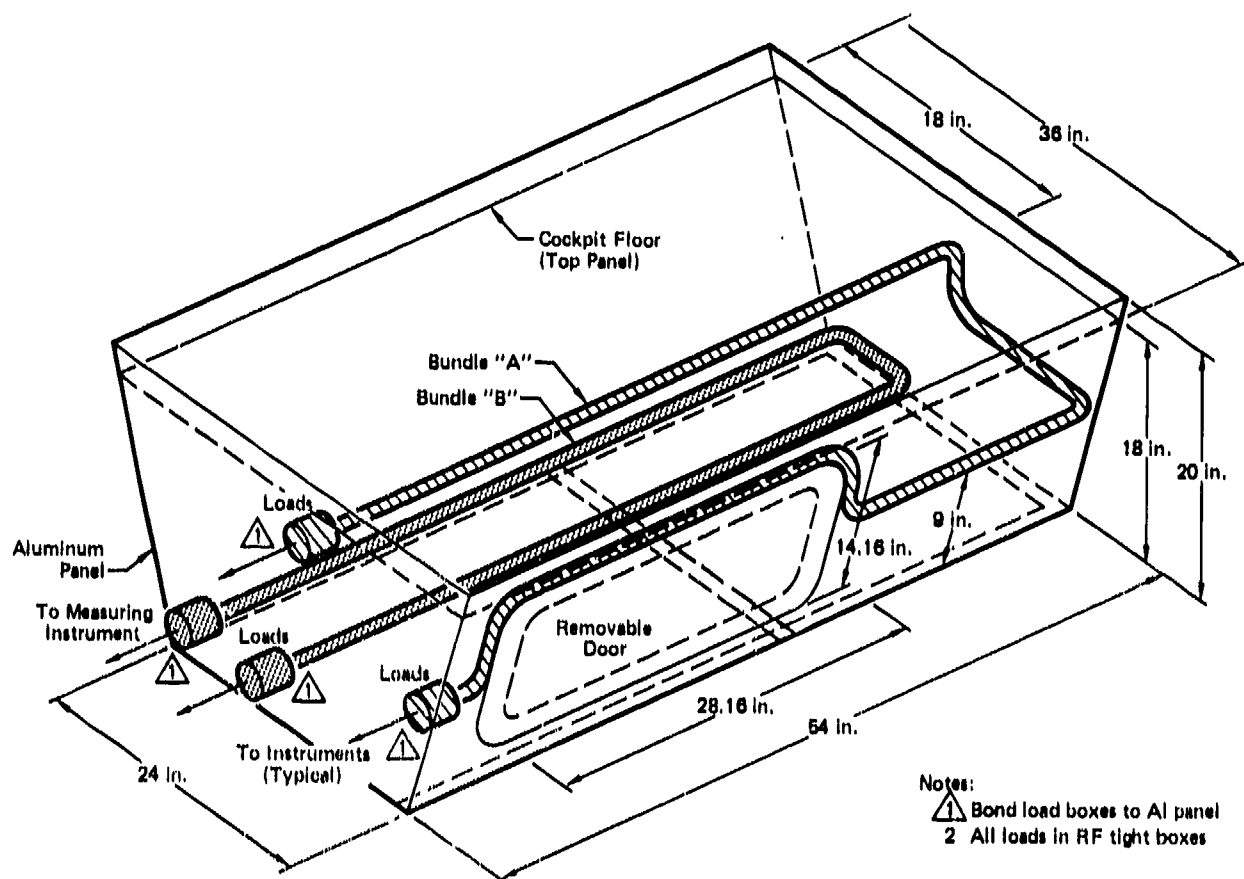


FIGURE 10 - TRIMETRIC VIEW OF WIRE ROUTING

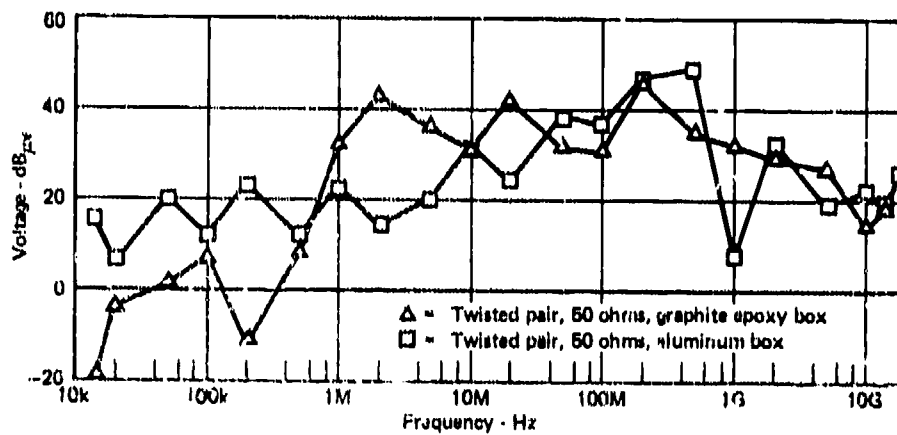
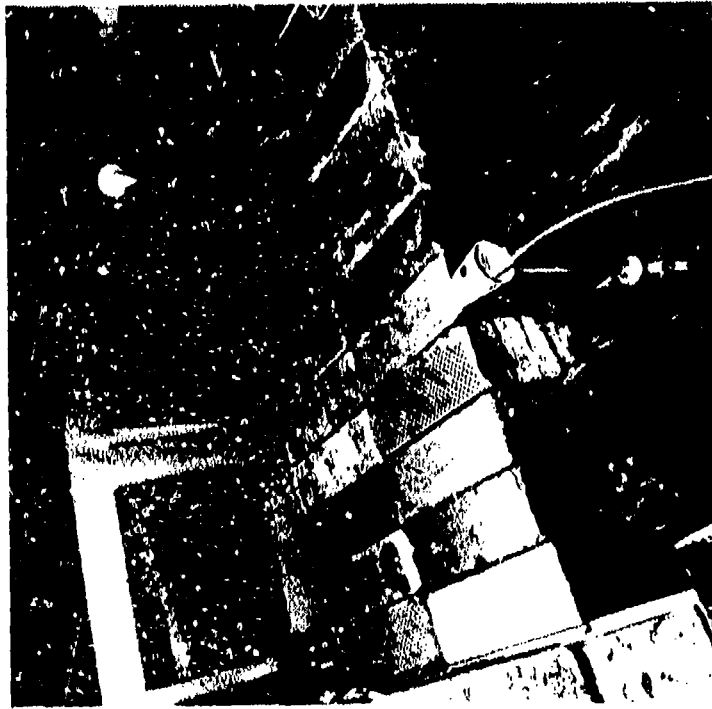
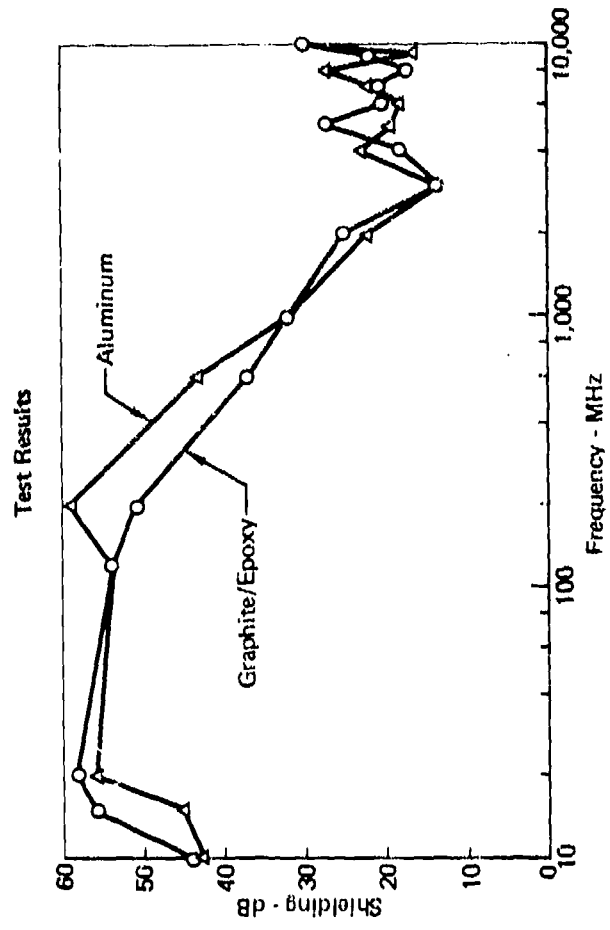


FIGURE 11 - INDUCED VOLTAGE ON TWISTED PAIR, 1 VOLT/METER FIELD

**Simulated Forward
Fuselage Structure
with Access Panel**



Test Setup



**FIGURE 12 - SHIELDING OF ALUMINUM AND COMPOSITE FIXTURES
Relative to Exposed Ground Return Wire**

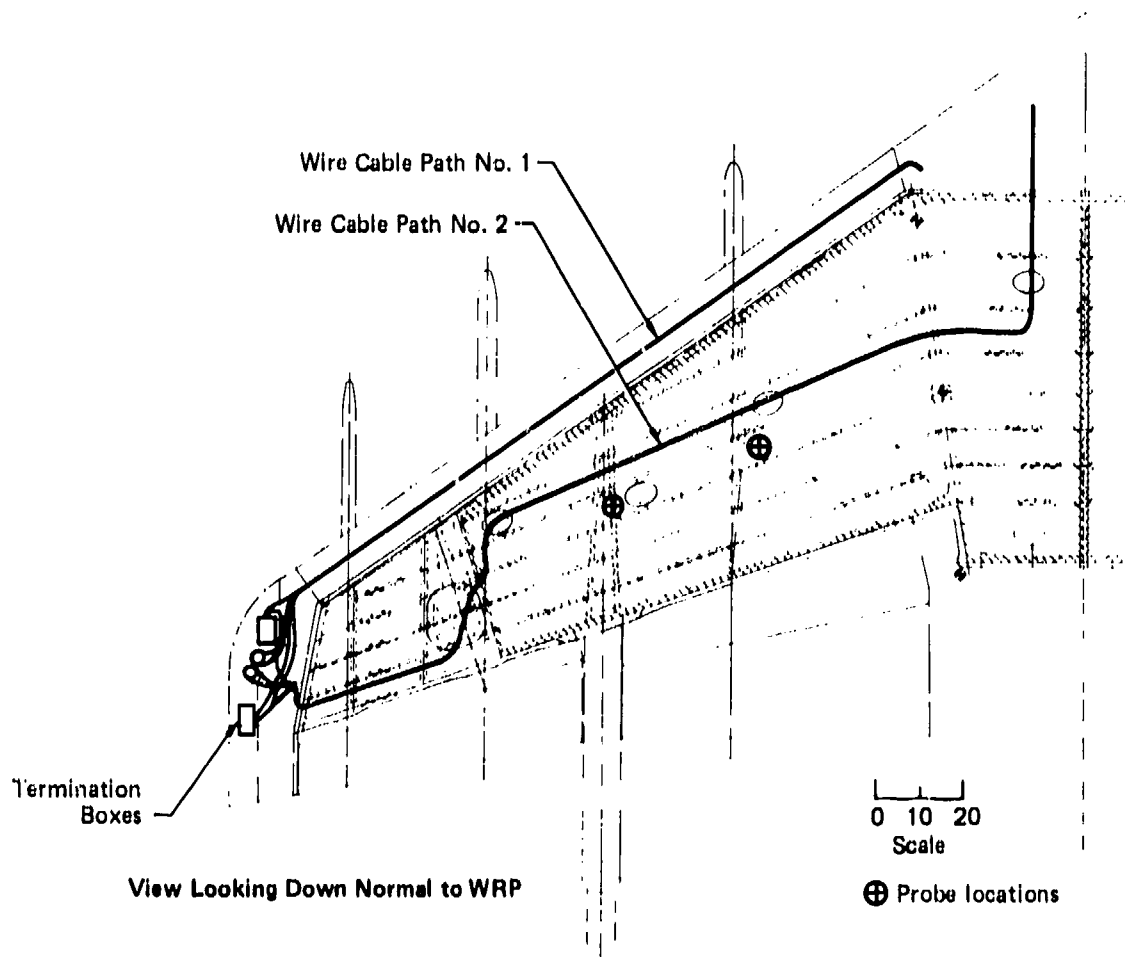
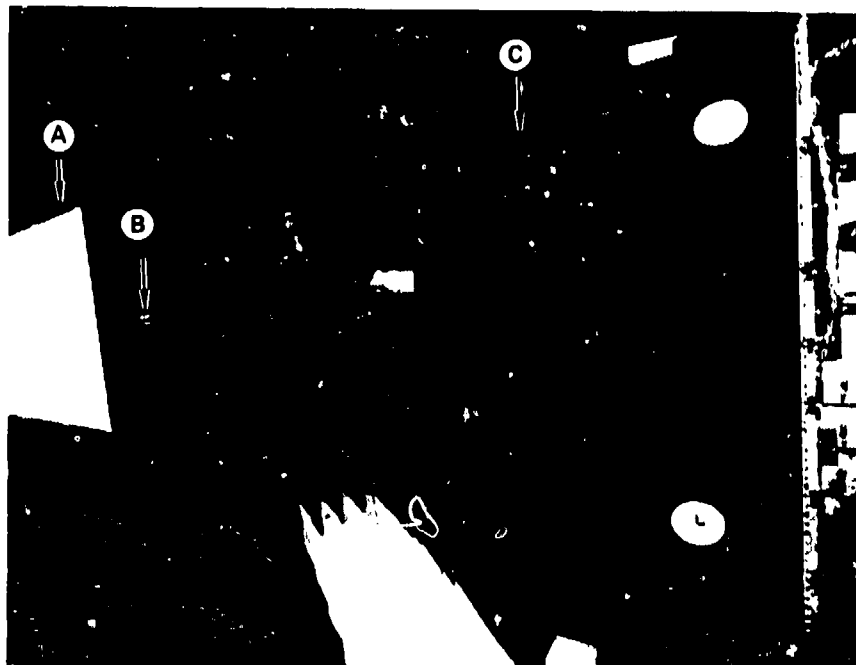


FIGURE 13 - EMI TEST ARTICLE

FIGURE 14 - EMI TEST SET UP IN ANECHOIC CHAMBER
(A) Antenna, (B) Field Meter, (C) Wing

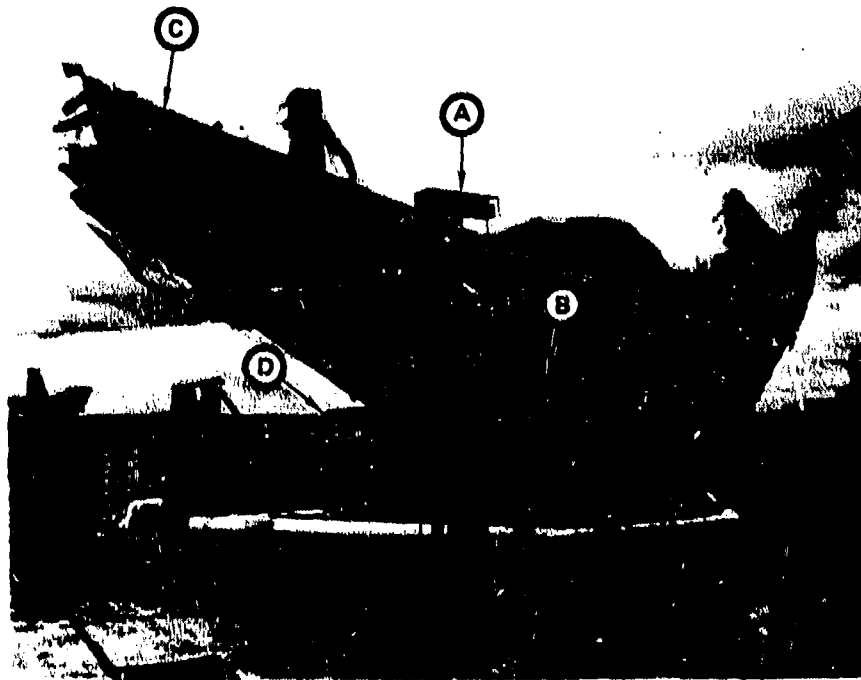


FIGURE 15 - EMI OUTDOOR TEST SETUP
(A) Antenna, (B) Field Meter, (C) Wing, (D) Instrumentation Box

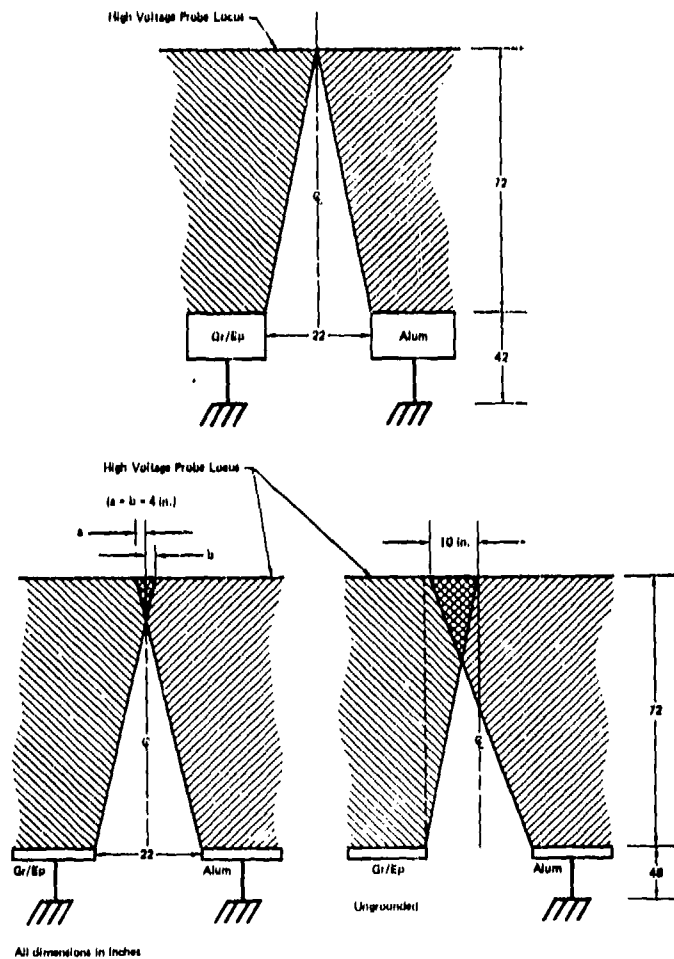


FIGURE 16 - ADJACENT GRAPHITE/EPOXY AND ALUMINUM LIGHTNING ATTACHMENT CHARACTERISTICS

ESSAIS EN VOL POUR L'ETUDE DES PERTURBATIONS RADIOELECTRIQUES
D'ORIGINE ELECTROSTATIQUE

P. Laroche
Office National d'Etudes et de Recherches Aérospatiales
92320 Châtillon - FRANCE

R. Weber
Société Nationale Industrielle Aérospatiale
92153 Suresnes - FRANCE

D. Gall
Centre d'Essais Aéronautiques de Toulouse
31056 Toulouse Cedex - FRANCE

RESUME

Les Services Officiels Français de l'Aéronautique sont à l'origine d'un programme d'essais en vol sur avion METEOR NF11 dont la finalité est la réduction des perturbations radioélectriques d'origine électrostatique. La protection antistatique d'un avion consiste à rendre les parties isolantes de la structure conductrices en surface et à installer des déperditeurs de potentiel. L'expérimentation en vol a été précédée par des essais au sol de polarisation haute tension, destinés à simuler les effets de la triboélectricité. Les déperditeurs de potentiel ont été expérimentés en rendant l'avion entièrement conducteur ; des panneaux diélectriques instrumentés ont ensuite été mis en place pour détecter l'apparition éventuelle de décharges électriques rampantes. Quelques résultats généraux concernant ces essais sont donnés dans cet article.

1 - INTRODUCTION

Les perturbations radioélectriques sur aéronefs consécutives à l'électrification par triboélectricité constituent des problèmes importants depuis plusieurs décades ; dès la fin de la seconde guerre mondiale, des études théoriques et expérimentales ont été entreprises sur ce sujet aux Etats Unis (Gun, 1946). Elles se sont concrétisées, dans les années 60, par la mise au point de déperditeurs passifs pour avion, assurant une évacuation des charges électrostatiques avec un bruit radioélectrique réduit (Nanevich, 1964). Depuis, les conditions de la circulation aérienne ont évolué vers une généralisation des procédures de vol aux instruments, donnant une plus grande importance aux moyens de radiocommunication et de radionavigation. Or, ce sont ces moyens qui sont susceptibles d'être perturbés par les précipitations statiques.

Les matériaux composites à base de fibres de verre ou de fibres de carbone interviennent de plus en plus dans la fabrication des éléments de structure des avions en raison de leur faible masse volumique et de leur grande résistance mécanique. Leur utilisation, sans protection antistatique appropriée, se traduit par un risque d'apparition de décharges électriques de surface très perturbantes.

Afin de définir concrètement les problèmes de perturbations d'origine électrostatique sur avion et d'évaluer les performances de différents dispositifs de protection antistatique, les Services Officiels Français de l'Aéronautique ont mis en place un programme d'expérimentation en vol. Les essais, dont la phase active a débuté en automne 1979, ont été effectués sous la direction de la DTCA (Direction Technique des Constructions Aéronautiques) et ont été coordonnés par le CEV (Centre d'Essais en Vol). Le CEAT (Centre d'Essais Aéronautiques de Toulouse) a assuré les essais de polarisation haute-tension au sol, la SNIAS (Société Nationale Industrielle Aérospatiale) a conduit l'expérimentation relative aux traitements antistatiques des parties structurales diélectriques et l'ONERA (Office National d'Etudes et de Recherches Aérospatiales) a été chargé de l'étude des performances des installations de déperditeurs de potentiel.

Après un bref rappel concernant la nature des problèmes traités, le programme d'essais et l'instrumentation mis en oeuvre sont décrits. Les essais en vol et leur exploitation n'étant pas terminés, seuls sont présentés les premiers résultats généraux.

2 - PROTECTIONS ANTISTATIQUES D'UN AVION

Trois types de phénomènes électrostatiques consécutifs à l'électrification d'un aéronef, peuvent être à l'origine de perturbations radioélectriques ; il peut s'agir soit d'arcs entre des surfaces métalliques isolées entre elles, soit de décharges rampantes sur des parois diélectriques, soit de décharges par effet couronné sur la structure métallique de l'avion.

Le risque d'apparition d'arcs électriques entre éléments structureaux métalliques non reliés est aisément supprimé par l'application d'une procédure de "métallisation" qui fixe les valeurs maximales des résistances admissibles entre différents points de l'avion.

Cependant, l'utilisation généralisée de produits tels que des mastics d'étanchéité ou des revêtements destinés à réduire les frottements sur axes et glissières rend plus critique l'application de cette procédure.

2.1 - Traitement des parties diélectriques

Les éléments diélectriques sur la surface d'un avion sont en général constitués par les ouvertures optiques (hublots, verrières,...), les panneaux de structures en matériaux composites (fibre de verre, de bore ou de carbone) et les carénages des antennes.

Les traitements antistatiques consistent à rendre ces éléments conducteurs en surface afin d'empêcher l'apparition de décharges rampantes. Les ouvertures optiques sont traitées au moyen de dépôts métalliques transparents ; les panneaux composites peuvent être recouverts par un "shoopage" (aluminium, zinc) ou par un clinquant métallique, ils peuvent être peints avec des produits comportant des pigments métalliques ou des particules de carbone; les carènes d'antenne sont traitées par des revêtements à haute résistivité superficielle (de l'ordre de quelques $M\Omega$ carré) de façon à conserver une radiotransparence compatible avec l'utilisation normale des aériens.

2.2 - Evacuation des charges électrostatiques

L'élévation du potentiel de l'avion, conséquence de la charge acquise par triboélectricité conduit inévitablement à l'apparition de décharges "couronne" sur des zones de la structure à faible rayon de courbure. Le signe de la charge étant en général négatif (Harper, 1967), les décharges "couronne" correspondent au régime impulsif de Trichel (Loeb, 1965). Le rôle des déperditeurs de potentiel passifs est d'organiser ces décharges en les découplant des antennes de réception. On peut concevoir des systèmes de déperditeurs actifs (Félici, 1979), mais étudiés essentiellement pour la protection des hélicoptères, leur utilisation à bord des avions ne se justifie pas.

Dans le cas des déperditeurs passifs, le découplage des décharges peut être obtenu grâce à trois procédés (figure 1) :

- le premier schéma(a) consiste à relier le point de décharge \textcircled{a} à la structure \textcircled{b} à l'aide d'une impédance répartie (résistance série, capacité parallèle)(Nanevicz, 1964) de manière à filtrer le courant émis par la structure et à réduire le couplage capacitif entre la décharge et les aériens ;

- le second consiste, en plus de la présence de l'impédance répartie, à diriger le courant j de la décharge orthogonalement au champ radioélectrique qui serait rayonné par les aériens en émission (schéma b) ; le principe de réciprocité prévoit, dans ce cas, que la décharge ne provoque pas de réponse aux bornes des antennes considérées (Nanevicz, 1964). Le dispositif A de la figure 1 est basé sur ces deux procédés de découplage ;

- enfin l'utilisation d'une résistance homogène et répartie de forte valeur (supérieure à $100 M\Omega$) (schéma c) empêche le développement complet de l'impulsion de Trichel, ce qui se traduit par une modification de la répartition spectrale du champ émis par la décharge : le spectre de raies disparaît au profit d'un fond continu de densité spectrale plus faible, ce qui est par conséquent favorable à la réduction du bruit parasite à l'entrée des récepteurs qui sont à bande passante réduite. Le dispositif B de la figure 1 applique ce procédé, le dispositif C est une version améliorée du dispositif B (Boulay, 1979).

3 - DEFINITION DU PROGRAMME D'EXPERIMENTATION EN VOL

3.1 - Objectifs

Les essais devaient mettre en évidence les perturbations radioélectriques provoquées par les phénomènes décrits précédemment et permettre d'effectuer une analyse quantitative de l'efficacité des protections antistatiques appliquées.

Ainsi, par adjonction systématique de panneaux diélectriques de structure, on provoque, dans des conditions d'électrisation élevée, l'apparition de décharges rampantes ; la perturbation qui en résulte est alors caractérisée et différentes protections sont ensuite mises en oeuvre dont l'efficacité peut être évaluée. Par ailleurs, à partir d'un avion à structure métallique, il est possible de mesurer l'efficacité d'une installation de déperditeurs sur l'équilibre électrostatique de l'avion et sur le niveau de bruit radioélectrique parasite. Les résultats obtenus au cours de ces essais doivent permettre une validation des techniques utilisées pour le choix des zones d'implantation des déperditeurs de potentiel sur avion.

L'avion utilisé pour ces essais est un biréacteur METEOR NF-11 (figure 2) ; bien qu'il soit de conception ancienne, les résultats obtenus peuvent être généralisés à d'autres avions de configurations plus modernes.

3.2 - Principe des essais

3.2.1 - Définition de l'état électrique de l'avion en vol

Le courant de charge lié à l'effet triboélectrique est indépendant du potentiel électrique de l'avion par rapport au milieu.

Le schéma électrique de l'avion chargé fait intervenir le courant d'impact total I_i ,

le courant I_d évacué par les déperditeurs de potentiel, le courant de décharge parasite par effet "couronne" I_c sur la structure et le courant I_m émis par les propulseurs (figure 3). En supposant l'avion équipotentiel, son état électrostatique est décrit par la relation suivante :

$$I_i - I_d(V) - I_m - I_c(V) = C \frac{dV}{dt}$$

C est la capacité propre de l'avion et V son potentiel.

Un état d'équilibre peut s'établir et est défini par la relation :

$$I_i - I_d(V_0) - I_m - I_c(V_0) = 0, V_0 \text{ étant le potentiel d'équilibre.}$$

I_c et I_d dépendent de la pression et de la température ; ils ne sont pas des fonctions simples de V . En fait, I_d peut être formulé ainsi :

$$I_d = \sum_{j=1}^N k_j(p, \theta) \cdot V(V - V_j) \text{ pour une installation de } N \text{ déperditeurs ;}$$

(V_j est le potentiel d'amorçage du déperditeur j , k_j est un coefficient de forme, p et θ sont la pression et la température) (Loeb, 1965). Une formulation identique peut être proposée pour I_c :

$$I_c = \sum_{i=1}^M A_i(p, \theta) \cdot V(V - V_i) \text{ dans le cas où } M \text{ points de la structure sont le siège d'une décharge "couronne".}$$

3.2.2 - Méthodologie

L'expérience a comporté quatre phases principales qui sont présentées ci-dessous dans l'ordre logique d'exécution.

- Les essais préliminaires au sol ont consisté à simuler, sur l'avion équipé de l'instrumentation de mesures définitive, des perturbations représentatives de celles qui devaient être analysées en vol, de manière à vérifier l'adéquation des instruments de mesure choisis.
- Les essais de polarisation haute tension au niveau du sol ont simulé l'effet sur le bruit radioélectrique du potentiel de l'avion et donc du courant échangé entre l'aéronef et le milieu ; cet essai était le seul permettant d'estimer, au sol, les performances des déperditeurs passifs (influence de leur nombre et de leur emplacement).
- Les essais en vol de l'avion "équipotentiel" sont intervenus ensuite pour l'étude des installations de déperditeurs passifs. Pour cette phase de l'essai, toutes les parties structurales extérieures de l'avion étaient conductrices (verrières, hublot, ...) et la totalité de la zone d'impact de l'appareil était couverte d'une peinture conductrice de faible résistivité. Toutes les antennes étaient carénées et traitées par une peinture antistatique à haute résistivité.

Dans cette configuration, le niveau de perturbation était tout d'abord mesuré sur l'avion non muni de déperditeurs ; les déperditeurs étaient ensuite progressivement implantés afin de rechercher les meilleures configurations de protection.

- Les essais en vol, concernant l'efficacité des protections antistatiques appliquées sur les surfaces diélectriques de l'avion, ont consisté à effectuer une implantation progressive de panneaux diélectriques à partir de l'avion en configuration équipotentielle et équipé de l'installation optimale de déperditeurs passifs. On a cherché dans ces conditions à caractériser les perturbations provoquées par les décharges rampantes et à localiser les endroits de la structure où elles apparaissaient ; ainsi sept panneaux métalliques étaient remplacés par leurs homologues en matériau composite, recouverts d'une peinture de finition isolante. Ces panneaux étaient instrumentés pour permettre la détection de charges d'impact d'origine triboélectrique ou celle de décharges rampantes et on cherchait également à mettre en évidence une augmentation des perturbations électromagnétiques directement liées à la nature diélectrique de l'avion. Le traitement antistatique des panneaux incriminés était ensuite réalisé et on vérifiait en vol, l'absence de perturbations en présence de précipitations statiques importantes.

4 - DESCRIPTION DE L'INSTRUMENTATION DE MESURE

L'implantation générale des capteurs est indiquée sur la figure 4.

4.1 - Mesure du potentiel électrique de l'avion

Lorsque l'avion évolue dans un nuage chargé à l'intérieur duquel règne un champ électrostatique et si ce champ inducteur est uniforme sur des distances grandes devant les dimensions de l'appareil, le champ en un point A quelconque de la surface de l'avion est une forme linéaire du champ extérieur et du potentiel propre de l'avion :

$$E_A = \alpha_A E_x + \beta_A E_y + \gamma_A E_z + \lambda_A V$$

(E_x , E_y , E_z sont les composantes du champ extérieur suivant un trièdre de référence lié à l'avion, V est le potentiel dû à la charge électrique portée par l'avion, α , β , γ , λ

sont des constantes). Pour déterminer les valeurs de V et de E , il suffit donc de mesurer le champ électrique en quatre points indépendants de la surface. En fait, pour valider les hypothèses sur la configuration électrique du milieu, la mesure est faite en cinq points.

Les capteurs utilisés sont du type "moulin à champ" (figure 5). Les coefficients α_A , β_A , γ_A et λ_A correspondant à chaque point A sont déterminés par des pesées électrométriques sur une maquette à échelle réduite de l'avion : une sphère d'épreuve métallique permet de prélever sur la maquette conductrice, placée dans une configuration de champ connue, une quantité de charge proportionnelle au champ local (figure 6).

4.2 - Évaluation du courant de charge d'origine triboélectrique

Le courant de charge est estimé en isolant des zones impactées de la structure et en les reliant à l'ensemble de cette structure au moyen d'un dispositif électronique de mesure de courant (convertisseur courant-tension). Trois sondes de courant d'impact ont été ainsi constituées sur l'avion : deux sondes identiques sur les bords d'attaque (surface droite $0,256 \text{ m}^2$) et une sur le radome (surface droite $0,64 \text{ m}^2$). Le revêtement des sondes de bords d'attaque était identique à celui de la partie frontale impactée de l'avion (peinture conductrice) ; le radome était traité par un revêtement antistatique radiotransparent.

La surface frontale totale de l'avion, pour une incidence faible correspondant au vol rectiligne est de $8,32 \text{ m}^2$; l'installation permet d'évaluer en principe des courants d'impact maximum compris entre $500 \mu\text{A}$ et $3,5 \text{ mA}$.

4.3 - Mesure des bruits radioélectriques parasites

Les bruits radioélectriques sont détectés à l'aide de récepteurs de laboratoire ou de bord. Ces derniers ne sont pas modifiés mais les informations caractéristiques de la valeur des perturbations sont prélevées sur chacun d'eux au moyen du circuit de contrôle automatique du gain. Les mesures sont effectuées dans les cinq bandes de fréquence suivantes :

- à 10 kHz (bande passante 500 Hz, fréquence de fonctionnement du système Oméga), par un récepteur de laboratoire dont le seuil est de $6 \mu\text{V}$ associé à un aérien capacitif dont la hauteur effective est d'environ 20 cm ;
- à 250 kHz (bande passante 3 kHz, fréquence radiocompas) par un récepteur de radiocompas (seuil voisin de $1 \mu\text{V}$) associé à une antenne de levée de doute de 10 cm de hauteur effective ;
- à 20 MHz (bande passante 3 kHz, radio-communication) par un récepteur BLU dont le seuil est de $1 \mu\text{V}$;
- à 130 et 390 MHz (VOR et ILS) par des récepteurs de communication à modulation d'amplitude (seuil voisin de $1 \mu\text{V}$) alimentés par une antenne V-UHF.

4.4 - Mesure des courants de déperditeurs

Chaque déperditeur de potentiel monté sur l'avion est relié électriquement à la structure au moyen d'une résistance de mesure, de faible valeur ($5 \text{ k}\Omega$) qui ne perturbe pas le fonctionnement du dispositif. L'installation doit permettre de mesurer un courant total des déperditeurs de l'ordre de 3 mA.

4.5 - Instrumentation des surfaces diélectriques

Le radome, différents panneaux de structure, le saumon, le volet d'intrades, le bord d'attaque vertical de la dérive, la glace frontale et un hublot latéral ont été instrumentés :

a) Mesure du potentiel de surface

Le "potentiel de surface" d'un panneau isolant est celui auquel il faut porter un panneau métallique de forme identique pour obtenir le même champ électrique sur un capteur situé à quelques centimètres sous le panneau. Cette grandeur est mesurée sous les panneaux isolants non traités qui peuvent se charger par triboélectricité ou par conduction (figure 7a). Le capteur utilisé est du type à lame vibrante et fonctionne suivant le principe général des "moulins à champ".

b) Mesure du courant de surface

Le courant circulant entre un panneau diélectrique et la structure peut être dû soit à un impact triboélectrique, soit à l'équilibrage par conductibilité de surface, provoqué par la variation du potentiel de l'avion, soit à une décharge rampante vers la structure. Ce courant est recueilli (figure 7b) par un encadrement conducteur placé à la périphérie du panneau.

c) Matériaux diélectriques et protections antistatiques

Les matériaux choisis pour les essais sont représentatifs de ceux utilisés actuellement dans l'aéronautique ; il s'agit de composite verre-résine drapé multi-plies et de composite carbone-résine tissé drapé.

Les protections appliquées sur ces matériaux sont des peintures fortement conductrices au carbone ($R < 10 \text{ k}\Omega$) dans le cas général et des peintures semi-conductrices pour les fenêtres électromagnétiques ($1 \text{ M}\Omega < R < 10 \text{ M}\Omega$).

Les glaces frontales de la verrière sont recouvertes d'un mylar métallisé par dépôt de nickel-chrome et les hublots sont recouverts d'un terfan métallisé par dépôt d'aluminium assurant une transparence dans le visible à 80 %.

5 - ESSAIS AU SOL

5.1 - Essais préliminaires

La partie la plus significative de ces essais consistait à provoquer des perturbations par décharges rampantes ou par effet "couronne". L'avion était posé sur des cales isolantes de 20 cm d'épaisseur ; il était relié à la masse par une impédance répartie de 15 MΩ afin de conserver un potentiel flottant pour les fréquences supérieures à 1 kHz.

Un déperditeur passif (ou une pointe métallique non protégée) était monté aux emplacements prévus sur l'avion. Une décharge "couronne" était alors provoquée sur l'extrémité, à l'aide d'un dispositif de polarisation découplé (figure 8a). Les courbes de la figure 8b montrent le niveau de bruit dû à une décharge négative non protégée à proximité de l'antenne 10 kHz et de l'aérien V.UHF ; une décharge "couronne" s'amorçant directement sur la structure provoque donc une perturbation notable à 10 kHz, 350 kHz et 130 MHz, si le couplage avec l'antenne de réception est élevé. Par contre, à la fréquence de 350 kHz, la perturbation est décelable quel que soit le point de l'avion où apparaît la décharge.

L'utilisation d'un éjecteur de particules chargées permettait de provoquer sur la peinture isolante recouvrant la structure métallique, des décharges rampantes répétitives. On a obtenu un faible niveau de perturbation à 10 kHz (20 dB au-dessus du bruit de fond) mais un niveau élevé à 350 kHz (supérieur à 1 mV ramené à l'entrée du récepteur).

5.2 - Essais de polarisation haute tension

Le principe de l'essai était de porter à une haute tension l'avion éloigné, autant que faire se peut, des masses électriques. Pour ce faire, l'avion, pesant 7 tonnes, a été placé sur des pieds de 2,5 m réalisés à partir d'isolateurs en céramique (figure 9). Le courant donné par l'avion et le potentiel de l'appareil étaient enregistrés à bord. Le générateur utilisé par le CEAT permettait d'appliquer une tension positive ou négative réglable entre 0 et 500 kV. Les essais ont été effectués initialement sans protection, à partir de l'avion équipotentiel, puis avec une implantation progressive de déperditeurs. De même, un montage progressif des panneaux diélectriques a permis de comparer l'effet des différents traitements antistatiques.

Les points essentiels alors mis en évidence sont les suivants :

- la caractéristique globale tension appliquée/courant évacué dépend peu, à forte tension (au delà de 100 kV), du nombre de déperditeurs, de leur emplacement et de leur type ;
- par contre, à faible niveau, le seuil d'apparition du courant est abaissé lorsque les déperditeurs sont montés et, à potentiel constant, le courant évacué est plus important ;
- des essais effectués dans l'obscurité ont montré que certains points de l'avion sont le siège de décharge "couronne" ; il s'agit des pitots qui sont installés sur le bord d'attaque (figure 4) et des carènes d'antennes V.UHF qui sont situées sur l'intrados en extrémité de voilure. La décharge "couronne" sur l'aérien V.UHF, qui est caréné et traité, est peu perturbante en basse fréquence (10 kHz, 250 kHz) sur le radiocompas ; par contre, la décharge aux extrémités des pitots provoque des perturbations très importantes en basse fréquence ;
- dans les conditions du montage, le seuil d'apparition des décharges "couronne" sur les pitots est voisin de 50 kV, un masquage de ces derniers et de l'extrémité des carènes d'antennes augmente le seuil d'apparition des décharges "couronne" jusqu'à 170 kV ;
- dans la configuration équipotentielle, les décharges "couronne" ne provoquent pas de perturbation en VHF et en UHF. Par contre, avec des panneaux diélectriques, les résultats ont été peu significatifs.

5 - ESSAIS EN VOL

Au cours d'environ 60 heures de vol, 9 heures utiles d'impact triboélectrique ont été obtenues ; ce programme d'essais n'est pas totalement achevé ; en effet, une partie importante des configurations diélectriques n'a pu être expérimentée.

Le phénomène d'impact a été recherché à l'intérieur de cirrus, entre 6000 et 10 000 m d'altitude, et aux sommets de nuages plus denses, glacés ou non, entre 3000 et 4000 m. Bien que des séquences d'impact intense aient été obtenues dans les cirrus, les nuages plus bas, tels que des altocumulus, ont donné lieu à des courants élevés plus fréquents. On note que, sauf pour de très rares périodes, le courant d'impact charge l'avion négativement, ce qui est conforme aux résultats déjà acquis dans ce domaine par d'autres expérimentateurs (Nanevicz, 1964).

6.1 - Mesure du potentiel de l'avion

En règle générale, le calcul du potentiel, effectué par la méthode décrite en 4.1, a donné des résultats satisfaisants car les valeurs déduites de la combinaison quatre par quatre des cinq mesures de champ sont sensiblement identiques. Toutefois, dans certaines configurations très perturbées (champ extérieur élevé et inhomogène), la correspondance entre les valeurs relevées n'est plus correcte et l'utilisation des cinq mesures est alors essentielle pour supprimer toute indication aberrante.

Le caractère essentiel de ces mesures est que, pour la majorité des vols réalisés, les hypothèses sur la nature électrique du milieu sont validées ; en particulier, ni la charge d'espace de signe contraire laissée par l'avion par triboélectricité, ni la charge d'espace créée par les déperditeurs de potentiel n'ont d'influence notable sur le champ électrique mesuré sur la structure.

6.2 - Mesure du courant d'impact

On a tout d'abord constaté en vol une même tendance entre les indications des trois sondes d'impact et la valeur du potentiel : même signe, même sens de variation. Cependant, le rapport entre les indications respectives de ces capteurs n'est pas constant ; les sondes situées sur les bords d'attaque, qui sont identiques, fournissent toujours des indications très voisines ; par contre, le courant recueilli sur la sonde de radome n'évolue pas dans un rapport constant avec celui des sondes latérales. Ainsi au cours d'une traversée à vitesse constante dans les précipitations, l'effet de l'inhomogénéité des constituants locaux a pu être observé par de brusques variations de régime entre les sondes latérales et la sonde frontale.

Toutefois, dans la plupart des cas, le régime de fonctionnement de ces sondes reste établi pendant la traversée du nuage, ce qui permet d'évaluer le courant total reçu par l'avion.

6.3 - Résultats obtenus

Plusieurs vols réalisés par beau temps ont montré que les propulseurs de l'avion n'ont pas d'influence sur le potentiel de l'aéronef.

Les courbes de la figure 10 montrent le bruit radioélectrique enregistré à 10 kHz et 350 kHz en fonction du potentiel avion et les courants d'impact pour un vol équipotentiel sans déperditeurs ; on distingue l'apparition brutale d'un bruit à 350 kHz lorsque le potentiel dépasse la valeur de 90 kV. Pour d'autres vols avec déperditeurs, on a remarqué que ce bruit apparaît sensiblement pour la même valeur du potentiel et ceci indépendamment du nombre et de l'emplacement des déperditeurs : ce point a permis ainsi de confirmer l'amorçage des pitots situés sur les voilures.

Afin de poursuivre utilement l'expérimentation dans des conditions d'électrisation plus sévères, une protection antistatique expérimentale des pitots a été mise en oeuvre. L'adjonction de ces protections a élevé le seuil d'apparition d'une décharge non protégée perturbante sur l'avion ; ce seuil est passé de 90 kV à 250 kV.

Les mesures de bruit radioélectrique dans la configuration équipotentielle ont mis en évidence les points suivants :

- a) pas de perturbations détectées dans le domaine VHF ou UHF, liées à l'apparition de décharges "couronne" sur la structure ;
- b) ces mêmes décharges "couronne" sur la structure provoquent un bruit de valeur moyenne élevée à la fréquence de 350 kHz (fréquence située dans la bande d'utilisation du radio-compass) ; elles provoquent une perturbation faible à 10 kHz même dans le cas d'un couplage important avec l'aérien de mesure (6 dB au-dessus du bruit extérieur) ;
- c) une première analyse des résultats portant sur l'efficacité des déperditeurs montre que pour de faibles valeurs du potentiel de l'avion, le nombre de déperditeurs intervient sur la valeur du courant évacué ; par contre, lorsque le nombre de déperditeurs est suffisant, l'efficacité de décharge n'en dépend plus ; ces résultats apparaissent clairement sur les courbes de la figure 11, les vols étant effectués sensiblement à la même altitude ;
- d) au cours d'un vol à 4000 m d'altitude, l'avion étant équipé d'une installation de déperditeurs, aucune décharge "couronne" parasite ne s'amorce sur la structure alors que le potentiel a atteint 300 kV pour un courant d'impact voisin de 1 mA ;
- e) une première comparaison entre les essais de polarisation haute tension réalisés au sol et les essais en vol peut être établie à l'aide des courbes de la figure 12 ; on constate que la caractéristique d'efficacité des déperditeurs en vol, correspond à un courant évacué nettement plus élevé qu'au sol. Deux effets sont à l'origine de cette différence d'efficacité :
 - les essais au sol ne font pas intervenir l'effet du vent sur le courant évacué par les déperditeurs ;
 - l'effet d'altitude correspond à une diminution de la pression et se traduit par une augmentation du courant évacué ;

- f) L'implantation de panneaux diélectriques non traités sur l'avion n'est caractérisée par l'apparition de décharges rampantes. Les courbes de la figure 13 montrent l'effet de ces décharges sur l'évolution du potentiel mesuré derrière deux panneaux particuliers traités ; ces décharges provoquent des perturbations à fréquences élevées (130 MHz et 390 MHz) ; ces résultats sont en cours d'analyse.

7 - CONCLUSIONS

Des essais en vol sur un avion METEOR ont permis de mettre en évidence l'importance des perturbations d'origine électrostatique, le domaine de fréquence le plus affecté étant celui correspondant au radio-compass. L'avion peut atteindre en vol des potentiels élevés dépassant 250 kV pour des courants d'impact de l'ordre de 1 mA. On a montré que, pour de tels courants, les déperditeurs de potentiel passifs fonctionnent sans provoquer de bruit radioélectrique sur les récepteurs de bord.

L'apparition de décharges rampantes sur des parois diélectriques non protégées a également été mise en évidence en vol. La réalisation d'essais complémentaires ainsi que l'exploitation des résultats de vol doit se poursuivre pendant l'année 1980.

REFERENCES

Boulay J.L., "Elimination des perturbations radioélectriques d'origine électrostatique sur avions". Recherche Aérospatiale n° 1979-2, pp. 101-120, 1979.

Gun R. et al, "Les précipitations atmosphériques et le brouillage radioélectrique à bord des avions". Traduction technique n° 946, G.R.A., 1976.

Harper W.R., "Contact and frictional electrification". Oxford Clarendum Press, 1967.

Félici N. et Larigaldie S., "Etude expérimentale d'un déchargeur électrostatique pour hélicoptère", Revue de Physique Appliquée, 15, pp. 81-91, 1980 et TP ONERA n° 1980-5.

Loeb L.B., "Electrical corona. Their basic physical mechanisms", University of California Press, 1965.

Nanevics J.E. and Tanner R.L., "An analysis of corona generated interference in aircraft" and "Some techniques for the elimination of corona discharge noise in aircraft". Proceedings of the IEEE, vol. 52, n° 1, 1964.

Robb J.D., ILS/VOR - Navigation and approach errors from precipitation static interference". AFAL TR 72-325 (AD 75 2551), Part I.

Truax R.L., AFAL TR 72-325, Part II.

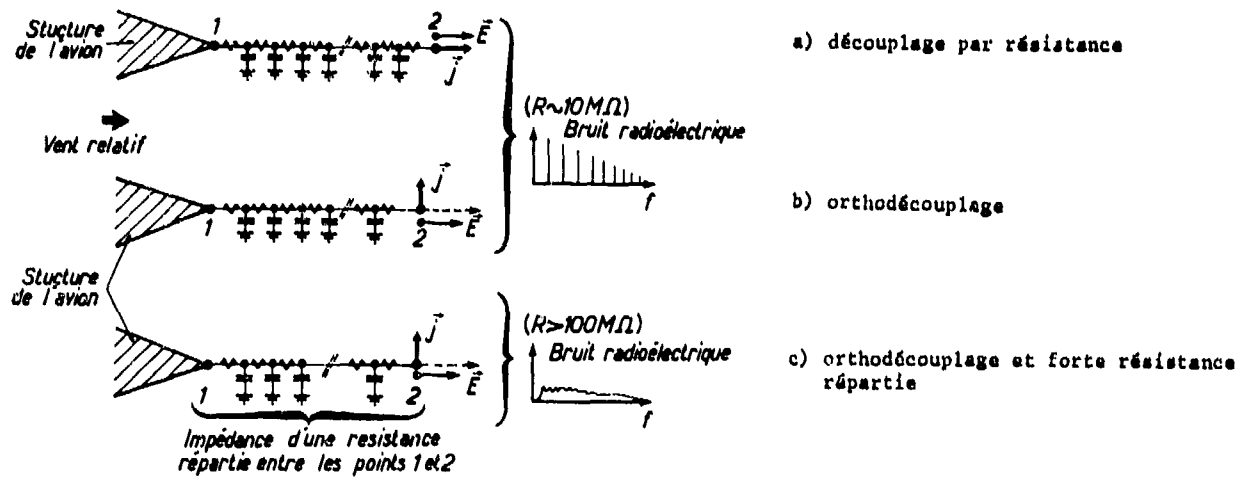


Fig. 1 - Déperditeurs passifs.

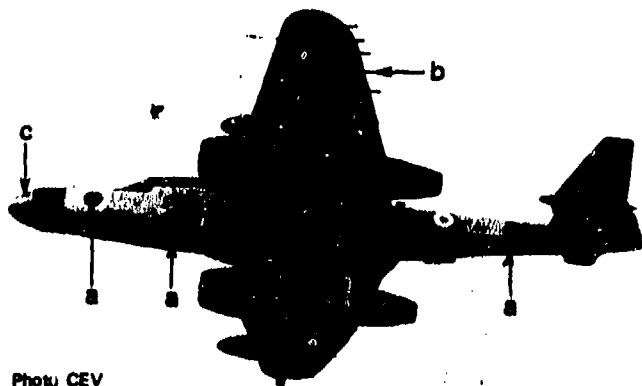
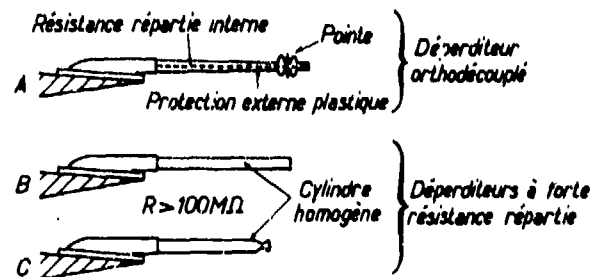


Photo CEV

Fig. 2 - Avion d'essai "METEOR NF 11-03".

- a) capteur de champ
- b) déperditeurs de potentiel
- c) sonde d'impact

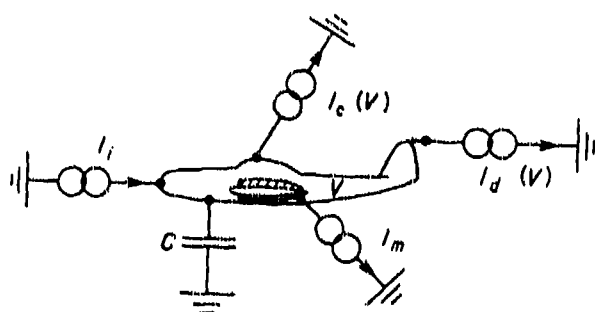


Fig. 3 - Schéma représentant l'état électrique de l'avion.

Fig. 4 - Instrumentation de l'avion d'essai

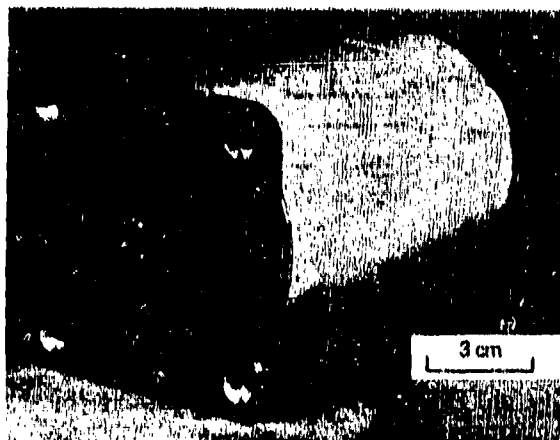
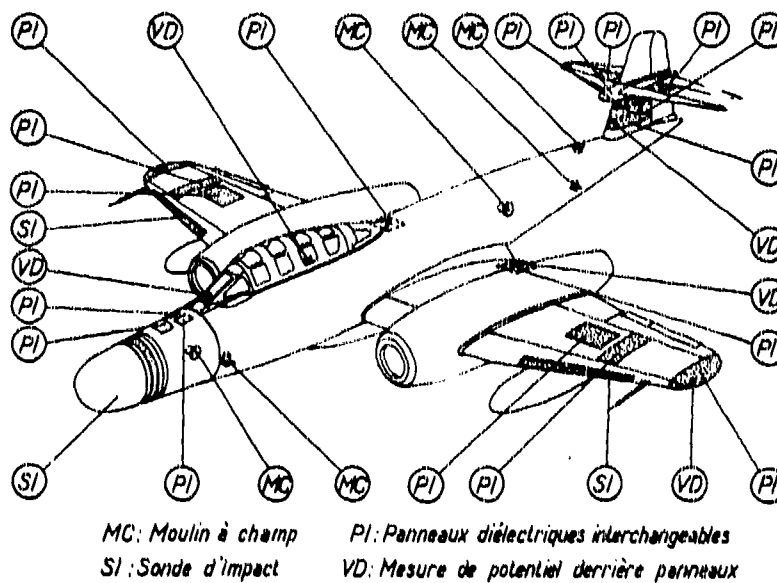
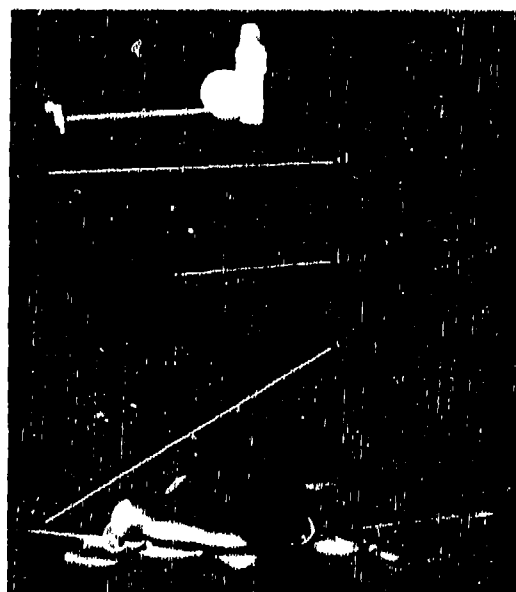
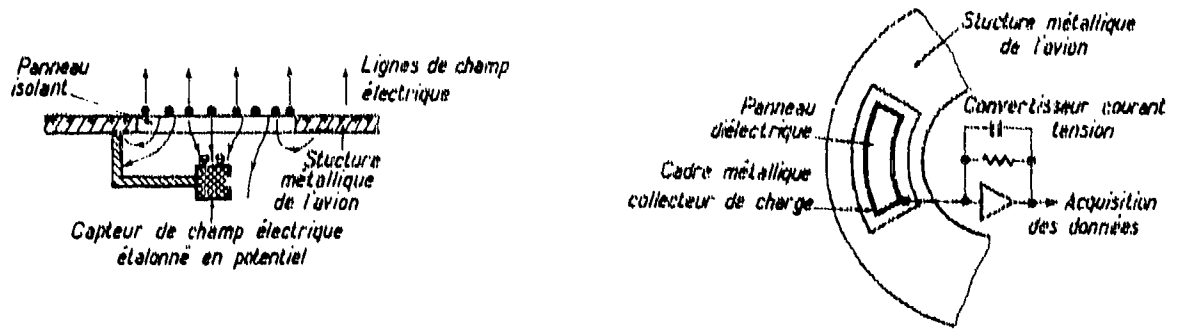


Fig. 5 - Moulin à champ embarqué sur l'avion METEOR

Fig. 6 - Mesure électrométrique sur une maquette conductrice de l'avion.

- a) pendule isolant
- b) plan inducteur
- c) sphère d'épreuve dorée \varnothing 6 mm

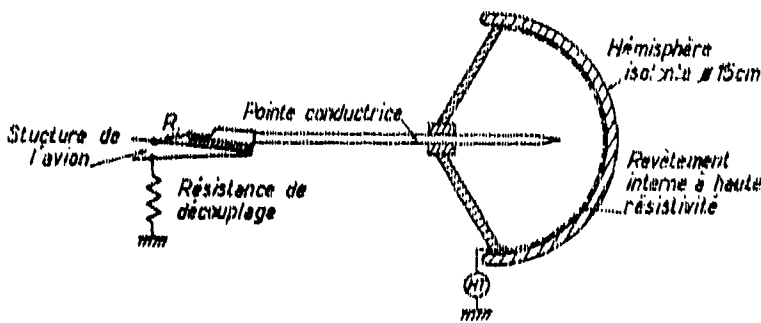




7a - Mesure du potentiel des panneaux induits.

7b - Mesure du courant de surface.

Fig. 7 - Instrumentation des panneaux diélectriques.



8a - Dispositif de polarisation des pointes et des dispersiteurs.

8b - Perturbation par une décharge "couronne" négative fortement couplée aux antennes

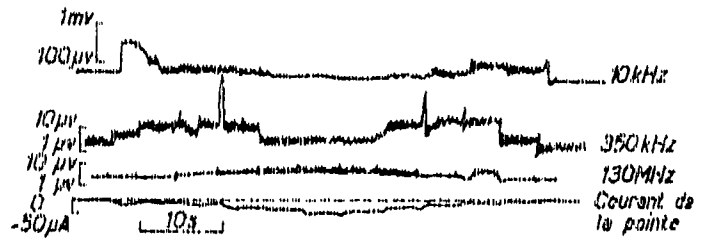


Fig. 8 - Essais préliminaires au sol.



Fig. 9 - Essais de polarisation haute tension au CEAT.

- Caractéristique de l'alimentation
- tension réglable de 0 à 500 kV,
 - courant : 50 mA max.
 - taux de régulation : 1 %
 - dispositif d'annulation des courants de fuite,
 - télécommande par pupitre.

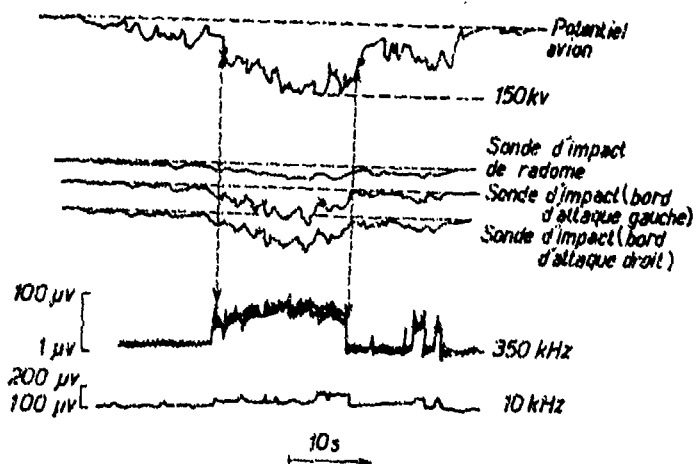


Fig. 10 - Séquence de vol avec l'avion équipotentiel sans déperditeur de potentiel.

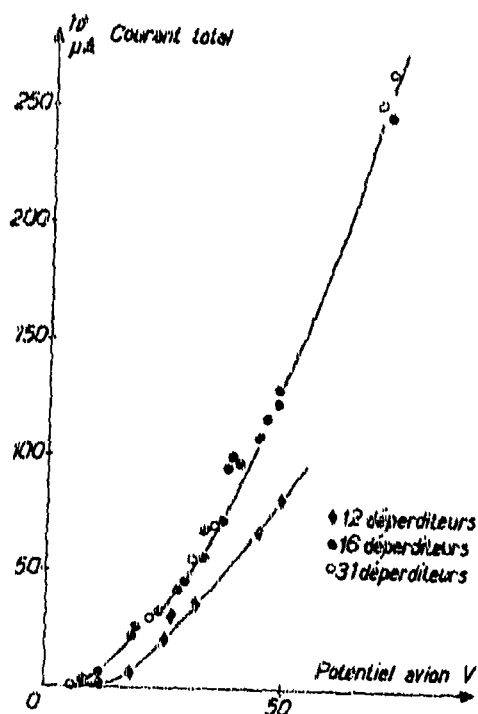


Fig. 11 - Efficacité de décharges des déperditeurs de potentiel.

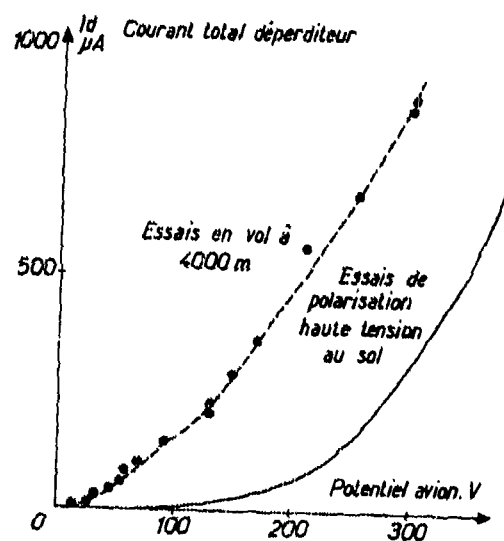


Fig. 12 - Comparaison de l'efficacité des déperditeurs au sol et en vol.

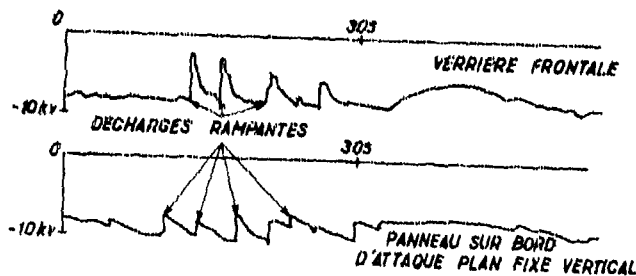


Fig. 13 - Détection en vol de décharges rampantes sur deux parois diélectriques non traitées.

THE BEHAVIOUR OF CFRP PANELS IN METAL
AIRCRAFT DURING SIMULATED LIGHTNING STROKES

B.J.C. Burrows and A.W. Hanson
UKAEA Culham Laboratory
Abingdon, Oxfordshire OX14 3DB
England

S U M M A R Y

The current flow-pattern in a CFRP panel and the surrounding metal skin changes significantly during a current pulse simulating a lightning stroke. Measurements of the current distribution changes are made and compared with a theoretical treatment. The effects of different lay-ups of CFRP and different methods of mounting the panel are described.

Observations are made of the influence of thin metal foils used to cover the outer surface on the screening provided by CFRP panels to simulated lightning current pulses. Screening by complex panels consisting of an aluminium honeycomb sandwiched between two CFRP skins is compared with these results. The direct damage suffered by both types of panels is also described, and their behaviour analysed theoretically.

1. I N T R O D U C T I O N

In parallel with research and development on the mechanical properties of carbon fibre reinforced plastic (CFRP) composites for aircraft use, the electrical properties are being examined in several centres. Lightning poses a special type of electrical threat to aircraft and must be considered where carbon fibre composite is used as a skin material. There is then the possibility of a direct lightning attachment to the CFRP panel, or more frequently, to a pulsed high intensity conducted current.

This paper reviews some of the contributions by Culham Laboratory Lightning Studies Unit on the electrical performance of CFRP skin panels in a metal aircraft, and discusses current flow, screening of induced voltages, protection techniques and direct damage.

2. C O M P A R I S O N O F M E T A L A N D C A R B O N F I B R E S T R U C T U R E S

An all metal fuselage of conventional construction uses aluminium alloy skinning, at the very least 1mm thick and more normally 2mm or more. Fortunately, aluminium is one of the best electrical conductors, endowing the aircraft with a very effective self-shielding to lightning current since the high amplitude fast rising pulses of current flow only on the outside skin ('skin effect') and neither magnetic flux nor current diffuse to the inside surface in times of interest. The current distribution around the fuselage is not resistively controlled, but inductively controlled and depends on the fuselage or wing cross section profile. For example a wing shows a larger surface current density J_s at the leading and trailing edges than at the mid-chord position by a factor of approximately 4, whereas the thickest metal and hence lowest resistance is in the centre box section. If current flow were resistively controlled, the box section would carry most. However, carbon fibre composites have a resistivity of three orders of magnitude (10^3) greater than aluminium and skin effect is not discernable below approximately 10MHz. (The diffusion time to the inside surface of a 2mm CFRP panel is a few nanoseconds only.)

Significant resistive voltages will be produced in a CFRP structure - up to 1000V/m. The diffusion flux will couple to circuits within the aircraft close to the skin, generating voltages of the same order in the wiring.

3. R E S I S T I V E A N D D I F F U S I O N F L U X I N D U C E D V O L T A G E S

As an illustration of the importance of resistive voltages in aircraft containing carbon fibre, Figure 1 shows a metal 'fuselage' with a carbon fibre skin panel. Diffusion flux is shown penetrating the carbon fibre panel, so that it enters and leaves the internal volume, but it does not cut the metal. The similarity between the flux patterns in Figures 1 and the open aperture flux in Figure 2 is clear.

However, the time variation of the flux within the interior is not the same in the two figures. In Figure 2, the rate of change of flux is proportional to the rate of change of lightning current. By contrast, $d\phi/dt$ within the interior of Figure 1 is proportional to v_R (the resistive voltage along the CFRP panel). This can be verified by considering a closed path ABCD and (ABC'D') on the inside surface of the metal and CFRP as in Figure 3. Path AB is in the centre of the panel. The total sum of pd's and induced emf's around the path ABCD must equal zero. Therefore the resistive pd along path AB must be balanced by an emf generated by the diffusion flux rate of change $d\phi_D/dt$ entering via ABCD and leaving via ABC'D' as in Figures 1 and 3. All other pd's in this loop are zero since skin effect in the metal keeps current mainly to the outside surface. Therefore

$$v_R = J_B \rho_m = \frac{d\phi_D}{dt} \quad (V/m) \quad (1)$$

J_B is the local bulk current density in the CFRP (assumed constant across the thickness of the panel) and ρ_m is the mean effective resistivity of the CFRP.

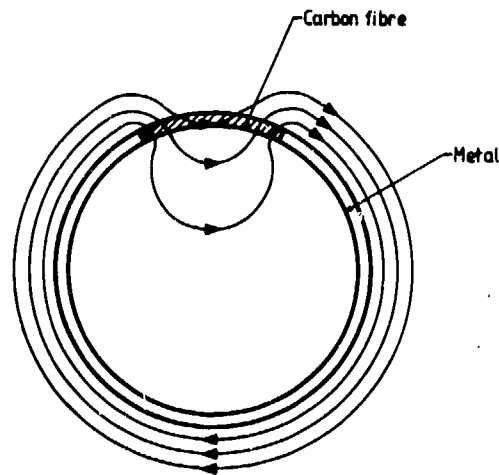


Fig. 1 Magnetic diffusion flux entering fuselage interior through carbon fibre composite panel. Field lines cut the CFRP but not the metal

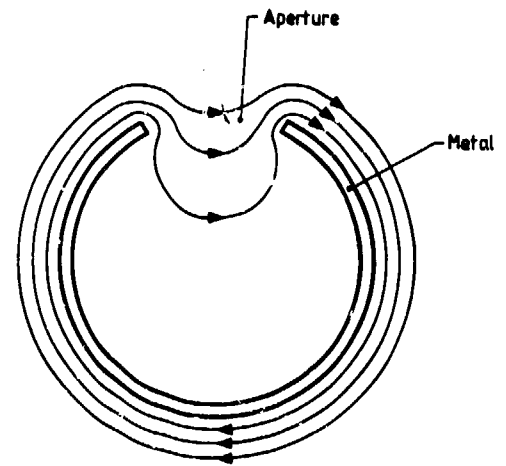


Fig. 2 Magnetic flux lines in an aperture of a metal structure

Two important conclusions from equation 1 are that diffusion flux induced voltages will have nearly the same waveform and spectrum as the current pulse, so lacking the high energy at high frequencies which aperture flux voltages exhibit, and that the maximum voltage which can be induced on a single turn loop by diffusion flux is equal to the

peak $J_B \rho_m$ voltage on the panel through which the diffusion flux is penetrating. Diffusion flux voltages can therefore be calculated quite simply from the resistive voltage as described previously. Thus it can be seen that if the CFRP panel is sufficiently thick $J_B \rho_m$ will be small so providing good screening against the changing magnetic field. Also, because CFRP is a conductor, it acts as a Faraday shield, it external electric fields and shields them effectively even in thin sheets.

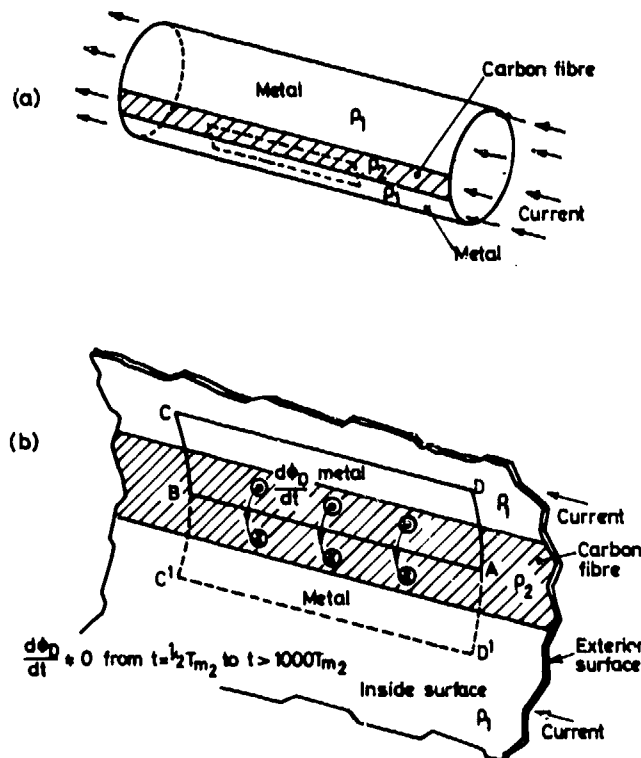


Figure 3 Interior flux distributions for cylindrical model (b) is an enlarged view from the inside of the cylinder, of the dashed loop shown in (a)

4.

CURRENT DENSITY IN CFRP PANELS

In considering CFRP metal structures we use J_B , the bulk or volume current density in (A/m^2) which is the appropriate current density for consideration of local voltages within the metal. The electric field along the surface of a conductor is $J_B \rho_m$ where J_B is the current density in the surface layer. However, in any discussion of skin effect and inductive current distribution, the surface current density J_S (A/m) is a useful concept. It is a measure of current flowing along a conductor per unit width. The two are related (in CFRP panels in which skin effect is negligible) by the following equation, in which h is the panel thickness:

$$J_B = \frac{J_S}{h} \quad (A/m^2) \quad (2)$$

Now, owing to the very fast diffusion time in CFRP referred to above, the value of J_B does not vary through the thickness of the panel for all the components of lightning less than about 1MHz, but at high frequencies skin effect is apparent. Above 10MHz appreciable variation of J_B will occur through the thickness of the skin material.

Regarding the low frequency current distribution across the width of a panel, measurements were made of the low frequency variation of J_S (and hence J_B) on a CFRP panel covering a square aperture in the Hawker Hunter fuselage using a fast pulse waveform. Current densities were obtained by taking measured values of voltages between three pairs of contact points as shown in Figure 4 and dividing by the mean bulk resistivity ρ_m , which had been established in previous work on a small test fixture (Burrows, Luther and Pownall 1977). For these panels which incorporated $8 \times 45^\circ$ plies and $8 \times 90^\circ$ plies $\rho_m = 7500 \times 10^{-8} \Omega m$. These values were then converted to the surface current density J_S .

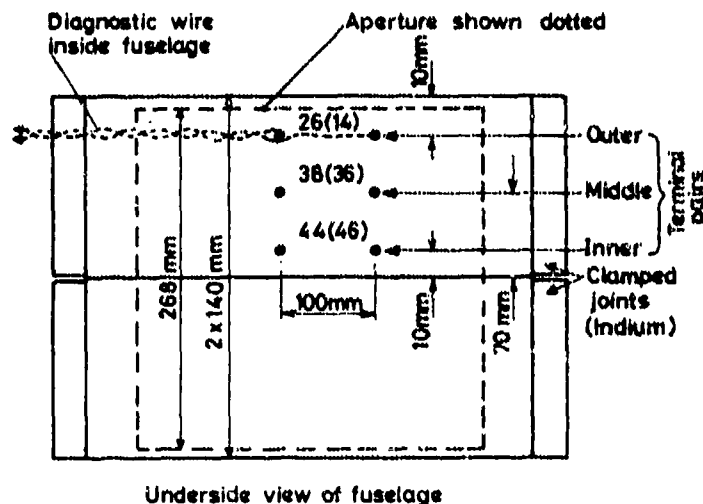


Fig. 4 Test arrangement for current density and voltage measurements

surprising at first, but an insight to this distribution can be obtained by consideration of the rectangular path ABCD of Figure 3. If flux is entering and leaving all over the area of the CFRP panel, then paths similar to ABCD, but with AB closer to the metal, will enclose less flux, and from equation 1, the local J_B (and hence J_S) will also be less, so giving the peaked profile observed.

The time variation of current distribution further complicates the analysis, and the above discussion applies to peak values. To understand the time variation, let us take a fast rising unidirectional pulse of current through the whole structure as in Figure 6 (lower trace).

The voltage along AB (Figure 3) has the form of the upper trace indicating a reversal in current flow at two divisions after the start. Although initially this is also surprising, clearly all the flux that diffuses in to give the pattern shown in Figure 1 has to diffuse out again when the current falls, so $d\phi/dt$ must change sign, and therefore J_S (or I) changes sign within the CFRP. This would not occur in a circular homogenous structure of CFRP but will occur in any representative structure in which high and low

Figure 5 shows the variation of peak current density over the panels as measured in the tests, assuming both halves of the panel are symmetric.

The dashed line indicates the mean surface current density J_S (mean) around the approximately circular fuselage estimated from:

$$J_S \text{ (mean)} = \frac{I_L}{\pi D}$$

$$\frac{58.3 \times 10^3}{\pi \times 1.3} = 14 \times 10^3 \text{ (A/m)} \quad (3)$$

The peak current density in the centre of the panel is seen to be very close to the mean current density around the fuselage so confirming the observation above that the inductive voltage from such a high di/dt pulse is sufficient to drive nearly the full average current through the highly resistive CFRP panel. Hence a first estimate, a 'worst case' figure, of maximum current density in the centre of a carbon fibre panel can assume inductive sharing of current around the fuselage or wing. The humped nature of the current distribution might seem

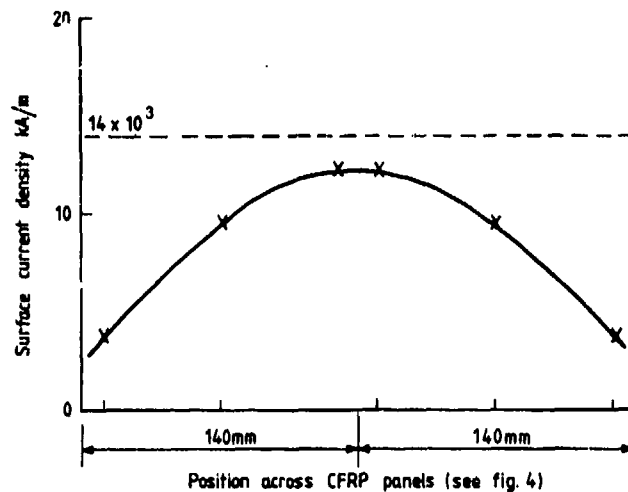


Fig. 5. Current density across CFRP panel

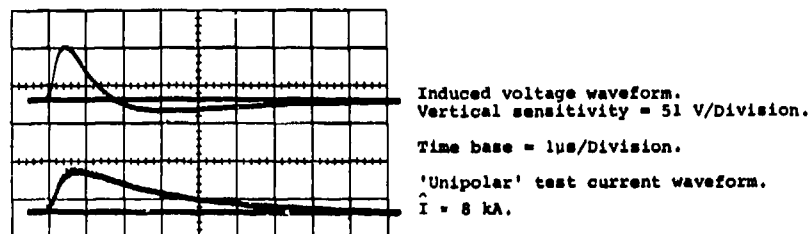


Fig 6 IR voltage measured as in Fig 4 showing current reversal. This occurs when the CFRP is shunted by metal structure.

5. EFFECTS OF CARBON FIBRE PLY LAY-UP ON RESULTS OF TESTS

The effective panel resistivity in the direction of current flow determines the magnitude of induced voltages and the magnitude of the internal flux densities. Basically panel resistivity depends on:-

1. Number of plies at 0° or 45° to direction of current flow (90° plies do not contribute to the conductivity):
2. Presence of a conducting honeycomb (see below):
3. Fixing techniques, i.e., whether countersunk screws, quick release fasteners, or simple hinges are used on the side perpendicular to the current flow direction.

6. FOIL SCREENING

Some work has been done on induced voltage reduction on carbon fibre panels using $5\mu\text{m}$ (0.2×10^{-3} inches) aluminium foils. In the tests, strips were stuck to the CFRP test panel measuring $.5\text{m} \times .5\text{m}$, both overlapping and butted. In some tests the foil joints were parallel to the current flow and in others perpendicular.

The results of the tests indicate that:-

1. For parallel strips, the induced voltage could be easily predicted from the combination of the parallel resistance of the foils and the CFRP panel, and the joint type was immaterial. $5\mu\text{m}$ foil improved the screening of a thin CFRP panel by a factor of 20.

conductivity materials are used, or where construction gives the possibility of current concentration e.g. at longerons. This effect has been observed in numerous tests.

2. For perpendicular joints in the foils, sparking occurred at both butted and overlap joints and the induced voltages on wires within were much higher than at one above and more variable from pulse to pulse.

7. ALUMINIUM HONEYCOMB/CARBON FIBRE PANELS

Aluminium honeycomb sandwich panels having carbon fibre skins provide much technical interest and complexity owing to the large number of variables:-

- a) Ply lay-up, thickness of skin, and orientation of laminae in the outer skin:
- b) Properties of any insulating layer between outer skin and aluminium.
- c) Thickness, density and ribbon orientation of honeycomb.
- d) Properties of any insulating layer between aluminium and second laminate.
- e) Ply lay-up etc. of inner skin.
- f) Design of close-outs.
- g) Fastening techniques.
- h) Moulding techniques.

Whereas carbon fibre laminates, within themselves are linear over more than five orders of magnitude of current density (Burrows, Luther and Pownall 1977) the joints to fasteners, CFRP/aluminium interfaces and the close-outs give considerable non-linearity in the V/I characteristic as a function of absolute amplitude (Burrows, Luther and Pownall 1977). For example, a certain type of joint design was shown to have a V/I characteristic as below:-

$$V \propto I^{0.85} \quad (4)$$

so dc testing will give misleading results since current densities have to be low to avoid heating. The characteristic given in equation (4) was obtained in fast pulse tests. More recent tests have shown that the ribbon orientation (ie., parallel to or perpendicular to current flow) and the extent to which the ribbons make contact with the fasteners determines the overall performance as lightning screen.

The non-linearity of this and other composite materials has important consequences regarding the testing of large structures, which require very high current pulses for realistic results (Burrows 1980).

8. NOMEX HONEYCOMB/CARBON FIBRE PANELS

Nomex honeycomb sandwich panels do not display the same complexity as aluminium honeycomb since nomex is an electrical insulator. Therefore the performance of the sandwich panel depends upon the CFRP skins only, and the close-out and fastening details. The same applies to all insulating honeycomb materials, e.g. the new glass fibre honeycomb.

9. DIRECT DAMAGE TO CFRP AND CFRP/HONEYCOMB PANELS

Direct damage to carbon fibre composites may occur as a result of:

- 9.1 Arc attachment damage.
- 9.2 Ohmic heating.
- 9.3 Sparking at glue lines or other insulating boundaries in either the CFRP itself or in metal components imbedded in it (e.g. aluminium honeycomb).

9.1 Arc Attachment Damage

As with metal skins, direct arc attachment to a CFRP skin causes arc root damage due to the intense local heating by the arc and by the high local current density. However, the laminated construction of CFRP helps to minimise burn through by the arc because of the electrical and thermal insulation between layers. Usually no more than three plies are burnt through, and the damage sustained is confined almost entirely to the surface. The resin is burnt away, the carbon fibres break, and this produces the typical tufted appearance of arc root damage. Thin panels can be punctured, or fractured by the acoustic and magnetic pressures caused by very high pulsed currents. This damage differs from that described above in that the resin is not burnt away, and the composite is delaminated, fractured, and splintered, but the splinters remain discrete pieces of composite complete with their resin. Should a high pulse current be followed by a continuing current, the splinters of composite will be subject to damage from the arc as will any material behind the panel such as the core of a sandwich panel.

9.2 Ohmic Heating

Ohm's law is obeyed in CFRP both for low dc currents and high pulse currents of short duration with low action integrals where the temperature rise is small. This is true over a very wide range of current densities. However, in 1977 Scruggs and Gajda observed that the temperature co-efficient of resistance of the fibres becomes negative above 65°C, and the bulk resistivity of their sample became non-linear at the transition temperature of the resin system used ($\approx 110^\circ\text{C}$). Relaxation of the interfibre contact pressures probably caused this non-linearity. Since CFRP laminates have an effective bulk resistivity of around 3000 to 3750 $\times 10^{-6} \Omega\text{m}$ ($\approx 10^3$ greater than aluminium) greater temperature rises will occur than would be experienced in a metal. Temperature rises should be kept to below 65°C.

9.3 Sparking at Glue Lines and Interfaces

Current crossing interfaces within the composite or at metal/composite joints is often forced to take a disadvantageous path through the CFRP e.g. crossing interlaminar boundaries. There is therefore a far greater potential hazard at such interfaces than exists at a metal/metal interface.

Particular care must be taken at glued interfaces where there is a possibility of current crossing the glue line. In such cases current will tend to concentrate in voids in the glue causing explosive expansion of the air in the void, and subsequent failure of the glue line.

In a similar manner aluminium honeycomb in CFRP sandwich panels can give rise to explosive delamination of the panel when current in the honeycomb crosses the honeycomb inter-foil glue lines. Aluminium honeycombs are very sensitive to this type of failure and a detailed investigation of the lightning hazards must be made if they are used in aircraft.

10. SURFACE PROTECTION OF CFRP WITH METALLIC LAYERS

Protection against the effects of arc root attachment damage can be achieved with little weight penalty, by the use of very thin surface layers of aluminium; flame sprayed or foil. This layer can be painted, and acts as a 'sacrificial' layer in the event of a lightning attachment, and is preferentially vaporised by the arc owing to its lower arc voltage than carbon rich arcs. Such a layer protects against both the arc root and the ohmic heating damage referred to above.

11. CONCLUSIONS

From the structural engineers standpoint, CFRP offers many advantages in terms of strength, weight, and stiffness. However, the electrical properties of carbon fibre are such that great care is needed in the application of CFRP to aircraft structures to avoid EMC and lightning problems. This paper has illustrated some of the characteristics, some problems and solutions which are important for proper use of CFRP.

To build safe aircraft, containing large amounts of composite, will require close co-operation between the electrical and structural engineers.

12. ACKNOWLEDGEMENTS

The authors acknowledge the support given by the Procurement Executive, UK Ministry of Defence for this work.

13. REFERENCES

Burrows B.J.C., Luther C.A., Pownall P. Resistive Measurements on Bulk CFRP and on Metal/CFRP Joints. Culham Lightning Studies Unit Memorandum Number 56 Culham Laboratory, England, 1977.

Scruggs L.A., Gajda W.J. Low Frequency Conductivity of Unidirectional Graphite/Epoxy University of Notre Dame Indiana. IEEE Conference on EMC Seattle, 1977.

Burrows B.J.C. The Role of Field Calculations in Simulated Lightning Testing. Symposium on Lightning Technology, NASA Langley Research Centre Hampton Virginia, April 1980.

APPENDIX TO PAPER 17Bibliography of Reports and Papers on CFRP Composites prepared solely or
jointly by Culham Lightning Studies Group, Culham LaboratoryAbingdon, Oxfordshire OX14 3DB U.K.

1. Pownall P. Preliminary Tests on the Screening Performance of Carbon Fibre Panels, CLSU Memo Number 51, June 1977.
2. Burrows B.J.C., Luther C.A. and Pownall P. Resistance Measurements on Bulk CFRP and on Metal/CFRP Panels, CLSU Memo Number 56, October 1977.
3. Burrows B.J.C., Luther C.A. and Pownall P. Further test on Screening due to CFRP Aperture Covers, CLSU Memo Number 59, November 1977.
4. Banks C. Investigation of the Uniformity of Resistivity of Carbon Fibre Composites, CLSU Memo Number 65, June 1978.
5. Burrows B.J.C. and Luther C.A. Summary of Theory of Induced Voltage Mechanisms, CLSU Memo Number 69.
6. Hanson A.W. Basic Research on Carbon Fibre Reinforced Plastic (Direct Effects), CLSU Memo Number 70, October 1978.
7. Pollard I. The Effects of Moisture Ingress on Low Current DC Resistance of CFC, Culham Publications CLM/RR/M13/1, October 1979.
8. Jones C.C.R. and Talbrys J.G. Comparative Tests on Arc Damage to Protected Carbon Fibre Panels from Hanover University, Culham Laboratory Report Number CLM/RR/M13/2.
9. Burrows B.J.C., Luther C.A. and Easton S. Prediction and Measurements of Lightning Induced Voltages behind a Comprehensive Range of CFC Panel Configurations, CLM/RR/M13/3.
10. Hanson A.W. and Jones C.C.R. A Review of Published work on Carbon Fibre Composites, Culham Laboratory Report Number CLM/RR/M13/5.
11. Wallace B.J., Burrows B.J.C., Zeitler R.T., Ledwig A.J. and Wiles K.G. Composite Forward Fuselage Systems Integration, Volume II, AFFDL - TR-78-110, September 1978.
12. Little P.F., Hanson A.W. and Burrows B.J.C. Test Techniques for Simulating Lightning Strikes to Carbon (graphite) Fibre Composite Structures, Federal Aviation Administration - Florida Institute of Technology Workshop on Grounding and Lightning Technology, Melbourne, Florida, March 1979.
13. Burrows B.J.C. Induced Voltage Hazards in Carbon Fibre Composite Structures, 15th European Conference on Lightning Protection, Uppsala, Sweden, June 1979.
14. Burrows B.J.C. and Hanson A.W. The Behaviour of CFRP Panels in Metal Aircraft during Simulated Lightning Strokes, Contributed paper to AGARD Avionics Panel Meeting, Lisbon, June 1980.

INFLUENCE ON ANTENNA GAIN AND POLARIZATION PURITY OF REFLECTORS
MANUFACTURED FROM CARBON FIBRE COMPOSITE MATERIALS

L. Heichele
MBB Antenna Department
Munich, Germany

SUMMARY

The effects on the RF-antenna performance of reflectors manufactured out of carbon fibre reinforced plastics (CFRP) have been investigated by experimental work. The test equipments used, are described and an extensive number of results are given in this paper. The measurements cover the frequency range from 2 GHz to 18 GHz. The polarization dependency of loss and the effects on the phase are given for different CFRP-types. The RF-tests of a realized offset reflector satellite antenna manufactured from CFRP with an aperture diameter of 2 m are described. The measured far field characteristics are shown and compared with theoretical results and CFRP sample measurements.

1. INTRODUCTION

The increasing interest in communication satellite systems has stimulated the development of new technologies for satellite reflector antennas. The demand for narrow spaced communication services and for frequency bandwidth has led to the development of antenna systems which have to achieve extremely high electrical performances. Therefore the trend in the design of advanced communication satellite antennas necessitates high efficient multiple beam - or shaped beam antennas using dual polarized feed systems. Particularly the most essential electrical characteristics which should be performed by these antennas are:

- high radiation efficiency (50 % - 60 %) in the single beams or shaped beam in order to minimize the necessary power supply
- low controlled sidelobe radiation (< -30 dB) to avoid interference between neighbouring communication services
- high polarization purity (< -35 dB) in order to allow frequency re-use within the same antenna beam or to provide high isolation between neighbouring beams operating in the same frequency band
- high pointing accuracy ($\approx 1/10$ of the half power beamwidth) is also important in order to perform accurate coverage of the service area and to avoid interference with other services

These stringent electrical requirements on the satellite reflector antennas are closely associated with the mechanical and thermal behaviour of the reflecting structures. A complex interrelation between electrical and mechanical properties has to be treated in order to find out the optimum design of an antenna for space applications. The main dependencies influencing the electrical and mechanical performance of a reflector antenna are shown in the block diagram of figure 1. It is obvious that the reflector material is of significant influence on the electrical performance in satellite antenna systems, where rigorous restrictions on mass exist. The important mechanical characteristics of a reflector like mechanical stiffness, surface accuracy and thermal behaviour usually can be improved by taking more mass into account, or by using new more advantageous reflector materials. The carbon fibre reinforced plastics (CFRP) appears to be a most favourable material for the construction of light-weight antenna reflectors. The use of CFRP-materials in reflector antennas leads to a considerable improvement in the requirements of low mass, accurate surface and high stiffness of the structure because of the low density, high modulus of elasticity combined with a low thermal expansion coefficient of the material. It was shown by recent measurements that the RF-reflectivity of these materials is close to that of metallic surfaces. However, these investigations have also pointed out that CFRP-materials can have serious losses and effects which are polarization-dependent caused by the structure of the fibres and from the manufacturing process.

2. CHARACTERISTICS OF CFRP-MATERIALS

2.1 Typical Mechanical Properties of Carbon Fibre Laminates

CFRP-materials consist of layers of thin carbon fibres incorporated in an epoxy resin system. Two types of carbon fibres are considered: the HM-fibre type having a high modulus of elasticity and the HT-fibres yielding high tensile strength.

Yarns of these fibres are tied together in manufacturing processes to mainly three CFRP-structures. These arrangements of the fibres are the unidirectional carbon fibre layers, carbon fibre skins which are produced by a filament winding procedure and the fibre materials woven like fabric. The surface structure of these types of carbon fibre materials are shown in figure 2.

In the manufacturing process for unidirectional composites two or more sheets of equal orientated fibres are deposited on one another. The angle between the direction of the fibre layers of the different sheets can be chosen in such a way that the CFRP-material performs orientation-independent mechanical characteristics. The unidirectional carbon fibre material is generally pre-impregnated with the epoxy resin system (Prepreg) and hardened under pressure in moulds at higher temperatures.

In the filament winding procedure, carbon fibre skins are deposited by winding fibre yarns on a large rotating drum. The axial traverse of the yarns produces a typical pattern on the rotating cylinder. After this procedure the cylindrical fibre skin is opened and can be cut in pieces for further manufacturing.

Common known pattern of fabric can also be produced with carbon fibre materials and pre-impregnated with the epoxy resin system. An example of perpendicular woven fibre tapes is shown in figure 2.

The mechanical and thermal performances of the CFRP-materials depend on the manufacturing process, on the structure and the thickness of the skin and on other specific mechanical and geometrical aspects. Therefore only some very typical average values can be given, describing the main mechanical properties of the CFRP-material.

Typical mechanical values of CFRP-skins:

fibre diameter	7 μm - 8 μm	
ply-thickness	0.5 mm - 0.05 mm	
fibre volume	50 % - 60 %	
thermal expansion coefficient	1 - 2 x 10 ⁻⁶ K ⁻¹	(22 x 10 ⁻⁶ K ⁻¹ AL)
temperature range	100 - 400 K	
density	1.6 g/cm ³	(2.7 g/cm ³ AL)

Young's modulus in fibre direction

HT-material	130 kN/mm ²	
HM-material	225 kN/mm ²	(70 kN/mm ² AL)

tensile strength in fibre direction

HT-material	1.6 kN/mm ²	
HM-material	1.4 kN/mm ²	(200 N/mm ² AL)

For some purposes it may be useful to compare the above values with those of aluminium. This comparison indicates the mechanical advantage which achieves the CFRP-material and which makes it to one of the most favourable materials for spacecraft reflector antennas.

2.2 Electrical Properties of CFRP

2.2.1 Measurements of the RF-Losses of Carbon Fibre Laminates

Recent publications have pointed out that the RF-reflectivity of carbon fibre laminates can be close to that of metallic surfaces. However, materials consisting of fibres or grids do not usually yield a homogenous surface for microwaves. In order to investigate the effect of carbon fibre layers on microwaves a number of different manufactured probes of carbon fibre laminates have been tested in the frequency band 2 GHz to 18 GHz. The general test equipment used for these investigations is shown in figure 3. The CFRP-probe was aligned accurately near the aperture of a small corrugated surface horn. Balancing the RF-bridge with the precision attenuator and the movable short located in the other arm of the bridge, the reflected wave can be determined from the position of the attenuator and the movable short. For the calibration of the bridge the probe was replaced by a polished aluminium plate of the same size. The magnitude and the phase of the RF-reflection factor of the probe material with respect to the aluminium surface was then calculated from the difference of the adjustment of the attenuator and the short. In order to prove an orientation dependency of the carbon fibre laminates the measurement was carried out several times aligning the probe in different angular positions with respect to the radiated electric field of the horn. A selection of the measured magnitude of the power reflection coefficients is given at discrete frequencies for meshed carbon fibre laminates in table 1 and for unidirectional CFRP in table 2.

The essential aspects which can be derived from the measurements are that carbon fibre laminates can perform extremely high reflectivity. But the investigations also point out that the RF-losses of carbon fibre layers show a more increasing tendency than metallic surfaces. This degradation from the RF-performance is mainly caused by the macrostructure of surface pattern of the layer and the microstructure of the carbon fibre epoxy resin system.

In general the properties of the investigations of carbon fibre laminates can be summarized as follows:

Meshed carbon fibre structures such as filament wound and carbon fibre fabric act as a homogenous surface at microwave frequencies. A condition for this behaviour is that the meshes of the structure are orthogonal symmetric and small compared with the wavelength. The measured frequency dependent reflection

coefficient for a typical example of a filament wound carbon fibre skin is shown in figure 4. The measured values are independent of the angular orientation of the probe with respect to the incident electric field. However, the shape of the phase indicates that the wave penetrates into the material. Therefore it can be assumed that the decrease in reflectivity is mainly caused by the losses of the epoxy resin.

Unidirectional carbon fibre layers generally produce an orientation dependent reflection loss and cannot be considered as homogenous materials in the microwave range. This effect is caused by the orientation dependent depth of penetration of the wave into the material. The experiments have pointed out that this depth of penetration and consequently the losses caused by the epoxy resin is a function of the fibre orientation, the thickness of the layers and the value of the fibre fraction in the layer. Figure 5 shows the measured orientation dependent reflection factor of a typical unidirectional carbon fibre material. Comparing the RF-reflectivity at one frequency point of unidirectional carbon fibre laminates with different ply thickness the measured values show approximately a linear dependency. For the frequency 12 GHz this was evaluated and drawn in figure 6. The dependency of the RF-reflectivity on orientation angle and ply thickness indicates that most of the carbon fibres are not in a conductive condition in the layer but are isolated by the epoxy resin. The microstructure of some carbon probes (figure 7) has shown that this assumption was realistic. In addition, areas of low fibre density can be found in the microstructure which allow also a penetration of the incident wave. In the case of the meshed carbon fibre materials the areas where the fibres cross mutually are filled at the surface with pure epoxy resin which causes remarkable higher losses at microwave frequencies.

The knowledge of the interdependence of the microstructure of CFRP-materials and the RF-losses can give hints for the manufacturing process of laminates of high RF-performance. The characteristic properties of these laminates should be:

- thin ply thickness of the surface layers 0.05 mm
- high fibre fraction in the surface layers 60 %
- smooth surface and avoidance of epoxy resin residues on the surface
- use of carbon fibres with high electrical conductivity (HM-fibres)

Recent publications [1,7] have pointed out that the DC-conductivities of the carbon fibre types show remarkable discrepancies.

The longitudinal conductivity values mentioned there are for the high tensile strength (HT) carbon fibres approximately $3 - 4 \times 10^4$ S/m and for the fibres with very high modulus of elasticity (HM) about $7 - 8 \times 10^4$ S/m.

The effect on the RF-reflectivity of these two fibre types was found by comparing the measurements of two probes manufactured with the same epoxy resin system. The measured magnitude of the reflection coefficient for a HM- and HT-fibre laminate shows the frequency dependent difference drawn in figure 8.

2.2.2 Measurement of CFRP-Effects on Polarization Purity

The orientation dependent surface loss of unidirectional carbon fibre laminates causes crosspolar components in a reflector system. In order to investigate the level and the angular dependencies of the effected depolarization of an incident wave on a carbon fibre surface a measurement was carried out which is sketched in figure 9. The test setup was a quasi-monostatic radar cross-section measurement system. The linearly polarized transmitted and received signal was separated by two closely located horns. The target was a plane disc of an unidirectional carbon fibre skin fixed on a turntable. The microwave circuit was calibrated by replacing the carbon fibre disc by an identical aluminium disc of the same size. Effects of the support structures have been cancelled by feeding a small signal with opposite phase in the receive channel. The test results for parallel and orthogonal linear polarizations of the two horn radiators dependent on the orientation of the surface fibre direction of the laminate are given in figure 10. These measurements verified the orientation dependency of the loss of these types of fibre laminates with orthogonal orientated fibre directions in the first two sheets. In addition the effect of depolarization with a maximum near the 45 degree plane could be demonstrated in a convincing manner.

3. THEORETICAL INVESTIGATIONS OF THE RF-EFFECTS OF CFRP-MATERIALS

3.1 Electrical Model for Carbon Fibre Laminates

Carbon fibre layers of the meshed type which have effected no orientation dependent RF-losses can be sufficiently considered taking an additional surface roughness and small ohmic surface losses of the reflecting layer into account.

The RF-reflectivity of unidirectional fibre structures depends on the orientation of the incident electric field in relation to the direction of the carbon fibres. Therefore this characteristic may be described approximately by defining an orientation dependent reflection factor. The electric field orientated in the plane of the reflecting carbon fibre surface can be separated in field components perpendicular and parallel to the direction of the fibres of the first layer. These field components are then multiplied by different reflection factors and transformed again to the original coordinate system. The mathematical relationship for a normal reflected wave can be given by a matrix equation for the complex components of the electric field.

$$\begin{pmatrix} E_{xR} \\ E_{yR} \end{pmatrix} = \begin{pmatrix} \cos\psi & \sin\psi \\ -\sin\psi & \cos\psi \end{pmatrix} \begin{pmatrix} r_p & 0 \\ 0 & r_o \end{pmatrix} \begin{pmatrix} \cos\psi & -\sin\psi \\ \sin\psi & \cos\psi \end{pmatrix} \begin{pmatrix} E_{x_i} \\ E_{y_i} \end{pmatrix}$$

E_{xR}, E_{yR} are the reflected field components parallel to the plane of the reflecting layer

E_{x_i}, E_{y_i} describe the incident field parallel to the plane of the reflecting layer

r_p, r_o are complex reflexion factors parallel and orthogonal to the carbon fibre orientation

ψ is the orientation angle of the carbon fibres in reference to the field coordinate system.

This theoretical approach was applied in the case of the plane CFRP-material with normal incidence of the electromagnetic wave. Using measured reflection coefficients for the two orthogonal planes sufficient agreement has been obtained with measured data (figure 10).

3.2 Theoretical Investigation of the Carbon Fibre Effects on a 2 m Diameter Offset Antenna

For the study of the effects of carbon fibre laminates on the RF-performances of a realistic reflector antenna a focus fed offset antenna configuration was selected. This configuration was chosen for realization in a feasibility study for a communication satellite system. The geometry of the reflector is sketched in figure 11. The main characteristics of the antenna configuration are:

- approximately circular aperture of 2 m diameter
- focal length 1.2 m
- the antenna is illuminated by a corrugated surface horn yielding a rotational symmetric pattern with -13 dB taper at the reflector edge
- frequency: 12.2 GHz
- for the reflector surface an unidirectional $0^\circ/90^\circ$ CFRP-material was assumed
- the fibre orientation was -45 degree with respect to the symmetrical plane of the reflector.

The reflector configuration was installed in a computer program using the physical optics approximation for the induced currents on the reflecting layer.

$$J = n \times (H_i + H_r)$$

with: J current density on the reflector
 n normal vector of the reflecting surface
 H_i, H_r magnetic field component of the incident and the scattered wave.

The incident electric field was described by the far field pattern of the corrugated surface horn and the reflected field of the former assumed by the scattered fields on a carbon fibre surface.

In addition it was assumed that the orientation dependent reflection coefficient shows also a dependency from the angle of incidence, different from the normal direction. The factor used for multiplication of the RF-losses and the path length of the wave in the surface layer was:

$$p = \frac{|n \cdot s|}{(n \cdot s)}$$

with: n = surface normal vector
 s = position vector of the surface point

This factor describes approximately the increasing depth of penetration of a part of the electromagnetic fields into a homogenous dielectric layer where the direction of incidence is different from the normal.

In order to compute the surface currents on the reflector, far field behaviour was assumed for the association of the magnetic and electric fields. Figure 12 shows the approximation of the reflector geometry in the electrical integration grid model.

The computations have been carried out for three types of reflector surfaces, the ideal reflector and two cases of high efficient unidirectional carbon fibre surfaces. The orientation dependent reflectivity derived from measurement was:

	in fibre direction /r/2 phase (deg.)		orthogonal /r/2 phase (deg.)	
ideal surface	1.00	0	1.00	0
CFRP-material model 1	0.99	0	0.98	2
CFRP-material model 2	0.99	0	0.97	3

The far field pattern have been calculated at the frequency 12.2 GHz for vertical linear polarization orientated at 45 degrees with respect to the fibre direction of the surface.

Comparing the results, it turned out that, the degradation in the copolar pattern is unessentially small if the considered high reflective CFRP-materials are assumed as reflector surfaces (figure 13).

The effects of the fibre surface can be seen more clearly regarding the crosspolarized pattern. In the symmetrical plane of the offset reflector where high crosspolarized levels usually exist also in the ideal reflector case, the crosspolarized pattern becomes asymmetric and the nulls are filled up by the effects of the fibre surface as can be seen in figure 14. In an ideal surface case only some crosspolarized radiation induced by the horn exists in the plane of asymmetry. Therefore the depolarization effects of unidirectional fibre surfaces can be immediately observed by the increasing beam of the crosspolarized component (figure 15).

Offset reflector antennas fed by a circularly polarized wave produce no crosspolarized waves, but a small beam squint of the copolar characteristic is effected by this configuration. The far field pattern of the considered offset antenna, fed by a circular horn was also computed assuming the same reflector surfaces as in the linear polarized case. The computed pattern of figure 16 and 17 show again only negligible effects of the fibre material on the copolar pattern but essential degradations of the crosspolar components. The essential values evaluated from the computation can be given in a short summarization:

	ideal surface	CFRP-material model 1	CFRP-material model 2
<u>linear polarized antenna</u>			
antenna gain	45.0 dBi	44.94 dBi	44.9 dBi
first sidelobe	-24.2 dB	-24.0 dB	-24.0 dB
crosspolarized	-19.0 dB	-18.3 dB	-18.0 dB
<u>circular polarized antenna</u>			
antenna gain	45.0 dBi	44.94 dBi	44.9 dBi
first sidelobe	-23.6 dB	-23.5 dB	-23.5 dB
crosspolarized	-50.0 dB	-35.2 dB	-31.8 dB
beam squint	0.09 deg.	0.09 deg.	0.09 deg.

4. COMPARISON OF THE RF-CHARACTERISTICS OF A REALIZED OFFSET ANTENNA WITH COMPUTED RESULTS

An antenna reflector of the dimensions under consideration has been available for electrical tests. This reflector shown in figure 18 has been designed and manufactured by Dornier Systems. Mechanical qualification tests have shown a very high surface accuracy with measured deviations from the ideal parabolic curvature of only 0.13 mm RMS. The carbon fibre material used for manufacturing the reflector was of a type with high electrical conductivity. The reflector surface consists of eight unidirectional layers with a ply thickness of only 0.05 mm. The carbon fibres of the surface layer have been orientated at 45 degrees with respect to the axis of symmetry of the offset configuration.

For the electrical performance tests a small corrugated surface horn with a rotationally symmetric radiation characteristic was installed in the antenna. The concept for the electrical tests was to rotate the linear polarized feed around its symmetry axis in discrete steps and to measure in each case the far field pattern. The expected discrepancy in these patterns should then indicate the polarization dependency of the antenna surface. Figure 19 shows the horn and its device for rotation. The measured RF-patterns of the horn are shown in figure 20. The measurements have been carried out at the frequency 12.2 GHz on the MBB far field antenna range 1000 m in length. However, despite taking care to align the horn, the carbon fibre antenna and the range antenna very accurately, an essential difference in the copolar pattern could not be noticed.

Nevertheless small polarization dependent effects could be found measuring the crosspolarized pattern. Figures 21, 22 and 23 compare measured patterns in the main axes of the antenna with values of one of the studied antennas. It can be seen that the co- and crosspolar pattern correspond very accurately. Therefore an estimation can be given for the polarization dependent reflectivity of the realized antenna surface. It can be confirmed that the reflecting carbon fibre layer has nearly an orientation independent reflectivity. The orientation dependent loss for the carbon fibre skin is less than -0.05 dB.

5. CONCLUSIONS

The investigations have shown that CFRP-material can have an extremely efficient RF-reflectivity up to frequencies of about 20 GHz. Especially laminates consisting of very thin layers of carbon fibres behave like metallic sheets at microwave frequencies. The degradation of the RF-performances observed in antenna reflectors manufactured from CFRP are mainly gain loss and depolarisation. These effects can be avoided by metallizing the surface or loading the epoxy resin of the surface layers with metal or graphite powder. But these procedures are difficult and would probably degrade the mechanical performances of the materials. The investigations have also indicated that the depolarization due to the inhomogeneous surface of CFRP is similar to the depolarization effects caused by poor adjustment of the horn or an unbalanced polarizer in the antenna feed system. Therefore the degradation from the polarization purity caused by the carbon fibre material can be compensated by tuning the feed system. On the other hand it should be mentioned that crosspolar components on the reflector can be improved by choosing a location dependent orientation of the carbon fibre layers. However, these compensation methods may be impracticable in dual polarized antenna systems.

REFERENCES

- (1) J.A. Dickinson
Final report for phase 1 of a study on the use of carbon-fibre-reinforced plastics in satellite structures. March 1974 ESTEC contract No. 1735/72
- (2) E.Y. Robinson, R.A. Stornier, C.L. Lofgren
Developments of a unique graphite/epoxy antenna subreflector.
Report of ASTM third conference 1974, pp. 632 - 650
- (3) K.M. Keen
Gain-loss measurements on a carbon-fibre composite reflector antenna.
Electronics letters May 1975 Vol. 11, No. 11, pp. 234, 235
- (4) H.L. Hillesland
Development of an advanced composite antenna reflector.
Proceedings of fourth national SAMPE technical conference 1972, 2, pp. 235, 248
- (5) MBB
Study of deployable antennas for satellites.
Second progress report, ESRO contract 2070/73 HP 1974
- (6) P.S. Hall
Measurements of reflection loss of carbon laminates for the Marots L-Band antenna
Marconi Space and Defence Systems Ltd.
Stanmore MAR/TM/UKS1/813/009
- (7) R.H. Knibbs, D.J. Baker, G. Rhodes
The thermal and electrical properties of carbon fibre unidirectional reinforced epoxy composites.
26th annual technical conference 1971, reinforced plastics/composite div.
The Soc. of Plastics Industry, Inc.
- (8) K. Keen, P. Molette, B. Pieper, C.M. Herkert, W. Schäfer
Development and testing of a new CFRP-antenna reflector for communication satellites
Raumfahrtforschung Band 20, Heft 4 Juli/August 1976

Probe Nr.	Carbon fibre type	Epoxy resin type	manufacturing process	fibre geometry number, direction and thickness of sheet	angle between electric field-fibre direction	frequency (GHz)								
						2	4	6	8	12	14	16	18	
1	TORAYCA M40-3000x40A	CIBA CY209/HT972	filament wound closed layer	1 x 0°/90° 0.55 mm	0°/90°	99.5	99.0	99.0	98.3	96.5	93.8	87.5	81.3	r/r^2
2	TORAYCA M40-3000x40A	CIBA CY209/HT972	filament wound open layer grid holes 1 x 1 mm	1 x 0°/90° 0.55 mm	0°/90°	99.5	99.0	99.0	98.2	97.5	93.3	87.0	84.5	
3	TORAYCA M40-3000x40A	CIBA CY209/HT972	filament wound open layer grid holes 2 x 2 mm	1 x 0°/90° 0.55 mm	0°/90°	98.4	98.0	97.0	96.5	95.5	88.5	80.0	68.0	
4	UCC THORNEL 75 S	CIBA CY209/HT972	filament wound closed layer	1 x ± 45° 0.45 mm 1 x ± 90° 0.45 mm	0°/90°	99.9	99.0	99.0	98.0	95.5	92.9	92.0	89.0	
5	UCC THORNEL 75 S	CIBA CY209/HT972	filament wound closed layer	2 x ± 45° 0.45 mm	0°/90°	99.3	99.5	98.8	98.4	93.2	89.9	82.0	73.0	
6	TORAYCA T300-3000x40A	CIBA CY209/HT972	filament wound closed layer	1 x 0°/90° 0.45 mm	0°/90°	98.8	98.2	98.0	97.0	96.0	95.0	93.0	91.5	
7	TORAY HT T300	Forthergill and Harvey Code 92	fabric prepreg	2 x 0°/90° 0.20 mm	0°/90°					96.0	94.9	93.0	91.0	

Table 1: Magnitude of the power reflection coefficient for meshed CFRP-samples

Probe Nr.	Carbon fibre type	Epoxy resin type	manufacturing process	fibre geometry number, direction and thickness of sheet	angle between electric field-fibre direction	frequency (GHz)								
						2	4	6	8	12	14	16	18	
8	TORAYCA M40-3000x40A	CIBA CY209/HT972	filament wound	0°, 90°, 90°, 0° 4 x 0.4 mm	90° 0°	98.5 100	97.5 100	97.0 99.5	97.0 99.5	88.0 99.5	77.0 98.0	64.0 98.0	49.0 97.0	r/r^2
9	UCC THORNEL 75 S	CIBA CY209/HT972	filament wound	+30°, -30°, 90°, -30° +30° 4 x 0.2 mm	90° 0°	98.5 100	98.0 100	97.0 99.0	97.0 98.5	88.0 98.0	77.0 98.0	72.0 98.0	62.0 96.0	
10	TORAYCA M40-3000x40A	CA 2000 TORAY	Prepreg	0°, 90°, 90°, 0° 4 x 0.25 mm	90° 0°	98.5 100	98.0 100	98.0 99.0	97.0 99.0	92.0 99.0	85.0 99.0	73.0 98.2	62.0 97.5	
11	TORAYCA T300-3000x40A	CA 2000 TORAY	Prepreg	90°, 0°, 0°, 90° 4 x 0.13 mm	90° 0°	98.5 99.5	98.5 99.5	98.0 98.5	97.7 98.5	90.0 97.0	85.5 98.0	79.5 93.5	72.0 91.5	
12	TORAYCA T300-3000x40A	CA 2000 TORAY	Prepreg smooth surface	0°, 90°, 90°, 0° 4 x 0.2 mm	90° 0°	98.0 99.0	98.0 99.0	98.0 99.0	96.5 98.5	92.0 97.0	88.0 95.5	84.0 93.7	80.0 92.0	
13	TORAYCA T300-3000x40A	CA 2000 TORAY	Prepreg rough surface	0°, 90°, 90°, 0° 4 x 0.2 mm	90° 0°	98.5 99.0	98.5 99.0	97.5 99.0	96.5 98.5	92.0 96.0	87.5 95.3	80.0 92.5	73.0 91.0	
14	Grafil HSS 3 mm	EPN 1138 HI 973	Prepreg short fibres of 3 mm length	+30°, -30°, 90°, -90° 5 x 0.12 mm	90° 0°	100 100	99.0 99.5	98.0 99.0	96.5 98.5	94.0 97.7	93.0 97.5	92.0 97.0	90.5 95.0	
15	Courtaulds HT-5 B	DX 210 BF ₃ MEA	Prepreg rough surface	+45°, -45°, -45°, +45° 4 x 0.37 mm	90° 0°	99.0 100	98.0 99.0	97.0 98.5	94.0 97.0	86.0 94.5	75.0 92.0	66.0 91.0	56.0 90.5	
16	TORAY HT T300 B	Code 92 Forthergill and Harvey	Prepreg	90°, 0°, 0°, 90° sym. 8 x 0.05 mm	90° 0°					97.0 99.0	96.0 98.0			
17	Courtaulds HM 180 SC 10 000	Code 92 Forthergill and Harvey	Prepreg	0°, +60°, -60° sym. 6 x 0.127 mm	90° 0°					94.0 97.0	93.0 96.0			

Table 2: Magnitude of the power reflection coefficient for unidirectional CFRP-material

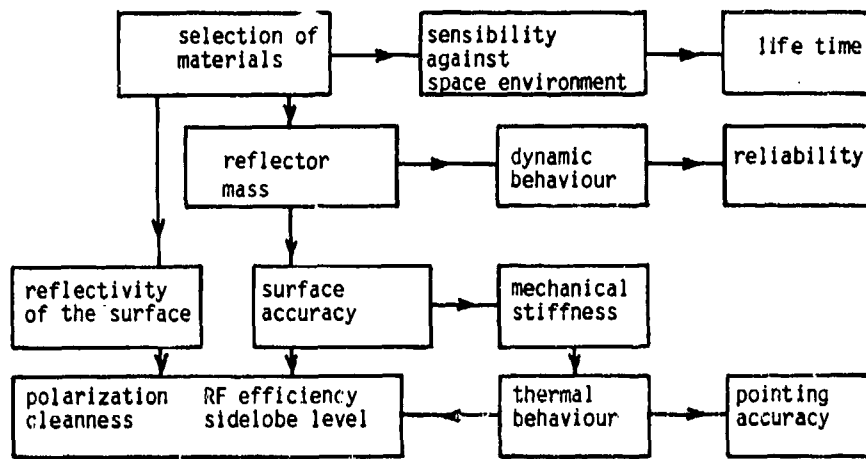


Figure 1: Main dependencies between mechanical, thermal and electrical performances of reflector antennas

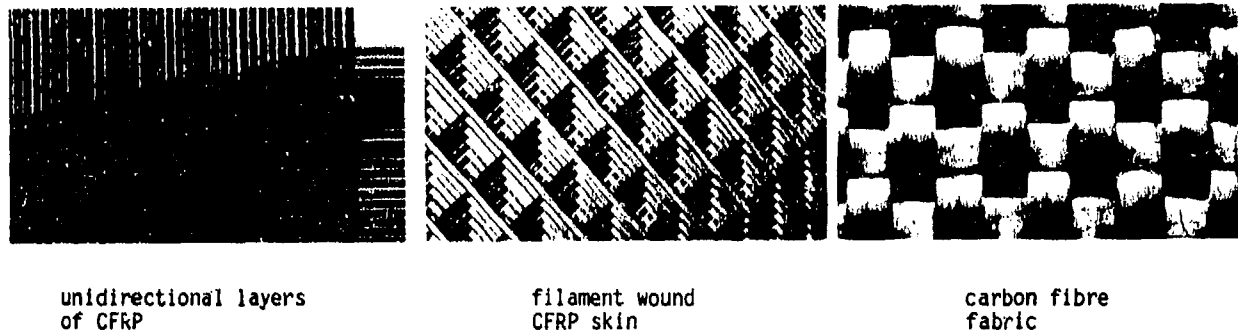


Figure 2: Types of carbon fibre laminates

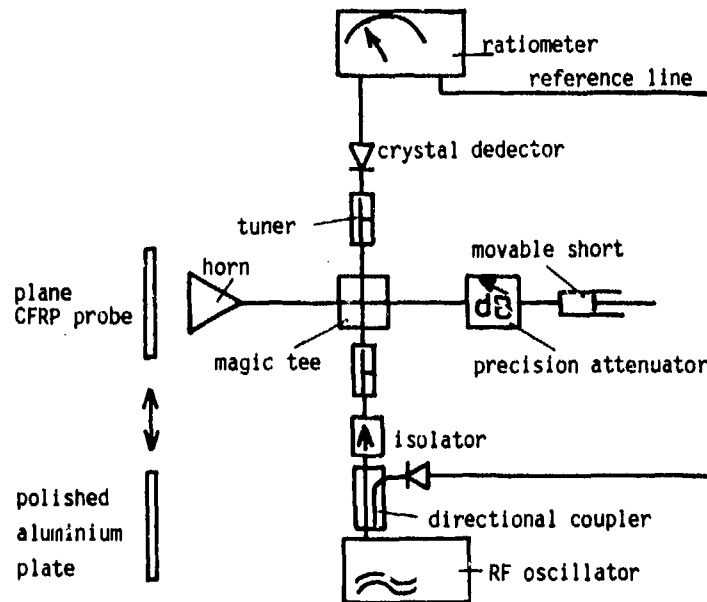


Figure 3: Arrangement for measuring the reflection coefficient of carbon fibre laminates

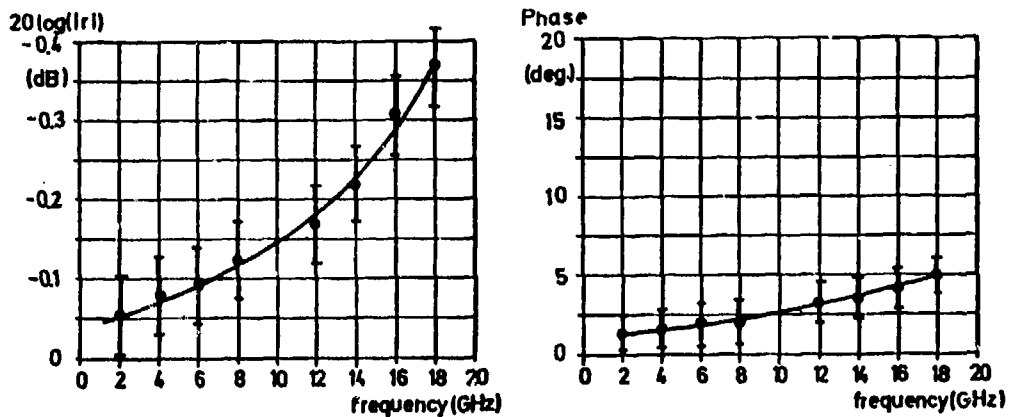


Figure 4: Amplitude and phase of the reflection coefficient of a filament wound CFRP-material.
 Carbon fibre: TORAYCA T 300-3000 x 40A, Epoxy resin: CIBA CY 209/HT 972
 one layer 0°/90°, thickness 0.45 mm
 orientation fibre direction - electric field 0°/45°/90°

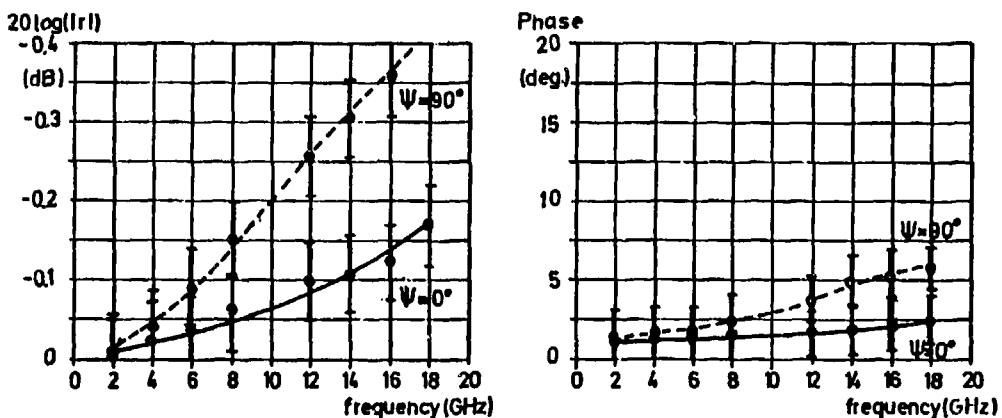


Figure 5: Amplitude and phase of the reflection coefficient of an unidirectional prepreg
 Carbon fibre: TORAYCA M 40-300 x 40A, Epoxy resin: Forthergill and Harvey Code 92
 4 layers 0°/90°/90°/0°, thickness 0.2 mm
 ψ = angle between fibre and electric field direction

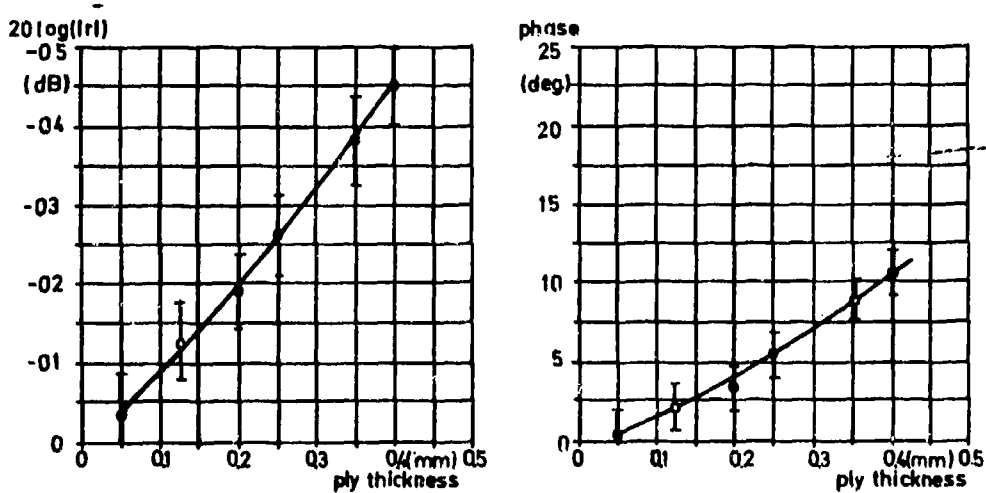


Figure 6: Dependence of the RF-reflection coefficient for a unidirectional carbon fibre surface from the ply thickness (12.0 GHz)

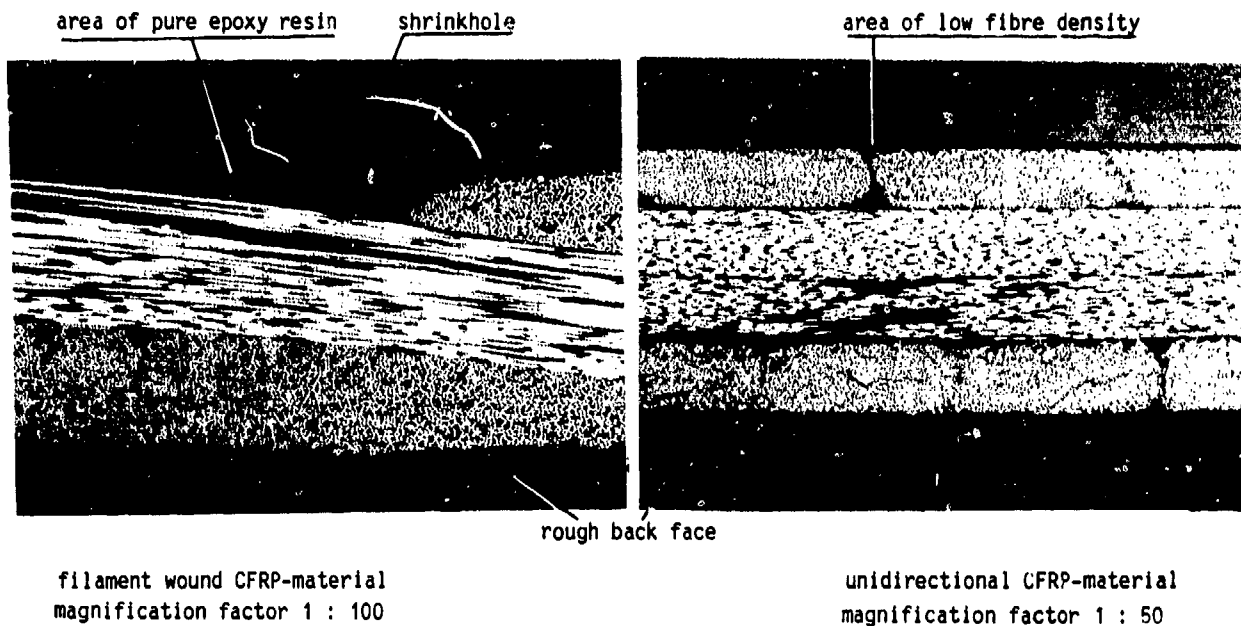


Figure 7: Photographs of the microstructure of carbon fibre laminates

Figure 8: Measured RF-reflectivity of HM- and HT-fibre laminates

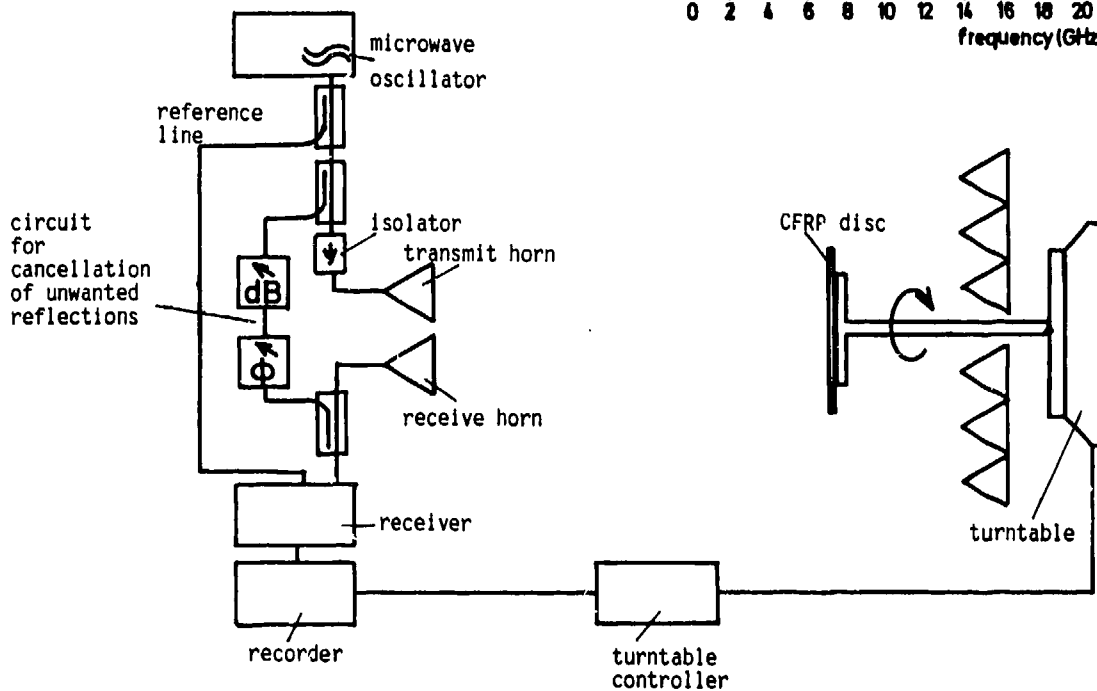
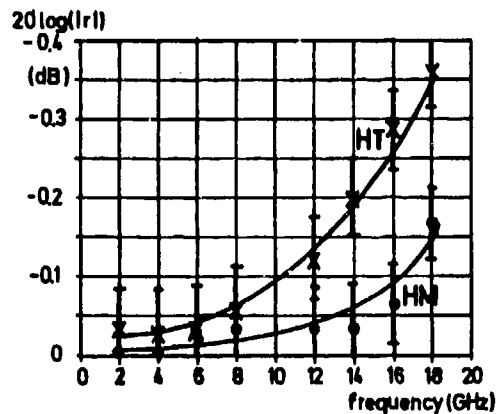


Figure 9: Microwave circuit for measurements of the orientation dependency of loss and crosspolarized level of CFRP-materials

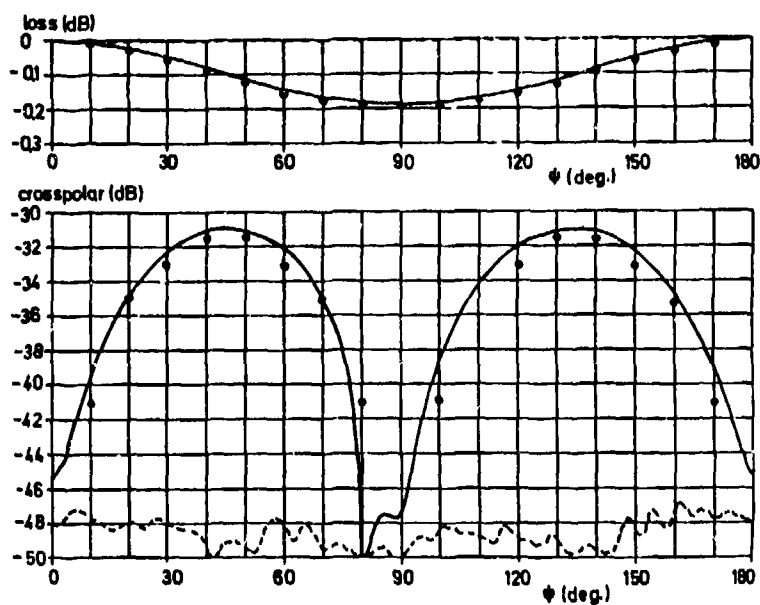


Figure 10: Orientation dependency of the loss and the effected crosspolarized level from an unidirectional carbon fibre laminate.

----- aluminium disc
 _____ unidirectional CFRP-disc
 ooooooo computed values

Figure 11: Geometry of the offset antenna configuration dimensions (mm)

$\psi = 45^\circ$ orientation of surface fibres

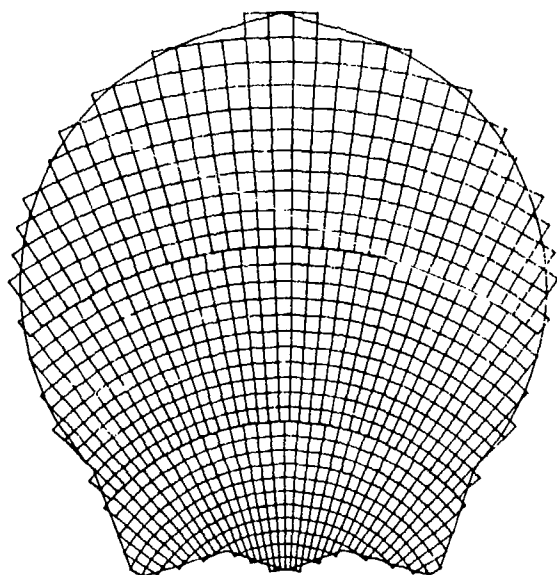
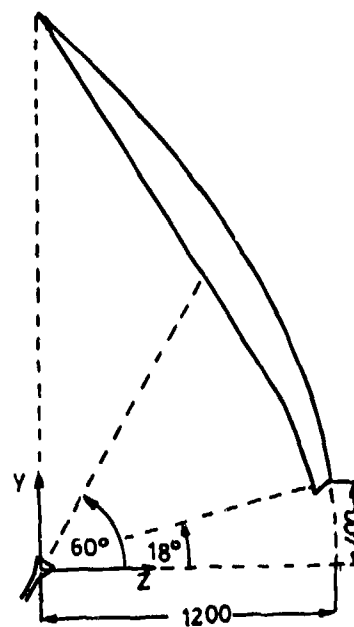
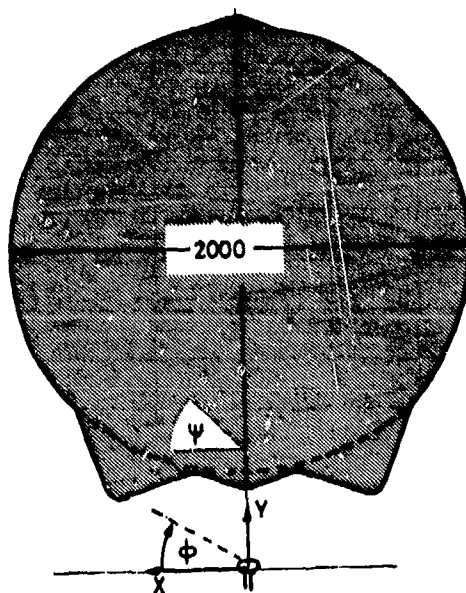


Figure 12: Approximation of the reflector geometry in the electrical grid model.

*

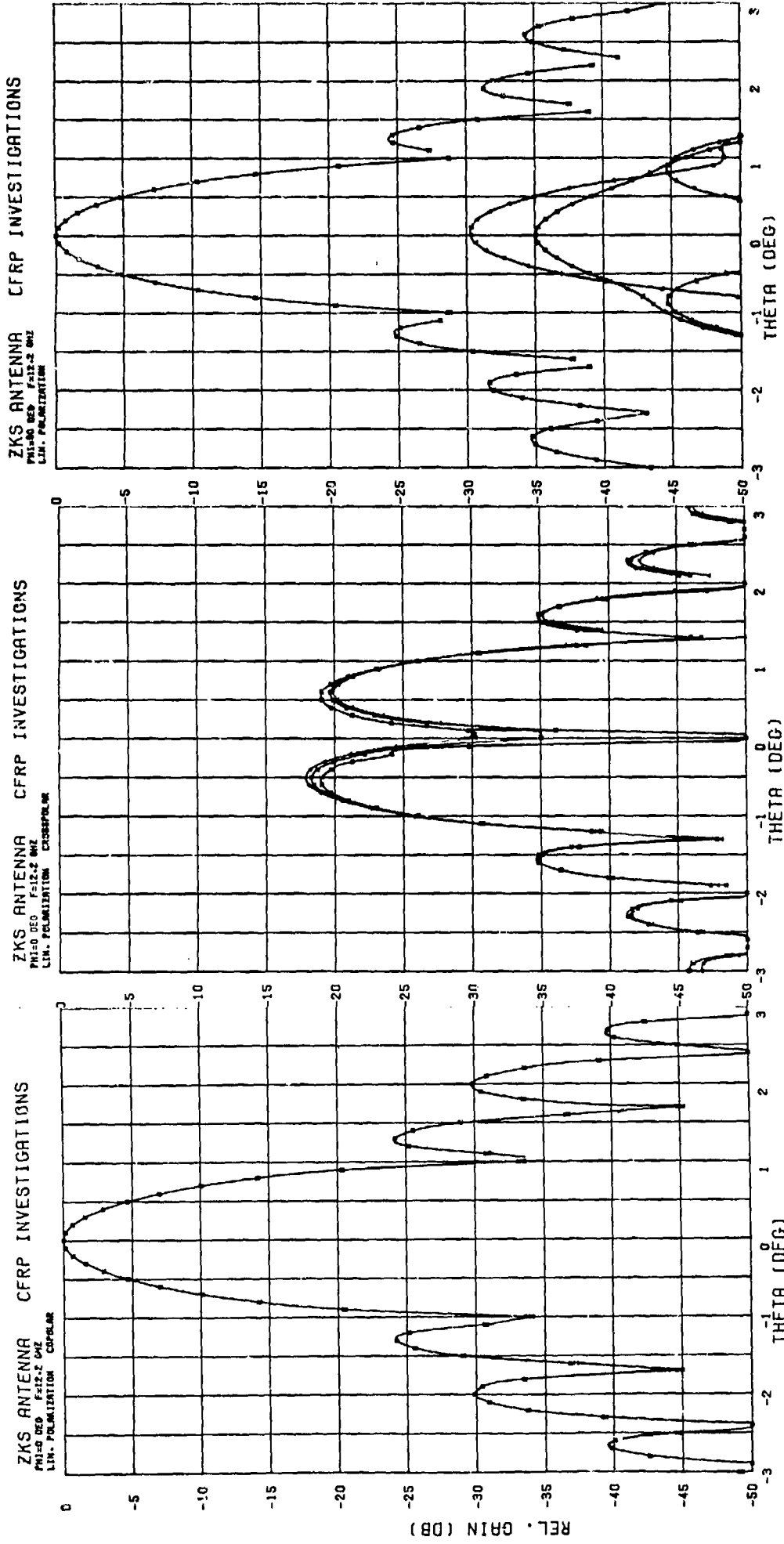


Figure 13

Figure 14

Figure 15

Computed far field patterns for linear polarization of two CFRP surface models and ideal reflector surface:

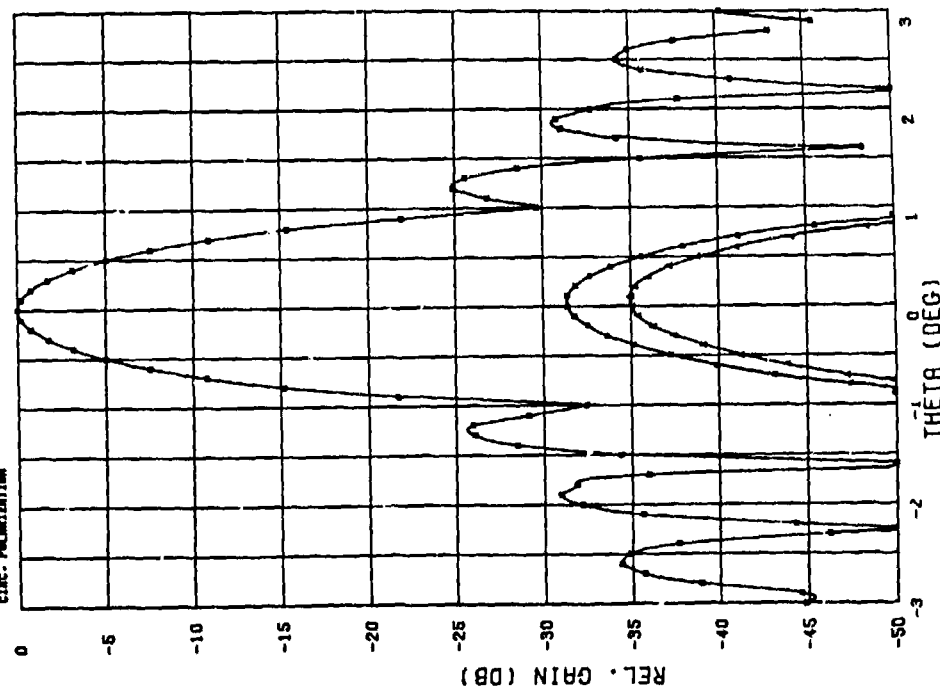
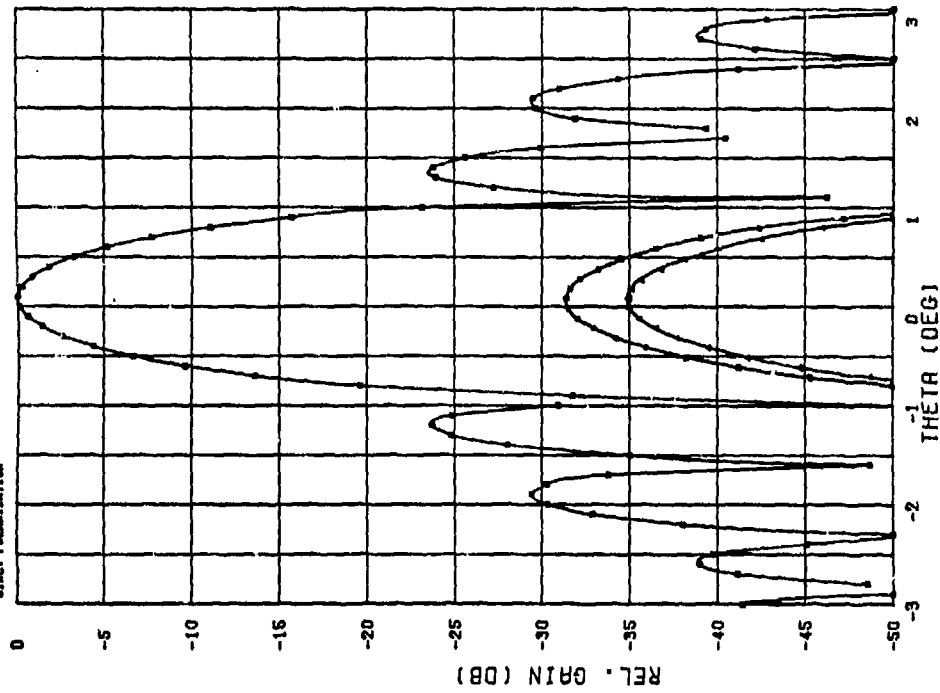
Figure 13: Copolar far field patterns $\theta = 0^\circ$

Figure 14: Crosspolar far field patterns

Figure 15: Co- and crosspolar far field patterns $\theta = 90^\circ$

ZKS ANTENNA
 PHU-80 DEG F412.2 MHz
 CIRC. POLARIZATION

ZKS ANTENNA
 PHU-80 DEG F412.2 MHz
 CIRC. POLARIZATION



Computed far field patterns for circular polarisation of two CFRP surface models and ideal reflector surface:
 Figure 16: Co- and crosspolar far field patterns $\theta = 90^\circ$
 Figure 17: Co- and crosspolar far field patterns $\theta = 0^\circ$

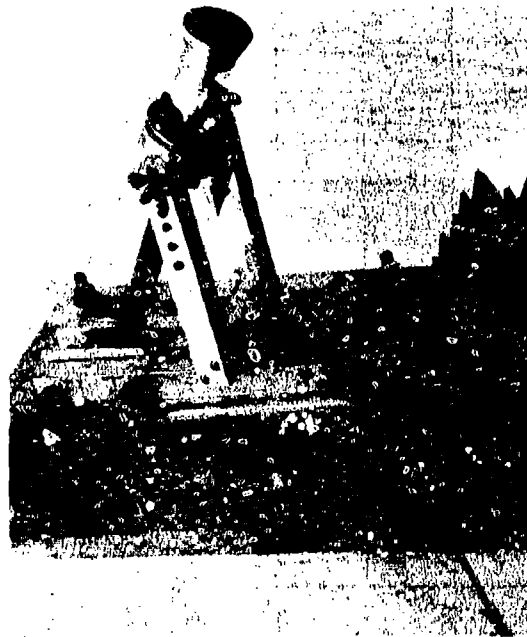


Figure 19: Corrugated surface horn adjusted in a device for purposes of axial rotation

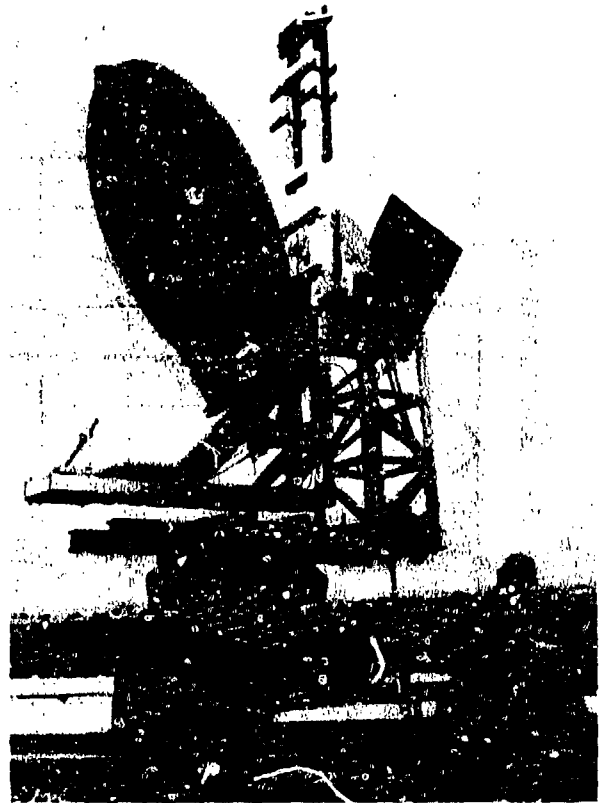


Figure 18: Focus fed offset reflector system on the antenna test site. (The reflector was manufactured by Dornier Systems)

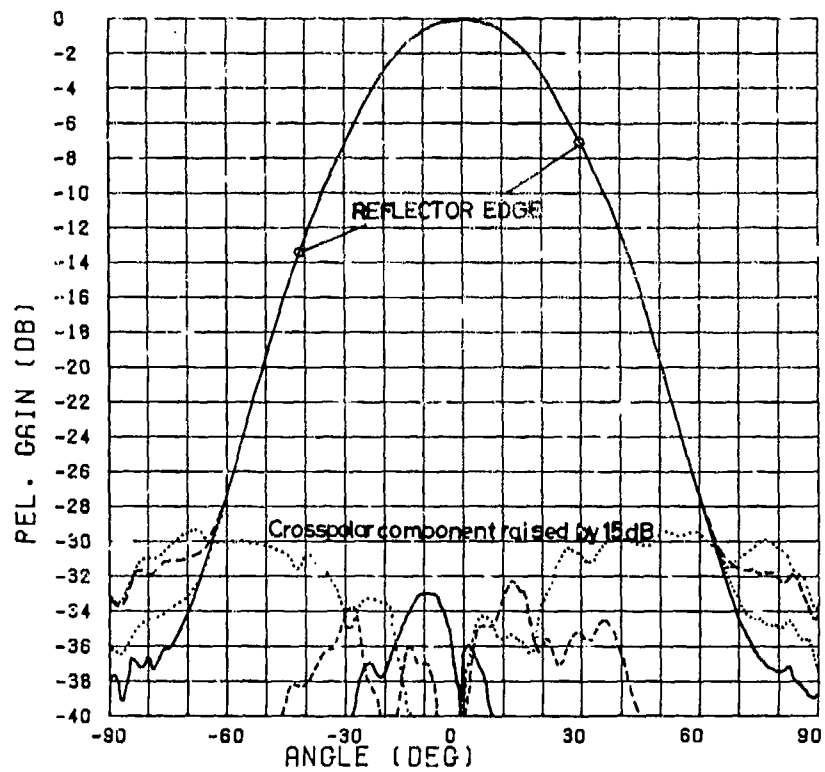


Figure 20: Radiation patterns in the E-, H- and diagonal planes exhibit identical beam symmetry

————— E-plane
 - - - - - H-plane
 diagonal plane

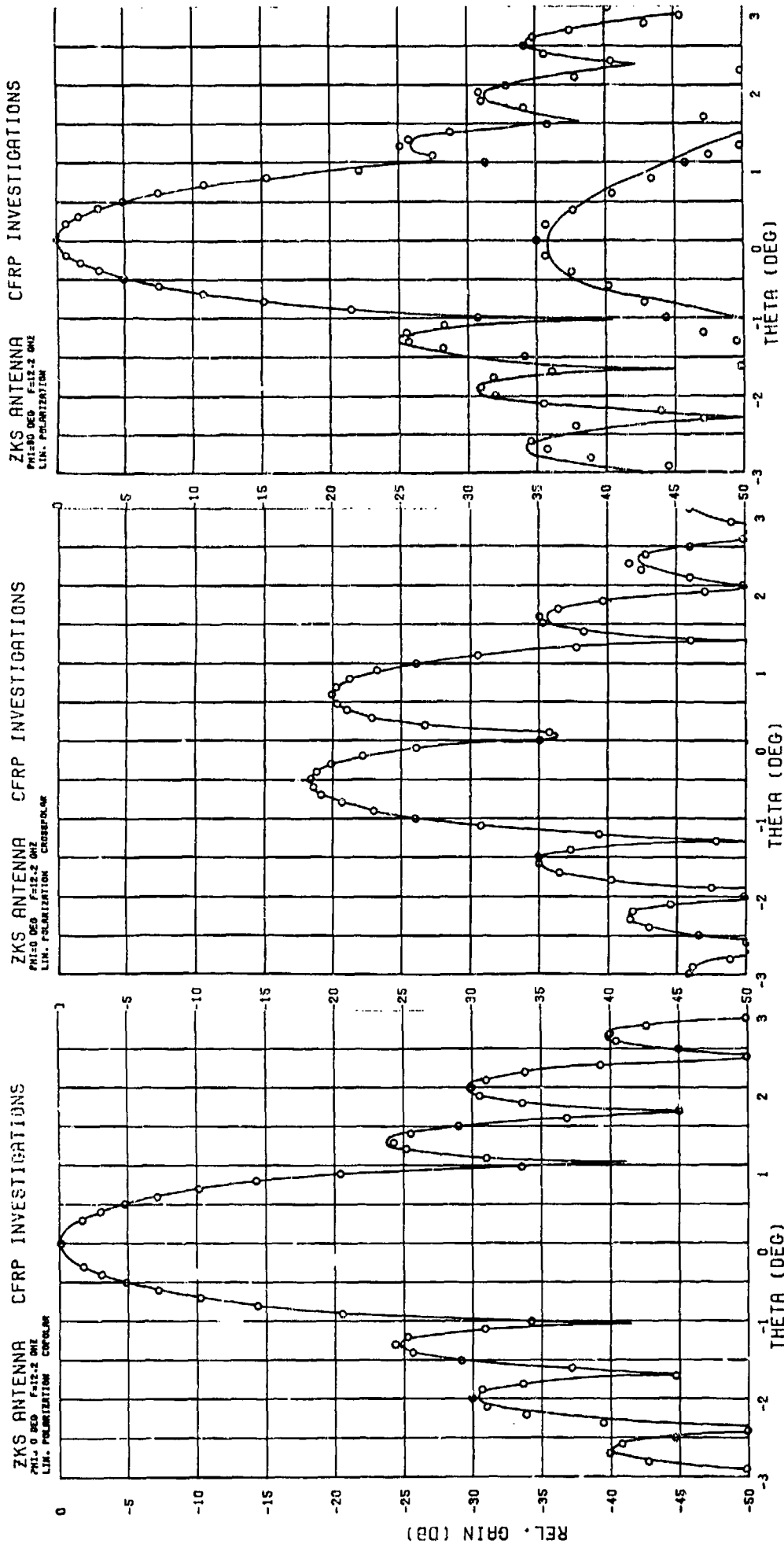


Figure 21

Figure 22

Figure 23

Comparison of the measured far field patterns (linear polarization) with the computed values of the CFRP surface mode: 1

Figure 21: Copolar far field patterns $\theta = 0$

Figure 22: Crosspolar far field patterns

Figure 23: Co- and crosspolar far field patterns $\theta = 90^\circ$

LIGHTNING THREAT DEFINITION FOR COMPOSITE AIRCRAFT

Dr. Preston Geren

Boeing Commercial Airplane Company

P.O. Box 3707, Seattle, Washington, USA

SUMMARY

An approach for calculating the transients induced in aircraft avionic systems by lightning is presented. The method has been applied to an aircraft geometry having various combinations of metal and graphite-epoxy structure. The effects of graphite-epoxy joints are considered. Results are shown for common mode open-circuit voltage and short-circuit current induced on two representative wire bundles (cockpit to tail and cockpit to wingtip). The approach employs standard analytical techniques from transmission line theory and antenna theory to obtain lightning-induced fields on the airframe surface, including the effects of airframe resonance. Both the directly attached and nearby lightning strikes are considered. A method for obtaining the concentration of fields as a result of noncylindrical geometries (e.g., along the leading and trailing edges of a wing) is described. The physical coupling mechanisms for penetration of exterior lightning-induced electromagnetic fields into the aircraft interior are explained.

The Pierce (or Bruce-Golde) waveform is used as an analytical tool to represent the lightning current in the channel and is related to lightning statistics for nominal severe and moderate strokes. Calculated results for an extremely severe stroke of 200-kA peak amplitude and 7.2×10^{11} A/s peak rate-of-rise are presented.

1. INTRODUCTION

At present, commercial and military aircraft have primarily metal structure. With the current trend toward the use of composite structural material, it is likely that future aircraft will use increasing amounts of nonmetallic structure. Aircraft with an all-composite fuselage are on the drawing boards today. Composite material has one major disadvantage for the EMI engineer: it has lower electrical conductivity than aluminum (e.g., about three orders of magnitude for graphite-epoxy) and provides poorer shielding against external interference sources, such as lightning. In parallel with this development in aircraft structure, avionic systems are becoming increasingly reliant upon the use of low-level digital circuits. The combination of the two trends, together with the incidence of lightning strikes to aircraft (about one per year for commercial and once every 10,000 to 30,000 hours for military), makes it essential that EMI engineers continue assessing the impact of the reduced shielding properties of composites upon avionic system performance. The first step in this assessment is prediction of the lightning EMI threat. With a realistic threat definition, one can then perform the necessary trade-offs between the advantages of composite structure and the penalties associated with its reduced shielding effectiveness.

The lightning threat may be divided into two categories: direct effects (physical damage to aircraft structure) and indirect effects (upset or damage of circuits). This paper will deal with indirect effects.

Figure 1 shows a flow chart for calculation of lightning-induced transients. The input to the analysis is the primary threat; i.e., the waveform of the current in the lightning channel at the altitude of the aircraft. The outputs are the transients induced at circuit loads.

The first step in the analysis is to obtain the current and charge distribution on the conducting external surfaces of the airplane. These external fields penetrate into the interior via joints and apertures as well as diffusion through conductive surfaces. In addition, some conductors may be directly exposed to the exterior fields (e.g., an electric windshield heater element). Given the electromagnetic fields incident upon the conductor of interest (usually an interconnecting wire bundle), one can then calculate the equivalent voltage and current sources by application of the reciprocity theorem. These source terms are then input into a transmission line model to obtain the transients at the terminating loads.

2. LIGHTNING THREAT

The cloud-to-ground lightning strike begins with the leader process; i.e., the formation of a plasma channel of ionized air. This is followed by a current surge, the return stroke. During the leader process, the average currents are on the order of 100A. Return stroke currents have peak values of tens of kiloamperes. A positive strike consists of a single return stroke; a negative strike will have from 3 or 4 to as many as 26 consecutive return strokes (Uman, 1969, P. 4) and has a duration on the order of tenths of a second.

Figure 2 depicts the two types of lightning threat--direct attachment of the lightning channel to the aircraft and a nearby strike. For the nearby strike, the dominant threat is the electromagnetic field associated with the main return stroke. For the directly attached case, there are two separate processes: initial leader attachment and return stroke (or strokes). The latter has much larger associated surface currents and is considered to be the dominant threat of the two. This paper will deal only with the return stroke threat, although the analysis methods are also applicable to leader attachment.

The starting point in threat definition is the lightning current waveform at the aircraft altitude. The most important lightning current parameters for induced effects analysis are peak amplitude, peak rate-of-rise, and total charge transfer for a single stroke.

Research scientists have been measuring lightning currents for many years, both directly (instrumented towers) and indirectly (magnetic fields). Unfortunately, all of the direct measurements and almost all of the indirectly measured data give information only on the current near the ground. Several U.S. agencies (NASA, NOAA, NSSL, and Air Force) are sponsoring in-flight measurement programs for the 1980 thunderstorm season. These in-flight programs will provide statistics for lightning currents at altitude, but a large data base is some years away. The lightning threat decreases with altitude. Until a complete in-flight data base is obtained, lightning protection design will be determined by the more severe ground-based data and, therefore, somewhat conservative.

As suggested by E. T. Pierce (Pierce, 1976), the double exponential waveform (see fig. 2) is a useful tool for calculating lightning-induced transients. This waveform is also referred to as the Bruce-Golde equation (Golde, 1977, p. 331). The three parameters of the double exponential are fit to the anticipated lightning current threat parameters (peak amplitude, peak rate-of-rise, and total charge) and then input into the analytical model to obtain predicted lightning-induced transients at the circuits.

For example, one may choose severe and moderate threats as follows:

Severe:

Peak current = 200 kA
Peak rate-of-rise = 2.1×10^{11} A/s
Total charge = 41C

Moderate:

Peak current = 20 kA
Peak rate-of-rise = 5.4×10^{10} A/s
Total charge = 1.6C

These two threats are composites based on statistics for cloud-to-ground positive strokes, negative first strokes, and negative subsequent strokes (Golde, 1977). Since all three categories of strokes are possible, the statistical data were treated independently.

It should be emphasized here that the double exponential is intended to simulate only the so-called "current peak" of the stroke (see Uman, 1969, pp. 131-133). The current peak has a duration of a few hundred microseconds and is followed by a slowly varying continuing current (also referred to as intermediate current) that lasts for several milliseconds. This low-frequency continuing current does not excite appreciable induced transients. It does, however, drive potentially damaging dc currents through circuits that use airframe for ground return. For circuits without dc conductive paths through airframe, the dominant threat is the current peak, and the intermediate currents may be neglected.

The severe stroke parameters chosen above fall in the upper 1% to 10% of the statistical distribution; the moderate stroke parameters are around the median. For example, the severe and moderate peak rate-of-rise values correspond to the upper 1% and upper 30%, respectively, for negative subsequent strokes (Golde, 1977, p. 326).

3. LIGHTNING-AIRFRAME INTERACTION

The lightning column-airframe interaction determines the current and charge densities over the conducting exterior surfaces of the airframe. These quantities are then used to obtain the fields at the location of wire bundles as described in section 4. There are two cases for which this interaction must be modeled: direct attachment and nearby strike.

3.1 Model for Direct Attachment

The lightning column has a diameter on the order of centimeters or less (Uman, 1969). When the small diameter lightning column attaches to a large diameter body such as a wing or fuselage, the impedance mismatch at the discontinuity causes reflections resulting in a high-frequency oscillatory waveform superimposed on the relatively low-frequency lightning current waveform. This effect may be approximated by modeling the airframe-lightning column as a mismatched transmission line (see fig. 3).

In figure 3,

- Z_L = characteristic impedance of lightning channel
- Z_{AC} = characteristic impedance of airplane
- I_L = lightning current waveform in the channel with the airplane removed
- L_{AC} = electrical length of current path through the airplane

This simple model gives the total current and charge in the airframe at any point along the current path. The surface current and charge are then obtained by calculating the effective circumference at the point of interest, using a two-dimensional field mapping. The current density on a conductor of elliptic cross section, for example, is given by the equation

$$J_s = \frac{I/C_{eff}}{\sqrt{a^2 - e^2 x^2}} 2\pi$$

where e = eccentricity, $2a$ = length of major axis, and x is the distance from the center along the major axis. Thus, the current and charge density along the leading and trailing edges of an aircraft wing (approximated as an ellipse) will be enhanced twofold or threefold above that for a cylinder of the same circumference.

3.2 Model for Nearby Strike

The surface currents and charges induced on an airframe by a nearby strike may be obtained by using a method of moments computer code to model the airframe. A simpler approximate model is to represent the fuselage or wings as an elliptic cylinder. The induced surface currents may be decomposed into common mode, obtained from the equations for an excited dipole, and differential mode, which may be obtained from the expression for an elliptic cylinder excited by an incident plane wave. Below dipole resonance, the differential mode dominates. The lightning fields incident upon the aircraft are obtained by modeling the lightning column as a long straight wire.

4. COUPLING MECHANISMS

Four basic coupling mechanisms for induced transients are listed below:

- a. Exposed conductors--conductors directly exposed to the lightning fields
- b. Apertures--nonconductive portions of airplane exterior (Some examples are the cockpit canopy, windows, and fiberglass access doors.)
- c. Joints--electrical discontinuities in aircraft exterior; e.g., the narrow gap between a metallic access door and underlying airframe or the interface between two graphite-epoxy panels
- d. Diffusion--low-frequency penetration of fields into the interior of metallic or graphite-epoxy fuselage, wings, etc.

The first three coupling mechanisms are important for both aluminum and composite aircraft. Diffusion is more important for composites than aluminum because of its lower conductivity.

The analysis methods employed for the various coupling mechanisms are as follows:

- a. Exposed wires. Using the method described in section 3, one obtains the fields directly. For more complicated structure, such as landing gear, it is necessary to do further analysis to obtain the fields on structural members protruding from the basic airframe.
- b. Apertures. When a conducting surface is interrupted by openings, the exterior surface fields penetrate into the interior (see fig. 4). At low frequencies, this coupling mechanism may be decomposed into magnetic and electric coupling (Vance, 1978), or, equivalently, stray inductance and capacitance between conductors in the interior of the body and the exterior surface. The magnetically and electrically coupled interior fields are proportional to the surface current and charge density that would appear on the shorted aperture. The magnetically coupled interior fields may be modeled, with certain restrictions, as those due to a magnetic dipole. Likewise, the electrically coupled interior fields may be modeled as those of an electric dipole, with similar restrictions. In the general case, one may solve for the interior fields by calculating the fields in the aperture and using the equivalent sources, distributed over the aperture, to solve the interior problem. The process is simplified by the fact that, for the lightning frequency spectrum, the apertures of interest are electrically small, reducing the problem to a quasi-static one.
- c. Joints. Joints may be divided into two categories: 1) slots and 2) strips having a constant admittance per unit length (see fig. 5). On equipment bay doors, for example, the hinge and latch sides make good electrical contact with structure, while the two other sides form narrow slot apertures. The fields of the slot may be modeled as those of a magnetic dipole. For wires lying across the slot, however, the voltage induced in the wire is simply the slot voltage at the wire location. The strip of constant admittance per length is quite similar, except that the voltage appearing across the strip is approximately constant along the strip as indicated in figure 5. For either type of joint, the interior fields may be obtained by using the fields in the opening to obtain the equivalent sources for solving the interior problem.
- d. Diffusion. This coupling mechanism is illustrated in figure 6. In the low-frequency limit, this mechanism is equivalent to what has been referred to in lightning studies (Fisher, 1977, p. 271) as the so-called "IR drop." For all-aluminum aircraft, this mechanism is important only for the low-frequency continuing current and is a threat only to circuits using structural return. For a graphite-epoxy aircraft, however, the electric fields associated with the high-frequency peak current can diffuse entirely through the structure, inducing considerable voltage in interior wiring. Figure 7 illustrates measured data for a typical graphite-epoxy transfer impedance. Comparing this with the lightning spectrum, it is apparent that the effective transfer impedance is well-approximated by the low-frequency asymptote, $1/(\text{conductivity} \times \text{thickness})$.

5. WIRE MODELING

The geometry of aircraft wiring lends itself naturally to transmission line analysis. Figure 8 is a lumped-element representation of a one-wire excited transmission line. Both electric and magnetic coupling may be important, but, for small gauge wiring, magnetic coupling dominates. Electric and magnetic coupling are inserted in the model as distributed current and voltage sources, respectively. See appendix A for proof.

Transmission line parameters are obtained from computing self and mutual inductances and capacitances for the individual wires in the bundle, along with wire and ground return resistance. These parameters are obtained from wire radius, wire-to-wire separation, height above ground plane, and dielectric constant of insulation, using textbook formulas.

Wire bundles having three or more conductors may often be modeled as random lay (i.e., wire-to-ground and wire-to-wire parameters the same for each wire and wire pair) with common mode sources. Differential mode effects are included by unequal loading at the bundle terminations.

6. PREDICTED INDUCED TRANSIENTS FOR COMPOSITE AIRCRAFT

The analysis methods described in sections 4 and 5 have been verified by comparison with measured data obtained from metal aircraft. At present, little or no data are available from composite-structure aircraft. There are substantial data, however, on the shielding properties of graphite and boron composites, as well as composites coated with shielding material. In addition, measurements of admittance for a variety of composite-to-composite and metal-to-composite joints have been obtained (see Strawe, 1975).

Using the data from Strawe, 1975, an analytical study was performed (Force, 1977) upon an idealized aircraft to scope the impact of graphite-epoxy upon avionic systems. The object of the study was an airplane of the size and shape indicated in figure 9, with two interior wires as shown. The wires were assumed to be single-wire transmission lines of 100 ohms characteristic impedance terminated at the wingtip and tail in 30-ohm loads. These wire models provide estimates of the common-mode threat to equipment in the cockpit in the form of open-circuit voltages and short-circuit current waveforms.

The common mode model provides estimates of the worst-case wire-to-ground threat to equipment. The common mode voltage V_{oc} approximates the maximum line-to-ground voltages in the corresponding cable bundle. The common mode current I_{sc} approximates the short-circuit bulk cable current. Individual wire current will normally be substantially less than the bulk current, although occasionally individual wire transient currents may equal or exceed the common mode current because of differential mode cable resonances.

Electronic equipment does not normally use structural ground as an equipment ground although connections to it are not uncommon. Ground or return wires (e.g., signal common) are normally provided. It is the wire-to-wire voltages and currents that represent the actual threats to circuits. Common mode responses (especially I_{sc}) tend to contain low-frequency tails of high energy content. These long-lasting responses are not often seen in the wire-to-wire voltages and currents because of the use of floating ground (return wires). The common mode responses for lightning are then excessive over estimates of circuit threats. Hence, for a more realistic threat definition, one must employ multiwire cable models so that both wire-to-wire and wire-to-ground response can be obtained.

Various composite and metal-composite configurations were compared in the study. An all-metal aircraft with electrically open cockpits was included for comparison. The configurations were as follows:

- An all-composite (graphite-epoxy) skin of uniform thickness (0.1 in = 0.0025m) and perfect electrical joints (This serves as a baseline comparison for other configurations.)
- An all-metal aircraft except for a composite (skin thickness = 0.1 in. = 0.0025m) vertical stabilizer, with perfect electrical joints
- An all-metal aircraft except for a composite (skin thickness = 0.1 in. = 0.0025m) right wing, with perfect electrical joints
- An all-metal aircraft with an imperfect resistive joint at the juncture of the vertical stabilizer and fuselage (The joint admittance was 15 mho/m.)
- An all-metal aircraft with an imperfect joint at the wing-fuselage juncture (the joint admittance was 15 mho/m.)

Tables 1 and 2 list the peak induced currents and voltages appearing on the two wires at the cockpit end. Figures 10 and 11 are representative waveforms. All transients were computed for an extremely severe stroke of 200 kA peak current and 7.2×10^{11} a/s peak rate-of-rise. For the nearby strike, a vertical lightning column at a distance of 100 meters was assumed.

Table 1. Peak Transients on nose-Tail Wire

NOTE: Values are given for open-circuit voltage (V_{oc}) and short-circuit current (I_{sc}) from wire to structural ground.

Threat	Transient type	Configuration			
		All-metal (open cockpit)	All composite	Composite tail Diffusion	Composite tail Joint
Nose-tail attachment	V_{oc}	4500V	32,000V	23,000V	2,100V
	I_{sc}	67A	1,100A	750A	70A
Nearby strike	V_{oc}	90V	250V	54V	21V
	I_{sc}	1.3A	8.2A	1.8A	0.70A

Table 2. Peak Transients on Nose-Wingtip Wire

NOTE: Values are given for open-circuit voltage (V_{oc}) or short-circuit current (I_{sc}) from wire to structural ground.

Theat	Transient type	Configuration		
		All composite	Composite wing Diffusion	Composite wing Joint
Nose-tail attachment	V_{oc}	6,500V	Not Applicable	Not Applicable
	I_{sc}	220A	Not Applicable	Not Applicable
Nose-wingtip attachment	V_{oc}	17,000V	11,300V	2,800V
	I_{sc}	550A	370A	95A

All the waveforms had the same shape as those of figure 10, except for aperture coupling through the cockpit, which is shown in figure 11.

7. CONCLUSIONS

General methods have been presented for the calculation of lightning-induced common-mode transients in composite aircraft. Results obtained from application of these methods to an idealized aircraft have been presented. As indicated in the text, these preliminary analyses considered only common-mode transients in the absence of nearby wiring. In real-world aircraft, the presence of nearby wire bundles, metal hydraulic lines, and other metallic components will partially shield the wiring, reducing the threat levels. A cost-effective protection system will take into account this gratis shielding. This does, however, complicate the analysis and requires measured data from full-scale low-level tests, as described in appendix B.

In summary, simple analyses provide design requirements for wire shielding and circuit protection. In order to take full advantage of the inherent protection afforded by the airframe and wire routing, it is necessary to obtain data from full-scale aircraft tests.

REFERENCES

1. Fisher, F. A., and Plumer, J. A., "Lightning Protection of Aircraft," NASA Reference Publication 1008, October 1977.
2. Force, R. D., Geren, W. P., Schneider, S. D., et al., "Investigation of Effects of Electromagnetic Energy on Advanced Composite Aircraft Structures and Their Associated Avionics/Electrical Equipment," Boeing Report D180-20186-4 prepared for Naval Air Systems Command contract NOC19-76-C-0497, September 1977.
3. Golde, R. H., Volume I, Physics of Lightning, Academic Press, 1977.
4. Pierce, E. T., et al., "Natural Lightning Parameters and Their Simulation in Laboratory Tests," SRI Project 3062, February 1976.
5. Strawe, D. F., and Piszker, L. D., "Interaction of Advanced Composites With Electromagnetic Pulse (EMP) Environment," AFML-TR-75-141, The Boeing Company, September 1975.
6. Uman, M. A., "Lightning," McGraw-Hill Advanced Physics Monograph Series, 1969.
7. Vance, E., "Coupling to Shielded Cables," Wiley-Interscience, 1978.
8. Weeks, W. L., "Electromagnetic Theory for Engineering Applications," John Wiley and Sons, 1964, ch. 2.
9. Young, D. E., and Piszker, L. D., "The Use of CW Test and Analysis Techniques in Lightning Vulnerability Assessment of Aircraft Systems," presented at the 1978 FAA and Georgia Tech Workshop on Grounding and Lightning Protection.

APPENDIX A

ELECTRIC AND MAGNETIC COUPLING FOR WIRES

Consider a wire loop shorted at both ends (fig. A-1) exposed to currents flowing through the ground plane. The short-circuit current in the wire at $x = 0$ is given by Weeks (1964) as

$$I_{SC} = \int_{z=0}^h E_z(0,0,z) G(0) dz + \int_{x=0}^L E_x(x,0,h) G(x) dx + \int_{z=h}^0 E_z(L,0,z) G(L) dz \quad (1)$$

where G is the appropriate Green's function.

$$\text{For } h \ll \lambda, \quad E_z(0,0,z) \approx E_z(0)$$

$$E_z(L,0,z) \approx E_z(L,0,0)$$

$$E_x(x,0,h) \approx h \delta E_x / \delta z$$

$$= h \left\{ \delta E_z / \delta x - j\omega B_y \right\}, \text{ so} \quad (2)$$

$$\int_{x=0}^L E_x G dx = -j\omega h \int B_y G dx - h \int E_z \frac{\delta G}{\delta x} dx \quad (3)$$

$$+ h \int_{x=0}^L E_z(x,0,0) G(x) dx$$

$$(1), (2), (3) = \Rightarrow I_{SC} = -j\omega h \int B_y G dx - h \int E_z \frac{\delta G}{\delta x} dx \quad (4)$$

In equation (4), the first term is the magnetic coupling term, while the second is electric coupling. The Green's functions correspond to those for distributed voltage and current sources (Weeks, 1964), hence the identification of magnetic and electric coupling with voltage and current sources.

APPENDIX B

TEST METHOD FOR LIGHTNING COUPLING ANALYSIS

The Boeing Company has developed a method for performing low-level measurements to obtain transfer functions for lightning coupling (Young, 1978).

Figure B-1 illustrates the electronics; a typical test configuration is depicted in fig. B-2. The system may be thought of as an FM transmitter and receiver, with the receiver phase-locked to the narrow-band transmitter. As the transmitter sweeps through the frequency range, the received signals are plotted as functions of frequency. Transfer functions may be measured directly by comparison of the drive and response channels (A and B in fig. B-1). As is apparent in figure B-2, the test configuration affects the distribution of currents and charges on the airframe. Field mapping of the airframe may be used to measure this effect. To apply the measurements to the in-flight case, one modifies the ground-based data, using a combination of analysis and field map data.

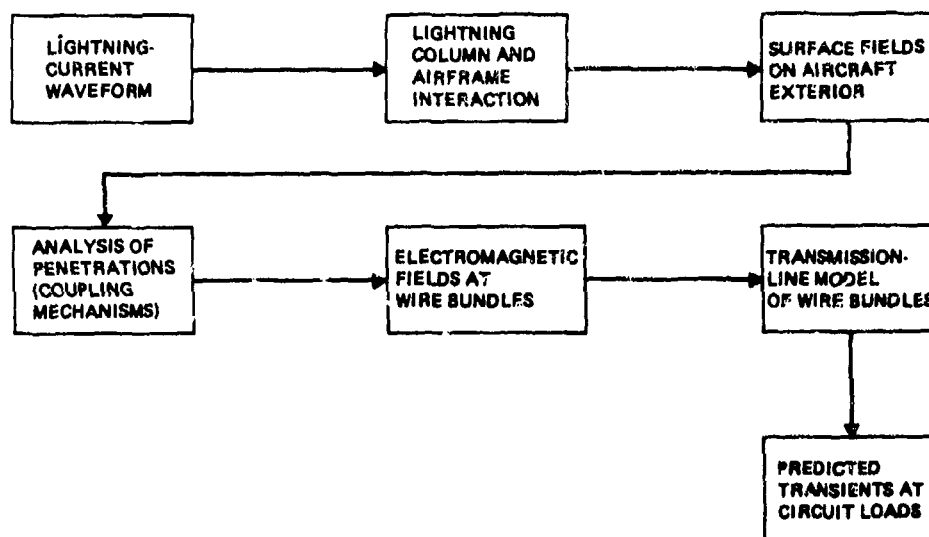


Figure 1. Flow Chart for Calculation of Lightning-Induced Transients

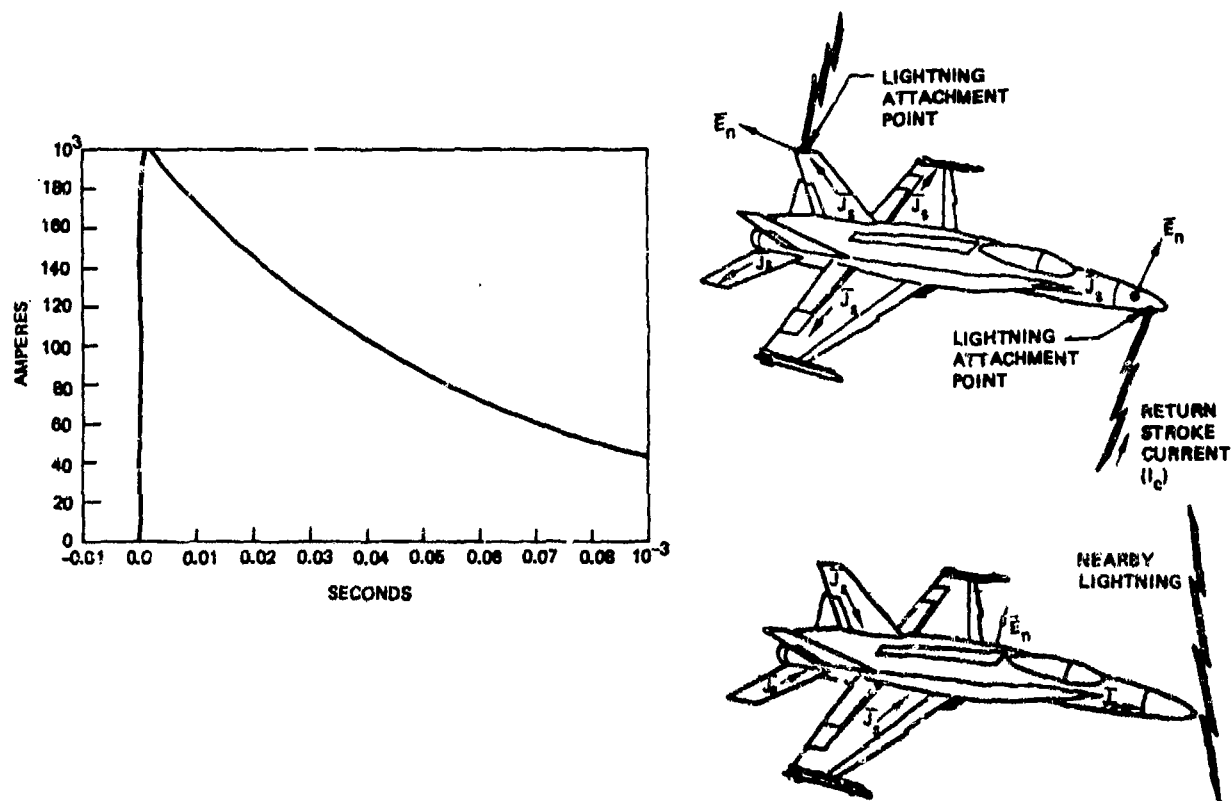


Figure 2. Lightning Threat to Aircraft

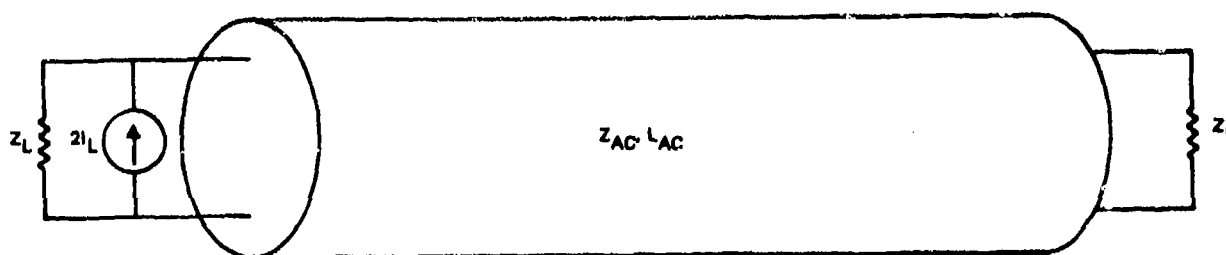


Figure 3. Transmission-Line Model for Aircraft and Lightning Column Interaction

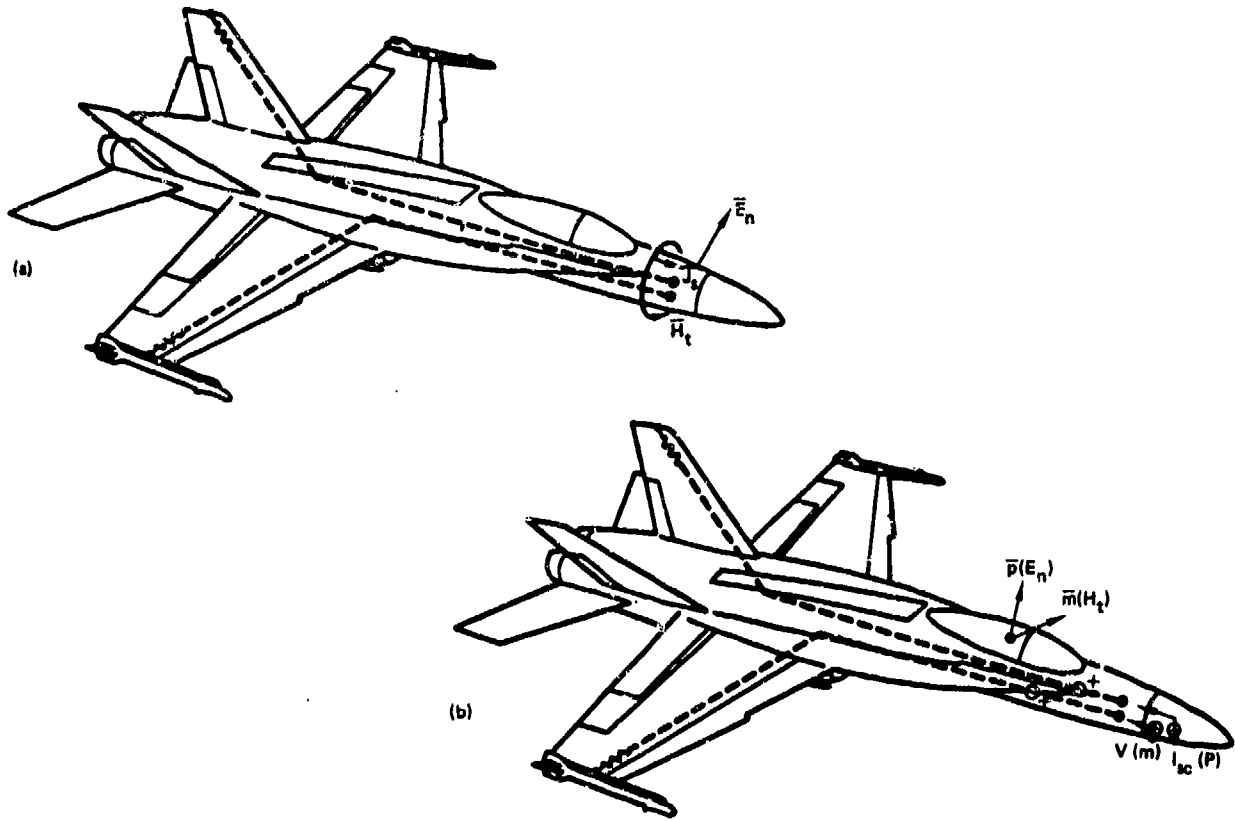
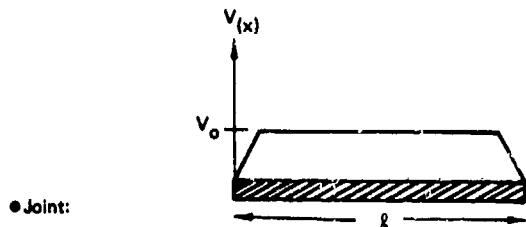


Figure 4. Apertures Coupling



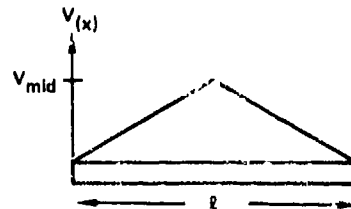
● Joint:

● Voltage distribution

● Impedance $V_0 = J/Y_j$

Y_j = joint admittance

J = surface current density



● Slot:

● Voltage distribution

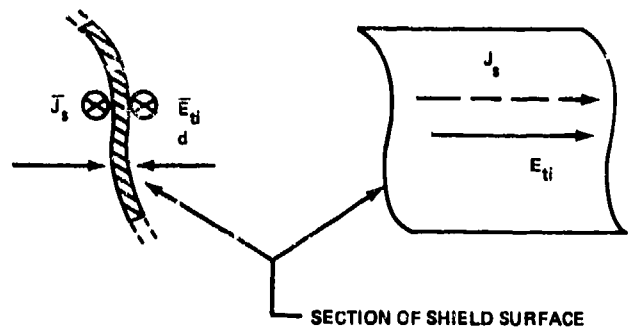
● Impedance

$$V_{mid} = Z_{slot} \times I_{eff} \times J_{sc}$$

$$Z_{slot} = Z_0^2 / 4Z_{dipole} \quad Z_0 = 120\pi$$

Z_{dipole} = impedance of complementary dipole

$$I_{eff} = \int_0^l V(x) dx / V_{mid}$$



$$E_{ti} = Z_{sd} J_s$$

E_{ti} (inner surface tangential electric field)

$$Z_{sd} = \frac{E_{ti}}{J_s} \text{ (outer surface skin current)}$$

● Thin surface:

$$Z_{sd} = \frac{\eta}{\sinh \gamma d}; \quad \eta = \sqrt{\frac{j\omega\mu}{\sigma}}; \quad \gamma = \sqrt{j\omega\mu\sigma}$$

Figure 5. Joint and Slot Coupling (Low Frequency Approximation)

Figure 6. Diffusion Coupling

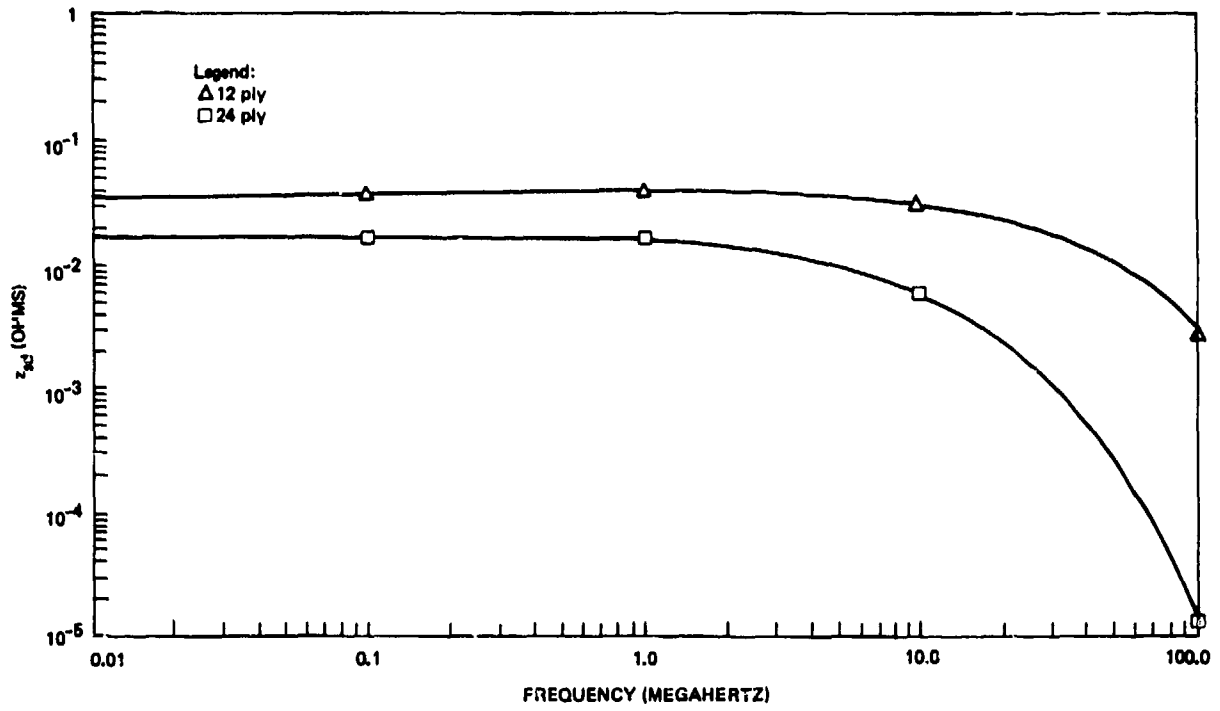


Figure 7. Transfer Impedance for Graphite Epoxy

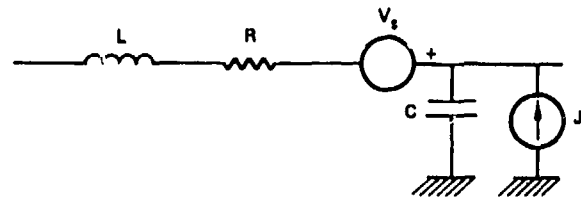


Figure 8. Transmission-Line Model for Aircraft Wiring

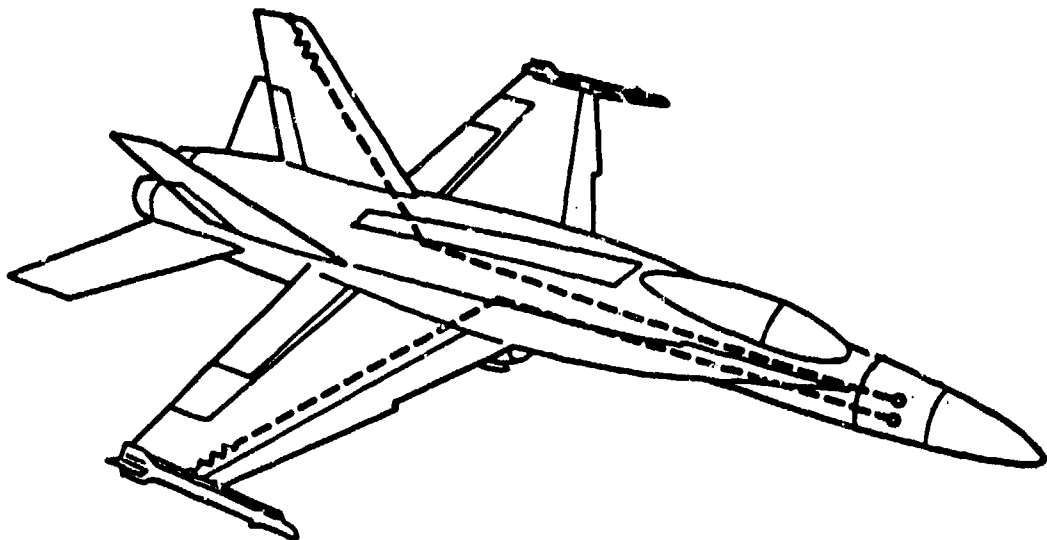


Figure 9. Idealized Aircraft for Lightning Study

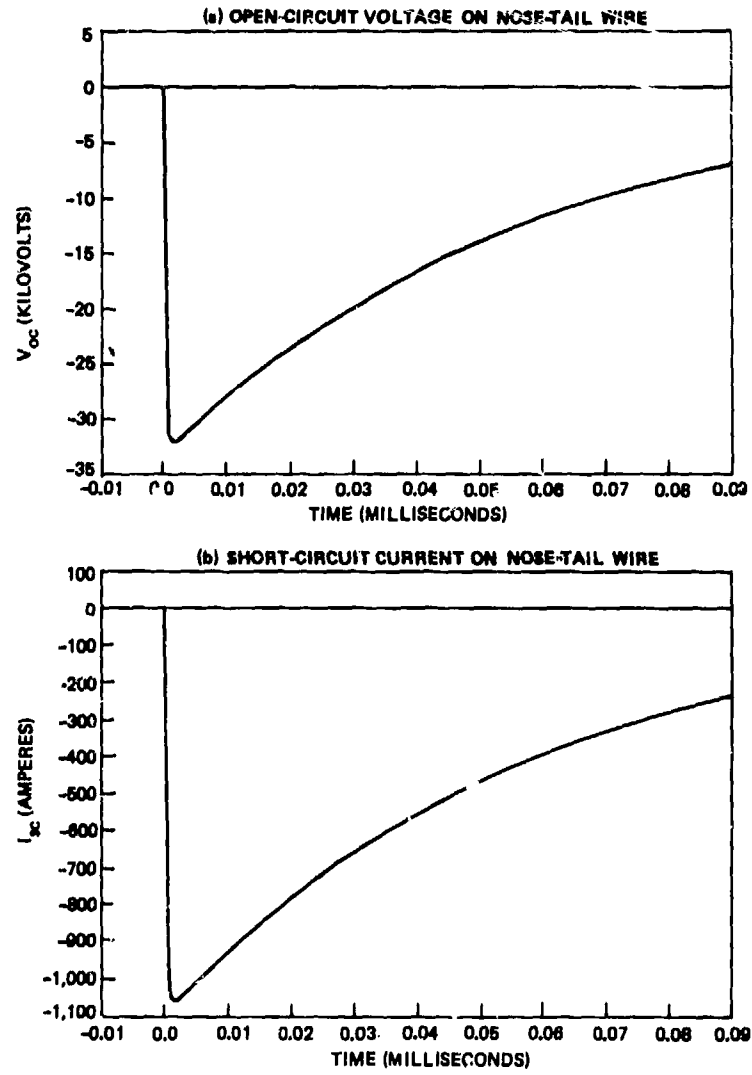


Figure 10. Transients on Nose-Tail Wire for Nose-Tail Lightning Strike—All-Composite Aircraft

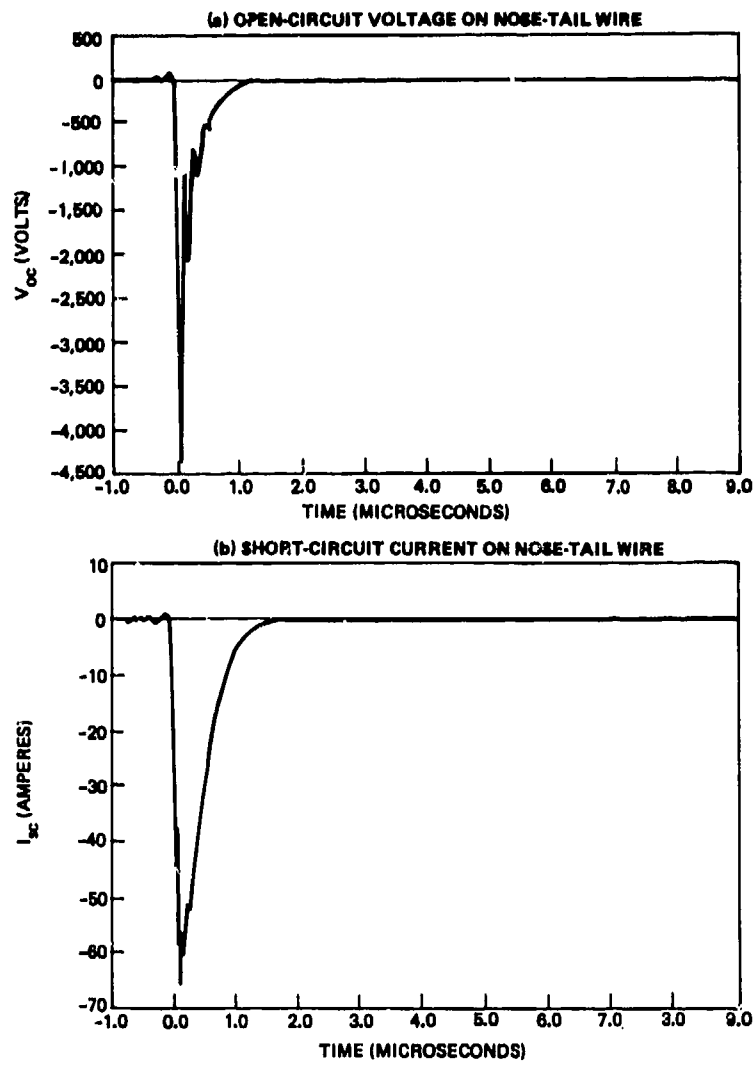


Figure 11. Transients on Nose-Tail Wire for Nose-Tail Lightning Strike—Coupling Through Cockpit Aperture

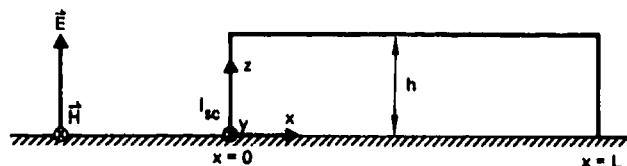


Figure A-1. Geometry for Excited Wire

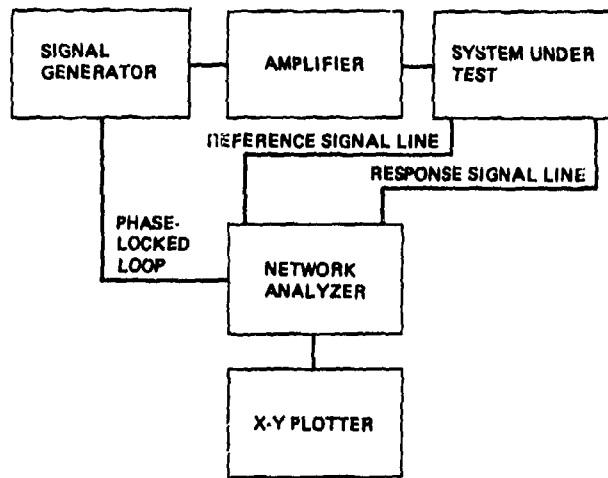


Figure B-1. Swept Continuous-Wave (CW) Measurement System

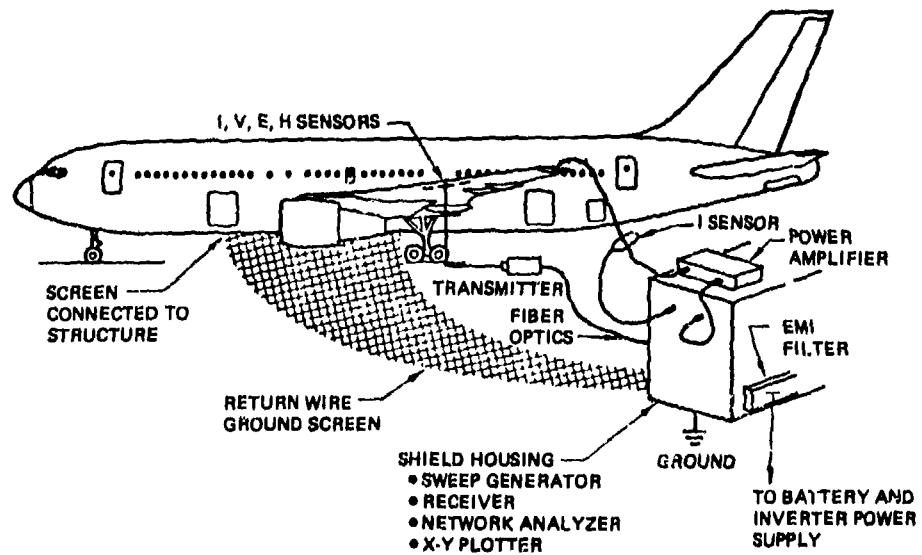


Figure B-2. Continuous-Wave (CW) Test Configuration

ELECTRICAL/ELECTROMAGNETIC CONCERNS ASSOCIATED WITH ADVANCED COMPOSITE
MATERIALS IN AEROSPACE SYSTEMS

CHRISTOPHER L. BLAKE
JOHN C. CORBIN, JR.

Aeronautical Systems Division
Directorate of Avionics Engineering
Wright-Patterson AFB, Ohio 45433

SUMMARY

This paper presents an assessment of the potential electrical/electromagnetic impacts created by the application of advanced composite materials to aerospace systems that was conducted by the United States Air Force 1979. Technical specialists from three Air Force organizations (Aeronautical Systems Division, Air Force Wright Aeronautical Laboratories, and Space and Missile Systems Organization) comprised a working group that elicited responses from specific Government agencies and aerospace contractors involved in the application or studies of composite materials. In addition to onsite visits and briefings to obtain information, a major source of data used in formulating the assessment was responses received to a broadly defined questionnaire sent to involved organizations. The assessment was specifically limited to two predominantly used varieties of graphite composite materials, GY-70 and T-300, and to Kevlar. The GY-70 has the higher conductivity and is used primarily on missiles and spacecraft. The T-300 grade has a slightly lower conductivity than GY-70 and is the material commonly applied to aircraft based upon its mechanical properties. Kevlar, a dielectric material, has varied aircraft, missile and spacecraft application. Specific areas of electrical/electromagnetic concern were surveyed. As a result of the survey, a number of significant concerns were defined. There are, however, no "show stoppers" in the use of composite materials. Leading concerns include shielding effectiveness (a lack of standardized material characterization within acceptable and defined error bounds), joint design (bonding of joints and seams), fuel tank design (spark-free fuel tanks), power system grounding, low frequency antenna performance, analytical techniques (lack of validated computer codes for designers), combined space environment effects, and design guides (lack of handbook information on composite materials). Recommended actions include technology development programs and the establishment of a combined Tri-Service/NASA effort to address the composite electrical/electromagnetic technical base and to collect, analyze, and distribute related data, establish standard test methods, develop design guides/handbooks, and develop applicable specifications/standards.

1. INTRODUCTION

Advanced composite materials in the form of fiber-reinforced matrix compounds (e.g., graphite/epoxy, Kevlar/epoxy) are being used in increasing amounts as structural and surface members in aerospace systems (aircraft, missiles, spacecraft). This growth has progressed over the past decade from limited use in empennage and secondary structure to major use in body enclosure and primary load bearing sections. The drive behind this transition from metals to composites has been the markedly improved strength-to-weight ratios of these composite materials. As composites are used to reduce the weight in major elements, a combination of increased performance, greater payload, and/or fuel savings can be realized.

As designs transition from metal to composites, electromagnetic characteristics of the aircraft can substantially change. Largely taken-for-granted features of the all-metal aircraft such as (1) readily available "common ground" return paths for signal and power, (2) a low impedance, high conductivity outer skin for carrying direct lightning strike currents and dissipating precipitation static charges, (3) shielding of 20 db or more between the external electromagnetic environment and internal aircraft electronics, and (4) relatively unbroken counterpoise systems for aircraft antennas will have to be re-examined. A new technology data base will have to be established if design changes have to be made to assure safe and satisfactory aircraft operation.

2. INITIATION OF STUDY

As a result of concern within the Air Force that the electrical/electromagnetic (E/EM) issues were not being adequately addressed in balance with associated structural development technology, an assessment study was requested by Air Force Headquarters. An Assessment Group representing the Aeronautical Systems Division (ASD), Air Force Wright Aeronautical Laboratories (AFWAL), and Space and Missile Systems Organization (SAMSO), all of the Air Force Systems Command (AFSC), accomplished the study.

The primary objective of the assessment was to determine the status of advanced composite material development in areas associated with possible E/EM impacts to aerospace systems. Fundamental to this effort was an examination of the potential E/EM susceptibilities of aerospace systems which utilize advanced composite materials. With an understanding of the possible system susceptibilities, the study centered on the research and development balance between structural and E/EM issues and on the evolution of a technology data base needed to support composite systems acquisition activities.

A further goal of the study was to involve a large cross section of the composite and electrical communities in order to determine a balanced consensus and also to learn minority opinions. A very significant result of the study was the exchange of data, information, and ideas among researchers and users.

3. CONDUCT OF STUDY

The study was conducted over a six month period from April to September 1979. A questionnaire was prepared and sent to Government agencies and companies known to be involved in composite activities. Responses were received from twenty-four separate organizations. These responses represented a major source of data used in formulating the assessment conclusions. In addition to the questionnaire, visits were made to ten organizations for in-depth discussions of specific sensitive areas and precise interpretation of written responses to the questionnaire received earlier.

On 22-23 June 1979, the Assessment Group sponsored a joint Government/Industry meeting at Wright-Patterson AFB which consisted of a series of invited technical presentations, a presentation of consolidated questionnaire responses, and an exposition of preliminary findings and probable recommendations.

A final briefing was prepared in September. Formal briefings up to Headquarters Air Force and Office of the Secretary of Defense level were given from September to December 1979.

4. SCOPE OF STUDY

The Assessment Group was tasked to assess the status of research and development efforts associated with the application of advanced composite materials to aircraft, missiles, and space systems.

Key to the study was a close examination of the basic technology issues (e.g., defining the appropriate E/EM environment, acquiring the technology data base, transitioning the data to the user, and educating the designer in the use of composite materials for various system/subsystem applications). By examining a broad spectrum of responses to questions on these issues, the Assessment Group established a sound base on which to make recommendations for future actions.

To limit the study to a manageable size, two widely used graphite epoxy composites (T-300/AS and GY-70) and a glass laminate composite (Kevlar) were chosen for evaluation. This limitation of materials restricted the electrical/electromagnetic concerns to two different conductive varieties of composites, the graphite epoxies, and to a nonconductor (Kevlar) with electrical properties similar to fiberglass. GY-70, a high modulus of elasticity material, is typically used in missile, spacecraft, and specialized aircraft applications. GY-70 is characterized as conductive, since it is only 10^{-3} less conductive than aluminum. T-300, a high strength material, is generally applied to aircraft and is only slightly less conductive than GY-70.

All other available epoxy composite materials have conductivities which are bounded by the graphite composites and Kevlar. In addition, there is a basically linear relationship between conductivity and modulus of elasticity which will be discussed later.

Topics surveyed were generally grouped under the major headings of implementation issues, E/EM concerns, and future development needs. Implementation issues involved design capability and design data. E/EM concerns included the direct and indirect effects of lightning, antenna performance, effects of static electricity, radar cross section (RCS), electromagnetic interference (EMI), electromagnetic compatibility (EMC), nuclear electromagnetic pulse (NEMP), power subsystem design, system generated EMP, other nuclear effects, and space environmental effects. Development needs considered both long and short term goals.

5. TOPICS SURVEYED

5.1 Implementation Issues

The current capability for design of an advanced composite aerospace system which requires an extensive data base on material characterization, acceptable design approaches, and life cycle acceptability of design methods was one target for examination of this study. The other study target, E/EM concerns, will be discussed later.

5.2 Design Capability

As should be expected, the E/EM data base supporting composite application is fragmented because the pieces have been generated by many different, essentially unrelated research and development programs. Although a great deal of data exists, the lack of necessary data collation and distribution of these resources is an obvious weakness in this development process. No formalized guidelines or utilization documents are available which address electrical or electromagnetic topics. A document of E/EM information would be invaluable to provide design alternatives, a basis for risk assessment, and an education tool for the inexperienced composite user. An existing document, the DOD/NASA Composite Design Guide, might be expanded to include this information.

From available data, deviations to EM-related specifications and standards necessary for controlled composite application are understood. However, the evaluations required to identify resulting implications of these deviations are yet to be accomplished (e.g., the 2.5 milliohm bonding requirement of MIL-B-5087B cannot be attained; however, it probably need not be an absolute requirement).

Computer programs, used extensively in the engineering design process, involve obvious assumptions of metal-peculiar characteristics requiring reconsideration. Computer codes developed by the Nuclear Electromagnetic Pulse (NEMP) community can be adapted to composite system evaluations by factoring in conductivity changes. Those codes used by the Electromagnetic Interference and Compatibility community (e.g., IEMCAP, SEMCAP, etc.) are not capable of considering composite uniquenesses (Note: Unfortunately, this is an insignificant point because these codes are not mature for metal systems).

An underlying awareness which surfaced during this study was a lack of maturity of E/EM supporting technology involving durability, maintenance and configuration control issues. Although solutions to

technical problems are, or can be, readily available, premature utilization of unproven or unverified technology could create long term risks.

5.3 Design Data

Three major elements of an electromagnetic design data base which most concern composite users are material properties, configuration parametric description, and life cycle information.

Many different composite materials appear to be available for the aerospace application. However, based on mechanical characteristics, only certain materials are being used or considered for use. Kevlar applications utilize fiberglass electrical protection technology based on conductivity similarities. Graphites, on the other hand, are much nearer in conductivity to aluminum (10^{-3} as conductive) and need not rely on fiberglass technology. The modulus of elasticity, which is basically linear with conductivity, is a well controlled parameter of graphite epoxy composites and thereby effectively limits variations in conductivity.

Good material characterization is required to define system parameters. Information available on conductivity has yielded many different descriptions of system parameters such as shielding effectiveness, joint impedance, or transfer impedance. A major dilemma exists because there are no uniform definitions or standard measurement techniques for these parameters. The varied data available from composite research programs are not universally accepted for this reason. In fact, one company can't, or won't, use another's data due to lack of standardization.

With respect to life cycle cost issues (e.g., producibility, maintainability, durability, repairability, etc.), little effort has been expended to assure reasonable design considering life cycle tradeoffs. Although some programs have addressed limited aspects, there are no guidelines for building cost effective composite systems. Again, this is not to imply an inability to produce a design, only to indicate an area requiring development to reduce long term acquisition risks.

Composite material E/EM technology has matured sufficiently so that researchers have begun identifying tradeoffs between structural hardening, subsystem hardening and interface hardening. The limitations caused by issues previously mentioned and by some as yet unresolved E/EM concerns still impede this effort.

5.4 Electrical and/or Electromagnetic (E/EM) Concerns

Table I categorizes the E/EM concerns into five levels - insignificant, minor, intermediate, major or unknown on the basis of current understanding and risk associated with the application of composite materials to aerospace systems. The text supports and explains the various categorizations. The E/EM concern is also identified in Table I in terms of conductivity, transfer impedance, joint impedance, and grounding.

5.4.1 Lightning Direct Effects

Natural lightning presents a very large, potentially damaging electrical event to aerospace vehicles. Currents from direct lightning attachments can burn, pit, arc and cause significant damage to the aerospace structure. Entry of lightning energy into the vehicle can damage internal subsystems. Further, arcing and/or local heating may result in fires or explosions in fuel systems. Such lightning effects, however, present manageable challenges to designers of metal technology aircraft. Using composite materials complicates the designer's task.

Lightning interaction with fuel systems may be the most serious complication resulting from composite applications. (Golam, G. ... 1978). Specific concerns are possible dangerous voltage potentials caused by end-to-end I-R voltage drops, arcing between conductive plumbing lines permitted by increased bonding resistance, or possible hot spot (point of attachment) release of heated material causing vapor ignition. Specific development activity will be required to fully resolve these issues.

With respect to other direct lightning effects, intensified research accomplished in the early seventies has led to a relatively good definition and understanding of the potential physical damage mechanisms involving composite structure. A variety of options has been developed which provides designers with guidelines for selection of particular design approaches (Schneider, S. D. ... 1978; Fisher, F. A. ... 1973; Quinlivan, J. J. ... 1971; Brick, R. O. ... 1972). In essence, the need for lightning protection of composite structures of aerospace systems can be determined and, if needed, effectively provided.

5.4.2 Lightning Indirect or Induced Effects

Lightning induced effects refer to the responses within the aerospace system caused by electromagnetic energy released during a lightning event. The technologies associated with characterization of the lightning event, the analytical prediction of effects, and the prevention of unacceptable responses are immature. Government sponsored R&D programs have recently evolved a number of techniques which offer potentially valuable guidance to designers of composite vehicles in providing resistance to lightning induced energy (Wallace B. J. ... 1978, Wallace, B. J.; Burrows, B. J. C. ... 1978). Much of the basic work necessary to develop protection techniques for the induced lightning threat has either been completed or is being addressed in continuing and proposed programs (Wallace, B. J. ... 1978; Wallace, B. J.; Burrows, B. J. C. ... 1978; Air Force Flight Dynamics Laboratory, 1978). However, due to the inability of designers to analytically determine hardness margins (measure of immunity to electromagnetic effects), the application of protection techniques cannot now be optimally matched to protection requirements. The application of graphite epoxy composite in areas on aerospace systems which contain electronics or wiring reduces material conductivity and increases structural joint impedance, resulting in a reduction in the shielding ability of the structure. Once provided with the basic data and methodology needed to perform tradeoffs, system designers may combat increased levels of electromagnetic energy by either increasing the immunity of subsystems or improving the shielding properties of the structure.

TABLE I

	I	II	III	IV	V	A	B	C	D
LIGHTNING DIRECT EFFECT									
Structural Effects		X				X			
Fuel System Effects			X			X		X	X
LIGHTNING INDIRECT EFFECTS			X			X	X	X	X
ANTENNA PERFORMANCE									
HF & LF			X					X	X
VHF - L Band		X						X	X
Above L Band			X			X		X	
STATIC ELECTRICITY		X						X	
RADAR CROSS SECTION		X				X			
Low RCS Observable Case			X					X	
EMI/EMC/EMP			X			X	X	X	X
POWER SYBSYSTEM			X			X		X	X
SYSTEM GENERATED EMP					X	X			
OTHER NUCLEAR EFFECTS					X				
SPACE ENVIRONMENTAL EFFECTS					X				

I - INSIGNIFICANT - No implication due to composites.

II - MINOR Sufficient data available to allow design alternatives.

III - INTERMEDIATE - A data base exists; however, R&D is necessary prior to or during development program.

IV - MAJOR - Insufficient data available to preclude high risk application, or data indicate significant risk.

V - UNKNOWN - impact unknown since no data are available.

A - CONDUCTIVITY - Concern relative to increased impedance.

B - TRANSFER IMPEDANCE - Concern relative to conductivity changes resulting in reduced shielding effectiveness.

C - JOINT IMPEDANCE - Concern relative to reduced joint conductivity, (involving electrical continuity and electrochemical isolation).

D - GROUNDING - Concern involving electrical signal reference to composite.

The Air Force Flight Dynamics Laboratory has prepared a Technology Program Plan (Air Force Flight Dynamics Laboratory, ... 1978) which specifically addresses the induced lightning problem with the goal of demonstrating protection technology for tomorrow's aerospace systems. This program has added importance in that it addresses other primary concerns identified by the assessment.

5.4.3 Antenna Performance

The impact of composite materials on the performance of antennas varies depending on the type of antennas involved and on the type of material. Nonconductive composites, such as fiberglass or kevlar, may use metallic surface treatments to preclude antenna impact. However, graphite epoxy materials serve as adequate ground planes for some antennas (Skoby, C. C. ... 1975; Hudson, J. L. ... 1974). Little data exist as to the performance of antennas operating above one GHz and below 30 MHz. Increased joint impedance will likely affect HF and LF antenna current circulation and, therefore, the performance of those antennas.

The many varied potential composite applications involving spacecraft antennas require significant examination to preclude inappropriate use of fiberglass technology and to retain weight savings benefits.

5.4.4 Static Electricity

The potential for encountering static electricity problems is a surface conductivity issue. For the boundary cases, Kevlar requires a surface treatment while graphites do not in themselves affect the charging character of aerospace systems. Graphites are sufficiently conductive to preclude charge storage; however, a fundamental conflict between conductivity and corrosion control may present a significant task to the designer. A potential electrochemical corrosion problem with the aluminum to graphite joint is solved by electrical isolation which is contrary to most electrical design approaches. The development of conductive, non-corrosive joints will preclude any static problems. Relative to conductivity, the benefit of properly designed joints to other electrical issues should be obvious.

5.4.5 Radar Cross Section (RCS)

RCS (a measure of radar power reflected from a structure back to the radar transmitting antenna proportional to the area of a sphere which when radiated produces the same return power as that of the structure) was anticipated to be significantly impacted by the application of graphite composites to the aerospace structure. Tests comparing aluminum to graphite, however, have shown no significant difference in RCS (Hudson, J. L. ... 1974).

Low RCS observable requirements may be cause for concern because the joints in the material may produce larger radar returns than those in metal structures. The level of concern is low due to factors associated with reducing other more significant return sources. However, if a low RCS observable design is to be realized utilizing graphite composites, the joint question should be answered.

5.4.6 Electromagnetic Interference (EMI), Electromagnetic Compatibility (EMC) and Nuclear Electromagnetic Pulse (NEMP)

These issues embody the fundamental concerns associated with the use of composite materials. The technical disciplines of EMI, EMC and NEMP are all directly related by the same physical laws and are controlled by the same design concepts. In a very general sense EMI, EMC and NEMP involve the generation of, detection of, susceptibility to, and protection from electromagnetic energy associated with electrical and electronic subsystems, natural sources and nuclear events. The design of the structure, which contains electrical or electronic equipments, is of primary importance given that most control techniques are associated with or referenced to the system structure. Fundamental tools of the EM designer are the equipotential ground plane and "Faraday Cage" typically provided by metal structure as mentioned earlier. When the metal structure, or portions thereof, is replaced by graphite epoxy, these fundamentals may be degraded. Again, the reduced material conductivity and joint impedance are the sources of concern. The impacts may include reduced shielding effectiveness of the structure; degraded electrical filter operation; increased bonding resistance for boxes and signal and shield terminations; degraded interface references; etc. (Wallace, B. J. ... 1978; Wallace, B. J. ... 1978; Skoby, C. D. ... 1975; Hudson, J. L. ... 1974; Force, R. ... 1977; Maxwell, K. J. ... 1979; Kim, D. G. ... 1974). The severity of such impacts depends heavily on the configuration of the material and the structural concepts utilized. A correct interpretation of available data is necessary to define degrees of concern with particular issues, eg., shielding effectiveness may be reduced significantly at specific frequencies but may be "as-good-as-metal" at others or the insertion loss of a filter may be reduced an order of magnitude at a specific frequency but may be adequate to ensure proper operation. Taken individually, these issues are not major concerns; however, the combined effects should be taken seriously. Given sufficient attention, many EMI, EMC and NEMP problems may be precluded. However, the fact that graphite composites present a reduction in the ability to control the effects associated with these EM sources must be a consideration in applications until defined control techniques are available. Further, trends toward more sensitive electronics and more powerful EM sources add an additional complication to this issue.

5.4.7 Power Subsystem Design

The lifeblood of the electrical and electronic subsystems is electrical power. In the aerospace vehicle the electrical power distribution systems are relatively complex and significant portions of the hardware. The supply of direct or alternating current to equipments is accomplished with a large amount of wire with the current returned typically through the structure. Because of the low resistance/impedance of metallic structure, the losses associated with this technique of power distribution are manageable. The increase in resistance/impedance due to composite materials results in additional distribution losses which range from marginal to unacceptable relative to system performance

(Wallace, B. J. ... 1978). Alternative design concepts may be available that provide acceptable performance given due consideration to system tradeoffs involving net weight savings.

Lightning induced effects are particularly critical because of the large voltage created on the power wires during lightning events. Experiments have shown that designs using structural return are likely to encounter large I-R voltages created by the resistance of the composite material (Wallace, B. J. ... 1978). The currents which result from direct or nearby lightning events exist in metal and composite structure, but due to the increased composite resistance, the resultant voltage is much higher in composites. The obvious concern is overvoltage to subsystems or the need for special design methods to preclude a major problem.

5.4.8 System Generated EMP (SGEMP)

SGEMP (Secondary electron emission resulting from free electron release caused by radiation effects) is a real concern for metal aerospace structures. However, for composite structures, the emphasis shifts to internal radiation effects at the box level. Little is apparently known relative to SGEMP impacts on equipment; therefore, the level of concern has not been established.

5.4.9 Other Nuclear Effects

This area has been left as a catch-all for nuclear effects produced by gamma radiation, X-ray radiation, etc., which may or may not degrade the effectiveness of hardness measures applied to aerospace systems. The level of concern is low based on anticipated hardening approaches. However, it is an issue which should be considered since little data currently exist.

5.4.10 Space Environmental Effects

The concern here is, in practical terms, essentially identical to that of Other Nuclear Effects, with the exception of space charging. Very little is known of potential EM interactions of the environmental degrading effects encountered in space. There are programs underway to address these issues, since experience has shown definite cause for concern.

6. STUDY FINDINGS

Of the issues considered, the leading concerns were:

- Lightning spark free fuel system designs
- Lightning indirect effects
- Bonding of joints and seams
 - Corrosion control
 - Electrical durability
 - Structural integrity
 - Producibility
- Power system grounding
- HF and LF antenna performance
- Combined space environment effects
- Specific data on parametric values
- Transition of technology

These leading concerns are direct reflections of differences between the properties of composites and metals and of limited data and experience. The property differences resulting from decreased conductivity, reduced shielding effectiveness, and increased joint impedance are major factors in all the concerns mentioned.

The level, or ranking, of concern over various topics between industry and Government engineers is primarily dependent on their experience with these topics. The more experience engineers have with the E/EM topics, the fewer their concerns. An unfortunate fallout of such experience has been the development of pockets of company-owned data unavailable to the general engineering public. The feeling of a need to develop company-owned data bases can only be eliminated by providing a common data base and means for distribution of available information.

7. CONCLUSIONS

Even with the changing roles of materials, the use of more sensitive electronics, and potentially more severe electromagnetic environments, the engineering community as a whole is optimistic that the benefits afforded by using composites can be sustained. Although E/EM development appears to be lagging structural development, it is considered in balance as compared to any normal development effort. There are no show stoppers precluding the use of advanced composite materials in aerospace systems. There are, however, specific areas requiring clarification and development. Based on the findings, a series of recommendations to Air Force activities responsible for research and development have been made. The study group concluded that technology development is essential in five major areas:

1. Shielding characterization and standardization are necessary to provide the user with basic electrical characterizations of designs and with universally accepted data (to eliminate the "not measured here" issue).

2. Effective, durable, maintainable, producible electrically conductive joint technology is necessary to allow accurate design characterization and to eliminate many design concerns.

3. A lightning proof fuel system design is required. In addition to the usual problems of arcing and sparking, the problem of hot spot ignition is of major concern.

4. Design alternatives require definition and demonstration to preclude distribution loss and lightning induced transient problems with sensitive, critical electronic systems and power system returns.

5. Because little data are currently available, the effects of the space environment on the material and E/EM related design features require definition.

Obviously, other technical areas are involved (e.g., EMI filter efficiency, signal return impedance, chassis ground impedance, etc.); however, these are secondary because the assurance of good conductivity, via good joint designs, can be expected to preclude many secondary problems.

Based on available research data, the revision to current specifications and standards should resolve to a numbers game (increasing bonding values, increasing permitted voltage losses, etc.). The data necessary to take an initial cut at these changes, while examining implications, are available.

Finally, to preclude duplication and assure a close working relationship, a dedicated tri-service/NASA/FAA working group is necessary. Primary responsibilities would include program coordination, development of design guides and handbooks, information exchange, development of specifications/standards or changes, and development of standard test methods for critical areas such as shielding measurement.

The Air Force has taken an active interest in this subject and indications are that Command support for necessary research and development is likely. Current Air Force activity includes a planning effort to scope necessary development and produce a roadmap outlining Command responsibilities. A key to successful composite utilization on aerospace systems will be initiative and cooperation on the part of the total composites community, structural and electrical, contractors and Government.

REFERENCES

1. Air Force Flight Dynamics Laboratory, 1978, "Atmospheric Electricity Hazards Protection (AEHP) of Advanced Technology Aircraft (Electrical/Electronic Subsystems), "Air Force Wright Aeronautical Laboratories.
2. Brick, R. O.; King, C. H.; Quinlivan, J. J., 1972, Technical Report AFML-TR-70-303 - Part II, Coatings for Lightning Protection of Structural Reinforced Plastics, Boeing Company, Seattle.
3. Fisher, F. A., 1973, Technical Report AFAL-TR-72-5, Lightning Effects Relating to Aircraft Part IV - Structural Properties of Graphite Fiber Epoxy and Polyimide Composites After Exposure to Simulated Lightning, General Electric Environmental Electromagnetics Unit.
4. Fisher, F. A.; Fassel, W. M., 1972, Technical Report AFAL-TR-72-5 Lightning Effects Relating to Aircraft Part I - Lightning Effects on and Electromagnetic Shielding Properties of Boron and Graphite Reinforced Composite Materials, General Electric High Voltage Laboratory and Philco-Ford Corporation Aeronautics Division.
5. Force, R.; Geren, P.; Strawe, D., Schmidt, A., 1977, Boeing Report D180-20186-4 Investigation of Effects of Electromagnetic Energy on Advanced Composite Aircraft Structures and Their Associated Avionics/ Electrical Equipment Volume I, Boeing Company Seattle.
6. Gajda, W. J., 1979, Technical Report RADC-TR-79-203 Measurement of the Electrical Properties of Composite Materials in the Frequency Range of DC to 30 MHz, Syracuse University.
7. Golam, G.; Carri, R.; Dastin, S., 1978, Fourth Quarterly Progress Report Protection Optimization for Advanced Composite Structures, Grumman Aerospace Corporation.
8. Golam, G.; Carri, R.; Dastin, S., 1978, Fifth Quarterly Progress Report Protection Optimization for Advanced Composite Structures, Grumman Aerospace Corporation.
9. Hudson, J. L.; Sneed, J. W.; Avery, L. R., 1974, Technical Report AFML-TR-71-41 Advanced Composite Technology Fuselage Program, General Dynamics Fort Worth.
10. Kim, G. D.; Dubro, G. A.; Beaven, R. C., 1974, Technical Report AFFDL-TR-74-30 Measurement of Advanced Composite Materials Shielding Effectiveness, Air Force Flight Dynamics Laboratory.
11. Maxwell, K. J.; Mangold, V. L., 1979, Technology Report AFFDL-79-69-FES Measurements of Shielding Effectiveness and Static Charge Characteristics of Various Composite/Aluminum Joint Combinations, Technology Scientific Services, Inc. and Air Force Flight Dynamics Laboratory.
12. Quinlivan, J. J.; Kuo, C. J.; Brick, R. O.; 1971, Technical Report AFML-TR-70-303 Part I Coatings for Lightning Protection of Structural Reinforced Plastics, Boeing Company Seattle.
13. Schneider, S. D.; Hendricks, C. L.; Olson, C. O.; 1978, Technical Report AFFDL-TR-77-127 Vulnerability of Composite Structures Lightning Strike (Program Results), Boeing Commercial Airplane Company.
14. Skouby, C. D., 1975, McDonnell Aircraft Company Report MDC-A3441 Electromagnetic Effects of Advanced Composites, McDonnell Aircraft Company.
15. Walker, W. F.; Heintz, R. E.; 1979, Technical Report RADC-TR-79-255 Measurement of Electrical Conductivity in Carbon/Epoxy Composite Material over the Frequency Range 75 MHz to 2.0 GHz, Syracuse University.
16. Wallace, B. J.; Burrows, B. J. C.; Zeitler, R. T.; Ledwig, A. J.; Wiles, K. G.; 1978, Technical Report AFFDL-TR-78-110 Volume II Composite Forward Fuselage Systems Integration, General Dynamics Fort Worth.
17. Wallace, B. J.; Zeitler, R. T.; Roberts, R. H.; Smith, B. R.; Wiles, K.C.; 1978, Technical Report AFFDL-TR-78-110 Volume I Composite Forward Fuselage Systems Integration, General Dynamics Fort Worth.

IN DEPTH STUDIES OF
COMPOSITE AIRCRAFT ELECTROMAGNETIC PERFORMANCE

BY

J. A. Birken
Naval Air System Command
Washington, D.C. 20361

SUMMARY

Five years ago the development of Naval aircraft with composite materials replacing selected metallic areas prompted the initiation of the program "Electromagnetic Characteristics of Composite Aircraft Structures and Electronics (EMCCASE)". Two years ago a parallel program "Composite Aircraft Generic Electromagnetic Protection (CAGEMP)" was begun which employs the data acquired from the EMCCASE program to optimize weight penalties required for composite aircraft electromagnetic protection. The program further investigates the structural-material-electromagnetic interactions experienced by protective coatings in severe Naval aircraft carrier electromagnetic environment and overall life cycle modification. Two avenues being used to disseminate knowledge gained from these programs are a composite aircraft electromagnetic design manual and the incorporation of electromagnetic effect parameters into currently employed aircraft structure/material design programs. While voids remain, this paper demonstrates that thin metal coatings are a weight efficient means of improving graphite/epoxy low frequency performance.

1. INTRODUCTION

Last generation aircraft designs utilized small amounts of different composite materials. Current airframes entering the production phase commence construction of major structural areas from graphite/epoxy material. Projections (Stansberg, 1979) indicate that 55% of all aircraft, helicopters and missiles will be constructed from composite materials. While future designs may tend toward new developed materials, graphite/epoxy is currently the dominant material whose utilization will continue for many years.

Composite material electromagnetic properties differ substantially from established aluminum electromagnetic properties. This paper will review the electromagnetic properties of various aircraft materials with primary concern given to graphite/epoxy. It will be shown that the low frequency transfer impedance of graphite/epoxy is 3800 fold less than an equal thickness of aluminum thereby significantly reducing the low frequency airframe shielding customarily provided by aluminum airframes. The electrical conductance across the joining of a graphite/epoxy panel to an aluminum panel cannot be as easily defined. Some joint designs have a dielectric coating placed between the metal and the composite material to prevent galvanic corrosion, thereby forming a slot antenna. Other joint designs use a poorly conducting adhesive to connect the composite material to aluminum causing similar leakage. Joint designs most currently encountered connect the graphite/epoxy to aluminum with titanium rivets. These offer limited conductivity ranging from .06 to .006 ohm-M with significance dependence on manufacturing. Electrically invisible joints can be formed by co-curing metal tabs into the composite material. Strawe successfully used this method to measure EMP and microwave joint behavior but this has yet to receive widespread application in the aerospace community due to its impact on manufacturing. Current composite joints exhibit poor electromagnetic integrity and fail to satisfy existing military specifications. Diffusion coupling through graphite/epoxy is inversely proportional to frequency and dominates joint coupling below approximately 0.5 MHz. How to compensate the increased composite airframe electromagnetic coupling requires the ability to describe each contributing parameter at all frequencies of interest. Such information combined with weight, cost, manufacturing and environmental considerations is required to determine the final aircraft design.

The interdependency of today's new disciplines no longer allows isolated structural-avionic-electromagnetic design until the detailed design phase at which point only minor variations in their mating can be made without significant cost overruns. Modern technology requires consideration of all disciplines in the preliminary design stage to prevent many expensive design iterations. Today, with the exception of joint coupling, graphite/epoxy electromagnetic properties are adequately understood to allow very early interdisciplinary design iterations to be mathematically performed. Such design algorithms are one avenue the United States Navy is employing to disseminate its composite material electromagnetic data base for use in early aircraft design to prevent costly later stage redesign. Two other avenues being used are the compilation of composite material electromagnetic design guidelines and specifications/standards. Table 1 provides the current outline for the composite material design guidelines. The refinement of certain graphite/epoxy parameters and protection techniques combined with the parameters of emerging composite materials will require periodic updating of the guidelines. An overview of some of the well understood graphite/epoxy electromagnetic parameters and the void regions which constitute current areas in need of investigation follows.

The open circuit black box voltage V_{oc} induced by an external electromagnetic field may be estimated from $V_{oc} = D(f) \pi^2 T_n(f)$ with the seven frequency dependent parameters $D(f)$, $T_1(f)$, $T_2(f)$, ..., $T_6(f)$ shown in Figure 1. $D(f)$ is the frequency dependent intensity of the external electromagnetic environment; $T_1(f)$, the frequency dependent air-

frame material electromagnetic shielding transfer function; $T_2(f)$, the shielding influence of the airframe shape; $T_3(f)$, the frequency dependent joint leakage term; $T_4(f)$, the cable shielding transfer function; $T_5(f)$, the frequency dependent subsystem susceptibility transfer function; and $T_6(f)$, is the additional protection transfer function required to reduce the aircraft internal electromagnetic field to tolerable levels. Knowledge of each of these terms allows evaluation of avionic subsystem open circuit voltage which must be kept adequately small to prevent avionic subsystem temporary upset or permanent burnout. Each of these terms will be discussed to form the foundation for composite aircraft electromagnetic protection, and weight penalty tradeoffs. To date studies reveal that protective metallic coatings on graphite/epoxy can conveniently provide one-hundred fold improvement in low frequency shielding without significantly affecting the weight or structural advantage of graphite/epoxy. The corrosion and other life-cycle degradation of such coatings, have had limited investigation. Efforts to fill these voids are underway. Further considerations must be given to coating manufacturing feasibility before optimum protective techniques from weight, cost and time perspectives may be determined.

The need of a protective metallic coating for a graphite/epoxy material airframe stems from the material's 3800 times higher resistance or 3800 lower conductivity than aluminum. Table II lists the conductivities in mhos/meter for aluminum, graphite/epoxy, boron/epoxy and kevlar. As illustrated in Table II, graphite/epoxy is the highest conducting composite material in production. Among all materials, graphite/epoxy ranks as a fair conductor. Indeed it is vastly better than kevlar which ranks as a dielectric with a conductivity 6.10^{-9} mhos/M. Initial investigations into the variation on graphite/epoxy 10,000 mhos/M average bulk conductivity due to manufacturing processes have revealed a +2 to -4 fold variance. Current Naval objectives are to determine avionic voltages and currents within an order of magnitude. As the conductivity variance is as much as 4 fold, measurement of samples from production lines can reduce the uncertainty for each company. Implementation of protection techniques discussed later in the paper will negate the effect of material conducting variance.

2. INTERNAL FIELD DEPENDENCE ON MATERIAL AND AIRCRAFT SHAPE

The effect different airframe material conductivities have on magnetic shielding effectiveness (G. Dike, R. Wallenberg and J. Birken, 1979 and R. Wallenberg et. al. 1980) $S_H(f) = H_{\text{external}}/H_{\text{internal}}$ of a small cylindrical 8 ply thick (.00107M) test sample is illustrated in Figure 2. The lower the conductivity of the material, the poorer the magnetic shielding and the higher the frequency beneath which the shielding is negligible. Shielding is a frequency dependent variable with significant changes from VLF to microwave which cannot be represented by a single number. Aluminum, the traditional airframe material exhibits excellent shielding properties. It has excellent shielding for almost the entire portion of the spectrum. Composite materials have an unshielded low frequency window below .1 MHz for graphite/epoxy and below 100 MHz for boron/epoxy. Kevlar with 10^{10} fold lower conductivity than graphite/epoxy possesses negligible shielding throughout the spectrum.

The magnetic shielding effectiveness discussed in the above paragraph was for a particular shape with a specific volume to surface ratio. Neither magnetic shielding effectiveness nor electrical shielding effectiveness $S_E(f) = E_{\text{external}}/E_{\text{internal}}$ can be measured on the single size sample and then be used for all other shapes and sizes constructed from the same composite material. Figure 3 shows the significant shielding effectiveness differences of different canonical shapes composed of the same material. The large variance between the flat plate and other sample shapes stems from the lack of circulating currents induces on a flat plate. A flat plate sample is a finite section of a cylinder whose infinite radius does not exist in the real world. The closed real world approximation to a single finite plate sample is a pair of parallel plates whose boundaries are electrically coupled. At low frequencies an aircraft wing is a close approximation to the parallel plate canonical case. As Figure 3 illustrates parallel plate representation of a wing does not exhibit the abnormally high shielding effectiveness implied by the measurement of a single plate. To account for aircraft shapes other than magnetic field codes are being adapted to allow accurate calculation of composite aircraft electromagnetic performance. The extremely low frequency large wavelengths in comparison to an aircraft size reduce the difference between the shielding of a circular and elliptical cylinder. Where the wavelength approximates .1 resonance, aircraft low frequency canonical approximations must be superceded by more precise code calculations. The significance in aircraft current density J_g variance due to airframe doors, apertures and joints will be determined this year when actual aircraft configurations are modeled with detailed codes. The significant shielding variation for different volume to surface ratios for an all graphite/epoxy cylinder is depicted in Figure 4.

Figure 4 again emphasizes the non-uniqueness of shielding $S_E(f)$ and $S_M(f)$ and the consequential difficulty of comparing different measurement experiments. The figure further shows that the frequency beneath which negligible magnetic shielding is exhibited becomes lower as volume to surface ratio increases. Consequently, large aircraft structures have better magnetic shielding than small missiles. A collection of published data on graphite/epoxy shielding is shown in Figure 5. The different values obtained by various parties may be correct for their test configuration, however, not realizing the dramatic differences caused by different measurement setups, has caused confusion in comparing test sample data.

To avoid this confusion by obtaining an unique material shielding parameter requires the introduction of terms other than S_H and S_E . The EMP community has long used the term

transfer impedance Z_{ST} to uniquely describe material shielding properties. Transfer impedance

$$Z_{ST}(f) = \frac{E_{\tan}^{\text{internal}}(f)}{J_{\text{surface}}^{\text{external}}(f)} \quad (1)$$

determines the internal tangential electric field normalized to the surface current density distribution. This removes the drastic effect the different shape current distributions shown in Figure 3 have on $S_H(f)$ and $S_E(f)$. For low frequencies the asymptotic of $Z_{ST}(f)$ is accurately represented by

$$Z_{ST} = 1/\sigma d \quad (2)$$

where σ is the material conductivity discussed earlier and d the material thickness. The J_S independence of equation (2) allows it to serve as a material shielding property which different parties can measure in different facilities and be able to compare their data without being puzzled why two carefully done experiments produce very different answers. The effect on the current distribution perturbations caused by apertures, joints and aircraft body shape can be evaluated for low frequencies with method of moments and finite element codes which have been developed for metal aircraft. The conductivity of graphite/epoxy is adequately higher than most joint and aperture impedances to allow surface current calculations to be performed similar to metal calculations. Boron/epoxy conductivity is too low for the convenient metal approximation $Z_{\text{material}} \ll Z_{\text{joint}}$.

Transfer impedances $Z_S(f)$ for different aircraft materials with a common .00107 meter thickness (the thickness of 8-ply graphite/epoxy) are shown in Figure 6. The transfer impedance value is unique for all shapes. Efforts are underway to adopt it as a standard measurement of shielding in the United States. With composite materials receiving widespread aviation industry application in the 1980's efforts should be put towards making transfer impedance a NATO standard. The low frequency asymptote of Figure 6 is simply $\lim_{f \rightarrow \text{VLF}} Z_{ST}(f) = 1/\sigma d$. The remainder of the transfer impedance curve is:

$$Z_{ST} = (\sqrt{\omega\mu/\sigma}) \sin(\sqrt{\omega\mu\sigma}d) \quad (3)$$

where ω , μ , σ and d are respectively, the angular frequency, permeability, conductivity, and thickness of the airframe.

3. JOINT LEAKAGE

The third contributing coupling mechanism $T_3(f)$ shown in Figure 1 is the electromagnetic leakage through joints. A joint is formed by the joining of two originally separate aircraft components by adhesive or rivets. Both joining methods generally create a significantly lower conductivity than that of the panels being joined. The presence of lower conducting boundaries on an airframe's surface impede current density J_S in certain directions. The greater the J_S disturbance, the greater the electromagnetic energy coupled into the aircraft interior. The disturbed currents create spatial variant J_S terms which can further increase coupling into the interior of the aircraft. An avionic bay door composed of graphite/epoxy with poorly conducting joints can force current to circulate about it forming a "magnetic well". Indeed graphite/epoxy possessing a conductivity 3.8×10^3 lower than surrounding aluminum can substantially alter aircraft surface current distribution even with ideal joints. The significance of the two dimensional joint effect is frequency dependent. Skin depth $\delta = 2/\omega\mu\sigma$ in graphite/epoxy and aluminum differ, as $1 - e^{-1}$ of the current travels above skin depth. Current reactive and cavity properties have been found to substantially reduce the two dimensional J_S above 1 MHz.

To describe joint leakage, (Strawe, D. R., 1980) and paper number 4 of this conference defines joint impedance as

$$\Delta V_{\text{joint}} = Z_j J_s \quad (4)$$

where V_{joint} is the contribution to V_{ij} , caused by the higher joint impedance Z_j per unit width through which surface current density J_s flows. Figure 7 illustrates three joint designs and the joint admittance $Y_j = 1/Z_j$ variance resulting from the different mechanical designs. The skirt joint shown in Figure 7, which adhesively connects two graded material sections offers little opportunity for the electrically conducting graphite fibers to contact the other section. Consequently, its electromagnetic properties are undesirable. A joint connected with fasteners is the most frequently employed aircraft joint design. This joint's electromagnetic properties can be improved by the use of special fasteners designed to provide contact to the graphite fibers and by considering the electromagnetic consequences imposed in the manufacturing processes. A frequently occurring joint design problem arises from the differences in electromotive series of the two jointed materials. The galvanic voltage generated in the humid environment electrolyte experienced by aircraft carriers produces corrosion. Graphite/epoxy, aluminum or cadmium plated steel produce approximately 1 volt accompanied by a 15 ampere per square centimeter current flow. A dielectric coating is frequently placed between the different materials to inhibit the corrosion. Such a coating prevents corrosion but creates significant electromagnetic leakage through the non-conducting dielectric electrical cracks. The but joint shown in Figure 7 with titanium rivets correctly inserted in manufacturing are one means of offering a pathway to electromagnetic

current flowing along an aircraft fuselage with dielectrically isolated joints. Measurements of new uncorroded joints when manufactured for high electromagnetic integrity can exhibit low frequency asymptote joint impedances as low as 5 to 10 milliohms/meter. Without special manufacturing considerations typical Z_j values lie in the 50 to 100 milliohms/meter range. Joints designed for electromagnetic integrity exhibit a low frequency asymptote $Z_j .01 - 0.1$ milliohms/meter. The above values show that the United States Military Standard Specification requirement of 2.5 milliohms is only satisfied in graphite/epoxy joints with specially designed joints.

All the above values are for new uncorroded joints. The difficulty of freshly produced composite joints to satisfy military bonding specifications has overshadowed consideration of environmentally degraded joints. Graphite to graphite bonding diminished 100 times when aged with humidity salt spray over a 30 day period. Further efforts are required in this area to produce a sufficient data base, however well established metal to metal joint environmental degradation combined with the significant graphite/epoxy aluminum galvanic corrosion indicates this to be an area of concern.

The study by Strawe, D. F. and Piszker, L. D., 1980 was initiated to determine the capability of different composite material and composite joint measuring techniques. It was well established at the onset of the effort that graphite/epoxy transfer impedance $Z_{GT}(f)$ could accurately be predicted with equations (2) and (3). However, it was originally felt that joint admittance $Y_j(f)$ would have to be determined empirically. To optimize selection of a test facility and firmly establish each facility's behavior each approach was analyzed. The results of this effort are included in paper number 4 of this meeting. Table III summarizes the frequency range, $Z_{GT}(f)$ and $Y_j(f)$ parameter sensitivity, dynamic range, estimated measuring time and estimated accuracy for each test facility. The maximum frequency is f_m (MHz). As one would expect the least expensive Flat Plate Tester (FPT) provides the minimal frequency range and sensitivity. It does offer the advantages of expedient testing of simple flat plate samples. The most expensive are the quadrax and stripline (Whitson, A. L. and E. F. Vance, 1977) which offer the highest sensitivities. The principle drawback of the quadrax is its requirement for cylindrical test samples. This prevents it from being used to examine samples directly from the production line. It should be noted that even though the remaining test facilities are capable of measuring flat samples, co-curing of metal strips into these samples for intimate external electrical continuity is required. This can easily be accomplished by selecting production line samples before they are wired and adding the metal strips. The lack of microwave coupling data through graphite/epoxy joints resulted in the decision to build the anechoic facility. Results from this effort plus (Harrington, R. F. and Aukland, D. T., 1979) and (Wallenberg, R., et. al.) have revealed current composite-aluminum joints to be severely resistive damped. This inhibits resonances to play a dominant role in the microwave region. Wallenberg shows this resistive damped. This inhibits resonances to play a dominant role in the microwave region. Wallenberg shows this resistive damped joint admittance to take the form

$$Y_i = \frac{\eta_a \eta_c \eta_a \eta_b}{\eta_a \lambda_a + \eta_c \lambda_c} - \frac{2j \ln [CH_a W]}{\lambda_a \eta_a} - \frac{2j \ln [CH_c W]}{\lambda_c \eta_c} \quad (5)$$

4. CABLE AND SUBSYSTEM TERMS

The transfer function $T_4(f)$ for different cable configurations is available from (Vance, E. F. 1974), (Frankel, S., 1974), (Fisher, F. A., 1977) and (Kaden, H., 1959). As with airframe shielding it is important to evaluate the shield current flow from which the internal wire field may be evaluated. Of similar importance is the connector transfer function and its grounding configuration. The high shielding values obtained under laboratory conditions are not found in the less than ideal configurations exhibited by the multiple wires with different shielding characteristics that are bundled together inside airframes. Fiber-optics offer high electromagnetic immunity if the avionics box is not contaminated by its unshielded power cables.

Figure 8 depicts subsystem susceptibility transfer function $T_5(f)$ and airframe material trends over the last 30 years. (Entner, R., Birken, J., 1977). The pre-1950 vacuum tube upset voltages were 250 volts. Upset voltages diminished to 12-23 volts with discrete transistor deployment. Progress in providing many transistors on a single integrated circuit (IC) chip further lowered the upset voltage to 5 volt region. The upset voltage remained nearly constant with the development of Large Scale Integration (LSI) in the late 70's. However, the significantly larger number of devices per ship reduced the total energy required to burnout different LSI functional regions. Upcoming Very Large Scale Integration (VLSI) is expected to diminish the upset voltages to the 1 to 2 volt region and further reduce required burnout energy.

As eluded to above, both upset voltage as well as the energy delivered to the device must be considered in protecting graphite/epoxy aircraft avionics from high level electromagnetic environments. Software techniques such as circumvention can reduce the probability of short term lightning (LEMP) and nuclear electromagnetic pulse (NEMP) upsets from threatening the aircraft's safety. If, however, the short term pulse is very intense, semi-conductor devices will be burnt out rendering circumvention ineffective. Figure 9 (E. Blume and M. Rose, 1975) provides the upset and burnout energy for a wide spectrum of electronic components. Key facts to be noted are that digital integrated circuits are the most susceptible and the $E_{upset} = 0.1 E_{burnout}$.

5. UNPROTECTED AIRCRAFT PERFORMANCE

The proceeding discussion provides the parameters needed to evaluate the ij subsystem open circuit voltage V_{ij} and short circuit current I_{ij} . The airframe surface current distribution $J_s(r, \theta, z, f)$ is evaluation for the aircraft of interest using Method of Moment (MOM) or Finite Difference Techniques. These techniques require input regarding the physical location of the metal and composite sections, joints, aircraft shape geometry, and cable routing. Analysis of a direct lightning strike is simplified by the major lightning energy content lying in the very low frequency region (centered about 50 kHz). Consequently, lightning, whose intense energy wavelengths $\lambda \gg L_{aircraft}$, is almost quasi-static. While new lightning threat data indicates higher HF ($f > 1$ MHz) energy content, the low frequency susceptibility of graphite/epoxy causes the intense $f < 50$ kHz region to be of primary concern. Aluminum aircraft exhibiting 3.8×10^3 greater conductivity than graphite/epoxy are not VLF susceptible. Consequently, metal impedance aircraft joints are the major electromagnetic coupling mechanism causing lightning HF content to be of concern for metal aircraft.

Table IV lists voltage, currents as well as energies lightning and nuclear electromagnetic pulses couple onto an unshielded wire the length of the composite aircraft. An all aluminum aircraft struck by full level lightning produces 10.1 volts at .3 amp on a common mode wire inside fighter size aircraft. The same size aircraft constructed with graphite/epoxy produces 32,000 volts at 1100 amps under the above cited conditions. The lower conductance of graphite/epoxy creates a low frequency transfer impedance ratio $Z_{GT}^{e/zAl} = (\sigma d)_{Al} / (\sigma d)_{G/E} = 3168$ times as discussed earlier. Lightning 100 meters from aircraft will induce approximately 250 volts at 8.2 amps. Table IV lists voltages currents, maximum power and energies caused by LEMP and NEMP external fields in aluminum and graphite aircraft with different quality joints. Figure 10 shows voltage caused by direct lightning attachment studies to a graphite/epoxy forward fuselage (Borrows, BJC 1978). Evaluation of the tested configuration of Figure 10 with the same equations used to produce Table IV provides excellent agreement. Careful use of protection devices could protect most avionics. The United States is currently considering a 500 volt avionics box hardening specification. Alone it would not suffice hardening for NEMP through a cockpit aperture or direct lightning strike voltage. NEMP aperture coupling is not unique to graphite/epoxy aircraft as diffusion and joint coupling. The remainder of the paper will deal with graphite/epoxy protective trade-off techniques that result in significant protection for direct strike and nearby LEMP, NEMP, radar, and laser protection.

6. PROTECTION TRADEOFFS

The destructive avionic system voltages selected electromagnetic threats can create in a graphite/epoxy skin aircraft has prompted the United States to initiate significant protective technique efforts. $T_6(f)$ is composed of the subgroups $T_6 = T_{16}^{material} + T_{36}^{joints} + T_{46}^{cable} + T_{56}^{box}$ where each of the T_{m6} terms is the improvement in electromagnetic vulnerability resulting from different protection. The introduction of composite materials has altered $T_{16}^{material}$, T_{36}^{joint} , and T_{56}^{box} whereas alteration of the remaining parameters is caused by other technology advances. To compensate this, primary Naval efforts are being directed in hardening the material and joint configurations and developing electromagnetic hard fiber optic lines. The Air Force is actively engaged in developing device hardening techniques which is also needed to suffice metallic aircraft EMP hardness requirements.

In the following discussion it will be shown that current material hardening can offer 50 to 300 fold improvement without imposing significant weight penalties. If we assume a 100 fold improvement due material and joint designs the remaining 38 fold can easily be obtained by specifying currently available fiber optics and protective devices. The Navy has begun work on a material shielding specification. This needs to be extended to other United States services and NATO countries. Likewise the Navy intends to actively participate in box hardening specification development which should also be extended to NATO countries. The combination of material hardening and box hardening will offer significant electromagnetic hardening for present and upcoming threats. Material hardening also corrects composite water absorption and lightning fuel tank spark ignition.

Figure 11 depicts the electromagnetic hardness of composite and metallic materials. All values are calculatable from equations 2 or 3 and have been confirmed by measurement. Low frequency lightning directly striking an aircraft produces the highest avionic voltages from the threats considered in this paper. Consequently, the low frequency asymptotic Z_{GT} values represent maximum lightning energy transfer shown in Figure 11 are design standards. Note the 75 dB higher voltages graphite/epoxy allows to be induced on wires than an equal thickness aluminum. To compensate this deficiency electromagnetic protection methods must be invoked. Recalling EM protection $T_6 = T_{16}^{material} + T_{36}^{joint} + T_{46}^{cable} + T_{56}^{box}$ maximization of payload necessitates minimizing the weight of T_6 , retaining adequate protection, and preventing protection life cycle degradation.

Figure 12 illustrates how much EM protection different coatings provide. A 4 mil coating of copper diminishes the internal field (E_{tan}) 325. An equal thickness of aluminum reduces the internal field and resulting avionic voltages 140 fold. Nickel and tin coatings respectively reduce avionic voltage 58 and 40 fold. The attributes of Nickel and Tin are their low corrosiveness with graphite/epoxy. Implementation of aluminum on copper coatings require anti-corrosive measures. The United States Navy is currently developing highly conductive non-corrosive coatings. Aluminum 120 mesh, aluminum flame spray and titanium coatings, 4 mils thick, do not significantly diminish avionic volt-

ages. The lightweight character of aluminum flame spray is attractive if techniques to increase its conductivity can be developed.

The 150 fold reduction in avionic voltage provided by aluminum would reduce the 36,000 volts resulting from a direct lightning strike to 240 volts. Increasing the coating thickness to 8 mils would further reduce the voltage to 120 volts. Further coating thickness increases begin to impose excessive weight penalties for fighter size aircraft. Consequently, wire shielding, fiber-optics and/or protection devices must be added to reduce the avionic voltages below the approximate LSI 2.5 volts or average 26 volt respective upset and burnout levels. Mission critical systems which cannot tolerate logic being changed for the duration of lightning impose the severest protection requirements and are best served by fiber-optic immunity. The isolation between well-shielded fiber-optic signal lines and unshielded power cables must be accounted for as poor lower line to signal line isolation will allow large powerline transients to appear at the signal lines via intra-box coupling.

Figure 13 depicts the weight penalties and weight density imposed by the coatings illustrated in Figure 12. The 100 square foot surface area was selected due to its numerical convenience and close approximation to a graphite/epoxy fuselage under development. While copper provides the most protection per unit of thickness, it also offers the highest weight penalty. Copper locating a 100 square foot aircraft area adds 18.4 lbs. weight. Constructing 100 square foot fuselages from graphite/epoxy provides an approximate 36 lbs. weight savings over the same fuselage constructed from aluminum. Adding a 4 mil copper coating imposes a 52% weight savings penalty. Aluminum foil offers the next best electromagnetic protection from the considered materials. For the fuselage area under discussion adding 4 mils of aluminum foil diminishes avionic voltage 141 fold. Such an aluminum coating imposes 5.52 lb. weight penalty or 15.3% reduction in composite material weight savings. This weight penalty is based on an eight ply thick graphite/epoxy fuselage. Graphite/epoxy wing designs have thickness from 24 to beyond 96 ply. Assuming an average 24 ply wing, a 4 mil aluminum foil protective coating imposes only a 5.1% weight savings reduction. Losing only 5 to 15% composite material weight savings for 100 fold electromagnetic immunity improvement is an affordable weight penalty. Studies have shown that metallic coated graphite/epoxy exhibits significantly less water absorption than uncoated G/E as well as being a vastly superior lightning fuel tank ignition design. A greater weapon immunity is also acquired by the use of metallic coatings. Weight penalties for the remaining materials in Figure 12 are shown in Figure 13. The very low weight penalty of aluminum flame is intriguing if its conductivity could be increased. Methods of realizing this are under discussion.

Shielding merit, SM, the avionic voltage diminishment per weight of one square foot of coating material is shown in Figure 14. SM is simple

$$SM = \frac{E_{g/e}/E_{tan}^{coated}}{J_s \sigma_s dS} \quad (6)$$

where σ is the protective material volume weight density. In terms of the surface density σ_s of Figure 13 it becomes $(E_{g/e}/E_{tan}^{coated})/\sigma_s d$. The lightweight high shielding of aluminum foil causes aluminum foil to offer the greatest shielding per unit weight. The high conductivity of copper overshadows its high weight. Aluminum flame spray due to its very lightweight exhibits the third highest shielding merit. Increasing aluminum flame spray conductivity as little as 3 fold would place it as the leading protective metal coating. The remaining coatings which exhibit less corrosive properties do not exhibit the excellent low weight penalty and shielding offered by copper or aluminum. An aluminum foil protected graphite/epoxy has recently been developed which is expected to be corrosive tolerant. Further electromagnetic, structural, and life cycle degradation of this design will be performed in 1980.

Highly conductive surface coatings composed of the material described above can only provide from 50-500 fold reduction in avionic voltage. To optimize the weight penalty imposed by such coatings the minimum manufacturing feasible thickness should be used. Such a thickness lies in the 4 mil inch region. Thin coatings are optimum since the first few mils of say aluminum reduces avionic voltage 140 fold at a 5.6 lb. per hundred square foot weight penalty.

Greater aluminum foil thicknesses of 8 and 16 mils would provide 280 and 560 fold voltage reduction at respective weight penalties of 10.8 and 21.6 lbs. Above the minimal thickness a 6 dB reduction in voltage doubles the weight penalty of conducting coatings. The 140 fold reduction is well justified by the 5.4 lb. weight penalty while the 21.6 lbs. weight is far less attractive. Continued protective coating thickening turns a composite aircraft into a metallic aircraft. Further work is underway to select optimum protective coating thickness. The remainder of the required protection will be provided by T_{46} cable and T_{56} box protection (Table V (Corbin, J.C., 1978)). Metallic coatings need to be complemented by hardened joints. If one commences graphite/epoxy aircraft design with a metallic coating the design of hardened joints will be significantly simplified. The United States Navy is pursuing a program which will use developed hardened joints for metallic coated composites.

CONCLUSIONS

In summary, unprotected graphite/epoxy aircraft avionics are significantly more vulnerable to lightning strikes than metallic aircraft while only slightly more vulnerable to nuclear EMP. The addition of a thin highly conductive metallic coating on the surface of the aircraft can significantly reduce this vulnerability. The additional reduction may be readily obtained with currently available box hardening devices. Composite aircraft hardening solely with devices is questionable. The use of a minimal weight savings penalty selection of coatings, hardened joints, and device hardening will result in aircraft electromagnetically safe from radar, nuclear EMP, lightning and severe future electromagnetic environments.

REFERENCES

- Birken, J.A., 1980, "Electromagnetic Effects of Advanced Composite Materials: Measurement and Models II", NAVAIR Rpt. 520-1, Naval Air Systems Command, Arlington, VA.
- Borrows, B.J.C., 1978, "Composite Forward Fuselage Systems Integration", Vol. II, AFFDL-TR-78-110, Air Force Flight Dynamic Lab, Ohio, Contract F33615-76-C-5439.
- Corbin, J.C., 1978, "Protection/Hardening of Aircraft Electronic Systems Against the Indirect Effects of Lightning", Proceedings from the Conference on Certification of Aircraft for Lightning and Atmospheric Electricity Hazards, Oneva-Chatillon, France.
- Dairiki, E., and Vance, E.F., "Cable System Analysis", AFWL TR-71-100, Air Force Weapon Labs, Albuquerque, N.M., AD-887-452.
- Dastin, S.; Carri, R. & Craft L., 1978, "Protection Optimization for Advanced Composite Structures", Air Force Flight Dynamics Labs, Wright Patterson Air Force Base, Ohio, Contract F33615-77-C-5169.
- G. Dike, R. Wallenberg, and Birken, J., 1979, "Electromagnetic Relationships between Shielding Effectiveness and Transfer Impedance", San Diego, CA, Proceedings IEEE EMC Symposium.
- Fisher, F.A. and Plummer, J.A., 1977, "Lightning Protection of Aircraft", Washington, D.C., NASA Reference Publication 1008.
- Frankel, S., "Cable and Multiconductor Transmission Line Analysis", 1974, Washington, D.C., Harry Diamond Labs Report HDL-TR-091-1, AD/A-000-848.
- Harrington, R.F. and Aukland, D.T., 1980, "Electromagnetic Transmission Through Narrow Slots in Thick Conducting Screens", to be published in IEEE Transactions of Antennas and Propagation.
- Kaden, H., 1959, "Wirbelstromer and Schirmung in der Hochfrequenztechnik", Springer-Verlag, Berlin.
- Stansbarger, D.L., 1979, October 8, "Materials Technology", Aviation Week and Space Technology, Washington, D.C., page 68.
- Stratton, R., et. al., 1978, "Electromagnetic Properties and Effects of Advanced Composite Materials: Measurement and Models I", Rome Air Development Center, Rome, New York, Report RADC-TR-78-156.
- Strawe, D.F., and Piszker, L.D., 1980, "Investigation of Penetration of Electromagnetic Energy Through Joints in Advanced Composite Structures", The Boeing Co., Seattle, Washington, Rpt. No. D180-25240-2, Naval Air Systems Command under Contract N00019-79-C-0058.
- Whitson, A.L. and Vance, E.F., 1977, "Bolt Lapped - Joint EMP Shields", Defense Nuclear Agency, Washington, D.C., Rpt. No. DNA 4472F.

TABLE I

Composite Aircraft Electromagnetic Design Guidelines

- 1.0 Introduction
- 2.0 Electromagnetic Threats
- 3.0 Impact on EM Performance
- 4.0 Present and Future Composite Material Applications
- 5.0 Intrinsic Material Properties
- 6.0 External to Internal Coupling Phenomena
- 7.0 Component & Subsystem Susceptibility
- 8.0 System Analysis/System Tradeoffs
- 9.0 Measurement Test and Evaluation
- 10.0 Protection Methods and Techniques
- 11.0 Design Guidelines

TABLE II

Material Conductivity

Low Composite Material Electrical Conductivity Provides Low Electromagnetic Shielding.

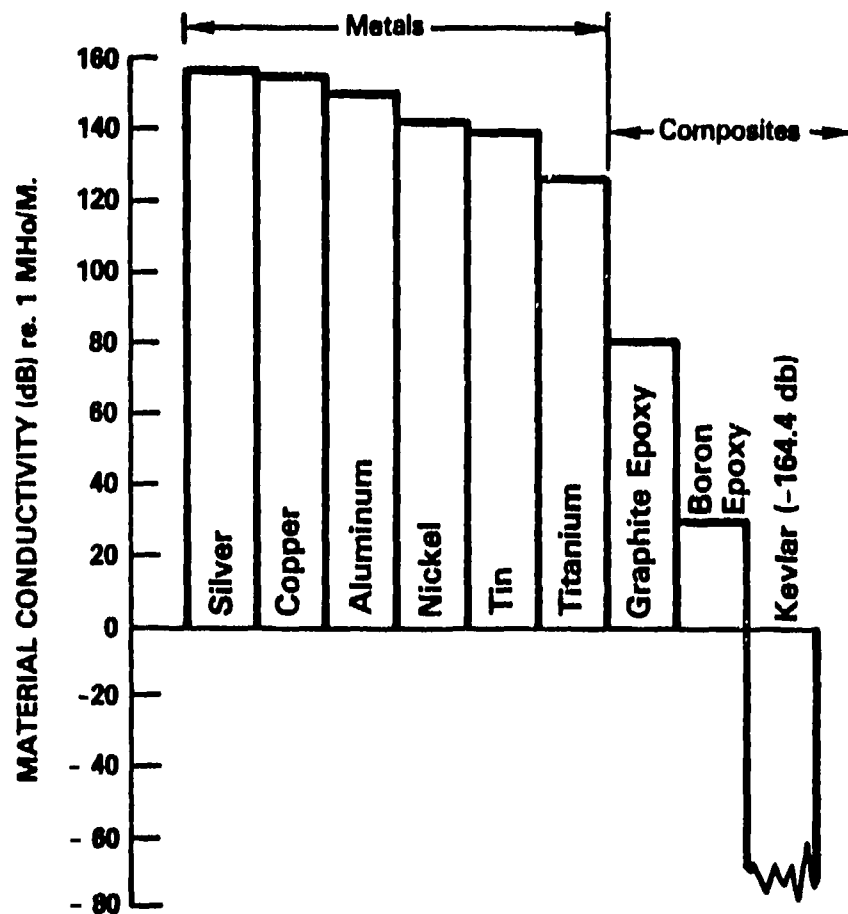


TABLE III

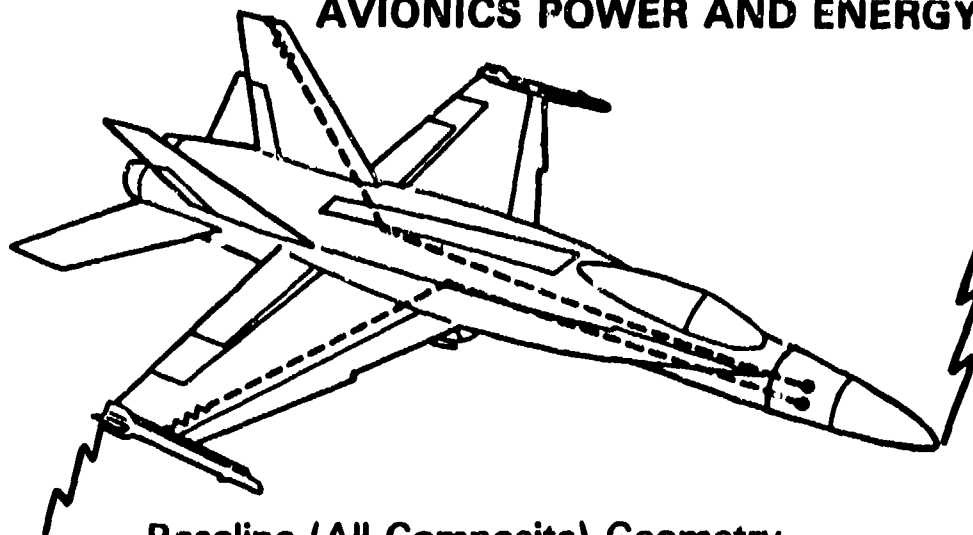
Estimated Performance

Facility	Current Frequency Range	Probable Frequency Extension	Parameter Sensitivity		Dynamic Range	Estimated Measurement Time	Estimated Measurement Accuracy
			γ_j (a/m)	z_s (a)			
Quadrox	.001-100 MHz	1000 MHz	4×10^5	2×10^{-6}	130 dB	2 Samples/Day	2 dB (6 dB)
FPT	.001-100 MHz	300 MHz	$\frac{4 \times 10^4}{ 1 + j \frac{f_m}{20} }$	$4 \times 10^{-6} 1 + j \frac{f_m}{20} $	70 dB	12 Samples/Day	3 dB (6 dB)
Stripline	.001-100 MHz	1000 MHz	$\frac{3 \times 10^4}{ 1 + j \frac{f_m}{25} }$	$7 \times 10^{-6} 1 + j \frac{f_m}{25} $	95 dB	6 Samples/Day	3 dB (6 dB)
Anechoic*	1-18 GHz	-----	300	2×10^{-2}	80 dB	6 Samples/Day	6-10 dB

TABLE IV

Voltage, Current, Power and Energies Caused by LEMP, NEMP External Fields in Aluminum and Graphite Epoxy

AVIONICS POWER AND ENERGY



Baseline (All Composite) Geometry

Peak Power and Maximum Energy

Direct Strikes	V_H (Volts)	i_H (Amps)	P_H^{peak} (Kilowatts)	E_H (Joules)
Nose/Tail Wire (Nose/Tail Attachment)	32,000	1,100	3,520	1035.2 J
(Nearby Strike)	250	8.2	2	0.059 J
Nose/Wing Tip (Nose/Tail Attachment)	6,500	220	1,430	42.06 J
Wire (Nose/Wing Tip Attachment)	17,000	550	9,350	275.0 J

TABLE V

Filter Comparison Matrix

FILTER CLASS	FILTER TYPE *	USEFUL FREQUENCY RANGE (Hz)	SIGNIFICANT ADVANTAGES	SIGNIFICANT DISADVANTAGES
Discrete R, L, C	1, 2, 3, 4	to 10^6	Versatile Low Cost	Large for Low Frequency Low Q
Ferrite Beads	1.	$10^3 - 10^6$	Versatile Dissipative With Low Pass Band Loss	Spurious Resonances Saturation
Filter Connector	1	$10^3 - 10^6$	Design Integra- tion Simpli- city Dissipative	Spurious Resonances Saturation
Coaxial	1, 2, 3, 4	$10^7 - 10^9$	High Frequency Use Low Parasitics	Large Size
Crystal	3, 4,	$5 \times 10^4 - 1.5 \times 10^8$	High Q Small Size	Spurious Resonances High Cost
Ceramic	3	$10^3 - 10^7$	High Q Small Size	Spurious Resonances Not IC Compatible
Mechanical	3, 4	.1 - 2×10^6	High Q	Limited Range Not IC Compatible High Insertion Loss
Active	1, 2, 3, 4	to 10^8	Small Size Gain Provision	Power Requirement Limited Range Damage Susceptibility

* 1 - Low pass; 2 - High Pass; 3 - Bandpass; 4 - Band Reject

TABLE VI

Comparative Values of Several Surge Protection Devices

PARAMETER	SPARK GAPS	VARISTOR DEVICES	ZENER DIODES
Typical surge current capability (Amps)	10,000	1,000	500
Response Time (Sec)	10^{-6}	10^{-6}	10^{-6}
Capacitance (fd)	10^{-12}	10^{-10}	10^{-10}
Voltage Range (Volts)	90 and higher	40-700	2-300
Insulation Resistance	High (10^9 ohm)	Medium	Medium
Bi-Polar Operation	Yes	Yes	No
Failure Mode	Short	Short	Short
Activated State	Short Circuit	Clamped	Clamped

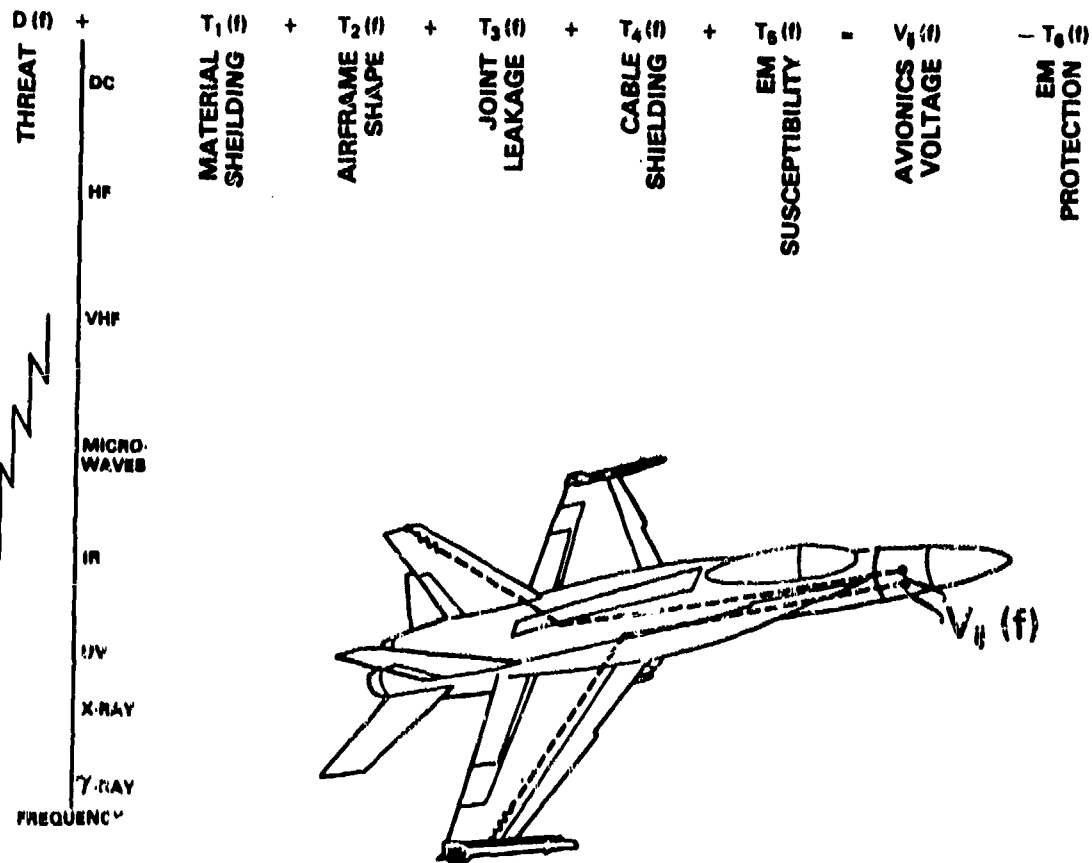


Fig.1 Electromagnetic system parameters

MATERIAL SHIELDING (T_1)

Composite Material Electromagnetic Shielding

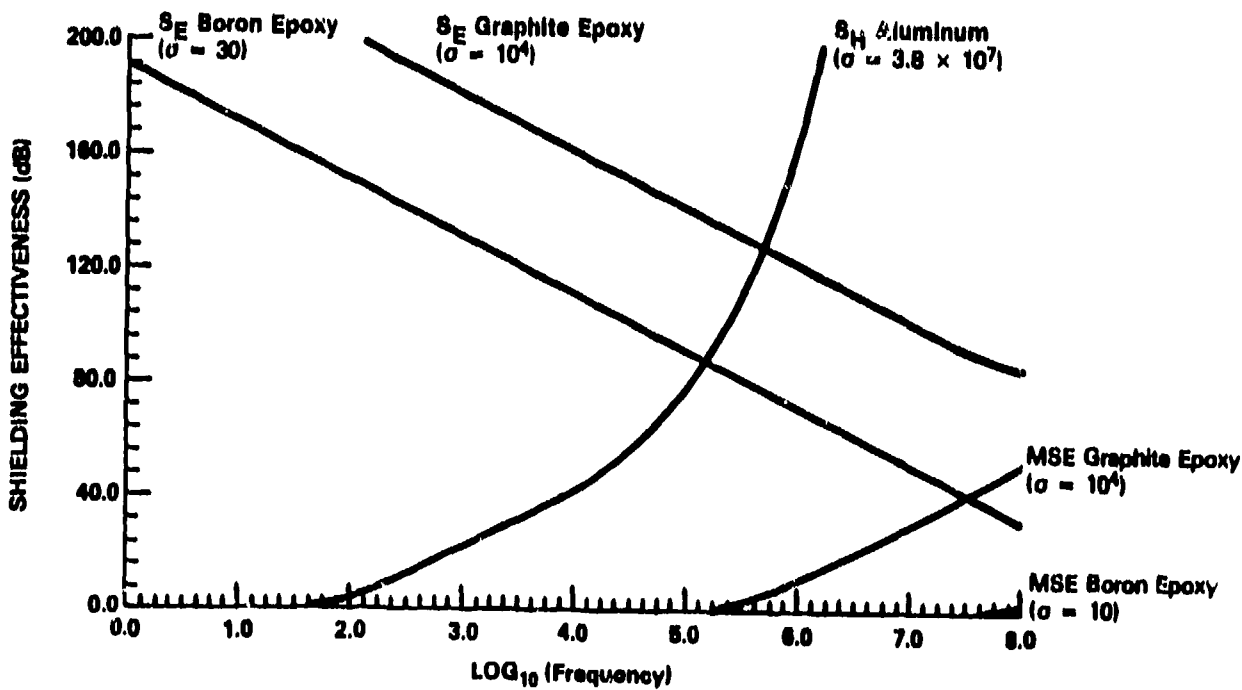


Fig.2 Magnetic and electrical shielding effectiveness for various materials

AIRFRAME SHAPE (T₂)

The Shape of an Aircraft Influences EM Coupling

MAGNETIC SHIELDING EFFECTIVENESS for a Uniform Incident Magnetic Field. SHIELD CONDUCTIVITY = $10^4 \Omega/m$. Shield Thickness = 0.00107 m (CORRESPONDING TO 8 PLY Composite Material at 0.00525 In/Ply)

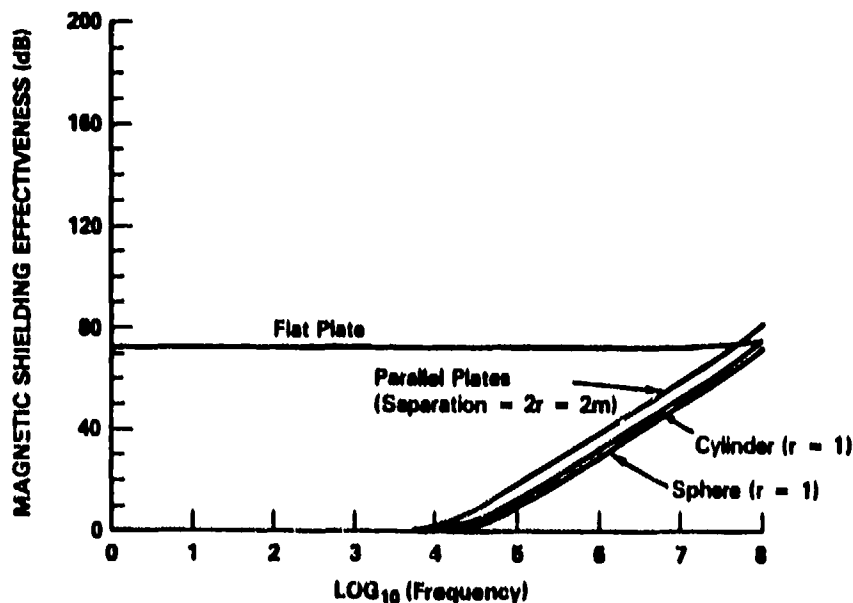


Fig.3 Magnetic shielding effectiveness for various shapes

AIRFRAME SHAPE (T₂)

MAGNETIC SHIELDING EFFECTIVENESS of an Enclosure Under a Uniform Magnetic Field as a Function of Volume-To-Surface Ratio. SHIELD CONDUCTIVITY = $17500 \Omega/m$. Shield Thickness = 0.00107 m (CORRESPONDING TO 8 PLY Composite Material at 0.00525 In/Ply)

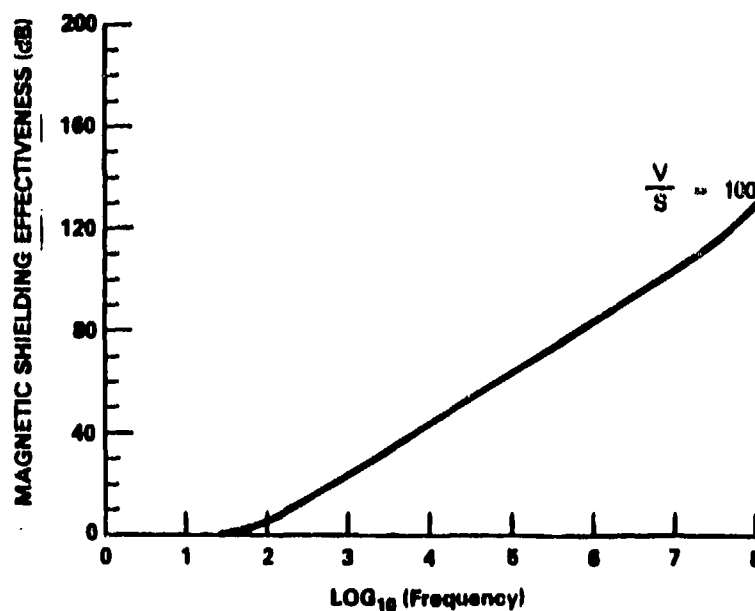


Fig.4 Magnetic shielding effectiveness as a function of volume to surface ratio

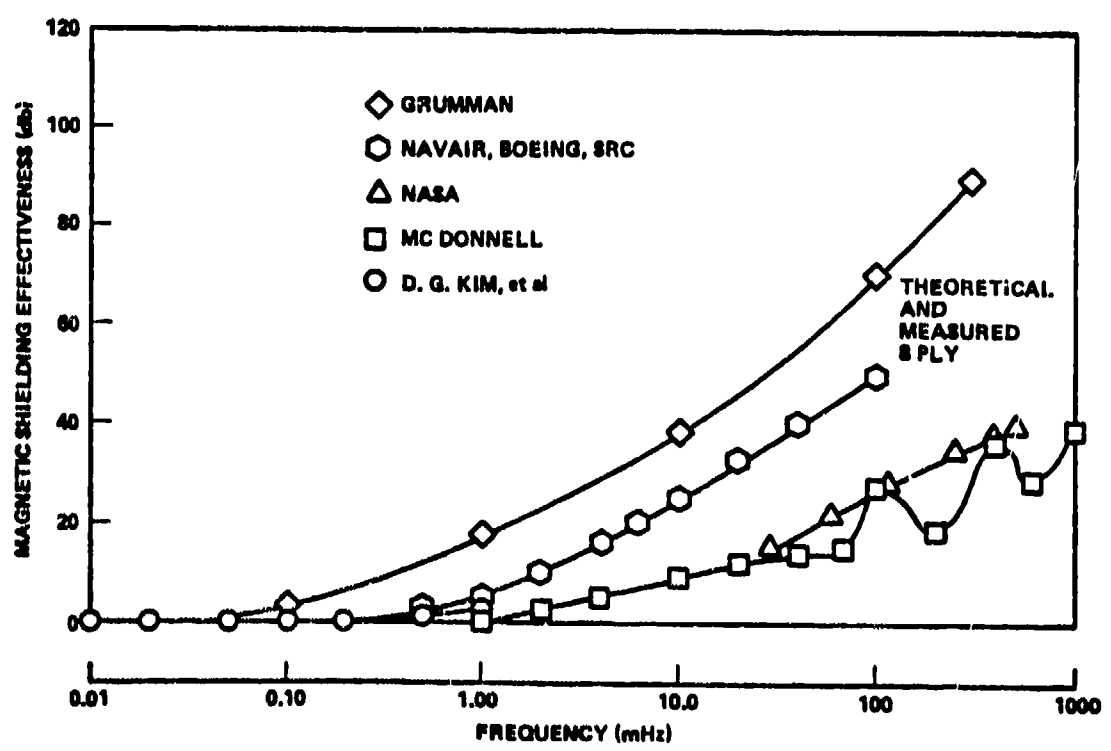
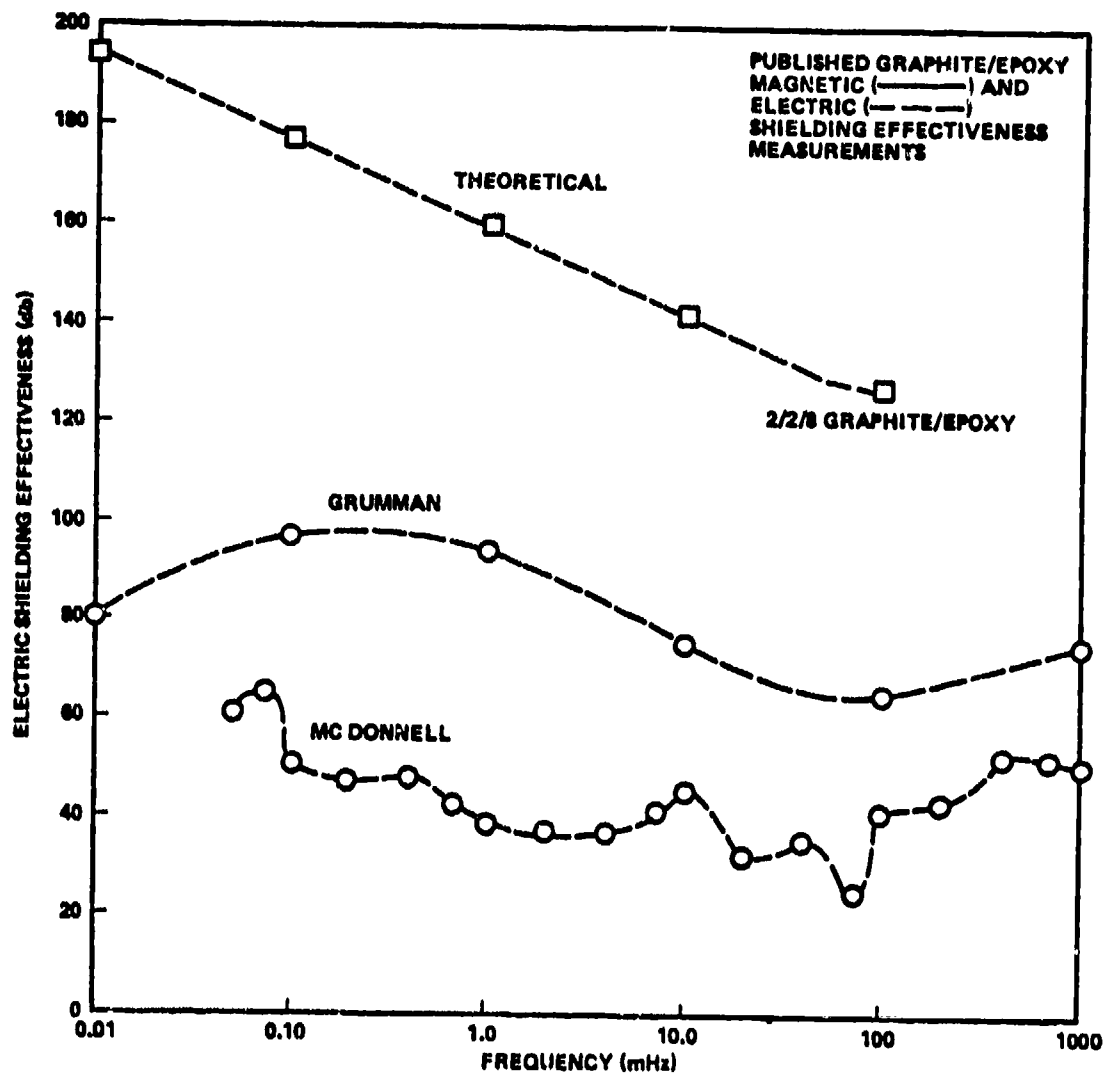


Fig.5 Published graphite/epoxy magnetic and electric shielding effectiveness

MATERIAL THICKNESS CORRESPONDS TO 8 PLY COMPOSITE
MATERIAL AT 0.00525 IN/PLY

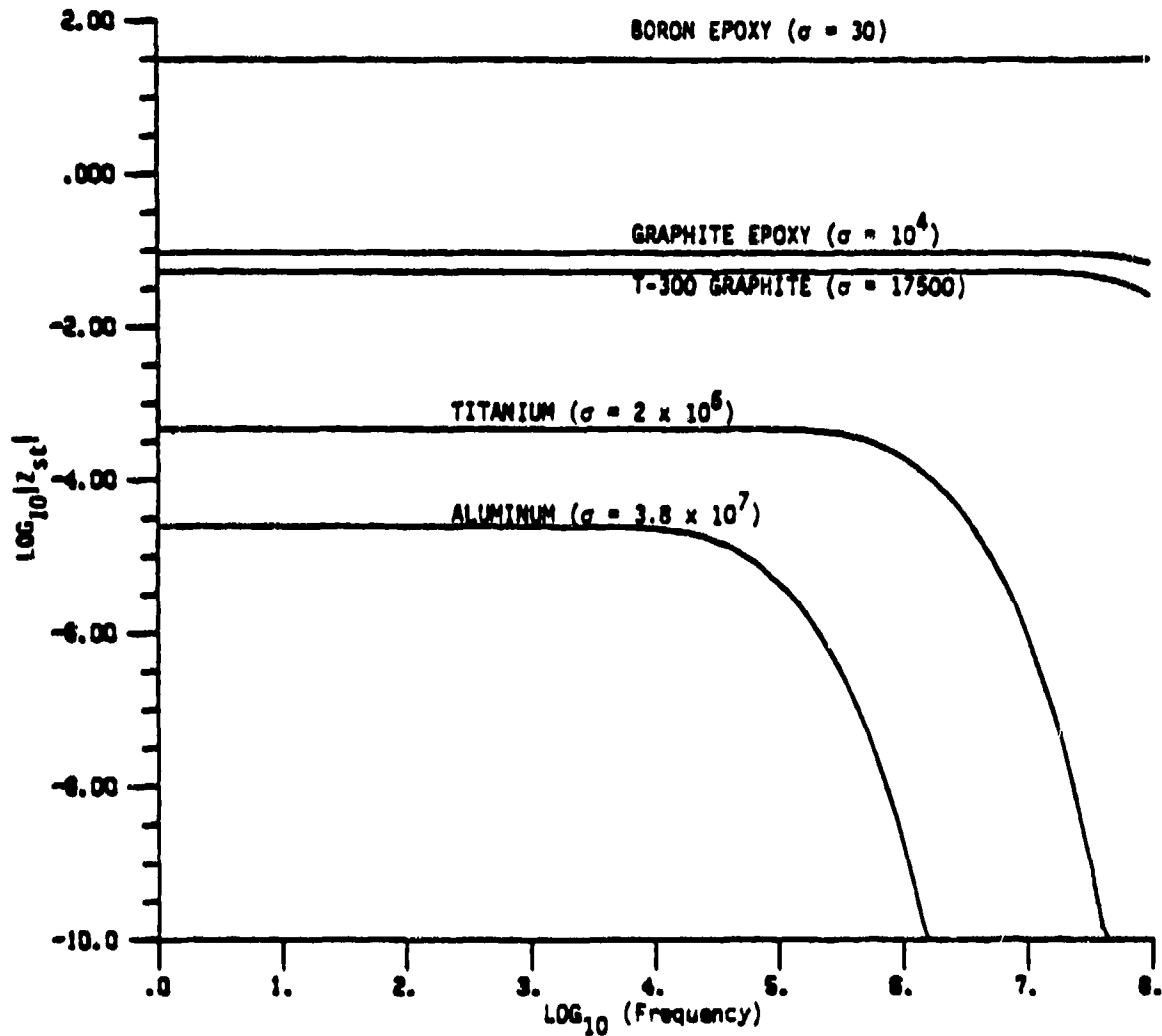


Fig.6 Surface transfer impedances for different materials

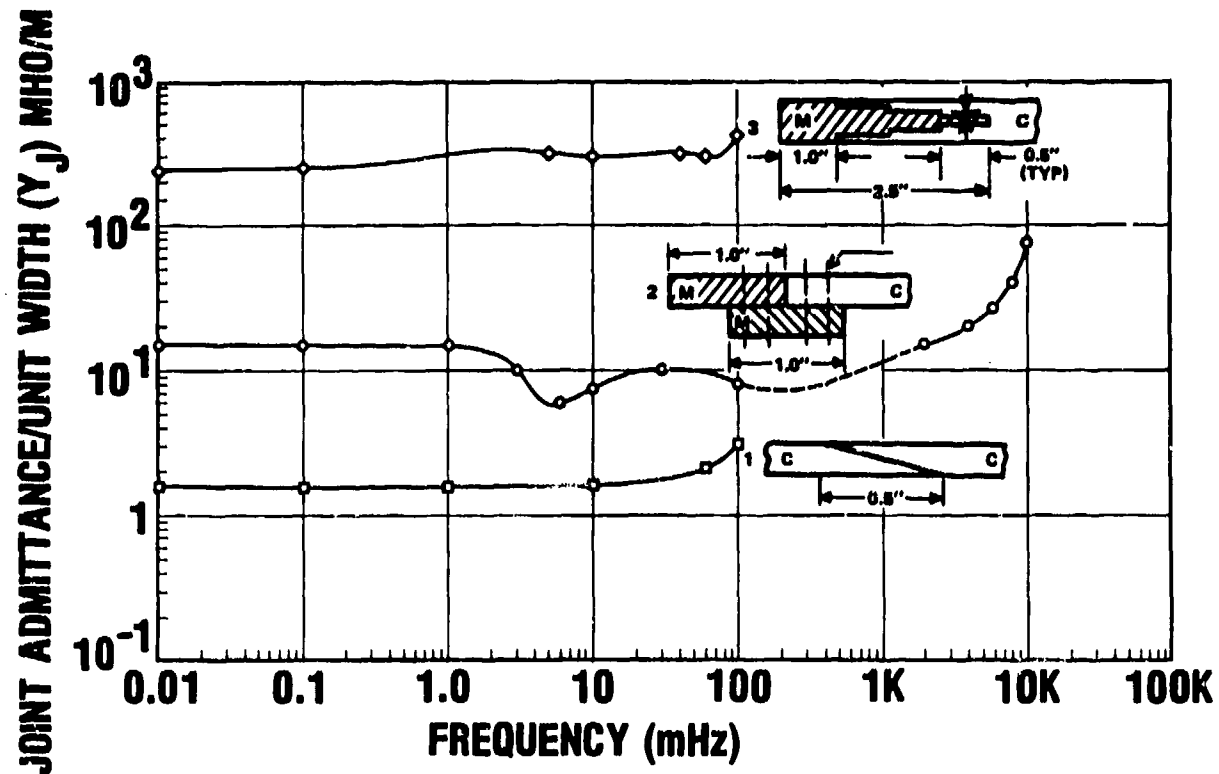


Fig.7 Joint admittance/unit width as a function of frequency






TUBES	DISCRETE TRANSISTORS	INTEGRATED CIRCUITS (IC)	LARGE SCALE INTEGRATED CIRCUITS (LSI)	VERY LARGE SCALE INTEGRATED CIRCUITS (VLSI)
 250V 1 WATT/DEVICE	 TO-5 12V-24V 10 ⁻¹ -10 ⁻² WATTS/DEVICE	 FLAT PACK 5V-12V 10 ⁻² -10 ⁻³ WATTS/TRANS	 DIP 5V-7V 10 ⁻³ -10 ⁻⁴ WATTS/TRANS	 CHIP CARRIER 1.5V-3V 10 ⁻⁵ -10 ⁻⁹ WATTS/TRANS
GLASS/ METAL/ CERAMIC	METAL/ CERAMIC	METAL/ CERAMIC/ EPOXY	METAL/ CERAMIC/ EPOXY	CERAMIC/ EPOXY
F-9	F-4	F-14	F-18	VSTOL
ALUMINUM	ALUMINUM	ALUMINUM/TITAN	GRAPHITE-EPOXY ALUMINUM	GRAPHITE-EPOXY ?
PRE-1950's	1950's	1960's	1970's	1980's

Fig.8 Aerospace technology trends

EM SUSCEPTABILITY (T_g)

Upset and Burnout Energies for Various Circuit Elements.

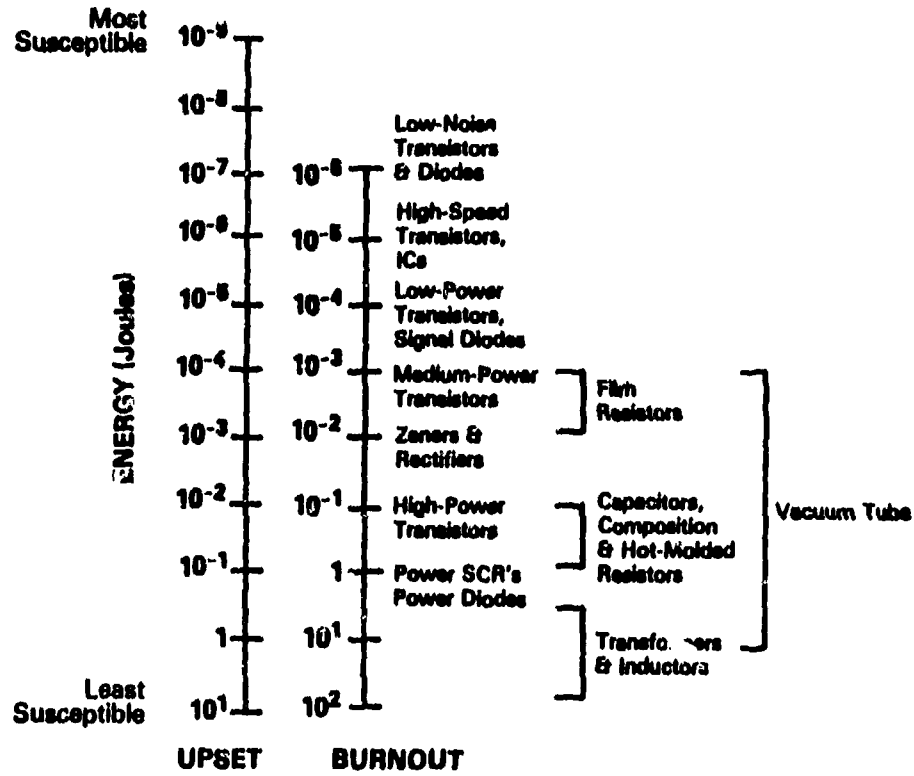


Fig.9 Electronic component upset and burnout energies

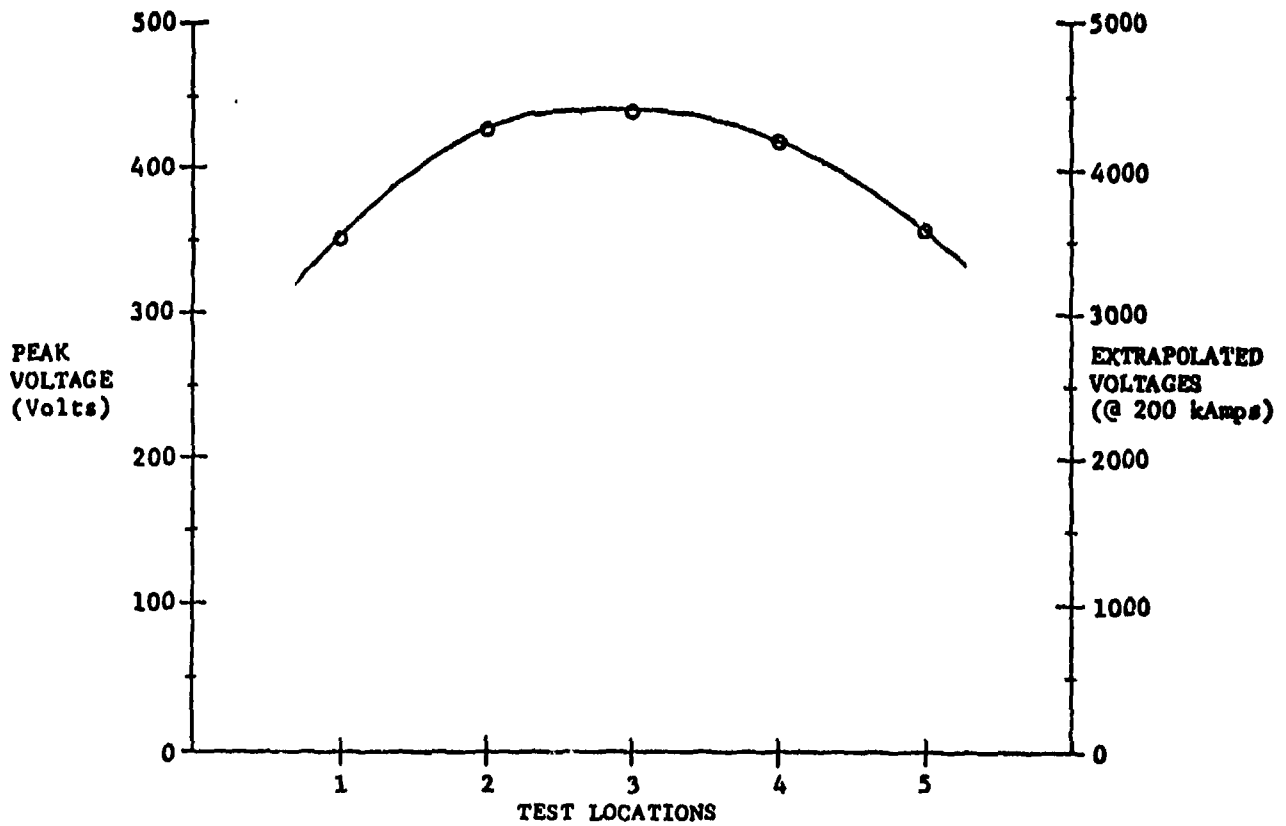


Fig.10 Lightning test induced voltages

EM PROTECTION OF METALS AND COMPOSITES (T_d)

Transfer Impedance Shielding of Structural Materials and Protective Electromagnetic Coatings

(Valid for Frequencies Below 10^5 Hz)

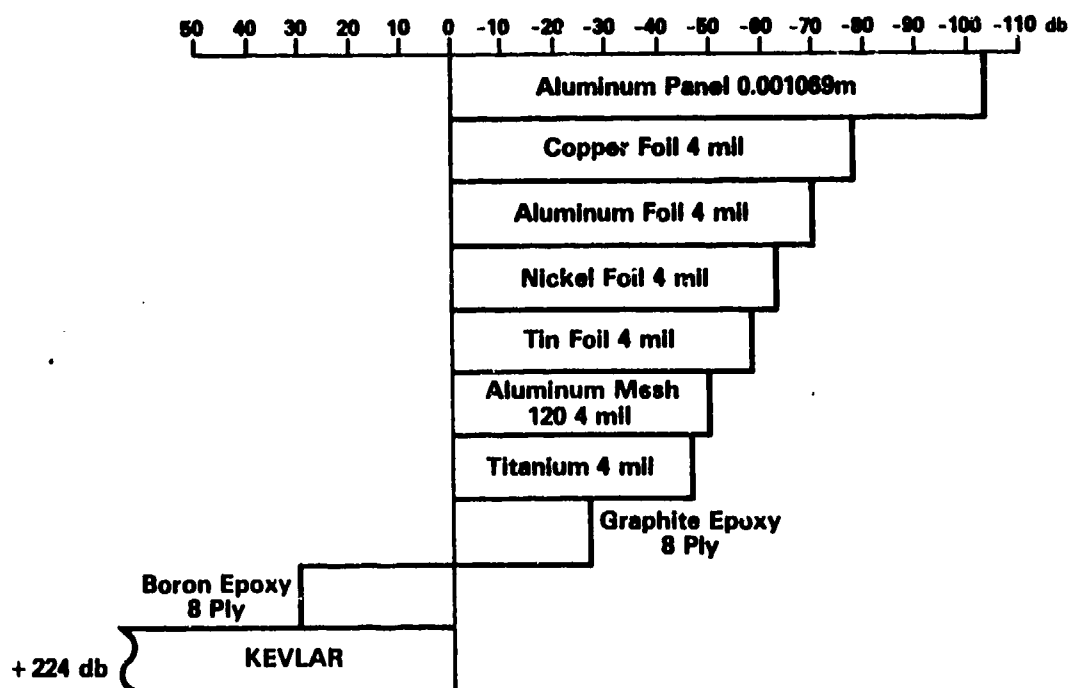


Fig.11 Transfer impedance shielding of structural materials and protective EM coatings

EM PROTECTION (T_g)

Protective Coatings Improvement Relative to 8-Ply G/E

(Valid for Frequencies Below 10^5 Hz)

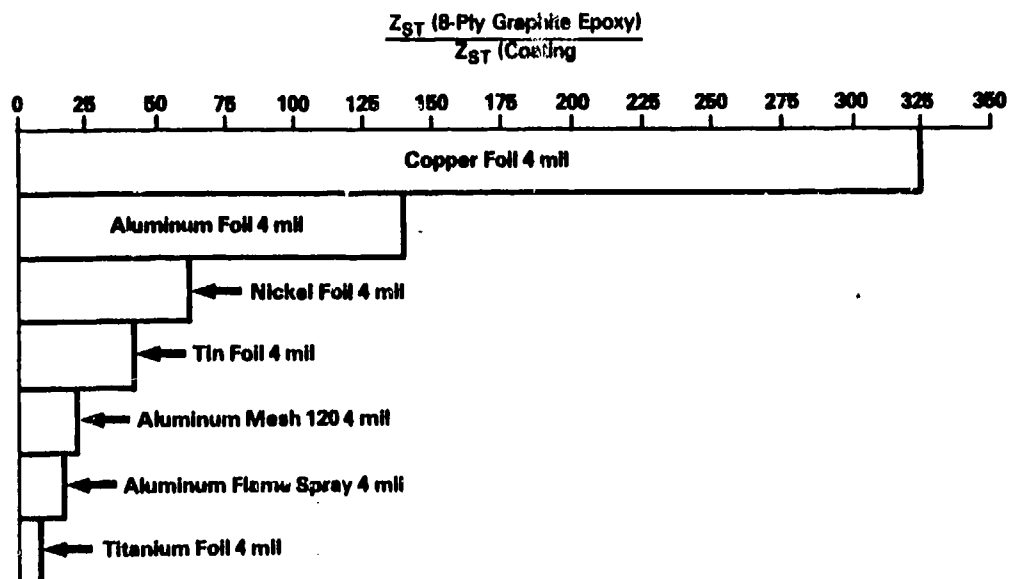


Fig.12 Improvement protective coatings provided relative to 8-ply graphite/epoxy

EM PROTECTION WEIGHT PENALTIES (T₆)

Forward Fuselage AV-8B (Area - 100 Ft²) Weight Penalty (Pounds) Imposed by Electromagnetic Protective Coatings

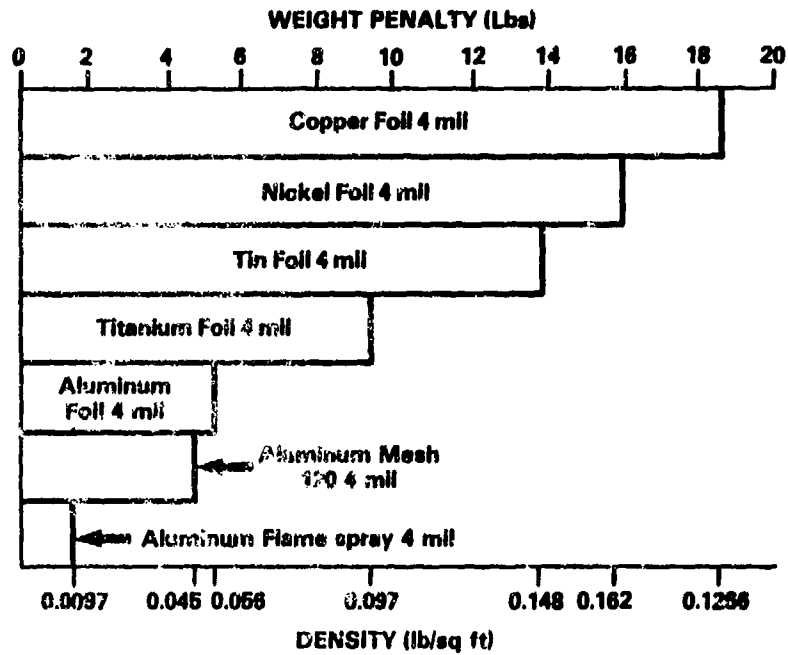


Fig.13 Weight penalty imposed by protective coatings

EM PROTECTION (T₆)

Weight Shielding Figure of Merit

(Protection Beyond 8-Ply G/E Provided by the Weight of 1 Square Foot of Protective Coating)

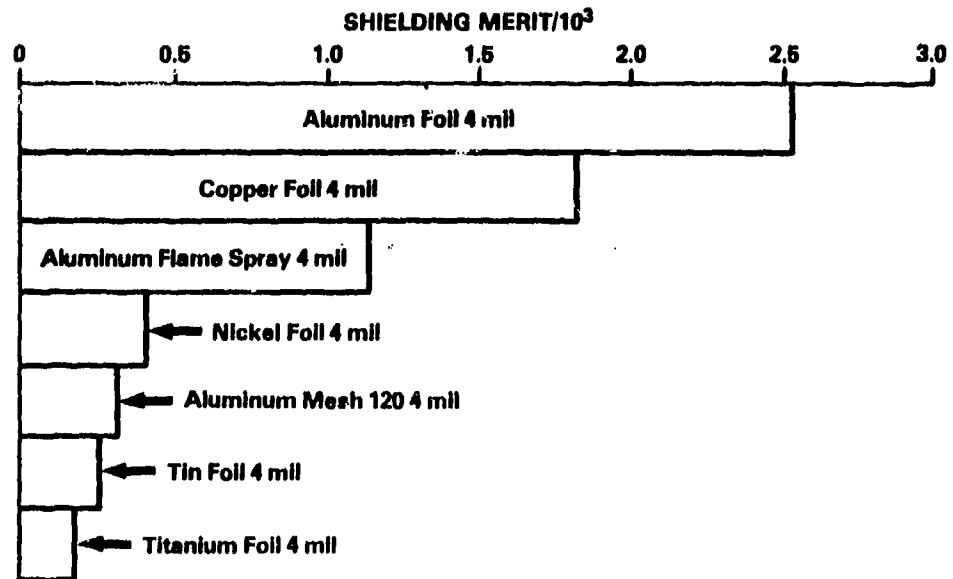


Fig.14 Weight/shielding figure of merit of EM protective coatings

**ELECTROMAGNETIC COUPLING TO ADVANCED COMPOSITE
AIRCRAFT WITH APPLICATION TO TRADE-OFF AND
SPECIFICATION DETERMINATION**

by

R. Wallenberg
E. Burt
G. Dike
Syracuse Research Corporation
Merrill Lane
Syracuse, New York 13210

SUMMARY

A major concern with the increasing use of composite materials and low voltage electronics is the amount of electromagnetic coupling to the interior of an aircraft and to the cables and electronic devices within it. This paper describes simple methods for determining the shielding provided by an aircraft's exterior surface and the coupling of the interior fields to cables and transmission lines within aircraft cavities. The results can be used to determine trade-offs between electromagnetic shielding, weight, and cost.

The expected threat to a US Navy advanced composite aircraft is defined. The concept of transfer impedance is used to decouple the interior problem from the exterior. Penetration through joints in composites is discussed. Upper bounds are obtained on the open-circuit voltage, short-circuit current, power, and energy at the terminals of an unshielded transmission line. Comparisons are made to typical device upset and burnout levels.

1. INTRODUCTION

A major concern with the increasing use of composite materials and low voltage electronics is the amount of electromagnetic coupling to the interior of an aircraft and to the cables and electronic devices within it. This paper describes simple methods for determining the shielding provided by an aircraft's exterior surface and the coupling of the interior fields to cables and transmission lines within aircraft cavities. The results can be used to determine trade-offs between electromagnetic shielding, weight, and cost.

As a starting point, the expected threat to a US Navy advanced composite aircraft is defined. This includes direct strike and nearby lightning, the nuclear electromagnetic pulse (EMP), and the radio frequency (RF) shipborne threat.

A formulation will be presented for coupling to the interior of a composite shell. Approximations will be made which decouple the interior problem from the exterior problem by the use of a surface transfer impedance. The transfer impedance concept is applicable to shells whose local radius of curvature is large with respect to the wavelength in the shell material and which are thin with respect to the free-space wavelength.

The other exterior surface coupling mechanism which will be discussed is penetration through joints or seams between composite-composite or composite-metal surfaces. A model which describes the penetration will be formulated and examples will be given which can be related to measurements of shielding effectiveness or joint admittance. Coupling by composite joint penetration to the interior of a cavity containing obstacles that might represent an avionics bay will also be discussed.

Given an estimate of the interior field levels caused by diffusion or joint penetration, simple expressions will be presented for upper bounds on the open-circuit voltage, short-circuit current, power, and energy at the terminals of a shielded or unshielded transmission line. Examples will be illustrated for lightning, nuclear EMPs, and radar pulses. Finally, typical device upset and burnout levels will be shown and comparisons will be made.

2. ELECTROMAGNETIC THREAT

A brief description is given of the threats considered against a US Navy advanced composite aircraft. The threats considered include nearby and direct strike lightning, the nuclear EMP, and the RF threat to aircraft aboard US aircraft carriers caused by navigation aides, high frequency (HF) communications, and carrier-based radars.

Direct Strike Lightning (LEMP) (FISHER, F.A., 1977)

It is the return strike current which dominates the overall lightning flash current waveform, and which is often modeled when effects due to lightning are being analyzed. A double exponential of the form

$$I(t) = I_0(e^{-\alpha t} - e^{-\beta t}) \quad (1)$$

where $I_0 = 206 \text{ kA}$, $\alpha = 1.7 \times 10^4 \text{ s}^{-1}$, and $\beta = 3.5 \times 10^6 \text{ s}^{-1}$ are often used to represent the return strike. A peak amplitude of 200 kA translates roughly into an axial surface current density of $200 \text{ kA}/2\pi r \approx 64 \text{ kA/m}$ for an average aircraft fuselage radius of 0.5 m.

Nearby Lightning Strike:

The fields produced by a lightning strike near an aircraft can be approximated by those due to an infinite cylindrical current column with the same current as in the direct strike case. The magnetic field is given by $H = I/2\pi r$, where I is the current waveform and r is the distance from the lightning strike to the aircraft. In particular, if $R = 150$ m and $I_{\max} = 200$ kA, we have $H_{\max} \approx 320$ A/m. The induced surface current density would then be $J_{\max} = 2 H_{\max} = 0.64$ kA/m. This is two orders of magnitude smaller than the surface current due to a direct strike. Generally, the currents induced by a nearby lightning strike can be expected to be small when compared to the currents due to a direct strike.

Nuclear EMP Threat (NEMP):

A nuclear detonation is accompanied by an EMP, generally referred to as EMP or NEMP. This EMP should be distinguished from other nuclear, shorter wavelength, electromagnetic radiation associated with a nuclear detonation such as visible light, X-rays, or gamma rays. The EMP threat studied here is the high altitude burst threat which is commonly used in the open literature. The incident field is assumed to be a plane wave with an electric field waveform given by a double exponential function. Analytically, this waveform is given by Equation 1 with I_0 replaced by E_0 and we will use the following typical values for the parameters: $E_0 = 58.15$ kV/m, $\alpha = 6.3$ s⁻¹, and $\beta = 189$ s⁻¹. This waveform has a peak value of 50 kV/m with a rise to peak time of 0.019 μ s and a time to half-peak amplitude of 0.185 μ s. The H-field is assumed to be given by $H = E_0/\eta_0$, where $\eta_0 = 377 \Omega$ is the impedance of free space. It is interesting to note the difference between this threat and the double exponential LEMP threat. The time scale of the LEMP is about 100 times that of the EMP. It is really this difference in time scale that makes the two threats appear so different with regard to threat analysis. This difference shows up clearly in the frequency domain. A comparison of the lightning and nuclear spectra show that the nuclear EMP waveform has a much higher frequency content than the LEMP waveform. These results tend to verify that for an aircraft size target, the LEMP can be treated fairly accurately using low frequency techniques whereas the EMP threat cannot. For example, at 100 MHz (corresponding to a wavelength of ~ 10 ft) the amplitude of the EMP is about $10^{-2.5}$ times its peak value. The LEMP amplitude at this frequency is down from its peak by a factor of 10^{-7} .

Shipborne RF Threat:

An unclassified threat level presented by McDonnell Douglas Corp., St. Louis, Missouri, is shown in Figure 1. It shows the peak values of the carrier deck environment expressed in V/m. Only the more powerful aircraft carrier transmitters are shown: a navigation aid at 300 to 500 kHz, HF communications at 2 to 30 MHz, and radars at UHF (200 and 450 MHz) and microwave frequencies (greater than 1 GHz). Many other emitters of lower power are not known.

Radar and communication sources are specified in terms of their effective radiated power (ERP). The peak ERP is available on many emitters. This quantity can be measured on non-cooperative emitters and it can also be estimated fairly accurately from knowledge of transmitter output, line losses, and antenna gain. The peak ERP represents the peak power in a pulse or continuous wave/amplitude modulation waveform and the average power in a continuous wave/frequency modulation waveform. The average ERP is calculated by multiplying the peak ERP by the duty cycle for a pulsed radar. Both peak and average ERP are useful for studying electromagnetic interferences, with the peak being used to estimate the voltage spikes induced in the electronics and the average being used to determine heating or burnout levels. ERP has the units of power (watts, kilowatts, etc.) and is frequently expressed in decibels referred to a milliwatt (dBm), so 1 W = 10^3 mW = +30 dBm. Typical pulse widths are around 0.4 μ s and pulse repetition frequencies can vary between 10 and 100 pps up to thousands depending on the application.

3. Penetration of Electromagnetic Waves through Lossy Shells (HARRINGTON, R.F., 1980)

Consider the problem of field penetration into an interior region completely enclosed by a sheet of lossy matter. For simplicity, we will consider the lossy matter to be linear, homogeneous, and isotropic. Figure 2a illustrates the general problem to be considered. A time-harmonic electromagnetic field E^i, H^i is incident on a body defined by the external surface S_1 and internal surface, S_2 . Loss is taken into account by letting ϵ and/or μ be complex. We next divide the problem into three equivalent problems, one for each region. They are shown in Figures 2b, 2c, and 2d. The equivalent electric and magnetic currents on the surfaces satisfy the following operator equations:

$$\begin{aligned}
\mathcal{L}_{11}^a(\underline{J}_1, \underline{M}_1) + \mathcal{L}_{11}^b(\underline{J}_1, \underline{M}_1) - \mathcal{L}_{21}^b(\underline{J}_2, \underline{M}_2) &= \underline{E}_{\tan}^i s_1 \\
\mathcal{M}_{11}^a(\underline{J}_1, \underline{M}_1) + \mathcal{M}_{11}^b(\underline{J}_1, \underline{M}_1) - \mathcal{M}_{21}^b(\underline{J}_2, \underline{M}_2) &= \underline{H}_{\tan}^i s_1 \\
-\mathcal{L}_{12}^b(\underline{J}_1, \underline{M}_1) + \mathcal{L}_{22}^b(\underline{J}_2, \underline{M}_2) + \mathcal{L}_{22}^c(\underline{J}_2, \underline{M}_2) &= 0 \\
-\mathcal{M}_{12}^b(\underline{J}_1, \underline{M}_1) + \mathcal{M}_{22}^b(\underline{J}_2, \underline{M}_2) + \mathcal{M}_{22}^c(\underline{J}_2, \underline{M}_2) &= 0
\end{aligned} \tag{2}$$

These equations result from satisfying boundary conditions on tangential \underline{E} and \underline{H} at the boundaries. The symbol \mathcal{L} denotes an electric-field operator and \mathcal{M} denotes a magnetic-field operator. It should be apparent that, in the notation \mathcal{L}_{pq}^x : x denotes the constitutive parameters ϵ_x and μ_x ; p denotes the surface S_p on which the currents reside; and q denotes the surface S_q on which the tangential components of \underline{E} are evaluated. Similar notation applies to the \mathcal{M}_{pq}^x operator for the tangential components of \underline{H} .

The \underline{E}^i , \underline{H}^i are continuous across S_1 , hence we have dropped the superscript on S_1 in the right-hand terms of the first two equations. The operators \mathcal{L} and \mathcal{M} are known, but complicated. Equations 2 are general in that they apply to any shell of linear, homogeneous, and isotropic matter. It should be pointed out that there are other surface formulations for the problem (HARRINGTON, R.F., 1961) equivalent to the one we have discussed.

Thin Highly Conducting Shells:

Composite materials such as graphite/epoxy have a high conductivity ($\sigma \sim 10^4$) and are used extensively in military aircraft construction. We have considered some approximate formulations for thin highly conducting shells.

For very low frequencies, that is, when the wavelength in the shell is large compared to shell thickness d , we can use an impedance sheet approximation. In this case, the problem reduces to that of a loaded body, for which the operator equation is (HARRINGTON, R.F., and MAUTZ, J.R., 1975)

$$\mathcal{L}(\underline{J}) + \mathcal{Z}_L \underline{J} = \underline{E}^i \tan s \tag{3}$$

Here we have considered S_1 and S_2 to be approximately the same surface S , supporting an electric current \underline{J} . The load impedance for this case is $\mathcal{Z}_L \approx 1/\sigma_b d$. Since the shell is highly conducting, this solution is valid only at very low frequencies.

For higher frequencies we can consider region "b" to support traveling waves and a transmission line model. Consider a section of the shell between surfaces S_1 and S_2 , assumed to be locally plane. The intrinsic impedance of the shell, $\eta_b = \sqrt{j\omega\mu/\sigma_b}$ is normally much smaller in magnitude than η_a and η_c (usually free space). Hence, region "a" sees almost a short circuit at S_1 , and region "b" sees almost an open circuit at S_2 . Thus, in region "b", we have

$$\begin{aligned}
H_t &= J_1 \frac{\sinh \gamma_b (d-z)}{\sinh \gamma_b d} \\
E_t &= \eta_b J_1 \frac{\cosh \gamma_b (d-z)}{\sinh \gamma_b d}
\end{aligned} \tag{4}$$

where γ_b is the intrinsic propagation constant in the shell, $\gamma_b = \sqrt{j\omega\mu\sigma_b}$, and z is the distance from S_1 in region "b". The impedance seen at S_1 is

$$\mathcal{Z}_L = \left. \frac{E_t}{H_t} \right|_{z=0} = \eta_b \coth \gamma_b d = \begin{cases} \frac{1}{\sigma_b d} & \text{as } d \rightarrow 0 \\ \eta_b & \text{as } d \rightarrow \infty \end{cases} \tag{5}$$

The interior fields are found by considering the boundary conditions at $z = d$. An approximate solution for \underline{M}_1 is not needed for the internal problem. The \underline{M}_1 ensures that the wave in the equivalent problem of Figure 2c travels only inward; i.e., there is zero field external to region "b". Setting $z = d$ in Equation 4, and using approximate equalities because we have used the approximation that region "b" sees an open circuit at S_2 , we have

$$\begin{aligned}
\underline{n} \times \underline{H}^b &= \underline{J}_2 \approx 0 \\
\underline{E}^b \times \underline{n} &= \underline{M}_2 \approx \frac{-\eta_b}{\sinh \gamma_b d} \underline{n} \times \underline{J}_1 \approx -Z_{st} \underline{n} \times \underline{J}_1
\end{aligned} \tag{6}$$

where the surface transfer impedance Z_{st} will be discussed in Section 4.

For a better approximation to \underline{J}_2 we could use the wave impedance looking into region "c" to relate \underline{J}_2 to \underline{M}_2 . For this, we could use \underline{M}_2 as known in the third equation of Equations 2 with $\chi_{12}^b = 0$ to determine \underline{J}_2 . Alternatively, we could use \underline{M}_2 as known in the fourth equation of Equations 2 with $\chi_{12}^b = 0$ to determine \underline{J}_2 . If necessary, we could also take \underline{J}_1 and \underline{M}_1 as known quantities in either of these two equations. For a cruder, but easier, approximation we could assume plane waves at S_2 in region "c" and obtain

$$\underline{J}_2 \approx \frac{Z_{st} \underline{J}}{\eta_c} \quad (7)$$

Since $1/\eta_c \ll 1$ usually, \underline{J}_2 is small compared to \underline{M}_2 , but not zero as implied by the first of Equations 5.

4. RELATIONSHIP OF MATERIAL PROPERTIES AND TRANSFER IMPEDANCE TO ELECTROMAGNETIC SHIELDING

The electromagnetic protection offered by a shield is generally specified in terms of the electric and magnetic shielding effectiveness (ESE and MSE) of the shield, which is defined by

$$\text{MSE} = 20 \log_{10} |\text{MSR}^{-1}| \quad (8)$$

where

$$\text{MSR}^{-1} = \frac{H_{\text{INCIDENT}}}{H_{\text{INTERNAL}}}$$

and

$$\text{ESE} = 20 \log_{10} |\text{ESR}^{-1}| \quad (9)$$

where

$$\text{ESR}^{-1} = \frac{E_{\text{INCIDENT}}}{E_{\text{INTERNAL}}}$$

The quotients of the interior and incident fields are referred to as the magnetic and electric shielding ratios.

The basic problem with such shielding specification is one of uniqueness. In general, the interior fields are not spacially uniform even when the incident fields are. There are certain geometries for which a spacially uniform incident field will produce a uniform interior field. These geometries include electrically small spherical and cylindrical shells as well as two parallel slabs. For these cases, the shielding effectiveness definitions are unique.

Shield Effectiveness for a Uniform Magnetic Field:

For a uniform magnetic field, the magnetic shielding effectiveness is a function of the shield material parameters (σ , μ , ϵ , d), the frequency of the impinging wave, and the shield geometry. The shielding effectiveness formula for single flat plate shielding is given by (LEE, K.S.H. and BEDROSIAN, G., 1976)

$$\text{MSR}^{-1} = \cosh(\gamma d) + Z_0/2\eta \sinh(\gamma d) \quad (10)$$

and for the enclosure geometries mentioned above at low frequencies by

$$\text{MSR}^{-1} = \cosh(\gamma d) + (V/S)\gamma \sinh(\gamma d) \quad (11)$$

where $\gamma = [j\omega\mu\sigma]^{1/2}$, $\eta = [j\omega\mu/\sigma]^{1/2}$, $Z_0 = \sqrt{\mu_0/\epsilon_0} = 377$, d is the shield thickness, and V/S denotes the volume-to-surface ratio for the geometries of Figure 3. Figure 3 illustrates the low frequency magnetic shielding effectiveness available for aluminum, titanium, and mixed-orientation graphite/epoxy composite enclosures with $V/S \approx 1$ and a shield thickness of 0.00107 m (corresponding to 8-ply composite material at 0.00525 in/ply thickness). It should be stressed that these shielding results are valid for the enclosures described only when the incident field is a uniform magnetic field. Similar formulas have been derived for the magnetic shielding effectiveness of an infinite flat plate with an incident nonuniform magnetic field generated by a nearby loop antenna (DIKE, G., 1979).

Electric Shielding:

For enclosures of the type previously mentioned, the inverse electric shielding ratio is (KADEN, H., 1959), where λ_0 is the wavelength in free space:

$$\text{ESR}^{-1} = \frac{\gamma \sinh(\gamma d)}{(4\pi/\lambda_0)^2 (V/S)} \quad (12)$$

Figure 4 illustrates the typical form of the frequency dependence of electric shielding effectiveness for an 8-ply mixed-orientation graphite/epoxy enclosure and similar aluminum enclosure of the same thickness.

For fixed frequency, conductivity, and shield thickness, the electric shielding effectiveness decreases with increasing volume-to-surface ratio. This is in contrast to the magnetic shielding effectiveness which increases with increasing volume-to-surface ratio.

Electromagnetic Relationships Between Shielding Effectiveness and Transfer Impedance:

The difficulty with expressions for electric and magnetic shielding effectiveness is the strong dependence of the shielding effectiveness on the nature of the incident field and on the geometry of the shield (i.e., they must be used for those basic geometries for which they were derived). Similarly, the extensive laboratory measurements of electric and magnetic shielding effectiveness that have been made over the spectrum of composite materials of current interest are valid only for the geometry of the test fixture. It is difficult to extend the test results to more complicated geometries.

For shields whose local radius of curvature is large with respect to the wavelength in the shell, a measurement of the degree of electromagnetic protection offered by the shield, independent of geometry and incident field type, is the surface transfer impedance of the shield material. This impedance is defined to be the ratio of the interior tangential electric field to the surface current density which would exist on the exterior shell surface if it were a perfect conductor. The surface transfer impedance, Z_{st} , of a homogeneous conducting shield (including mixed-orientation graphite/epoxy composites) is determined by the material conductivity and thickness, and the frequency of the incident field.

Figure 5 illustrates the dependence of the surface transfer impedance on the material thickness and material conductivity, respectively, as a function of frequency. The low frequency asymptote to the surface transfer impedance is $Z_{st} = 1/\sigma d$.

For homogeneous conducting shields with a geometry of the types discussed above under a uniform magnetic field, the surface transfer impedance can be related to the magnetic shielding effectiveness as (DIKE, G., 1979)

$$MSE = 20 \log_{10} |Z/Z_{st}| \quad (13)$$

over a frequency interval dependent upon the shield geometry, conductivity, and thickness where $Z = (V/S)j\omega\mu$ for a cylindrical, spherical, or parallel plate enclosure with volume-to-surface ratio (V/S) under a uniform magnetic field.

Similarly, for a homogeneous conducting enclosure of the type discussed above, the electric shielding effectiveness can be related to the surface transfer impedance as

$$ESE = 20 \log_{10} |Z'/Z_{st}| \quad (14)$$

over a frequency interval dependent upon the shield geometry, conductivity, and thickness, where $Z' = j[8\pi cf(V/S)]^{-1}$.

These relationships provide a means for extending the application of laboratory measurements of the magnetic shielding effectiveness of a homogeneous conducting material to locally planar homogeneous conducting shields, in general, through the concept of surface transfer impedance. Conversely, laboratory measurements of the surface transfer impedance of a homogeneous conducting shield of arbitrary locally planar geometry can be used to determine the associated magnetic shielding effectiveness for shields of the basic geometries and associated incident field types discussed. These relationships are valid over a frequency interval dependent on the shield geometry, conductivity, and thickness.

An immediate corollary to the relationship $MSE = 20 \log_{10} |Z/Z_{st}|$, valid for the frequency intervals over which the relationships hold, is as follows:

For two shields of the same geometry with conductivities and shield thickness (σ_1, d_1) , respectively, with $i = 1, 2$, the difference in the magnetic shielding effectiveness offered by the shields is

$$MSE(\sigma_1, d_1) - MSE(\sigma_2, d_2) = 20 \log_{10} \left| \frac{Z_{st}(\sigma_2, d_2)}{Z_{st}(\sigma_1, d_1)} \right| \quad (15)$$

This corollary also holds for ESE. This relationship provides a "back-of-the-envelope" solution to the gain or loss in magnetic shielding effectiveness when conducting films are added to shields or when different materials are used for the shield.

5. JOINT COUPLING

Definition of Joint Admittance:

Skin currents flowing across a joint in the aircraft skin induce electric fields in the aircraft interior. These fields in turn induce transients on interior wiring. The maximum voltage which can be induced on an interior wire is the voltage drop across the joint, namely, $V_j = J/Y_j$, where J is the surface current density at the joint and Y_j is the joint admittance per unit length.

Well-formed joints in shield material (those of uniform construction and good electrical contact and without cracks or apertures) can be described in terms of a distributed joint transfer admittance per unit of joint length. The exterior surface current density flowing across the joint produces a voltage V_j across the joint on the inside. For a linear joint contact impedance, the interior joint voltage is proportional to exterior surface current and inversely proportional to joint width. A typical joint construction is shown in Figure 6. Corresponding measured joint admittances are in Figures 7a and 7b.

Joint Model:

Harrington (HARRINGTON, R.F. and AUCKLAND, D.T., 1979) defines the joint admittance in a similar manner but identifies it as a transfer admittance. For the simple butt joint of width W and depth d , transmission line theory and circuit theory applied to the equivalent circuit yield

$$Y_j = (Y^a + Y^0) \cosh \gamma_b d - (Y_0 + \frac{Y^a Y^0}{Y_0}) \sinh \gamma_b d \quad (16)$$

Here Y^a is the aperture admittance of a thin slot opening into half space region "a". It is given by the equation

$$Y^a = \frac{1}{\eta_a \lambda_a} [\pi - 2j \ln(Ck_a W)] \quad (17)$$

where η_a , λ_a , k_a are the impedance, wavelength, and wave number in region "a", and C is a constant ($C = 0.2226$). The Y^0 term has the same form, but the a 's are replaced by 0 's. The term $Y_0 = 1/W\eta_b$ is the characteristic admittance of a parallel-plate transmission line.

For a highly lossy slot, $\gamma_b = \sqrt{j\omega\mu\sigma}$ and $\eta_b = \sqrt{\frac{j\omega\mu}{\sigma}}$. If $\gamma_b d \rightarrow 0$, Equation 16 becomes independent of frequency. This is the behavior shown over low frequencies in Figure 7a for the joint shown in Figure 6.

The power transmitted through the aperture is equal to the power dissipated in Y^0 of the equivalent circuit; that is,

$$P_t = \left| \frac{I^1}{Y_{12}} \right|^2 R_e(Y^0) \quad (18)$$

where $I^1 = 2H^1$ for the simple butt joint.

6. COUPLING OF ELECTROMAGNETIC FIELDS TO TRANSMISSION LINES (BURT, E.C., 1979)

An isolated two-wire transmission line is illuminated by a uniform electromagnetic field. The line lies in the x - z plane, parallel to the z -axis with terminations parallel to the x -axis and is of length L . The incident field propagates in the x -direction with the E -field parallel to the line for maximum coupling. The open-circuit voltage and short-circuit current as a function of time can be written as

$$V_{oc}(t) = I_0(t) + \sum_{n=1}^{\infty} \Gamma^n (I_{2n} - I_{2n-1}) \quad (19a)$$

$$Z_0 I_{sc}(t) = I_0(t) + \sum_{n=1}^{\infty} (-\Gamma)^n (I_{2n} + I_{2n-1}) \quad (19b)$$

where

$$I_n(t) = v \int_{nT_0}^{(n+1)T_0} E_0(t - \tau) d\tau \quad (19c)$$

where v is the velocity of propagation on the line, $E_0(t)$ is the amplitude of the incident field, $T_0 = L/v$ and Γ is the voltage reflection coefficient at the terminated end of the line. Each of the terms in these expressions can be interpreted as a (multiple) reflection of an excitation arising from the incident field at some past time.

Similar expressions can be derived where the field is incident on only a portion of the line. This allows one to approximate the case of a nonuniform field due to coupling

through a joint between composite material. In particular, if we assume as before that the incident field is parallel to the line, with no z-dependence, and only affects the line between z_1 and z_2 , $0 \leq z_1 < z_2 \leq L$, then

$$V_{oc}(t) = I_o^s(t) + \sum_{n=1}^{\infty} \Gamma^n (I_{2n}^s - I_{2n-1}^s) \quad (20a)$$

$$z_o I_{sc}(t) = I_o^s(t) + \sum_{n=1}^{\infty} (-\Gamma)^n (I_{2n}^s + I_{2n+1}^s) \quad (20b)$$

where

$$I_{2n}^s(t) = v \int_{2nT_o + t_1}^{2nT_o + t_2} E_o(t - \tau) d\tau \quad (20c)$$

and

$$I_{2n-1}^s(t) = v \int_{2nT_o - t_2}^{2nT_o + t_1} E_o(t - \tau) d\tau \quad (20d)$$

Using the expressions for $V_{oc}(t)$ and $I_{sc}(t)$ as given in Equation 19 (or 20) various upper bounds can be found for the open-circuit voltage and short-circuit current. The accuracy of these estimates depends on the form of the incident field. If a particular incident field is assumed, then better estimates can be made.

We can sum Equation 19 if we assume $I_n(t)$ is positive for each n and define $I_{max} = \max_t I_o(t)$ to give

$$|V_{oc}^{peak}| \leq I_{max} / (1 - |\Gamma|) \quad (21)$$

and

$$|z_o I_{sc}^{peak}| \leq I_{max} (1 + |\Gamma|) / (1 - |\Gamma|)$$

I_{max} can be computed for a given incident field or estimated by $I_{max} \leq L E_{max}^i$, where $E_{max}^i = \max_t E_o(t)$.

For an incident field with a very rapid rise and decay such as a nuclear EMP, the peak voltage and current will occur shortly after the commencement of the incident field. If the rise time to peak for the field is comparable to the length of the line then only the first several terms of Equation 19 will be nonzero at the time the peak occurs. Therefore,

$$|V_{oc}^{peak}| \leq I_{max} (1 + |\Gamma|) \quad (22)$$

and

$$|z_o I_{sc}^{peak}| \leq I_{max} (1 + |\Gamma|)$$

If a resistance R is placed across the terminals of our transmission line model, then the delivered instantaneous power, $P(t)$, can be bounded in three ways:

$$P(t) \leq V_{oc}^2(t) / R \quad (23)$$

$$P(t) \leq I_{sc}^2(t) R \quad (24)$$

$$P(t) \leq V_{oc}(t) I_{sc}(t) \quad (25)$$

It can easily be seen that Equation 23 will give the best estimate if $R > V_{oc}(t) / I_{sc}(t)$ and Equation 24 will be best if $R < V_{oc}(t) / I_{sc}(t)$. If $R = V_{oc}(t) / I_{sc}(t)$, then all three bounds are equal. If no specific value of R is known, then Equation 25 should be used.

Using Equation 25, together with our previous estimates for V_{oc}^{peak} and I_{sc}^{peak} , we have

$$P^{peak} \leq V_{oc}^{peak} I_{sc}^{peak} \leq \frac{I_{max}^2 (1 + |\Gamma|)}{z_o (1 - |\Gamma|)^2} \quad (26)$$

An upper bound for the maximum energy which the incident field can deliver to the line can be obtained as

$$E \leq \frac{L^2 ||E^i||^2 (1 + |\Gamma|)}{z_0 (1 - |\Gamma|)^2} \quad (27)$$

where $||E^i||$ is the L^2 norm of the incident electric field.

For an incident field of the double exponential form given in Equation 1, the calculations involved in evaluating Equation 19 for the open-circuit voltage and short-circuit current can be carried out exactly for any given value of t . Unfortunately, because only a finite number of terms in these series are nonzero and this number changes with time, simple closed form expressions for $V_{oc}(t)$ and $I_{sc}(t)$ do not result. However, the resultant expressions can be incorporated into a computer program to efficiently calculate these quantities. In order to check the validity of the expressions given in Equation 19 and also check the accuracy of the estimates, comparisons were made with results obtained by a much more detailed analysis. In particular, in (FORCE, R.; et al., 1977), an elaborate computer simulation is described. This simulation uses a wire grid model of an F-18 to predict through a moment method code the fields incident on internal wires. The open-circuit voltage and short-circuit current are then calculated. Comparisons were performed to check against this reference. Close agreement was obtained in all cases checked.

7. CIRCUIT DAMAGE AND SUSCEPTIBILITY

Wunsch Model for Semiconductor Vulnerability:

The model used to predict device burnout as a function of electromagnetic pulsewidth is the Wunsch model, given by

$$P = K T_d^{-1/2} \quad (28)$$

P is the power required for junction failure, K is the damage constant determined by junction properties and geometry, and T_d is the square pulse time to failure.

This is an experimentally derived relationship. At pulse durations in excess of about 10 μ s, the amount of power required for damage is set by the rate at which heat can be conducted away from the hot spot.

Integrated Circuit Susceptibility:

Some information has been gathered by McDonnell Douglas in the susceptibility of individual integrated circuits over the frequency region from 200 MHz to 10 GHz (ROE, J.M., 1978). The sample curves shown represent only a small portion of the data available from the source documents. The data in Figure 8a shows that the most sensitive devices are operational amplifiers, followed by multi-pin regulators and TTL devices. The worst-case susceptibility, in terms of absorbed power to cause a minimal interference, covers a range of almost three orders of magnitude. The three-pin regulator and the CMOS circuitry are less susceptible than the TTL and multi-pin regulator.

In the experiments and analyses performed, the shielded cabling presented a worst-case aperture of a half-wave dipole ($0.13\lambda^2$), so that the power absorbed by the cabling, P , without considering losses can be related to the incident power density, P_d , at the cabling by

$$P = 0.13\lambda^2 P_d \quad (29)$$

where λ is the wavelength of operation. Using this relationship with the curves shown in Figure 8a (WIDMANN, L., BARRETT, J., 1980) the worst-case power density susceptibility shown in Figure 8b was obtained. These curves exhibit a very wide range of power density susceptibility over the frequency range. Using these curves with the environmental RF threat provides a means for assessing the increased shielding required. As an example, the power density at a range of 1 nmi from a 10 kW transmitter with a 40 dB gain antenna is shown in dotted lines across the top of Figure 8b. At the 220 MHz end of the spectrum, over 60 dB increases in shielding might be required. Even an increase in distance from the antenna to 10 nmi would only reduce the requirements to 40 dB more shielding. The requirement is considerably less at the higher frequencies due to the inverse frequency square properties of the dipole absorption apertures.

Integrated Circuit Damage:

The preceding information pertains to interference susceptibility which goes away when the interfering source is removed. However, permanent damage results at some level higher than the interference level. Depending upon the effect on performance, it would be classified as degradation or catastrophic failure. The failure mechanism is due to the increase in temperature caused by the absorption of power (energy) reaching a damaging level in the silicon junctions, the metalization stripes, or the bond wires. The thermal dissipation time constant of the devices is such that pulse durations in excess of 30 μ s has the same effect as CW signals. At pulse durations in excess of 30 μ s, the peak power times pulse duration times pulse repetition frequency product (i.e., the energy absorbed) is the critical issue since the effect is thermal destruction. The data shows that a minimum of 0.5 W of absorbed power is required to cause burnout. Using the half-wave dipole aperture absorption model, the CW power density for burnout ranges from 0.43 W/m^2 (0.043 mW/cm^2) at 100 MHz to 4273 W/m^2 (0.43 W/cm^2) at 5.6 GHz.

The failure mechanism due to the EMP generated by nuclear blasts is reported to be dominantly due to semiconductor junction failure. For integrated circuits, a model paralleling that for the semiconductors was empirically generated. This model is $P = K T^{-B}$. The data found experimentally by McDonnell Douglas for microwave power absorption shows a value for B of 0.5. The range of Wunsch constants for various devices has been published in many sources. Typical values are in the range from 0.01 to 50 $W \cdot s^{1/2}$ for transistors and 0.0002 to 20 $W \cdot s^{1/2}$ for diodes. Integrated circuits lie in the range from 0.0005 to 0.2 $W \cdot s^{1/2}$.

8. EQUIVALENT SQUARE-WAVE POWER PULSES (BURT, E.C., 1979)

The Wunsch damage constant for semiconductor junction devices used in estimating the vulnerability of electronic devices to burnout is obtained under the assumption of a square-wave power pulse. In order to use the Wunsch damage constant for other power pulses, it is useful to relate a given waveform to a rectangular pulse with the same peak amplitude which produces the same or greater device damage. For a general power waveform, $P(t)$, whose peak amplitude is P_0 , we can define an equivalent square-wave pulse which has the same energy content as $P(t)$. We denote the duration of this energy equivalent pulse by T_e . This energy equivalent time may be used in $K = P_0 T_e^{1/2}$ to calculate the smallest allowable Wunsch damage constant a device can have and still withstand burnout when subjected to a power pulse $P(t)$.

Lightning or nuclear EMP threats may be described by a simple exponential which describes the threat for large time, and in fact is an upper bound for the double exponential waveform for all t . For this case, $T_e = 1/2\alpha$. Applying this result, it is possible to bound the energy delivered to a device due to coupling to a transmission line. In particular,

$$E \leq V_{oc}^{peak} I_{sc}^{peak} T_e \quad (30)$$

9. EXAMPLES

The concepts and formulas of the previous sections have been applied to determine the threat to circuits terminating transmission lines within composite aircraft. Comparisons are shown for aluminum and graphite/epoxy coverings.

The parameters used to develop the curves of Figures 9 and 10 were as follows. For diffusion coupling, graphite/epoxy was assumed to have a conductivity of $\sigma = 10^4$ mhos/m, the composite thickness was taken as 0.0025 m or approximately 10 plies. Threat parameters were taken as described in Section 2. The characteristic impedance, Z_0 of the transmission line was taken as 100 ohms with $|\Gamma| = 0.54$. The integral I_{max} was taken as $L E_{max}^2$. Upper bounds on V_{oc} , I_{sc} , $P(t)$ were computed as a function of effective length L of exposed line.

The minimum allowable Wunsch constant of devices that will survive these threats was also plotted. The equivalent square pulse length for the shipborne radar threat was taken as 400 μs with an amplitude of 400 V/m. The results of Figures 9 and 10 may be compared with device susceptibility data to determine the amount of shielding that must be provided by coating the graphite/epoxy skin with a metallic coating or by shielding the transmission lines. The upper bounds for direct strike and near miss lightning coupled through aluminum are included as a reference.

Below 100 MHz the joint admittance was taken as constant at 15 mhos/m. Upper bounds on the parameters of interest are tabulated below for frequencies below 100 MHz.

	V_{oc} (V)	I_{sc} (A)	Power (W)	Wunsch Constant ($W \cdot s^{1/2}$)
Direct Strike Lightning	9.5×10^3	150	1.4×10^6	0.76×10^4
Near by Lightning (20 m)	460	7.1	3.2×10^3	18
NEMP	27.7	0.2	7.37	0.0029
Shipboard RF	0.306	0.0047	1.44×10^{-3}	0.000028

Above 2 GHz, the results vary with frequency as the joint admittance changes as shown in Figure 7b. Upper bounds in the parameters are shown in Figure 11 for the shipboard threat, take as 4000 V/m. Results for the power coupled to the transmission line termination using Equations 18 and 29 are included as is the minimum Wunsch constant of devices that will survive this threat. The power curves of Figure 11 can be overlaid on the curves of Figure 8a to compare the threat at the cable termination to the integrated circuit susceptibility power level.

10. REFERENCES

1. BURT, E.C., 1980, "Coupling of Electromagnetic Fields to Transmission Lines," Interim Report, Advanced Composite Aircraft Electromagnetic Design and Synthesis, prepared by the Syracuse Research Corporation for the Naval Air Systems Command and the Office of Naval Research under Contract N00014-78-C-0673, SRC TN 79-490.

2. DIKE, G., Relationships of Material Properties to Electromagnetic Shielding, prepared by the Syracuse Research Corporation for the Naval Air Systems Command and the Office of Naval Research under Contract N00014-78-C-0673, SRC TN 79-037.

ALSO:

BIRKEN, J., DIKE, G., and WALLENBERG R., 1979, "Electromagnetic Relationships Between Shielding Effectiveness and Transfer Impedance," IEEE International Symposium on Electromagnetic Compatibility, 79CH1383-9 EMC, pp. 133-138.

3. FISHER, F.A., and PLUMER J.A., 1977, Lightning Protection of Aircraft, prepared by the General Electric Company for NASA Lewis Research Center, NASA Reference Publication 1008.

4. FORCE R.; GEREN, P.; STRAWE, D.; and SCHMIDT, A., 1977, Investigation of Effects of Electromagnetic Energy in Advanced Composite Aircraft Structures and Their Associated Avionics/Electrical Equipment, Phase II, Vol. 1, presented by the Boeing Corporation for Naval Air Systems Command, Final Report under Contract N00019-76-C-0497, Final Report D18-20186-4.

5. HARRINGTON, R.F., 1961, "Time-Harmonic Electromagnetic Fields," McGraw-Hill Book Co.

6. HARRINGTON, R.F., 1980, "Penetration of Electromagnetic Waves Through Lossy Shells," Advanced Composite Aircraft Electromagnetic Design and Synthesis, Interim Report prepared by the Syracuse Research Corporation for the Naval Air Systems Command and the Office of Naval Research under Contract N00014-78-C-0673, SRC TN 79-490.

7. HARRINGTON, R.F., and AUCKLAND, D.T., 1979, "Electromagnetic Transmission Through Narrow Slots in Thick Conducting Screens," submitted for publication in IEEE Transactions on Antenna and Propagation.

8. HARRINGTON, R.F., and MAUTZ, J.R., 1975, "An Impedance Sheet Approximation for Thin Dielectric Shells," IEEE Transactions, Vol. AP-23, No. 4, pp. 531-534.

9. KADEN, H., 1959, "Wirbelströme und Schirmung in der Nachrichtentechnik," Springer-Verlag, Berlin.

10. LEE, K.S.H., and BEDROSIAN, G., 1979, "Diffusive Electromagnetic Penetration into Metallic Enclosures," IEEE Transactions, Vol. AP-27, No. 2, pp. 194-198.

11. ROE, J.M., et al., 1978, Integrated Circuit Electromagnetic Susceptibility Handbook, Phase III, prepared by McDonnell-Douglas Astronautics Company for the Naval Surface Weapons Center under Contract N60921-76-C-A030, MDC E1929.

12. STRAWE, D.F., and PISZKER, L.D., 1980, "Investigation of Penetration of Electromagnetic Energy Through Joints in Advanced Composite Structures," The Boeing Co., Seattle, Washington, prepared for the Naval Air Systems Command, D180-25240-2.

13. WIDMANN, L., and BARRETT, J., 1980, "Integrated Circuit Electromagnetic Susceptibility," Advanced Composite Aircraft Electromagnetic Design and Synthesis, Interim Report prepared by the Syracuse Research Corporation for the Naval Air Systems Command and the Office of Naval Research under Contract N00014-78-C-0673, SRC TN 79-490.

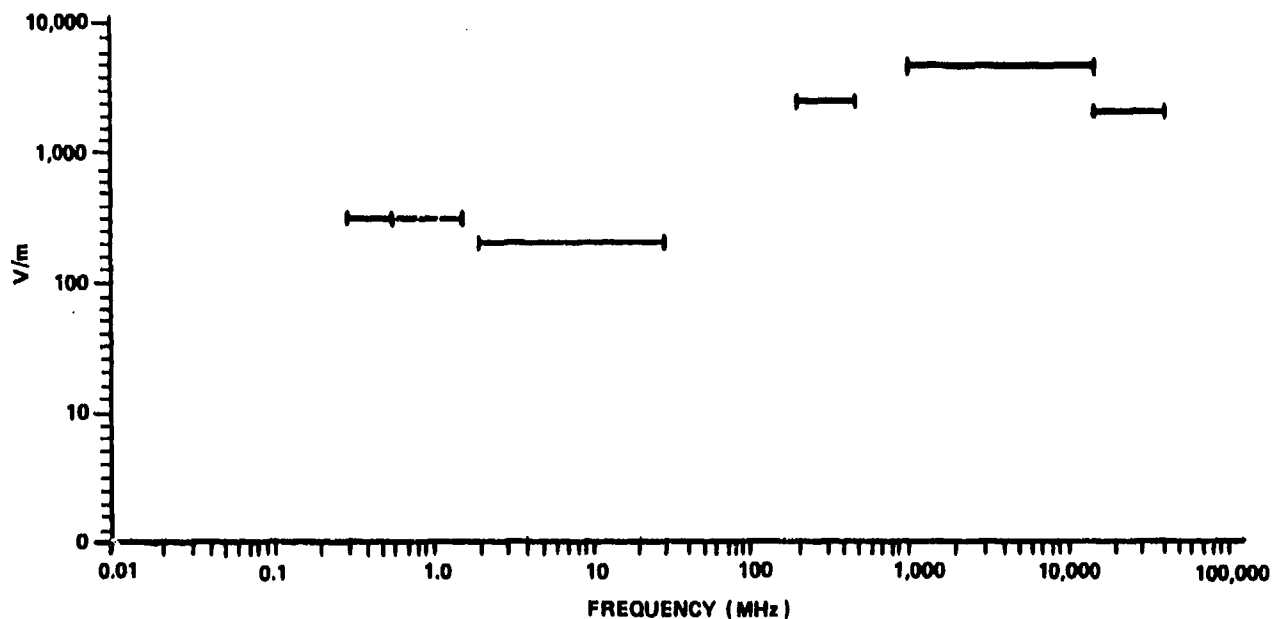


Fig.1 Transmitter field strength on carrier flight deck

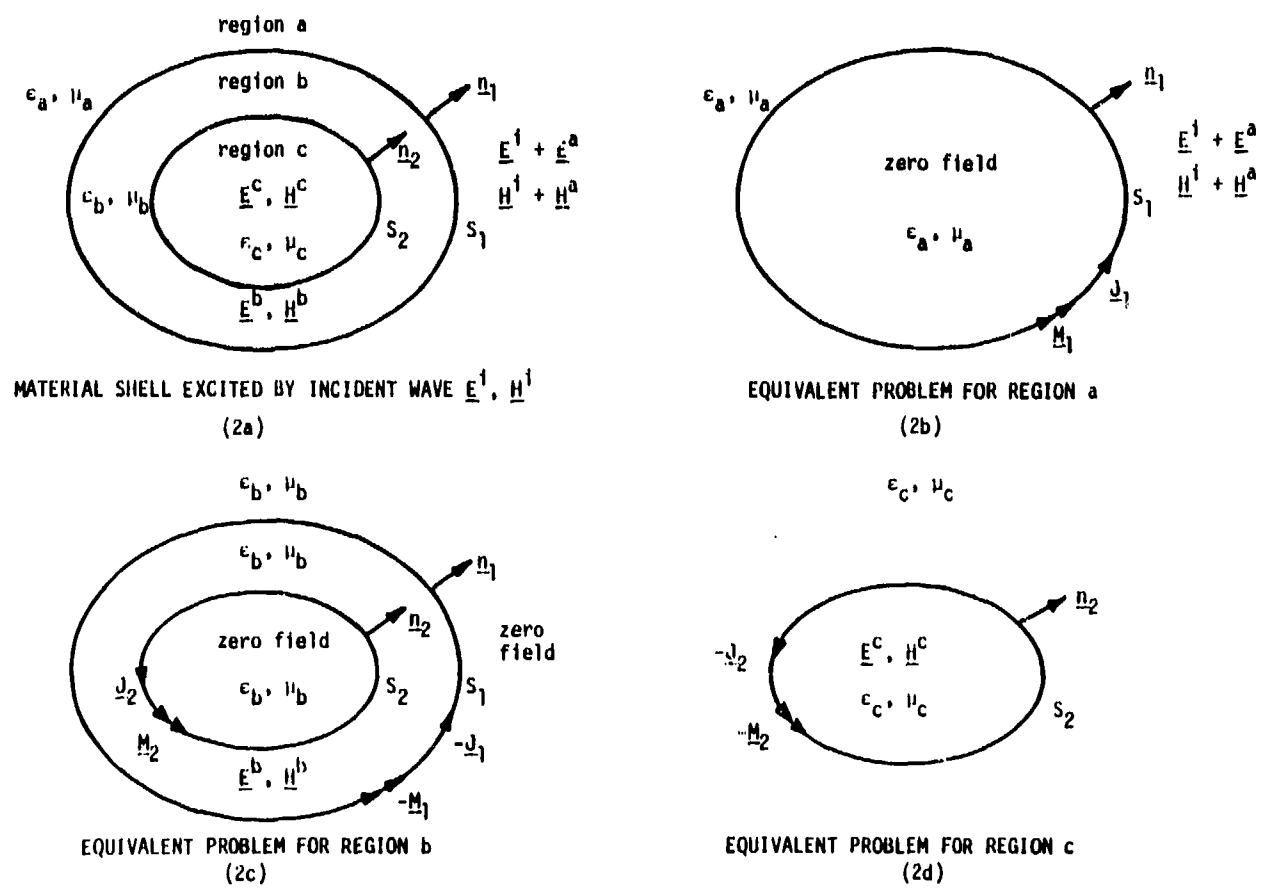


Fig.2 A material shell excited by an incident wave and equivalent problems

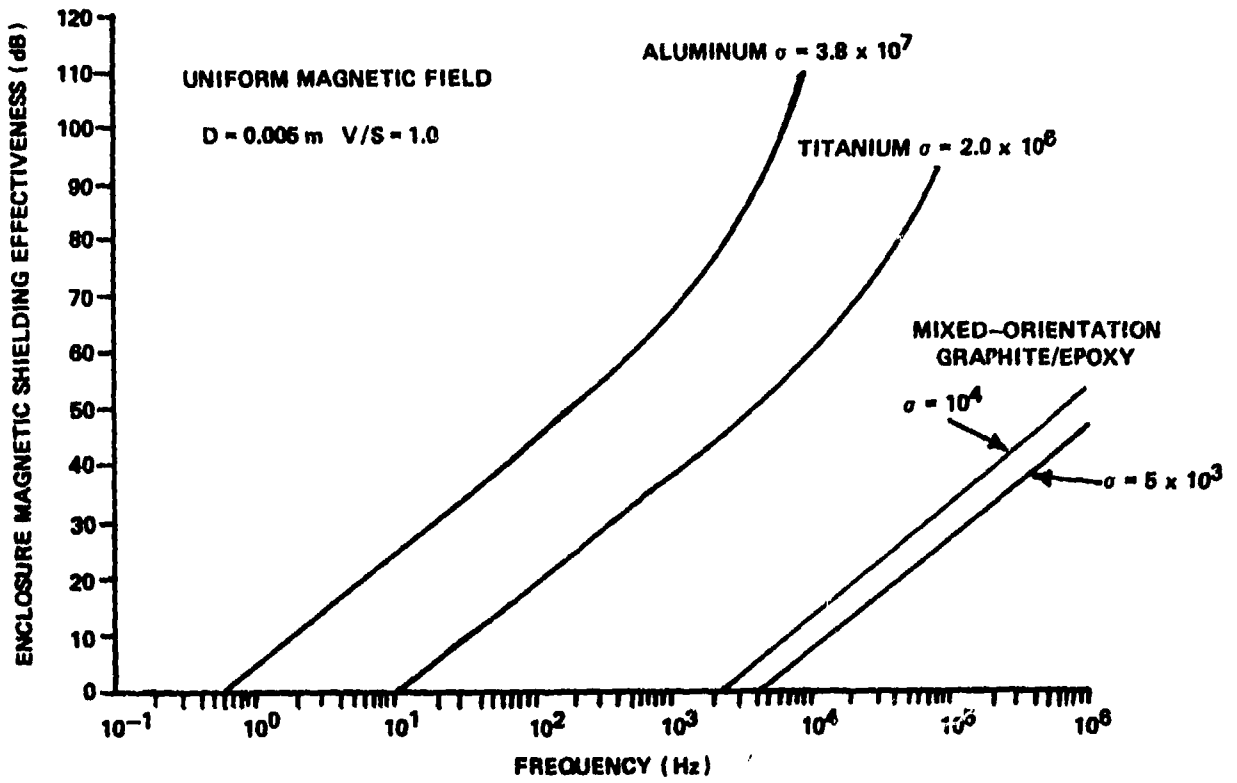


Fig.3 Magnetic shielding effectiveness for an enclosure

V/S = 1

SHIELD THICKNESS CORRESPONDS TO 8-PLY COMPOSITE MATERIAL OF 0.00525 IN/PLY

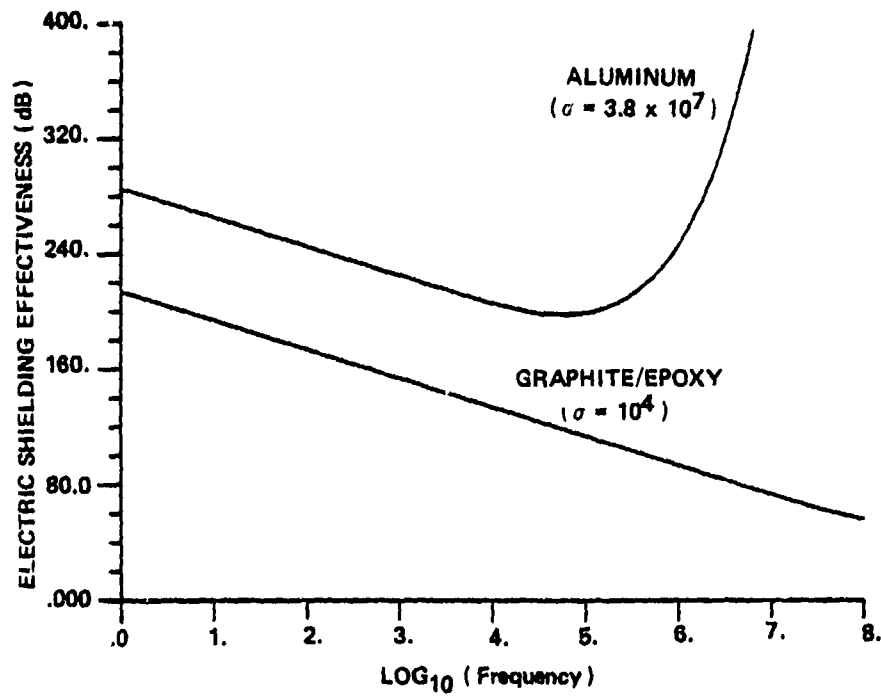


Fig.4 Electric shielding effectiveness of an enclosure under a uniform electric field

MATERIAL THICKNESS CORRESPONDS TO 8-PLY COMPOSITE MATERIAL AT 0.00525 IN/PLY

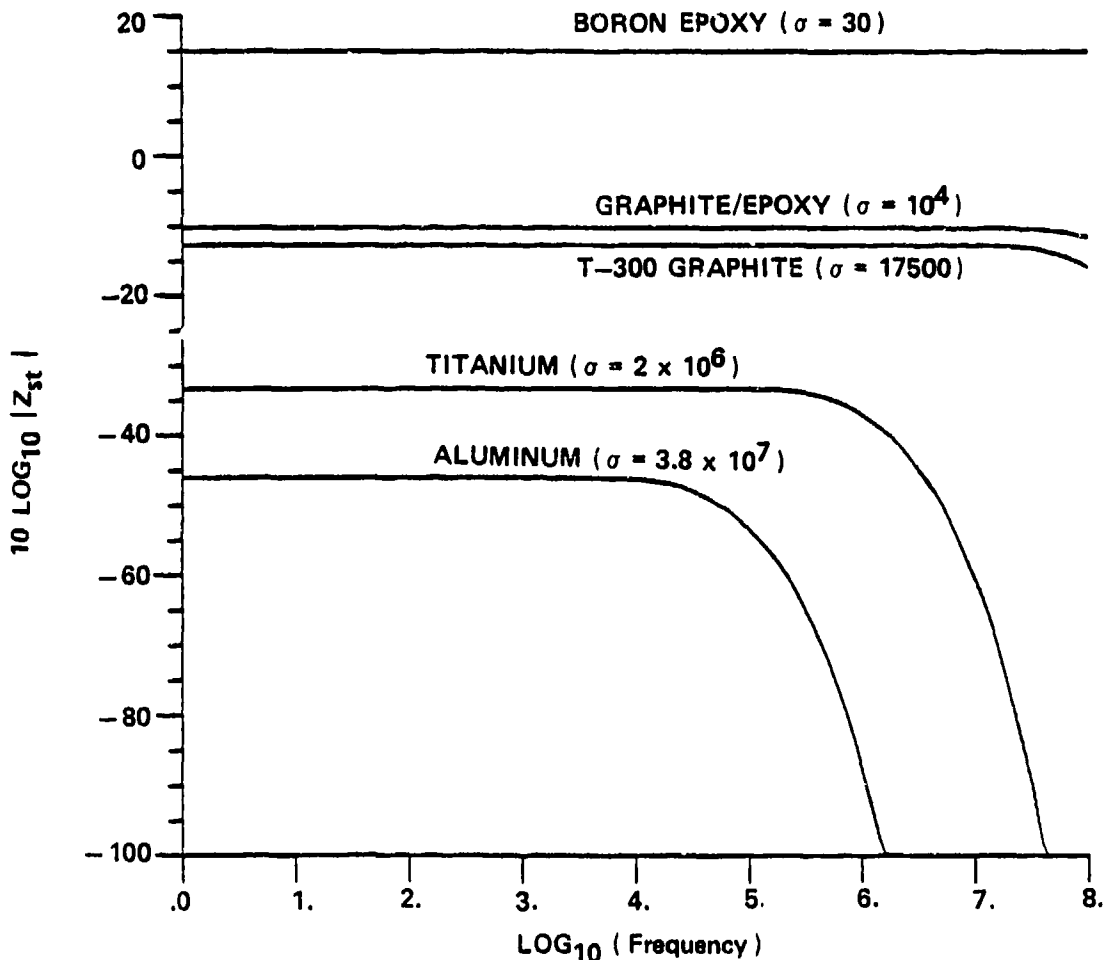


Fig.5 Surface transfer impedance as a function of frequency

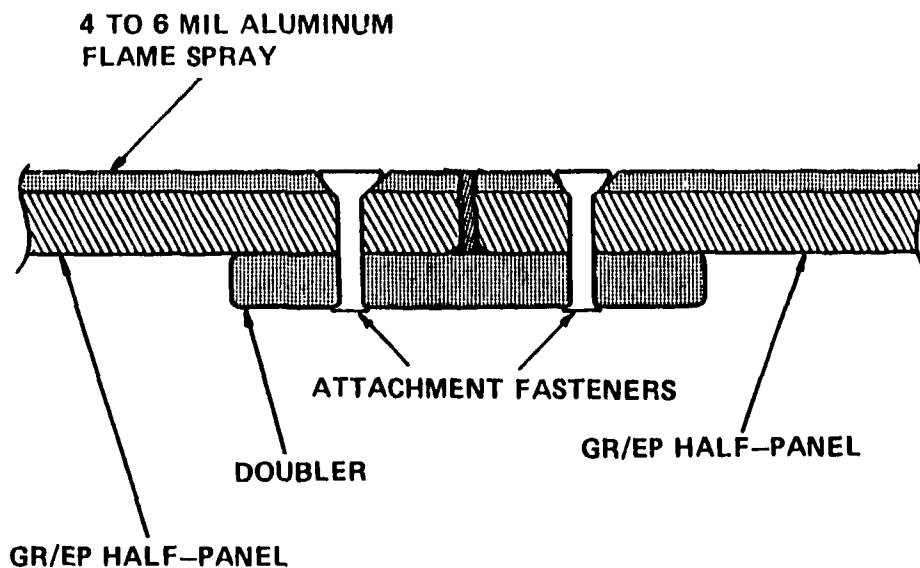


Fig.6 Cross-section of graphite/epoxy joined panel (not to scale)

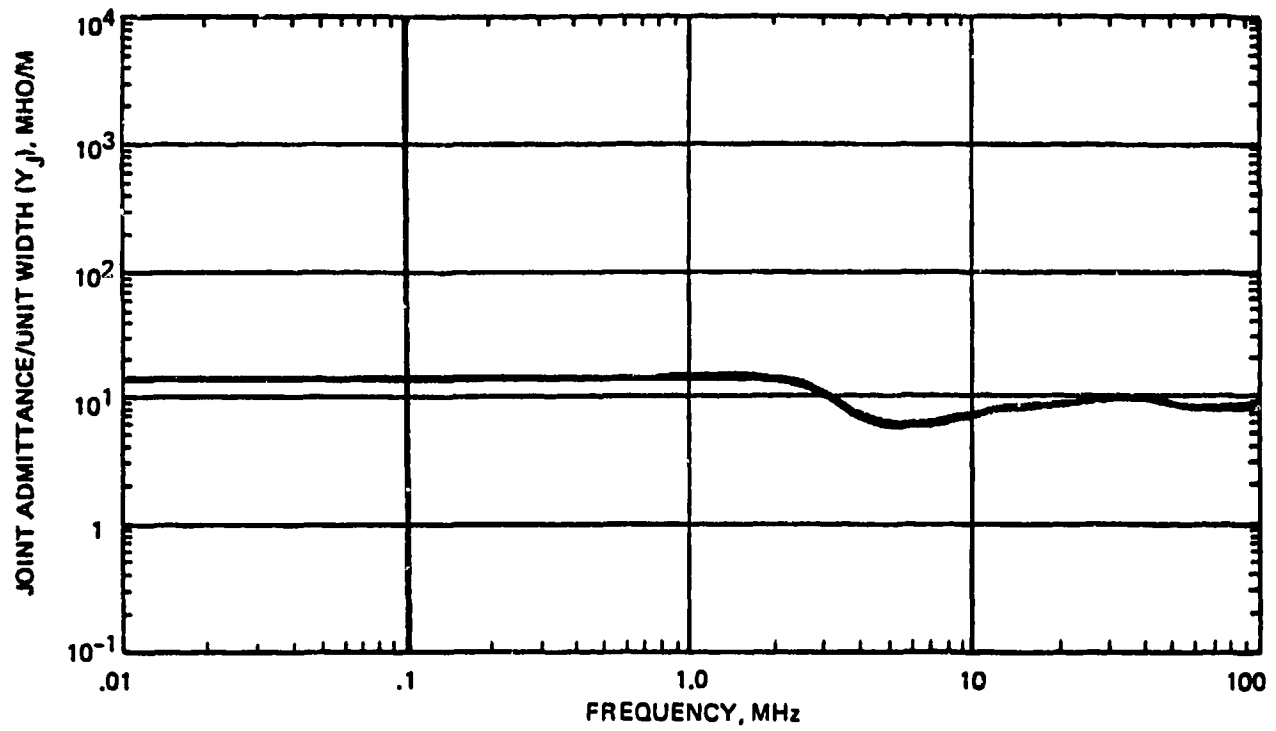


Fig.7a Low frequency measured joint admittance
(Force, R.; Green, P.; Strawe, D.; 1977)

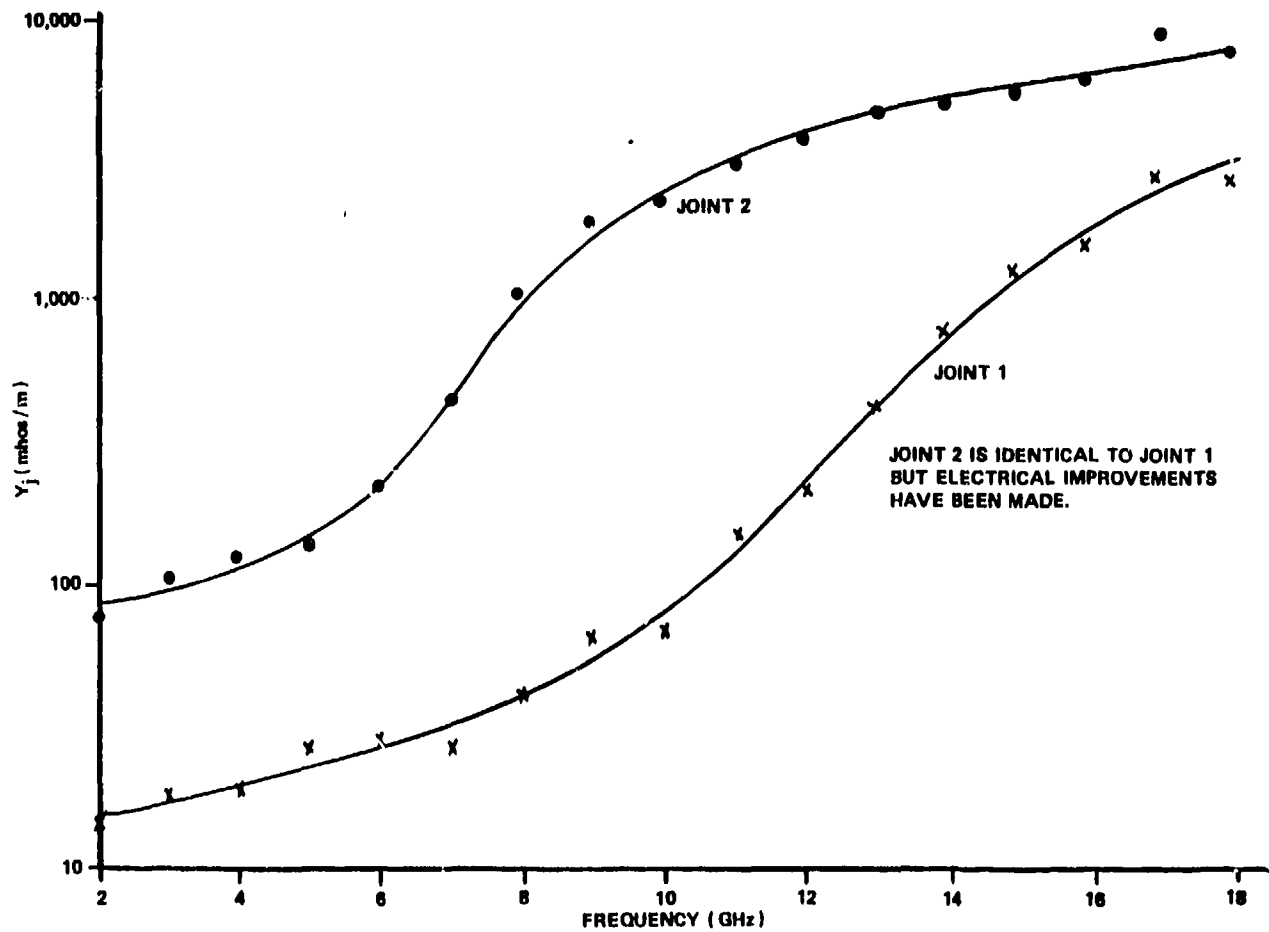


Fig.7b High frequency measured joint admittance
(Strawe, D. and Piszker, L.; 1980)

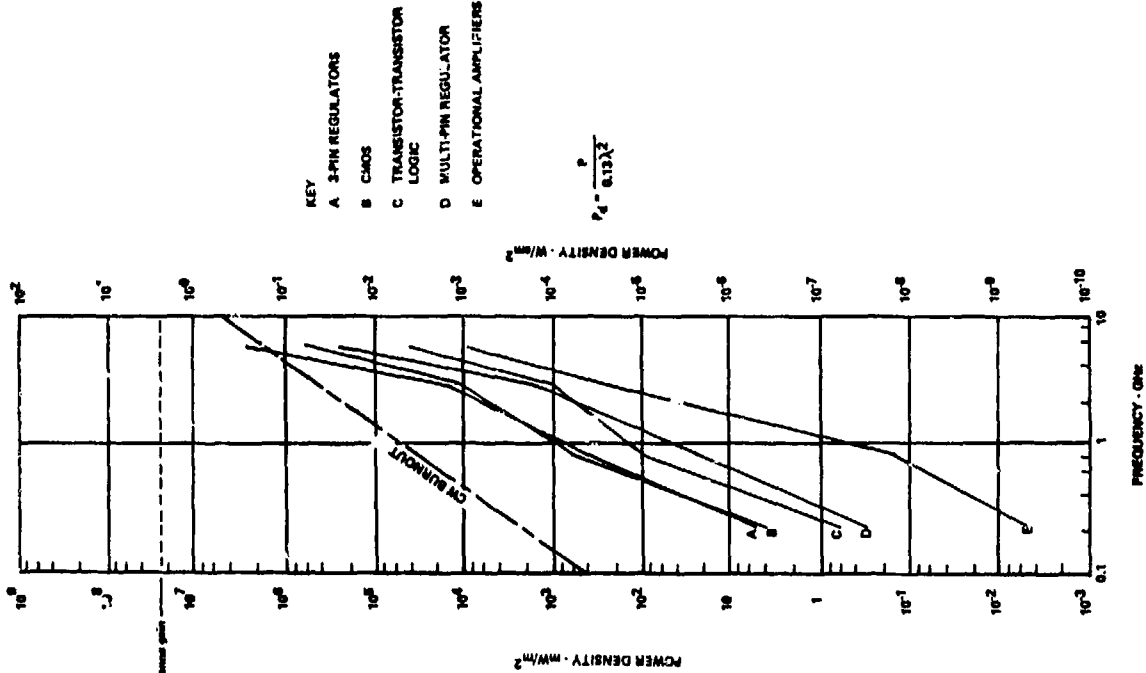


Fig.8a Worst-case absorbed power susceptibility (Roe, J.M., et al., 1978)

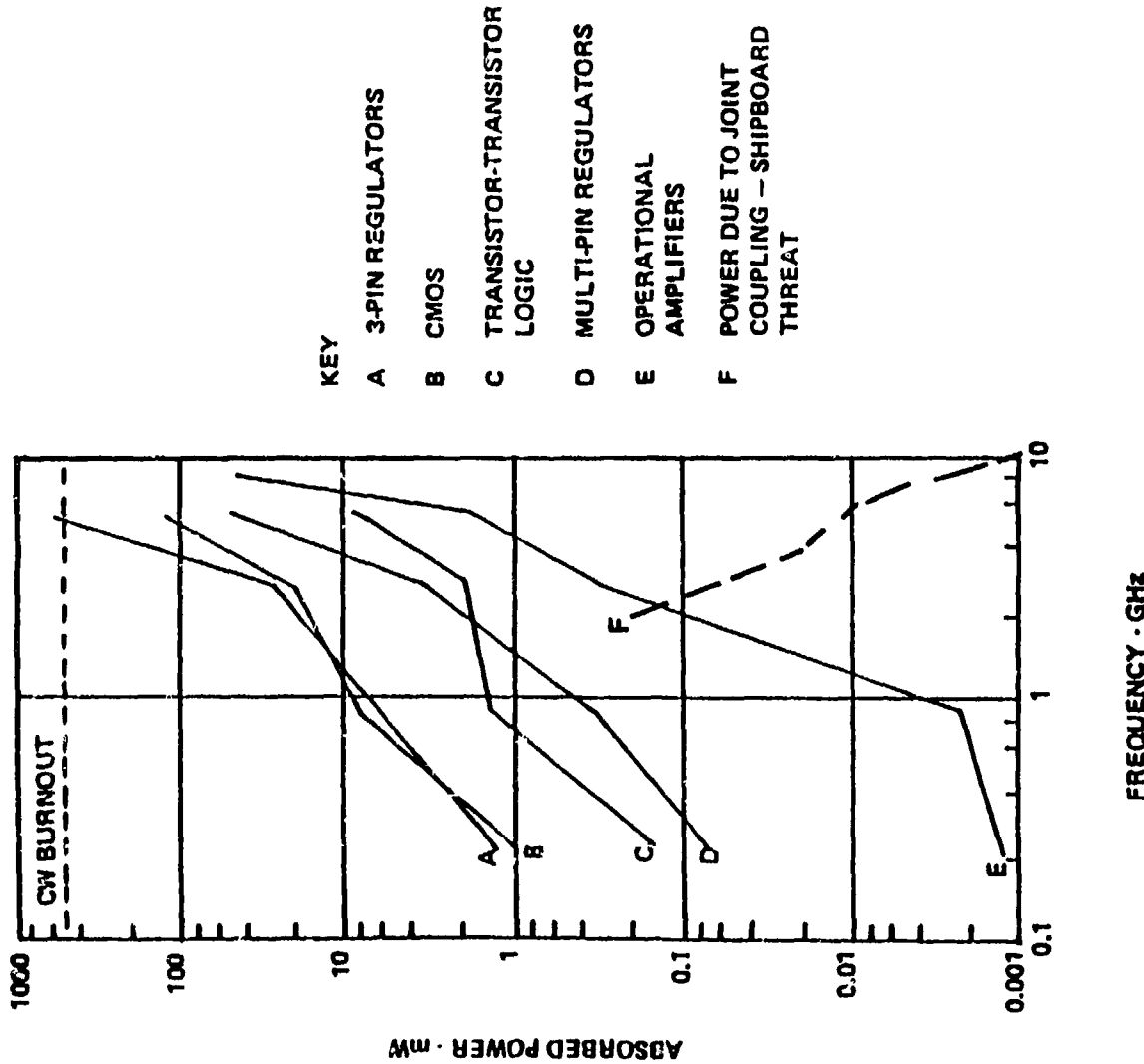


Fig.8b Worst-case power density susceptibility values assuming λ/2 aperture (Widmann, L., 1979)

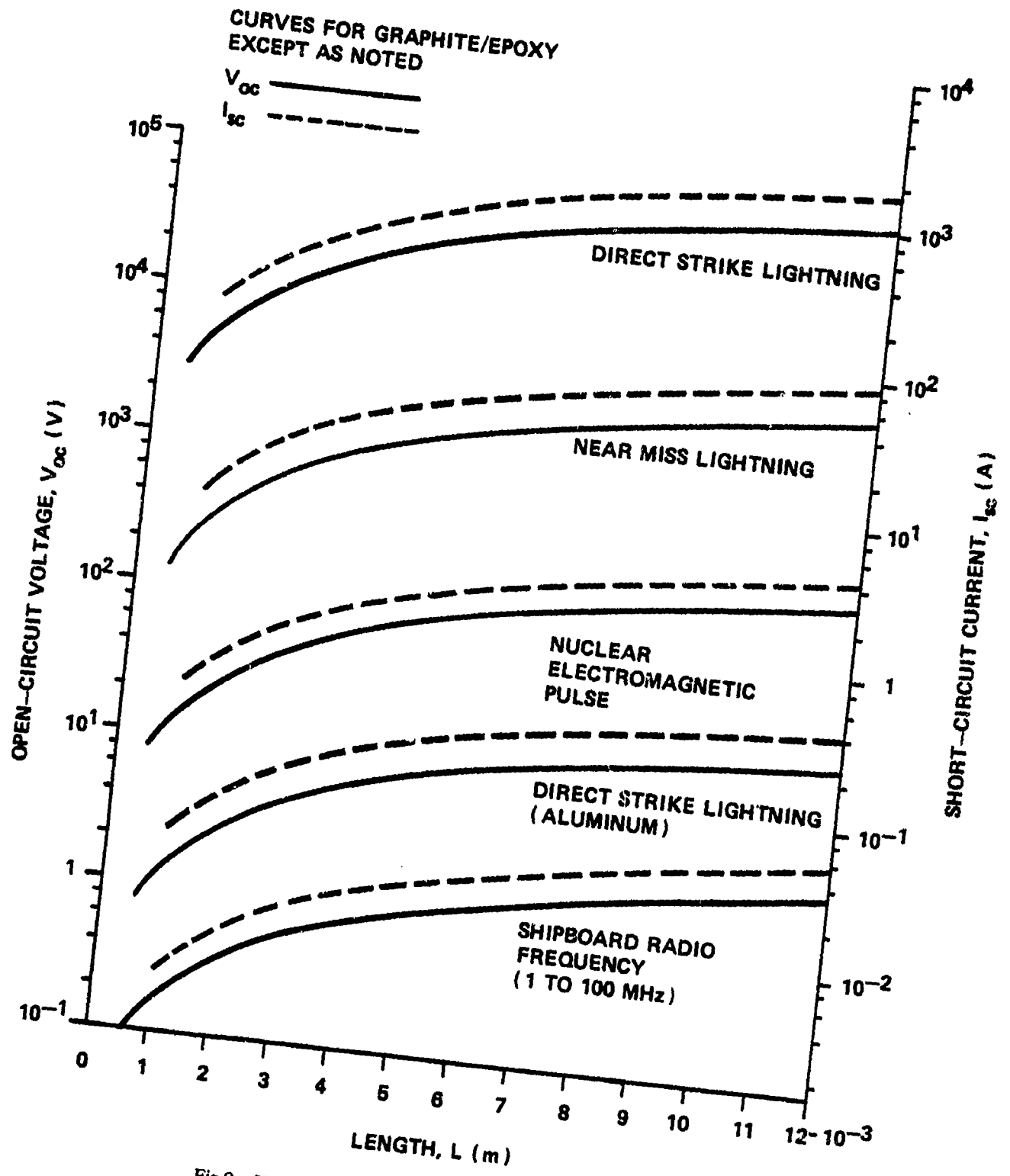


Fig.9 Upper bounds on open-circuit voltage and short-circuit current due to diffusion through graphite/epoxy

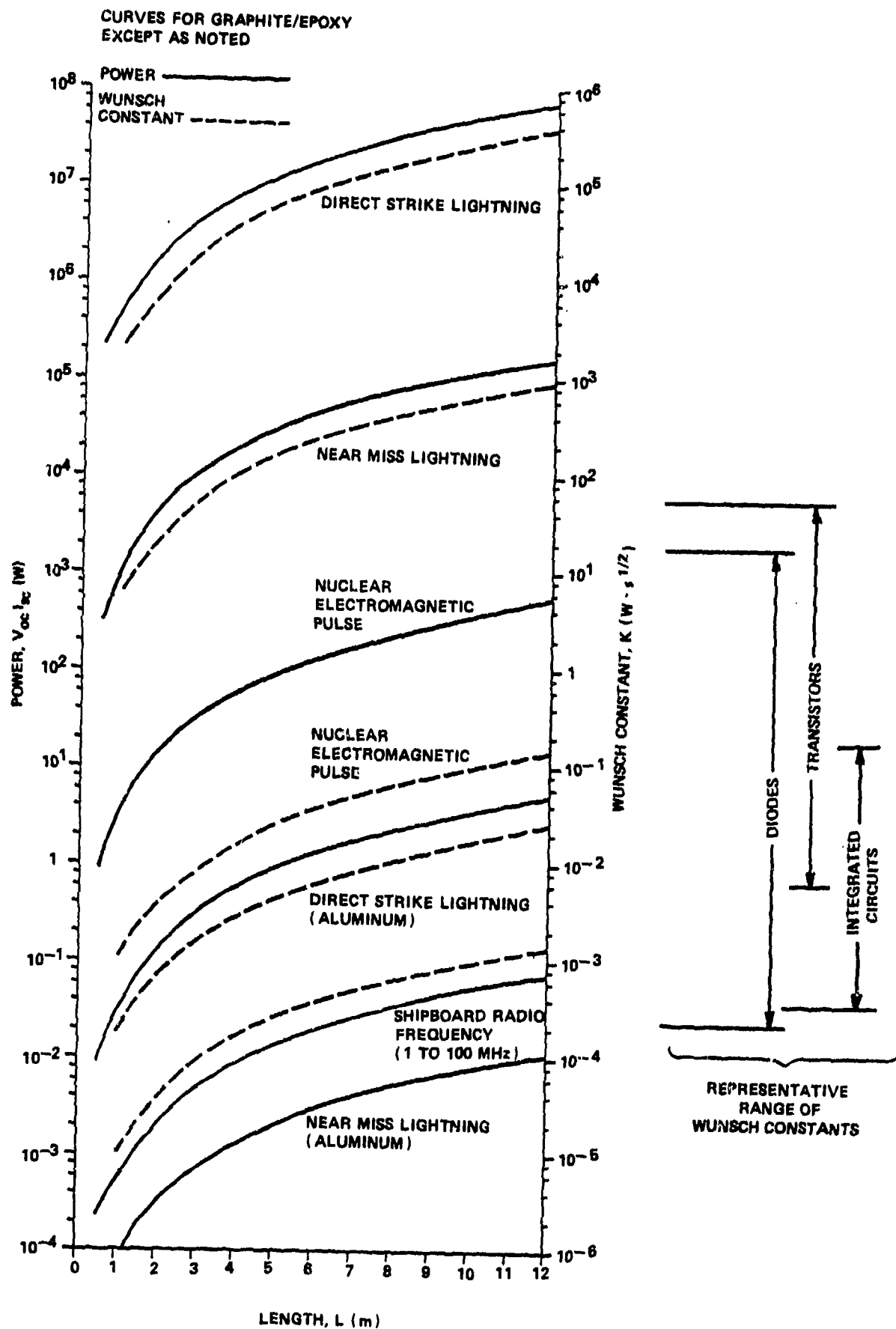


Fig.10 Upper bounds on power delivered to transmission line termination; minimum Wunsch constant of devices that will survive threat

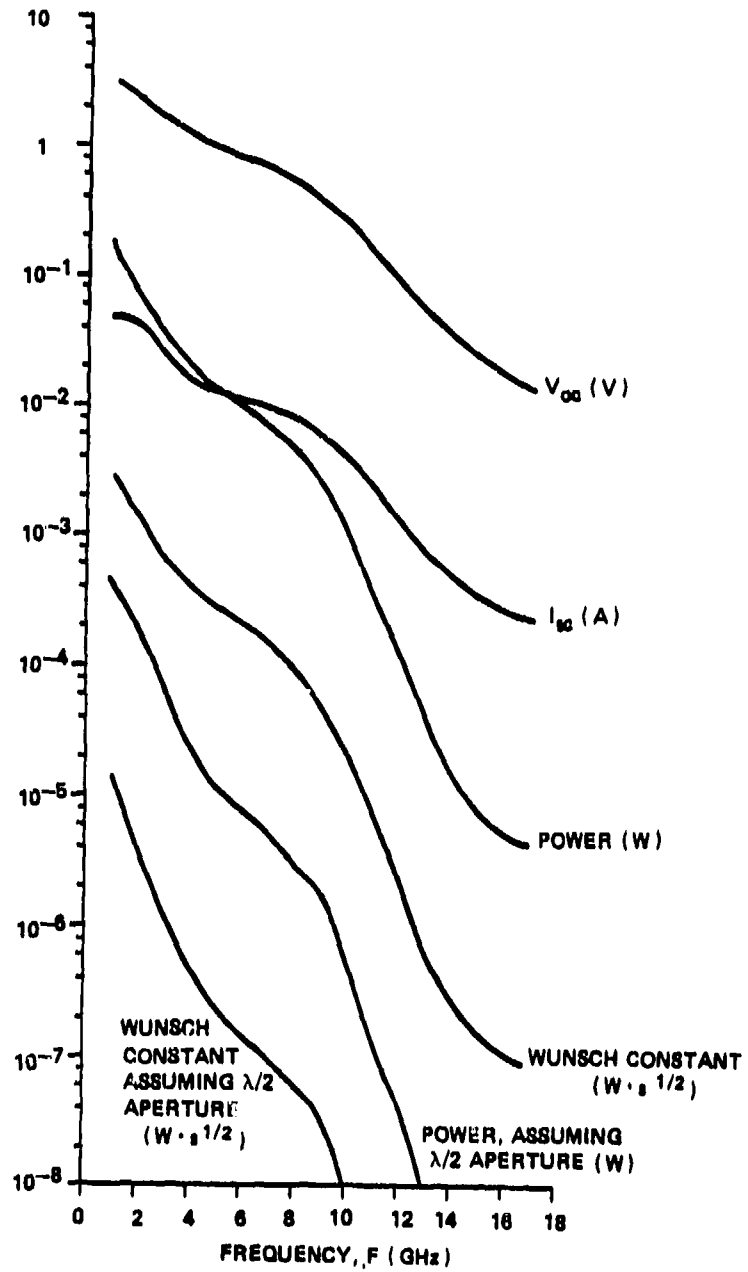
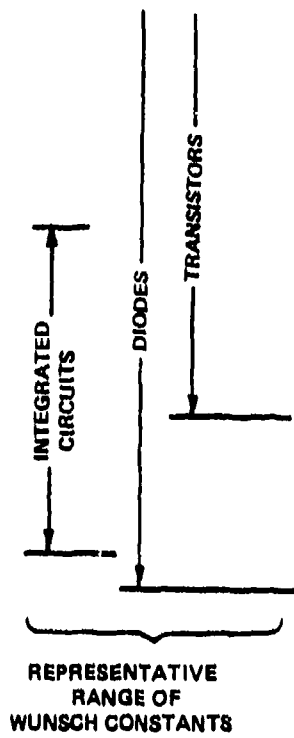


Fig.11 Upper bounds, due to joint coupling, on open-circuit voltage, short-circuit current, and power delivered to transmission line termination; minimum Wunsch constant of devices that will survive threat

APPENDIX A

Some additional data on shielding and the possible trade-offs when coatings are used on composites is shown in Figures A-1 through A-5. A breakdown of burnout constants for various kinds of devices is provided in Figure A-1 (Widmann, 1980). Figure A-2 illustrates the gain in magnetic shielding effectiveness over graphite/epoxy when coated with different materials. The separation between the curves would remain the same versus frequency if plotted for electric shielding effectiveness although the shape of the curves would change.

Figure A-3 shows bar graphs of the improvement protective coatings provide relative to 8-ply graphite/epoxy as measured by the low frequency approximation to the ratio of transfer impedances. The bar graphs show the variation with coating thickness and material.

Figure A-4 demonstrates the figure of merit based on weight density and transfer impedance for 4 mils of coating on 8-ply graphite/epoxy. The figure of merit is simply the shielding improvement as measured by the ratio of the transfer impedances of the coated and uncoated materials divided by the weight density of the coatings.

Finally, Figure A-5 presents bar graphs of coating thickness and the weight penalty for coating with a sufficient thickness of material to make the equivalent transfer impedance of coated material equal to -60 dB if 100 square feet of surface is coated.

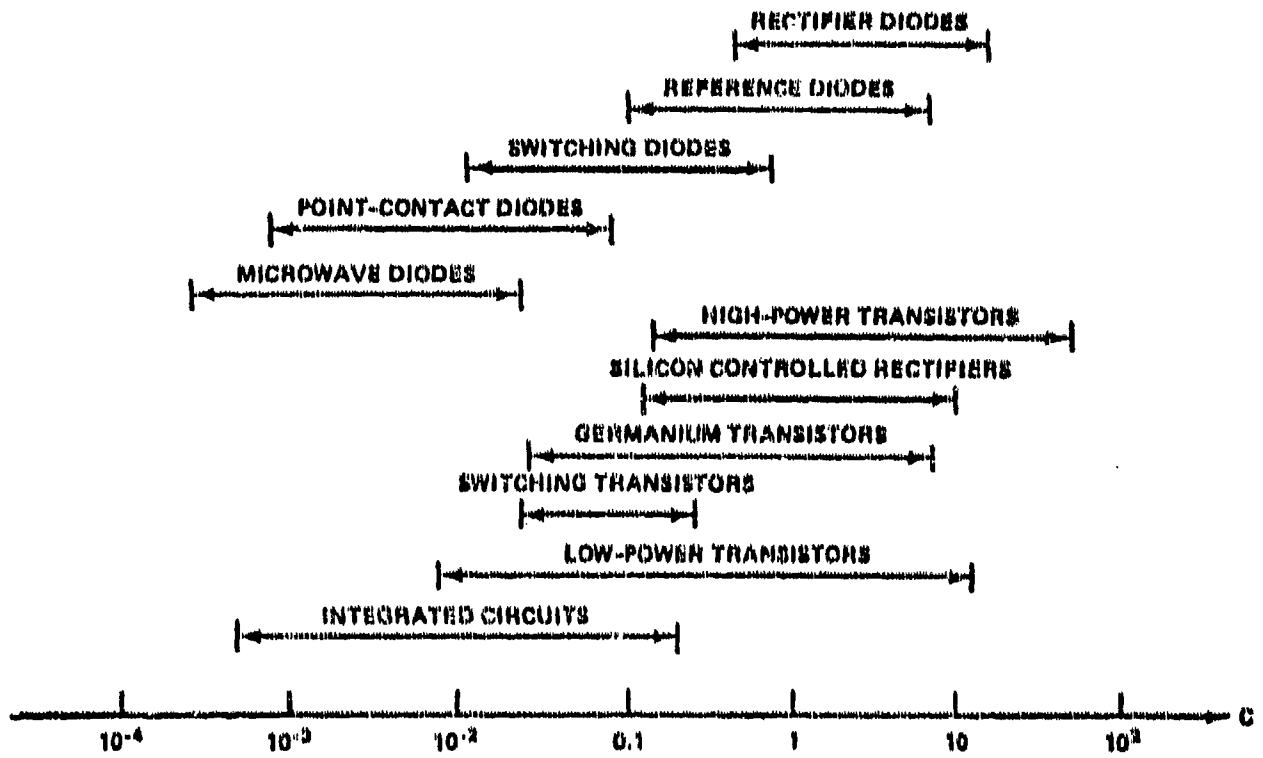


Fig.A-1 Ranges of (or Wunsch K) for various device families

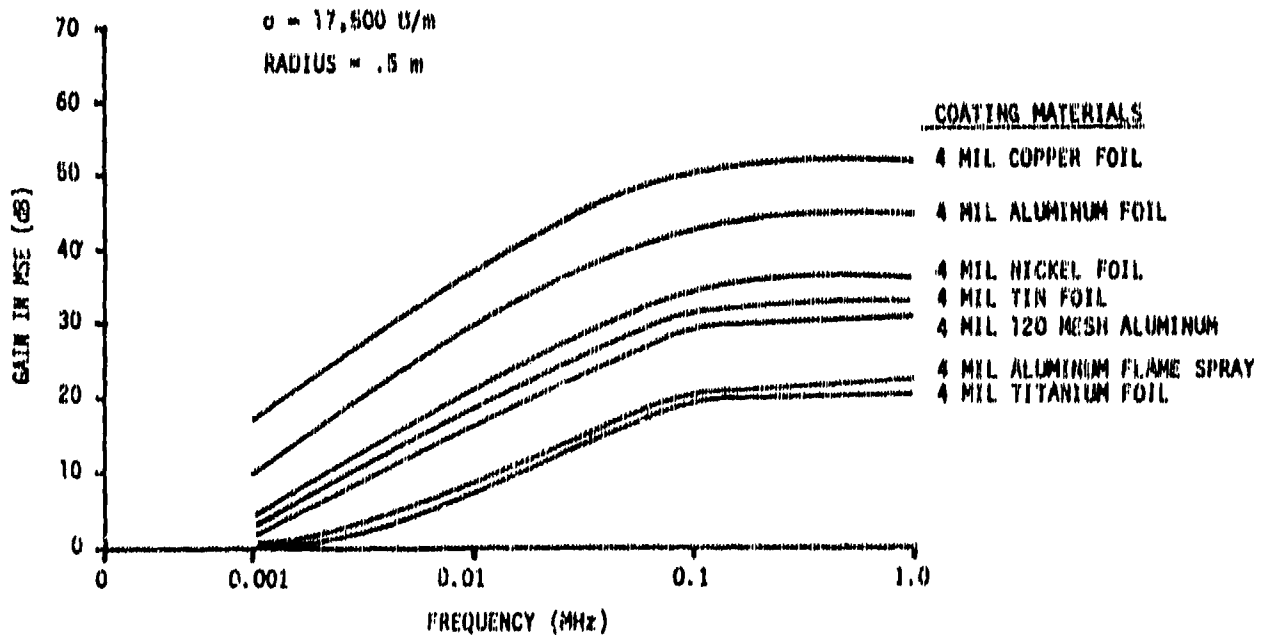


Fig.A-2 Gain in magnetic shielding effectiveness over an 8-ply mixed orientation G/E cylinder under a uniform magnetic field

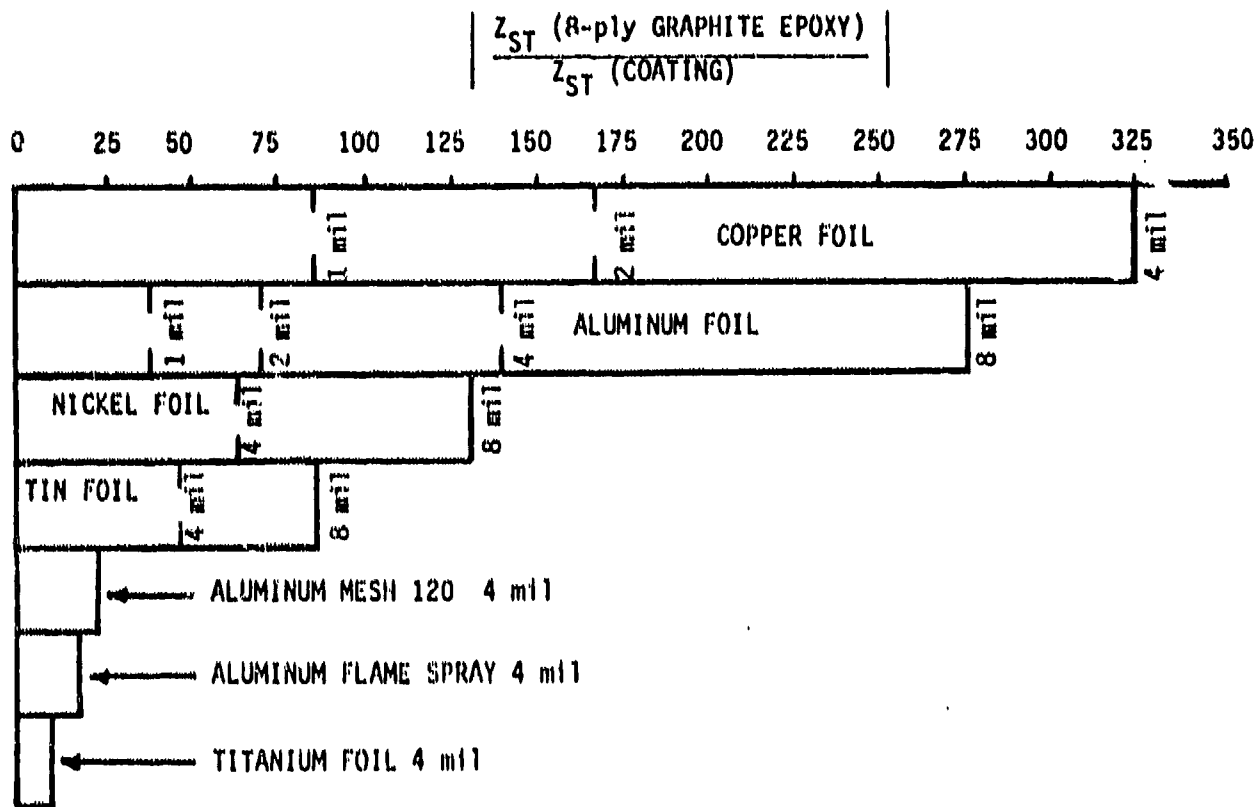


Fig.A-3 Improvement protective coatings provide relative to 8-ply G/E
(Valid for frequencies below 10^4 Hz)

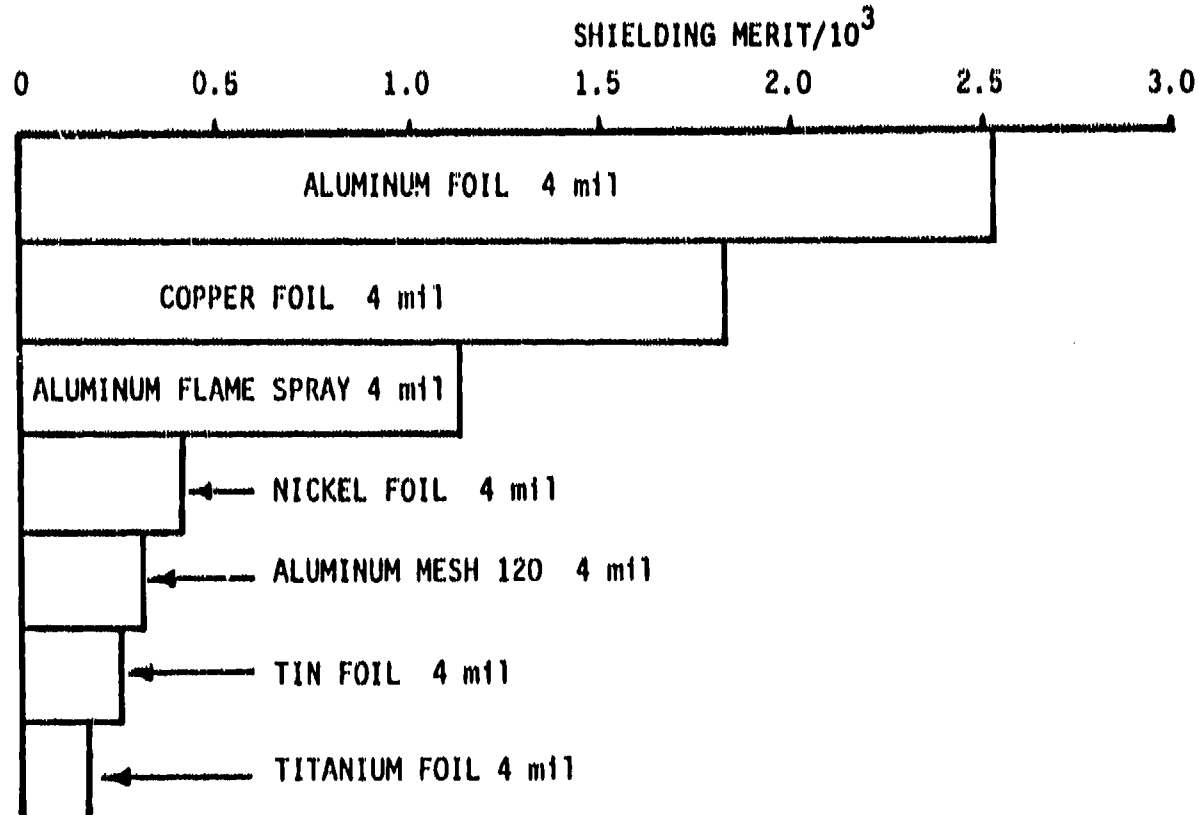


Fig.A-4 Weight shielding figure of merit (shielding beyond 8-Ply G/E)
of electromagnetic protective coatings

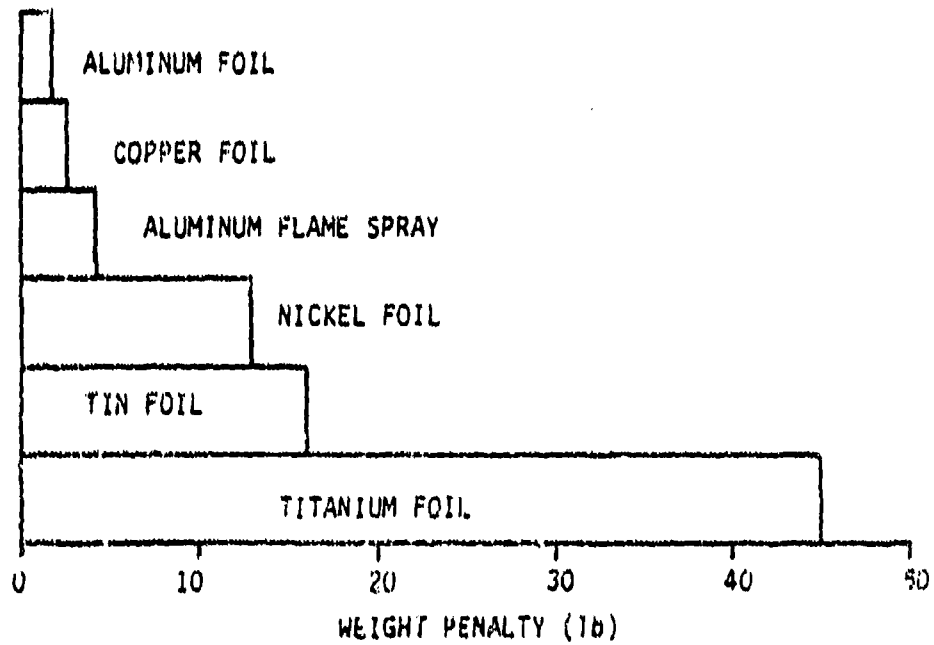
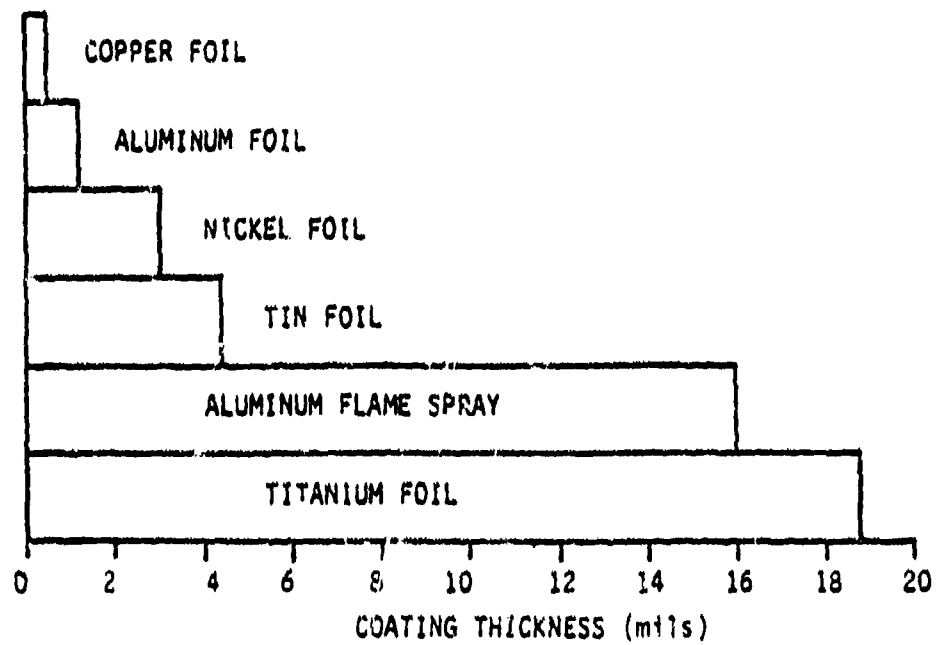


Fig.A-5 Coating thickness and weight penalty for $\alpha_{st} = 60$ dB at low frequency

DISCUSSIONS

SESSION I

REFERENCE NO OF PAPER 1/3
 DISCUSSOR'S NAME - K F ROGERS
 AUTHOR'S NAME - T SHARPLES

COMMENT: Do you see any applications for higher temperature resins, for example the polyimides, in the future structures you will be building; applications such as higher temperature ducting etc.

AUTHOR'S REPLY: We shall be interested in any modified or new system which could give cost or weight benefits. At the moment we are looking for a less moisture sensitive material and one which has a simplified cure cycle. Polyimides are not yet figuring strongly in our plans for the near future, but we shall be keeping an interest at laboratory level.

COMMENT ON REPLY: I would not wish to add anything to your excellent reply; except to note that there may be in the future areas where epoxies can not be used.

REFERENCE NO OF PAPER 1/3
 DISCUSSOR'S NAME - P F LITTLE
 AUTHOR'S NAME - T SHARPLES

COMMENT: Lightning attachments to metal conductors outside a CFC skin which penetrates the skin to an aluminium honeycomb beneath will allow currents to flow in the honeycomb rather than the skin. This could be dangerous if the material is employed in positions where the high current component of the lightning stroke can flow. The risk depends on detail design and the positioning of the component, and the degree of risk should be considered at an early stage in the structural design phase. One safe way always would be to replace the conducting honeycomb by nomex or other insulating material, but this may not be necessary.

AUTHOR'S REPLY: We at BAe have not seen any evidence which shows that damage from lightning strikes is unacceptable. Evidence can be seen at "Aerospatiale" shows the damage to be minimal.

Each component should be treated on its merits, taking into account the probability of sustaining a lightning strike; for example a taileron may be protected by a swept wing.

We have used aluminium alloy honeycomb because of cost considerations and it is a material which we are used to handling. But, if evidence is available which shows that this is not acceptable for production use, then we will take this into account in deciding upon a design standard.

REFERENCE NO OF PAPER 1/3
 DISCUSSOR'S NAME - G BARTON
 AUTHOR'S NAME - T SHARPLES

COMMENT: With reference to problems with the CFC skins/aluminium honeycomb: I consider the problem is not as great as expected. One has only to consider where the structure is and its layup. The problem only occurs on say thin panels, in direct lightning zones.

REFERENCE NO OF PAPER 1/3
 DISCUSSOR'S NAME - WALTER VOGL MBB, MUNICH
 AUTHOR'S NAME - T SHARPLES

COMMENT: Under the assumption that all precautions are taken at manufacturing to minimise the environmental degradation, what is the experience so far on the life time of composites, taking into account the change of the chemical structure of the material under the various stress conditions, (static and dynamic)?

AUTHOR'S REPLY: The experience to date is very encouraging in that no problems appear to be occurring in service which can be attributed to unforeseen physical degradation. It should be noted, however, that in order to obtain this sort of information, full knowledge of the environmental conditions, including stress levels and loading spectra, would be required. This is no small task.

Reference should be made to the recent AGARD meeting in Athens where the USAF and Navy stated that their in-service experience was favourable and that they are becoming quite relaxed about using aircraft containing CFC.

REFERENCE NO OF PAPER 1/1
DISCUSSOR'S NAME - B J C BURROWS
AUTHOR'S NAME - LEONARD & MULVILLE

COMMENT: In comments on the composite AV8B wing it was stated that lightning current would flow down the aluminium front leading edge. It is a fact that the high count pulses of current flow distribute initially inductively around the wing - so a large current will flow down the near edge too.

AUTHOR'S REPLY: The point is that no special lightning protection provisions are made beyond reliance on the metal leading edge and tip structure, and the conductivity of the carbon composite itself, including the composite trailing edge. (See the additional reply by G Weinstok.)

REFERENCE NO OF PAPER 1/1
DISCUSSOR'S NAME - G WEINSTOK
AUTHOR'S NAME - R W LEONARD

COMMENT: In a reply to questions of lightning current distribution on the AV8B wing (question by Burrows)

As a representative of McDonnell Aircraft Co, the manufacturer of the AV8B, it was recognised that some lightning current would flow through the AV8B composite wing. The design of the wing is such that there is sufficient cross-sectional area in the wing to carry the lightning current without damage. Extensive tests have proved this design.

REFERENCE NO OF PAPER 1/1
DISCUSSOR'S NAME - F S STRINGER
AUTHOR'S NAME - R W LEONARD

COMMENT: DC10 illustration. I was concerned that the damage shown by lightning does not appear to have been discovered until some time after the occurrence. Does this mean that strikes are a more serious problem where CFC is applied?

AUTHOR'S REPLY: I doubt that the late discovery by itself implies serious CFC problems. Rather, it underscores the benign nature of the damage incurred and, perhaps, the conservative structural design of the DC10 CFC rudder. The fact that attachment occurred certainly implies a deficiency in either the lightning protection system design or its application. Moreover, if a certain degree of mechanical damage can be incurred and only discovered after many flight cycles, design of highly stressed primary structure for durability must account for such damage and required inspection intervals.

REFERENCE NO OF PAPER 1/1
DISCUSSOR'S NAME - B J C BURROWS
AUTHOR'S NAME - R W LEONARD

COMMENT: You showed the picture of a tail fin of an aircraft which suffered a direct strike which the operators knew nothing about. It was unlikely to have been a swept stroke, and the extent of the damage indicates a Zone 1B attachment point, ie an initial attachment with hand-on.

It is not unknown for strikes to have occurred to aircraft and the crew being unaware of them. Lightning strike statistics are probably incomplete because of this reason.

AUTHOR'S REPLY: The incident was characterised by airline and Douglas personnel as attachment of a swept stroke. The point of damage is at the forward edge of a (about) 5-inch-wide fibreglass trailing edge wedge where it is relative, with titanium rivets, to the aft flange of the carbon/epoxy rear spar of the DC10 upper aft rudder. It lies about 20 inches below the lower end of a "grounded" trailing-edge metal strap with the static discharge pointer. Deposits on the trailing-edge wedge clearly mark the horizontal air flow.

REFERENCE NO OF PAPER 1/2
DISCUSSOR'S NAME - K F ROGERS
AUTHOR'S NAME - G JUBÉ

COMMENT: Est ce qu'il y avait à Athenes un rapport ou une discussion au sujet de la réparation des structures en plastiques renforcée de fibres de carbone, le réparation générale, pas seulement des pâles d'hélicoptère?

AUTHOR'S REPLY: Le sujet des réparations n'a pas fait l'objet d'un rapport particulier et n'a été que cité brièvement dans plusieurs communications. En général la réparation consiste à enlever la partie endommagée et à rétablir la continuité du composite par des couches de matériau préimprégné convenablement décalées. Le durcissement s'opère par un chauffage local.

REFERENCE NO OF PAPER 1/3
 DISCUSSOR'S NAME - G ORION AMD. BA.
 AUTHOR'S NAME - T SHARPLES

COMMENT: In your cost and weight saving study, you did not consider the impact of solutions you will have to introduce to protect the aircraft against lightning and electro magnetic effects. Do you intend to introduce this in your study at a later date?

AUTHOR'S REPLY: We have to consider the problems of:-

Screening and Bonding - We do not expect any cost or weight implications coming from the solutions to these problems, especially since the same problems appear to be occurring with the current metal structures.

REFERENCE NO OF PAPER 1/3
 DISCUSSOR'S NAME - PRESTON GEREN
 AUTHOR'S NAME - T SHARPLES

COMMENT: How do you design joints with good RF shielding properties? Will adequate joint design significantly impact weight/cost advantages of CFC?

AUTHOR'S REPLY: We are under the impression that RF shielding is a fairly local problem and that this depends mainly on the efficiency of Avionics bay door joints. As these joints will be made with metal fittings and are stated to be independent of the CFC part of the structure, then the solutions which have to be applied to current metal problems will also apply to the CFC structures. The RAE will be discussing this at a later stage in the Symposium.

REFERENCE NO OF PAPER 1/3
 DISCUSSOR'S NAME - J A PLUMER, LIGHTNING TECHNOLOGIES, INC, USA
 AUTHOR'S NAME - T SHARPLES

COMMENT: Some of the lightning protection methods that are available involve the application of aluminium strips or coatings to carbon composites (in places where protection against severe direct strike effects is necessary). The possibility of corrosion at aluminium-graphite interfaces has often been raised. What are your opinions regarding such possibilities?

AUTHOR'S REPLY: We have no long term experience of this particular problem, but we are well aware of and concerned with, problems of corrosion.

If we were to use aluminium strips then these would be laid up with the composite and therefore well protected, but we would certainly like to hear from anyone who has any relevant experience.

FURTHER COMMENT BY G WEINSTOCK: On the question regarding corrosion of aluminium and carbon composite material, because of the possibility of corrosion, we at McDonnell Aircraft have used TIN instead of aluminium for lightning protection. We have found that tin presents no corrosion problems when applied to aluminium.

SESSION II

REFERENCE No. OF THE PAPER: 2/5
 DISCUSSOR'S NAME: B.W. Smithers (ERA Technology Ltd)
 AUTHOR'S NAME: D.C. Brewster

COMMENTS:

Commenting on a question to the author from another delegate, the CFC sample referred to by the author is sample D, (see Table 1 of our Paper No. 6 for details of number of plies and lay angles). The fibres are made by Courtaulds Ltd, and the resin by Pothergill and Harvey Ltd.

The fibre volume fraction is not known but was found to be 0.62 for another CFC sample from the same source. The last reference in our Paper, (WHITNEY J.M., 1978), contains the statement that volume fractions vary from about 0.60 to 0.65.

REFERENCE No. OF THE PAPER: 2/5
 DISCUSSOR'S NAME: Borgonovo - Italy

COMMENTS:

Very little has been said about interference problems to be expected from new digital avionics (ARINC 700 series), due to the very low shielding properties of composite materials. This aspect should be worth attention in the general discussion.

REFERENCE No. OF THE PAPER: 2/6
 DISCUSSOR'S NAME: G. Weinstock
 AUTHOR'S NAME: D.A. Bull, G.A. Jackson and B.W. Smithers

COMMENTS:

Does 20 dB of shielding present a problem?

AUTHOR'S REPLY:

No.

1. Existing metal aircraft use non-conductive metal seals and do not necessarily provide 20 dB of shielding.
2. Many sensitive digital equipments are installed in locations on aircraft where no shielding occurs. These are cockpit areas, engine electronics, wheel wells. These equipments can easily be designed to operate properly.
3. 20 dB shielding presents no problem just normal EMC Design Procedures.

REFERENCE No. OF THE PAPER: 2/6
 DISCUSSOR'S NAME: G.A. Du Bro
 AUTHOR'S NAME: Bull, Jackson and Smithers

COMMENTS:

The measurement of shielding effectiveness properties should be viewed as only a relative number. Such measurements are dependent upon the test set-up as well as various parameters within such a test set-up. Measurements made by different authors may yield results not comparable in an absolute manner.

AUTHOR'S REPLY:

Inevitably screening measurements must to some extent be dependent on the test arrangement. Nevertheless, the results quoted, see Figures 14 and 17 of Paper 6 demonstrate good agreement between near and distant field tests and it is therefore considered that these results can be applied with confidence to the practical aircraft structures and are not "only relative numbers".

REFERENCE No. OF THE PAPER: 2/6
 DISCUSSOR'S NAME: J. Birken
 AUTHOR'S NAME: D.A. Bull, G.A. Jackson and B.W. Smithers

COMMENTS:

Electrical $S_E(f)$ and Magnetic $S_H(f)$ Shielding Effectiveness has been theoretically derived and measured with excellent agreement in papers by Strawe, D., Wallenberg, Dike and Birken at this meeting. As G. Du Bro, AFFDL stated, many shielding efforts have been conducted and are difficult to compare. For this reason the US Navy is now using transfer impedance $Z_{st}(f)$ which is not dependent on the instrument measuring volume. $S_E(f)$ is very high at low frequencies. Because of this S_E measurements are often incorrect as the energy coupled into the box is through the joining to the box not through the materials.

In regard to the question 'Will the reduced electrical conductivity of composite cause EMC problems?' US Naval studies have shown direct lightning strikes can cause problems, while high frequency coupling problems are not significantly worse than metal aircraft problems.

AUTHOR'S REPLY:

The relationship between surface transfer impedance and overall attenuation is complex. Z_{st} can give an indication of attenuation by reflection but will not necessarily give a good indication of absorption loss.

Considerable care was taken in the measurements described to ensure that penetration or coupling through imperfections in the structure was negligible. The results show that attenuation in the magnetic mode at frequencies less than 30 MHz is significantly lower than for a metal structure, and it therefore seems likely that EMC problems will arise in the HF band.

REFERENCE No. OF THE PAPER: 2/7
 DISCUSSOR'S NAME: B.W. Smithers (ERA Technology Ltd)
 AUTHOR'S NAME: W.F. Walker

COMMENTS:

Question 1: What is the resistivity of the carbon fibres and what is their type?
 Question 2: Is the technique employed of use with CFC materials other than unidirectional?
 Question 3: What is the effect of varying the width (and hence aspect ratio) of cross-section of the sample in the transmission line?

AUTHOR'S REPLY:

Answer 1: Prof. W. Gajda has data on the T300 material used.
 Answer 2: Possibly, although a theoretical description of behaviour would be difficult.
 Answer 3: Very little effect.

REFERENCE No. OF THE PAPER: 2/7
 DISCUSSOR'S NAME: J.L. van Lidth de Jeude (Fokker Aircraft Co.)
 AUTHOR'S NAME: W. Walker

COMMENTS:

It was suggested by a number of the audience during the discussion, that taking care of good shielding performance of the aircraft structure would relax our shielding requirements on the avionics equipment and system itself. This cannot be true however as the equipment should withstand the interference generated within the aircraft itself. The conducted interference over the power lines probably belong to the worst of all.

AUTHOR'S REPLY:

I think that this comment may have been intended for one of the other speakers - whose papers dealt more directly with shielding effectiveness.

Nevertheless, I agree with the comment - but I do not know anyone who expects the aircraft structure (particularly if made of CFC) to satisfy all shielding requirements.

REFERENCE No. OF THE PAPER: 2/7
 DISCUSSOR'S NAME: Dr J. Birken
 AUTHOR'S NAME: Prof. J. Walker

COMMENTS

Regarding the question of material, Prof. Walker measured conductivity of fibre which Prof. Gadjio built. (Type T-300 material 20,000 mhos/M.) Details are in books by Roy Stratton, Rome Air Development Centre, Rome N.Y. or J. Birken, Naval Air System Command, Washington DC 20361 entitled Composite Electromagnetic Design Guidelines Handbook.

REFERENCE No. OF THE PAPER: 2/8
 DISCUSSOR'S NAME: J.M. Thomson (Royal Aircraft Establishment, UK)
 AUTHOR'S NAME: D. Jaeger, K. Rippl

COMMENTS:

With respect to the part of your paper discussing EMC emission and susceptibility standards, I follow the flow of your analysis. UK experience is also that one of the biggest differences between OFC and conventional aluminium alloys is that there is less attenuation to magnetic fields at HF and below. Therefore if it was necessary to prepare an equipment test specification today we would have to think seriously about increasing the susceptibility requirements and reducing the emission requirements. However, we heard a good deal of discussion yesterday about the problems of relating laboratory measurements of shielding effectiveness to the aircraft case. In particular, if there is a mixture of OFC and metal in the aircraft structure, then the pattern of skin current distribution, and hence penetration, is changed: but the shielding is not necessarily worse, just different. Therefore, in the UK we consider it very important to back such analysis as yours with experimental work. At ERA Technology, for example, we have a Wessex helicopter fuselage in which composite panels can be mounted, so that we can measure the changes in shielding effectiveness.

Is your analysis backed up by any such practical work on large structures?

AUTHOR'S REPLY: K. Rippl

We at MBB Munich have not yet performed similar measurements on large aircraft structures; but theoretically an influence of OFC panels against aluminium panels is evident if they are mounted at a critical place where shielding effectiveness plays a significant role. Nevertheless we consider your tests as a good approach to the problem and intend to perform similar tests in the future.

REFERENCE No. OF THE PAPER: 2/8
 DISCUSSOR'S NAME: Audone
 AUTHOR'S NAME: K. Rippl

COMMENTS:

1. How have the curves of shielding effectiveness of aircraft structures against magnetic fields been obtained?
2. Why is the magnetic field effectiveness related to electric field tests (REO2) and no mention given to the relevant magnetic field tests (REO1, RSO1)?
3. Why is the shielding effectiveness of the aircraft structure related to tests which should deal with interactions between equipment installed within the structure?

AUTHOR'S REPLY:

1. They are obtained from practical measurements and are also comparable to theoretical considerations.
2. The comparison to REO2 was used as an example only - other comparisons to tests as REO1/RSO1 could be done, but it must be considered that the limits of these tests are not applicable to aircraft.
3.
 - a. External EMC should also be considered in establishing new limits.
 - b. Structural parts also exist between equipment within the aircraft eg antenna/equipment interactions.
 - c. Limits concerning equipment must always be seen against the background of the system problems.

REFERENCE No. OF THE PAPER: 2/8
 DISCUSSOR'S NAME: G. Weinstock
 AUTHOR'S NAME: D. Jaeger, K. Rippl

COMMENTS:

With reference to comments made by the author as to need for new EMC requirements. We at McDonnell Aircraft Co. have increased requirements relative to EMI/EMC/LIGHTNING and defined design approaches for composite aircraft. The following have proved successful on aircraft that are 50% composite.

1. Magnetic/Low frequency - require use of balanced circuits and twisted pair wiring.
2. Magnetic/electric mid frequency - use shielded wires and cable and discrete RLC filters.
3. High frequencies above 10 MHz - extensive use of filter pin connectors and small feed-through filters on signal lines.

The RSO3 requirements have been greatly increased over MIL-STD-461 also transient and ground plane interference tests have been added.

AUTHOR'S REPLY:

I agree in principle with your approach. You established more stringent requirements in advance although relevant specifications are missing to date.

REFERENCE No. OF THE PAPER: 2/9
 DISCUSSOR'S NAME: J. Birken, NAWAIR USA
 AUTHOR'S NAME: K. Lodge, Plessey Research UK

COMMENTS:

How are you compensating for galvanic corrosion with copper treated graphite? Copper is further apart from carbon on the valence chart and consequently should produce a larger galvanic voltage.

AUTHOR'S REPLY:

We are not compensating for galvanic corrosion of copper and graphite. Copper work was purely from an experimental electrical viewpoint.

REFERENCE No. OF THE PAPER: 2/9
 DISCUSSOR'S NAME: T. Sharples
 AUTHOR'S NAME: Brettle, Lodge and Poole

COMMENTS:

Can you please explain your statement that protective treatment to prevent electrolytic corrosion will be detrimental to the electrical properties? (Is your experience such that you can state that the use of conventional protective treatments is not acceptable?)

AUTHOR'S REPLY:

Not all methods of preventing electrolytic corrosion depend on electrically isolating the components, for example, sacrificial coatings may actually improve the conduction across the interface. However, many of the methods we have examined, for example, the rivetted joints and the joints made with sealants (Figs 8, 9 and 14 in the written paper) have significantly degraded the electrical properties of joints. It should be noted that the provision of a low resistance current path across a joint may be detrimental to the corrosion protection system used.

REFERENCE No. OF THE PAPER 2/9
 DISCUSSOR'S NAME: T. Sharples, BAe Warton
 AUTHOR'S NAME: R. Poole, Plessey

COMMENTS:

What do the changes of resistance mean in terms of acceptance levels. Is there a maximum value above which the joint is unacceptable?

Does a well-tightened bolt cancel out the effect of a "bad hole"?

AUTHOR'S REPLY:

The lowest resistance value obtained by the passage of a current through one of our joints was about 400 mΩ. There is, as far as I know, no suitable level of acceptability for joint resistance in CFC, but we would expect a sensible level to be in the milliohm or tens of milliohm range rather than hundreds of milliohms. These acceptance levels would, of course, change with the electrical requirements of the joint.

As is seen in Figure 8 in the written paper, tightening the bolt up does not overcome the damage caused by poor hole drilling. We are currently working on a method of joint construction which will obviate the electrical need for accurate hole drilling.

REFERENCE No. OF THE PAPER 2/9
 DISCUSSOR'S NAME: G. Barton
 AUTHOR'S NAME: K. Lodge

COMMENTS:

The work reported was on bolted and adhesive joints, have you done any work on percussion rivetted type joints and if so are these electrically better or worse?

AUTHOR'S REPLY:

The only work we have carried out on rivetted CFC joints was an examination of some joints made by an aircraft manufacturer. The electrical resistance of the individual CFC/rivet joints varied by up to 3 orders of magnitude. Overall, they were electrically much worse than bolted joints.

REFERENCE No. OF THE PAPER 2/9
 DISCUSSOR'S NAME: K.F. Rogers
 AUTHOR'S NAME: J. Brettle and K. Lodge

COMMENTS:

Would you care to comment, please, on the change of joint resistance with structural loading.

AUTHOR'S REPLY:

Only rough, qualitative tests have been carried out on mechanically fastened joints, but it would appear that it is possible to produce erratic results by flexing the joints. It is intended to examine this problem more fully in the second phase of this work.

REFERENCE No. OF THE PAPER: 2/9
 DISCUSSOR'S NAME: T.A. Collings
 AUTHOR'S NAME: K. Lodge

COMMENTS:

On the adhesive joint, where did the adhesive burning occur in the joint? It is not surprising that lap joints are not significantly affected structurally if the burning occurs at the centre of the joint. The load transfer across an adhesive joint is not linear. Load is mainly taken at the ends of the lap joint due to differential straining of the adhesive.

AUTHOR'S REPLY:

On our sample, the burnt area was on the edge of the overlap, but the other sample was damaged close to the centre of the joint.

REFERENCE No. OF THE PAPER: 2/9
 DISCUSSOR'S NAME: C.M. Heruert MBB
 AUTHOR'S NAME: K.J. Lodge

COMMENTS:

The given values are valid for low continuing currents. What results would you expect for high frequent currents due to a lightning stroke?

AUTHOR'S REPLY:

From work done at Plessey Electronic Systems Research, it would appear that the joint impedance is relatively independent of the method of joint construction at frequencies involved in lightning strikes, above about 300 kHz. Extrapolating the values shown in Fig 22 of the written paper, we would expect the value of ESR to be about 10 Ω at 500 MHz.

From results given at this meeting by Mr B.J. Burrows of Culham Laboratories, it would appear that it is possible to alter the joint resistance by the passage of a lightning stroke.

REFERENCE No. OF THE PAPER: 2/9
 DISCUSSOR'S NAME: K. Rippl
 AUTHOR'S NAME: K. Lodge

COMMENTS:

Concerning the test arrangements particularly the contacts between CFC and the measuring electrode. Can you describe the hardware used? How did you manage to get a good contact between the electrodes and the CFC material?

AUTHOR'S REPLY:

The equipment used is described in section 2.3 of the written paper. In addition several signal sources were used including a custom built 12 V, 8 A, 50 Hz power supply, a WAVETEK Model 143 0-20 MHz function generator and a Marconi TF 144 H/4 standard signal generator. Voltage monitoring was by Levell ac broad band voltmeters Type TM3B and TM6B and Racal RF Millivolt meter type 9301A.

The contacts were made by plating the exposed CFC with copper plating as described in section 2.2 of the written paper. The details of the plating solutions are given in the appendix of paper 6 of this conference.

REFERENCE No. OF THE PAPER: 2/9
 DISCUSSOR'S NAME: P.F. Little
 AUTHOR'S NAME: K.J. Lodge (presenter)

COMMENTS:

What area of overlap was employed and what area was burnt out by your continuous 8 Amp current?

AUTHOR'S REPLY:

The two samples of adhesively bonded lap joints which had 8 Amps passed through them had areas of 225 and 102 mm². The visibly burnt areas were 4.16 and 6.56 mm² respectively.

REFERENCE No. OF THE PAPER: 2/9
 DISCUSSOR'S NAME: J.H. Ashworth, BAe Woodford
 AUTHOR'S NAME: K.J. Lodge

COMMENTS:

Can you please comment on measurements on bolted joints other than those measured at dc.

AUTHOR'S REPLY:

Both the impedance and the effective series resistance of the joints have been measured at frequencies up to 50 MHz and the results given in sections 5.1 and 5.2 of the written paper. In general, the dc values were retained up to about 10 MHz. The effective series resistance of all joints tended to be in the range 0.5-1.5 Ω at 50 MHz.

REFERENCE NO. OF THE PAPER: 2/5

DISCUSSOR'S NAME: C. M. Herkert (MBB)

AUTHOR'S NAME: D. C. Brewster

COMMENTS:

Concerning the CFC materials, which type of fibre did you consider at which volume fraction and what thickness of the single layer?

The fibres considered, of UK origin, were "Super a" fibers with resistivity approximately $1.3 \times 10^{-2} \Omega \cdot \text{m}$. The resin was 851914C. The volume fraction was approximately 62%. We considered single layer thicknesses from 11mm to 18 mm.

REFERENCE NO. OF THE PAPER: 2/5

DISCUSSOR'S NAME: G. Barton & I. Mac Diarmid

COMMENTS: You stated that CFC ground planes should behave the same as metal ones. Does this include H. F.? Experimental results show shielding of CFC to be poor and one would therefore expect poor performance in the HF Band. It is possible that it is incorrect to view CFC as a perfect conductor of HF because of the losses involved in the currents flowing in either a CFC ground plane or air-frame. This applies both to wire antennas and notch antennas. Antennas of higher frequencies should be less affected because their smaller size implies lower losses in the CFC.

REFERENCE NO. OF THE PAPER: 2/5

DISCUSSOR'S NAME: B. Audone

COMMENTS:

What is the correlation between theory and your experiments?

Our experimental program is continuing but at present there is some disagreement between theory and experiment. We have not arrived at any definite conclusions yet.

SESSION III

REFERENCE No. OF THE PAPER: 3/10
 DISCUSSOR'S NAME: G. Barton
 AUTHOR'S NAME: J.M. Thomson and R.H. Evans

COMMENTS:

The information required by Industry does not appear to be coming from any guidelines provided by the programme outlined. Timescales do not refer to the structural programme. This is of great concern to me.

AUTHOR'S REPLY:

Thank you for your opinion.

It is one of my personal hobby-horses to distil the information from the research programmes into a form suitable for industry to use. As you know I have sought sympathy and backing from your side of the fence for this idea.

I would agree that, apart from lightning protection, the UK CPO structural demonstrators programmes have not been influenced in the slightest by electrical considerations.

REFERENCE No. OF THE PAPER: 3/10
 DISCUSSOR'S NAME: R.B. Rowley
 AUTHOR'S NAME: J.M. Thomson and R.H. Evans

COMMENTS:

Table 2 shows bonding and jointing as a major problem but non-linear effects (such as intermodulation product generation) is classed as a minor problem. I would have expected the two aspects to be related and hence fall into the same category. Would Dr Thompson please comment on why they are apparently unrelated?

AUTHOR'S REPLY:

Non-linear effects are classed as a minor problem because our research programme leads us to this conclusion (see Paper No.9). If they occurred in practice then an ad hoc solution would have to be sought.

We classify bonding as a major problem because it affects many areas besides non-linear effects. As outlined in our paper these include shielding to RF, EMP and lightning, and aerial installation. All these affect the safety or mission success, or both, of the complete weapon system.

REFERENCE No. OF THE PAPER: 3/10
 DISCUSSOR'S NAME: W. Bascom
 AUTHOR'S NAME: J.M. Thomson and R.H. Evans

COMMENTS:

On the question of poor information transfer from research to design then to specification, there is also poor communication on a "horizontal" level. For example, we have heard little said about what happens to joint strength when it is modified for better electrical transfer. In general there is a continuing need for communication between materials, electronic scientist, and design engineers.

AUTHOR'S REPLY:

We also recognise the need for "horizontal" communication. With regard to bond strength my colleague Kevin Lodge briefly mentioned this in his presentation. Such considerations are always uppermost in our minds and I think that we have been reasonably successful in stimulating contact between all parties, both in Defence and Industry, in the UK.

REFERENCE No. OF THE PAPER: 3/10
 DISCUSSOR'S NAME: B.J.C. Burrows
 AUTHOR'S NAME: J.M. Thomson and R.H. Evans

COMMENTS:

1. Carbon Fibre fuselage tests. It is our experience at Culham that aluminium honeycomb drastically affects the screening performance. Was the fuselage tested made with aluminium honeycomb, and is this construction intended for a composite aircraft? Are the results of this test applicable to nomex honeycomb structures?
2. Fuel systems. I would have liked fuel system safety to be specially mentioned in your list of priorities.
3. System grounding. Power system grounding insofar as it is subject to lightning strikes is a severe problem owing to the large voltage difference which may be seen between grounding points. Do you not think it should be given higher priority?

AUTHOR'S REPLY:

1. The 'shielding' is a function of the total shape and construction, as well as the construction of individual sections, so strictly the results apply only to the particular structure tested, which in this case had certain parts constructed of aluminium honeycomb. However, combined with results from other structures and laboratory experiments an overall trend appears, which is described in the paper. I would expect similar results from nomex honeycomb structures.
2. We will amend our paper to take account of this.
3. Our paper, and that by McDiarmid and Barton, suggests that for an all-CFRP aircraft, a separate, internal, grounding system will be required. Our paper classified direct lightning effects as minor but recognised the problems of induced voltages from lightning and other sources at HF and below, although we probably did not sufficiently emphasise resistive coupling from lightning currents as distinct from inductive (magnetic field) coupling. Mr Burrows' own paper (No.17) draws attention to resistive effects.

REFERENCE No. OF THE PAPER: 3/12
 DISCUSSOR'S NAME: K. Rippl
 AUTHOR'S NAME: G. Barton

COMMENTS:

Have you any experience with rotor blade modulation in using CFRP rotor blades?

AUTHOR'S REPLY:

This problem has not been experienced to date by WIL with metal rotor blades; however if there is a problem with rotor blade modulations it should be reduced with the introduction of composite blades.

Author's footnote: The introduction of de-icing systems, high pulsed currents on the rotor blade; could possibly make blade modulation a problem in the future.

REFERENCE No. OF THE PAPER: 3/12
 DISCUSSOR'S NAME: G.M. Herkert, MBE
 AUTHOR'S NAME: G. Barton

COMMENTS:

The two slides shown for protection of CFRP with Al-flame-sprayed and foil material did show low damage between screws and protection system. Could you explain or show how the electrical bonding between surface protection and bolt is solved?

AUTHOR'S REPLY:

There was no electrical bonding to the surface protection as we were considering lightning strike protection only and from the work undertaken in the past it did not make any appreciable difference to the results if the protection surface was electrically isolated or not. It must also be noted that because of the position of the panels on the aircraft these panels were only subjected to strike and swept current tests.

REFERENCE No. OF THE PAPER: 3/12
 DISCUSSOR'S NAME: L. Skorosewaki, British Aerospace
 AUTHOR'S NAME: G. Barton, I. McDiarmid

COMMENTS:

The author concentrated on power supply wiring and the need to provide earth return cabling/metal to compensate for the fact that a GFC fuselage would not provide the path normally provided by a metal aircraft.

Has any attempt been made to assess the increase in signal cable remaining mass resulting from adoption of GFC structure?

AUTHOR'S REPLY:

The study was carried out in such a way that signalling cables were separated out because it was felt that on a future aircraft extensive use of a data bus system would dramatically reduce the cable weight due to signalling cables.

REFERENCE No. OF THE PAPER: 3/12
 DISCUSSOR'S NAME: G. Orion
 AUTHOR'S NAME: G. Barton, I. McDiarmid

COMMENTS:

Problems of developing an HF notch antenna in case of GFC aircraft have been recognized. From your programme, did you propose solutions to solve the problem? Do you intend to have a special HF programme to make in-depth investigations?

AUTHOR'S REPLY:

I believe this is a problem, however we have no contract to consider the problem further. It should be addressed and given the necessary resources for a programme with realistic objectives, so the problem can be overcome.

REFERENCE No. OF THE PAPER: 3/13
 DISCUSSOR'S NAME: J.B. Stringer
 AUTHOR'S NAME: Kwor

COMMENTS:

Reaction of aircraft manufacturers was invited to the background cost and effort to be expected from the use of boron fibres. [Editor's Note: No response was received.]

REFERENCE No. OF THE PAPER: 3/13
 DISCUSSOR'S NAME: G. Barton
 AUTHOR'S NAME: Kwor

COMMENTS:

Mr Barton requested more information about the treating and doping of boron fibres. The reply indicated that some results so far were encouraging but research is needed to enhance conductivity. Mr Birken added a comment that work was in hand at the University of Pennsylvania where graphic/epoxy information could be sought. The structural integrity after treatment is not yet understood fully.

REFERENCE No. OF THE PAPER: 3/13
 DISCUSSOR'S NAME: J.H. Ashworth
 AUTHOR'S NAME: Kwor

COMMENTS:

Why use carbon as a dope instead of other materials?

The presenter of the paper was unable to give an authoritative answer. Mr Ashworth was invited to write to the author for a considered reply.

REFERENCE No. OF THE PAPER: 3/15
 DISCUSSOR'S NAME: G. Orion
 AUTHOR'S NAME: G.L. Weinstock

COMMENTS:

Low frequency equipment is less protected by carbon structures than with metal. In your case did you consider the use of ADF or QMGSA systems?

We considered only frequencies down to HF.

REFERENCE No. OF THE PAPER: 3/15
 DISCUSSOR'S NAME: W. Vogl, NEEB
 AUTHOR'S NAME: G.L. Weinstock

COMMENTS:

On the understanding that the results stem primarily from ground tests and from in-flight tests, you obviously must rely upon crew reports:

1. Have you experienced any environmental impact, under extreme conditions as of temperature, dust and boundary effects, etc?
2. Did the crew report on their subjective impressions, or was there any measurable basis for the comparison with "better" circumstances in the cockpit?

AUTHOR'S REPLY:

Yes. Most measurements were made on the ground.

1. No, the tests were not conducted under environmental conditions. We have found no adverse in-flight environmental effects such as those from temperature or dust.
2. Test pilots have not reported any problems related to composites, for instance, they did not report any problems when flying near radar or due to static.

REFERENCE No. OF THE PAPER: 3/15
 DISCUSSOR'S NAME: J.G. Kleins, ESG, Munchen
 AUTHOR'S NAME: G.L. Weinstock

COMMENTS:

In which frequency range and at which field strength were tests on the F18 performed without noticing effects on the avionic equipment that could be identified as being caused by using the carbon fibre material?

Which equipment did show any effect at all?

The frequencies checked were those from low HF to high K band radar. There were no effects caused by use of carbon fibre composites.

REFERENCE No. OF THE PAPER: 3/15
 DISCUSSOR'S NAME: J.H. Ashworth, EAs
 AUTHOR'S NAME: G. Weinstock

COMMENTS:

You mentioned in your talk that in your tests you were not able to detect any change in antenna performance on an aircraft regardless of the adequacy of the bond from the antenna base to the local CFRP area.

Could you please offer an explanation? This is certainly not my experience on metal aircraft at V & UHF.

We have extensively tested the gain, pattern and VSWR of blade antennas at 400 MHz, 1 GHz and 10 GHz and have found no significant difference between metal and carbon fibre composite ground planes.

REFERENCE No. OF THE PAPER: 3/15
 DISCUSSOR'S NAME: Audone
 AUTHOR'S NAME: G.L. Weinstock

COMMENTS:

Early in the meeting we heard about problems expected by aircraft manufacturers in the application of CFC. The author of this paper now claims that there is no problem. Is this because the equipment standard was improved to meet the new situation?

AUTHOR'S REPLY:

Wiring was very carefully shielded. Additional equipment requirements were added also; they included transformer coupling. Effort was made to improve fuselage bonding on the F18. Problems could have been expected but the engineers were forewarned and designs were arranged to meet likely problem areas. Weight rather than price was a major consideration; equipment weight is especially important in the AV8-B aircraft. Precautions were taken therefore.

REFERENCE No. OF THE PAPER: 3/15
 DISCUSSOR'S NAME: J.H. Ashworth
 AUTHOR'S NAME: G.L. Weinstock

COMMENTS:

It has been stated that there was no detectable difference if the antenna ground plates were grounded to CFC or not. If this is true it is very puzzling. Can the author explain?

AUTHOR'S REPLY:

The author stated that he was not an antenna expert. He suggested that the available ground plane need not be a good conductor but performance would depend on the antenna type. Tests were performed for the US Navy during 1974-75.

In a further comment the British Aerospace attendee from Woodford UK claimed that metal aircraft experience had shown that an adequate bond was essential.

REFERENCE No. OF THE PAPER: 3/15
 DISCUSSOR'S NAME: F.S. Stringer
 AUTHOR'S NAME: G.L. Weinstock

COMMENTS:

What is the true cost of the F18 exercise so far as systems are concerned to solve the problems imposed by the use of CFC? Would a lot of man-hours be required at significant cost to prepare the total aircraft to meet the electromagnetic problems?

AUTHOR'S REPLY:

The cost to obtain system compatibility in the F18 as a result of using CFC is not known exactly, but it is estimated to be very small in relation to total program costs.

REFERENCE No. OF THE PAPER: 3/15
 DISCUSSOR'S NAME: J.M. Thomson (UK)
 AUTHOR'S NAME: G.L. Weinstock

COMMENTS:

What radio transmitters do your aircraft carry? In particular, do you carry HF sets operating in the 2-30 MHz band? If you do not, is this the reason you do not have EMC problems? Do you have any intention of installing HF systems and do you foresee any problems?

AUTHOR'S REPLY:

Our aircraft carry radio transmitters using frequencies of 30 MHz and higher. We carry no 2-30 MHz transmitter. However, extensive radiated susceptibility tests were performed by the US Navy in the HF range (2-30 MHz) and NO EMC problems were noticed. If our customers specify HF radios we will provide them in our aircraft. Until tests are performed, it is difficult to estimate if any problems will occur.

D-16

REFERENCE No. OF THE PAPER 3/15
DISCUSSOR'S NAME: J.C. Kleins
AUTHOR'S NAME: G.L. Weinstock

COMMENTS:

Were field strength effects noted on the F18 or not, due to carbon fibre composite application?

AUTHOR'S REPLY:

There were no serious problems. The F18 has landed successfully on an aircraft carrier. Some minor problems such as ground power supply were experienced.

REFERENCE No. OF THE PAPER: 3/15
DISCUSSOR'S NAME: G. Orion
AUTHOR'S NAME: G.L. Weinstock

COMMENTS:

What measurements were made to check that the value of 20 dB was satisfactory? It seems to be a low figure, why could it not be improved? I think that you will need to introduce a conductive bond; you could get a much better value without undue difficulty.

AUTHOR'S REPLY:

It is difficult to make measurements inside an aircraft. The real value was perhaps better than 20 dB. The design figure was 26 dB and in fact it may have been 30-40 dB on test.

REFERENCE No. OF THE PAPER: 3/15
DISCUSSOR'S NAME: G. Orion
AUTHOR'S NAME: G.L. Weinstock

COMMENTS:

In your presentation, you mentioned that fuel system has to be grounded.

Because part of the fuel circuitry is routed underneath carbon panels, did you introduce new lightning protections? (ie larger tube section). We know that a large amount of current could transfer through the pipes instead of flowing through the structure as it is the case with an all-metal aircraft.

We did introduce a better protected fuel gauging system and improved its resistance to induced voltages

REFERENCE No. OF THE PAPER: Session II and III - Overall Discussion
DISCUSSOR'S NAME: B.J.C. Burrows
AUTHOR'S NAME: G. Weinstock

COMMENTS:

The importance of geometry in screening is equally valid for wires behind carbon doors, as for wires in aperture regions, as the cockpit. Much of the present success in introducing carbon fibre materials to aircraft and lack of EMC and lightning problems probably comes from the natural screening provided by the metal structure.

Do McDonnell ground their twisted pair wiring screens both ends, and if not, how do you relieve the problem of common mode voltages; by transformers?

AUTHOR'S REPLY:

I agree with the first comment.

Yes, we ground twisted pair wiring screens at both ends.

REFERENCE No. OF THE PAPER: 3/15
 DISCUSSOR'S NAME: F. Hildebrandt, MEB
 AUTHOR'S NAME: G. Weinstock

COMMENTS:

For the trials you compared Al samples with carbon fibre ones, with respect of shielding capability. Was the thickness of carbon fibre samples made according to stress requirements or electric conductivity etc requirements (taking into account your mentioning of practically no difference in electric performance)?

AUTHOR'S REPLY:

The thickness of the carbon composite material was for the most part determined by structural requirements. Some testing was performed however, on thin 1 or 2 ply material for comparison purposes.

REFERENCE No. OF THE PAPER: Session II and III - Overall
 DISCUSSOR'S NAME: C. Blake, USAF

COMMENTS:

Relative to modifications to Military Standards or Specifications the comment was that the modifications are definitely necessary, eg bond specification changes; however, insufficient data exists on which to base such changes. Rather, as peculiar deviations are necessary, they must typically be handled as one-time changes.

It is unlikely that, given good definition of necessary changes, the specifications and standards would be rapidly modified.

REFERENCE No. OF THE PAPER: Session II and III - Overall
 DISCUSSOR'S NAME: R.H. Evans

COMMENTS:

I agree that many specifications on EMC and lightning have not yet been revised in line with recent advances in technology. However, the NATO Air Electrical Working Party on Standardisation is actively considering a new lightning testing standard, based on documents issued by SAE in USA and the Culham Laboratory in UK. Also I understand that SAE are drawing up recommendations for the revision of the EMC Specification MIL 461/462, and the UK is taking part in these discussions. In the meantime, specifications for new aircraft projects use existing general specifications so far as this is possible, but with some of the test methods and test limits changed to correspond to present-day needs.

REFERENCE No. OF THE PAPER: Session II and III - Overall
 DISCUSSOR'S NAME: G. Du Bro

COMMENTS:

1. I should like to make a point concerning the need for careful and validated design for aircraft utilizing composites. When measurements for shielding effectiveness were made by Air Force Flight Dynamics Laboratory, samples for honeycomb enclosed composites indicated that E-M energy was enhanced rather than attenuated, in a frequency range 10-50 kHz, a range which reflects a maximum power spectral density (energy) for a lightning direct stroke. No matter whether the measurements were properly made with or without proper grounding techniques, the mere occurrence of such phenomena shows an especially unexpected negative result.

2. Secondly, I wish to emphasize strongly a perception stated in this meeting. Composites are not a problem. In fact, they afford substantial benefits -

increased strength-to-weight ratio
 improved energy efficiency.

The issue is how to address an integration of new emerging technologies without excessive cost or decreased performance.

SESSION IV

REFERENCE No. OF THE PAPER: 4/16

DISCUSSOR'S NAME: R.H. Evans

AUTHOR'S NAME: R. Weber

COMMENTS:

Would the speaker please say what changes in the electrostatic characteristics of aircraft are likely to be introduced by the use of carbon fibre composites.

AUTHOR'S REPLY:

On ne peut pas donner un avis définitif pour un matériau aussi hétérogène que le composite carbone. Nos fabrications actuelles conduisent à des épaisseurs de résine en surface tellement peu épaisses que les fibres de carbone permettent toujours une certaine conductivité - le processus de conductivité est le même que celui permettant à des charges électrostatiques de traverser une peinture isolante déposée sur une surface métallique.

REFERENCE No. OF THE PAPER: 4/16

DISCUSSOR'S NAME: G. Orion

AUTHOR'S NAME: R. Weber

COMMENTS:

1. Des techniques existent aujourd'hui pour protéger les surfaces optiquement transparentes lorsque celles-ci sont réalisées en verre. A ce jour, on ne connaît pas de traitement pour les surfaces réalisées avec des matériaux plastiques (cas des verrières) qui soit, sous l'aspect de la résistance à l'érosion, acceptable.

2. VHF. Bien que les bruits d'origine électrostatique soient réduits par rapport à ceux observés en plus basse fréquence, il existe néanmoins des cas où les perturbations dans la communication VHF et celles engendrées dans les systèmes de radio navigation VHF sont très pénalisantes et nécessitent l'application de techniques de protection.

3. VLF. Un moyen de réduire l'influence des perturbations dans cette gamme est d'utiliser des antennes captant le composante magnétique du champ.

AUTHOR'S REPLY:

1. Tout à fait d'accord mais il semble qu'il existe une possibilité consistant à placer dans le plastique, aussi près que possible de la surface extérieure, une traine métallique similaire à celle utilisée pour certains réseaux chauffants de dégivrage.

2. Le traitement qui sera appliqué pour les basses fréquences conviendra également aux hautes fréquences.

3. Il est très probable que de nouvelles antennes, captant le composante magnétique du champ seraient beaucoup moins perturbées. Mais sont-elles au point actuellement?

REFERENCE No. OF THE PAPER: 4/16

DISCUSSOR'S NAME: Borgonovo - Italy

AUTHOR'S NAME: R. Weber

COMMENTS:

What type of static protection has been used to drain static charges from windshields and other cockpit transparencies? How much were the optical properties of the transparencies degraded?

AUTHOR'S REPLY:

Les pare-brise en verre sont traités par dépôt à chaud d'oxyde d'étain - la transparence reste très bonne, probablement de l'ordre de 80 à 90%. Les pare-bris en plastique ne sont pas actuellement traités, mais il semble que des solutions soient possibles, par exemple en utilisant à proximité immédiate de la surface extérieure, des grillages métalliques tels que ceux utilisés pour les réseaux chauffants de dégivrage.

REFERENCE No. OF THE PAPER: 4/17
 DISCUSSOR'S NAME: G. Barton
 AUTHOR'S NAME: B.J.C. Burrows

COMMENTS:

Induced voltage levels of 1000 V/m were predicted for a CFC fuselage and it was further stated that it is a low frequency problem and therefore isolating transformers in equipment can be used. I doubt this is true because when considering 1000 V/m the possible induced current levels could be in excess of 100 A on all wires, ie Power, Signal and Control.

AUTHOR'S REPLY:

The 1000 V/m is a worst case figure assuming wire routes do not make use of available screening from metal and other high conductivity regions. Clearly this level may well be too severe for long routes (say greater than 1 m). Hence wire routing is important and part of the design problem is to use routes which have low common mode voltages. For reasonable values of CM voltage, isolating transformers may well be satisfactory, eg for data bus lines. By this means, or some other, common mode voltage isolation will have to be provided.

REFERENCE No. OF THE PAPER: 4/17
 DISCUSSOR'S NAME: G. Orion
 AUTHOR'S NAME: B.J.C. Burrows

COMMENTS:

Use of metal honeycomb with glass fibre skins is not recommended as far as lightning protection is involved.

By comparing lightning behaviour of metal honeycomb with glass fibre skins and metal honeycomb with carbon fibre skins, is your recommendation not to use metal honeycomb with carbon fibre skins?

AUTHOR'S REPLY:

I have no experience of glass fibre skinned aluminium honeycomb sandwich panels. However regarding the lightning threat there should be no physical damage problem with it so long as the electrical insulation of the glass fibre prevents all risk of current flowing in the honeycomb.

As a general reply I should like to say that aluminium honeycomb can be successfully used both in glass fibre and carbon fibre, but each application must be considered on its merit for safety.

REFERENCE No. OF THE PAPER: 4/18
 DISCUSSOR'S NAME: Little
 AUTHOR'S NAME: Heichele

COMMENTS:

Thin aluminium foil (~10 μm) or a similar covering vacuum-deposited would give a smoother profile than the carbon fibres themselves because the aluminium would lie on top of the epoxy resin surface. The mechanical properties should not be much affected by such a thin layer: would the performance as an antenna be improved? Are there any extra problems that would result?

AUTHOR'S REPLY:

A smooth cover of aluminium foil or vacuum-deposited aluminium usually improves the RF performance of the CFRP-surface. But there are many problems which have to be considered. Metallic surfaces of high accuracy focus the sunlight in the paraboloid. Therefore the reflector has to be covered by paints diffusing the sunlight in order to avoid heating and destruction of the fuel system.

Another aspect is that from the connections between CFRP and aluminium problems arise because of the different thermal expansion coefficients. Therefore it is difficult to arrange contact of aluminium foils on the CFRP material so that the connection can withstand the space environmental thermal conditions.

A third aspect is that facilities for vacuum depositing of metal on large reflectors are not available.

REFERENCE No. OF THE PAPER: 4/18
 DISCUSSOR'S NAME: Hildebrandt, MBB - Hamburg
 AUTHOR'S NAME: Heichele, FRG

COMMENTS:

Were measurements made of the quality of geometry of reflector under different temperature conditions?

AUTHOR'S REPLY:

The mechanical qualification tests of the CFRP antenna have been carried out by Dornier Systems. I personally have no knowledge of measurements of the antenna geometry under different temperature conditions. Dornier Systems have calculated the thermal distortions of the antenna structure assuming different cases of temperature distributions on the structure which can be expected in space. The maximum computed degradation of the antenna geometry from the ideal parabolic curvature was about 0.2 mm.

REFERENCE No. OF THE PAPER: 4/19
 DISCUSSOR'S NAME: J.C. Kleine ESG - Munchen
 AUTHOR'S NAME: Dr. P. Geren

COMMENTS:

Do we have to consider new and more effective measures to protect the pilot inside an all-composite aircraft?

AUTHOR'S REPLY:

Possibly wires attached at one end to the airframe will experience large voltages at the open end.

REFERENCE No. OF THE PAPER: 4/19
 DISCUSSOR'S NAME: G.W. Underwood
 AUTHOR'S NAME: Dr. P. Geren

COMMENTS:

The use of a fibre optics data bus might appreciably reduce the problems of EMC and EMP - both for the systems engineer and the structures engineer. Is Boeing interested in applying this technology and, if so, within what timescale could one expect to see it adopted?

AUTHOR'S REPLY:

My Group, Systems Technology, is investigating the applications of Fibre Optics (F/O) to avionics. As a Group, we are promoting the incorporation of F/O into future Boeing aircraft. I believe that F/O will be included in the successor to the 767/757, provided there are no insurmountable reliability/maintenance problems.

REFERENCE No. OF THE PAPER: 4/19
 DISCUSSOR'S NAME: B.J.C. Burrows
 AUTHOR'S NAME: Dr. P. Geren

COMMENTS:

1. You mentioned the need for calculating the additional effect of screening by control wires, metal hydraulic pipes etc. For 2D geometry this can be accomplished now (for the lightning frequency range up to ~1 MHz) by the use of Culham's computer program INDGAL.
2. Does the swept CW system enable you to measure really low interference levels in wires, since, for the test current used, you need to measure signal levels in the region of microvolts, which is below the noise level of the receiver?

AUTHOR'S REPLY:

1. The additional screening I described is generally due to aspects of the geometry which may not be treated as 2-D structures.
2. In our swept-CW tests, we systematically perform coherent noise measurements. We consider a signal/coherent noise ratio of 20 dB acceptable.

REFERENCE No. OF THE PAPER: 4/19
 DISCUSSOR'S NAME: G. Weinstock
 AUTHOR'S NAME: Dr. P. Geren

COMMENTS:

Reduction of lightning induced voltage by using twisted pair balanced wiring as opposed to a single wire has been found to be 60 to 80 dB reduction. I think the 40 dB reduction mentioned by the Author to be very conservative. Our test results show 60 to 80 dB for our wire and cable methods.

AUTHOR'S REPLY:

The 40 dB figure was a pessimistic guess. I am pleased to note that you found a 60 to 80 dB reduction in actual installations. Undoubtedly the circuits were very well balanced.

REFERENCE No. OF THE PAPER: 4/19
 DISCUSSOR'S NAME: C. Blake
 AUTHOR'S NAME: Dr. P. Geren

COMMENTS:

Could you describe the extent of the conservatism implied by assuming single-ended structural return wiring. What is a number that would be expected in a more realistic design?

AUTHOR'S REPLY:

A pessimistic guess is 40 dB reduction for differential mode voltage with twisted pair wiring and balanced loads. G. Weinstock's experience with the F18 is 60 to 80 dB reduction

REFERENCE No. OF THE PAPER: 4/19
 DISCUSSOR'S NAME: Jacobsen, AUP Member Germany
 AUTHOR'S NAME: Dr. P. Geren

COMMENTS:

To what extent does the pitot tube on the aircraft nose pose a lightning threat?

AUTHOR'S REPLY:

Considerably. The pitot boom will undoubtedly be an attachment point for lightning. The boom must be grounded to the airframe by a heavy galvanized conductor. Pitot heater wiring must be protected by routing it inside the lightning ground strap.

SESSION V

REFERENCE No. OF THE PAPER: 5/20
 DISCUSSOR'S NAME: K.F. Rogers
 AUTHOR'S NAME: Blake/Corbin

COMMENTS:

Thank you for a most interesting paper. It is most useful to see the problems set out systematically in this way. Hopefully, members of the audience will be able to supply some of the answers. There is one aspect that you touched upon indirectly under corrosion, and that is the behaviour of the composite in a wet environment, about which we have heard very little at this Conference. As we know, it can affect us by changing the electromagnetic properties of the composite, or by accelerating electrochemical effects at joints. May I ask that we should determine definitely whether a problem exists, and that the problem should not be lost in a gap between this Conference and the Athens meeting?

AUTHOR'S REPLY:

I agree that the environment is important relative to degradation. This is to be included in our recommended programme to Headquarters A.F. Also, relative to repair technology the broad subject is little known to the author; however, I agree that it is an issue which must be dealt with and will assure its inclusion in our proposal for follow-on work.

REFERENCE No. OF THE PAPER: 5/20
 DISCUSSOR'S NAME: G. Barton
 AUTHOR'S NAME: Blake/Corbin

COMMENTS:

When are the electromagnetic problems going to be addressed and will they be compatible with the mechanical and structural programmes? Will the production of Specifications, standards to assist in the solution of possible EMC problems, be within the timescales of those structural programmes?

AUTHOR'S REPLY:

We are involved in the EMC problems of metal aircraft. We do not have enough quantitative data yet to provide Specifications to meet the CFC situation. We are addressing the problem however. It is a matter of cataloguing all the available data and applying it systematically.

REFERENCE No. OF THE PAPER: 5/20
 DISCUSSOR'S NAME: K. F. Rogers
 AUTHOR'S NAME: Blake/Corbin

COMMENTS:

May I raise the problem of repair, which was not included in your paper. For example, if repairs are effected to composites skins in the field, how do you ensure that electrical bonding is effected across the repair? If this is not adequate the EM properties of the skin will be altered and the positions of maximum field intensity within the aircraft may be redistributed. Do you have any plans for work in this area?

AUTHOR'S REPLY:

This topic has been raised many times. It has been addressed and was unfortunately not included in the paper. It will be covered adequately in future however.

REFERENCE No. OF THE PAPER: 5/20
 DISCUSSOR'S NAME: B.W. Smithers (ERA Technology Ltd., UK)
 AUTHOR'S NAME: C.L. Blake

COMMENTS:

A Vu-graph shown by the Author, but not reproduced in his paper, was a lucid flow chart, part of which emphasised the need for adequate characterisation of CFC constituents and properties.

We support this view, which has also long been held by Mr K. F. Rogers of Materials Department, RAE, UK. We therefore ask all who present fundamental electrical data on CFC, (eg resistivity, screening performance etc), to identify fibre type and resistivity and the resin type wherever possible.

Fibre volume fraction is also valuable and when, for example, combined with dc resistance values on test samples of unidirectional material, (current flow in direction of fibres), can add immense support to the plausibility of resistivity values quoted at high frequencies.

AUTHOR'S REPLY:

The transcript indicated that the author was of the opinion that this matter is one for the standardisation organisation, to be included in future specifications.

REFERENCE No. OF THE PAPER: 5/21
 DISCUSSOR'S NAME: G. Weinstock
 AUTHOR'S NAME: J. Birken

COMMENTS:

With reference to the statement that AV-8B used aluminum foil for EM protection; actually there is no Al foil on the AV-8B for EM protection - a spray is used for lightning protection only, not for EM shielding.

AUTHOR'S REPLY:

I stand corrected on the statement that Al foil is used on the AV-8B. Tin spray is used as you say, imposing a greater weight penalty than Al foil to avoid corrosion. Our definitions of shielding differ. Any means that modifies aircraft surface current distribution Js alters the internal electromagnetic field hence this may be construed as shielding.

REFERENCE No. OF THE PAPER: 5/21
 DISCUSSOR'S NAME: W. Bascom
 AUTHOR'S NAME: J. Birken

COMMENTS:

I understood that the butt joint involves using bolts through the composite section. Although CFRP is very tough in the 'through fibre' direction the interlaminar toughness of epoxy-graphite composites is very low; slightly higher than the epoxy itself. The probability of fatigue interlaminar crack growth is very great and, although laboratory tests of bolted material may be satisfactory, it is my opinion that the risk is very real. The cost of the stop joint may not be all that high in the long term.

AUTHOR'S REPLY:

Extensive examination of joints commonly being used for production aircraft as well as composite joints for future composite aircraft quickly demonstrated that butt-joints are the prime joint generic family.

REFERENCE No. OF THE PAPER: 5/21
 DISCUSSOR'S NAME: T.A. Collings
 AUTHOR'S NAME: J. Birken

COMMENTS:

It is implied that bolted joints in CFRP are inefficient. Work at RAE Farnborough has shown that statically CFRP joints are more efficient on a specific strength basis than other methods. Evidence exists to suggest that they are also better in fatigue.

REFERENCE No. OF THE PAPER: 5/21

DISCUSSOR'S NAME: L. Skorozewski

AUTHOR'S NAME: J. Birken

COMMENTS:

1. The trend in component technology seems to be towards lower power, higher density, more sensitive devices (eg silicon components).

Is the author confident that, in the absence of effective airframe shielding due to increased use of GFC material, the alternative protection methods referred to (twin twisted wire, balanced loads, cable screening) will be sufficient.

2. Are additional protection methods required?

3. Should we be looking towards inherently harder devices?

AUTHOR'S REPLY:

1,2. Yes, the protection technology is available. The key problem is that of deciding how much protection is needed.

3. Designing hardness into devices is desirable, however, satisfying the high density required by likely future devices makes this difficult.

REFERENCE No. OF THE PAPER: 5/21

DISCUSSOR'S NAME: C. Blake

AUTHOR'S NAME: J. Birken

COMMENTS:

A question relative to the ability to deal with increasingly sensitive electronic circuits or components. The comment made was that a joint (combined) USAF, NAVY, NASA and FAA programme on Atmospheric Electricity Hazards Protection is intended to deal with this, including the effects of lightning induced energy. This programme will cover composite structures as well as metals.

AUTHOR'S REPLY:

The Author meets with the questioner at these Atmospheric Electricity Hazards meetings and is Director on the Naval portion of their programme.

REFERENCE No. OF THE PAPER: 5/21

DISCUSSOR'S NAME: T.A. Collings

AUTHOR'S NAME: J. Birken

COMMENTS:

Can the author be more explicit about moisture absorption in CFRP. Moisture can be absorbed in many ways and moisture gradients can be formed in the composite that can be as large as 2% at the surface to zero at the centre. The average moisture soak-up for CFRP for an aircraft service life is given as 1%, which is a quasi-steady state that is fairly stable throughout the composite thickness. To reach an average of 1% in the laboratory is difficult and accelerated ageing can result in a non-representative average of 1%.

In looking at EMC problems with wet laminates it is important that this difference in obtaining the 1% moisture level should be noted. Since laminates soak up moisture from the time they are cured then moisture content should be another material parameter that is quantified and stated as well as fibre volume fraction and orientation etc.

Thermal spiking of CFRP can cause laminate cracking, this can lead to further moisture being retained in the micro cracks. Both the process of cracking and further moisture pick-up may have implications on EMC effects.

AUTHOR'S REPLY:

Limited data is available. The current US Navy programmes will include an investigation of this topic.

REFERENCE No. OF THE PAPER: 5/22
 DISCUSSOR'S NAME: J.M. Thomson
 AUTHOR'S NAME: R. Wallenburg et al

COMMENTS:

The last viewgraph you showed had details of weight penalties for a given shielding effectiveness. This does not appear in the Conference pre-print. Can you arrange for it to appear in the Conference proceedings, please?

AUTHOR'S REPLY:

The information will be sent to AGARD.

REFERENCE No. OF THE PAPER: 5/22
 DISCUSSOR'S NAME: K.F. Rogers
 AUTHOR'S NAME: R. Wallenburg

COMMENTS:

May I ask again a question I asked Dr Lodge on the first day. Regarding Fig 7, have you considered the effect of mechanical loading and fatigue on the admittances of joints in composites?

AUTHOR'S REPLY:

At this point in time, I have not, but Boeing Aerospace Co. may have data.

REFERENCE No. OF THE PAPER: 5/22
 DISCUSSOR'S NAME: K.F. Rogers
 AUTHOR'S NAME: R. Wallenburg

COMMENTS:

Just to note that, in reply to the previous discussion, the erosion protection in structures such as, for example, the projected DC 10 fin is provided by a sheet metal wrap-round leading edge strip, and the question of further lightning protection does not arise.

REFERENCE No. OF THE PAPER: 5/22
 DISCUSSOR'S NAME: G. Barton
 AUTHOR'S NAME: R. Wallenburg

COMMENTS:

With reference to the threat levels to components and the method of defining susceptibility of the components; has any thought been put into employing similar tests to equipment EMC qualification tests to provide susceptibility criteria of the equipment rather than just a NO,GO test?

AUTHOR'S REPLY:

I do not have data. Integrated circuit susceptibility (degradation) is based on approximately 0.2 volt change in output.

REFERENCE No. OF THE PAPER: 5/22
 DISCUSSOR'S NAME: I.P. MacDermid
 AUTHOR'S NAME: R. Wallenburg and G. Dike

COMMENTS:

Without any information about the size of the enclosure I was a little unsure as to whether the rise in shielding effectiveness was due to some resonance of the enclosure with the wavelength.

AUTHOR'S REPLY:

The enclosure was of cylindrical, spherical or parallel plate design. The volume to surface ratio (VS = 1) specified the size of the enclosure.

REFERENCE No. OF THE PAPER: 5/22
DISCUSSOR'S NAME: Hildebrandt
AUTHOR'S NAME: R. Wallenburg

COMMENTS:

The Boeing representative was asked to describe the Company experience with erosion of protective coatings.

AUTHOR'S REPLY:

The Al foil shielding for lightning induced transients is placed on the inside surface, out of the air flow. A flame spray, added for protection from direct damage effects and P-static reduction, has been shown to be adequate from the in-service record. I believe it is also a maintenance item.

REFERENCE No. OF THE PAPER: 5/22
DISCUSSOR'S NAME: I.P. MacDiarmid
AUTHOR'S NAME: R. Wallenburg and G. Dike

COMMENTS:

What did you use as your criterion for component upset?

AUTHOR'S REPLY:

A change of 0.2 volts at the output of the integrated circuit.

REFERENCE No. OF THE PAPER: 5/22
DISCUSSOR'S NAME: J. Birken
AUTHOR'S NAME: R. Wallenburg

COMMENTS:

Joint admittance of operational degradation Y_j has received a limited amount of attention. A short examination of Y_j revealed a 10-fold reduction under vibration.

REFERENCE No. OF THE PAPER: 5/23
DISCUSSOR'S NAME: B.W. Smithers (ERA Technology Ltd., UK)
AUTHOR'S NAME: Prof. F. Lincoln Vogel

COMMENTS:

We have noted the work done by Gajda, published in 1978 involving intercalation of carbon fibres by antimony pentafluoride and hydrofluoric acid. Fibre breakage was a problem and he discontinued his work in view of the effort underway at the University of Pennsylvania and the Naval Research Laboratory.

I, like many others, was intrigued to hear you speak of your work at the University of Pennsylvania in producing intercalated fibres using nitric acid or arsenic pentafluoride, with electrical conductivities exceeding that of copper and undegraded mechanical properties.

- Q1. Is there a significant toxicity hazard in a fire or crash involving an aircraft containing such materials, and what is the proportion of arsenic involved?
- Q2. Are there significant toxic hazards to operatives during manufacture and assembly of these materials?
- Q3. Are increased corrosive effects observed with these doped materials when used with fasteners of, say, monel or titanium?
- Q4. Are there any deleterious effects on cable sheaths or insulants in contact with such doped CFC?

AUTHOR'S REPLY:

- A1. The arsenic content is 2% to 3% and a hazard could arise. This hazard could be avoided by the use of the nitric acid treated material.
- A2. Simple precautions and protective equipment are required for operatives.
- A3. No corrosive effects with monel fasteners. Effects with titanium are not known at present.
- A4. No deleterious effects on cable sheaths or insulants are expected.

Addendum

ELECTRICAL CONDUCTIVITY OF INTERCALATED GRAPHITE FIBERS
AND ORGANIC MATRIX COMPOSITES MADE THEREFROM

by

Glenn Davis and F. Lincoln Vogel
Moore School D-2
University of Pennsylvania
Philadelphia, PA 19104
USA

It has been shown that acceptor intercalation compounds of graphite which are synthesized in well structured crystals have electrical conductivities which are comparable, and even higher, than that of copper at room temperature. High strength, high modulus carbon/graphite fibers demonstrate an increase of conductivity on intercalation similar to that in well structured crystals except that since the initial conductivity of the virgin fiber is lower than that of the crystal, is correspondingly lower in the final intercalated material. The intercalated fibers can be used to reinforce epoxy matrix composites thereby increasing the conductivity of the latter by several orders of magnitude. Furthermore, new high conductivity carbon/graphite fibers have been prepared which are expected to exhibit even higher conductivity in the organic composites.

1. INTRODUCTION

Carbon/graphite fibers are finding increasing applications as the reinforcing component in epoxy matrix composites because of their very high specific modulus and tensile strength. Fibers of the type that are used to reinforce epoxy matrix composites are characterized by the crystal structure and properties of a highly defected graphite^{1,2}. The crystallites are highly oriented with the crystallographic *a* axis parallel to the longitudinal axis of the fiber and *c* axis normal thereto.

The need for a more highly conducting composite stems from the trend currently in progress to replace metals in aircraft structures with graphite fiber reinforced composites which have strength, weight, and stiffness advantages over metallic materials but which possess lower electrical conductivity. As a larger fraction of the aircraft is fabricated from graphite reinforced composite it becomes vulnerable from various sources:

Lightning Stroke. In order for aircraft to escape serious damage from lightning stroke, the electrical path between the points of impact and discharge must be of relatively low resistance³ — a condition not satisfied by present composites lacking metallic content.

Static Discharge. Under certain conditions, which cannot always be avoided by military aircraft, an electric charge develops on the craft which on reaching a sufficiently high potential discharges with unpleasant, sometimes disastrous results.

Electronic Ground Plane. The electronic communications and navigations equipment in aircraft require a common ground connection maintained by a low resistance path. This is more difficult to provide as a larger fraction of the structure becomes non conducting.

Shielding. The sensitive electronic equipment inside an aircraft is protected from electromagnetic interference (EMI) and electromagnetic pulses (EMP) by the conducting skin which in the case of present composites would be of much reduced effectiveness.

In the general electronics area an urgent need is developing because of the convergence of three factors. First, electronic computer controls, now becoming widespread in use, are increasingly sensitive to minute currents and voltages. Present generation MOS circuitry can change its state with currents as small as 10^{-12} amperes and currents of 10^{-16} amperes are expected to be effective in operation of this type of circuit in the future. This means that very small induced currents can disrupt sensitive control mechanisms. Second, the space around us is being filled with electromagnetic

radiation from a wide variety of sources and having a broad spectrum of characteristics^{5,6,7}. This can have a relatively modest effect such as may be encountered by a home computer⁸ or a mobile communications system, or it may be critical such as on the flight deck of an aircraft carrier where the atmosphere is literally charged with signals of all descriptions. Third, there is a trend to replace metals with reinforced plastics, polymers and epoxies. As a result of the lower electrical conductivity of these organic materials the protection afforded by the metals to the transmission of electromagnetic radiation is absent and thus the hazard goes unabated.

All of the problem areas delineated above benefit from the advent of highly conducting graphite fibers with good mechanical properties which could be used as reinforcing for organic matrix composites.

2. TECHNICAL BACKGROUND

2.1 Graphite Fibers

Graphite, a semi-metal, is a moderately good conductor of electricity with a conductivity σ_a (300K) — $2.55 \times 10^4 \Omega^{-1} \text{cm}^{-1}$ (Refs 9, 10), the subscript "a" indicating a measurement parallel to the hexagonal planes. This value results from a mobility $\mu \sim 1.2 \times 10^4 \text{cm}^2/\text{volt-sec}$ and an equal density of holes and electrons of $n(300\text{K}) = p = 6.7 \times 10^{18}/\text{cm}^3$. The conductivity of highly oriented pyrolytic graphite (HOPG) in the direction normal to the planes is less by a factor of about 3000, with σ_c in the range of 1 to $10 \Omega^{-1} \text{cm}^{-1}$ (Refs 3, 4) the variation probably being caused by variations in planar defects parallel to the hexagonal planes.

Carbon/graphite fibers demonstrate a much lower electrical conductivity than three dimensional crystals ranging from $25 \Omega^{-1} \text{cm}^{-1}$ for very poorly structured carbon fibers made from pitch to $3000 \Omega^{-1} \text{cm}^{-1}$ for the most highly graphitic commercial fibers¹¹. This relationship between structural order as determined by elastic modulus and the electrical conductivity has been known for some time^{12,13}. Bright and Singer¹⁴ studied the relationship between structural perfection as determined by x-ray diffraction and electrical conductivity for various temperatures of treatment of pitch precursor fibers. For their highest temperature of treatment, 3000°C , the electrical conductivity was in excess of $6000 \Omega^{-1} \text{cm}^{-1}$. In a further paper, Bright¹⁵ analyzed resistivity and magnetoresistance data using a development of Yazawa's model¹⁶. He was able to explain in a semi-quantitative way the unusual negative magnetoresistance of poorly graphitized fibers and the change to positive magnetoresistance as the heat treatment temperature (HTT) increased, bringing about a more nearly three dimensional (3-D) structure.

A significant piece of research on fibers done in Japan by Endo and his colleagues at Shinshu University has received scant notice in this country but has produced some startling results. Endo's fibers are grown on ceramic or graphite substrates by thermal decomposition of vaporized hydrocarbon such as benzene at $\sim 1100^\circ\text{C}$ using metal particles as catalysts¹⁷. The fibers range in diameter from 3 to $100 \mu\text{m}$ and length from 10 to 23 cm. The electrical resistivity, tensile strength and Young's modulus were found to be $1-2 \times 10^{-3} \text{ohm-cm}$, $>50,000 \text{psi}$ and $25 \times 10^6 \text{psi}$ respectively. Scanning electron microscopy revealed a scroll type structure and the x-ray orientation was determined to be \vec{a} parallel to the longitudinal axis of the fiber and \vec{c} in the radial direction. In common with either PAN based fiber or the pitch based kind, the properties of interest are improved by heating the vapor grown fibers in the range 2000° to 3000°C for 30 minutes. On heating to about $2600-2800^\circ\text{C}$ the vapor grown fibers undergo an increase in perfection which is shown by the $\circ\circ\circ$ x-ray diffraction lines¹⁸. The graphite lattice constant, C_0 , decreases from its starting value of 6.90\AA to 6.72\AA indicative of a conversion from a two dimensional (2-D) to a three dimensional (3-D) graphite structure. Under the same conditions the C_0 of a PAN fiber decreases from 6.90\AA to 6.82\AA .

The ideal C_0 for graphite is 6.70\AA . This conversion to a perfected 3-D graphitic structure brings with it other property changes such that a fiber with $10 \mu\text{m}$ diameter displays a tensile strength of $625,000 \text{psi}$ and a Young's modulus of $38 \times 10^6 \text{psi}$ (Ref.19). The resistivity of the high temperature heat treatment vapor grown fibers is $60-100 \mu\text{m cm}$ (Ref.19) — the lowest values ever reported for a graphite fiber and a close approach to the ideal graphite \vec{a} axis resistivity, $\rho_a = 40 \times 10^{-6} \Omega \text{cm}$.

The property values quoted for this vapor grown fiber after high temperature heat treatment give a firm indication that this fiber has a highly perfected 3-D structure which makes it a good candidate as a starting material for intercalation to achieve high electrical conductivity. Furthermore, the ratio of the Young's modulus to the tensile strength of this fiber indicates a larger strain to fracture for this fiber than is generally experienced with the PAN or pitch based variety. This characteristic presages favorable mechanical properties.

Based on several types of physical property measurement, we may summarize the properties of carbon fibers of interest at $\sim 300\text{K}$ in the following way:

- (1) Graphite planes are approximately aligned along the axis of the fiber. C-axes are therefore perpendicular to the fiber axis, but are more-or-less randomly oriented in the perpendicular plane. The manner in which the c-axes are aligned with respect to each other in this plane varies considerably. In the present case i.e. vapor grown fibers, a "scroll" structure has been observed. In some commercial fibers a somewhat similar arrangement of c-axes outwards from the fibers axis has been observed (radial structure) while in others the c-axes are nearly random.

- (2) Although the heat treatment temperature (HTT) is generally not a sufficient parameter for specifying the physical properties of fibers, it has been found that materials prepared from the same precursor, and treated under similar conditions, have properties which vary in a sensible way with HTT. In particular, with higher HTT the graphitization process becomes more complete. These changes in structure are reflected in the resistivity of the fiber, and it has been suggested^{12,13} that many properties such as fiber strength, can be correlated better with either the electrical resistivity, or its temperature dependence than HTT.
- (3) The stacking of planes within a region characterized by a given C-axis is sufficiently random for poorly graphitized fibers, that the electronic overlap parameter γ_2 (Ref.3) is essentially zero, and the band structure is more nearly that of two-dimensional graphite. This 2D nature is particularly associated with negative magnetoresistance^{15,16}. In the 2D case the valence and conduction bands do not overlap but just touch.

However, the Fermi-level is depressed from the intrinsic value by the presence of acceptors (related to defects), so that the number of free carriers in the conductivity formula:

$$\sigma = ne\mu$$

is controlled by the defects. For very defective (poorly graphitized) fibers the relaxation time is so short ($\sim 10^{-15}$ secs) that the electronic states are broadened considerably as shown in Figure 2(d).

- (4) Fibers with heat treatment at 2600–2800°C prepared by decomposition of benzene or other hydrocarbon vapors appear to develop electronic characteristics of 3D graphite. This must be related to the improved stacking of adjacent planes in the regular – ABAB – sequence of crystalline graphite. Accordingly, the electronic structure might more nearly be that which has a Fermi level depressed by the presence of acceptors. For these 3D fibers the magnetoresistance becomes positive in all temperature and magnetic field ranges studied.²⁰
- (5) Although the properties of the fibers will be inhomogeneous on a microscopic scale, it is reasonable to assume that they are homogeneous on a macroscopic scale, e.g. along the length of the fiber.

The defects will control the scattering of the current carriers for poorly graphitized fibers, since the mean free path for scattering by defects, λ_d , will be much shorter than the intrinsic value due to phonon scattering λ_p

$$\lambda_d \ll \lambda \text{ (300K)} \quad \text{(poorly graphitized fibers) .}$$

For material with prolonged heat treatment at 3000°C, however, Bright¹⁵ suggests that the mobility at 4K is $\sim 1.1 \times 10^4$ cm²/v-sec, which is almost identical with that of crystalline graphite at 300K. In this case.

$$(\lambda_d \sim \lambda_p) \text{ 300K} \quad \text{(well graphitized fibers) .}$$

It is this observation that gives us particular reason to suspect that intercalated fibers may be prepared with very high conductivities.

2.2 The Electrical Conductivity of Intercalated Compounds

When pure graphite crystals are intercalated with donor alkali metals,^{21,22,23} such as Li or K, both the a-axis and the c-axis conductivities are observed to increase, the former by a factor of five, reducing the anisotropy to about 30. Acceptors on the other hand produce much higher a-axis conductivities as shown in the following table.

TABLE I
Selected Conductivity Values of Acceptor Intercalation
Compounds of Graphite

Compounds and Stage	σ_a $\Omega^{-1} \text{cm}^{-1}$	σ_c $\Omega^{-1} \text{cm}^{-1}$	References
HNO ₃ -1	1.7×10^5	2	24
HNO ₃ -2	3.3×10^5	—	24
HNO ₃ -3	2.9×10^5	—	24
HNO ₄ -4	2.4×10^5	—	24
AsF ₅ -1	5.0×10^5	0.23	25
AsF ₅ -2	6.2×10^5	0.24	25
AsF ₅ -3	5.8×10^5	0.26	25
SbF ₅ -1	3.5×10^5	—	26
SbF ₅ -2	4.0×10^5	—	26
SbF ₅ -3	1.0×10^6	—	27
SbF ₅ -6	5.8×10^6	—	26
FeCl ₃ -1	1.1×10^5	10	28
FeCl ₃ -2	2.5×10^5	—	28

Several other generalities can be taken from the table above. In all known cases involving the acceptor compounds, the maximum conductivity does not occur at stage 1 but at some higher stage, usually 2 or 3. Also, in connection with the experiments on AsF_5 intercalated graphite²⁵ continuous data were taken on samples simultaneously registering the thickness and conductivity as intercalation occurred from pure graphite to stage 1. While there was an orderly progression of conductivity with stage, between stages the conductivity was observed to drop precipitously²⁹.

Therefore, the most important experimental results can be summarized as follows:

- (1) Higher conductivities are found in *strong, acid* (acceptor) compounds, rather than either weak acceptor or donor compounds.
- (2) Maximum conductivity is apparently found for second stage compounds, *at stoichiometry*.
- (3) Generally the anisotropy of principal conductivities *increases* for acceptor compounds but *decreases* for donor compounds.

Relatively little is known about the electronic structure of the acid compounds. We make the following conjectures to explain the high conductivity in these compounds:

- (1) Because of the strong acid nature of the intercalants there is a charge transfer between the graphite lattice and the acid creating an ion which has a highly localized negative charge compared to the graphite wherein the charge (positive) is delocalized. This charge transfer produces an increase of two orders of magnitude in the carrier density of the graphite.
- (2) The mobility of the charge carrier in the case of the acceptor compounds is reduced only moderately compared to that in the pure graphite³⁰.

2.3 Intercalation of Carbon/Graphite Fibers

Several attempts have been made to intercalate carbon/graphite fibers but the values reported in the literature to date barely match that of pristine graphite crystals ($\sigma_a = 2.5 \times 10^4 \Omega^{-1} \text{cm}^{-1}$). In 1976 the author reported a value of $1.8 \times 10^4 \Omega^{-1} \text{cm}^{-1}$ (Ref.31) on fiber specially prepared by Dr Herbert Ezekiel of the Air Force Materials Laboratory, and intercalated to stage 2 with nitric acid. Recently in the Graphite Intercalation Laboratory at University of Pennsylvania several highly structured, high modulus PAN based, pitch based fibers have been intercalated with the following results.

TABLE 2
Electrical Conductivities of Selected Intercalated Fibers

Fiber Type	Starting Conductivity $\Omega^{-1} \text{cm}^{-1}$	Intercalated Conductivity			Resistance Ratios After Intercalation		
		$\Omega^{-1} \text{cm}^{-1}$			HNO_3	$\text{HNO}_3/\text{AsF}_5$	AsF_5
		HNO_3	$\text{HNO}_3/\text{AsF}_5$	AsF_5			
Union Carbide (UC) Type P	2.0×10^3	1.8×10^4	5×10^4		9.0	11.4	31
Celanese-GY70	2.5×10^3	2.2×10^4	2.4×10^4	4.5×10^4	11.1	12.1	27.2

That the conductivities of the UC type P and Celanese GY-70 approach those of intercalated crystals is undoubtedly due to the critical role played by defects in these materials:

- (1) The degree of intercalation can be strongly affected by the density and type of defects present.
- (2) The mobility at ambient temperature can be controlled by defect scattering, rather than electron-phonon scattering, suggested in Section 2.1 for virgin fibers.

Accordingly, the primary requirement for the preparation of a highly conducting fiber is that the defect concentration be reduced as much as is practicable.

2.4 Carbon/Graphite Fiber Composites

The conductivity in a well graphitized commercial fiber is approximately an order of magnitude less than that of the a-axis conductivity in graphite crystal, fiber = $2.5 \times 10^3 \Omega^{-1} \text{cm}^{-1}$ (Ref.14). The elastic modulus and tensile strength of the well-graphitized fibers are in the range of $15-125 \times 10^6$ psi and $14.5-105 \times 10^5$ psi (Ref.14), respectively, which accounts for their use in epoxy composites of very high specific strength. Also, it has been shown that the electrical

resistivity of commercially available fibers can be reduced by greater than one order of magnitude, Table 2, by nitric acid intercalation without significantly affecting the mechanical properties.

The electrical conductivity of some typical laboratory fabricated composites is displayed in Figure 1. For the pristine fibers two types of laminations are shown: one where the plies are all parallel, marked 180° (unidirectional) and one where they are alternated $\pm 45^\circ$, marked 90° . The conductivities of these materials with 55% vol % fiber ($\sigma = 1.9 \times 10^3 \Omega^{-1} \text{ cm}^{-1}$) in 45 vol. % epoxy are $1 \Omega^{-1} \text{ cm}^{-1}$ and $10 \Omega^{-1} \text{ cm}^{-1}$, respectively, the higher conductivity resulting from better contact between fibers with crossed plies.

Also shown in Figure 1 is the conductivity for a composite fabricated from fibers intercalated with HNO_3 to an average conductivity of $\sigma = 8.3 \times 10^3 \pm 5\%$, an increase over the pristine fiber conductivity by about a factor of 4.5. For the same filling factor, however, the composite conductivity is increased by more than an order of magnitude.³²

Recent work in the Graphite Intercalation Laboratory at the University of Pennsylvania makes the fabrication of a highly conducting carbon/graphite fiber composite a very real possibility. Intercalated fibers have yielded σ 's of $> 50,000 \Omega^{-1} \text{ cm}^{-1}$. Using a simple linear relationship from the data presented in the previous paragraph³², a composite of $\sigma > 10000 \Omega^{-1} \text{ cm}^{-1}$ is quite realistic. This level of conductivity would yield ~ 45 db of attenuation at 1 MHz when laid up in a 9 mm thick pane³³. Such a composite when layed up in a slightly thicker dimension would yield correspondingly better attenuation. This composite would present a significant step in solving the previously mentioned problems of lightning stroke, static discharge, electronic ground plane, and shielding for EMI and EMP

3. REFERENCES

1. N.W.Reynolds, Chem and Phys Carbon Vol. 11, Ed. P.L.Walker and P.A.Thrower, Marcel Dekker, New York 1965.
2. Ian L.Spain, Chem and Phys Carbon Vol. 15, Ed. P.L.Walker and P.A.Thrower, Marcel Dekker, New York 1980.
3. Franklin A.Fisher and J.Anderson Plumer, "Lightning Protection of Aircraft", NASA Reference Publication 1008, 1977, p.85.
4. R.A.Perala, K.Lee and R.Cook, Third Symposium on Electromagnetic Compatibility, Rotterdam, May 1977, p.421.
5. Lowell Ponte, Readers Digest, January 1980, p.165.
6. Estimates of Maximum Electric Field Strengths, NTIA Report 79-16.
7. D.G.Bodnar and B.M.Jenkins, Army Materials and Mechanics Research Center Tech. Report, 79-49.
8. Federal Communication Commission Report, 79-555, 14686, Released Oct. 11, 1979.
9. I.L.Spain, Chem. and Phys. Carbon, 8, 1, 1973.
10. C.Zeller, G.M.T.Foley and F.L.Vogel, J. Mat. Sci., 13, p.1114 (1978).
11. F.L.Vogel, Proc. Fourth London International Conference on Carbon and Graphite, 1974, p.332.
12. H.Ezekiel, J. Appl. Phys. 41, 5351, 1970.
13. D.Robson, F.Y.I.Assabghy, E.G.Cooper, D.J.E.Ingram, J. Phys., D.6, 1822, 1973.
14. A.A.Bright and I.S.Singer, "The Electronic and Structural Characteristics of Carbon Fibers from Mesophase Pitch", Carbon.
15. A.A.Bright, "Negative Magnetoresistance in Pregraphitic Carbons", Carbon.
16. K.Yazawa, J. Phys. Soc., Japan 26, 1407, 1969.
17. T.Koyama, M.Endo and Y.Onuma, Japanese Jour. Appl. Phys. 11, 445, 1972.
18. M.Endo, T.Koyama and Y.Hishiyama, Japanese Jour. Appl. Phys. 15, 2073, 1976.
19. T.Koyama, M.Endo and Y.Hishiyama, Japanese Jour. Appl. Phys. 13, 1933, 1974.
20. M.Enō, T.Mori, T.Koyamo and M.Inagaki, Trans. Electrical Eng. Japan A98, 294, 1978.
21. A.R.Ubbelohde and F.A.Lewis, "Graphite and Its Crystal Compounds", Oxford University Press, London 1960.

22. Many relevant references can be found *Mats. Sci. and Engr.*, Vol.31, 1977. (Special edition – "Proceedings of the LA Napoule Conference on Intercalation Compounds of Graphite".)
23. J.E.Fischer, T.E.Thompson, *Physics Today*, July 1978, p.36, "Graphite Intercalation Compounds".
24. F.L.Vogel, H.Fuzellier, C.Zeller and E.McRae, *Carbon*.
25. G.M.T.Foley, C.Zeller, E.R.Falardeau and F.L.Vogel, *Sol. State Comm.* 24, 371, 1977.
26. F.L.Vogel, J.Gan and T.C.Wu, Fifth Lond International Conference on Carbon and Graphite, September 1978.
27. F.Lincoln Vogel, *J. Mat Sci* 12, 982, 1977.
28. Jean Perrachon, Masters Thesis, Univ. of Pennsylvania, August 1978.
29. Claude Zeller, private communication.
30. F. Lincoln Vogel, *Molecular Metals*, p.261 in et seg., Ed William, E.Hatfield Plenum Press, New York, 1978.
31. F. Lincoln Vogel, *Carbon* 14, 1975, 1976.
32. F.L.Vogel and W.C.Forsman, Tech. Rept Air Force Materials Laboratory TR 79-4034 May 79, p.22.
33. D.G.Bodnar and B.M.Jenkins Tech Rept. Army Materials and Mechanics Research Center DAAG46-77-C-0027, Dec. 78, p.7-8.

DISCUSSION

Question:

While intercalation can improve material conductivity what does it do to the structural properties of the graphite/epoxy?

Answer:

The structural properties, tensile strength and modular are largely unaffected. The fibers themselves undergo a slight (20%) increase in modular and a slight (10%) decrease in tensile strength as a result of the intercalation. When these intercalated fibers are incorporated into an epoxy matrix composite no difference is observed compared to an epoxy matrix composite made with unintercalated carbon/graphite fibers.

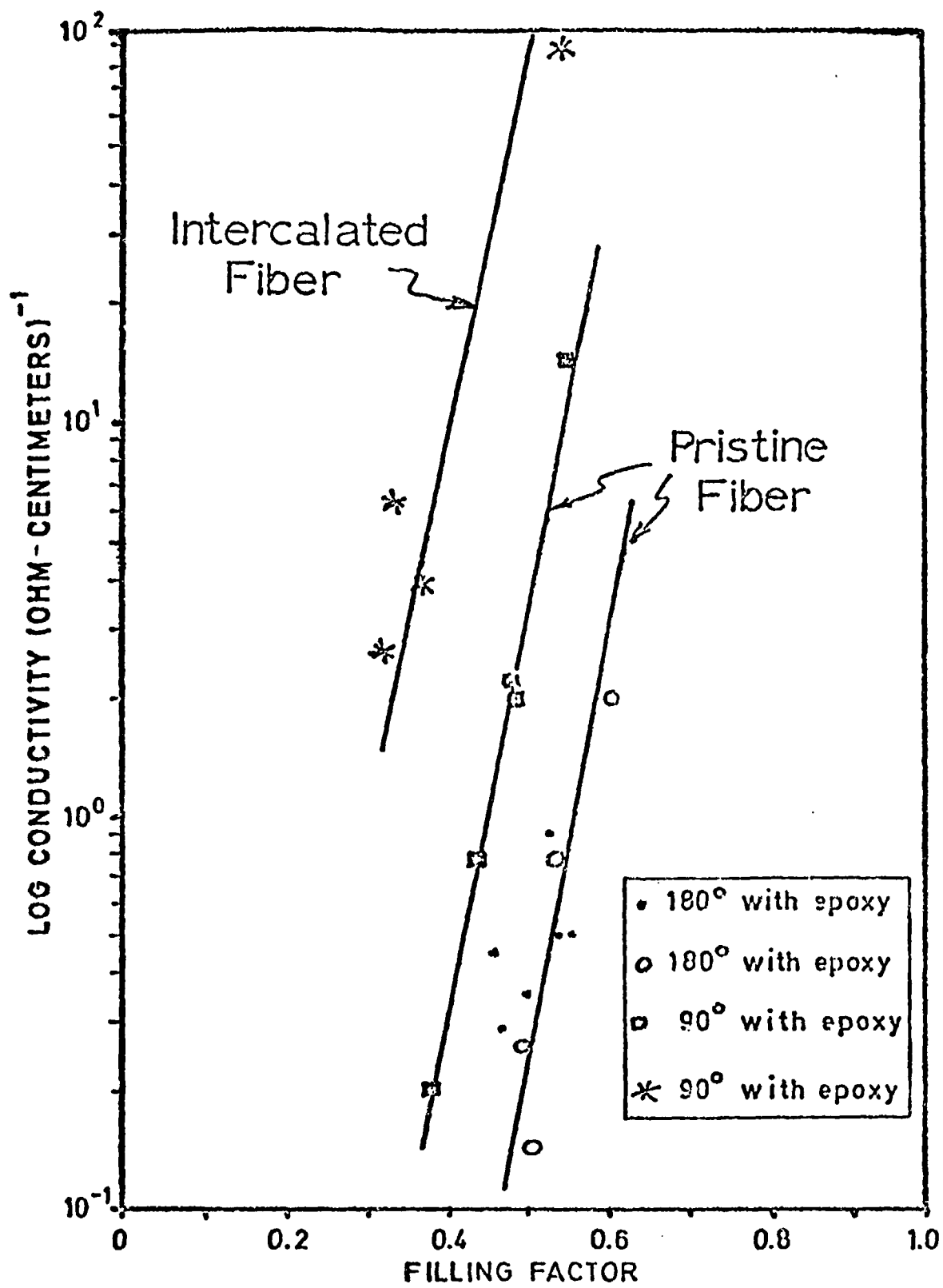


Fig.1 Composite conductivity vs. filling factor

APPENDIX

LIST OF ATTENDEES

ALLIOT, J.C. Mr	ONERA, 92320 Châtillon-sous-Bagneux, France
ASHWORTH, J.H. Mr	Avionics Design, British Aerospace, Woodford nr Stockport, Cheshire, UK
AUDONE, B. Mr	Settore Avionics, Caselle Torinese (10072), Torino, Italy
BALL, W.F. Mr Panel Member	Acting Head, Avionic Facilities Division, (Code 311) Naval Weapons Center, China Lake, CA 93555, USA
BARTON, G. Mr	Westland Helicopters Ltd, Yeovil, Somerset, BA20 2YB, UK
BASCOM, W.D. Dr	Office of Naval Research, London Branch, 223 Old Marylebone Rd, London NW1 5TH, UK
BIRKEN, J.A. Dr	Naval Air Systems Command (AIR-5162G2) Department of the Navy, Washington, D.C. 20361, USA
BLAKE, C.L. Mr	ASD/ENAMA, WPAFB, OH 45433, USA
BOES, G. Mr	Institut für Plasmaphysik der Universität Hannover, Callinstr. 38, D-3000 Hannover, FRG
BOBILLOT, G. Mr	ONERA, 29, Avenue de la Division Leclerc, 32320, Châtillon, France
BORGOVONO, G. Dr	SIAI MARCHETTI S.p.A. Via Indipendenza 2, Sesto Calende, Italy
BRAULT, Y. Mr Panel Deputy Chairman	Thomson CSF, Division Equipements Avioniques & Spatiaux, 178 Bld Gabriel Péri, 92240 Malakoff, France
BRAUN, C. Mr	FhG-INT, Appelsgarten 2, D-5350 Euskirchen, FRG
BREWSTER, D.C. Dr	GEC Marconi Electronics Ltd, West Hanningfield Road, Chelmsford, CM2 8HN, UK
BUNT, G.E. Mr	British Aerospace Aircraft Group, Kingston Brough Division, Richmond Rd, Kingston-upon-Thames, Surrey KT2 5QS, UK
BURROWS, B.J.C. Mr	Culham Laboratory, Abingdon, Oxford, OX14 3DB, UK
CELLETTI, L. Dr Panel Member	Scuola di Ingegneria Aerospaziale, Centro Ricerca Aerospaziale, Via Salaria 581, 00199, Roma, Italy
COLLINGS, T.A. Mr	Structures Department, X 34 Bldg, Royal Aircraft Establishment, Farnborough, Hampshire, UK
CONTI, D.A. Mr	British Aerospace Dynamics, P.B. 161, Site "A", Six Hills Way, Stevenage, Herts, UK
COOPER, C.W. Mr	Head, Airborne Radar Group, R.S.R.E., St Andrews Road, Malvern, Worcs WR14 3PS, UK
DAWSON, D.B. Mr	Procurement Executive, MOD, Castlewood House, 77-91, New Oxford Street, London WC1A 1DT, UK
DIAMOND, F.I. Dr Panel Member	Communications and Control Division, Rome Air Development Center/DC, Griffiss AFB, N.Y. 13441, USA
DOVE, B.L. Mr Panel Member	Head, Avionics Systems Branch, Electronics Directorate, NASA Langley Research, Mail Stop 4777, Hampton, VA 23665, USA
DUBRO, G. Mr	AFAL/FIESL, Wright Patterson AFB, OH 45433, USA
EVANS, R.H. Mr	Engineering Physics Department, Royal Aircraft Establishment, Farnborough, Hants, UK
FERNANDES, Albano Candido de Nogueira TCOR	IGFA/GPA, Av. Leite Vasconcelos Alfragide, 2700 Amadora, Portugal

GALL, D. IEAT	CEAT, 23, Avenue Henri Guillaumet, 31056 Toulouse, France R.S.R.E., St Andrews Road, Malvern, Worcs WR14 3PS, UK
GERHARDT, L.A. Prof. Panel Member	Professor and Chairman, Dept of Electrical and Systems Engineering, Rensselaer Polytechnic Institute, Troy, N.Y. 12181, USA
HAGEMANN, B. Mr	Dornier GmbH, Postfach 1420, D-7790, Friedrichshafen, FRG
HEICHELE, L. Mr	MBB, Antenna Department, Postfach 80 11 40, D-8000 München 80, FRG
HERKERT, C.M. Mr	c/o Messerschmitt Bölkow Blohm, Postfach 80 11 40, D-8000 München 80, FRG
HILDEBRANDT, F. Mr	c/o MBB-Hamir Flugzeugbau, Postfach 950 01 09, 2103 Hamburg 95, FRG
JACOBSEN, M. Mr Panel Member	AEG Telefunken, N14 V3, Postfach 1730, D-7900 Ulm, FRG
JUBE, M.G. Mr	Sous Directeur de la Prospective Aérospatiale, 37, Bld Montmorency, 75016 Paris, France
KLEINE, J. Mr	ESG Elektronik System GmbH, Postfach 80 05 69, 8000 München, FRG
KLISCH, E. Mr	Airbus Industrie, B.P. No.33, 31700 Blagnac, France
KOHL, W. Dr	MBB, Postfach 80 11 60, 8000 München 80, FRG Podensewerk, Postfach 1120, 7770 Ueberlingen, FRG
KUNZMANN, R.G. Mr	FA Eltro GmbH, Entzickungsvertrieb, Kurpfalzring 106, 6900 Heidelberg, FRG
LE BLANC, R. Ing.	Aérospatiale DSBS, Sub-Systèmes, Route de Verneuil, Les Mureaux, 78130, France
LEONARD, R.W. D.	NASA Langley Research Center, MIS 458, Hampton, Virginia 23665, USA
LITTLE, P.F. Dr	Culham Laboratory, Abingdon, Oxford OX14 3DB, UK
LODGE, K.J. Dr	Plessey Research (Caswell) Ltd, Caswell, Towcester, Northants, UK
LUEG, H. Prof. Dr Panel Member	Institut für Technische Elektronik RWTH, Templergraben 55, D-5100 Aachen, FRG
MACDIARMID, I.P. Mr	British Aerospace Aircraft Group, Warton Aerodrome, Preston, Lancashire, PR14 1AX, UK
MASCARENHAS, J.M.B.G. Capt. Panel Member	Direcção do Serviço de Electricidade e Telecomunicações da FA, Rua Escola de Exército, 13, Lisbon, Portugal
MOHR, P. Mr	MBB, Dept. F 2386, Postfach 80 11 60, 8000 München 80, FRG
MOREAU, C. Ing. en Chef Panel Member	STTE/PNI, 129, rue de la Convention, 75731 Paris Cedex 15, France
MULVILLE, D.R. Dr	Naval Air Systems Command, (Air 320B) Department of the Navy, Washington D.C. 20361, USA
ORION, G. Mr	AMD, BA, 78 Quai Carnot, 92 St Cloud, France
PLUMER, J.A. Mr	Lightning Technologies Inc., 560 Hubbard Ave., Pittsfield, MA 01201, USA
PRESTON GEREN, W. Dr	Boeing Commercial Airplane Company, Mail Stop 47-31, Box 3707, Seattle, Washington 98124, USA
PRÜGEL, E. Mr	MBB, Postfach 80 11 60, 8000 München 80, FRG
KANNOU, J. Mr	Thomson CSF, 178 Bld Gabriel Péri, 92240 Malakoff, France
RIPPL, K. Dips. Ing.	MBB, Ottohann, Abt AE224, Postfach 80 11 49, D-8000 München 80, FRG
RODE, R. Mr	MBB Dept. F 2386, Postfach 90 11 60, 8000 München 80, FRG
ROGERS, K.F. Mr	Materials Dept., Royal Aircraft Establishment, Farnborough, Hants, UK
ROWLEY, R B. Mr	"Malunda" 67 Ash Street, Ash, Aldershot, Hants GU12 6LG, UK
RYLES, J.C. Dr Panel Member	Chief Scientist, Air Force Avionics Lab/CA Wright Patterson AFB, Ohio 45433, USA
SANCHES, A. José Ferreira	OGMA ALVERCA, Portugal
MAI. FÜGEL	
SCHRADER, H.G. Dr	c/o Messerschmitt Bölkow Blohm, Postfach 80 11 40, D-8000 München 80, FRG

SHARPLES, T. Mr	Technical Manager, Advanced Structures, British Aerospace Aircraft Group, Warton Division, Warton Aerodrome, Preston, Lancashire, PR4 1AX, UK
SKETCH, H. Mr	MOD, Room 422, St Giles Court 1-13, St Giles High Street, London WC2H 8LD, UK
SKORCZEWSKI, L. Mr	Advanced Projects, British Aerospace, Aircraft Group, Warton Division, Warton Aerodrome, Preston, PR4 1AX, Lancs, UK
SMITH, R.H. Mr	EMC Systems Engineer, EASAAMS Ltd, 86 Shepherds Lane, Guildford, Surrey, GU2 6S10, UK
SMITHERS, B.W. Dr	ERA Technology Ltd., Cleeve Road, Leatherhead, Surrey, UK
SPORRER, F. Ing.	Deutsche Airbus GmbH, Arabellastr. 30, 8000 München 81, FRG
STEYLAERS-SCHMIDT, D.S. Lt. C.	Director Air Armament, Postfach: 902500/501/14, 5000 Köln, 90 FRG
STEWART, C.V. Lt. Col.	Assistant Professor of Electrical Eng., USAF Academy/DFEE, Colorado 80840, USA
STRAHLE, U.D. Mr	Bundesministerium der Verteidigung, RüFo 2, Postfach 1388, 5300 Bonn 1, FRG
STRINGER, F.S. Mr Panel Member	ADXR/FS, Flight Systems Dep., Royal Aircraft Establishment, Farnborough, Hants, UK
TAILLET, J. Dr Panel Member	ONERA, 92320 Châtillon-sous-Bagneux, France
THOMSON, J. Dr	MOD (PE) Royal Aircraft Establishment, Engineering Physics Dept, Farnborough, Hants, UK
TIMMERS, H.A.T. Ir. Panel Member	National Aerospace Laboratory, NLR, Anthony Fokkerweg 2, 1059, CM, Amsterdam, Netherlands
UNDERWOOD, G.W. Mr	Aerospace Aircraft Group, Richmond Road, Kingston-upon-Thames, Surrey, UK
UNTERHITZENBERGER, J. Mr	Messerschmitt-Bölkow-Blöhm, 8012 Ottobrunn, FRG
VAGNARELLI, F. Lt. Col. Panel Member	Aeronautica Militare-Ufficio del Delegato Naz. AGARD, 3 P. le K. Adenauer, 00144, Roma, Italy
VAN KEUK, G. Dr Panel Member	Head of Department, SuS, Forschungs-Institut für Funk und Mathematik, Königstrasse 2, D-5307 Wachtberg-Werthhoven, FRG
VAN LIDTH DE JEUDE, J.L. Mr	Fokker - VFW, B.V. Postbox, 7600, 1117 ZJ, Schiphol Oost, Netherlands
VILLEMEJANE, C. Mr	1, rue du Tourmalet à l'Union, 31240, France
VINGUT, Mr	SNIAS, B.P. No.13, 13722 Marignane, France
VOGEL, F.L. Prof.	The Moore School of Electrical Eng. D.2, University of Pennsylvania, Philadelphia, PA 19104, USA
VOGEL, M. Dr Panel Chairman	DFVLR, NE-HF, D-8031, Oberpfaffenhofen, FRG
VOGL, W. Mr	MBB, Dept. 382, Postfach 80 11 60, 8000 München 80, FRG
WAGEWOORT, M.R.H. Maj. Ir.	Postbus 5953, 2280 42 Ryswyk, Netherlands
WALKER, W.F. Dr	Electrical Engineering Dept., Rochester Institute of Technology, Rochester, N.Y. 14623, USA
WALLENBERG R.F. Dr	Syracuse Research Corporation, Merrill Lane, Syracuse, N.Y. 13210, USA
WEBER, R. Mr	SNIAS, 12, rue Pasteur, 92150, Suresnes, France
WEINSTOCK, G. Mr	Dept. 313, Bld 33, McDonnell Aircraft Co, Box No.516, St Louis, MO 63166, USA
WEISS, M.T. Dr Panel Member	Vice President, General Manager, The Aerospace Corporation, P.O. Box 92957, Los Angeles, CA 90009, USA
WENTZEL, Mr	V.F.W., Hünelndstr. 1-5, D-2800 Bremen 1, FRG
WOITHE, K. Mr	IABG-TFS Hünelndstr. 20, D-8012 Ottobrunn, FRG

REPORT DOCUMENTATION PAGE

1. Recipient's Reference	2. Originator's Reference	3. Further Reference	4. Security Classification of Document
	AGARD-CP-283	ISBN 92-835-0277-9	UNCLASSIFIED
5. Originator	Advisory Group for Aerospace Research and Development North Atlantic Treaty Organization 7 rue Ancelle, 92200 Neuilly sur Seine, France		
6. Title	ELECTROMAGNETIC EFFECTS OF (CARBON) COMPOSITE MATERIALS UPON AVIONICS SYSTEMS		
7. Presented at	the 39th Technical Meeting of the Avionics Panel of AGARD, held in Lisbon, Portugal on 16-19 June 1980.		
8. Author(s)/Editor(s)	Various	Edited by F.S.Stringer	9. Date October 1980
10. Author's/Editor's Address	Various	See Fly Leaf	11. Pages 382
12. Distribution Statement	This document is distributed in accordance with AGARD policies and regulations, which are outlined on the Outside Back Covers of all AGARD publications.		
13. Keywords/Descriptors	Composite materials Avionics Aircraft Fuselages		
14. Abstract	<p>These Conference Proceedings consist of the papers and discussions from the 39th Meeting of the Avionics Panel of the Advisory Group for Aerospace Research and Development-NATO. Subject of the Meeting was the effects of introduction of composite materials on Avionics Systems. The meeting addressed the overall impact of composites electronically as well as providing some review of state of the art in use of composites in aircraft. Three papers were on materials and applications, 6 on characteristics, measurements, modelling and standards, 6 on specific research programs, 4 on electromagnetic effects on radiation patterns and lightning problems, and four on protection and tradeoff methods.</p>		

<p>AGARD Conference Proceedings No.283 Advisory Group for Aerospace Research and Development, NATO ELECTROMAGNETIC EFFECTS OF (CARBON) COMPOSITE MATERIALS UPON AVIONICS SYSTEMS Edited by F.S.Stringer Published October 1980 382 pages</p> <p>These Conference Proceedings consist of the papers and discussions from the 39th Meeting of the Avionics Panel of the Advisory Group for Aerospace and Development-NATO. Subject of the Meeting was the effects of introduction of composite materials on Avionics Systems. The meeting addressed the overall impact of composites</p> <p>P.T.O.</p>	<p>AGARD-CP-283</p> <p>Composite materials Avionics Aircraft Fuselages</p>	<p>AGARD-CP-283</p> <p>Composite materials Avionics Aircraft Fuselages</p>	<p>AGARD-CP-283</p> <p>Composite materials Avionics Aircraft Fuselages</p>	<p>AGARD Conference Proceedings No.283 Advisory Group for Aerospace Research and Development, NATO ELECTROMAGNETIC EFFECTS OF (CARBON) COMPOSITE MATERIALS UPON AVIONICS SYSTEMS Edited by F.S.Stringer Published October 1980 382 pages</p> <p>These Conference Proceedings consist of the papers and discussions from the 39th Meeting of the Avionics Panel of the Advisory Group for Aerospace and Development-NATO. Subject of the Meeting was the effects of introduction of composite materials on Avionics Systems. The meeting addressed the overall impact of composites</p> <p>P.T.O.</p>	<p>AGARD-CP-283</p> <p>Composite material Avionics Aircraft Fuselages</p>
<p>AGARD Conference Proceedings No.283 Advisory Group for Aerospace Research and Development, NATO ELECTROMAGNETIC EFFECTS OF (CARBON) COMPOSITE MATERIALS UPON AVIONICS SYSTEMS Edited by F.S.Stringer Published October 1980 382 pages</p> <p>These Conference Proceedings consist of the papers and discussions from the 39th Meeting of the Avionics Panel of the Advisory Group for Aerospace and Development-NATO. Subject of the Meeting was the effects of introduction of composite materials on Avionics Systems. The meeting addressed the overall impact of composites</p> <p>P.T.O.</p>	<p>AGARD-CP-283</p> <p>Composite materials Avionics Aircraft Fuselages</p>	<p>AGARD-CP-283</p> <p>Composite material Avionics Aircraft Fuselages</p>	<p>AGARD-CP-283</p> <p>Composite materials Avionics Aircraft Fuselages</p>	<p>AGARD Conference Proceedings No.283 Advisory Group for Aerospace Research and Development, NATO ELECTROMAGNETIC EFFECTS OF (CARBON) COMPOSITE MATERIALS UPON AVIONICS SYSTEMS Edited by F.S.Stringer Published October 1980 382 pages</p> <p>These Conference Proceedings consist of the papers and discussions from the 39th Meeting of the Avionics Panel of the Advisory Group for Aerospace and Development-NATO. Subject of the Meeting was the effects of introduction of composite materials on Avionics Systems. The meeting addressed the overall impact of composites</p> <p>P.T.O.</p>	<p>AGARD-CP-283</p> <p>Composite material Avionics Aircraft Fuselages</p>

<p>electronically as well as providing some review of state of the art in use of composites in aircraft. Three papers were on materials and applications, 6 on characteristics, measurements, modelling and standards, 6 on specific research programs, 4 on electromagnetic effects on radiation patterns and lightning problems, and four on protection and tradeoff methods.</p> <p>Copies of papers and discussions presented at the 39th Technical Meeting of the Avionics Panel of AGARD, held in Lisbon, Portugal on 16-19 June 1980.</p> <p>ISBN 92-835-0277-9</p>	<p>electronically as well as providing some review of state of the art in use of composites in aircraft. Three papers were on materials and applications, 6 on characteristics, measurements, modelling and standards, 6 on specific research programs, 4 on electromagnetic effects on radiation patterns and lightning problems, and four on protection and tradeoff methods.</p> <p>Copies of papers and discussions presented at the 39th Technical Meeting of the Avionics Panel of AGARD, held in Lisbon, Portugal on 16-19 June 1980.</p> <p>ISBN 92-835-0277-9</p>
<p>electronically as well as providing some review of state of the art in use of composites in aircraft. Three papers were on materials and applications, 6 on characteristics, measurements, modelling and standards, 6 on specific research programs, 4 on electromagnetic effects on radiation patterns and lightning problems, and four on protection and tradeoff methods.</p> <p>Copies of papers and discussions presented at the 39th Technical Meeting of the Avionics Panel of AGARD, held in Lisbon, Portugal on 16-19 June 1980.</p> <p>ISBN 92-835-0277-9</p>	<p>electronically as well as providing some review of state of the art in use of composites in aircraft. Three papers were on materials and applications, 6 on characteristics, measurements, modelling and standards, 6 on specific research programs, 4 on electromagnetic effects on radiation patterns and lightning problems, and four on protection and tradeoff methods.</p> <p>Copies of papers and discussions presented at the 39th Technical Meeting of the Avionics Panel of AGARD, held in Lisbon, Portugal on 16-19 June 1980.</p> <p>ISBN 92-835-0277-9</p>

4

AGARD

NATO  OTAN

7 RUE ANCELLE · 92200 NEUILLY-SUR-SEINE
FRANCE

Telephone 745.08.10 · Telex 810176

**DISTRIBUTION OF UNCLASSIFIED
AGARD PUBLICATIONS**

AGARD does NOT hold stocks of AGARD publications at the above address for general distribution. Initial distribution of AGARD publications is made to AGARD Member Nations through the following National Distribution Centres. Further copies are sometimes available from these Centres, but if not may be purchased in Microfiche or Photocopy form from the Purchase Agencies listed below.

NATIONAL DISTRIBUTION CENTRES

BELGIUM

Coordonnateur AGARD - VSL
Etat-Major de la Force Aérienne
Quartier Reine Elisabeth
Rue d'Evere, 1140 Bruxelles

CANADA

Defence Science Information Services
Department of National Defence
Ottawa, Ontario K1A 0K2

DENMARK

Danish Defence Research Board
Østerbrogades Kaserne
Copenhagen Ø

FRANCE

O.N.E.R.A. (Direction)
29 Avenue de la Division Leclerc
92320 Châtillon sous Bagneux

GERMANY

Fachinformationszentrum Energie,
Physik, Mathematik GmbH
Kernforschungszentrum
D-7514 Eggenstein-Leopoldshafen 2

GREECE

Hellenic Air Force General Staff
Research and Development Directorate
Holargos, Athens

ICELAND

Director of Aviation
c/o Flugrad
Reykjavik

UNITED STATES

National Aeronautics and Space Administration (NASA)
Langley Field, Virginia 23365
Attn: Report Distribution and Storage Unit

THE UNITED STATES NATIONAL DISTRIBUTION CENTRE (NASA) DOES NOT HOLD STOCKS OF AGARD PUBLICATIONS, AND APPLICATIONS FOR COPIES SHOULD BE MADE DIRECT TO THE NATIONAL TECHNICAL INFORMATION SERVICE (NTIS) AT THE ADDRESS BELOW.

PURCHASE AGENCIES

Microfiche or Photocopy

National Technical
Information Service (NTIS)
5285 Port Royal Road
Springfield
Virginia 22161, USA

Microfiche

Space Documentation Service
European Space Agency
10, rue Mario Nikis
75015 Paris, France

Microfiche

Technology Reports
Centre (DTI)
Station Square House
St. Mary Cray
Orpington, Kent BR5 3RF
England

Requests for microfiche or photocopies of AGARD documents should include the AGARD serial number, title, author or editor, and publication date. Requests to NTIS should include the NASA accession report number. Full bibliographical references and abstracts of AGARD publications are given in the following journals:

Scientific and Technical Aerospace Reports (STAR)

published by NASA Scientific and Technical
Information Facility
Post Office Box 8757
Baltimore/Washington International Airport
Maryland 21240, USA

Government Reports Announcements (GRA)

published by the National Technical
Information Services, Springfield
Virginia 22161, USA



Printed by Technical Editing and Reproduction Ltd
Herford House, 7-9 Charlotte St, London W1P 1HD

ISBN 92-835-0277-9